CONFERENCE PROCEEDINGS

5th INTERNATIONAL CONFERENCE ON COMPUTATIONAL MATHEMATICS AND ENGINEERING SCIENCES

08-10 June,
2021 Van, TURKEY

ISBN
77733

THE FIFTH INTERNATIONAL CONFERENCE ON COMPUTATIONAL MATHEMATICS AND ENGINEERING SCIENCES (CMES-2021), VAN/TURKEY, JUNE 08-10 2021

The **Fifth International Conference on Computational Mathematics and Engineering Sciences (CMES-2021)** will be held in Van Yüzüncüyil University from **June 08-10, 2021 in Van, Turkey.** It provides an ideal academic platform for researchers and professionals to discuss recent developments in both theoretical, applied mathematics and engineering sciences. This event also aims to initiate interactions among researchers in the field of computational mathematics and their applications in science and engineering, to present reccent developments in these areas, and to share the computational experiences of our invited speakers and participants.

Organizing Committee

Chairs of Committee

Hasan Bulut, Firat University, Elazig, Turkey

Zakia Hammouch, Ecole NormaleSuperierue de Meknes, Moulay Ismail University, Morocco

Mohammed Ouazzani Jamil, Universite Privee de Fes, Morocco

Carlo Cattani, Tuscia University, Viterbo, Italy

Haci Mehmet Baskonus, Harran University, Sanliurfa, Turkey

MESSAGE FROM THE GENERAL CHAIRS


Dear Conference Attendees,

We would like to welcome you to the **5th International Conference on Computational Mathematics and Engineering Sciences (CMES-2021)** at Van Yüzüncüyıl University from June 08-10, 2021 in Van, Turkey. This year, the conference includes 300 extended abstracts, out of 300 submissions received in response to the call for papers, selected by the Program Committee. The program features keynote talks by distinguished speakers such as Abdon Atangana from Free State University, South Africa, Dumitru Baleanu, from Institute of Space Sciences, Magurele-Bucharest, Romania, Carlo Cattani from Tuscia University, Viterbo Italy, Juan Luis García Guirao from Technical University of Cartagena, Spain. Oscar Castillo from Tijuana Institute of Technology, Tijuana, Mexico, Ali Yousef from Kuwait College of Science and Technology, Kuwait, Vatan Karakaya from Yildiz Technical University, Istanbul, Turkey, Ali Rostami Photonics and Nanocrystals Research Lab (PNRL), University of Tabriz, Tabriz, Iran. The conference also comprises contributed sessions, posters sessions and research highlights.

We would like to thank the Program Committee members and external reviewers for volunteering their time to review and discuss submitted abstracts. We would like to extend special thanks to the Honorary, Scientific and Organizing Committees for their efforts in making CMES-2021 a successful event. We would like to thank all the authors for presenting their research studies during our conference. We hope that you will find CMES-2021 interesting and intellectually stimulating, and that you will enjoy meeting and interacting with researchers around the world.

.

Hasan Bulut, Firat University Elazig, Turkey.

Zakia Hammouch, École Normale supérieure, Moulay Ismail University of Meknès, Morocco
Harran University, Sanliurfa, Turkey
Thu Dau Mot University, Binh Duong Province, Vietnam
China Medical University Hospital Taichung 40402, Taiwan.

TOPICS

Applied Mathematics,
Financial Mathematics,
Control Theory,
Game Theory
Modeling of Bio-systems for Optimization and Control,
Linear and Nonlinear programming and Dynamics,
Artificial Intelligence,
Geometry and Its Applications,
Analysis and Its Applications,
Statistics and Its Applications,
Mathematics Education and Its Applications,
Algebra and Its Applications.
Engineering Sciences
Computer Science

Information technology
Electrical and Electronic Engineering
Ordinary, Partial, Stochastic and Delay Differential Equations
Chaos and Dynamical Systems
Numerical methods and scientific programming
Fractional Calculus and Applications,
Cryptography and its applications
Computational Fluids mechanics, Heat and Mass Transfers.
Economics and Econometric Studies
Topology and Its Application
Education Sciences
Economics and Econometric Studies
Topology and Its Application

CHAIRS OF COMMITTEE

Prof.Dr.Hasan Bulut, Firat University Elazig, Turkey
Prof.Dr.Zakia Hammouch, Ecole Normale Supérieure of Meknes, Moulay Ismail University Morocco

CO-CHAIRS OF COMMITTEE

Prof.Dr.Mohammed Ouazzani Jamil, Universite Privee de Fes, Morocco
Prof.Dr.Carlo Cattani, Tuscia University, Viterbo, Italy
Assoc.Prof.Dr.Haci Mehmet Baskonus, Harran University, Sanliurfa, Turkey

HONORARY COMMITTEE

SCIENTIFIC COMMITTEE

Mustafa Açıkkar (Adana Science and Tec.University, Turkey)
Bülent Tavlı (TOBB Economics and Tec.University, Turkey)
Halis Yılmaz (Dicle University,Turkey)
Yasin Kaya (Dicle University, Turkey)
Sunil Kumar (National Institute Of Tech. Jamshedpur, India)
Hatun Özlem Güney (Dicle University, Turkey)
Sedat İlhan (Dicle University, Turkey)
Arife Atay (Dicle University, Turkey)
Seçil Yalaz (Dicle University, Turkey)
Özge Kuran (Dicle University, Turkey)
Damla Barlak (Dicle University, Turkey)
Mahmut Isık (Harran University, Sanlıurfa,Turkey)
Tamer Uğur (Ataturk University /Turkey)
Muzaffer Aşkın (Munzur University,Tunceli,Turkey)
Elman Hazar (Igdır University, Turkey)
Fariba Bahrami (University of Tabriz Iran)
Mehrdad Lakestani (University of Tabriz Iran)
Sedaghat Shahmorad, (University of Tabriz Iran)
Serap Şahinkaya (Tarsus University)
Naci Genc (Van Yüzüncü Yıl University, Turkey)
Remzi Tuntas (Van Yüzüncü Yıl University, Turkey)
Kadriye Aydemir (Amasya University,Turkey)
Yadigar Sekerci (Amasya University,Turkey)
Hayati Olgar (Gazi Osman Paşa University,Turkey)
Semih Çavusoglu (Gazi Osman Paşa University,Turkey)
Nagehan Kılınc Gecer (Kırsehir Ahi Evran University,Turkey)
Cem Oguz (Kırsehir Ahi Evran University,Turkey)
Arzu Denk Oguz (Atılım University,Turkey)
Erhan Pişkin (Dicle University,Diyarbakır,Turkey)
Aynur Yalcıner (Selcuk University,Konya,Turkey)
S. Khodayifar (Institue for Adv.Studies in Basic Sciences,Iran)
Javid Ali (Aligarh Müslim University,India)
Hamit Mirtagiloğlu (Bitlis Eren University,Bitlis,Turkey)
Heybetkulu Mustafayev (Yüzüncüyıl University, Turkey)
Cesim Temel (Yüzüncüyıl University, Turkey)
Mehmet Mendeş (Canakkale 18 Mart University, Turkey)
Çağrı KARAMAN (Atatürk University – Erzurum, Turkey)
Ceren KINA (Malatya Turgut Özal University, Turkey)
Harun KAYA (Malatya Turgut Özal University, Turkey)
Olha Ivanyshyn (Izmir Institute of Technology,Izmir, Turkey)
Ozlem Ertekin (Munzur University, Tunceli, Turkey)
Onur Alp İlhan (Erciyes University, Turkey)
Danyal Soybaş (Erciyes University, Turkey)
Fatma Berna Benli (Erciyes University, Turkey)
Inan Ünal (Munzur University, Turkey)
Kemal Aydın (Selçuk University /Turkey)
Dursun Taşçı (Gazi University /Turkey)
Hakan Şimşek (Kırıkkale University /Turkey)
Bilal Şenol (İnönü University, Malatya)
Sertaç GÖKTAŞ (Mersin University, Mersin, Turkey)
Ali Akgül (Siirt University /Turkey)
Esra Karataş Akgül (Siirt University /Turkey)
Abdulkadir Karakaş (Siirt Üniversity,Turkey)
Murat Sat (Erzincan Binali Yıldırım University, Turkey)
İsmail Onur Kıymaz (Ahi Evran University / Turkey)
Ayşegül Çetinkaya (Ahi Evran University / Turkey)
Nergiz (ÖNEN) POYRAZ (Çukurova University, Turkey)
Ozen Ozer (Kırklareli University, Turkey)
Sinan Çalık (Firat Univeristy,Elazıg,Turkey)
Murat Karakaş (Bitlis Eren Univeristy,Bitlis,Turkey)
Ayşe Metin Karakaş (Bitlis Eren Univeristy,Bitlis,Turkey)
Ahmet Yıldız (İnönü Univeristy,Malatya,Turkey)
Aynur Keskin KAYMAKÇI (Selcuk University, Konya)
Nejmi Cengiz (Ataturk University, Turkey)
Abdullah Kopuzlu (Ataturk University, Turkey)
Kürşat Akbulut (Ataturk University, Turkey)
Mesut Karabacak (Ataturk University, Turkey)
Yeşim Saraç (Ataturk University, Turkey)
Sıdıka Şule Şener (Ataturk University, Turkey)
Sait Taş (Ataturk University, Turkey)
Fatma Taşdelen Yeşildal (Ankara University, Turkey)
Şevket Gür (Sakarya Univercity, Turkey)
Serdal Pamuk (Kocaeli Univercity, Turkey)
Fethiye Müge Sakar (Dicle University, Turkey)
Ceren Sultan Elmalı (Erzurum Technical University, Turkey)
Muhammed Yiğider (Erzurum Technical University, Turkey)
Sibel Turanlı (Erzurum Technical University, Turkey)
Ömür Deveci (Kafkas University, Turkey)
Hatıra Günerhan (Kafkas University, Turkey)
Murat Çağlar (Kafkas University, Turkey)
Erhan Deniz (Kafkas University, Turkey)
Nizami Mustafa (Kafkas University, Turkey)
Nigar Yıldırım Aksoy (Kafkas University, Turkey)
M. Ali Dokuyucu (Agrı İbrahim Cecen University, Turkey)
Ahmet Ocak Akdemir (Agrı İbrahim Cecen University, Turkey)
Talat Körpinar(Muş Alparslan University, Turkey)
Selçuk Baş (Muş Alparslan University, Turkey)
Rıdvan Cem Demirkol (Muş Alparslan University, Turkey)
Zeliha Körpinar (Muş Alparslan University, Turkey)
Evrim Toklu (Agrı İbrahim Cecen University, Turkey)
Serhan Eker (Agrı İbrahim Cecen University, Turkey)
Kadirhan Polat (Agrı İbrahim Cecen University, Turkey)
Abdullah Çağman (Agrı İbrahim Cecen University, Turkey)
Erhan Set (Ordu University, Turkey)
Selahaddin Maden (Ordu University, Turkey)
Yıldıray Çelik (Ordu University, Turkey)
Mehmet Korkmaz (Ordu University, Turkey)
Süleyman Şenyurt (Ordu University, Turkey)
Erdal Ünlüyol (Ordu University, Turkey)
Yusuf Pandır (Bozok University – Turkey)
Cemil İnan (Mardin Artuklu University, Turkey)
Çetin Kürşat Bilir (Ahi Evran University, Turkey)
Alper Ekinci (Bandırma 17 Eylul University, Turkey)
Hayriye Esra Akyüz (Bitlis Eren University,Bitlis,Turkey)
Fahrettin Özbey (Bitlis Eren University,Bitlis,Turkey)
Hatice Kuşak Samancı (Bitlis Eren University,Bitlis,Turkey)
Akbar Barati Chiyaneh (Yüzüncüyıl University,Bitlis,Van)
Ufuk Kaya (Bitlis Eren University,Bitlis,Turkey)
M. Tuncay Gençoğlu (Fırat University, Elazığ, Turkey)
Berivan Polat (Munzur University, Turkey)
Alper Polat (Munzur University, Turkey)
Şükran Konca (Bitlis Eren University, Bitlis,Turkey)
Ali Çakmak (Bitlis Eren University, Bitlis,Turkey)
Unal İç (Firat Üniversity, Elazıg)
Burcu Gürbüz (Üsküdar University, Turkey)
Mahir Murat Cengiz (Ataturk University /Turkey)
Şebnem Yıldız (Kırşehir Ahi Evran University /Turkey)
Fatma Sağsöz (Atatürk Üniversity, Turkey)
Semra Yurttancıkmaz (Atatürk Üniversity, Turkey)
Nguyen Huy Tuan (Thu Dau Mot university, Vietnam)

ORGANIZING COMMITTEE

Hasan Bulut (Chair) Firat University, Turkey
Zakia Hammouch (Chair) Ecole Normale Supérieure of Meknes, Moulay Ismail University Morocco
Haci Mehmet Baskonus (Co-Chair) Harran University, Turkey
Mohammed Ouazzani Jamil (Co-Chair) Universite Privee de Fes, Morocco
Carlo Cattani (Co-Chair) Tuscia University, Italy
Fevzi Erdogan (Co-Chair) (Yüzüncüyıl University, Turkey)
Mikail Et (Fırat University, Turkey)
Mehmet Bektaş (Fırat University, Turkey)
Ercan Çelik (Atatürk University, Turkey)
Alaattin Esen (İnönü University, Turkey)
Mir Sajjad Hashemi (University of Bonab, Iran)
Murat Kayri (Yüzüncüyıl University, Van,Turkey)
Musa Çakır (Yüzüncüyıl University, Turkey)
Esin İnan Eskitascıoğlu (Yüzüncüyıl University, Turkey)
Şenay Baydaş (Yüzüncüyıl University,Van,Turkey)
Hakkı Duru (Yüzüncüyıl University, Turkey)
Bülent Taşel (Final International University, Girne, Cyprus)
M. Giyas Sakar (Yüzüncüyıl University, Turkey)
Sebaheddin Şevgin (Yüzüncüyıl University,Van,Turkey)
Onur Saldır (Secretary, Yüzüncüyıl University ,Van)
Aysenur Akkılıç (Fırat University, Elazığ)
Bahar Acay (Fırat University, Elazığ)
Sibel Tarla (Fırat University, Elazığ)

LOCAL COMMITTEE

Hikmet Kemaloğlu (Fırat University, Elazığ)
Çiğdem Bektaş (Fırat University, Elazığ)
Handan Öztekin(Fırat University, Elazığ)
Alper Osman Öğrenmiş (Fırat University, Elazığ)
Mihriban Külahcı (Fırat University, Elazığ)
Münevver Yıldırım Yılmaz (Fırat University, Elazığ)
Yavuz Altın (Fırat University, Elazığ)
Reşat Yılmazer (Fırat University, Elazığ)
Erdal Baş (Fırat University, Elazığ)
Hıfsı Altınok (Fırat University, Elazığ)
Ayşegül Gökhan (Fırat University, Elazığ)
Mehmet Karay (Final Int. University, Girne, Cyprus)
Gülnür Yel (Final Int.l University, Girne, Cyprus)
Emrah Yılmaz (Fırat University, Elazığ)
T.A. Sulaiman (Federal University Dutse, Jigawa)
Mustafa Yeneroglu (Fırat University, Elazığ)
Münevver Tuz (Fırat University, Elazığ)
Gülden Altay Suroglu (Fırat University, Elazığ)
Pervin Taşel (Final Int.l University, Girne, Cyprus)
Fatma Erdogan (Fırat University, Elazığ)
Tolga Aktürk (Ordu University, Turkey)
Asif Yokuş (Fırat University, Elazığ)
Ebru Cavlak Aslan (Fırat University, Elazığ)
Ş. T. Demiray (Osmaniye Korkut Ata Univ., Turkey)
M. Evren Aydın (Fırat University, Elazığ)
Tüba Gülşen (Fırat University, Elazığ)
Hatice Aslan (Fırat University, Elazığ)
Alev Kelleci (Fırat University, Elazığ)
Ramazan Özarslan (Fırat University, Elazığ)
Ahu Ercan (Fırat University, Elazığ)
Berat Karaagac (Adıyaman University, Adıyaman)
Asst. Prof. Dr. Ezgi Kaya (Igdır University, Igdır)
İsmail Hakkı Denizler (Van Yüzüncüyıl Univ., Turkey)
Turgut Hanoymak (Van Yüzüncü Yıl Univ., Turkey)
Ramazan Yazgan (Van Yüzüncü Yıl Univ., Turkey)
Nagehan Akgün (Van Yüzüncü Yıl University, Turkey)
Mehmet Şerif Aldemir (Van Yüzüncü Yıl Univ., Turkey)
Mehmet Açil (Van Yüzüncü Yıl University, Turkey)
Mahmut Karakuş (Van Yüzüncü Yıl University, Turkey)
Hatice Taşkesen (Van Yüzüncü Yıl University, Turkey)
Fatih Kutlu (Van Yüzüncü Yıl University, Turkey)
Cemil Büyükadalı (Van Yüzüncü Yıl University, Turkey)
Mahmut İhtiyaroğlu (Van Yüzüncü Yıl Univ., Turkey)
Şakir İşleyen (Van Yüzüncü Yıl University, Elazığ)
Yener Altun (Van Yüzüncü Yıl University, Elazığ)
İbrahim Enam İnan (Fırat University, Elazığ)
Gökhan Gökdere (Fırat University, Elazığ)
Dilek Günaydın (Fırat University, Elazığ)
Betül Demirdağ (ODTÜ University, Ankara)
Tugba Yazgan (Atatürk University, Erzurum)
Sibel Şehriban Ataş (Fırat University, Elazığ)
Aslı Alkan (Fırat University ,Elazığ)
Beyhan Kemaloğlu (Fırat University, Elazığ)
Mucahit Saydam (Fırat University, Elazığ)
Çağrı Yılmazer (Fırat University, Elazığ)
Merve Zeynep Gecmen(Atatürk University,Erzurum)
Bahar Kalkan (Van Yüzüncü Yıl University, Turkey)
Ömer Küsmüş (Van Yüzüncü Yıl University, Turkey)
Murat Luzum (Van Yüzüncü Yıl University, Turkey)
Hayri Topal (Van Yüzüncü Yıl University, Turkey)
Osman Tunç (Van Yüzüncü Yıl University, Turkey)
Necati Erdoğan (Van Yüzüncü Yıl Üniversity,Van)
Fatih Uludağ (Van Yüzüncü Yıl Üniversity,Van)
Asuman Duva (Van Yüzüncü Yıl Üniversity,Van)
H.Kavurmacı Önalan (Van Yuzuncu Yil Univ.,Turkey)

LANGUAGE EDITORIAL COMMITTEE

Erkan Yuce (Nevsehir Hacı Bektas Veli University, Nevsehir, Turkey)
Suheyla Demirkol Orak (Firat University, Elazıg, Turkey)

PROCEEDINGS

Extended abstracts will be published in some Special Volumes of famous journals. Procedure, Guidelines and Checklist for the preparation and submission of a paper for the Proceedings of CMES-2021 can be found in the journals websites. The journals in which selected and peer-reviewed full papers of CMES-2021 will be published are follows:

1. ABSTRACT [Free]
If Authors submit ABSTRACT TEXTS, then, after getting referees evaluations for these abstracts, they will be published in ABSTRACT PROCEEDING BOOK of CMES-2021 before 30 October 2021. For FULL TEXT PAPERS, Authors have to submit their FULL TEXT PAPERS online via submission system of CMES-2021 untill 20 November 2021. These FULL TEXT PAPERS will be published in FULL TEXT PROCEEDING BOOK of CMES-2021 after getting at least two positive reports.

2. FULL TEXT PROCEEDING BOOK [Free]
At the beginning, if Authors submit FULL TEXT PAPERS, then, after getting at least two positive referee reports, FULL TEXT PAPERS will be published in FULL TEXT PROCEEDING BOOK of CMES-2021 with ISBN:77733 number. Therefore, Abstracts of these FULL TEXT PAPERS will **NOT** be published in ABSTRACT PROCEEDING BOOK of CMES-2021.

3. FRACTAL AND FRACTIONAL [SCI-E],
Seletec paper from CMES-2020 will be published in a special issue dedicated to the Conference entitled "**New Challenges Arising in Engineering Problems with Fractional and Integer Order**".https://www.mdpi.com/journal/fractalfract/special_issues/EPFIO2020
This journal is indexed by Clarivate as SCI-E.

4.Turkish Journal of Science, [Free]
"Participants of CMES 2020 can submit their good quality papers to Turkish Journal of Science. After the peer review process, the papers will be published at TJOS. The authors must write "CMES 2021" as comments to the editor.
(Editor in Chief: Dr. Ahmet Ocak AKDEMİR) For on-line submission: https://dergipark.org.tr/tr/pub/tjos

5.Turkish Journal of Inequalities, [Free]
"Participants of CMES 2021 can submit their good quality papers to Turkish Journal of Inequalities. Selected papers will be published at TJI after the peer review process. The participants can send their papers to erhanset@tjinequality.com. The authors must write "CMES 2021" as the subject.
(Editor in Chief: Prof. Dr. Erhan SET) http://tjinequality.com/

6. MATHEMATICS IN NATURAL SCIENCE (MNS)
*Authors can submit their full text paper directly to the journal by using the following link https://www.isr-publications.com/mns

7. Mathematics in Engineering, Science and Aerospace (MESA), [Free, Scopus]
"Selected papers will be published after peer review in the Journal of Mathematics in Engineering, Science and Aerospace (MESA)"
(Editor in Chief: Prof. Seenith Sivasundaram)
http://nonlinearstudies.com/index.php/mesa

8. Applied Mathematics and Nonlinear Sciences, [Scopus]
Participants of CMES 2021 can submit their high quality full text papers to Applied Mathematics and Nonlinear Sciences by selecting CMES-2021 under the Select Article Type Menu.
(https://www.editorialmanager.com/amns/default.aspx)

9.International Journal of Cognitive Computing in Engineering.
Special Issue on Innovative Developments in Mathematical Simulations for Computational and Engineering **Problems** in the journal of
International Journal of Cognitive Computing in Engineering.
http://www.keaipublishing.com/en/journals/international-journal-of-cognitive-computing-in-engineering/call-for-papers/si-on-innovative-developments-in-mathematical-simulations/

PLENARY & INVITED SPEAKERS TALKS

FRACTIONAL DIFFERENTIATION AND INTEGRATION ABOVE POWER LAW SOME NEW DEVELOPMENTS

Abdon Atangana
University of the Free State, South Africa
abdonatangana@yahoo.fr
athematiCs

Abstract

To capture more complexities in nature some new differential and integral operators were suggested very recently. These differential operators are defined as fractal derivative of order beta of a convolution of power law, exponential decay and the generalized Mittag-Leffler function. I will represent some new theoretical results and their applications to capture nature.

Keywords: Generalized Mittag-Leffler function

REFERENCES

1. A Atangana, D Baleanu, New fractional derivatives with nonlocal and non-singular kernel: Theory and application to heat transfer model, Thermal Science, 2016.

SOME NEW TRENDS IN FRACTIONAL CALCULUS

Dumitru Baleanu [1,2]

[1] Department of Mathematics, Cankaya University, Balgat 06530, Ankara, Turkey

[2] Institute of Space Sciences, Magurele-Bucharest, Romania

Abstract

Fractional calculus is an emerging field of mathematics with important applications in many branches of science and engineering. In this talk some basic problems of the fractional calculus will be reviewed and some new trends will be presented. Illustrative examples from fractional mathematical biology will be given.

Keywords: Fractional calculus***,*** fractional mathematical biology.

REFERENCES

1. D.Baleanu, K.Diethelm, E.Scalas, J.J.Trujillo, Fractional Calculus: Models and Numerical Methods(Series on Complexity, Nonlinearity and Chaos), 2012, World Scientic.

A REVIEW ON WAVELET FRACTIONAL CALCULUS

Carlo Cattani
Engineering School, DEIM, Tuscia University, Italy
cattani@unitus.it

Abstract

In this talk a review on wavelets and their application in fractional calculus, will be discussed. The main properties of the most popular wavelet families will be given, by taking into account of their characteristic features in the Fourier domain. It will be shown that the fractional operators based on wavelets have a very simple expression thus opening new frontiers in the solution of fractional differential problems.

Keywords: Wavelets, local fractional derivative, wavelet series

REFERENCES

[1] D.Baleanu, K.Diethelm, E.Scalas, J.J.Trujillo, Fractional Calculus: Models and Numerical Methods(Series on Complexity, Nonlinearity and Chaos), 2012, World Scientic.
[2] C.Cattani, “Harmonic Wavelets towards Solution of Nonlinear PDE”, Computers and Mathematics with Applications, 50, 8-9 (2005), 1191-1210.
[3] C. Cattani, “Local Fractional Calculus on Shannon Wavelet Basis”, in Fractional Dynamics, C. Cattani, H. Srivastava, X.J. Yang (Eds.) , De Gruyter, Krakow, chp. 1, 2015.
[4] C. Cattani, “Sinc-Fractional operator on Shannon Wavelet Space”, Frontiers in Physics, vol. 6, art.118, (2018) pp. 1-16.
[5] Heydari, M.H. , Hooshmandasl, M.R. , Cattani, C., and Maalek Ghaini, F.M., “An efficient computational method for solving nonlinear stochastic Ito integral equations: Applicationfor stochastic problems in physics”, Journal of Computational Physics, vol. 283, (2015) 148-168.
[6] Heydari, M.H. , Hooshmandasl, M.R. , Shakiba, A. and Cattani, C., “Legendre wavelets Galerkin method for solving nonlinear stochastic integral equations", Nonlinear Dynamics, vol. 85, n.2 (2016),1185-1202.
[7] D.E. Newland, “Harmonic wavelet analysis”, Proc.R.Soc.Lond. A, 443, (1993) 203-222.

SHANNON–WHITTAKER–KOTEL’NIKOV’S THEOREM GENERALIZED

JUANLUİS GARCÍA GUİRAO
Technical University of Cartagena, Spain
juan.garcia@upct.es
http://www.jlguirao.es

Abstract The aim of the present contribution provide a generalization of the classical Shannon-Whittaker-Katel’niko’s theorem for a class of non band-limited signals which plays a central role in the signal theory, the Gaussian map is the unique function which reachs the minimum of the product of the temporal and frecuential width. This solves a conjecture stated by Boas in 1972.

Keywords: Shannon–Whittaker–Kotel’nikov’s Theorem; recomposi- tion of chemical products, signal theory.

REFERENCES

[1]R.P. Boas Jr., Summation formulas and band--limited signals, Tohoku Math. J., 24, (1972), 121-125.

OPTIMIZATION OF TYPE-2 FUZZY SYSTEMS: THEORY AND APPLICATIONS

Oscar Castillo
Tijuana Institute of Technology, Tijuana, Mexico.
ocastillo@tectijuana.mx

Abstract
Type-2 fuzzy systems are powerful intelligent models based on the theory of fuzzy sets, originally proposed by Prof. Zadeh. Most real-world applications up to now are based on type-1 fuzzy systems, which are built based on the original (type-1) fuzzy sets that extend the concept of classical sets. Type-2 fuzzy sets extend type-1 fuzzy sets by allowing the membership to be fuzzy, in this way allowing a higher level of uncertainty management. Even with the current successful applications of type-1 fuzzy systems, now several papers have shown that type-2 is able to outperform type-1 in control, pattern recognition, manufacturing and other areas. The key challenge in dealing with type-2 fuzzy models is that their design has a higher level of complexity, and in this regard the use of bio-inspired optimization techniques is of great help in finding the optimal structure and parameters of the type-2 fuzzy systems for particular applications, like in control, robotics, manufacturing and others. Methodologies for designing type-2 fuzzy systems using bio-inspired optimization in different areas of application are presented as illustration. In particular, we will cover Bee Colony Optimization, Particle Swarm Optimization, Gravitational Search and similar approaches to the optimization of fuzzy systems in control applications, robotics and pattern recognition [1, 2, 3, 4, 5]. Finally, we will also consider using fuzzy logic for enhancing the performance of metaheuristics, where also good results have been achieved.

Keywords: Type-2 Fuzzy Logic, Optimization, Fuzzy Logic, Metaheuristics

REFERENCES

[1] Melin, P., Sanchez, D.: Multi-objective optimization for modular granular neural networks applied to pattern recognition**.**Information Sciences 460-461, 594-610 (2018).

[2] Olivas, F., Valdez, F., Castillo, O., Melin, P.: Dynamic parameter adaptation in particle swarm optimization using interval type-2 fuzzy logic. Soft Comput. 20(3): 1057-1070 (2016).

[3] Castillo, O., Castro, J.R., Melin, P., Rodriguez Dias, A. Application of interval type-2 fuzzy neural networks in non-linear identification and time series prediction. SoftComput. 18(6): 1213-1224 (2014).

ASYMPTOTIC CHARACTERISTICS OF THE THREE-STAGE PROCEDURE WHEN THE NORMAL COEFFICIENT OF VARIATION IS KNOWN WITH SIMULATION

Ali Yousef
Faculty of Engineering, Kuwait College of Science and Technology, Safat 13133, Kuwait
a.yousef@kcst.edu.kw

Abstract

This paper studies the three-stage[Hall, Ann Stat 9(6):1229–1238, 1981]sequential procedure's asymptotic characteristics when the normal population coefficient of variation is known. We estimate the population mean of the normal distribution using the Searls estimator [Searls, J. Amer Statist Ass 59, 308: 1225-1226, 1964]. We tackle three estimation problems; first, minimum risk point estimation using a squared-error loss function plus linear sampling cost, where we find the asymptotic risk and regret. Second, we find the asymptotic fixed-width confidence interval for the mean, and third, we discuss the sensitivity of the procedure to detect any potential shift that occurs in the population mean by finding the asymptotic operating characteristic function. The theoretical results reveal that the asymptotic characteristics of the three-stage procedure depend on the numerical value of the coefficient of variation. A Monte Carlo simulation is conducted using Microsoft Developer Studio software to study the procedure's performance using different values of the coefficient of variation. The simulation results agree with the theoretical findings.

Keywords: Confidence interval, loss function, minimum risk point estimation, operating characteristic function, risk, Searls estimator, a three-stage procedure

REFERENCES

1. Hall P (1981) Asymptotic theory and triple sampling of sequential estimation of a mean. Ann Statist 9: 1229-1238.
2. Searls DT (1964) The utilization of a known coefficient of variation in the estimate procedure. J Amer Statist Ass 59, 308: 1225-1226.
3. Yousef A, Hamdy H (2019a) Three-stage estimation of the mean and variance of the normal distribution with application to inverse coefficient of variation. Mathematics 7(9), 831.
4. Yousef A, Hamdy H (2019b) Three-stage sequential estimation of the inverse coefficient of variation of the normal distribution. Computation 7(4), 69.

THE FORMATION STAGES OF MATHEMATICAL MODELING IN TERMS OF MATH PHILOSOPHY

Vatan KARAKAYA
Department of Mathematical Engineering, Yildiz Technical University, Istanbul, Turkey
Ahi Evran University, Kirsehir, Turkey
vkkaya@yahoo.com

Abstract

The perception of mathematical objects by the human mind has been one of the fundamental questions of philosophy in general and of philosophy of mathematics in particular throughout history. Many schools of thought have put forward different opinions on how the concepts of number and geometric, which are abstaract entities, are perceived by the human mind in the form of "counting" and "measuring". In the philosophical trend led by Descartes, the mathematical verification and model resource was Analytic geometry, which is formed by the combination of algebra and geometry. In this trend, mathematical verification has turned into a verification method in the form of Clarity, Analysis, Synthesis, and Counting. Kant was also one of the philosophers who opened a detailed discussion on how mathematical concepts are formed. Describing mathematical objects as synthetic a priori, Kant claimed that the information obtained by man through the five senses in the body, world turns into perception and then becomes an abstract entity through perception. He argued that both numbers and geometric objects transform from the object to the abstract being and from the abstract being into the objective rules with the relationship of the visible and conceivable realm. However, Frege, one of Kant's followers, defended the thesis that, unlike Kant, numbers are a logical inference, therefore should be analytical a priori, not synthetic a priori. Frege defended the thesis that numbers can be constructed by purely logical rules without a visual space and that "the object of the mind is the mind." Under this view, he argued that the geometric concepts of mathematics require a sensory perception, on the other hand numbers can be deduced by the rules of logic without sensory perception, and this constructed system can represent the relations of real life. In terms of mathematical philosophy, numbers and geometric shapes, which are mathematical objects, have been described as entities designed in the human mind, dependent or independent on human sense perceptions, but have a representation in the material world with a model. This phenomenon will be tried to be explained through the abstract representation of the triangle, which consists only of points as an abstract entity, and its models as representing the triangle in the visible world.

Keywords: Noumenon, Phenomenon, Counting, Measuring

REFERENCES

[1] Alfred North Whitehead, Bilim ve Modern Dünya, 1925 Lowell Dersleri, Öteki Yayınevi, İstanbul, 2018.
[2] Gottlob Frege, Aritmetiğin Temelleri, Sayı Kavramı Üzerine Mantıksal-Matematiksel Bir İnceleme, Yapı Kredi Yayınları, İstanbul, 2020.
[3] Heinz Heimsoeth, Kant'ın Felsefesi, Doğu Batı Yayınları, Ankara, 2014.
[4] Ludwig Wittgenstein, Tractatus Logico-Philosophicus, Metis Yayınları, İstanbul, 2018.
[5] René Descartes, Yöntem Üzerine Konuşma, Alfa Yayınları, İstanbul, 2019.
[6] Ş. Teoman Duralı, Aklın Anatomisi, Salt Aklın Eleştirisinin Teşrihi, Dergah Yayınları, İstanbul, 2013.

Investigation of Solitary Wave Solutions of Nonlinear Partial Differential Equation by Modified Exponential Function Method

Mahşure Kübranur DİKİCİ[1], Tolga AKTÜRK[2]

[1]Department of Mathematics, Faculty of Science, Ordu University, Turkey

[2]Department of Mathematics and Science Education, Faculty of Education, Ordu University, Turkey

[1]kubradikici.55@hotmail.com , [2]tolgaakturkk@gmail.com;

Abstract

In this article, traveling wave solutions of the (1+1)-dimensional nonlinear the medium equal width equation(MEWE) are found using the improved exponential function method (MEFM). Different traveling wave solutions are obtained by giving appropriate values to the parameters in the explicit solution. Two-three dimensional and contour graphs of these solutions are drawn with the help of software program by determining appropriate parameters.

Keywords: The nonlinear partial differential equation; the medium equal width equation; the modified exponential function method.

1.Introduction

Mathematical models are expressed in nonlinear partial differential equations in many fields such as nuclear physics, wave mechanics, engineering, and medicine. The solutions of equations of this structure are essential, but obtaining exact solutions to these equations is quite difficult. By applying different approaches, our chances of finding close solutions are increasing. In the literature, different methods have been used to solve these equations: the first integral method [1-5], G′/G-expansion method for nonlinear evolution equation [6-9], application of the new function method [10-13], Galerkin method for the numerical solution [14], Sine–Cosine method [15], Sub-Equation method [16], The modified exponential function method (MEFM) [17] was used in our study. The MEWE we apply the method is as follows [18-23].

$$u_t + u^2 u_x - u_{xxt} = 0. \tag{1}$$

The traveling wave solutions of the equation are obtained using the modified exponential function method (MEFM). These wave solutions help us better understand physical events. In this study, the method used in the second part is mentioned. In the third chapter, wave solutions of the MEWE are obtained. Two-three dimensional and contour graphs are drawn. In the fourth episode, the results were evaluated.

METHOD

2. Modified Exponential Function Method

The general form of the nonlinear partial differential equation based on the solution function $u(x,t)$ of two variables is as follows:

$$P\left(u,u_x,u_t,u_{xx},u_{xxt},\ldots\right)=0. \tag{2}$$

Step 1: If the wave transformation is applied to the $u(x,t)$ function:

$$u(x,t)=u(\xi),\quad \xi=k\left(x-ct\right). \tag{3}$$

If the u function required in equation (1) and u derivative concepts connected to ξ are written in equation (2):

$$N\left(u,u^2,u',u''',\ldots\right)=0. \tag{4}$$

The general state of the nonlinear ordinary differantial equation is obtained.

Step 2: If the solution function u is accepted as follows:

$$u(\xi)=\frac{\sum\limits_{i=0}^{n} A_i[e^{-\vartheta(\xi)}]^i}{\sum\limits_{j=0}^{m} B_j[e^{-\vartheta(\xi)}]^j}=\frac{A_0+A_1e^{-\vartheta}+\ldots+A_ne^{-n\vartheta}}{B_0+B_1e^{-\vartheta}+\ldots+B_me^{-m\vartheta}}, \tag{5}$$

where $A_i,B_j,(0\le i\le m,\ 0\le j\le n)$. m , n are positive integers found using the balancing principle. $\vartheta(\xi)$ functions in equation (5) are determined using the following solution families [25].

Family 1: When, $\mu\ne 0,\lambda^2-4\mu>0,$

$$\vartheta(\xi)=ln(\frac{-\sqrt{\lambda^2-4\mu}}{2\mu}tanh(\frac{\sqrt{\lambda^2-4\mu}}{2}(EE+\xi))-\frac{\lambda}{2\mu}). \tag{6}$$

Family 2: When, $\mu\ne 0,\ \lambda^2-4\mu<0,$

$$\vartheta(\xi)=ln(\frac{\sqrt{-\lambda^2+4\mu}}{2\mu}tan(\frac{\sqrt{-\lambda^2+4\mu}}{2}(EE+\xi))-\frac{\lambda}{2\mu}). \tag{7}$$

Family 3: When, $\mu=0,\lambda\ne 0,\ \lambda^2-4\mu>0,$

$$\vartheta(\xi)=-ln(\frac{\lambda}{e^{\lambda(EE+\xi)}-1}). \tag{8}$$

Family 4: When, $\mu\ne 0,\lambda\ne 0,\ \lambda^2-4\mu=0,$

$$\vartheta(\xi)=ln(-\frac{2\lambda(EE+\xi)+4}{\lambda^2(EE+\xi)}). \tag{9}$$

Family 5: When, $\mu=0,\lambda=0,\ \lambda^2-4\mu=0,$

$$\vartheta(\xi) = ln(EE+\xi). \tag{10}$$

3. Application

In this section, we use the modified exponential function method (MEFM) to find the traveling wave solutions of the (1+1) dimensional nonlinear MEWE,

$$u_t + u^2 u_x - u_{xxt} = 0. \tag{11}$$

When we apply the traveling wave transformation as $u(x,t)=u(\xi), \quad \xi = k\left(x-ct\right)$, we get the nonlinear ordinary differantial equation as following,

$$-cku' + u^2 ku' + ck^3 u''' = 0. \tag{12}$$

In order to get the solution function, integral must be taken in equation (12).

$$-3cu + u^3 + 3ck^2 u'' = 0. \tag{13}$$

If the balancing procedure is applied to the equation (14), if $m=1$ is selected $n=2$ is obtained,

$$\mathrm{u}(\xi)=\frac{A_0 + A_1 e^{-\theta} + A_2 e^{-2\theta}}{B_0 + B_1 e^{-\theta}}. \tag{14}$$

Derivative terms required for equation (12) are obtained from equation (14). By substituting these terms (12) in the equation, an algebraic equation system consisting of coefficients is obtained. When this system of algebraic equations is solved, the following cases are obtained.

Case 1;

$$A_0 = \frac{\sqrt{3}\sqrt{c}\lambda B_0}{\sqrt{\lambda^2 - 4\mu}};$$

$$A_1 = \frac{\sqrt{3}\sqrt{c}(2B_0 + \lambda B_1)}{\sqrt{\lambda^2 - 4\mu}};$$

$$A_2 = \frac{2\sqrt{3}\sqrt{c}B_1}{\sqrt{\lambda^2 - 4\mu}};$$

$$k = -\frac{1}{\sqrt{-\frac{\lambda^2}{2} + 2\mu}};$$

These coefficients are substituted in the equation (14) and the following conditions are get.

Family 1: When, $\mu \neq 0,\ \lambda^2 - 4\mu > 0$,

$$u_{1.1}(x,t)=\frac{\sqrt{3}\sqrt{c}\left(\lambda^2-4\mu+\lambda\sqrt{\lambda^2-4\mu}Tanh\left[\frac{1}{2}\sqrt{\lambda^2-4\mu}\left(EE+\xi\right)\right]\right)}{\sqrt{\lambda^2-4\mu}\left(\lambda+\sqrt{\lambda^2-4\mu}Tanh\left[\frac{1}{2}\sqrt{\lambda^2-4\mu}\left(EE+\xi\right)\right]\right)}. \tag{15}$$

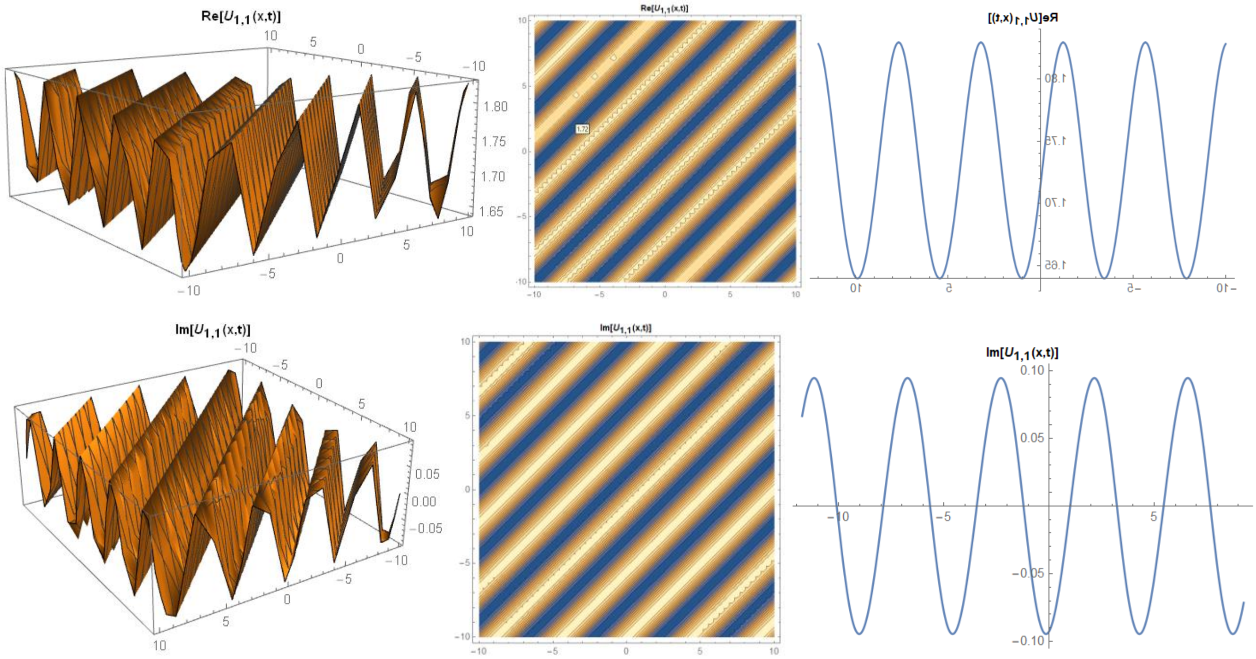

Figure-1: Two and three dimensional, contour graphs of the real and imaginary parts of equation (15) in $c=1,\ \lambda=3,\ \mu=1,\ k=i\sqrt{\frac{2}{5}},\ EE=0.75$ and $t=1$.

Family 2: When, $\mu\neq 0,\ \lambda^2-4\mu<0$,

$$u_{1.2}(x,t)=\frac{\sqrt{3}\sqrt{c}\left(-\lambda^2+4\mu+\lambda\sqrt{-\lambda^2+4\mu}Tan\left[\frac{1}{2}\sqrt{-\lambda^2+4\mu}\left(EE+\xi\right)\right]\right)}{\sqrt{\lambda^2-4\mu}\left(\lambda-\sqrt{-\lambda^2+4\mu}Tan\left[\frac{1}{2}\sqrt{-\lambda^2+4\mu}\left(EE+\xi\right)\right]\right)}. \tag{16}$$

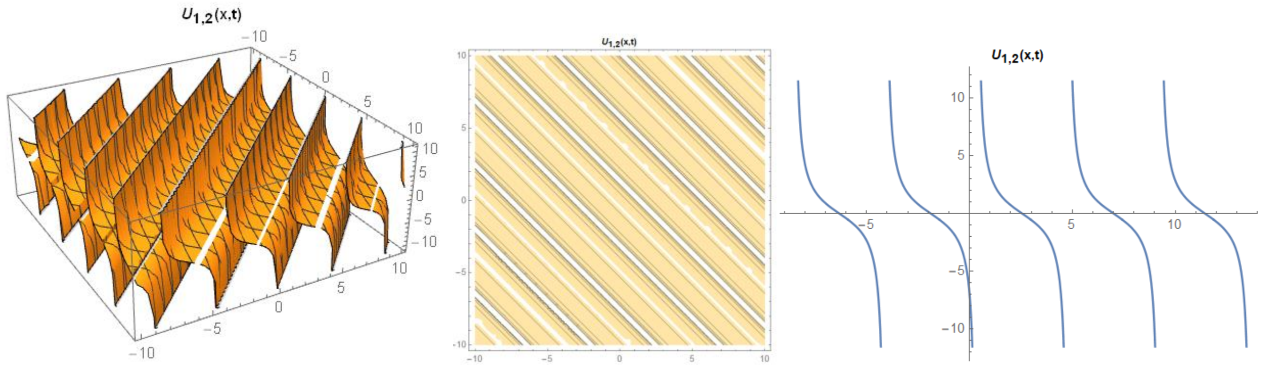

Figure-2: Two and three dimensional, contour graphs of the equation (16) in $c=-1,\ \lambda=1,\ \mu=3,\ k=-\sqrt{\frac{2}{11}},\ EE=0.75$ and $t=1$.

Family 3: When, $\mu=0,\lambda\neq 0,\ \lambda-4\mu>0,$

$$u_{1.3}(x,t)=\frac{\sqrt{3}\sqrt{c}\lambda Coth\left[\frac{1}{2}(EE+\xi)\lambda\right]}{\sqrt{\lambda^2}}. \tag{17}$$

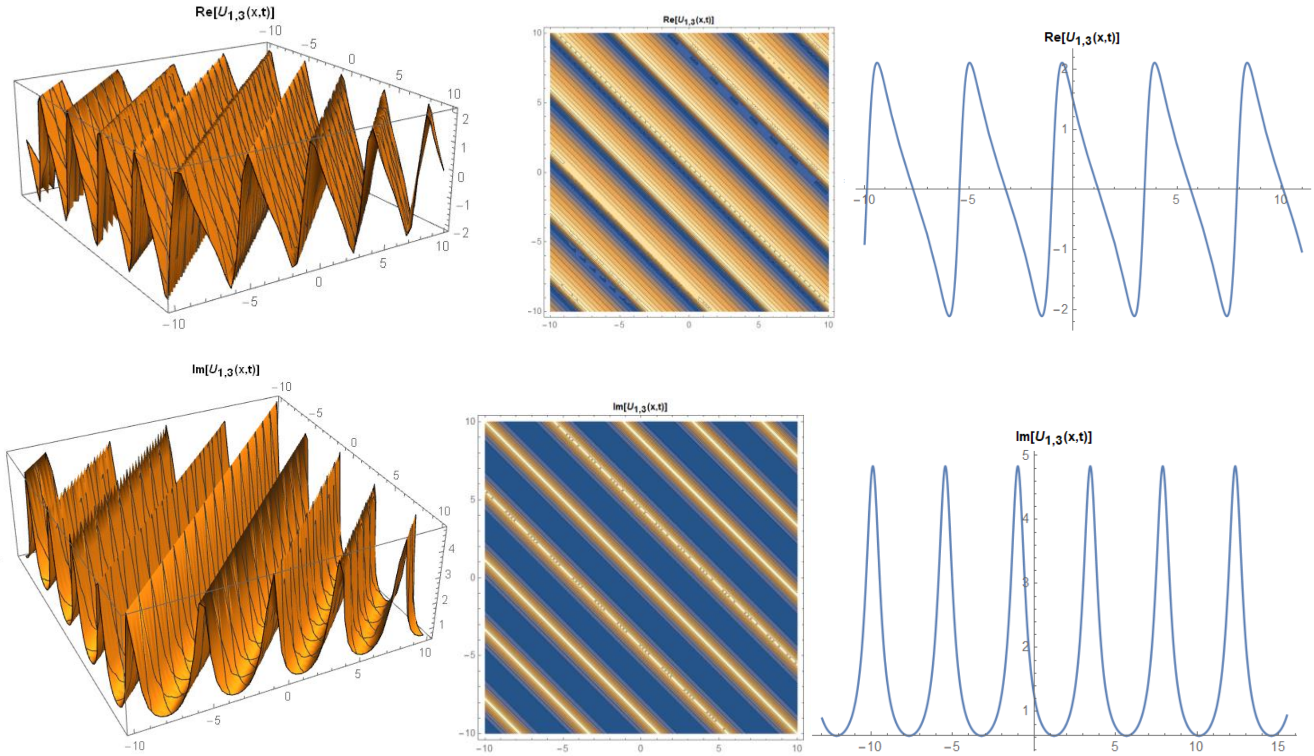

Figure-3: Two and three dimensional, contour graphs of the real and imaginary parts of equation (17) in $c=-1,\ \lambda=1,\ \mu=0,\ k=i\sqrt{2},\ EE=0.75$ and $t=1$.

Family 4 and 5 are undefined because they do not provide the equation.

Case 2;

$$A_0=-\frac{\sqrt{-3cB_0^4+\frac{9}{2}c\mu B_0^2B_1^2}}{\sqrt{-B_0^2+\mu B_1^2}};$$

$$A_1=\frac{B_1\sqrt{-3cB_0^4+\frac{9}{2}c\mu B_0^2B_1^2}\left(3\mu B_1^2+B_0\left(-2B_0+\sqrt{-2B_0^2+3\mu B_1^2}\right)\right)}{\sqrt{-B_0^2+\mu B_1^2}\left(2B_0^3-3\mu B_0B_1^2\right)};$$

$$A_2=\frac{B_1{}^2\sqrt{-3B_0^4+\frac{9\mu B_1^2}{2}}\sqrt{-2cB_0^4+3c\mu B_0{}^2B_1^2}}{\sqrt{-B_0^2+\mu B_1^2}\left(2B_0^3-3\mu B_0B_1^2\right)};$$

$$\lambda=\frac{2\sqrt{-2B_0^2+3\mu B_1^2}}{B_1};$$

$$k=\frac{B_1}{2\sqrt{B_0^2-\mu B_1^2}};$$

Solutions written in the equation of these coefficients (14) are obtained.

Family 1: When, $\mu \neq 0,\ \lambda^2 - 4\mu > 0$,

$$u_{2.1} = \frac{\sqrt{-3cB_0^4 + \frac{9}{2}c\mu B_0^2 B_1^2 (-2B_0^2\psi + \mu B_1(-2\sqrt{-2B_0^2 + 3\mu B_1^2} + 3B_1\psi))}}{(B_0(2B_0^2 - 3\mu B_1^2)\sqrt{-B_0^2 + \mu B_1^2}\psi}. \tag{18}$$

$$\left(\psi = \lambda + \sqrt{\lambda^2 - 4\mu}Tanh\left[\frac{1}{2}\sqrt{\lambda^2 - 4\mu}\left(EE + \xi\right)\right]\right)$$

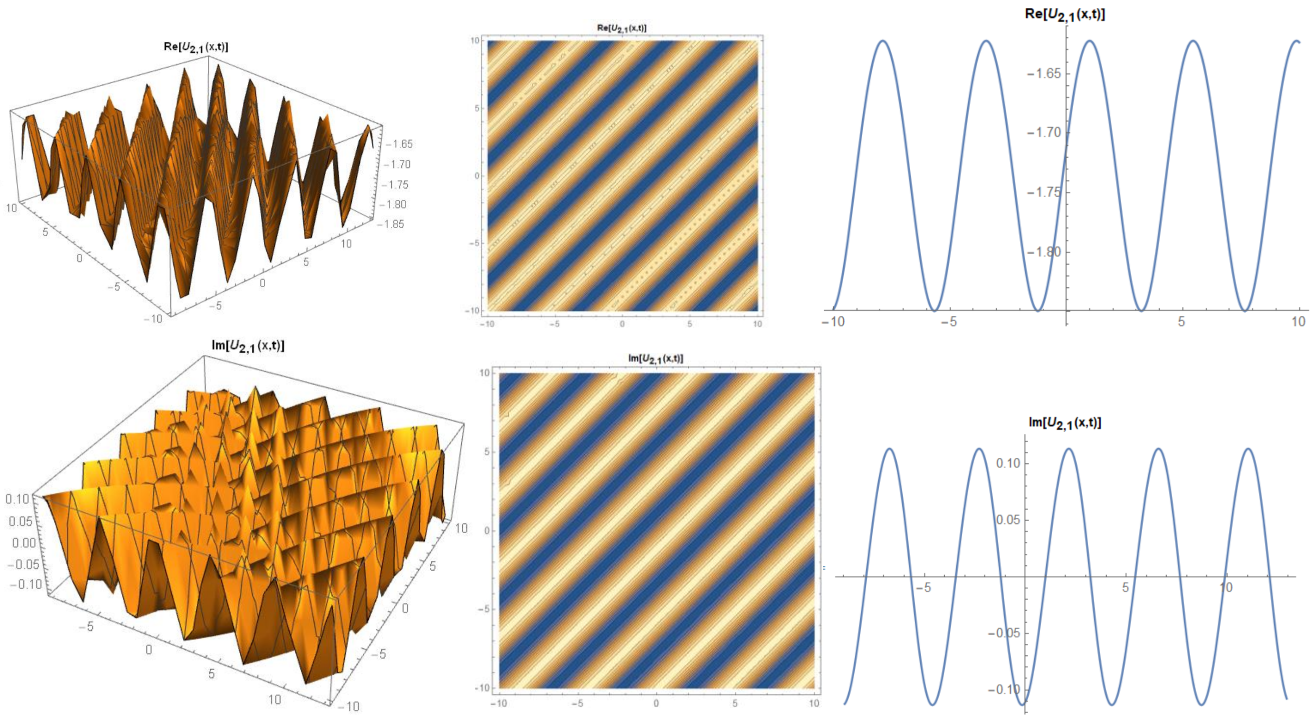

Figure-1: Two and three dimensional, contour graphs of the real and imaginary parts of equation (18) in $B_1 = 3,\ B_0 = 2,\ c = 1,\ \lambda = \frac{2\sqrt{19}}{3},\ \mu = 1,\ k = -\frac{3i}{2\sqrt{5}},\ EE = 0.75$ and $t = 1$.

Family 2: When, $\mu \neq 0,\ \lambda^2 - 4\mu < 0$,

$$u_{2.2} = \frac{\sqrt{-3cB_0^4 + \frac{9}{2}c\mu B_0^2 B_1^2 (-2B_0^2\sigma + \mu B_1(-2\sqrt{-2B_0^2 + 3\mu B_1^2} + 3B_1\sigma))}}{(B_0(2B_0^2 - 3\mu B_1^2)\sqrt{-B_0^2 + \mu B_1^2}\sigma}. \tag{19}$$

$$\left(\sigma = \lambda - \sqrt{-\lambda^2 + 4\mu}Tan\left[\frac{1}{2}\sqrt{-\lambda^2 + 4\mu}\left(EE + \xi\right)\right]\right)$$

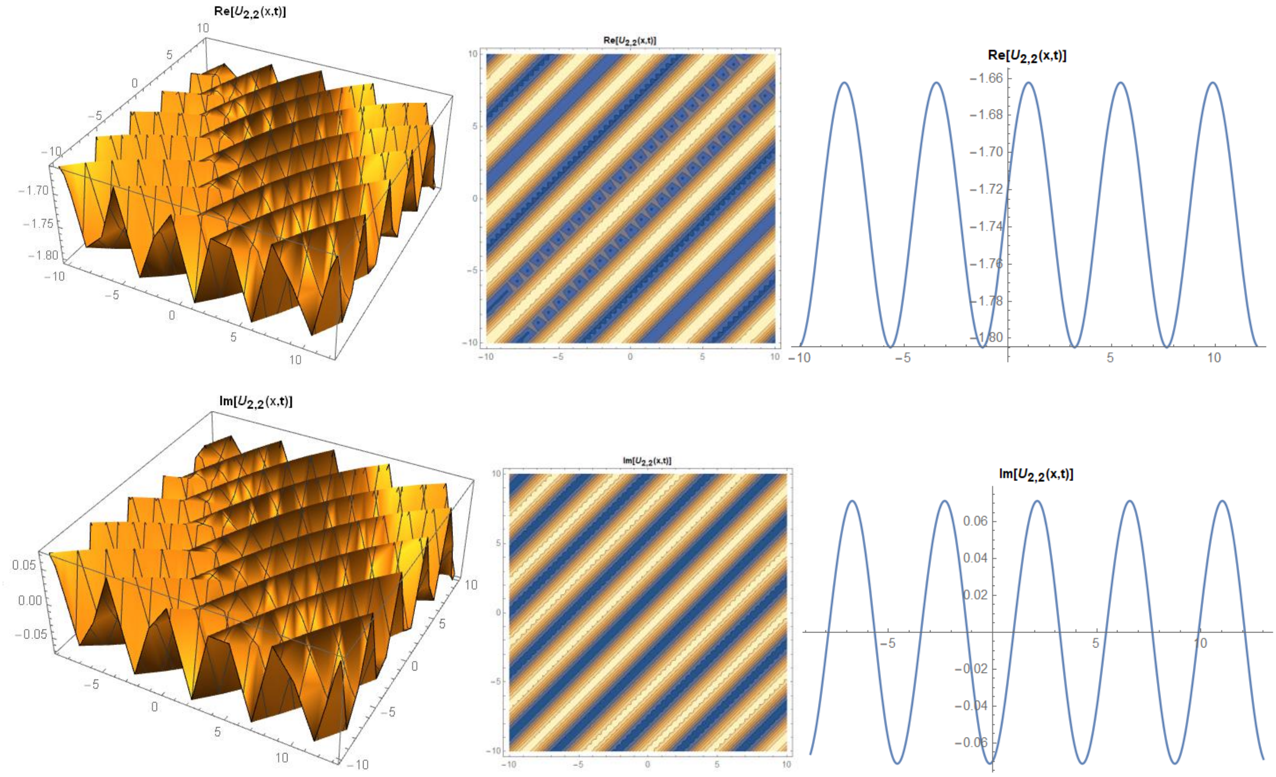

Figure-2: Two and three dimensional, contour graphs of the real and imaginary parts of equation (19) in $B_1 = 1,\ B_0 = 1,\ c = 1,\ \lambda = 4,\ \mu = 2,\ k = -\frac{i}{2},\ EE = 0.75$ and $t = 1$.

Family 3: When, $\mu = 0, \lambda \neq 0,\ \lambda - 4\mu > 0,$

$$u_{2.3}(x,t) = \frac{\sqrt{3}\sqrt{-cB_0^4}\left(2\sqrt{-B_0^2} + \frac{\sqrt{2}\lambda B_1}{-1+e^{(EE+\xi)\lambda}}\right)}{2B_0^3}. \tag{20}$$

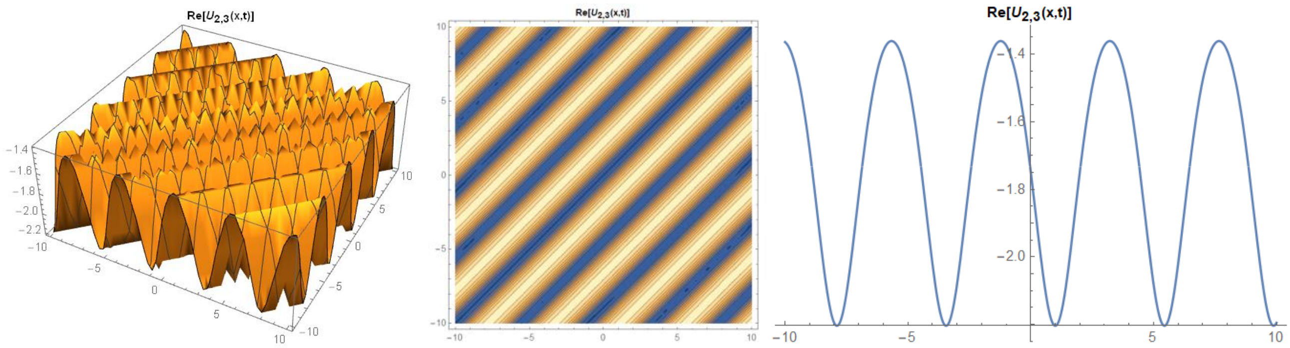

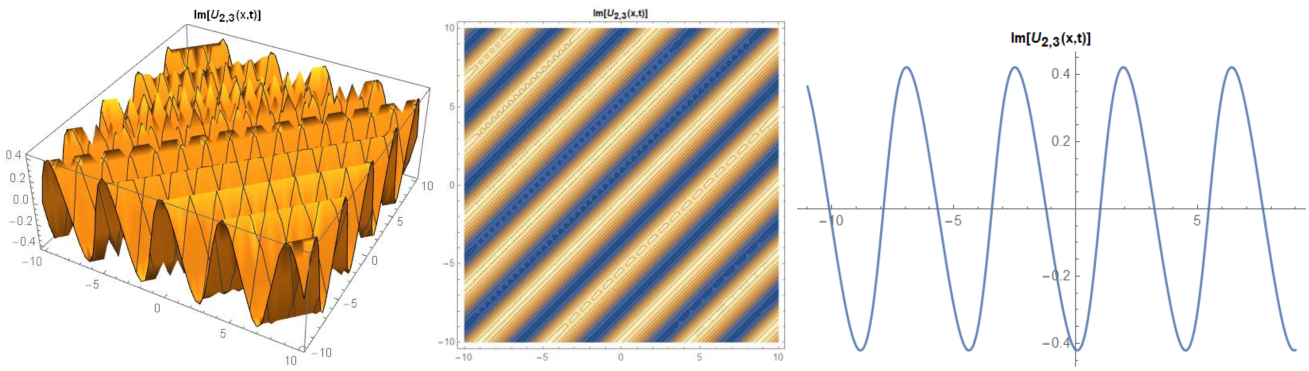

Figure-3: Two and three dimensional, contour graphs of the real and imaginary parts of equation (20) $B_1 = i,\ B_0 = 1,\ c = 1,\ \mu = 0,\ \lambda = 2\sqrt{2},\ k = \frac{i}{2},\ EE = 0.75$ and $t = 1$.

Family 4 and 5 are undefined because they do not provide the equation.

4.Conclusions

In this study, traveling wave solutions were obtained by applying the modified exponential function method to the MEWE. These wave solutions show that the partial differential equation is very suitable for wave solutions. The control of the solutions was made with the help of software program. Two-three dimensional and contour graphs were drawn.

5.References

1. Zhaosheng Feng, The first-integral method to study the Burgers–Korteweg–de Vries equation, Journal of Physics A, Mathematical and General, Vol:35, No:2, 343, 2002.
2. Zhaosheng Feng, Exact solution to an approximate Sine-Gordon equation in (n+1)-dimensional space, Physics Letters A, Vol:302, No: 2-3, 64-76, 2002.
3. Zhaosheng Feng, Wang Xiaohui, The first integral method to the two-dimensional Burgers–Korteweg–de Vries equation, Physics Letters A, Vol:308, No:2-3, 173-178, 2003.
4. K. R. Raslan, The first integral method for solving some important nonlinear partial differential equations, Nonlinear Dynamics, Vol:53, No:4, 281-286, 2008.
5. Rui, Weiguo, et al., Integral bifurcation method and its application for solving the modified equal width wave equation and its variants. In Rostocker Mathematisches Kolloquium, Vol:62, 87-106, 2007.
6. Wang Mingliang, Li Xiangzheng, Zhang Jinliang, The (G′/G)-expansion method and travelling wave solutions of nonlinear evolution equations in mathematical physics, Physics Letters A, Vol:372, No:4, 417-423, 2008.
7. Duran, S, Extractions of travelling wave solutions of (2+ 1)-dimensional Boiti–Leon–Pempinelli system via (G′/G, 1/G)-expansion method. Optical and Quantum Electronics, 53(6), 1-12, 2021.
8. Yokuş, A., Durur, H., & Duran, S, Simulation and refraction event of complex hyperbolic type solitary wave in plasma and obtical fiber for the perturbed Chen-Lee-Liu equation, 2021.

9. Durur, H, Different types analytic solutions of the (1+ 1)-dimensional resonant nonlinear Schrödinger's equation using (G′/G)-expansion method. Modern Physics Letters B, 34(03), 2050036, 2020.
10. Hasan Bulut, Tolga Aktürk, Yusuf Gürefe, An application of the new function method to the generalized double sinh-Gordon equation, AIP Conference Proceedings, AIP Publishing LLC, Vol:1648, No:1, 2015.
11. Hasan Bulut, Sibel Sehriban Atas, Haci Mehmet Baskonus, Some novel exponential function structures to the Cahn–Allen equation, Cogent Physics, Vol:3, No:1, 1240886, 2016.
12. Shikuo Liu, Jacobi elliptic function expansion method and periodic wave solutions of nonlinear wave equations, Physics Letters A, Vol:289, No:1-2, 69-74, 2001.
13. Tolga Aktürk, Yusuf Gürefe, Yusuf Pandır, An application of the new function method to the Zhiber–Shabat equation, An International Journal of Optimization and Control, Theories & Applications (IJOCTA), Vol:7, No:3, 271-274, 2017.
14. Turabi Geyikli, S. Battal Gazi Karakoç, Petrov-Galerkin method with cubic B-splines for solving the MEW equation, Bulletin of the Belgian Mathematical Society-Simon Stevin, Vol:19, No:2, 215-227, 2012.
15. E. Yusufoğlu, A. Bekir, M. Alp, Periodic and solitary wave solutions of Kawahara and modified Kawahara equations by using sine–cosine method, Chaos, Solitons & Fractals, Vol:37, No:4, 1193-1197, 2008.
16. Duran, S., & Karabulut, B, Nematicons in liquid crystals with Kerr Law by sub-equation method, Alexandria Engineering Journal, 2021.
17. Tolga Aktürk, Hasan Bulut, Gülnur Yel, An Application of the Modified Expansion Method to Nonlinear Partial Differential Equation, Turkish Journal of Mathematics and Computer Science, Vol:10, 202-206, 2018.
18. Alaattin Esen, A numerical solution of the equal width wave equation by a lumped Galerkin method, Applied mathematics and computation, Vol:168, No:1, 270-282, 2005.
19. Alaattin Esen, A lumped Galerkin method for the numerical solution of the modified equal-width wave equation using quadratic B-splines, International Journal of Computer Mathematics, Vol:83, No:5-6, 449-459, 2006.
20. Bülent Saka, Algorithms for numerical solution of the modified equal width wave equation using collocation method, Mathematical and Computer Modelling, Vol: 45, No:9-10, 1096-1117, 2007.
21. Junfeng Lu, He's variational iteration method for the modified equal width equation, Chaos, Solitons & Fractals, Vol:39, No:5, 2102-2109, 2009.
22. Alaattin Esen, Selçuk Kutluay, Solitary wave solutions of the modified equal width wave equation, Communications in Nonlinear Science and Numerical Simulation, Vol:13, No:8, 1538-1546, 2008.
23. T. Mohyud-Din, et al., Numerical solution of modified equal width wave equation, World Applied Sciences Journal, Vol:8, No:7, 792-798, 2010.
24. Yokuş, A., Durur, H., Nofal, T. A., Abu-Zinadah, H., Tuz, M., & Ahmad, H, Study on the applications of two analytical methods for the construction of traveling wave solutions of the modified equal width equation, Open Physics, 18(1), 1003-1010, 2020.
25. Hasibun Naher, Abdullah Farah Aini, New approach of (G′/G)-expansion method and new approach of generalized (G′/G)-expansion method for nonlinear evolution equation, AIP Advances, Vol:3, No:3, 032116, 2013.

The Solution of The Linear Delay Differential Equations with Aboodh Transform

Özgür KOTAN[1]*, Ercan CELIK* and Naiyer Mohammadi LANBARAN*

**Ataturk University Faculty of Science, Department of Mathematics, Erzurum-TURKEY*

Ozgurkotan2525@gmail.com, ercelik@atauni.edu.tr, nil98100@gmail.com

Abstract:

In this paper, we apply Aboodh transform to solve linear delay differential equations. Firstly, The basic properties of the Aboodh Transform are given. Secondly, Existence of the Aboodh transform proved. Then, the two linear delay differential equations are solved by Aboodh transform. This means that Aboodh transform is a powerful tool for solving linear delay diffferential equations.

Keywords: Linear Delay Differential Equations, Aboodh Transform, Existence of the Aboodh Transform.

1. Introduction

The Aboodh Transform is integral transform. There are many integral transforms in the literature. Some of these transformations are Laplace Transform, Fourier Transform, Sumudu Transform, Elzaki Transform, ZZ Transform [1-8]. These transformations are used to solve for differential equations and integral equations. The most common of these transformations is Laplace transform. The Aboodh transform was first presented by Khalid Aboodh in 2013[9-12]. This transformation has also been applied to the solution of ordinary differential equations and partial differential equations. The purpose of this paper is to solve the linear delay differential equations with the Aboodh transform. The Aboodh transform is obtained from the standard Fourier integral. Based on the mathematical simplicity and basic features of the Aboodh Transform. This transformation facilitates the process of solving ordinary and partial differential equations.

Delay Differential equations are used to define many physical phenomena in medicine, engineering, economics, biology, physics, and chemistry. Many methods have been developed to solve these equations[13-15].

---

[1] Corresponding author

This article was planned as follows: In section second part, the basic properties and existence of the Aboodh transformation are given. In the third part, application was given. In the fourth part, the result is given, respectively.

2. The Aboodh Transform:

The Aboodh transform defined for $t \geq 0$. Let $f(t)$ be an exponential order function in the set A as

$$A = \{f(t): \exists\, M, k_1, k_2 > 0,\ |f(t)| < Me^{-vt}\}.$$

Where, the constant M is finite number and k_1, k_2 are finite or may be infinite numbers. Then the Aboodh transform is,

$$\mathcal{A}[f(t)] = A(v) = \frac{1}{v}\int_0^\infty f(t)e^{-vt}dt\ , t \geq 0, k_1 \leq v \leq k_2\ . \quad (1)$$

The unique function $f(t)$ in (1) is called the inverse transform of $A(v)$ is indicated by

$$f(t) = \mathcal{A}^{-1}[A(v)]\ .$$

2.1. The Aboodh Transform of Some Required Functions

Theorem 1.

1. $\mathcal{A}(1) = \frac{1}{v^2}$

2. $\mathcal{A}(t^n) = \frac{n!}{v^{n+2}}$

3. $\mathcal{A}(e^{at}) = \frac{1}{v^2 - av}$

4. $\mathcal{A}(sinat) = \frac{a}{v(v^2+a^2)}$

5. $\mathcal{A}(cosat) = \frac{1}{(v^2+a^2)}$

6. $\mathcal{A}(t^n e^{at}) = \frac{n!}{v(v-a)^{n+1}}$

7. $\mathcal{A}\big(u(x-a)\big) = \frac{e^{-av}}{v^2},\ \ v > 0$

$\vdots$

Proof 2. Let $f(t) = t^n$, where $t \geq 0$, then Aboodh transform of this function can be written as

$$\mathcal{A}(t^n) = \frac{1}{v}\int_0^\infty f(t)e^{-vt}dt = \frac{1}{v}\int_0^\infty t^n e^{-vt}dt$$

$$\mathcal{A}(t^n) = \frac{1}{v}\int_0^\infty t^n e^{-vt}dt = \frac{1}{v}\left[\frac{-t^n e^{-vt}}{v}\Big|_0^\infty + \frac{n}{v}\int_0^\infty t^{n-1}e^{-vt}dt\right]$$

$$\mathcal{A}(t^n) = \frac{1}{v}\left[\frac{n}{v}\mathcal{A}(t^{n-1})\right] = \frac{1}{v}\left[\frac{n!}{v^{n+1}}\right] = \frac{n!}{v^{n+2}} \ .$$

3. Let $f(t) = e^{at}$, where $t \geq 0$, where a is a constant, then Aboodh transform of this function can be written as

$$\mathcal{A}(e^{at}) = \frac{1}{v}\int_0^\infty f(t)e^{-vt}dt = \frac{1}{v}\int_0^\infty e^{at}e^{-vt}dt = \frac{1}{v}\int_0^\infty e^{(a-v)t}dt$$

$$= \frac{1}{v}\int_0^\infty e^{-(v-a)t}dt = \frac{1}{v}\frac{e^{-(v-a)t}}{-(v-a)}\Big|_0^\infty = \frac{1}{v^2 - av} \ .$$

Others can be proof similarly.

2.2. Existence of the Aboodh Transform

Theorem 2.

If $f(t)$ is piecewise continuous in every finite interval $0 \leq t \leq K$ and of exponential order γ for $t > K$, Then its Aboodh transform $A(f(t))$ exists for all $v > \gamma$.

Proof:

We have for every positive number K .

$$\frac{1}{v}\int_0^\infty f(t)e^{-vt}dt = \frac{1}{v}\int_0^K f(t)e^{-vt}dt + \frac{1}{v}\int_K^\infty f(t)e^{-vt}dt$$

Since $f(t)$ is piecewise continuous in interval $0 \leq t \leq K$, there is the first integral on the right. Also there is the second integral on the right. So $f(t)$ is of exponential γ for order $t > K$. To see this we have only to observe that in such case:

$$\left|\frac{1}{v}\int_K^\infty f(t)e^{-vt}dt\right| \leq \frac{1}{v}\int_K^\infty |f(t)e^{-vt}|dt \leq \frac{1}{v}\int_0^\infty e^{-vt}|f(t)|dt$$

$$\leq \frac{1}{v}\int_0^\infty e^{-vt}Me^{\gamma t}dt \leq \frac{M}{v}\int_0^\infty e^{-vt}e^{\gamma t}dt \leq \frac{M}{v}\int_0^\infty e^{-(v-\gamma)t}dt$$

$$= \frac{M}{v}\left|\frac{e^{-(v-\gamma)t}}{-(v-\gamma)}\right|_0^\infty = \frac{M}{v}\frac{1}{v-\gamma} = \frac{M}{v(v-\gamma)} \ .$$

Teorem 3.

i. Let $\mathcal{A}\{u(t)\} = \bar{u}(v)$, then

$\mathcal{A}\{u(t+1)\} = \frac{e^v}{v}[\bar{u}(v) - u_0\bar{V}_0(v)], \quad u(0) = u_0$

Proof

i. $\mathcal{A}\{u(t+1)\} = \frac{1}{v}\int_0^\infty e^{-vt}\, u(t+1)dt$

$$= \frac{e^v}{v}\int_1^\infty e^{-v\tau}u(\tau)\, d\tau$$

$$= \frac{e^v}{v}\left[\bar{u}(v) - u(0)\int_0^1 e^{-v\tau}d\tau\right]$$

$$= \frac{e^v}{v}[\bar{u}(v) - u_0\bar{V}_0(v)],$$

ii. $\mathcal{A}\{u(t+2)\} = \frac{e^v}{v}[\mathcal{A}\{u(t+1)\} - u(1)\bar{V}_0(v)]$

$$= \frac{e^{2v}}{v}[\bar{u}(v) - u(0)\bar{V}_0(v)] - e^v u_1\bar{V}_0(v)$$

$$= \frac{e^{2v}}{v}[\bar{u}(v) - (u_0 + u_1e^{-v}\bar{V}_0(v)] \qquad u(1) = u_1,$$

iii. $\mathcal{A}\{u(t+3)\} = \frac{e^{3v}}{v}[\bar{u}(v) - (u_0 + u_1e^{-v} + u_2e^{-2v})\bar{V}_0(v)],$

Generally

iv. $\mathcal{A}\{u(t+k)\} = \frac{e^{kv}}{v}\left(\bar{u}(v) - \bar{V}_0(v)\sum_{r=0}^{k-1} u_r e^{-rv}\right).$

2.3. Remark

Let $H(t)$ is Heaviside unit step function, then

$$V_n(t) = H(t-n) - H(t-n-1), \;\; n \le t < n+1.$$

The Aboodh Transform of $V_n(t)$ is

$$\bar{V}_n(v) = \mathcal{A}\{V_n(t)\}$$

$$= \frac{1}{v}\int_0^\infty e^{-vt}\{H(t-n) - H(t-n-1)\}dt$$

$$= \frac{1}{v}\int_n^{n+1} e^{-vt}dt$$

$$= \frac{1}{v^2}(1 - e^{-v})e^{-nv}$$

$$= \bar{V}_0(v)\, e^{-nv}.$$

Where

$$\bar{V}_0(v) = \frac{1}{v^2}(1 - e^{-v}).$$

2.4. The Aboodh Transform of Derivatives

Teorem 4.

Let $A(f(t))$ is Aboodh transform of $f(t)$, then

1. $\mathcal{A}[f'(t)] = vA(v) - \frac{f(0)}{v}$

2.$\mathcal{A}\ [f''(t)] = v^2A(v) - \frac{f'(0)}{v} - f(0)$

Generally

3. $\mathcal{A}[f^n(t)] = v^nA(v) - \sum_{k=0}^{n-1} \frac{f^k(0)}{v^{2-n+k}}$

4. (i) $\mathcal{A}\{tf(t)\} = -\frac{d}{dv}A(v) - \frac{1}{v}A(v)$

(ii) $\mathcal{A}\big(tf'(t)\big) = -\frac{d}{dv}\left[vA(v) - \frac{f(0)}{v}\right] - \frac{1}{v}\left[vA(v) - \frac{f(0)}{v}\right]$

(iii)$\mathcal{A}\{tf''(t)\} = -\frac{d}{dv}\left[v^2A(v) - \frac{f'(0)}{v} - f(0)\right] - \frac{1}{v}\left[v^2A(v) - \frac{f'(0)}{v} - f(0)\right]$

(iv) $\mathcal{A}\{t^2f'(t)\} = v\frac{d^2A(v)}{dv^2} + 4\frac{dA(v)}{dv} + \frac{2}{v}A(v)$

(v) $\mathcal{A}\{t^2f''(t)\} = v^2\frac{d^2A(v)}{dv^2} + 6v\frac{dA(v)}{dv} + 6A(v)$

$\vdots$

Proof

1. $\mathcal{A}[f'(t)] = \frac{1}{v}\int_0^\infty e^{-vt}\, f'(t)dt$

$\mathcal{A}[f'(t)] = \frac{1}{v}\left[e^{-vt}f(t)|_0^\infty - \int_0^\infty -ve^{-vt}\, f(t)dt\right]$

$\mathcal{A}[f'(t)] = vA(v) - \frac{f(0)}{v}$

4. i) $\mathcal{A}[f(t)] = A(v) = \frac{1}{v}\int_0^\infty f(t)e^{-vt}dt\ \ t \geq 0, k_1 \leq v \leq k_2$

$$\frac{d}{dv}A(v) = \frac{d}{dv}\left(\frac{1}{v}\int_0^\infty f(t)e^{-vt}dt\ \right) = -\frac{1}{v^2}\int_0^\infty e^{-vt}f(t)dt - \frac{1}{v}\int_0^\infty te^{-vt}f(t)dt$$

$$-\frac{d}{dv}A(v) - -\frac{1}{v^2}\int_0^\infty f(t)e^{-vt}dt = \frac{1}{v}\int_0^\infty te^{-vt}f(t)dt$$

$$\mathcal{A}[tf(t)] = -\frac{d}{dv}A(v) - \frac{A(v)}{v}\ .$$

Others can be proof similarly.

2.5. Linearity Property of Aboodh Transforms

If $\mathcal{A}\{f(t)\} = A(v)$ and $\mathcal{A}\{g(t)\} = B(v)$ then

$\mathcal{A}\{af(t) + bg(t)\} = a\mathcal{A}\{f(t)\} + b\mathcal{A}\{f(t)\} = aA(v) + bB(v)$,

where a, b are arbitrary constants.

3. Applications

In this section, we will use the Aboodh transformation to find solutions of two the linear delay differential equations.

Application 1:

Consider linear delay differential eqaution

$$u'(t) = u(t-1), \qquad (2)$$

with the initial conditions

$$u(0) = 1.$$

Solution:

Taking the Aboodh transform of equation (2), we get

$$\mathcal{A}[u'(t)] = \mathcal{A}[u(t-1)]$$

$$vu(v) - \frac{u(0)}{v} = \frac{e^{-v}}{v}[u(v) - u_0\bar{V}_0(v)]$$

$$vu(v) - \frac{1}{v} = \frac{e^{-v}}{v}\left[u(v) - \frac{1}{v^2}(1 - e^{-v})\right]$$

$$vu(v) - \frac{1}{v} = \frac{e^{-v}}{v}u(v) + \frac{e^{-2v}}{v^3} - \frac{e^{-v}}{v^3}$$

$$u(v)\left[v - \frac{e^{-v}}{v}\right] = \frac{1}{v} + \frac{e^{-v}}{v^3}(e^{-v} - 1)$$

$$u(v) = \frac{v^2 - e^{-v}}{v^2(v^2 - e^{-v})} + \frac{e^{-2v}}{v^2(v^2 - e^{-v})}$$

$$= \frac{1}{v^2} + \frac{e^{-2v}}{v^4\left(1 - \frac{e^{-v}}{v^2}\right)}$$

$$= \frac{1}{v^2} + \frac{e^{-2v}}{v^4}\left(1 + \frac{e^{-v}}{v^2} + \frac{e^{-2v}}{v^4} + \frac{e^{-3v}}{v^6} + \cdots + \frac{e^{-nv}}{v^{2n}} + \cdots\right)$$

$$= \frac{1}{v^2} + \frac{e^{-2v}}{v^4} + \frac{e^{-3v}}{v^6} + \frac{e^{-4v}}{v^8} + \frac{e^{-4v}}{v^{10}} + \cdots + \frac{e^{-nv}}{v^{2n}} + \cdots \quad .$$

Where $u(v)$ is the Aboodh Transform of function $u(t)$. Now taking the inverse Aboodh Transform, we get

$$\mathcal{A}^{-1}[u(t)] = \mathcal{A}^{-1}\left[\frac{1}{v^2}\right] + \mathcal{A}^{-1}\left[\frac{e^{-2v}}{v^4}\right] + \mathcal{A}^{-1}\left[\frac{e^{-3v}}{v^6}\right] + \mathcal{A}^{-1}\left[\frac{e^{-4v}}{v^8}\right] + \mathcal{A}^{-1}\left[\frac{e^{-4v}}{v^{10}}\right] + \cdots$$
$$+ \mathcal{A}^{-1}\left[\frac{e^{-nv}}{v^{2n}}\right] + \cdots$$

$$u(t) = 1 + \frac{(t-2)^2}{2!} + \frac{(t-3)^4}{4!} + \frac{(t-4)^6}{6!} + \cdots + \frac{(t-n-1)^{2n}}{(2n)!} + \cdots \quad ,t > n$$

where

$$\mathcal{A}^{-1}\left\{\frac{e^{-av}}{v^{2n}}\right\} = \frac{(t-n-1)^{2n}}{\Gamma(2n+1)} .$$

Application 2:

Consider linear delay differential eqaution

$$u'(t) - \alpha u(t-1) = \beta, \tag{3}$$

with the initial conditions

$$u(0) = 0 .$$

Solution:

Taking the Aboodh transform of equation (3), we get

$$\mathcal{A}[u'(t)] - \mathcal{A}[u(t-1)] = \mathcal{A}[\beta]$$
$$vu(v) - \frac{u(0)}{v} - \alpha\frac{e^{-v}}{v}[u(v) - u(0)\bar{u}(v)] = \frac{\beta}{v^2}$$
$$vu(v) - \alpha\frac{e^{-v}}{v}\big(u(v)\big) = \frac{\beta}{v^2}$$
$$u(v)\left(v - \alpha\frac{e^{-v}}{v}\right) = \frac{\beta}{v^2}$$
$$u(v) = \frac{\beta}{v^2}\left(\frac{v}{(v^2 - \alpha e^{-v})}\right)$$
$$u(v) = \frac{\beta}{v^3\left(1-\alpha\frac{e^{-v}}{v^2}\right)}$$

$$u(v) = \frac{\beta}{v^3}\left(1 + \frac{\alpha e^{-v}}{v^2} + \frac{\alpha^2 e^{-2v}}{v^4} + \frac{\alpha^3 e^{-3v}}{v^6} + \cdots + \frac{\alpha^n e^{-nv}}{v^{2n}} + \cdots\right)$$
$$u(v) = \beta\left(\frac{1}{v^3} + \frac{\alpha e^{-v}}{v^5} + \frac{\alpha^2 e^{-2v}}{v^7} + \frac{\alpha^3 e^{-3v}}{v^9} + \cdots + \frac{\alpha^n e^{-nv}}{v^{2n+3}} + \cdots\right).$$

Where $u(v)$ is the Aboodh Transform of function $u(t)$. Now taking the inverse Aboodh Transform, we get

$$\mathcal{A}^{-1}[u(v)] = \beta\left(\mathcal{A}^{-1}\left[\frac{1}{v^3}\right] + \mathcal{A}^{-1}\left[\frac{\alpha e^{-v}}{v^5}\right] + \mathcal{A}^{-1}\left[\frac{\alpha^2 e^{-2v}}{v^7}\right] + \mathcal{A}^{-1}\left[\frac{\alpha^3 e^{-3v}}{v^9}\right] + \cdots + \mathcal{A}^{-1}\left[\frac{\alpha^n e^{-nv}}{v^{2n+3}}\right] + \cdots\right)$$

$$u(t) = \beta\left[t + \frac{\alpha(t-1)^3}{3!} + \frac{\alpha^2(t-2)^5}{5!} + \frac{\alpha^3(t-3)^7}{7!} \ldots + \frac{\alpha^n(t-n)^{2n+1}}{(2n+1)!} + \cdots\right]$$

where

$$\mathcal{A}^{-1}\left\{\frac{e^{-av}}{v^{2n+3}}\right\} = \beta\left[\frac{(t-n)^{2n+1}}{\Gamma(2n+2)}\right].$$

4. Conclusion

The main features of the Aboodh transform are presented in this article. We applied a new integral transform, the Aboodh transform, to solve two the linear delay differential equations. We proved the existence of the Aboodh transformation. Some examples in applications are given to demostrate the effectiveness of Aboodh transform. As a result, the Aboodh transform reveals that it is very effective, simple and can be applied to the linear delay differential equations.

5. References

[1] Lokenath Debnath and D. Bhatta. Integral transform and their Application Second Edition, Chapman & Hall /CRC, 2006.

[2] G.K.Watugala.(1998), simudu transform- a new integral transform to Solve differential equation and control engineering problems, Math .Engrg Induct .6 ,no 4,319-329.

[3] Hassan Eltayeb and Adem Kilicman. (2010), A Note on the Sumudu Transforms and differential Equations, Applied Mathematical Sciences, VOL, 4, no.22,1089-1098.

[4] Tarig M. Elzaki. (2011), The New Integral Transform "Elzaki Transform" Global Journal of Pure and Applied Mathematics, ISSN 0973-1768, Number 1, pp. 57-64.

[5] Mohand M. AbdelrahimMahgob and Tarig M. Elzaki.(2015), Elzaki Transform And Power Series Expansion On A Bulge Heaviside Step Function, Global Journal of Pure and Applied Mathematics. ISSN 0973-1768 Volume 11, Number 3, pp. 1179-1184,.

[6] Tarig M.Elzaki, Salih M. Elzaki. (2011), On the Elzaki Transform and Ordinary Differential Equation With Variable Coefficients, Advances in Theoretical and Applied Mathematics. ISSN 0973-4554 Volume 6, Number 1, pp. 13-18.

[7] Zain Ul Abadin Zafar, ZZ Transform method, IJAEGT, 4(1), 1605-1611, 2016.

[8] R Najafi, GD Küçük, E Çelik.(2017), Modified iteration method for solving fractional gas dynamics equation, Mathematical Methods in the Applied Sciences 40 (4), 939-946.

[9] K. S. Aboodh. (2013), The New Integral Transform "Aboodh Transform" Global Journal of Pure and Applied Mathematics, 9(1), 35-43.

[10] K. S. Aboodh. (2014), Application of New Transform "Aboodh transform" to Partial Differential Equations, Global Journal of Pure and Applied Math, 10(2),249- 254.

[11] Abdelilah K. Hassan Sedeeg and Mohand M. Abdelrahim Mahgoub. (2016), Aboodh Transform Homotopy Perturbation Method For Solving System Of Nonlinear Partial Differential Equations, Mathematical Theory and Modeling Vol.6, No.8.

[12] Abdelbagy A. Alshikhand Mohand M. Abdelrahim Mahgoub. (2016), A Comparative Study Between Laplace Transform and Two New Integrals “ELzaki” Transform and “Aboodh” Transform, Pure and Applied Mathematics Journal, 5(5): 145-150.

[13] F. Shakeri and M. Dehghan. (2008), Solution of delay differential equations via a homotopy perturbation method, Mathematical and Computer Modelling, vol. 48, no. 3-4, pp. 486–498.

[14] Z. K. Wu. (2009), Solution of the enso delayed oscillator with homotopy analysis method, Journal of Hydrodynamics, vol. 21, no. 1, pp. 131–135.

[15] A. K. Alomari, M. S. Noorani, and R. Nazar. (2009), Solution of delay differential equation by means of homotopy analysis method, Acta Applicandae Mathematicae, vol. 108, no. 2, pp. 395–412.

A FUZZY-STOCHASTIC MATHEMATICAL PROGRAMMING APPROACH FOR AN INTEGRATED LOT-SIZING AND SUPPLIER SELECTION PROBLEM WITH QUANTITY DISCOUNTS AND BACKORDERING OPTIONS

Bilge Varol, Kemal Subulan, Ali Serdar Taşan

Dokuz Eylül University, Faculty of Engineering, Department of Industrial Engineering, Izmir, Turkey

bilgeevarol@gmail.com; kemal.subulan@deu.edu.tr; serdar.tasan@deu.edu.tr

Abstract

This study addresses an integrated lot-sizing and supplier selection problem with multiple items, time periods, quantity discounts and backordering options under uncertain environments. The main purpose of this study is to cope with mixed fuzzy and stochastic uncertainties embedded in demands, budget limits and storage capacities. Because, these data cannot be determined precisely in most of the real-life applications. Based on this motivation, a fuzzy-stochastic mixed-integer linear programming (FS-MIP) model is developed in order to handle stochastic demands, fuzzy budget limits and storage capacities. The original model of the stated problem was formerly proposed by Alfares & Turnadi (2018) based on a case study of a petrochemical company which operated in a process industry. The proposed fuzzy-stochastic model aims to minimize total cost which consists of ordering, purchasing, transportation, inventory holding and shortage costs. By making use of the well-known transformation approaches in the literature, the proposed fuzzy-stochastic MIP model is converted to its crisp equivalent form and then illustrated by a hypothetical example.

Keywords: Integrated lot-sizing & supplier selection problems, all-units quantity discount, shortages, backordering and fuzzy-stochastic mixed-integer programming.

I. INTRODUCTION

Lot-sizing (LS) is one of the well-known production and inventory control problems in the literature. In general, when calculating the lot size, average inventory level, ordering frequency and order size are utilized to satisfy the demands with minimum total cost. In fact, the main goal of the lot-sizing problems is to determine economic order quantities (EOQs) by minimizing the total cost which generally includes inventory holding, purchasing and ordering costs. In determining the lot size and ordering frequency, primary objective of the production and inventory control systems is to satisfy customer demands for one or several items. Furthermore, in case of several suppliers are available, the classical LS problem should be integrated with supplier selection (SS) problem. In particular, if there are quantity discounts, suppliers should also be selected in addition to determine the order quantities and frequencies. In the existing literature, primitive versions of the integrated LS & SS models are developed just for a single item and only one time period without considering the shortages and quantity discounts. Based on this motivation, multiple time periods, shortages and all-unit quantity discounts are taken into account in this study. This expansion makes the classical LS & SS problems much more difficult due to the inclusion of several additional decision variables in the developed mathematical models. As highlighted by Rezaei & Davoodi (2016), well-constructed mathematical models can be very useful for solving these types of problems instead of applying heuristic/metaheuristic based solution approaches. An overview of the recent articles in which integrated LS & SS problems were studied can be summarized as follows: Rezaei & Davoodi (2016) developed multi-objective, mixed-integer non-linear programming models for the lot-sizing problems with multiple products, periods and several suppliers. A novel mixed-integer programming model was also presented by Alfares & Turnadi (2018) for an integrated LS & SS problem which includes multiple items, multiple time periods, quantity discounts and shortages. All-units incremental quantity discounts were also taken into consideration. They applied modified silver-meal heuristic and a genetic algorithm based metaheuristic for solving larger scale problem instances. In this study, the deterministic mathematical model which was proposed by Alfares & Turnadi (2018) is extended by considering stochastic demands, fuzzy budget limits and fuzzy storage capacities. Because, most of the real-life production and inventory control problems may have different types of uncertainties, i.e., fuzziness, stochasticity and dynamism, simultaneously. Therefore, hybrid fuzzy-stochastic programming based approaches may be useful to revise these deterministic models by taking the dynamism into account for better reflection of the real-world applications. Based on these facts, Kasilingam & Lee (1996) proposed a MIP model which considers stochastic demands to select vendors and determine order quantities instantaneously. They also took into account the quality of supplied parts with their lead time requirements, costs of purchasing/transportation, fixed costs for established vendors and the cost of receiving poor quality parts as well. Kumar, Vrat & Shankar (2004) employed a fuzzy goal program for solving a multi-objective vendor selection problem in a supply chain network. They formulated a multi-objective MIP model so as to minimize net rejection, total cost and late deliveries.

In this research, an integrated LS & SS problem is addressed with multiple time periods, all-units quantity discounts and backordering. For better reflection of the real-life applications, demands are considered as stochastic data and a single-stage stochastic programming approach is utilized. Additionally, budget limits and storage capacity of the manufacturer are also taken as uncertain parameters and represented by fuzzy numbers. The proposed fuzzy-stochastic programming model is converted into its crisp equivalent form by using well-known transformation approaches in the literature.

II. PROBLEM DESCRIPTION AND THE PROPOSED FUZZY-STOCHASTIC MODEL

In the integrated LS & SS problems, it is targeted to find a better inventory plan for a finite time horizon. Actually, order quantities will be determined by considering shortages and all-units quantity discounts. According to the quantity discounts of different suppliers, supplier selection is also carried out. The main objective is to provide minimum total cost which includes inventory holding, shortage, transportation, purchasing and ordering costs. The original model of that problem was generated by Alfares & Turnadi (2018) based on a case study of a petrochemical company that operated in a process industry. That’s why demands are stated as continuous. Furthermore, there are three different cases of inventory levels for calculating the holding costs. These cases are displayed in the following Fig. 1. Unlike the study of Alfares &

Turnadi (2018), this study assumes that demands have randomness in nature. After performing input analysis with the deterministic problem data, the best fit probability distribution is determined as triangular distribution. Since the problem data is based on a case study of a petrochemical company, demands are not discrete, they represented by a continuous random variable. Moreover, total budget for replenishment and storage capacity are also considered as fuzzy parameters and represented by triangular fuzzy numbers. Because, the values of these critical parameters cannot be known with certainty and may have some sort of ambiguity.

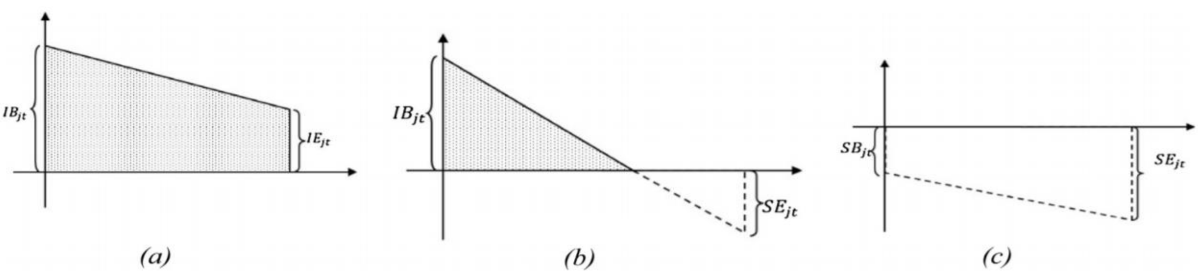

Figure 1. Different cases of inventory levels in the integrated LS & SS problem (Alfares & Turnadi, 2018).

A. Modelling assumptions

The customer demands are not known precisely. Since they may have randomness, the stochastic nature of the demands is handle by a single-stage stochastic program. Each item can be ordered at most once per time period. Each item is sold by several suppliers and they offer all-units quantity discounts. The lead-time is certainly known and constant, and each order is fully received at the start of the given time period. Either inventory or shortage is possible in any time period. Unit inventory holding cost per time period is known and constant. In detail, it does not depend on the unit price. Unit shortage cost per time period is also known and constant. Each vehicle can transport several items according to its storage capacity. Many orders can be given from several suppliers. Otherwise, only one supplier should be selected for any given order. The planning horizon is known and finite. The initial levels of both inventory and shortage are set to zero. All shortages must be fulfilled at the end of the planning horizon. Total budget for replenishment and total storage capacity are not known certainly, they are considered as ambiguous parameters and represented by triangular fuzzy numbers.

Table 1. Mathematical nomenclature for the MIP formulation of the examined problem.

Indices & sets	
t	Time periods ($t = 1,2, \dots, T$), where T is the planning horizon.
i	Suppliers ($i = 1, 2, \dots, I$)
j	Items ($i = 1, 2, \dots, J$)
k	Price levels for quantity discount policy ($k = 1, 2, \dots, K$)
Deterministic parameters	
h_j	Holding cost for item j per unit per time period
l_j	Shortage cost for item j per unit per time period
o_{ij}	Ordering cost per order for item j from supplier i
c_i	Container volume per vehicle from supplier i
v_j	Volume per unit of item j
s_i	Transportation cost per vehicle from supplier i
p_{ijk}	Purchasing cost of item j from supplier i at price level k
q_{ijk}	Maximum order size of item j from supplier i at price level k; p_{ijk}, If ($q_{ijk-1} \le QP_{ijt} \le q_{ijk}$)
M	A huge positive number

Fuzzy parameters	
$\widetilde{w_t}$	Fuzzy total budget for replenishment in period t
$\tilde{y}$	Fuzzy total storage capacity
Stochastic parameter	
φ_{jt}	Stochastic demand for item j in period t
φ_{jt}^{l}	Lowest value of the demand for item j in period t
φ_{jt}^{m}	Middle value of the demand for item j in period t
φ_{jt}^{u}	Highest value of the demand for item j in period t
Decision variables	
TC	Total cost of the entire planning horizon
QP_{ijt}	Order quantity for item j from supplier i in period t
CO	Total ordering cost for the planning horizon
CP_{ijtk}	Total purchase cost of item j from supplier i in period t at price level k
CI_{jt}	Inventory cost for item j in period t
CS_{jt}	Shortage cost for item j in period t
N_{it}	Number of vehicles used by supplier i in period t
IB_{jt}	Beginning inventory level for item j in period t
IE_{jt}	Ending inventory level for item j in period t
SB_{jt}	Beginning shortage level for item j in period t
SE_{jt}	Ending shortage level for item j in period t
AB_{jt}	1 If there is inventory of item j at the beginning of period t; 0 otherwise
AE_{jt}	1 If there is inventory of item j at the end of period t; 0 otherwise
BB_{jt}	1 If there is shortage of item j at the beginning of period t; 0 otherwise
BE_{jt}	1 If there is shortage of item j at the end of period t; 0 otherwise
F_{it}	1 If a purchase is made from supplier i in period t
U_{ijtk}	1 If item j is purchase from supplier i in period t at price level k

B. *Mathematical formulation*

Based on these information, a fuzzy-stochastic mathematical programming model of the integrated LS & SS problem is presented in Eqs. (1) – (24) by using the mathematical nomenclature in the above Table 1. The objective function given in Eq. (1) is to minimize total cost which is the summation of the ordering, purchasing, transportation, inventory holding and shortage costs, respectively.

$$Minimize\ TC = CO + \sum_{i=1}^{I}\sum_{j=1}^{J}\sum_{t=1}^{T}\sum_{k=1}^{K} CP_{ijtk} + CT + \sum_{j=1}^{J}\sum_{t=1}^{T} CI_{jt} + \sum_{j=1}^{J}\sum_{t=1}^{T} CS_{jt} \tag{1}$$

Subject to:

$$CO = \sum_{t=1}^{T}\sum_{j=1}^{J}\sum_{i=1}^{I} o_{ij}.F_{it} \tag{2}$$

$$CP_{ijtk} \geq p_{ijk}.QP_{ijt} - (1 - U_{ijtk}).M \qquad \forall i \in I,\ j \in J,\ t \in T,\ k \in K \tag{3}$$

$$\sum_{k=1}^{K} q_{ijk-1}.U_{ijtk} \leq QP_{ijt} \qquad \forall i \in I, j \in J, t \in T \tag{4}$$

$$\sum_{k=1}^{K} U_{ijtk} = 1 \qquad \forall i \in I, j \in J, t \in T \tag{5}$$

$$\sum_{j=1}^{J} QP_{ijt} \leq F_{it}.M \qquad \forall i \in I, t \in T \tag{6}$$

$$CT = \sum_{t=1}^{T}\sum_{i=1}^{I} s_i . N_{it} \tag{7}$$

$$CI_{jt} \geq \frac{h_j}{2}.\left(IB_{jt} + IE_{jt}\right) - BE_{jt}.M \qquad \forall j \in J, t \in T \tag{8}$$

$$CI_{jt} \geq \frac{h_j.(IB_{jt}+\varphi_{jt})}{2} - (1 - BE_{jt} + BB_{jt}).M \qquad \forall j \in J, t \in T, \varphi_{jt} \sim Triangular\left(\varphi_{jt}^{l}, \varphi_{jt}^{m}, \varphi_{jt}^{u}\right) \tag{9}$$

$$CS_{jt} \geq \frac{l_j}{2}.\left(SB_{jt} + SE_{jt}\right) - AB_{jt}.M \qquad \forall j \in J, t \in T \tag{10}$$

$$CS_{jt} \geq \frac{l_j.\left(SB_{jt} + \varphi_{jt}\right)}{2} - (1 - AB_{jt} + AE_{jt}).M \quad \forall j \in J, t \in T, \varphi_{jt} \sim Triangular\left(\varphi_{jt}^{l}, \varphi_{jt}^{m}, \varphi_{jt}^{u}\right) \tag{11}$$

$$IE_{jt} - SE_{jt} = IB_{jt} - SB_{jt} - \varphi_{jt} \qquad \forall j \in J, t \in T, \varphi_{jt} \sim Triangular\left(\varphi_{jt}^{l}, \varphi_{jt}^{m}, \varphi_{jt}^{u}\right) \tag{12}$$

$$IB_{jt} - SB_{jt} = IE_{jt-1} - SE_{jt-1} + \sum_{i=1}^{I} QP_{ijt} \qquad \forall j \in J, t \in T \tag{13}$$

$$\sum_{j=1}^{J} v_j . QP_{ijt} \leq N_{it} . c_{it} \qquad \forall i \in I, t \in T \tag{14}$$

$$AB_{jt} + BB_{jt} = 1 \qquad \forall j \in J, t \in T \tag{15}$$

$$AE_{jt} + BE_{jt} = 1 \qquad \forall j \in J, t \in T \tag{16}$$

$$IB_{jt} \leq AB_{jt}.M \qquad \forall j \in J, t \in T \tag{17}$$

$$SB_{jt} \leq BB_{jt}.M \qquad \forall j \in J, t \in T \tag{18}$$

$$IE_{jt} \leq AE_{jt}.M \qquad \forall j \in J, t \in T \tag{19}$$

$$SE_{jt} \leq BE_{jt}.M \qquad \forall j \in J, t \in T \tag{20}$$

$$\sum_{i=1}^{I}\sum_{t=1}^{T} QP_{ijt} \geq \sum_{t=1}^{T} \varphi_{jt} \qquad \forall j \in J, \varphi_{jt} \sim Triangular\left(\varphi_{jt}^{l}, \varphi_{jt}^{m}, \varphi_{jt}^{u}\right) \tag{21}$$

$$\sum_{i=1}^{I}\sum_{j=1}^{J} CP_{ijtk} \leq \widetilde{w_t} \qquad \forall k \in K, t \in T \tag{22}$$

$$\sum_{j=1}^{J} IB_{jt} \leq \tilde{y} \qquad \forall t \in T \tag{23}$$

$U_{ijtk}, F_{it}, AB_{jt}, AE_{jt}, BB_{jt}, BE_{jt} \in \{0,1\}, N_{it} \geq 0$ integer and all variables are nonnegative (24)

According to constraint in Eq. (2), one can calculate the ordering cost. Similarly, purchasing costs with all-units quantity discount can be computed by Eq. (3). Constraint set in Eq. (4) ensures that when calculating the purchasing cost, purchase quantity is used appropriately. Constraint set in Eq. (5) ensures that every item should have only one price level from each supplier at each time period. Constraint set in Eq. (6) allows purchasing if an order has been placed. Transportation cost can be calculated by Eq. (7). One can calculate the inventory holding cost by making use of constraint sets in Eqs. (8) and (9). In detail, holding cost for item j in time period t, i.e., CI_{jt}, is obtained by multiplying the unit holding cost h_j with average beginning and ending inventory levels as formulated in Eq. (8). As mentioned before, there are three different cases as shown in Fig. 1. For the first case (a), $BB_{jt} = BE_{jt} = 0$, and only the constraint set in Eq. (8) is active. For the second case (b), $BB_{jt} = 0$, $BE_{jt}=1$, and only the constraint set in Eq. (9) is active. For the last case (c), $BB_{jt}=1$, $BE_{jt}=1$, and both of the constraint sets in Eq. (8) and (9) are inactive because there is no excess inventory. It should also be emphasized here that apart from the deterministic demands in the study of Alfares & Turnadi (2018), stochastic nature of the customer demands are taken into consideration in Eq. (9). By making use of the constraint sets in Eq. (10) and (11), shortage cost can be calculated. Actually, the shortage cost, i.e., CS_{jt}, is obtained by multiplying the unit shortage cost (l_j) with the average beginning and ending shortage levels. In a similar manner, there are also three possible cases as shown in Fig. 1. For the first case (a), AB_{jt}=AE_{jt}=0, and only the constraint set in Eq. (10) is active. For the second case (b), AB_{jt}=1, AE_{jt}=0, and only the constraint set in Eq. (11) is active. For the final case (c), AB_{jt}=1, AE_{jt}=0, and both of the constraint sets in Eq. (10) and (11) are inactive because there is no shortage (Alfares & Turnadi, 2018). Constraint set in Eq. (12) ensures that inventory balance is accomplished. Eq. (13) is also formulated for satisfying the inventory balance and calculating the beginning inventory levels. Eq. (14) guarantees that order quantity for any supplier at each time period cannot exceed the transportation capacity of that supplier. The logical constraints of the model are also formulated in Eqs. (15) - (20). The probabilistic demand satisfaction constraint is given in Eq. (21). According to constraint set in Eq. (22), fuzzy budget limits cannot be surpassed. Similarly, fuzzy capacity constraint on the storage volume is formulated in Eq. (23). Finally, binary and integer decision variables of this mathematical model are defined in Eq. (24).

C. The crisp equivalent formulations of the fuzzy constraints

In this sub-section, transformation of the fuzzy constraints in Eqs. (22) – (23) into their crisp equivalent forms is presented. Since only the right hand side values of these constraints are represented by fuzzy numbers, it is classified as Type-2 fuzzy mathematical programs by Baykasoğlu & Göçken (2008). In order to solve this kind of fuzzy mathematical programs, Verdegay's (1982) and Werners's (1987) approaches were generally preferred to use in the literature. For applying these approaches, tolerance values (p_i) should be previously known or determined by the decision maker. In fact, Verdegay's (1982) approach focused on a non-symmetric model where only the right hand side parameters, i.e., $\tilde{b}$ are fuzzy. On the other hand, Werners's (1987) approach justifies that the objective function will also be fuzzy because of the uncertainty in right hand side parameters, and a symmetrical model has been introduced. Moreover, Verdegay's (1982) approach is based on α-cuts. In other words, the crisp equivalent form is an α-parametric model where α is a measure of the fuzziness in the mathematical model. This parameter also represents the satisfaction degree of the fuzzy constraints. Furthermore, another term, i.e., $\theta = 1 - \alpha$ is also used by Verdegay's (1982) approach. If $\theta = 0$, then $\alpha = 1$ and the constraint satisfaction degree will be 100%. If $\theta = 1$, then $\alpha = 0$ which corresponds to the maximum tolerance in the fuzzy constraints. Before applying these transformation approaches, membership functions of the fuzzy constraints are formulated in Eq. (25).

$$\mu(Ax)_i = \begin{cases} 0 & if\ (Ax)_i > b_i + p_i \\ 1 - \frac{(Ax)_i - b_i}{p_i} & if\ b_i \le (Ax)_i \le b_i + p_i \\ 1 & if\ (Ax)_i < b_i \end{cases} \tag{25}$$

Through the Eq. (25), the crisp equivalent forms of fuzzy constraints (22) - (23) are provided by using Verdegay's (1982) approach as in Eqs. (26) – (27).

$$\sum_{i=1}^{I}\sum_{j=1}^{J} CP_{ijtk} \leq w_t + (1-\alpha) * p_i \qquad \forall k \in K, t \in T \tag{26}$$

$$\sum_{j=1}^{J} IB_{jt} \leq y + (1-\alpha) * p_i \qquad \forall t \in T \tag{27}$$

As mentioned previously, Werners's (1987) approach is based on a symmetric model or a non-parametric method. Actually, if the right hand side of a constraint is considered as fuzzy, the objective function value (aspiration level) is also required to be fuzzy (symmetric). In that approach, lowest and highest tolerances on the objective value could be first determined. Afterwards, membership functions for both fuzzy objective and constraints should be formulated as Eq. (25) and Eq. (28):

$$\mu_0(c^T x)_i = \begin{cases} 1 & if\ c^T x \geq Z^1 \\ 1 - \frac{Z^1 - c^T x}{Z^1 - Z^0} & if\ Z^0 \leq c^T x \leq Z^1 \\ 0 & if\ c^T x \leq Z^0 \end{cases} \tag{28}$$

Based on these information, crisp equivalent forms of the fuzzy objective function and the constraints in Eqs. (22) - (23) can be yielded by using Werners's (1987) approach as follows:

$$\text{Max} \quad \alpha \tag{29}$$

$$TC \leq z^1 - (z^1 - z^0)(1-\alpha) \tag{30}$$

$$\sum_{i=1}^{I}\sum_{j=1}^{J} CP_{ijtk} \leq w_t + (1-\alpha) * p_i \qquad \forall k \in K, t \in T \tag{31}$$

$$\sum_{j=1}^{J} IB_{jt} \leq y + (1-\alpha) * p_i \qquad \forall t \in T \tag{32}$$

It is obviously seen in Eqs. (29) – (32) that satisfaction degree of the least satisfied fuzzy objective (or constraint) is targeted to maximize in that approach.

III. NUMERICAL EXAMPLE

In order to see the validation and verification of the proposed fuzzy-stochastic MIP model and test its performance, a numerical example which was taken from Alfares & Turnadi (2018) is presented. In this example, there are 2 suppliers (A and B), 2 items, 4 quantity discounts, and 5 periods, respectively. This numerical example is also based on the data of Lee et al. (2013). However, the values of shortage cost and volume per item are not given by both of these articles. Moreover, numerical examples given in these articles just considered a single item whereas this study present a numerical example with multiple items. Therefore, shortage costs, volume per units are solved by using different values. As a result, shortage cost is determined as \$0.2, and volume per item is determined as 1 unit. Furthermore, customer demands for all items are assumed to have triangular distribution in which demands of these items are distributed triangularly with the parameters of Tria(255, 368, 405). In this study, all quantity discounts are considered as all-units quantity discounts for each supplier. Schematic depiction of the examined problem is also presented in Figure 2. It shows the decision flow from suppliers to a buyer/customer. Inventory holding costs are determined for each item as h_j= \$0.11 and \$0.21, respectively. Moreover, shortage costs are specified as l_j= \$0.2 and \$0.3.

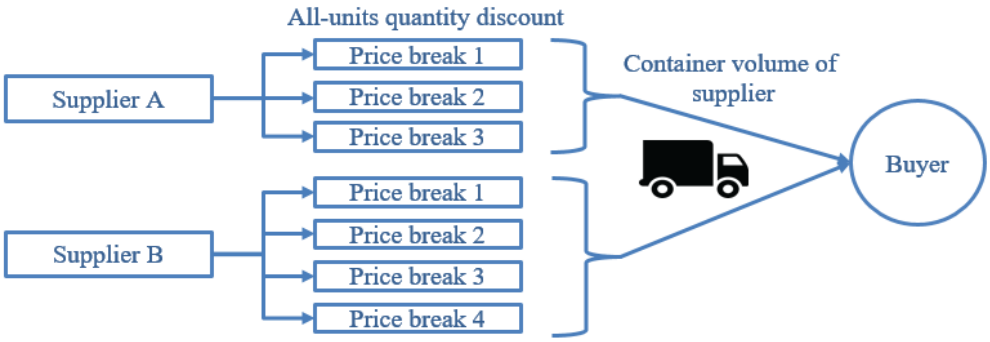

Figure 2. A schematic depiction of the stated problem.

Furthermore, transportation costs are $21 and $22 for suppliers A and B, respectively. Ordering costs for the first item are equal to $250 for supplier A and $220 for supplier B; Ordering costs for the second item are $220 for supplier A and $200 for supplier B. Additionally, each item can also be purchased from the same supplier. Container volume per vehicle from the supplier is c_i= 25 m^2. The volume per item is equal, v_j =1 for all items. The total budget for replenishment is taken as w_t= $30000. The tolerance value for this fuzzy input parameter $\widetilde{w_t}$ is p=$10000 for all items. Storage capacity is specified as y=3000 m^2. Besides, the tolerance value for this fuzzy parameter $\tilde{y}$ is taken as p=1000 m^2. The discount schedule of the supplier A for the all items with all-units quantity discounts are given in Table 2.

Table 2. Discount schedule of supplier A for the items.

Item 1			Item 2		
Price break (k)	Purchase quantity (q_{i1k})	Price per unit (p_{i1k})	Price break (k)	Purchase quantity (q_{i2k})	Price per unit (p_{i2k})
1	0-2000	$2.99	1	0-1500	$3.50
2	2001-3899	$2.85	2	1501-3500	$3.25
3	3900 or more	$2.74	3	3500 or more	$3.00

The discount schedule of the supplier B for the all items with all-units quantity discounts are also presented in Table 3.

Table 3. Discount schedule of supplier B for the items.

Item 1			Item 2		
Price break (k)	Purchase quantity (q_{i1k})	Price per unit (p_{i1k})	Price break (k)	Purchase quantity (q_{i2k})	Price per unit (p_{i2k})
1	0-1100	$3.00	1	0-1000	$3.75
2	1101-2200	$2.93	2	1001-2000	$3.45
3	2201-3400	$2.82	3	2001-4000	$3.15
4	3401 or more	$2.75	4	4000 or more	$2.85

IV. Optimization Results

The proposed fuzzy-stochastic mathematical programming model is solved by the stochastic programming solver of LINGO 18.0 optimization software. In the single stage stochastic program, the sample size or the number of scenarios is set to 2. The optimization results of these scenarios are shown in Tables 4 - 5. Both of Verdegay's (1984) and Werner's approaches (1987) are applied to fuzzy components of the model for converting it to its crisp equivalent form. The expected value of the total cost objective is equal to $14879.10 when the α-cut level is set to zero. This means that total cost value will be probably $14879.10 when the maximum tolerance is considered in satisfying the fuzzy constraints. On the other hand, the expected value of the total cost objective is equal to \$14726.78 in case of the α-cut level is set to one. This means that in the absence of tolerance on the fuzzy constraints, objective value will be \$14726.78. These values are also used in applying Werner's approach (z^0 =\$14726.78.17 and z^1=\$14879.10).Furthermore, the proposed model is also solved with different α-cut values to investigate how the model will behave under different levels of uncertainty.

Table 4. Optimization results of the scenario-1.

α-*cuts*	Objective value	Time periods (t)	1	2	3	4	5	Elapsed runtime (sec.)
0	14759.91	d_{1t}	335.69	360.96	333.95	394.17	330.37	337.80
		d_{2t}	383.21	363.68	335.16	341.49	312.33	
		QP_{11t}	0	1030.60	0	0	724.54	
		QP_{12t}	0	1110.42	0	0	625.46	
1	14588.80	d_{1t}	335.69	360.96	333.95	394.17	330.37	1028.99
		d_{2t}	383.21	363.68	335.16	341.49	312.33	
		QP_{11t}	0	0	1755.14	0	0	
		QP_{12t}	0	0	1735.88	0	0	

Table 5. Optimization results of the scenario-2.

α-*cuts*	Objective value	Time periods (t)	1	2	3	4	5	Elapsed runtime (sec.)
0	14998.29	d_{1t}	358.19	328.79	379.79	340.62	370.06	337.80
		d_{2t}	343.60	320.56	371.32	373.72	367.48	
		QP_{11t}	0	686.98	0	1090.47	0	
		QP_{12t}	0	664.15	0	1112.52	0	
1	14864.76	d_{1t}	358.19	328.79	379.79	340.62	370.06	1028.99
		d_{2t}	343.60	320.56	371.32	373.72	367.48	
		QP_{11t}	0	0	1777.45	0	0	
		QP_{12t}	0	0	1776.67	0	0	

Fuzzy optimization results obtained from Verdegay's approach are shown in Tables 6 under different α-cuts. Details of the fuzzy optimization results provided by Werner's approach are also given in Table 7. In summary, the expected objective value provided by Werner's approach is equal to 1.0 for both scenarios as displayed in Table 7. In addition, total cost is also calculated as \$14879.10 when Werner's approach is applied.

Table 6. Fuzzy optimization results by using Verdegay (1982) approach under different uncertainty levels.

α-cuts	Total expect cost	Objective of Scenario-1	Objective of Scenario-2
0	\$14879.10	\$14759.91	\$14998.29
0.2	\$14793.54	\$14588.80	\$14998.29
0.4	\$14726.78	\$14588.80	\$14864.76
0.6	\$14726.78	\$14588.80	\$14864.76
0.8	\$14726.78	\$14588.80	\$14864.76
1.00	\$14726.78	\$14588.80	\$14864.76

Table 7. Details of the fuzzy optimization results obtained from Werners's approach (1987).

Objectives of scenarios (α)	Time periods (t)	1	2	3	4	5	Elapsed runtime (sec.)
1.00	d_{1t}	335.69	360.96	333.95	394.17	330.37	351.61
	d_{2t}	383.21	363.68	335.16	341.49	312.33	
	QP_{11t}	0	696.65	0	1058.49	0	
	QP_{12t}	0	619.37	0	1116.51	0	
1.00	d_{1t}	358.19	328.79	379.79	340.62	370.06	351.61
	d_{2t}	343.60	320.56	371.32	373.72	367.48	
	QP_{11t}	0	0	1781.77	0	0	
	QP_{12t}	0	0	1776.67	0	0	

It should also be emphasized here that supplier A is selected in every situation. All QP_{2jt} values take the value zero in all situations. According to the above results, total expected cost will be between $14726.78 and $14879.10. Therefore, decision maker(s) should take into account this objective range while controlling the production and inventory system. In addition, this solution report can also be send to supplier B for the quantity discounts and some arrangements can also be made to offer alternative discounts.

V. CONCLUSION AND FUTURE RESEARCH

In this study, an integrated lot-sizing and supplier selection problem (LSS/SS) is addressed with multiple items, time periods, quantity discounts and backordering options under different types of uncertainties, i.e., fuzziness and stochasticity. Indeed, the original deterministic MIP model of Alfares & Turnadi (2018) is extended by using stochastic and fuzzy mathematical porgramming approaches simulatenaoulsy Because most of the real-life inventory control problems may have stochastic demands, fuzzy budget limits and storage capacities. The proposed fuzzy-stochastic model aims to provide minimum total expected cost, which includes ordering, transportation, holding, shortage and purchasing cost items. Moreover, purchasing cost is handled under all-units quantity discounts for different suppliers. As a result, with the help of the proposed model, order quantities, supplier selection and time to orders which provides the minimum total expect cost, can be obtained.

In the future, metaheuristic algorithms can be applied for solving larger size problem instances within reasonable computing times. Because, MIP models may not be useful in case of big data. Briefly, solving an integrated lot-sizing & supplier selection problem with multiple items, time periods, quantity discounts, backordering, and stochastic demands by making use of metaheuristic algorithms can be scheduled as a future work.

REFERENCES

1. Alfares, H., & Turnadi, R. (2018). Lot sizing and supplier selection with multiple items, multiple periods, quantity discounts, and backordering. *Computers & Industrial Engineering, 116*, 59-71.
2. Baykasoğlu, A., & Göçken, T. (2008). A review and classification of fuzzy mathematical programs. *Journal of Intelligent & Fuzzy Systems, 19*, 205-229.
3. Kasilingam, R., & Lee, C. (1996). Selection of Vendors - A Mixed-Integer Programming Approach. *Computers & Industrial Engineering, 31*, 347-350.
4. Kumar, M., Vrat, P., & R., S. (2004). A fuzzy goal programming approach for vendor selection. *Computers & Industrial Engineering, 46*, 69-85.
5. Rezaei, J., & Davoodi, M. (2016). Inventory lot-sizing with supplier selection under non-stationary stochastic demand. *International Journal of Production Research, 54*, 2459-2469.
6. Verdegay, J. (1982). Fuzzy mathematical programming. *Fuzzy Information and Decision Processes*, 231-237.
7. Vergeday, J. (1984). A Dual Approach to Solve the Fuzzy Linear Programming Problem. *Fuzzy Sets and Systems, 14*, 131-141.
8. Werners, B. (1987). An Interactive Fuzzy Programming System. *Fuzzy Sets and Systems, 23*, 131-147.

Investigation of the Wave Solutions of the Nonlinear Partial Differential Equations with the Modified Exponential Function Method

Hasan BULUT[1], Tolga AKTÜRK[2], Aslı ALKAN[3]

[1]Department of Mathematics, Faculty of Science, Fırat University, Turkey

[2]Department of Mathematics and Science Education, Faculty of Education, Ordu University, Turkey

[3]Department of Mathematics, Faculty of Science, Fırat University, Turkey

[1]hbulut@firat.edu.tr, [2]tolgaakturkk@gmail.com, alkanasli47@gmail.com;

Abstract

In this study, the wave solutions related to the Dullin-Gottwold-Holm equation were obtained using the modified exponential function method (MEFM). Solution functions obtained as a result of calculations include hyperbolic, trigonometric, and rational functions. Two-dimensional, three-dimensional, contour graph and density graphs representing the characteristic feature of the solution functions obtained by determining the appropriate parameters are drawn.

Keywords: The wave solutions; the Dullin-Gottwold-Holm equation; the modified exponential function method.

1. Introduction

Nonlinear partial differential equations (NPDEs) appear in many different fields such as chemistry, biology, optics, hydrodynamics, economy, meteorology, plasma physics and engineering. Therefore, there are various methods in the literature for obtaining solutions of these equations. Some of these, the (G'/G) expansion method [1], the new function methods [2], the generalized Kudryashov method [3], the sine-Gordon expansion method [4], the $\partial-$ dressing method [5], the homotopy perturbation method [6] and so on. In this study, we apply the modified expansion function method (MEFM) [7-8] to solve a nonlinear Dullin-Gottwald-Holm (DGH) equation and find new interactions among travelling wave solutions.

The Dullin-Gottwald-Holm equation can be defined as follow [9],

$$u_t + c_0 u_x + 3uu_x - \alpha^2 (u_{xxt} + uu_{xxx} + 2u_x u_{xx}) + \gamma u_{xxx} = 0. \tag{1}$$

2. Modified Expansion Function Method

In this section, we will be given information about MEFM.

Consider the following nonlinear partial differential equation;

$$P(u, u_x, u_t, u_{xx}, u_{xxx}, u_{tt}, u_{tx}, \dots) = 0, \tag{2}$$

where $u(x,t)$ is unknown function, P is a polynomial in $u(x,t)$ and its derivatives.

Step 1: The following traveling wave transformation:

$$u(x,t) = u(\xi), \xi = k(x - ct), \tag{3}$$

where k, c are constants and can be determined later.

Substituting Eq. (3) into Eq. (2), it gives the following nonlinear ordinary differential equation;

$$N(u,u',u'',u''',,\dots) = 0. \tag{4}$$

Step 2: We assume that according to the MEFM the requested solution is as follows:

$$u(\xi) = \frac{\sum_{i=0}^{n} A_i\left[\exp\left(-\Omega(\xi)\right)\right]^i}{\sum_{j=0}^{m} B_j\left[\exp\left(-\Omega(\xi)\right)\right]^j} = \frac{A_0 + A_1 e^{-\Omega} + \cdots + A_m e^{-n\Omega}}{B_0 + B_1 e^{-\Omega} + \cdots + B_n e^{-m\Omega}}, \tag{5}$$

where A_i $(0 \leq i \leq n)$ and B_j $(0 \leq j \leq m)$.

Using the balance principle, the m and n positive integer values are obtained.

$$\Omega' = e^{-\Omega(\xi)} + \mu e^{\Omega(\xi)} + \lambda. \tag{6}$$

Eq. (6) has the following families of solutions [10].

Family 1: When $\mu \neq 0, \lambda^2 - 4\mu > 0$,

$$\Omega(\xi) = \ln\left(\frac{-\sqrt{\lambda^2 - 4\mu}}{2\mu}\tanh\left(\frac{\sqrt{\lambda^2 - 4\mu}}{2}(\xi + EE) - \frac{\lambda}{2\mu}\right)\right). \tag{7}$$

Family 2: When $\mu \neq 0, \lambda^2 - 4\mu < 0$,

$$\Omega(\xi) = \ln\left(\frac{-\sqrt{\lambda^2 + 4\mu}}{2\mu}\tan\left(\frac{\sqrt{-\lambda^2 + 4\mu}}{2}(\xi + EE) - \frac{\lambda}{2\mu}\right)\right). \tag{8}$$

Family 3: When $\mu = 0, \lambda \neq 0, \lambda^2 - 4\mu > 0$,

$$\Omega(\xi) = -\ln\left(\frac{\lambda}{e^{\lambda(\xi + EE)} - 1}\right). \tag{9}$$

Family 4: When $\mu \neq 0, \lambda \neq 0, \lambda^2 - 4\mu = 0$,

$$\Omega(\xi) = \ln\left(-\frac{2\lambda(\xi + EE) + 4}{\lambda^2(\xi + EE)}\right). \tag{10}$$

Family 5: When $\mu = 0, \lambda = 0, \lambda^2 - 4\mu = 0$,

$$\Omega(\xi) = \ln(\xi + EE). \tag{11}$$

Where, EE is a integral constant.

Step 3: Substituting Eq. (5) and its derivatives into Eq. (4), we get an algebraic equation system. The Mathematica software program has solved this system, and then the solutions of the Dullin-Gottwald-Holm equation have been obtained.

3. Application

In this section, the modified expansion function method will be used to obtain solutions to the DGH equation. Consider the following traveling wave transformation:

$$u(x,t) = u(\xi), \xi = k(x - ct). \tag{12}$$

The following nonlinear ordinary differential equation is obtained,

$$(c_0 - c)u + \alpha^2 k^2 (cu'' - (u')^2 - uu'' + u') + \frac{3}{2}u^2 + \gamma k^2 u'' = R, \tag{13}$$

where R is integral constant. If the balancing procedure is applied to Eq. (12), we have the following relationship,

$$n = m + 2.$$

Choosing $m = 1$ we get $n = 3$, the Eq. (5) is obtained for m and n values as follows;

$$u(\xi) = \frac{A_0 + A_1 e^{-\Omega} + A_2 e^{-2\Omega} + A_3 e^{-3\Omega}}{B_0 + B_1 e^{-\Omega}}. \tag{14}$$

If Eq. (14) is regulated according to the necessary term in equation (13), then the following system of algebraic equations is obtained which consists of the coefficients of $e^{-\Omega(\xi)}$.

Some suitable coefficients obtained by using the Mathematica software program are given below.

Case-1:

$$A_0 = \frac{(-k^4\gamma^2(\lambda^2 + 8\mu)A_3 + \sqrt{k^4\gamma^2(6R + k^4\gamma^2(\lambda^2 - 4\mu)^2)A_3^2})B_0}{3k^2\gamma A_3},$$

$$A_1 = \frac{1}{12}\left((\lambda^2 + 8\mu)A_3 - \frac{\sqrt{k^4\gamma^2(6R + k^4\gamma^2(\lambda^2 - 4\mu)^2)A_3^2}}{k^4\gamma^2} - 48k^2\gamma\lambda B_0\right),$$

$$A_2 = \lambda A_3 - 4k^2\gamma B_0,$$

$$B_1 = -\frac{A_3}{4k^2\gamma},$$

$$c = \frac{\sqrt{k^4\gamma^2(6R + k^4\gamma^2(\lambda^2 - 4\mu)^2)A_3^2}}{k^2\gamma A_3} + c_0.$$

Substituting these coefficients into Eq. (13), the following solutions:

Family 1: When $\mu \neq 0, \lambda^2 - 4\mu > 0$, solution of Eq. (1),

$$u_{1,1}(x,t) = \frac{\left(Sech\left[\frac{1}{2}\Lambda\right]^2 (-k^4\gamma^2(\lambda^2 - 4\mu)(-10\mu + \Gamma + \lambda\Phi)A_3 + (2\mu + \Gamma + \lambda\Phi)\psi)\right)}{3k^2\gamma A_3\left(\lambda + \sqrt{\lambda^2 - 4\mu}\,Tanh\left[\frac{1}{2}\Lambda\right]\right)^2}. \tag{15}$$

Where, $\Lambda = (EE + \xi)\sqrt{\lambda^2 - 4\mu}$, $\Gamma = (\lambda^2 - 2\mu)Cosh[\Lambda]$, $\Phi = \sqrt{\lambda^2 - 4\mu}\,Sinh[\Lambda]$,

$\psi = \sqrt{k^4\gamma^2(6R + k^4\gamma^2(\lambda^2 - 4\mu)^2){A_3}^2}.$

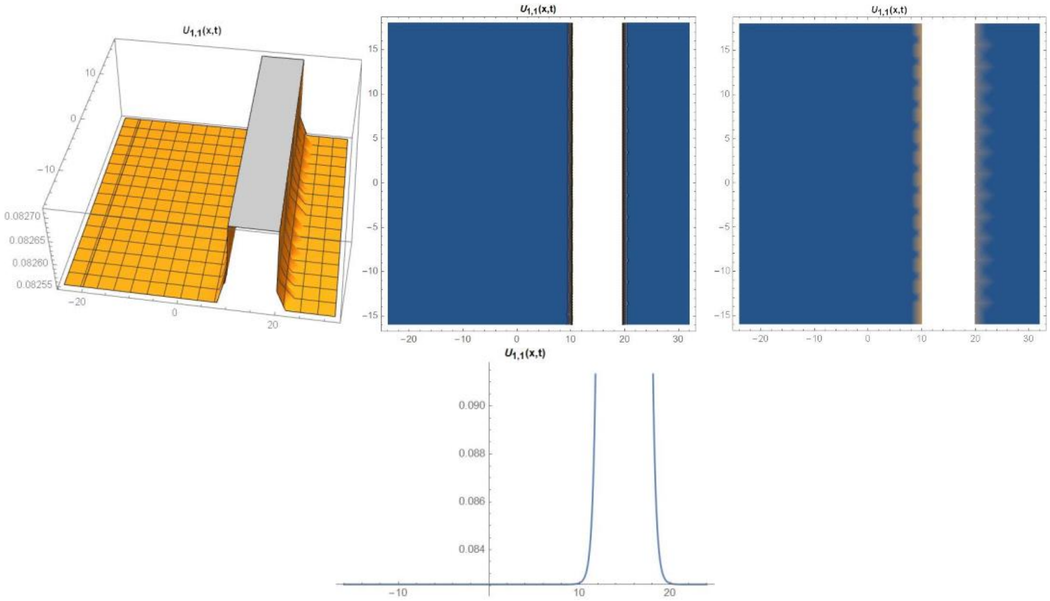

Figure 1: The 3D, density, contour graphics and 2D surface of Eq. (15) for $\lambda = 3, \mu = 1, c_0 = 0.25, \gamma = 2, k = 1.25, R = 1.3, c = 16.1226, A_1 = -6.00991, A_2 = 2, B_1 = -0.12, EE = 0.65, A_3 = 1.5, B_0 = 0.2, A_0 = -2.48349, t = 1$.

Family 2: When $\mu \neq 0, \lambda^2 - 4\mu < 0$, solution of Eq. (1),

$$u_{2,1}(x,t) = \frac{\left(Sec\left[\frac{1}{2}\vartheta\right]^2 (k^4\gamma^2(\lambda^2-4\mu)(10\mu-(\lambda^2-2\mu)Cos[\vartheta]+\lambda\beta)A_3+(2\mu+(\lambda^2-2\mu)Cos[\vartheta]-\lambda\beta)\psi)\right)}{3k^2\gamma A_3\left(\lambda-\sqrt{-\lambda^2+4\mu}Tan\left[\frac{1}{2}\vartheta\right]\right)^2}. \quad (16)$$

Where, $\vartheta = (EE + \xi)\sqrt{-\lambda^2+4\mu}, \beta = \sqrt{-\lambda^2+4\mu}Sinh[\vartheta]$

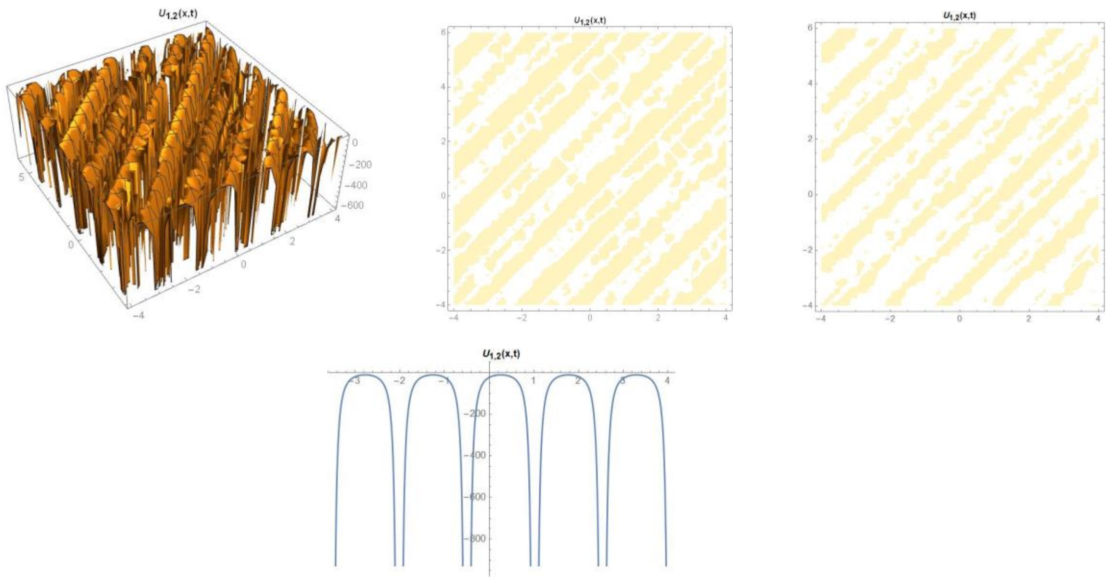

Figure 2: The 3D, density, contour graphics and 2D surface of Eq. (15) for $\lambda = 1, \mu = 3, c_0 = 0.25, \gamma = 2, k = 1.25, R = 1.3, A_3 = 1.5, \alpha = 0, B_0 = 0.2, A_0 = -2.90912, c = 34.7383, A_1 = -0.754531, A_2 = -1, B_1 = -0.12, EE = 0.65, t = 1$.

Family 3: When $\mu = 0, \lambda \neq 0,\ \lambda^2 - 4\mu < 0$, we get solution of Eq. (1),

$$u_{3,1}(x,t) = \left(\frac{ \frac{\lambda^3 A_3}{\delta^3} + \frac{(-k^4\gamma^2\lambda^2 A_3+\zeta)B_0}{3k^2\gamma A_3} + \frac{\lambda^2(\lambda A_3 - 4k^2\gamma B_0)}{\delta^2} + \frac{\lambda\left(\lambda^2 A_3 - \frac{\zeta}{k^4\gamma^2} - 48k^2\gamma\lambda B_0\right)}{12\delta} }{ -\frac{\lambda A_3}{4\delta k^2\gamma} + B_0 } \right). \tag{17}$$

Where, $\sigma = (EE + \xi)\lambda,\ \delta = -1 + e^{\sigma},\ \ \zeta = \sqrt{k^4\gamma^2(6R + k^4\gamma^2\lambda^4){A_3}^2}$

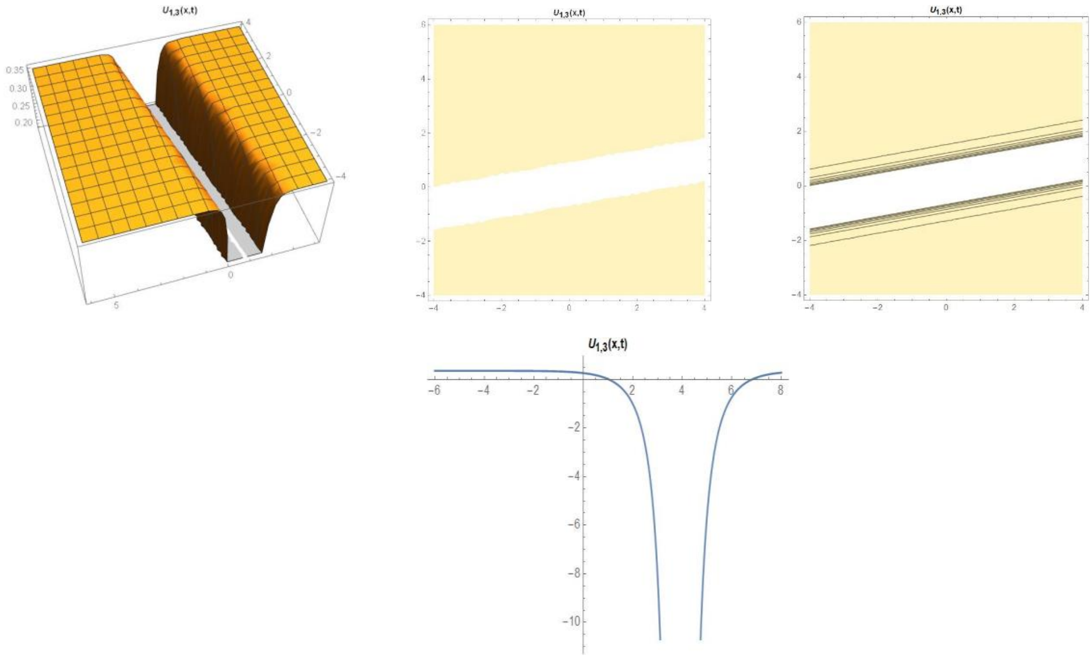

Figure 3: The 3D, density, contour graphics and 2D surface of Eq. (15) for $\lambda = 1, \mu = 0, c_0 = 0.25, \gamma = 2, k = 1.25, R = 1.3, A_3 = 1.5, \alpha = 0, B_0 = 0.2, A_0 = 0.0710758, c = 4.44114, A_1 = -2.54265, A_2 = -1, B_1 = -0.12, EE = 0.65, t = 1$.

Family 4: When $\mu \neq 0, \lambda \neq 0,\ \lambda^2 - 4\mu = 0$, we get solution of Eq. (1),

$$u_{4,1}(x,t) = \left(\frac{ \frac{\lambda^3 A_3}{\theta^3} + \frac{(-k^4\gamma^2\lambda^2 A_3+\zeta)B_0}{3k^2\gamma A_3} + \frac{\lambda^2(\lambda A_3 - 4k^2\gamma B_0)}{\theta^2} + \frac{\lambda\left(\lambda^2 A_3 - \frac{\zeta}{k^4\gamma^2} - 48k^2\gamma\lambda B_0\right)}{12\theta} }{ -\frac{\lambda A_3}{4\theta k^2\gamma} + B_0 } \right). \tag{18}$$

Where, $\sigma = (EE + \xi)\lambda,\ \theta = -1 + e^{\sigma},\ \zeta = \sqrt{k^4\gamma^2(6R + k^4\gamma^2\lambda^4){A_3}^2}$.

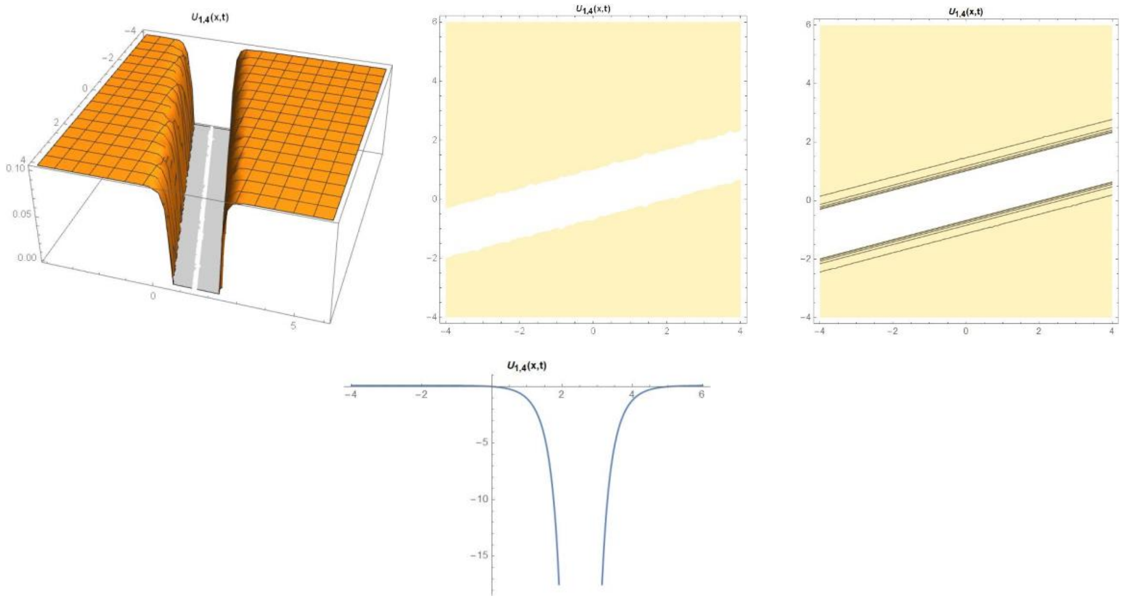

Figure 4: The 3D, density, contour graphics and 2D surface of Eq. (15) for $\lambda = 2, \mu = 1, c_0 = 0.25, \gamma = 2, \mathrm{k} = 1.25, \mathrm{R} = 1.3, A_3 = 1.5, \alpha = 0, B_0 = 0.2, A_0 = -2.31381, \mathrm{c} = 3.04285, A_1 = -3.61171, A_2 = 0.5, B_1 = -0.12, EE = 0.65.$

Family 5: When $\mu = 0, \lambda = 0, \lambda^2 - 4\mu = 0$, we get solution of Eq. (1),

$$u_{5,1}(x,t) = \left(\frac{-12k^4\gamma^2 A_3 + \sqrt{6}\sigma^2\sqrt{k^4 R\gamma^2 {A_3}^2}}{3k^2\sigma^2\gamma A_3} \right). \tag{19}$$

Where, $\sigma = (EE + \xi)\lambda$

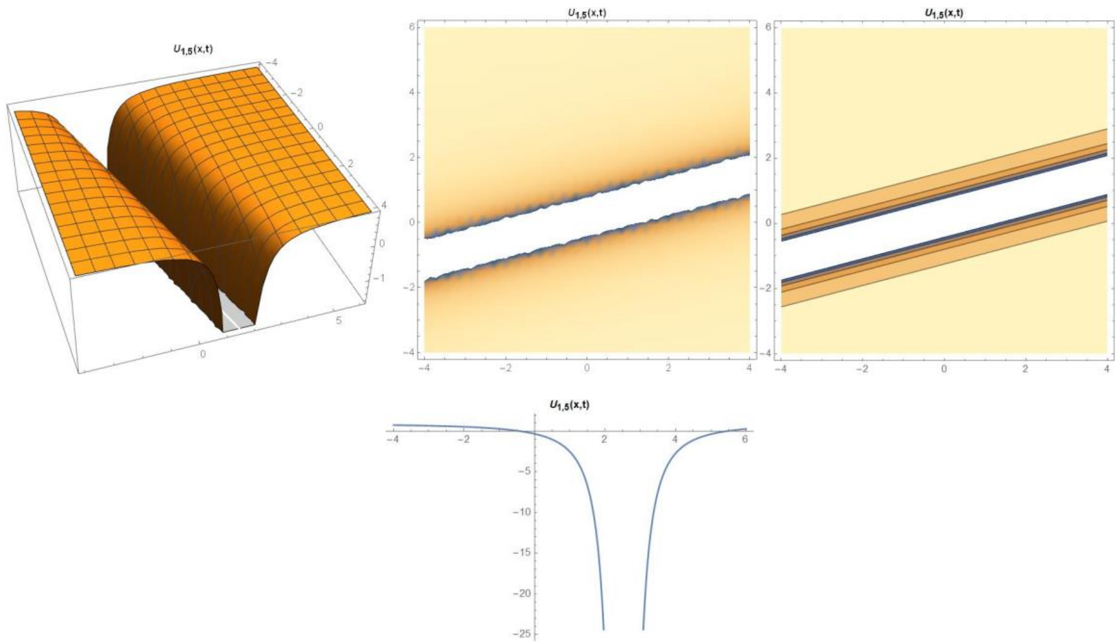

Figure 5: The 3D, density, contour graphics and 2D surface of Eq. (15) for $\lambda = 0, \mu = 0, c_0 = 0.25, \gamma = 2, \mathrm{k} = 1.25, \mathrm{R} = 1.3, A_3 = 1.5, \alpha = 0, B_0 = 0.2, A_0 = 0.18619, \mathrm{c} = 3.04285, A_1 = -0.111714, A_2 = -2.5, B_1 = -0.12, EE = 0.65.$

Case-2:

$$A_0 = \frac{B_0((\lambda^2 + 8\mu)A_3 + 4B_1(c - c_0))}{12B_1},$$

$$A_1 = \frac{1}{12}\left(A_3\left(\lambda^2 + 8\mu + \frac{12\lambda B_0}{B_1}\right) + 4B_1(c - c_0)\right),$$

$$A_2 = A_3\left(\lambda + \frac{B_0}{B_1}\right),$$

$$\gamma = -\frac{A_3}{4k^2B_1},$$

$$R = \frac{-(\lambda^2 - 4\mu)^2A_3^2 + 16B_1^2(c - c_0)^2}{96B_1^2},$$

$$\alpha = 0.$$

Substituting these coefficients into Eq. (14), the following solutions:

Family 1: When $\mu \neq 0, \lambda^2 - 4\mu > 0$, solution of Eq. (1),

$$u_{2,1}(x,t) = \frac{\left(Sech\left[\frac{1}{2}\Lambda\right]\right)^2((\lambda^2-4\mu)(-10\mu+(\lambda^2-2\mu)Cosh[\Lambda]+\lambda\Phi)A_3-4(-2\mu-(\lambda^2-2\mu)Cosh[\Lambda]-\lambda\Phi)B_1(c-c_0))}{12B_1\left(\lambda+\sqrt{+\lambda^2-4\mu}Tanh\left[\frac{1}{2}\Lambda\right]\right)^2}. \tag{20}$$

Where, $\Lambda = (EE + \xi)\sqrt{\lambda^2 - 4\mu}, \Phi = \sqrt{\lambda^2 - 4\mu}Sinh[\Lambda]$

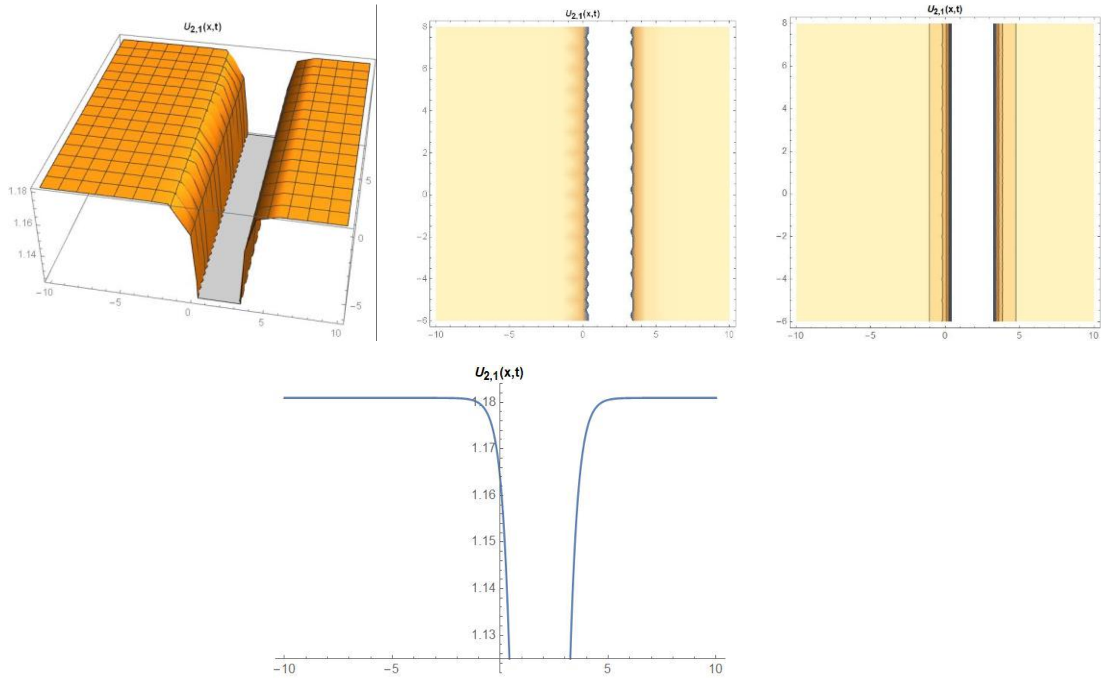

Figure 1: The 3D, density, contour graphics and 2D surface of Eq. (15) for $\lambda = 3, \mu = 1, c_0 = 0.25, \gamma = -0.096, k = 1.25, R = 1.3, A_3 = 1.5, \alpha = 0, B_0 = 0.2, A_0 = 0.0866667, c = 3.04285, A_1 = 1.44333, A_2 = 4.62, B_1 = 2.5, EE = 0.65, t = 1.$

Family 2: When, $\mu \neq 0, \lambda^2 - 4\mu < 0$, solution of Eq. (1),

$$u_{2,2}(x,t) = \left(\frac{Sec\left[\frac{1}{2}\vartheta\right]^2(\lambda^2-4\mu)(-10\mu+(\lambda^2-2\mu)Cos[\vartheta]+\lambda\beta)A_3-4(-2\mu-(\lambda^2-2\mu)Cos[\vartheta]-\lambda\beta)B_1(c-c_0))}{12B_1\left(\lambda-\sqrt{-\lambda^2+4\mu}Tan\left[\frac{1}{2}\vartheta\right]\right)^2}\right). \quad (21)$$

Where, $\vartheta = (EE + \xi)\sqrt{-\lambda^2 + 4\mu}, \beta = \sqrt{-\lambda^2 + 4\mu}Sinh[\vartheta]$

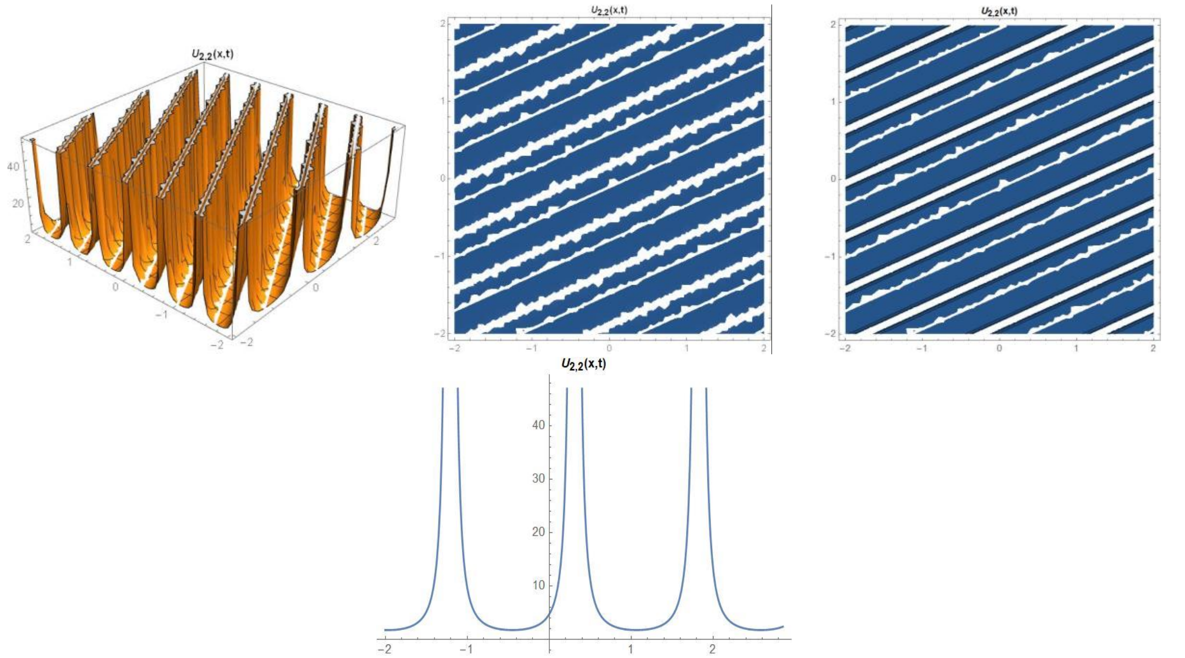

Figure 2: The 3D, density, contour graphics and 2D surface of Eq. (15) for $\lambda = 1, \mu = 3, c_0 = 0.25, \gamma = -0.096, k = 1.25, A_3 = 1.5, \alpha = 0, B_0 = 0.2, A_0 = 0.166667, c = 2.20333, A_1 = 1.62, A_2 = 4.62, B_1 = 2.5, EE = 0.65, R = -0.193333, t = 1$.

Family 3: When $\mu = 0, \lambda \neq 0,\ \lambda^2 - 4\mu < 0$, we get solution of Eq. (1),

$$u_{2,3}(x,t) = \left(\frac{1}{12}\left(\frac{\lambda^2(1+3\text{Csch}[2\sigma]^2)A_3}{B_1} + 4(c-c_0)\right)\right). \quad (22)$$

Where, $\sigma = (EE + \xi)\lambda$.

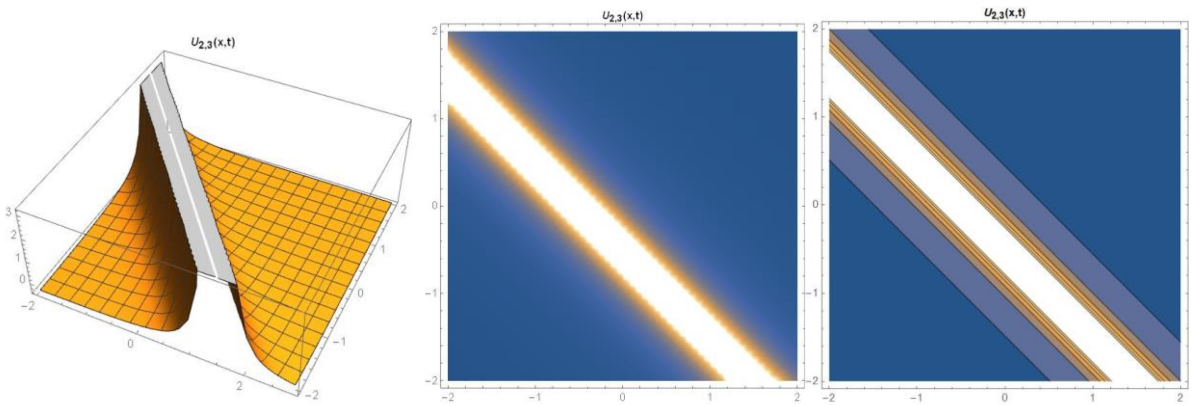

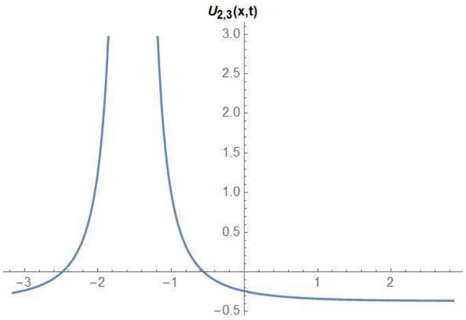

Figure 3: The 3D, density, contour graphics and 2D surface of Eq. (15) for $\lambda = 1, \mu = 0, c_0 = 0.25, \gamma = -0.096, \mathrm{k} = 1.25, A_3 = 1.5, \alpha = 0, B_0 = 0.2, A_0 = -0.0733333, \mathrm{c} = -1, A_1 = -0.796667, A_2 = 1.62, B_1 = 2.5, EE = 0.65, \mathrm{R} = 0.256667, t = 1.$

Family 4: When $\mu \neq 0, \lambda \neq 0,\ \lambda^2 - 4\mu = 0$, we get solution of Eq. (1),

$$u_{2,4}(x,t) = \frac{1}{6}\left(2c + \frac{\left(\frac{\lambda^2(2-\sigma)(4+\sigma)}{(2+\sigma)^2} + 4\mu\right)A_3}{B_1} - 2c_0\right). \tag{23}$$

Where, $\sigma = (EE + \ \xi)\lambda$.

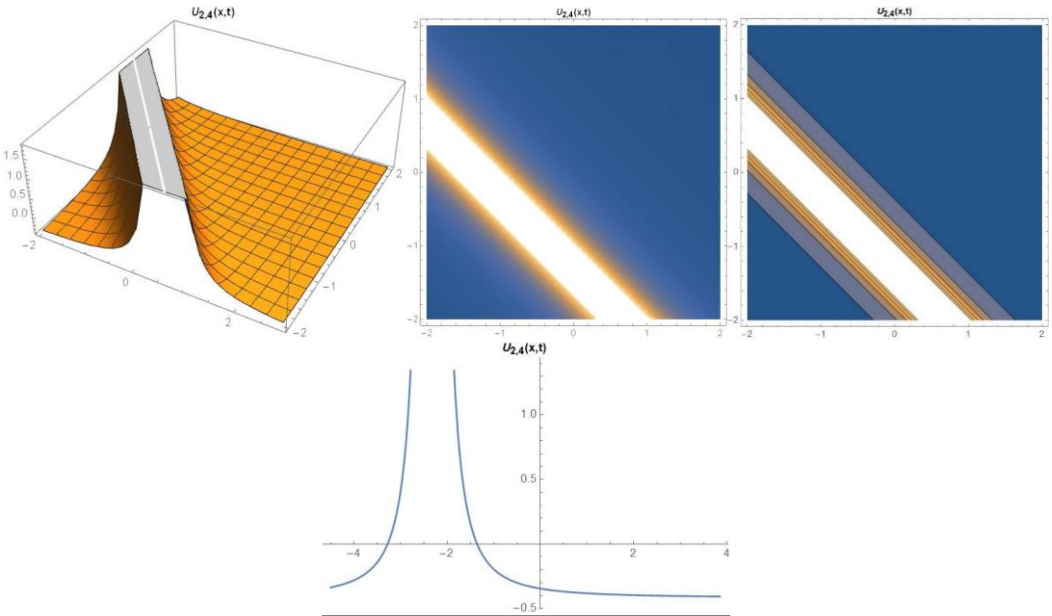

Figure 4: The 3D, density, contour graphics and 2D surface of Eq. (15) for $\lambda = 2, \mu = 1, c_0 = 0.25, \gamma = -0.096, \mathrm{k} = 1.25, A_3 = 1.5, \alpha = 0, B_0 = 0.2, A_0 = 0.0366667, \mathrm{c} = 2.20333, A_1 = 0.698333, A_2 = 3.12, B_1 = 2.5, EE = 0.65, \mathrm{R} = 0.260417, t = 1.$

Family 5: When $\mu = 0, \lambda = 0, \lambda^2 - 4\mu = 0$, we get solution of Eq. (1),

$$u_{5,1}(x,t) = \frac{A_3}{\left(\frac{\sigma}{\lambda}\right)^2 B_1} + \frac{1}{3}(c - c_0) \tag{24}$$

Where, $\sigma = (EE + \xi)\lambda$.

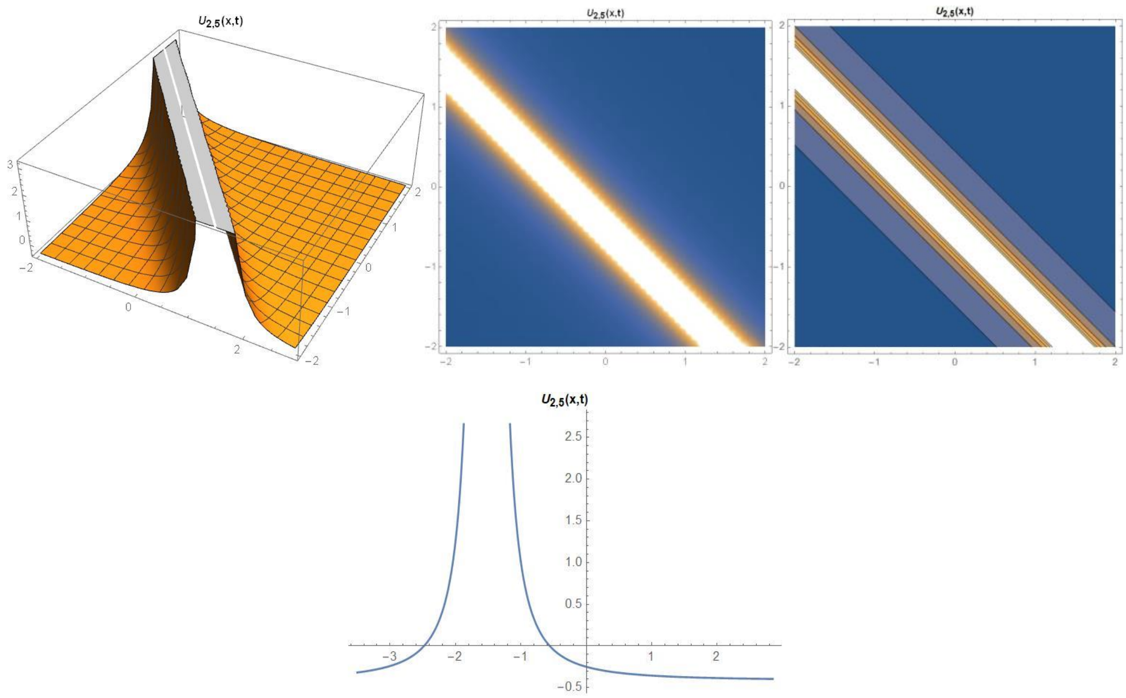

Figure 5: The 3D, density, contour graphics and 2D surface of Eq. (15) for $\lambda = 2, \mu = 1, c_0 = 0.25, \gamma = -0.096, k = 1.25, A_3 = 1.5, \alpha = 0, B_0 = 0.2, A_0 = -0.0833333, c = 2.20333, A_1 = -1.04167, A_2 = 0.12, B_1 = 2.5, EE = 0.65, R = 0.260417, t = 1$.

4. Conclusion

In this study, we have obtained traveling wave solutions of the Dullin-Gottwald-Holm equation by using the modified expansion function method. The results show that the modified expansion function method is a very effective mathematical method for solving nonlinear partial differential equations. The Mathematica program has checked the obtained solutions, and two-three-dimensional, density and contour graphs of the solutions were constructed using appropriate parameters.

References

[1] Hossain, A.K.S, Akbar, M.A., Closed form solutions of two nonlinear equation via the enhanced (G'/G) expansion method, *Cogent Mathematics and Statistics*, **4**(2017), 1355958.

[2] Akturk, T., Bulut, H., & Gurefe, Y. (2017). *An application of the new function method to the Zhiber-Shabat equation. An International Journal of Optimization and Control: Theories & Applications*, 7(3), 271-274.

[3] Baskonus, H.M., Bulut, H., New hyperbolic function solutions for some nonlinear partial differential equation arising in mathematical physics, Entropy, **17**(2015), 4255-4270.

[4] Chen, Y., & Yan, Z. (2005). New exact solutions of (2+ 1)-dimensional Gardner equation via the new sine-Gordon equation expansion method. Chaos, Solitons & Fractals, 26(2), 399-406.

[5] V. G. Dubrovsky and Y. V Lisitsyn, "The construction of exact solutions of two-dimensional integrable generalizations of Kaup–Kuperschmidt and Sawada–Kotera equations via ∂^{-}-dressing method," Phys. Lett. A, vol. 295, no. 4, pp. 198–207, 2002.

[6] Mohiud-Din, S.T., 2007. Homotopy perturbation method for solving fourth-order boundary value problems, Math. Prob. Engr., 1-15, Article ID 98602, doi:10.1155/2007/98602.

[7] Baskonus, H. M., Bulut, H., & Atangana, A. (2016). On the complex and hyperbolic structures of the longitudinal wave equation in a magneto-electro-elastic circular rod. *Smart Materials and Structures*, 25(3), 035022.

[8] Xu, F. (2008). Application of Exp-function method to symmetric regularized long wave (SRLW) equation. *Physics Letters A*, 372(3), 252-257.

[9] H. Dullin, G. Gottwald and D. Holm, An integrable shallow water equation with linear and nonlinear dispersion, Phys. Rev. Lett., 87(2001)194501-1-194501-4.

[10] Naher, H., & Abdullah, F. A. (2013). New approach of (G′/G)-expansion method and new approach of generalized (G′/G)-expansion method for nonlinear evolution equation. *American Institute of Physics Advances*, 3(3), 032116.

MATHEMATICAL MODELING FOR CYBER DEFENSE APPLICATIONS

Muharrem Tuncay GENÇOĞLU
Fırat University Technical Sciences Vocational School, Elazığ, Türkiye, mtgencoglu23@gmail.com

Abstract

With the development of technological developments in addition to internet technology, the necessity of cyber defense systems has emerged for the protection of valuable or valuable information stored in the cyber environment. It is important to understand the behavior of malicious objects with the increasing threat of cyber attacks in recent years. Mathematical modeling is required for this. In this study, a mathematical modeling process and a cyber defense system modeling principle are given. Since the attacks on the computer are completely stochastic, a Cyber Defense System Design Model based on the detection of the behavior of malicious objects with the help of the probability distribution function and differential equations has been proposed. This paper documents an epidemic model known as SIR (Susceptible – Infected – Removed units). We derive an approximated solution to the differential equations that define the SIR model. Unlike the exact SIR solution, the approximate solution is analytical and has a closed form expression. We use this approximate model as an inspiration to cyber defence. Such a model allows us to investigate the characteristics of the propagation of electronic viruses. That is, we can determine the number of susceptible units, the number of infected units and the number of removed units as a function of time. This information will eventually permit the defence to find ways to eradicate a virus attack and to show how viruses affect the defence effectiveness.

Keywords: Cyber Security, Mathematical Modelling Process, Cyber Security System Design.

1. Introduction

Advances in network technology in recent years have caused serious changes in data transfer and information exchange. Along with technological developments, internet technology has become more functional and developed. With these developments in internet technology, the necessity of cyber defense systems to protect valuable or insignificant information stored in the cyber environment has emerged seriously. To create cyber defense systems, some mathematical models have been suggested to search and figüre out diverse malicious objects and to detect and represent their behavior[1]. These models concentrate on the self-replication of some malicious objects.

2. Mathematical Modelling

Sometimes it may not be possible to implement a system in real environment due to high cost and excessive time requirement. In this case, it would be more appropriate to create a model and examine the manner of the system. Modeling is to replace and simplify a real system. If we take a look at some different models from here;

- Physical Model: Based on Mechanical, Electrical or Electric and Hydraulic systems.
- Mathematical Model: Systems body forth by mathematical equations.
- Physical Static Model: Systems whose behavior does not change over time.
- Physical Dynamic Model: Systems whose behavior changes over time.
- Mathematical Static Model: These are models that give a mathematical equation when the system is in balance.
- Mathematical Dynamic Model: Models that allow the change of system eigenvalues depending on a time function.
- Mathematical Static Numerical Model: Complex static mathematical models that can be resolved by simulation.
- Mathematical Static Analytical Model: These are small static mathematical models that can be resolved with basic mathematical methods.
- Mathematical Dynamic Analytical Model: These are minor dynamic mathematical models that can be resolved with basic mathematical methods.
- X. Mathematical Dynamic Numerical Model: Complex dynamic mathematical models that can be resolved by imitation[2]. These models are shown in fig. 1

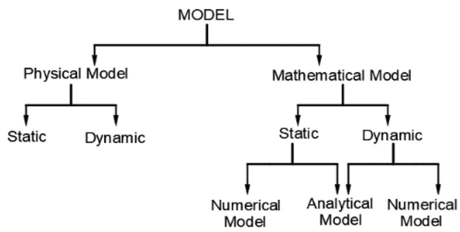

Fig. 1. Mathematical Models

3. Cyber Defense System Modelling Principle

Cyber assaults are the biggest issue in the modern world. Understanding the behavior of malicious objects is essential to overcome this problem. This is very important in mathematical modeling. Malicious objects such as Viruses, Worms, Trojans, Spam and certain technologies such as instant messaging, bots, phishing can be understood and defended against them using modeling. Situations can be determined where some necessary assumptions such as the lifetime of the data, the time of collection, the number of connections can be applied. Malicious objects; It should be estimated with the help of calculations to be made and mathematical equations representing the state of information. More exercises need to be done to make the security model adaptable[3]. Fig. 2 shows the defense system modeling process.

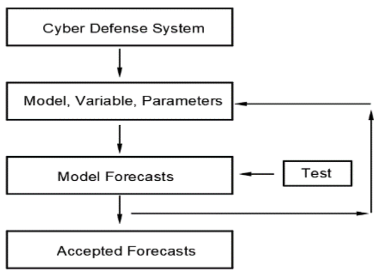

Fig. 2. Cyber Defense System Modeling Proces

4. Malware Objects and Defensive

Since the assaults on the computer are completely stochastic, we cannot know the real-time of the subsequent assault. Only through probability concepts in modeling the probability of the attack can we find it.

To express the attack time of the stochastic variable x_i $(i = 1,2,3,\ldots)$ the probability of x_i is expressed by $P(x_i)$. where n_i is the number of attacks from a certain source and N is the total number of attacks.

$$P(x_i) = \frac{n_i}{N} \tag{4.1}$$

Here, considering $P(x_i)$ as a set of numbers, $\int_R P(x_i)dx_i = 1$, that is, the area under the curve is 1. This We can express $\sum_{i=1}^{\infty} P(x_i) = 1$, which is the probability density function. There can also be a probability distribution function that gives the probability of small or equal stochastic attacks to a given value.

$$F(x_i) = \sum_{x_i \le x} P(x_i) \tag{4.2}$$

Different measurements of the probability function such as mean, mode, median, and standard deviation can be used to examine the stochastic system. Characteristic equation models can be Linear and Non-Linear. The non-linear system can be expressed by partial differential equations.

Let's assume that the malicious object has P spread feature due to diverse other factors such as A, B, C,…. In this case, it can be body forth by $P = f(A,B,C,\ldots)$. From here, taking the 1st and 2nd derivatives, respectively; velocity $\frac{\partial P}{\partial t} = \frac{\partial f(A,B,C,\ldots)}{\partial t}$, acceleration $\frac{\partial^2 P}{\partial t^2} = \frac{\partial^2 f(A,B,C,\ldots)}{\partial^2}$ is calculated.

The imitated conclusions acquired by using particular approximation techniques mentioned down can be used to complement the simulation-created data as well as verify.

4.1. Taylor Series Expansion

Any function with a derivative can be widened by the Taylor formula. In an area close , the function can be approached using the polynomial for the value of the independent variable .

$$F(x) = f(a) + f'(a)(x-a) + \frac{f''(a)}{2!}(x-a)^2 + \cdots + \frac{f^{(n)}(a)}{n!}(x-a)^n \tag{4.3}$$

4.2. Finite Difference Approach Methods

This method divides partial differential equations into small intervals. It does this in two ways;

I. Advanced Difference Approach:
Calculates the gradient of the function at diverse points with the formula

$$f^{\prime}(x_i) = \frac{(f(x_{i+1}) - f(x_i))}{\Delta x} \tag{4.4}$$

II. Backward Difference Approach:
Calculates the gradient of the function at various points with the formula

$$f^{\prime}(x_i) = \frac{(f(x_i) - f(x_{i-1}))}{\Delta x} \tag{4.5}$$

4.3. Higher-Order Derivatives
These derivatives can be used to express diverse significant points in the dispersion according to the formula below;

$$f^{(n)} = (f^{(n-1)})^{\prime}$$

Tests can be used to verify the model like polynomial regression tests. Thus, it can be determined whether the values can be placed in a polynomial. The characteristic equation is obtained, the conclusions can be verified experimental or analytical, according to existing standard math hypotheses. To validate the mathematical model, it is the first examination of dimensional homogeneity that requires each term to have the same mesh size. The second is to verify the quality and limit behavior of the models by checking. Apart from these, depending on how large the errors are, some issues such as accuracy and precision, the ability to prepare the data with mean, mode, median or standard deviation can be examined. These data are with ease comparable and can aid us to understand the attitude of malicious objects. For example, some definitions of the virus can be modeled as follows;
I. Let v be a simple virus that affects existent files and make them behave in the same way, a set of programs P, $v \in P$ and $p_i \in P$, $f(v)$, $f(p_i)$ and is the attitude of virus v and p_i , respectively;
II. Definition of the virus at a constant

$$T(v, p_i, e, t, S) = \log(\frac{f(v,e,t,S)}{f(p_i,e,t,S)} \tag{4.6}$$

Here $f(v, e, t, S)$ and $f(p_i, e, t, S)$ gives the attitude of programs v and p_i, in order of, at time t in S the system where e the event occurs.
Now if $T(v, p_i, e, t, S) = 0$ then the program v is a virus otherwise it is not.
III. Definition of the virus based on a continuous-time interval Δt

$$T(v, p_i, e, t, S) = \log(\frac{\int_{\tau_0}^{\tau_1} f(v,e,t,S)dt}{\int_{\tau_0}^{\tau_1} f(p_i,e,t,S)dt} \tag{4.7}$$

Here, the functions $\int_{\tau_0}^{\tau_1} f(v, e, t, S)dt$ and $\int_{\tau_0}^{\tau_1} f(p_i, e, t, S)dt$ respectively It gives the attitude of programs and in the time range $\Delta t = \tau_1 - \tau_0$ in S the system at the occurrence of e event. If $T(v, p\_i, e, t, S) = 0$ then program v is a virus otherwise it is not.
Now, to model a cyber defensive system, it is necessary to combine different components such as sensors and abuse, situational awareness, defense contraption, command and control, strategies and tactics, and science and engineering.
A cyber defense system design model using these components is given in fig. 3[4,5].

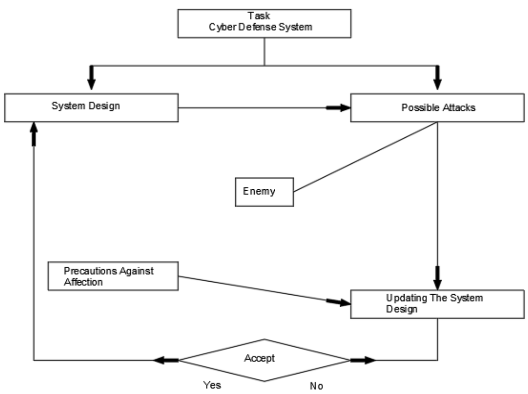

Fig. 3. Cyber Defensive System Design Model

5. Game Theory and Cyber Security[10]

Two broad categories of application of game theory in cyber security are:
1. The Cyber-Attack-Defense Analysis
2. The Cyber Security Assessment

By modeling the defense behaviors as games the actions of cyber attacker can be predicted in Cyber-Attack-Defense analysis. It also analyses the possible states of attack-defense equilibrium. The counter defense strategies can be determined ideally based on the state of equilibrium.

The equilibrium state of cyber-attack-defense can be scrutinized and the prognosis of the attack and defense strategies can be used as the rationalization of cyber security and assessment. Owing to the quantitative facets of game analysis security and reliability is viewed as a quantitative assessment which gives a computation of cyber security and reliability.

The classification of game theory methods in the field of cyber security has been classified as shown in the table [Table 1]. Cyber security adopts non cooperative dynamic game model. But in all the earlier researches all the non-cooperative models were classified under static models. But the attacker strategies in Cyber-attacks are not static and to achieve ideal effect analysis of dynamic model is very crucial because dynamic models are very much closer to real to time cyber security issues. And for Cyber-defense analysis purpose incomplete information game model is used [8].

Table 1. Game Theoretic Methods for Cyber Security[10]

Game Models			Application and Security Issues
Cooperative game models	Static game models		mobile ad hoc networks security
Non cooperative game models	Static game models		intrusion detection
			security investment optimization
	Dynamic game models	Complete information game models	security investment optimization
			security incentive mechanism
		Incomplete information game models	cyber attack-defence analysis

5.1. Game Theory Methods for Cyber Security Applications

Game Theory for cyber security applications can be divided into six categories:

1. Physical Layer Security.
2. Self-Organised Network Security.
3. Intrusion Detection and Prevention.
4. Privacy preservation and Anonymity.
5. Economics of Cyber Security
6. Cloud Computing Security.

For our discussion purpose we shall consider Self-Organized Network Security and Cloud computing Security.

Self-Organised Network Security (SON): Game theoretic approaches that are used for designing security protocols for SONs are Vehicular Networks (VANETs), Wireless Sensor Networks and Mobile Ad Hoc Networks (MANETs). Most of the game theoretic approaches consider that only two players will be there in the game.

Attacker: The attacker is an opponent who makes malicious entry into the system with the intendment of threatening its security. The strategies of the attacker can vary from a single action to a sequence of differed counter activities. In this study, we limit our interests to such attacks that consist of a series of activities that directs towards an ultimate goal.

Defender: The defender on the other side is responsible for applying proper defense techniques to secure the system from various malicious attacks from attacker. The defender has a set of counter strategies to monitor and protect the system. The main aim of this player is to make pre-emptive responses in a manner where he has limited knowledge of the system status, purely relying on the counter strategies. These assumptions on players are not practical in MANETs. The strategic decisions of each node in MANETs can be computed in a fully distributed approach, where the decision can be made without centralized administration and each node only needs to know the information of its own state and thereby aggregate effect of the other node in the MANET[5]. In few networks Digital signature is widely used, it may provide security but it introduces delay due to signature verification which in turn reduces Quality of Service QoS.

Cloud Computing Security: Traditional security is not suitable for Cloud computing concepts such as multi-tenancy, resource sharing and resource outsourcing. These are the new challenges for security researches. Security-aware virtual machines (VM) have been proposed by researchers with the combination of game theory in public cloud, where multiple Nash Equlibria has been included for security game in public cloud i.e., defender has counter actions for each one of the attackers strategies. Nash Equilibrium is a combination of Set of strategies and payoffs which results in stable state where no player has benefit when there is change in strategies on any player in the game. Scalable security risk assessment model using game theory has also been proposed for cloud computing in order to evaluate the risk. Main aim of this risk assessment is to decide who should fix the risk in the system i.e. by the cloud provider or tenant of the system [9].

6. Approximated Differential Equations to The Sır Epidemic Model[11]

We note that from Equations (6.11), R is uniquely determined by I . So we focus on S and I because once we solve for S and I , we can readily solve for R . The first two equations of Equation (6.1) can be combined to give:

$$S' = -\,aSI$$

$$I' = aSI - bI \tag{6.1}$$

$$R' = bI$$

$$I' = -S' - bI \tag{6.2}$$

We define

$$f(\,t) = \int_0^1 I\; t\; dt \;\geq\; 0 \tag{6.3}$$

Integrating Equation (6.2), we get:

$$S = -I - \; b.f + C \tag{6.4}$$

If we assume that there is 0 I infection at time zero and there are no removed units then these are the boundary conditions:

$$f(\,0) = \int_0^0 I\; t\; dt \;=\; 0$$

$$f' = I(0) = I_0$$

$$S(0) = S_0 \tag{6.5}$$

$$S_0 + I_0 = 1$$

$$R_0 = 0$$

This means that

$$A = S_0$$

$C = 1$ (6.6)

Hence,

$f' = 1 - bf - S_0\, e^{-af}$ (6.7)

We plot the exact df dt / in Equation (6.7) and the quadratic function in Equation (6.7) that approximates df dt / in fig. 4.

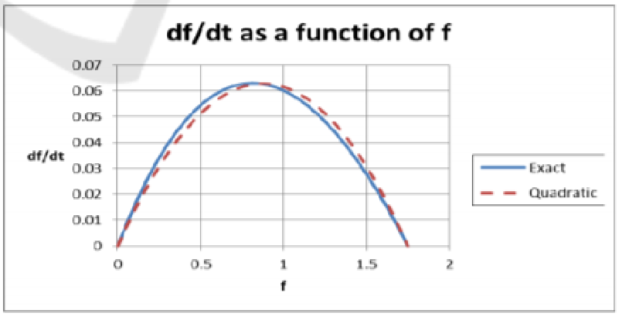

Fig. 4. Derivative of f .

For illustration, we assume the following values in fig. 3:

$$a = \frac{1}{2}, b = \frac{1}{3}$$

$S_0 = 0.99999$ (6.8)

$$f_1 = -5.99991.10^{-5}, f_2 = 1.74847$$

7. Conclusion

Although various models and solutions are presented, some problems still await solutions. These problems are mainly:
All properties of malicious objects must be body forth in the shape of mathematical equations to predict their future behavior. Also, a realistic model should be created to apply these characteristic equations in the current environment.
The accuracy of a model can be ensured after it has been analyzed and developed based on imitated conclusions. This verification assists to preserve the system against assault by malignant objects. Worms similar code red are modeled with high correctness and are now easily controllable. Although most models have certain verification limits, it is still possible for them to be developed[6].
Most malicious objects have an increase in their behavioral complexity, with a lot of features to be identified. Therefore, each feature should be generalized and the feature area should be narrowed[7].
Most cyber defense systems incur fixed expenses, such as packet length, increasing data length, or more expensive for comparison, which slows down the current system when implemented. For this reason, it is necessary to provide such a cyber defense system that does not create any more fixed costs. Defense systems that provide recovery for both pre-attack and post-attack must be highly verified and sufficiently predictable based on mathematical modeling.
It is hard to track down the attacker because of low cognizance in cyber defense. Therefore, we need to develop an appropriate policy and awareness to limit such malicious activity.
Game theory in literature has proven results for its capability in solving problems of applications like e-Commerce. With this background, the paper attempts to unfold the security issues, challenges and the research which are ongoing in the field of game theory to researchers.
The input parameters are shown in Equation (6.8). Note that we did not give a unit for the time as we do not know the coupling parameters a and b . Once we obtain the values for the coupling parameters, we will be able to extract the unit of time[11].

REFERENCES

[1] Saini, D. K. (2011). A Mathematical Model for the Effect of Malicious Object on Computer Network Immune System, Applied Mathematical Modeling, 35, ss. 3777-3787. DOI:10.1016/.2011.02.025

[2] Saini, D.K. (2012). Cyber Defense: Mathematical Modelling and Simulation, International Journal of Applied Physics and Mathematics, 2(5), ss. 312-315.

[3] Saini, D. K., Gupta, N. (2007). Fault Detection Effectiveness in GUI Components of Java Environment through Smoke Test, Journal of Information Technology, ISSN 0973-2896, 3(3), ss. 7-17.

[4] Saini, D. K., Saini, H. (2008). VAIN: A Stochastic Model for Dynamics of Malicious Objects, Journal of Systems Management, 6(1), ss. 14- 28.

[5] Saini, D. K., Mishra, B. K. (2007). Design Patterns and their effect on Software Quality, ACCST Research Journal, 5(1), ss. 356-365.

[6] Kalashinkov, A. O. (2014). Example of using game-theoretic approach in problems, Cybersecurity Issues, 1(2), ss. 49-54.

[7] Stasuk, O.I., Goncharova, L.L, (2017). Differential mathematical models to investigate the computer network architecture of an all-mode Systems of control over a distance of railways, Cybernetics and Systems Analysis, 53(1), ss. 157-164.

[8] Owen, G. (2001). Game Theory, New York: Academic Press, 3rd ed.

[9] Kwiat, L. et al., (2015). Security-aware virtual machine allocation in the cloud: a game theoretic approach. Proc. IEEE 8th Int'l Conf. on Cloud Computing.

[10] Patil, A. et al., (2018). Applications of Game Theory for Cyber Security System: A Survey. International Journal of Applied Engineering Research 13(17), 12987-12990.

[11] Nguyen, B. (2017). Modelling Cyber Vulnerability using Epidemic Models. In Proceedings of the 7th International Conference on Simulation and Modeling Methodologies, Technologies and Applications (SIMULTECH 2017), 232-239.

Analysis of the Solution of Shallow Water Model

Tolga AKTÜRK[1], Mahşure Kübranur DİKİCİ[2]

[1]Department of Mathematics and Science Education, Faculty of Education, Ordu University, Turkey

[2]Department of Mathematics, Faculty of Science, Ordu University, Turkey

[1]tolgaakturkk@gmail.com, [2]kubradikici.55@hotmail.com;

Abstract

In this article, the traveling wave solutions of the shallow water like equation are obtained by using modified exponential function method. The resulting solution functions include hyperbolic and trigonometric functions. Two and three dimensional graphs were plot by determining the appropriate parameters for the solution functions.

Keywords: The nonlinear shallow water like equation; the modified exponential function method; traveling wave solutions.

1.Introduction

The physical phenomena of wave equations can be better understood with different methods. Mathematical models represent such as mathematical physics, geophysics, engineering. This is very important to resolve nonlinear differential equations representing these models. Because they model the rise, propagation, and scattered of nonlinear waves. Studies on wave solutions of partial differential equations increased in the 1900s. The generalized tanh method is proposed, aiming at the soliton-like solutions [1-3], G′/G-expansion method for nonlinear evolution equation [4-5], Bernoulli sub-equation function method [6-7], The first integral method [8-9], Modified exponential function method (MEFM) [10-13]. Thus, the physical phenomena of wave equations can be better understood with different methods.

$$u_{xxxy}+3u_{xx}u_{y}+3u_{x}u_{xy}-u_{yt}-u_{xz}=0. \tag{1}$$

The exponential function method (MEFM) was used to interpret the traveling wave equation better. In the second part, MEFM method was mentioned. In the third chapter, the shallow water-like equation was solved with the help of a mathematical package program. The solution functions were obtained with appropriate parameter values. Two-three dimensional and contour graphics were drawn with the help of the program. In the fourth chapter, the compatibility of the solutions found with wave equations was evaluated.

METHOD

2. Modified Exponential Function Method

The nonlinear partial Shallow Water-Like (SWL) differential equation based on $u(x,y,z,t)$ solution function its general shape is as follows:

$$P\left(u,u_{x},u_{y},u_{t},u_{xx},u_{xy},u_{yt},u_{xz},u_{xxxy}\right)=0. \tag{2}$$

Step 1: If wave transformation (3) is applied to the function u like $\xi\neq 0$ to obtain a traveling wave solution in equation (2);

$$u(x,y,t)=u(\xi),\quad \xi=k\left(x+ay+bz-ct\right). \tag{3}$$

By applying wave transformation to derivative terms in equation (1), the equation is obtained nonlinear ordinary differential equation:

$$N\left(u,u',(u')^2u'',u''',\ldots\right)=0. \tag{4}$$

Step 2: The solution functions are as follows;

$$u(\xi)=\frac{\sum_{i=0}^{n} A_i[e^{-\vartheta(\xi)}]^i}{\sum_{j=0}^{m} B_j[e^{-\vartheta(\xi)}]^j}=\frac{A_0+A_1e^{-\vartheta}+\ldots+A_ne^{-n\vartheta}}{B_0+B_1e^{-\vartheta}+\ldots+B_me^{-m\vartheta}}, \tag{5}$$

where $A_n\neq 0, B_m\neq 0$ are coefficients with $A_i, B_j, (0\le i\le n,\ 0\le j\le m)$. m, n using the balancing principle, positive integers are obtained. The solution functions of (5) equations are found by using the following solution families in accordance with the balancing principle (Naher, H.& Abdullah, F. A.[14]).

Family 1: When, $\mu\neq 0, \lambda^2-4\mu>0$,

$$\vartheta(\xi)=ln\left(\frac{-\sqrt{\lambda^2-4\mu}}{2\mu}tanh\left(\frac{\sqrt{\lambda^2-4\mu}}{2}(EE+\xi)\right)-\frac{\lambda}{2\mu}\right). \tag{6}$$

Family 2: When, $\mu\neq 0,\ \lambda^2-4\mu<0$,

$$\vartheta(\xi)=ln\left(\frac{\sqrt{-\lambda^2+4\mu}}{2\mu}tan\left(\frac{\sqrt{-\lambda^2+4\mu}}{2}(EE+\xi)\right)-\frac{\lambda}{2\mu}\right). \tag{7}$$

Family 3: When, $\mu=0,\ \lambda\neq 0,\ \lambda^2-4\mu>0$,

$$\vartheta(\xi)=-ln\left(\frac{\lambda}{e^{\lambda(EE+\xi)}-1}\right). \tag{8}$$

Family 4: When, $\mu\neq 0,\ \lambda\neq 0,\ \lambda^2-4\mu=0$,

$$\vartheta(\xi)=ln\left(-\frac{2\lambda(EE+\xi)+4}{\lambda^2(EE+\xi)}\right). \tag{9}$$

Family 5: When, $\mu=0,\ \lambda=0,\ \lambda^2-4\mu=0$,

$$\vartheta(\xi)=ln(EE+\xi), \tag{10}$$

where, EE is a integral constant.

Step 3: When the derivative concepts required in equation (4) are replaced in equation (1), an algebraic system of equations is obtained. This system is solved with the help of mathematica software program, and wave solutions of the nonlinear Shallow Water Like (SWL) equation are found.

3. Application

In this section, the modified exponential function method (MEFM) developed to find the traveling wave solutions of the nonlinear Shallow Water Like (SWL) equation is used. The Shallow Water Like (SWL) equation is as follows:

$$u_{xxxy}+3u_{xx}u_y+3u_xu_{xy}-u_{yt}-u_{xz}=0. \tag{11}$$

When we apply the travelling wave transformation as $u(x,y,t)=u(\xi),\quad \xi=k\left(x+ay+bz-ct\right)$. When the derivatives found with the help of the wave transformation if written instead in the equation (11):

$$ak^4u^4+6ak^3u''u'+cak^2u''-bk^2u''=0. \tag{12}$$

The integral should be taken in equation (12):

$$ak^3u'''+3ak\left(u'\right)^2+\left(ca-b\right)u'=0. \tag{13}$$

Applying the transformation $u'=v$ in equation (13);

$$ak^2v''+3akv^2+\left(ca-b\right)v=0. \tag{14}$$

It becomes a nonlinear ordinary differential equation. If the balancing procedure is applied to equation (14), if $m=1$ is selected, $n=3$ is obtained,

$$\text{u}(\xi)=\frac{A_0+A_1e^{-\theta}+A_2e^{-2\theta}+A_3e^{-3\theta}}{B_0+B_1e^{-\theta}}. \tag{15}$$

Case 1:

$A_0=-\frac{1}{3}B_0k\left(\lambda^2+2\mu\right);$

$A_1=-\frac{1}{3}k\left(B_1\left(\lambda^2+2\mu\right)+6B_0\lambda\right);$

$A_2=-2k\left(B_1\lambda+B_0\right);$

$\text{A}_3=-2k\text{B}_1;$

$b=a\left(c-k^2\left(\lambda^2-4\mu\right)\right);$

These coefficients are obtained from equation (15) with the following conditions.

Family 1: When, $\mu\neq 0,\ \lambda^2-4\mu>0$,

$$v_{1,1}=\left(-\frac{k\left(\lambda^2-4\mu\right)Sech^2\left(\frac{\vartheta}{2}\right)\left(\lambda\sqrt{\lambda^2-4\mu}Sinh\vartheta+\left(\lambda^2-2\mu\right)Cosh\vartheta-4\mu\right)}{3\left(\lambda+\sqrt{\lambda^2-4\mu}Tanh\left(\frac{\vartheta}{2}\right)+\lambda\right)^2}\right). \tag{16}$$

If $u'=v$ transform used in equation (15) is integrated with respect to v;

$$u_{1,1}=\left(\frac{1}{3}k(\lambda^2-4\mu)(-EE-\xi+\frac{3\lambda}{\lambda^2-2\mu+2\mu Cosh[\vartheta]})+\frac{2k\sqrt{\lambda^2-4\mu}\mu Sinh[\vartheta]}{\lambda^2-2\mu+2\mu Cosh[\vartheta]}\right). \tag{17}$$

$$\left(\vartheta=(\mathrm{EE}+\xi)\sqrt{\lambda^2-4\mu},\upsilon=(\mathrm{EE}+\xi)\sqrt{-\lambda^2+4\mu}\right).$$

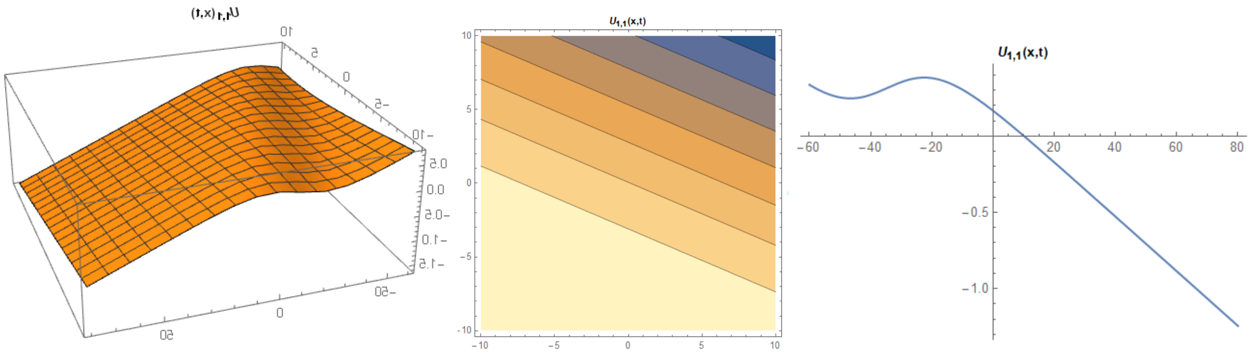

Figure-1: The 3D and 2D surfaces of Eq. (17) in $a=0.222, b=-0.169164, c=-0.52, \mathrm{EE}=0.75,$ $k=0.22, \lambda=3, \mu=1, y=1$ and $t=1$.

Family 2: When, $\mu\neq 0,\ \lambda^2-4\mu<0$,

$$v_{1,2}=\left(\frac{k\left(\lambda^2-4\mu\right)Sec^2\left(\frac{\upsilon}{2}\right)\left(\lambda\sqrt{4\mu-\lambda^2}Sin\upsilon-\left(\lambda^2-2\mu\right)Cos\upsilon+4\mu\right)}{3\left(\lambda-\sqrt{4\mu-\lambda^2}Tan\left(\frac{\upsilon}{2}\right)\right)^2}\right). \tag{18}$$

If $u'=v$ transform used in equation (15) is integrated with respect to v;

$$u_{1,2}=\left(\frac{1}{3}k\left(\lambda^2-4\mu\right)\left(\frac{3\lambda}{2\mu Cos\upsilon+\lambda^2-2\mu}-\mathrm{EE}-\xi\right)-\frac{2k\mu\sqrt{4\mu-\lambda^2}Sin\upsilon}{2\mu Cos\upsilon+\lambda^2-2\mu}\right). \tag{19}$$

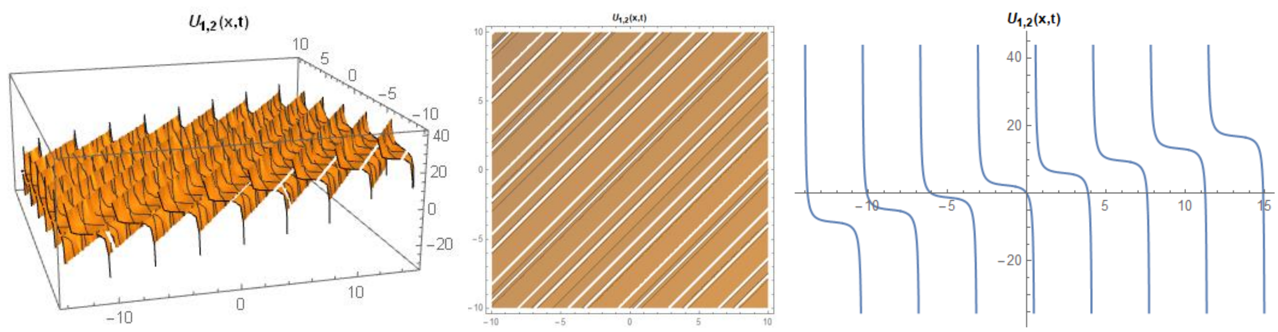

Figure-2: The 3D and 2D surfaces of Eq. (19) in $a=1, b=4, c=1, \mathrm{EE}=0.75, k=1, \lambda=1,\ \mu=1, y=1$ and $t=1$.

Family 3: When, $\mu=0, \lambda\neq 0,\ \lambda-4\mu>0$,

$$v_{1,3}=\left(-\frac{1}{6}k\left(3\lambda^2Csch^2\phi+2\lambda^2+4\mu\right)\right). \tag{20}$$

$$\left(\phi=\frac{1}{2}\lambda(\mathrm{EE}+\xi)\right).$$

If $u' = v$ transform used in equation (15) is integrated with respect to v;

$$u_{1,3}=\left(k\lambda Coth\phi-\frac{1}{3}k\xi\left(\lambda^2+2\mu\right)\right). \tag{21}$$

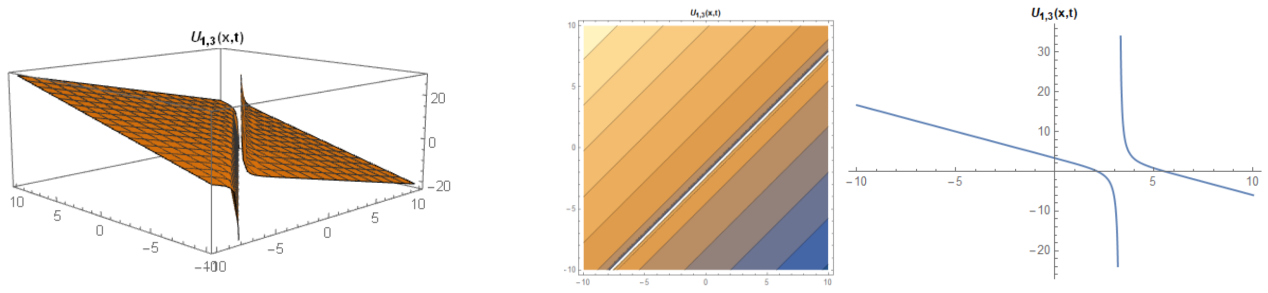

Figure-3: The 3D and 2D surfaces of Eq. (21) in $a=1, b=-3, c=1, \mathrm{EE}=0.75, k=1, \lambda=2, \mu=0, y=1$ and $t=1$.

Family 4: When $\lambda \neq 0$, $\mu \neq 0, \lambda^2-4\mu=0$,

$$v_{1,4}=\left(\frac{1}{6}k\left(\lambda^2\left(1-\frac{12}{(\lambda(\mathrm{EE}+\xi)+2)^2}\right)-4\mu\right)\right). \tag{22}$$

If $u' = v$ transform used in equation (15) is integrated with respect to v, we get,

$$u_{1,4}=\left(\frac{1}{6}k\left(\lambda(\lambda(\mathrm{EE}+\xi)+2)+\frac{12\lambda}{\lambda(\mathrm{EE}+\xi)+2}-4\mu\xi\right)\right). \tag{23}$$

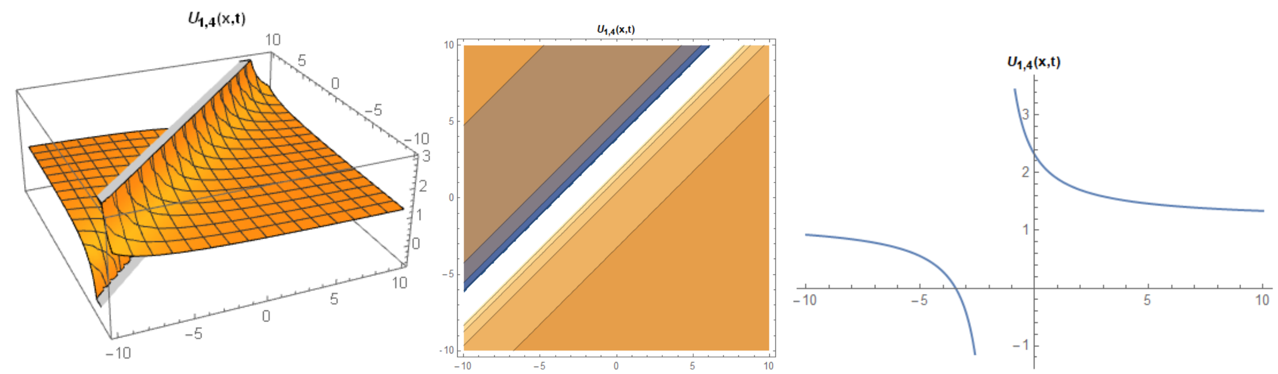

Figure-4: The 3D and 2D surfaces of Eq. (23) in $a=1, b=1, c=1, \mathrm{EE}=0.75, k=1, \lambda=2, \mu=1, y=1$ and $t=1$.

Family 5: When $\lambda=0, \mu=0, \lambda^2-4\mu=0$,

$$v_{1,5}=\left(-\frac{k\left((\mathrm{EE}+\xi)\left(\left(\lambda^2+2\mu\right)(\mathrm{EE}+\xi)+6\lambda\right)+6\right)}{3(\mathrm{EE}+\xi)^2}\right). \tag{24}$$

If $u' = v$ transform used in equation (15) is integrated with respect to v;

$$u_{1,5} = \left(-\frac{1}{3} k \left((\mathrm{EE}+\xi)\left(\lambda^2+2\mu\right) + 6\lambda \log(\mathrm{EE}+\xi) - \frac{6}{\mathrm{EE}+\xi} \right) \right). \tag{25}$$

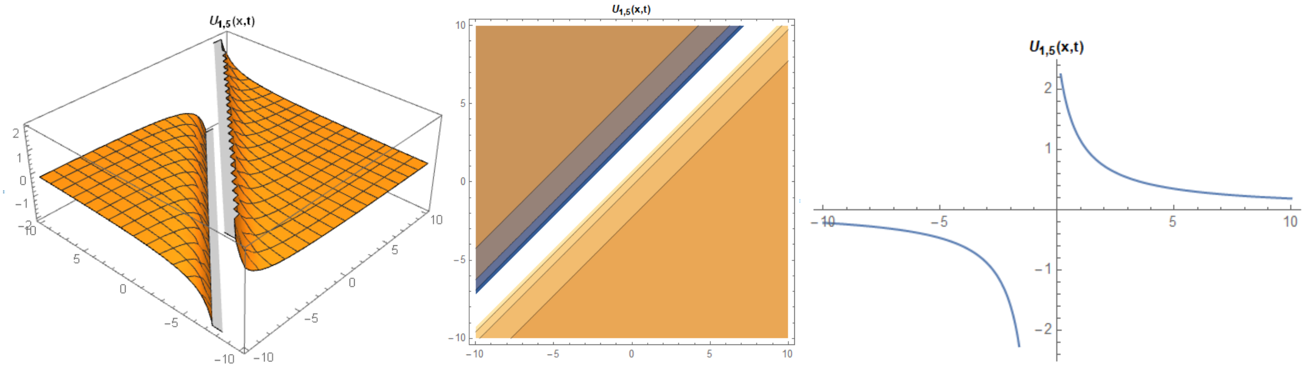

Figure-5: The 3D and 2D surfaces of Eq. (25) in $a=1, b=1, c=1, \mathrm{EE}=0.75, k=1, \lambda=0, \mu=0, y=1,$ and $t=1$.

Case 2

$$A_0 = \frac{B_0 B_1 (ac-b)}{aA_3} + \frac{A_3 B_0 \lambda^2}{4B_1};$$

$$A_1 = \frac{B_1^2 (ac-b)}{aA_3} + \frac{1}{4} A_3 \lambda \left(\frac{4B_0}{B_1} + \lambda \right);$$

$$A_2 = A_3 \left(\frac{B_0}{B_1} + \lambda \right);$$

$$k = -\frac{A_3}{2B_1};$$

$$\mu = \frac{B_1^2 (ac-b)}{aA_3^2} + \frac{\lambda^2}{4};$$

Solutions written in the equation of these coefficients (15) are obtained.

Family 1: When, $\mu \neq 0,\ \lambda^2 - 4\mu > 0$,

$$v_{2,1} = \left(\frac{Sech^2 \frac{\vartheta}{2} \left(aA_3^2 \left(\lambda^2 - 4\mu\right)\psi + 4B_1^2 (b-ac)\left(-\psi - 4\mu\right) \right)}{\left(4aA_3 B_1 \left(\sqrt{\lambda^2 - 4\mu}\, Tanh\left(\frac{\vartheta}{2}\right) + \lambda \right)^2 \right)} \right). \tag{26}$$

$\left(\psi = \lambda\sqrt{\lambda^2 - 4\mu}Sinh\vartheta + \left(\lambda^2 - 2\mu\right)Cosh\vartheta - 2\mu\right).$

If $u' = v$ transform used in equation (15) is integrated with respect to v;

$$u_{2,1} = \left(\frac{\dfrac{aA_3^2\sqrt{\lambda^2-4\mu}\left(\gamma\sqrt{\lambda^2-4\mu} - 4\mu Sinh\vartheta + 2\mu\vartheta Cosh\vartheta\right)}{\sigma} - 4B_1^2(\mathrm{EE}+\xi)(b-ac)}{4aA_3B_1}\right). \tag{27}$$

$\left(\gamma = (\lambda^2 - 2\mu)(\mathrm{EE}+\xi) - 2\lambda, \sigma = 2\mu Cosh\vartheta + \lambda^2 - 2\mu\right).$

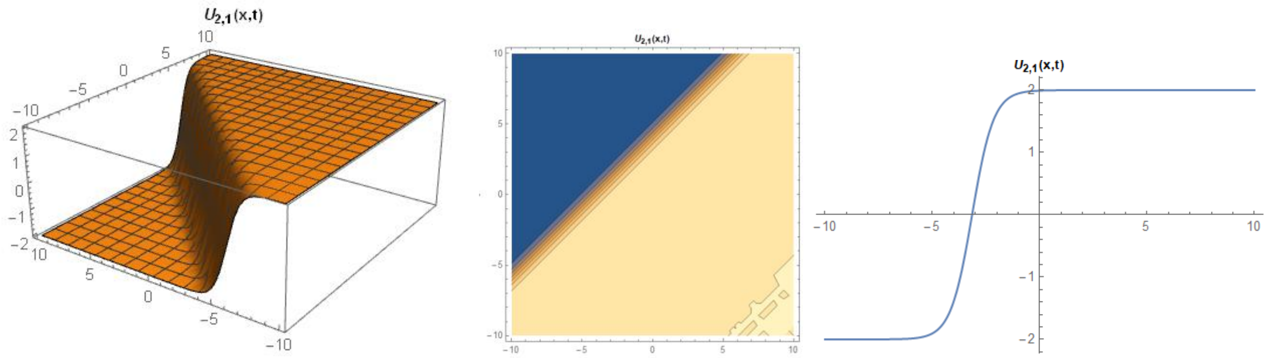

Figure-1: The 3D and 2D surfaces of Eq. (27) in $a=1, A_3=3, b=5, B_1=1, \gamma=1, c=1, \mathrm{EE}=0.75,$ $k=-1.5, \lambda=4, \mu=\dfrac{32}{9}, y=1$ and $t=1$.

Family 2: When, $\mu \neq 0,\ \lambda^2 - 4\mu < 0$,

$$v_{2,2} = \left(\frac{Sec^2\dfrac{\upsilon}{2}\left(aA_3^2\left(\lambda^2-4\mu\right)\left(-\varphi-2\mu\right) + 4B_1^2(b-ac)\left(\varphi-2\mu\right)\right)}{\left(4aA_3B_1\left(\lambda - \sqrt{4\mu-\lambda^2}Tan\dfrac{\upsilon}{2}\right)^2\right)}\right). \tag{28}$$

$\left(\varphi = \lambda\sqrt{4\mu-\lambda^2}Sin\upsilon - \left(\lambda^2-2\mu\right)Cos\upsilon\right).$

If $u' = v$ transform used in equation (15) is integrated with respect to v;

$$u_{2,2} = \left(\frac{B_1(\mathrm{EE}+\xi)(ac-b)}{aA_3} + \frac{A_3\left(\left(\lambda^2-4\mu\right)\left(\gamma + \ell(\mathrm{EE}+\xi)\right) + 4\mu\sqrt{4\mu-\lambda^2}Sin\upsilon\right)}{4B_1\left(\ell + \lambda^2 - 2\mu\right)}\right). \tag{29}$$

$\left(\ell = 2\mu Cos\upsilon\right).$

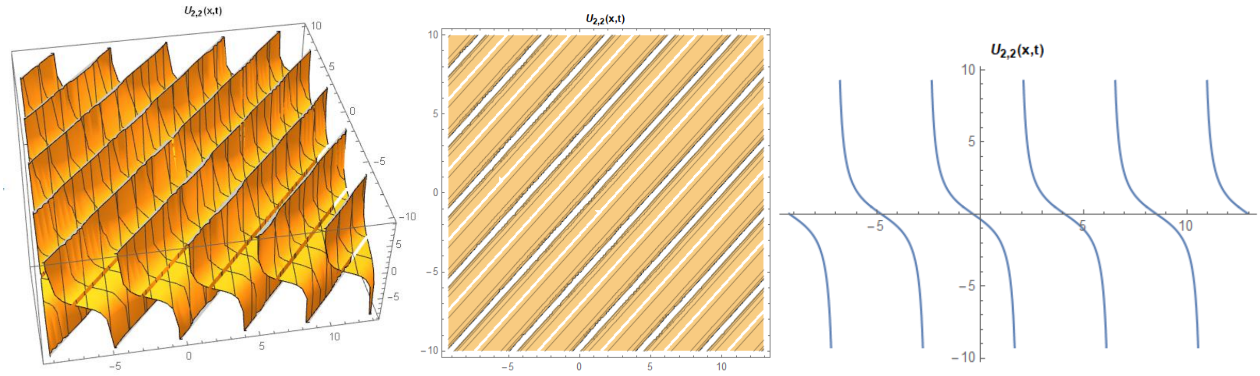

Figure-2: The 3D and 2D surfaces of Eq. (29) in $a=1, A_3=2, b=-1, B_1=1, \gamma=1, c=1, \mathrm{EE}=0.75,$ $k=-1, \lambda=1, \mu=\dfrac{3}{4}, y=1$ and $t=1$.

Family 3: When, $\mu=0, \lambda\neq 0,\ \lambda-4\mu>0,$

$$v_{2,3}=\left(\frac{B_1(ac-b)}{aA_3}+\frac{A_3\lambda^2 Coth^2\phi}{4B_1}\right). \tag{30}$$

If $u'=v$ transform used in equation (15)is integrated with respect to v;

$$u_{2,3}=\left(\frac{B_1\xi(ac-b)}{aA_3}+\frac{A_3\lambda\left(Tanh^{-1}\left(Tanh\phi\right)-Coth\phi\right)}{2B_1}\right). \tag{31}$$

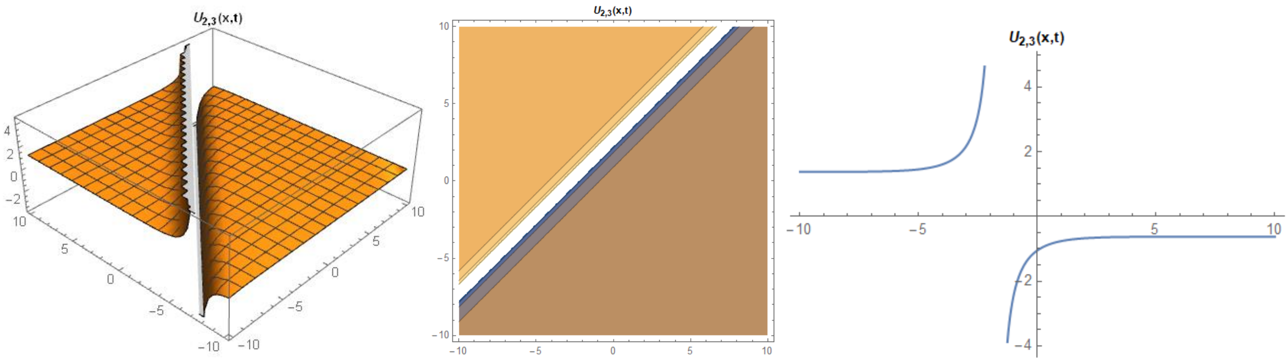

Figure-3: The 3D and 2D surfaces of Eq. (31) in $a=1, A_3=2, b=2, B_1=1, \gamma=1, c=1, \mathrm{EE}=0.75,$ $k=1, \lambda=1, \mu=0, y=1$ and $t=1$.

Family 4: When, $\lambda\neq 0,\ \mu\neq 0, \lambda^2-4\mu=0,$

$$v_{2,4}=\left(\frac{B_1(ac-b)}{aA_3}+\frac{A_3\lambda^2}{B_1(\lambda(\mathrm{EE}+\xi)+2)^2}\right). \tag{32}$$

If $u'=v$ transform used in equation (15) is integrated with respect to v;

$$u_{2,4}=\left(\frac{B_1\xi(ac-b)}{aA_3}-\frac{A_3\lambda}{B_1(\lambda(\mathrm{EE}+\xi)+2)}\right). \tag{33}$$

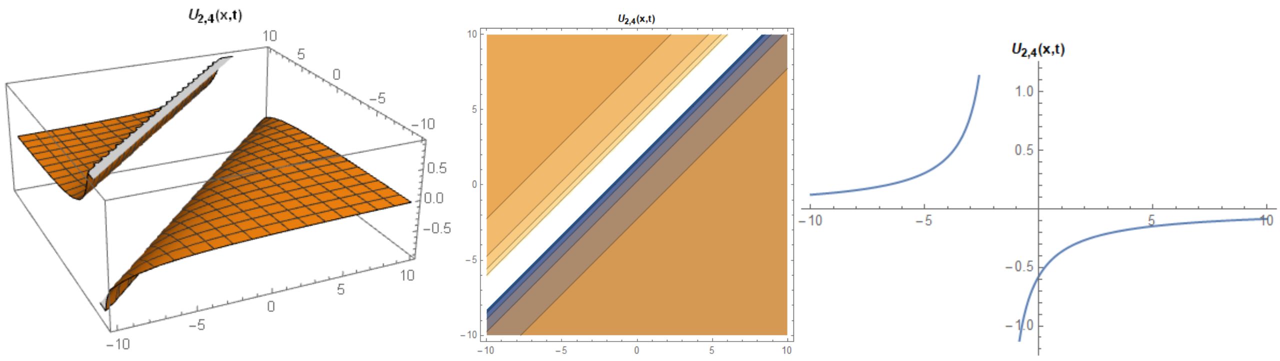

Figure-4: The 3D and 2D surfaces of Eq. (33) in $a=1, A_3=1, b=1, B_1=1, \gamma=1, c=1, \mathrm{EE}=0.75,$ $k=1, \lambda=2, \mu=1, y=1$ and $t=1$.

Family 5: When, $\lambda=0, \mu=0, \lambda^2-4\mu=0$,

$$v_{2,5}=\left(\frac{B_1(ac-b)}{aA_3}+\frac{A_3(\lambda(\mathrm{EE}+\xi)+2)^2}{4B_1(\mathrm{EE}+\xi)^2}\right). \tag{34}$$

If $u'=v$ transform used in equation (15) is integrated with respect to v;

$$u_{2,5}=\left(\frac{B_1\xi(ac-b)}{aA_3}+\frac{A_3\lambda^2(\mathrm{EE}+\xi)}{4B_1}+\frac{A_3\lambda\log(\mathrm{EE}+\xi)}{B_1}-\frac{A_3}{B_1(\mathrm{EE}+\xi)}\right). \tag{35}$$

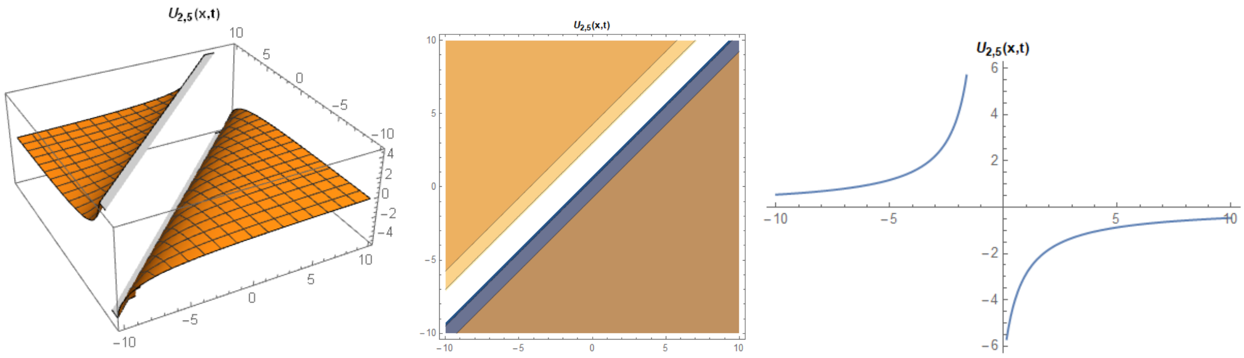

Figure-5: The 3D and 2D surfaces of Eq. (35) in $a=1, A_3=5, b=1, B_1=1, \gamma=1, c=1, \mathrm{EE}=0.75,$ $k=1, \lambda=0, \mu=0, y=1$ and $t=1$.

4.Conclusions

In this study, traveling wave solutions are obtained by applying the modified exponential function method to the Shallow Water Like (SWL) equation. These solutions show that they are well suited for wave solutions of the partial differential equation. The resulting solution functions include hyperbolic and trigonometric functions. Calculations were made with the help of the Mathematica package program. Two-three dimensional and contour graphics of the solutions found were drawn with the help of the program.

5.References

1. Mustafa Mizrak, Hiperbolik tanjant yönteminin klasik Boussinesq sistemine uygulanması, Dicle Üniversitesi Ziya Gökalp Eğitim Fakültesi Dergisi, Vol:10,159-171, 2008.
2. Bo Tian, Yi-Tian Gao, On the generalized tanh method for the (2+ 1)-dimensional breaking soliton equation, Modern Physics Letters A, Vol:10, No:38, 2937-2941, 1995.
3. Bo Tian, Yi-Tian Gao, Beyond travelling waves, a new algorithm for solving nonlinear evolution equations, Computer Physics Communications, Vol:95, No:2-3, 139-142, 1996.
4. Marwan Alquan, Aminah Qawasmeh, Soliton solutions of shallow water wave equations by means of (G/G)-expansion method, Journal of applied analysis and computation, Vol:4, No:3, 221-229, 2014.
5. Hülya Durur, Different types analytic solutions of the (1+ 1)-dimensional resonant nonlinear Schrödinger's equation using (G′/G)-expansion method, Modern Physics Letters B, Vol:34, No:03, 2050036, 2020.
6. Faruk Düşünceli, New exact solutions for generalized (3+ 1) shallow water-like (SWL) equation, Applied Mathematics and Nonlinear Sciences, Vol:4, No:2, 365-370, 2019.
7. Faruk Düşünceli, Exact Solutions for Generalized (3+ 1)-Dimensional Shallow Water-Like (SWL) Equation, Conference Proceedings of Science and Technology, Vol:2, No:1, 2019.
8. MTa Darvishi, et al.,Traveling wave solutions of a (2+ 1)-dimensional Zakharov-like equation by the first integral method and the tanh method, Optik, Vol:127, No:16, 6312-6321, 2016.
9. Weiguo Rui vd. Integral bifurcation method and its application for solving the modified equal width wave equation and its variants, Rostocker Mathematisches Kolloquium, Vol:62, 87-106, 2007.
10. Tolga Aktürk, Hasan Bulut, Gülnur Yel, An Application of the Modified Expansion Method to Nonlinear Partial Differential Equation, Turkish Journal of Mathematics and Computer Science, Vol:10, 202-206, 2018.
11. Tolga Aktürk, Yusuf Gürefe, Yusuf Pandır, An application of the new function method to the Zhiber–Shabat equation, An International Journal of Optimization and Control, Theories & Applications (IJOCTA), Vol:7, No:3, 271-274, 2017.
12. D.Kumar, M.T. Darvishi, A.K. Joardar, Modified Kudryashov method and its application to the fractional version of the variety of Boussinesq-like equations in shallow water, Optical and Quantum Electronics Vol: 50, No:3, 1-17, 2018.
13. Nikolai A. Kudryashov, Nadejda B. Loguinova, Be careful with the Exp-function method, Communications in Nonlinear Science and Numerical Simulation, Vol:14, No:5, 1881-1890, 2009.
14. Hasibun Naher, Abdullah Farah Aini, New approach of (G′/G)-expansion method and new approach of generalized (G′/G)-expansion method for nonlinear evolution equation, AIP Advances, Vol:3, No:3, 032116, 2013.
15. Emad HM Zahran, Mostafa MA Khater, Exact traveling wave solutions for the system of shallow water wave equations and modified Liouville equation using extended Jacobian elliptic function expansion method, American Journal of Computational Mathematics, Vol:4, No:05, 455, 2014.
16. Yakup Yıldırım, Emrullah Yasar, Adem Abdullahi Rashid, A multiple exp-function method for the three model equations of shallow water waves, Nonlinear Dynamics, Vol:89, No:3, 2291-2297, 2017.
17. Abdul-Majid Wazwaz, Solitary wave solutions of the generalized shallow water wave (GSWW) equation by Hirota's method, tanh–coth method and Exp-function method, Applied Mathematics and Computation, Vol: 202, No:1, 275-286, 2008.

Investigation of the Wave Solutions of the Double-Chain DNA Model by the Modified Exponential Function Method

Özlem KIRCI[1], Tolga AKTÜRK[2], Hasan BULUT[3]

[1]Department of Mathematics, Faculty of Arts and Sciences, Kırklareli University, Turkey

[2]Department of Mathematics and Science Education, Faculty of Education, Ordu University, Turkey

[3]Department of Mathematics, Faculty of Science, Fırat University, Turkey

[1]ozlem.isik@klu.edu.tr, [2]tolgaakturkk@gmail.com, [3]hbulut@firat.edu.tr,

Abstract

In this study, the wave solutions of the (2 + 1)-dimensional equation of the double-chain DNA model which is formulated mathematically as a nonlinear partial differential equation is found by using the modified exponential function method. The solution functions, obtained as a result of the all calculations, are revealed to be hyperbolic, trigonometric and rational functions. By determining the appropriate parameters for the obtained solution functions, two and three-dimensional graphs, contour graphs and density graphs are shown and these graphs represent the characteristic behavior of the solution functions.

Keywords: the (2 + 1)-dimensional equation of the double-chain DNA model; the wave solutions; the modified exponential function method.

1. Introduction

Many phenomena can be modelled by partial differential equations (PDEs) in applied sciences. Hence the solutions of these equations become important to comment the needed data or to make the solution of the problem easier. For this, various methods have been implemented such as exp-function method, modified $\exp(-\Omega(\xi))$-expansion function method, modified extended exp-function method [1-4], modified expansion method [5], $tan(F(\xi)/2)$-expansion method [6,7], (G′/G)-expansion method and generalized (G′/G)-expansion method [8], Modified simple equation method [9], the generalized Kudryashov method [10], the Hirota's bilinear transformation [11], the Backlaund transformation method [12], the homotopy perturbation method [13] and many more methods. One of the remarkable mathematical models of the nonlinear science is the dynamical DNA system. Some methods are applied to construct the wave solutions of this model such as (G′/G)-expansion method [14], Riccati parameterized factorization method [15], Riccati equation mapping method [16], Lie transformation method and singular manifold method [17], Φ^6-model expansion method [18], Conte's Painlev´e truncation expansion and the Pickering's truncation expansion [19], the generalized exponential rational function method [20], the new extended direct algebraic method and the generalized Kudryashov method [21] and so on.

In this study the (2+1)-dimensional double-chain nonlinear DNA model is considered and the modified exponential function method is applied to obtain the wave solutions of the nonlinear PDE formulating this model. The study progresses as follows. In section 2 the modified exponential-function method is given, in section 3 mathematical formulation of the double-chain DNA model is presented, in section 4 the method is applied for this model and the graphical results are shown, finally the study is ended with the conclusion in section 5.

2. The modified exp-function method

The steps of the modified exp-function method will be given for a nonlinear PDE. Let us consider the (2+1)-dimensional nonlinear partial differential equation

$$P(u,u_x,u_y,u_t,u_{xx},u_{xy},u_{yy},\ldots)=0, \tag{2.1}$$

where P is a function of $u=u(x,y,t)$ and its partial derivatives in which the highest order derivatives and nonlinear terms are involved.

Step1: Applying the wave transformation $\xi=k(x+y-ct)$ the equation (2.1) reduces to the nonlinear ordinary differential equation;

$$Q(U,U',U'',\ldots)=0, \tag{2.2}$$

where Q is a function of $U(\xi)$ and its derivatives with respect to ξ.

Step2: Suppose that the solution of (2.2) is in the form of

$$U(\xi)=\frac{\sum_{i=0}^{N}A_i\left[exp\left(-\Omega(\xi)\right)\right]^i}{\sum_{j=0}^{M}B_j\left[exp\left(-\Omega(\xi)\right)\right]^j}=\frac{A_0+A_1\left[exp\left(-\Omega(\xi)\right)\right]+\ldots+A_N\left[exp\left(-\Omega(\xi)\right)\right]^N}{B_0+B_1\left[exp\left(-\Omega(\xi)\right)\right]+\ldots+B_M\left[exp\left(-\Omega(\xi)\right)\right]^M}, \tag{2.3}$$

where A_i $(0\le i\le N)$ and B_j $(0\le j\le M)$ are constants to be determined with $A_N\neq 0$ and $B_M\neq 0$. The positive integers M and N appeared in (2.3) are specified by applying the balancing rule which is a relation between the highest order derivative and the highest nonlinear term in equation (2.2). Moreover the function $\Omega(\xi)$ satisfies the following nonlinear ordinary differential equation

$$\Omega'(\xi)=\mu exp(\Omega(\xi))+exp(-\Omega(\xi))+\lambda. \tag{2.4}$$

The solutions of (2.4) are given in [22] as in the following.

Family1: When $\mu\neq 0,\lambda^2-4\mu>0$,

$$\Omega(\xi)=ln\left(\frac{-\sqrt{\lambda^2-4\mu}}{2\mu}tanh\left(\frac{\sqrt{\lambda^2-4\mu}}{2}(\xi+E)\right)-\frac{\lambda}{2\mu}\right).$$

Family2: $\mu\neq 0,\lambda^2-4\mu<0$,

$$\Omega(\xi)=ln\left(\frac{\sqrt{-\lambda^2+4\mu}}{2\mu}tanh\left(\frac{\sqrt{-\lambda^2+4\mu}}{2}(\xi+E)\right)-\frac{\lambda}{2\mu}\right).$$

Family3: $\mu = 0, \lambda \neq 0, \lambda^2 - 4\mu > 0$,

$$\Omega(\xi) = -ln\left(\frac{\lambda}{exp(\lambda(\xi+E))-1}\right).$$

Family4: $\mu \neq 0, \lambda \neq 0, \lambda^2 - 4\mu = 0$,

$$\Omega(\xi) = ln\left(\frac{2\lambda(\xi+E)+4}{\lambda^2(\xi+E)}\right).$$

Family5: $\mu = 0, \lambda = 0, \lambda^2 - 4\mu = 0$,

$$\Omega(\xi) = ln(\xi+E),$$

where E is the integration constant.

Step3: Substituting (2.3) into the equation (2.2) results in a system of algebraic equations for powers of $e^{\Omega(\xi)}$ such that the coefficients of the exponential function have to vanish. Solving the system of equations gives the coefficients $A_0, A_1, \ldots, A_N, B_0, B_1, \ldots, B_M, \mu, \lambda$.

3. Mathematical model

The double-chain DNA model is used in [9],

$$u_{tt} - c_1^2 u_{xx} - c_1^2 u_{yy} = \lambda_1 u + \gamma_1 uv + \mu_1 u^3 + \beta_1 uv^2, \tag{3.1}$$

$$v_{tt} - c_2^2 v_{xx} - c_2^2 v_{yy} = \lambda_2 v + \gamma_2 u^2 + \mu_2 u^2 v + \beta_2 v^3 + c_0, \tag{3.2}$$

where $u(x, y, t)$ is the difference of the longitudinal displacements of the bottom and top strands and $v(x, y, t)$ is the difference of the transverse displacements of the bottom and top strands. $c_1, c_2, \lambda_1, \lambda_2, \gamma_1, \gamma_2, \mu_1, \mu_2, \beta_1, \beta_2$ and c_0 are constants and defined as;

$$c_1 = \pm\frac{\varepsilon}{\rho}, c_2 = \pm\frac{F}{\rho}, \lambda_1 = \frac{-2\mu}{\rho\sigma h}(c - I_0), \lambda_2 = \frac{-2\mu}{\rho\sigma}, \beta_1 = \beta_2 = \frac{4\mu I_0}{\rho\sigma h^3}, c_0 = \frac{\sqrt{2}\mu(h - I_0)}{\rho\sigma}, \gamma_1 = 2\gamma_2 = \frac{2\sqrt{2}\mu I_0}{\rho\sigma h^3},$$
$$\mu_1 = \mu_2 = \frac{-2\mu I_0}{\rho\sigma h^3}.$$

Here ρ is the mass density, σ is the area of the cross section, ε is the Young's modulus, F is the tension density of the strand, μ is the rigidity of elastic membrane, h is the distance between two strands, I_0 is the height of the membrane in the equilibrium position. (3.1) and (3.2) reduces to a single partial differential equation via the transformation $v = b_1 u + b_2$ and considering the constants b_2 and F to be $h/\sqrt{2}$ and ε, respectively. This single form of PDE is

$$u_{tt} - C_1^2 u_{xx} - C_1^2 u_{yy} - Au^3 + Bu^2 + Cu = 0, \tag{3.3}$$

where $A = \frac{\Omega}{h^3}(4b_1^2 - 2), B = \frac{6\sqrt{2}b_1}{h^3}\Omega, C = \frac{6\Omega}{h} - \frac{2\Omega}{I_0}, \Omega = \frac{\mu I_0}{\rho\sigma}, C_1 = C_2.$

4. Application of the method to the double-chain DNA model

As mentioned above the wave transformation $\xi = k(x+y-ct)$ is performed for the (2+1) dimensional nonlinear PDE (3.3) and as a result the nonlinear ODE

$$(k^2c^2 - 2S^2k^2)U'' - FU^3 + GU^2 + HU = 0, \tag{4.1}$$

is obtained. Indeed the coefficients in (4.1) are the same as (3.3) after the transformation, namely $S = C_1, F = A, G = B, H = C$. In (4.1) by applying the balance rule, the positive integers M and N can be determined as $M=1$, $N=2$. Hence by using this result and (2.3), the solution of (4.1) can be given as

$$U(\xi) = \frac{\sum_{i=0}^{2} A_i \left[exp\left(-\Omega(\xi)\right)\right]^i}{\sum_{j=0}^{1} B_j \left[exp\left(-\Omega(\xi)\right)\right]^j} = \frac{A_0 + A_1 exp\left(-\Omega(\xi)\right) + A_2\left[exp\left(-\Omega(\xi)\right)\right]^2}{B_0 + B_1 exp\left(-\Omega(\xi)\right)}. \tag{4.2}$$

Substituting (4.2) with the required derivatives into (4.1) and considering the solution of (2.4), a system of algebraic equations is obtained. The system is solved for $A_0, A_1, A_2, B_0, B_1, \mu, F, G, H, c, S$ with the assistance of Mathematica. The families of solutions are presented in each case. Some of the obtained cases and the corresponding solution families together with the graphics are given in the following.

<u>Case1:</u>

$$A_0 = \frac{\lambda^2 A_2}{4} + \frac{G\lambda B_1}{8F} - \frac{G\sqrt{4F^4(\lambda^2-4\mu)A_2^4B_1^2 + F^2G^2A_2^2B_1^4}}{24F^3A_2^2} + \frac{G^2B_1^3 - 3\lambda\sqrt{4F^4(\lambda^2-4\mu)A_2^4B_1^2 + F^2G^2A_2^2B_1^4}}{24F^2A_2B_1},$$

$$A_1 = \lambda A_2 + \frac{GB_1}{4F} - \frac{\sqrt{4F^4(\lambda^2-4\mu)A_2^4B_1^2 + F^2G^2A_2^2B_1^4}}{4F^2A_2B_1},$$

$$B_0 = \frac{FA_2B_1(6F\lambda A_2 - GB_1) - 3\sqrt{4F^4(\lambda^2-4\mu)A_2^4B_1^2 + F^2G^2A_2^2B_1^4}}{12F^2A_2^2},\ S = -\frac{\sqrt{-FA_2^2 + 2c^2k^2B_1^2}}{2kB_1},$$

$$H = \frac{2F^3(\lambda^2-4\mu)A_2^3 - FG^2A_2B_1^2 + G\sqrt{4F^4(\lambda^2-4\mu)A_2^4B_1^2 + F^2G^2A_2^2B_1^4}}{8F^2A_2B_1^2}.$$

For this case the solutions $U_{1,1}, U_{1,2}, U_{1,3}, U_{1,4}, U_{1,5}$ which correspond to Family-1, Family-2, Family-3, Family-4 and Family-5 respectively, are obtained as,

$$U_{1,1}=\frac{\left[\frac{\lambda^2 A_2}{4}+\frac{G\lambda B_1}{8F}-\frac{G\gamma}{24F^3A_2^2}+\frac{G^2B_1^3-3\lambda\gamma}{24F^2A_2B_1}+\frac{4\mu^2A_2}{\left(\lambda+\upsilon\right)^2}-\frac{2\mu\left(\lambda A_2+\frac{GB_1}{4F}-\frac{\gamma}{4F^2A_2B_1}\right)}{\lambda+\upsilon}\right]}{\left[\frac{FA_2B_1(6F\lambda A_2-GB_1)-3\gamma}{12F^2A_2^2}-\frac{4\mu B_1}{\lambda+\upsilon}\right]}, \tag{4.3}$$

where $\upsilon=\sqrt{\lambda^2-4\mu}tanh\left(0.5\left(E+\xi\right)\sqrt{\lambda^2-4\mu}\right)$, $\gamma=\sqrt{4F^4(\lambda^2-4\mu)A_2^4B_1^2+F^2G^2A_2^2B_1^4}$.

$$U_{1,2}=\frac{\left[\frac{\lambda^2 A_2}{4}+\frac{G\lambda B_1}{8F}-\frac{G\gamma}{24F^3A_2^2}+\frac{G^2B_1^3-3\lambda\gamma}{24F^2A_2B_1}+\frac{4\mu^2A_2}{\left(\chi\right)^2}+\frac{2\mu\left(\lambda A_2+\frac{GB_1}{4F}-\frac{\gamma}{4F^2A_2B_1}\right)}{\chi}\right]}{\left[\frac{FA_2B_1(6F\lambda A_2-GB_1)-3\gamma}{12F^2A_2^2}-\frac{2\mu B_1}{\chi}\right]}, \tag{4.4}$$

where $\chi=\lambda-\sqrt{-\lambda^2+4\mu}tanh\left(0.5\left(E+\xi\right)\sqrt{-\lambda^2+4\mu}\right)$.

$$U_{1,3}=\frac{\left[6F^3\omega^2A_2^3B_1+3F^2G\omega A_2^2B_1^2-GB_1v+FA_2\left(G^2B_1^3-3\omega v\right)\right]}{\left[2FB_1\left(FA_2B_1\left(6F\omega A_2-GB_1\right)-3v\right)\right]}, \tag{4.5}$$

where $v=\sqrt{4F^4\lambda^2A_2^4B_1^2+F^2G^2A_2^2B_1^4}$, $\omega=\lambda coth\left(0.5(E+\xi\lambda\right)$.

$$U_{1,4}=\frac{\left[\frac{\lambda^2A_2}{\left(2+E\lambda+\xi\lambda\right)^2}+\frac{G\lambda B_1}{4F\left(2+E\lambda+\xi\lambda\right)}-\frac{G\gamma}{24F^3A_2^2}+\frac{G^2B_1^3-\frac{6\lambda\gamma}{2+E\lambda+\xi\lambda}}{24F^2A_2B_1}\right]}{\left[\frac{\lambda B_1}{2+E\lambda+\xi\lambda}-\frac{GB_1^2}{12FA_2}-\frac{\gamma}{4F^2A_2^2}\right]}. \tag{4.6}$$

$$U_{1,5}=\frac{\frac{24A_2}{\left(E+\xi\right)^2}+\frac{G^2B_1^2}{F^2A_2}-\frac{G\sqrt{F^2G^2A_2^2B_1^4}}{F^3A_2^2}+\frac{6\left(FGB_1^2-\frac{\sqrt{F^2G^2A_2^2B_1^4}}{A_2}\right)}{F^2\left(E+\xi\right)B_1}}{24\left(\frac{B_1}{E+\xi}-\frac{FGA_2B_1^2+3\sqrt{F^2G^2A_2^2B_1^4}}{12F^2A_2^2}\right)}. \tag{4.7}$$

Moreover the solutions $U_{1,1}, U_{1,2}, U_{1,3}, U_{1,4}, U_{1,5}$ are substituted into the single form of equation (3.3) and it is observed that they satisfy the nonlinear PDE. The 2D and the 3D graphs of the related solutions with the density and the contour plots which indicate the behavior of the solution function in detail and the view from the top of the three-dimensional graph, respectively are presented below.

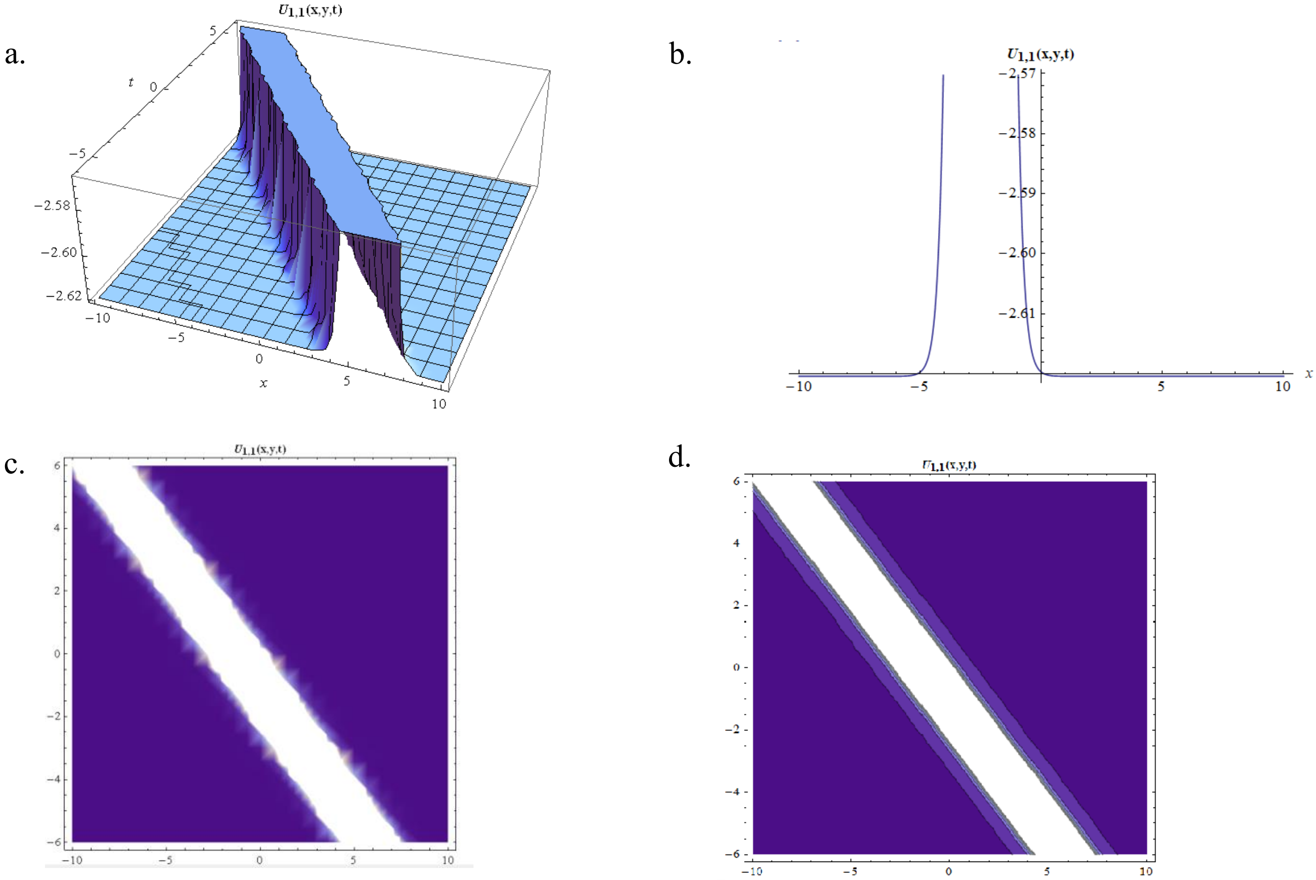

Figure1.1: In a, b, c, d the 3D, 2D, density and the contour graphs of $U_{1,1}$ for the values $\lambda = 3, \mu = 1, F = 1.8, G = 1.3, A_2 = 0.5, \alpha = 0, B_1 = 0.2, k = 2, B_0 = 1, c = 2$ and $t = 1$ for the 2D graph are given, respectively.

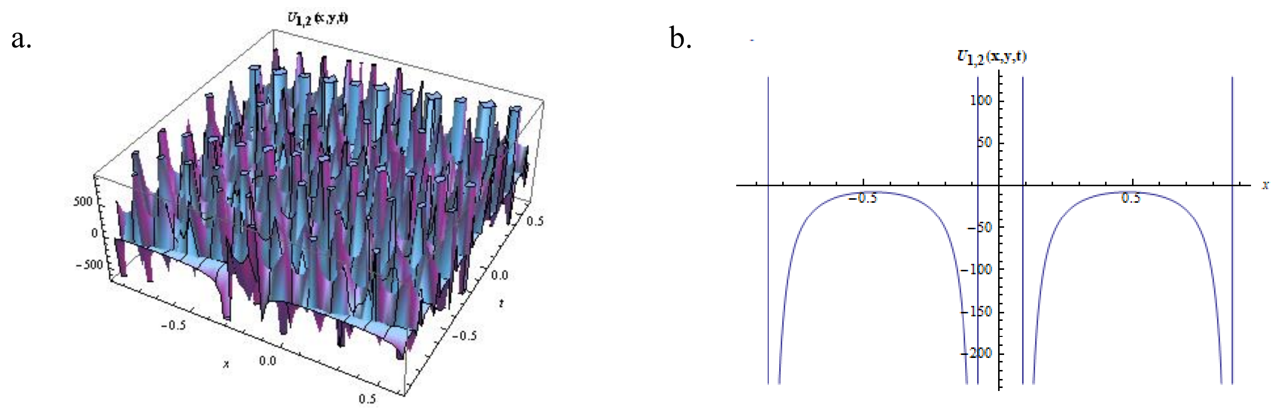

c.

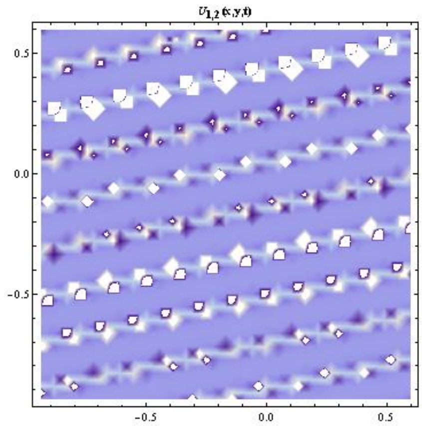

d.

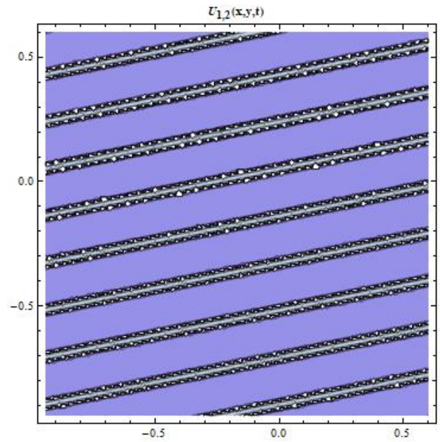

Figure1.2: In a, b, c, d the 3D, 2D, density and the contour graphs of $U_{1,2}$ for the values $\lambda = 1, \mu = 2, F = 0.1, G = 25, A_2 = 0.5, B_1 = 0.02, k = 2, B_0 = 1, c = 5$ and $t = 1$ for the 2D graph are given, respectively.

a.

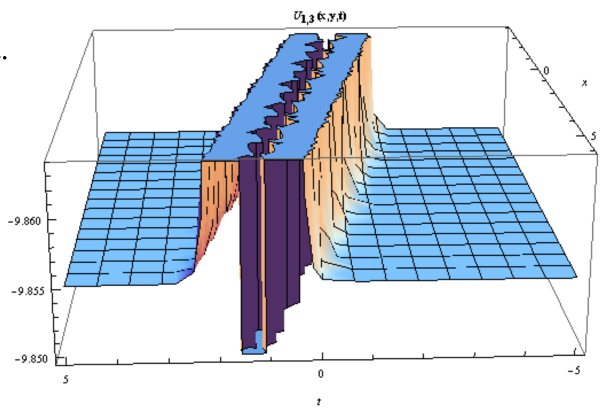

b.

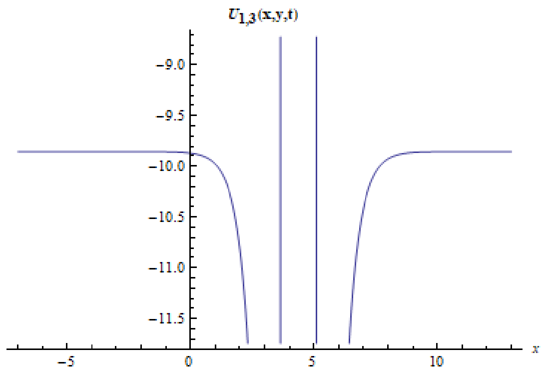

c.

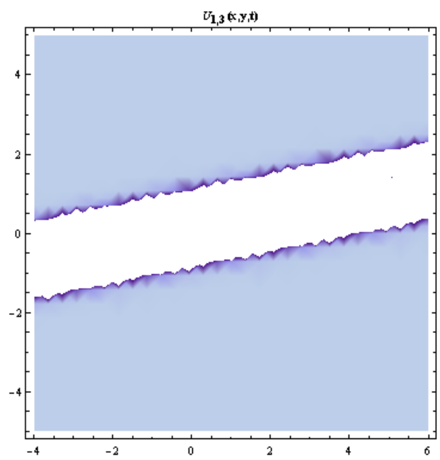

d.

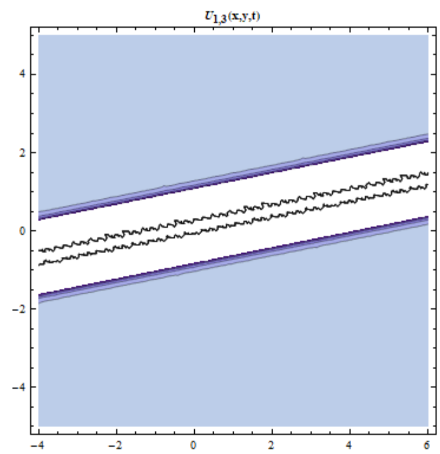

Figure1.3: In a, b, c, d the 3D, 2D, density and the contour graphs of $U_{1,3}$ for the values $\lambda = 1, \mu = 0, F = 0.1, G = 1.2, A_2 = 0.5, B_1 = 0.02, k = 2, B_0 = 1, c = 5$ and $t = 1$ for the 2D graph are given, respectively.

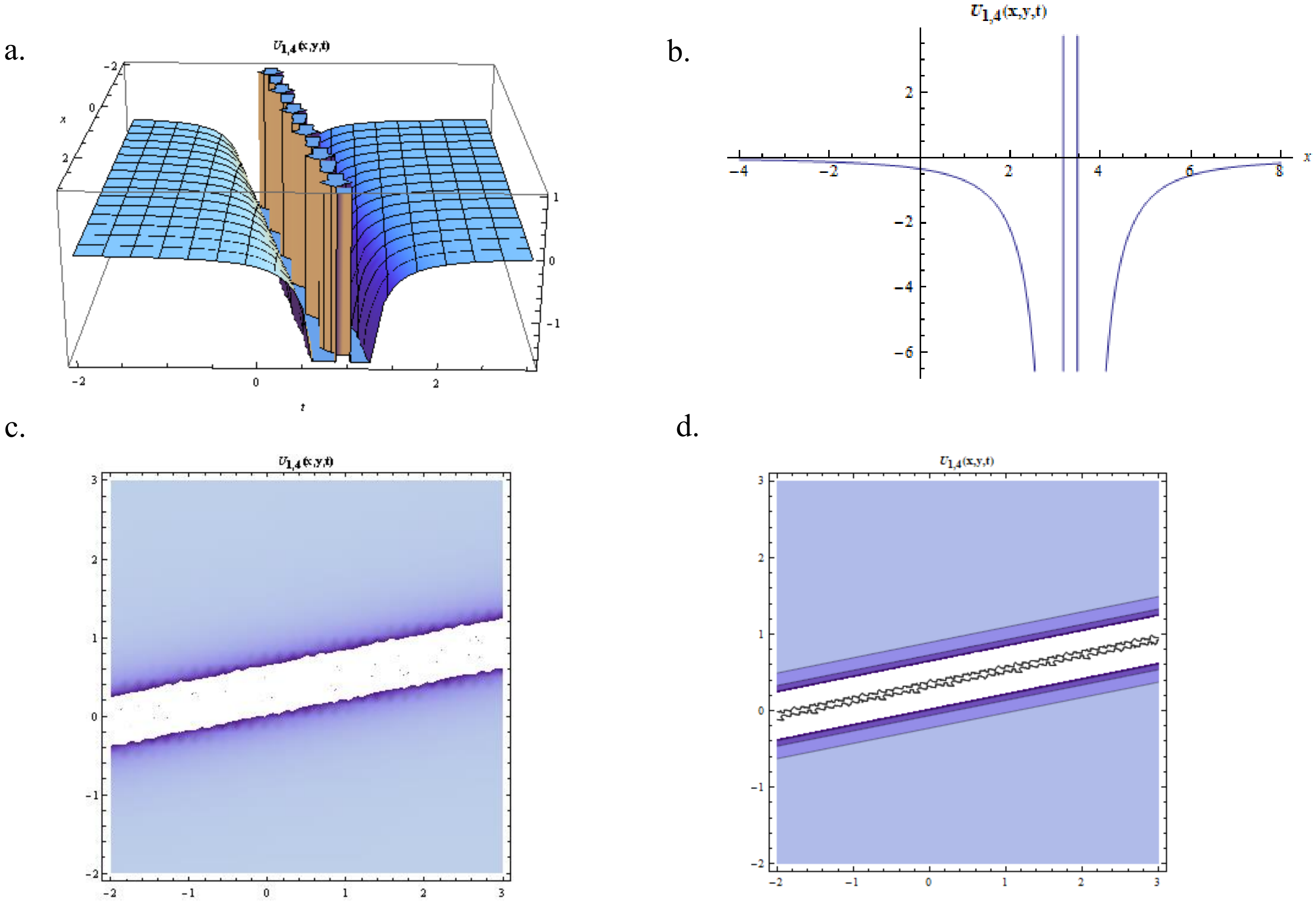

Figure1.4: In a, b, c, d the 3D, 2D, density and the contour graphs of $U_{1,4}$ for the values $\lambda = 2, \mu = 1, F = 0.01, G = 1.2, A_2 = 0.5, B_1 = 0.02, k = 2, B_0 = 1, c = 5$ and $t = 1$ for the 2D graph are given, respectively.

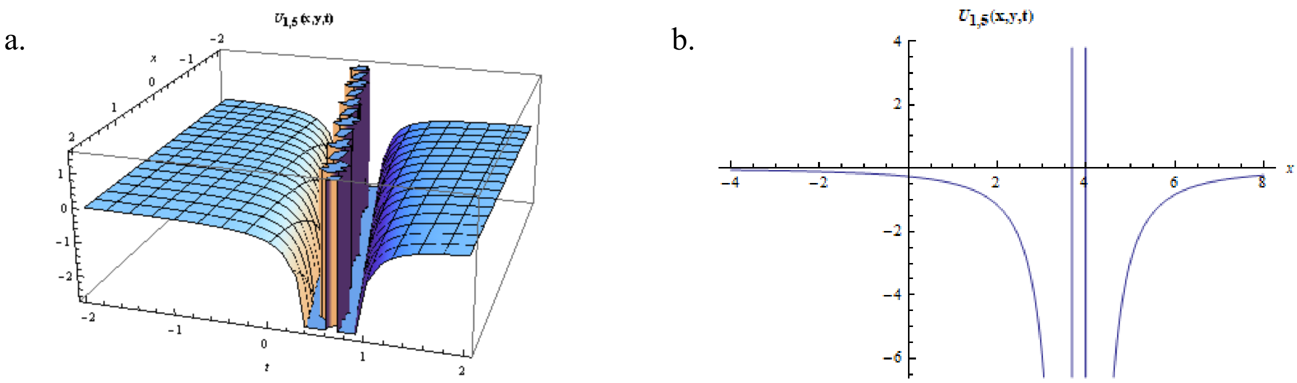

c. 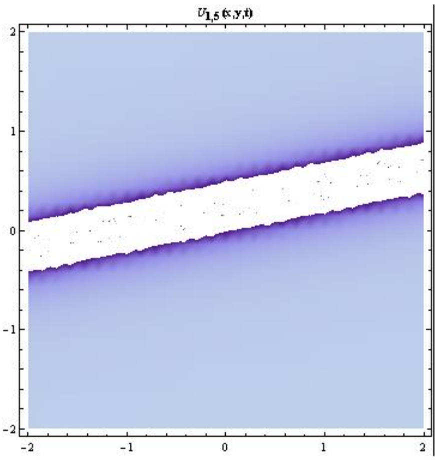

d. 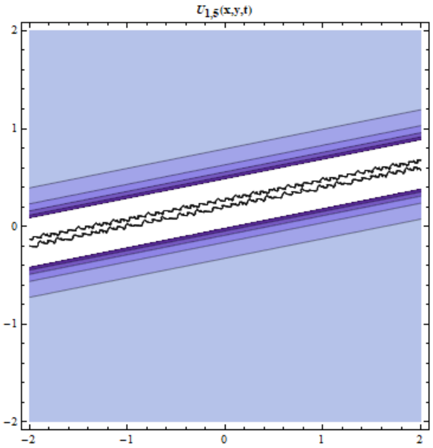

Figure1.5: In a, b, c, d the 3D, 2D, density and the contour graphs of $U_{1,5}$ for the values $\lambda = 0, \mu = 0, F = 0.01, G = 1.2, A_2 = 0.5, B_1 = 0.02, k = 2, B_0 = 1, c = 5$ and $t = 1$ for the 2D graph are given, respectively.

<u>Case2:</u> The solutions for Case2 are given as in the following.

$$A_0 = \frac{\left(5k^2\left(c^2-2S^2\right)\lambda B_1+\sqrt{10}\sqrt{-Hk^2\left(c^2-2S^2\right)B_1^2}\right)\left(k^2\left(c^2-2S^2\right)\lambda A_2 B_1^2+\sqrt{-Hk^2\left(c^2-2S^2\right)A_2^2B_1^4}\right)}{20k^4\left(c^2-2S^2\right)^2B_1^3},$$

$$A_1 = \frac{5\sqrt{-Hk^2\left(c^2-2S^2\right)A_2^2B_1^4}+A_2B_1\left(10k^2\left(c^2-2S^2\right)\lambda B_1+\sqrt{10}\sqrt{-Hk^2\left(c^2-2S^2\right)B_1^2}\right)}{10k^2\left(c^2-2S^2\right)B_1^2},$$

$$B_0 = \frac{\lambda B_1}{2}-\frac{HB_1^2}{\sqrt{10}\sqrt{-Hk^2\left(c^2-2S^2\right)B_1^2}}, \mu = \frac{1}{4}\left(\frac{H}{k^2\left(c^2-2S^2\right)}+\lambda^2\right), F = \frac{2k^2\left(c^2-2S^2\right)B_1^2}{A_2^2},$$

$$G = \frac{3\sqrt{-Hk^2\left(c^2-2S^2\right)A_2^2B_1^4}}{A_2^2B_1}.$$

For this case the solutions $U_{2,1}, U_{2,2}, U_{2,3}, U_{2,4}, U_{2,5}$ which correspond to Family-1, Family-2, Family-3, Family-4 and Family-5 respectively, are obtained as,

$$U_{2,1} = \frac{A_2\left(-\frac{HA_2B_1^2}{\sqrt{-Hk^2\left(c^2-2s^2\right)A_2^2B_1^4}}\right)+\frac{\lambda^2-4\mu+\lambda\gamma}{\lambda+\gamma}}{2B_1}, \tag{4.8}$$

where $\gamma = \sqrt{\lambda^2-4\mu}tanh\left(0.5\left(E+\xi\right)\sqrt{\lambda^2-4\mu}\right)$.

$$U_{2,2} = \frac{A_2\left(-\frac{HA_2B_1^2}{\sqrt{-Hk^2\left(c^2-2s^2\right)A_2^2B_1^4}}\right)+\frac{\lambda^2-4\mu-\lambda\upsilon}{\lambda-\upsilon}}{2B_1}, \tag{4.9}$$

where $\upsilon=\sqrt{-\lambda^2+4\mu}tan\left(0.5\left(E+\xi\right)\sqrt{-\lambda^2+4\mu}\right)$.

$$U_{2,3} = \frac{A_2\left(\lambda coth\left(0.5\left(E+\xi\right)\lambda\right)-\frac{HA_2B_1^2}{\sqrt{-Hk^2\left(c^2-2s^2\right)A_2^2B_1^4}}\right)}{2B_1}. \tag{4.10}$$

$$U_{2,4} = \frac{\lambda A_2}{\left(2+E\lambda+\xi\lambda\right)B_1}-\frac{\sqrt{H}A_2^2B_1}{2\sqrt{k^2\left(-c^2+2S^2\right)A_2^2B_1^4}}. \tag{4.11}$$

$$U_{2,5} = \frac{A_2}{\left(E+\xi\right)B_1}-\frac{\sqrt{H}A_2^2B_1}{2\sqrt{k^2\left(-c^2+2S^2\right)A_2^2B_1^4}}. \tag{4.12}$$

Moreover the solutions $U_{2,1}, U_{2,2}, U_{2,3}, U_{2,4}, U_{2,5}$ are substituted into the single form of equation (3.3) and it is observed that they satisfy the nonlinear PDE. The 2D and the 3D graphs together with the density and the contour plots of the related solutions are presented below.

a.

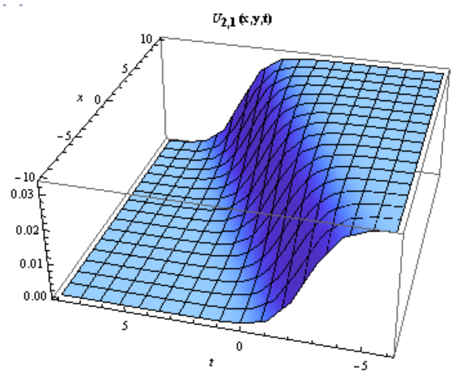

b.

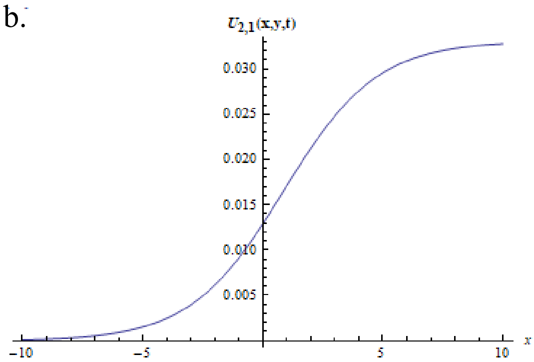

c. 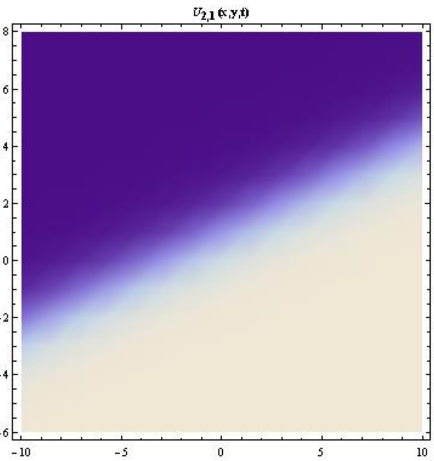

d. 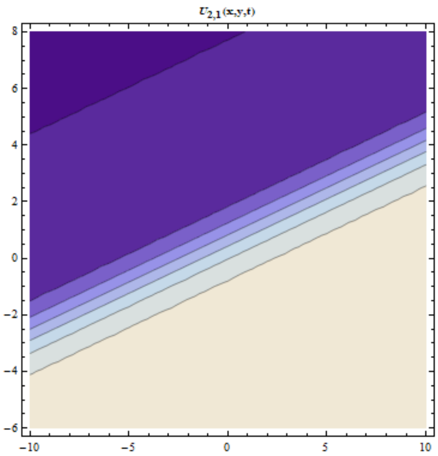

Figure2.1: In a, b, c, d the 3D, 2D, density and the contour graphs of $U_{2,1}$ for the values $\lambda = 3, k = 1.25, \mu = 2.20733, S = 1.5, c = 3, H = -1.2,\ A_2 = 0.2, B_1 = 2.5$ and $t = 1$ for the 2D graph are given, respectively.

a. 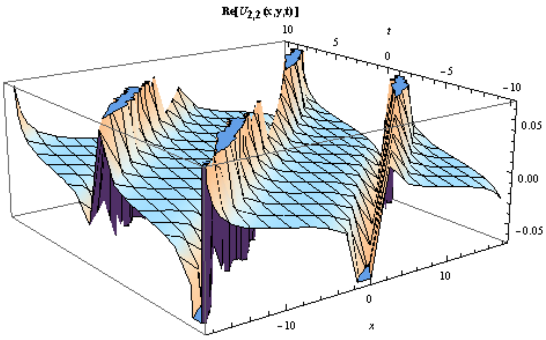

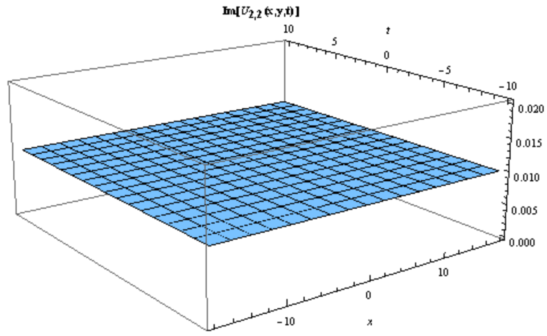

b. 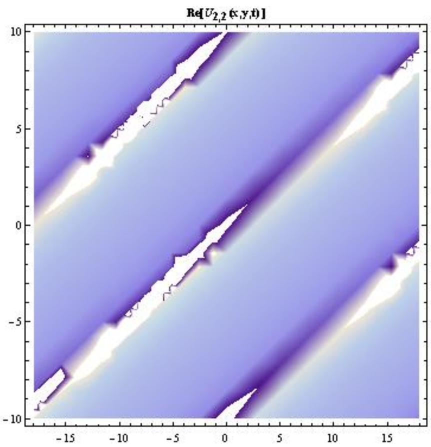

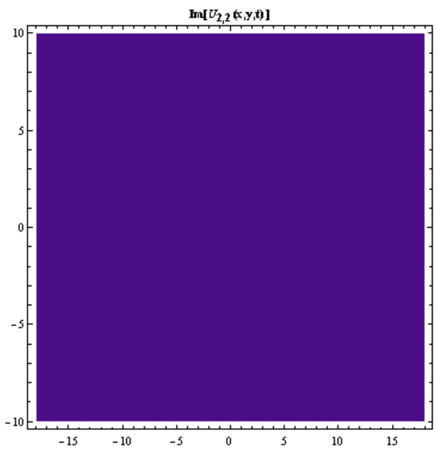

c.

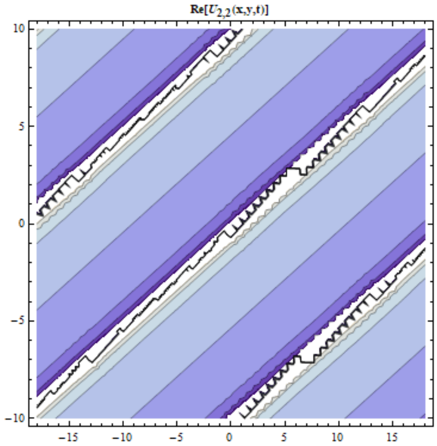

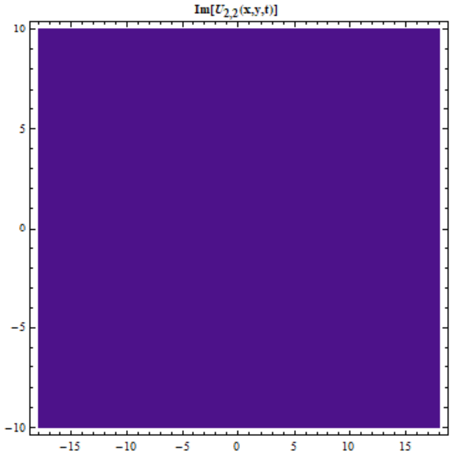

d.

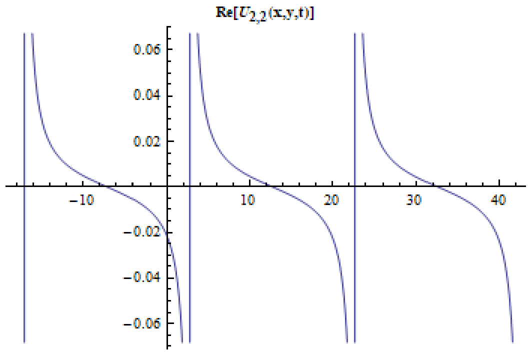

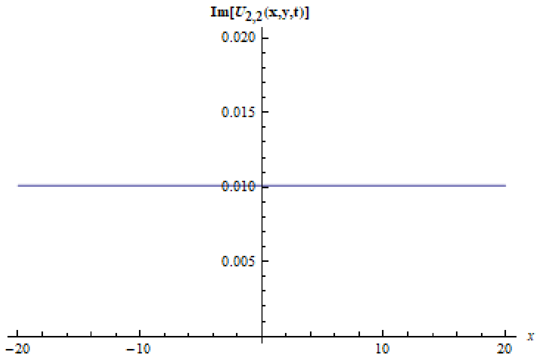

Figure2.2: In a, b, c, d the real and the imaginary parts of the 3D, 2D, density and the contour graphs of $U_{2,2}$ for the values $\lambda = 0.1, k = 1.25, \mu = 0.0185, S = 1, c = 2, H = 0.2,\ A_2 = 0.2, B_1 = 2.5$ and $t = 1$ for the 2D graph are given, respectively.

a.

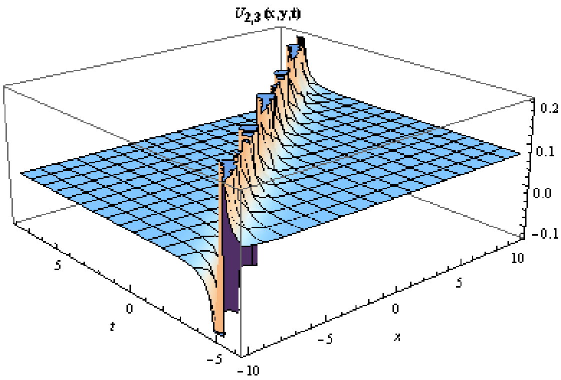

b.

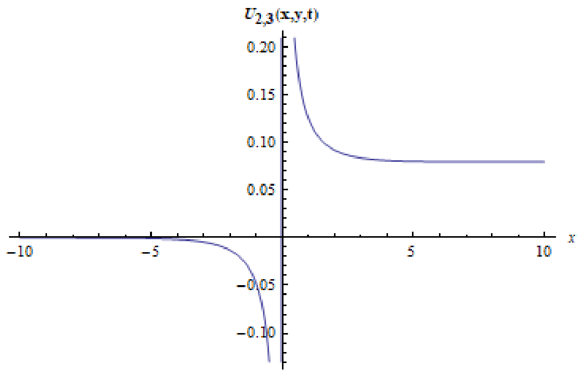

c.

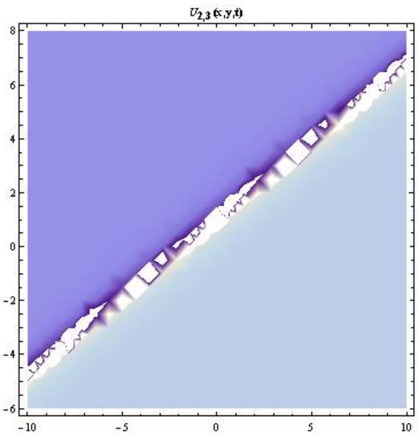

d.

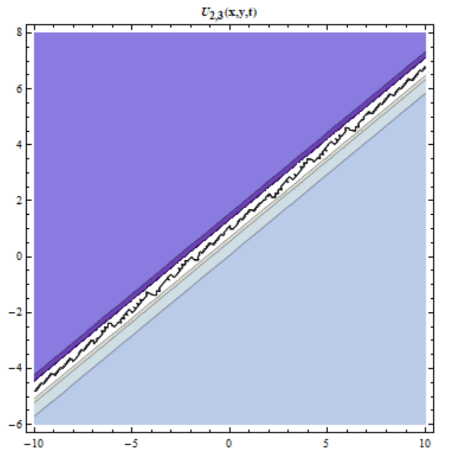

Figure2.3: In a, b, c, d the 3D, 2D, density and the contour graphs of $U_{2,3}$ for the values $\lambda = 1, k = 1, \mu = 0, S = 1, c = \sqrt{3}, H = -1,\ A_2 = 0.2, B_1 = 2.5$ and $t = 1$ for the 2D graph are given, respectively.

a.

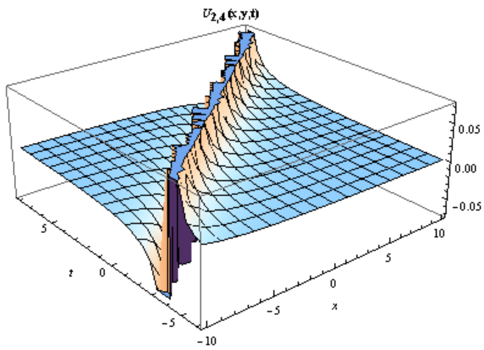

b.

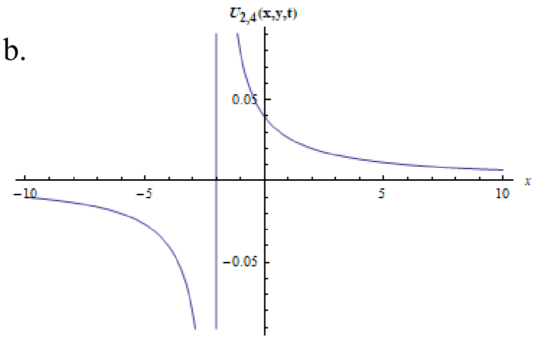

c.

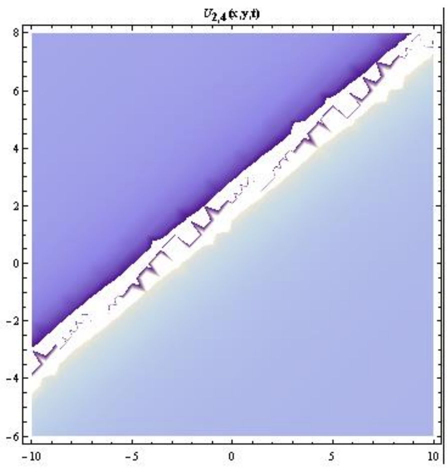

d.

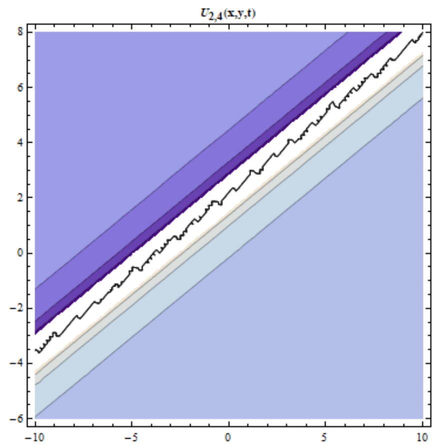

Figure2.4: In a, b, c, d the 3D, 2D, density and the contour graphs of $U_{2,4}$ for the values $\lambda = 1, k = 1, \mu = 0.25, S = 2, c = \sqrt{3}, H = 0,\ A_2 = 0.2, B_1 = 2.5$ and $t = 1$ for the 2D graph are given, respectively.

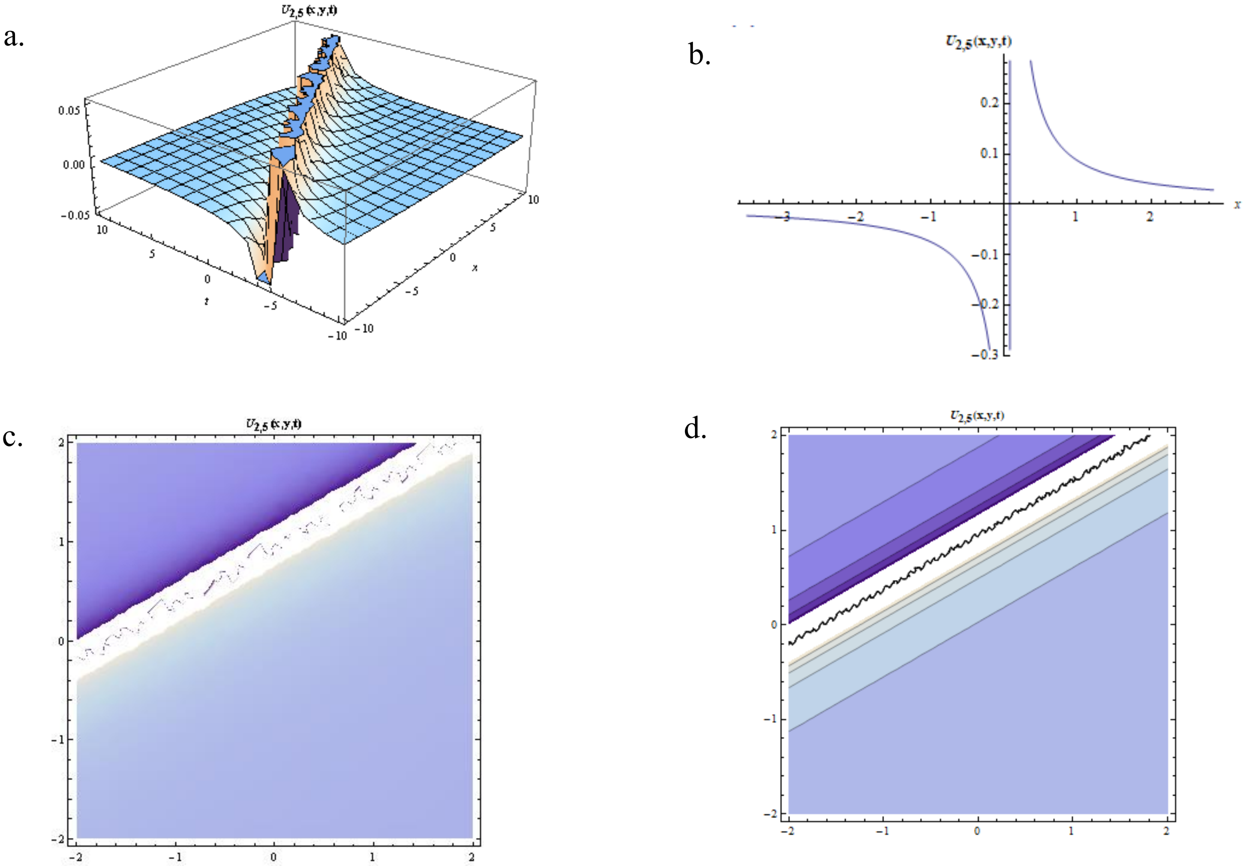

Figure2.5: In a, b, c, d the 3D, 2D, density and the contour graphs of $U_{2,5}$ for the values $\lambda = 0, k = 1, S\mu = 0, = 3, c = \sqrt{3}, H = 0,\ A_2 = 0.2, B_1 = 2.5, \mu = 0$ and $t = 1$ for the 2D graph are given, respectively.

5. Conclusion

The modified $\exp(\Omega(\xi))$-function method is applied to the double-chain DNA model which is given by a (2+1)-dimensional nonlinear PDE. The hyperbolic, trigonometric and the rational form of the solutions are obtained. Some of them are given and it is verified that those solutions satisfy their corresponding equations. The solutions are new kind when compared with the ones in [14-21]. In brief those studies present the soliton, kink, anti-kink, periodic and multi-soliton waves for transversal and longitudinal motion [14-18], the breather-type wave shape, Lump solitons shape, periodic multi-solitons shape, multiple solitons wave shape, and the singular periodic waves [20]. In this letter the generated solutions exhibited the effectiveness, power and the trustworthiness of the MEFM. The obtained solutions enable to expand the information of the governing equations and have applications in mathematical biology. Therefore this method can be applied to other nonlinear evolution equations and may provide new ideas in the biology based science.

REFERENCES

1. He, J. H., & Wu, X. H., Exp-function method for nonlinear wave equations, Chaos, Solitons & Fractals, 30(3), 700-708, 2006.

2. Özpinar, F., Baskonus, H.M., Bulut, H., On the Complex and Hyperbolic Structures for the (2 + 1)-Dimensional Boussinesq Water Equation, Entropy, 17(2), 2015.

3. Shakeel, M., Mohyud-Din, S.T., Iqbal, M.A., Modified extended exp-function method for a system of nonlinear partial differential equations defined by seismic sea waves, Pramana - J Phys, 91, 28, 2018.

4. Akturk, T., An application of the MEFM to the modified Boussinesq equation, An International Journal of Optimization and Control: Theories & Applications (IJOCTA), 9(1), 11-17, 2019.

5. Aktürk, T., Bulut, H., & Gülnur, Yel., An Application of the Modified Expansion Method to Nonlinear Partial Differential Equation, Turkish Journal of Mathematics and Computer Science, 10, 202-206, 2018.

6. Kırcı, Ö., Bulut, H., On the new solutions of (3+1)-dimensional Potential-YTSF equation by $\tan(\frac{F(\xi)}{2})$-expansion method, 4th International Conference on Analysis and Its Applications, Kırşehir, September 11-14, 2018.

7. Isik, O., Degirmenci, O.I., Bulut, H., Classifications on the travelling wave solutions to the (3+1)-dimensional generalized KP and Jimbo-Miwa equations, ITM Web of Conferences, Vol.13, 01021, 2017.

8. Naher, H., & Abdullah, F. A., New approach of (G′/G)-expansion method and new approach of generalized (G′/G)-expansion method for nonlinear evolution equation, American Institute of Physics Advances, 3(3), 032116, 2013.

9. Ilhan, O.A., Islam, M.N., Akbar, M.A., Construction of Functional Closed Form Wave Solutions to the ZKBBM Equation and the Schrödinger Equation, Iranian Journal of Science and Technology, Transactions of Mechanical Engineering, 45(3), 827-840, 2021.

10. Mahmud, F., Samsuzzoha, Md, Akbar, M. A., The generalized Kudryashov method to obtain exact traveling wave solutions of the PHI-four equation and Fisher equation, Results in Physics, 7, 4296-4302, 2017.

11. Hietarinta, J., Hirota's bilinear method and soliton solutions, Physics AUC, 15(1), 31-37, 2005.

12. Lu D, Hong B, Tian L. Backlund transformation and N-soliton-like Solutions to the Combined KdV-Burgers Equation with Variable Coefficients, International Journal of Nonlinear Sciences, 2(1):3–10, 2006.

13. Biazar, F. Badpeima, F. Azimi, F., Application of the homotopy perturbation method to Zakharov-Kuznetsov equations, Computers&Mathematics with Applications, 58(11-12), 2391 2009.

14. Mabrouk, S.M., Explicit Solutions of Double-Chain DNA Dynamical System in (2+1) - Dimensions, International Journal of Current Engineering and Technology, 9(5), 2019.

15. Alka, W., Goyal, A., Kumar, C.N., Nonlinear dynamics of DNA – Riccati generalized solitary wave solutions, Physics Letter A, 375, 480-483, 2011.

16. Zayed, E.M.E., Arnous, A.H., Many exact solutions for nonlinear dynamics of DNA model using the generalized Riccati equation mapping method, Scientific Research and Essays, Vol. 8(8), pp. 340 -346, 25 February, 2013.

17. Saleh, R., Mabrouk, S. M., & Wazwaz, A. M., Lie symmetry analysis of a stochastic gene evolution in double-chain deoxyribonucleic acid system, Waves in Random and Complex Media, 1-15, 2021.

18. Seadawy, A.R., Bilal, M., Younis, M., Rizvi, S.T.R., Althobaiti, S., Makhlouf, M.M., Analytical mathematical approaches for the double-chain model of DNA by a novel computational technique, Chaos, Solitons and Fractals, 144, 110669, 2021.

19. Qian, X., Lou, S., Exact Solutions of Nonlinear Dynamics Equation in a New Double-Chain Model of DNA*, Communications in Theoretical Physics 39(4): 501-505, 2003.

20. Kumar, S., Kumar, A., Kharbanda, H., Abundant exact closed-form solutions and solitonic structures for the double-chain deoxyribonucleic acid (DNA) model, Brazilian Journal of Physics 51:1043–1068, 2021.

21. Bilal, M., Younas, U., Ren, J., Dynamics of exact soliton solutions in the double-chain model of deoxyribonucleic acid, Mathematical Models in the Applied Sciences, 2021; 1-19. https://doi.org/10.1002/mma.7631

22. Bulut, H., Baskonus, H.M., New Complex Hyperbolic Function Solutions for the (2+1)-Dimensional Dispersive Long Water–Wave System, Mathematical and Computational Applications, 21(2), 6, 2016.

OPTICAL SOLUTIONS OF CONFORMABLE EXTENDED CALOGERO-BOGOYAVLENSKII-SCHIFF EQUATION

Gülnur YEL[1*], Nesrin GÜLLÜOĞLU[2], Hasan BULUT[3]

[1]Faculty of Education, Final International University, Kyrenia, Mersin 10, Turkey
[2]Sanlıurfa Technical Sciences Vocational School, Harran University, Sanlıurfa, Turkey
[3]Department of Mathematics, Firat University, Elazig, Turkey

gulnur.yel@final.edu.tr, ngulluoglu@harran.edu.tr, hbulut@firat.edu.tr

Abstract

We implement an analytical approach which is the sine-Gordon expansion method to the extended Calogero–Bogoyavlenskii–Schiff equation in conformable sense. By this way, we find out some optical soliton solutions which contain dark, bright, kink type soliton solutions. We give 3D, 2D and contour plots of waves for better understand physical behaviors in engineering and physics.

Keywords: The sine-Gordon expansion method; the conformable extended Calogero–Bogoyavlenskii–Schiff equation; optical soliton solutions.

1. Introduction

Nonlinear evolution equations have significant role for modelling various scientific phenomena in real-world. Especially, mathematicians and physicists have studied the nonlinear integrable equations in plasma physics, optics, fluid mechanics, electromagnetic, quantum physics, etc. To come out exact solutions of the nonlinear evolution equations (NLEEs), great numbers of powerful methods have been developed including the tan $\left(\phi(\xi)/2\right)$ -expansion method [1], the Hirota simple method [2,3], the Lie symmetry analysis [4,5,6], the extended sinh-Gordon equation expansion method [7], the extended direct algebraic method [8] and many other methods [9-18].

One of the nonlinear integrable equations is the Calogero–Bogoyavlenskii–Schiff (CBS) equation which is defined by Bogoyavlenskii and Schiff [22, 23]. They described the interaction of Riemann wave, which is one-dimensional traveling nonlinear waves in non-dispersive systems, extended along the two spatial dimensions, x-axis and y-axis. Dynamics of Riemann waves are studied in many physical fields such as surface waves in oceans, ion-sound waves in plasmas, optical tsunami in fibers, electromagnetic waves in lines. In 1998 [24], Yu et al. described integrable the (2+1)- dimensional model as,

$$u_{tx}+u_x u_{xy}+\frac{1}{2}u_{xx}u_y+\frac{1}{4}u_{xxxy}+\frac{1}{4}\partial_x^{-1}u_{yyy}=0, \tag{1}$$

where $u(x,y,t)$ is a function of x,y space and t temporal variables, $u_x u_{xy}, u_{xx}u_y$ are nonlinear terms.

The extended (2+1)- dimensional equation of Eq.(1) is presented by Wazwaz [25], adding the βu_{xy} planar flux term, where β is any constant.

$$u_{tx}+u_x u_{xy}+\frac{1}{2}u_{xx}u_y+\frac{1}{4}u_{xxxy}+\frac{1}{4}\partial_x^{-1}u_{yyy}+\beta u_{xy}=0. \tag{2}$$

The following equation is obtained by differentiating Eq.(2) with respect to x.

$$4u_{txx}+6u_{xx}u_{xy}+4u_x u_{xxy}+2u_{xxx}u_y+u_{xxxxy}+u_{yyy}+4\beta u_{xxy}=0. \tag{3}$$

We can see so many studies on the Calogero–Bogoyavlenskii–Schiff equation in the literature. For example, using the generalized bilinear method, the breather wave, periodic lump soliton, rational solutions of generalized Calogero–Bogoyavlenskii–Schiff equation have been obtained in [26]. Hammouch et al. have found some soliton solutions such as trigonometric, hyperbolic and exponential functions of the time-fractional nonlinear Calogero-Bogoyavlenskii-Schiff equation [27]. The (G'/G)- expansion method is implemented to the extended Calogero-Bogoyavlenskii-Schiff equation and one-soliton, kink, periodic and N-soliton solutions are presented [28]. Lie symmetries of the (2+1)-dimensional extended Calogero-Bogoyavlenskii-Schiff equation are derived and then three method are used to construct implicit solutions [29].

In this study, we suppose the conformable (2+1)-dimensional Calogero–Bogoyavlenskii–Schiff equation given as,

$$4u_{txx}^{\theta}+6u_{xx}u_{xy}+4u_x u_{xxy}+2u_{xxx}u_y+u_{xxxxy}+u_{yyy}+4\beta u_{xxy}=0, \tag{4}$$

where $0<\theta\le 1$ is order of conformable derivative, β is an arbitrary constant.

In second section, we give some fundamental theorems and definitions of conformable derivative. In section 3, basic steps are presented of the proposed method which is the sine-Gordon expansion method. Implementation and 3D, 2D, contour figures to the mentioned governing model are given in section 4. Finally, some conclusions and discussions corresponding to all solutions obtained are devoted in section 5.

2. Fundamental Properties of Conformable Derivative

In the literature, there are various fractional derivative definitions such as Riemann–Liouville, Caputo, Grünwald–Letnikov, Jumarie. A novel definition of the fractional derivative which is a conformable derivative that based on the basic limit definition of the derivative is presented by Khalila et al. [19].

In this section, we give some fundamental properties of conformable derivative.

Definition: Let $h:[0,\infty)\rightarrow\mathbb{R}$ be a given function, the conformable derivative of h of order α is defined as,

$$L_\alpha(h)(t)=\lim_{\varepsilon\rightarrow\infty}\frac{h\left(t+\varepsilon t^{1-\alpha}\right)-h(t)}{\varepsilon}.$$

For all $t>0,\ \alpha\in(0,1)$ [19].

Theorem: Let L_α be the derivative operator with order α and $\alpha\in(0,1)$ and h,k be $\alpha-$ differentiable at a point $t>0$. Then [19,20], we have the following

i. $L_\alpha(ah+bk)=aL_\alpha(h)+bL_\alpha(k),\quad \forall a,b\in R.$

ii. $L_\alpha\left(t^p\right)=p.t^{p-\alpha},\quad \forall p\in R.$

iii. $L_\alpha(hk)=hL_\alpha(k)+kL_\alpha(h).$

iv. $L_\alpha\left(\frac{h}{k}\right)=\frac{kL_\alpha(h)-hL_\alpha(k)}{k^2}.$

v. $L_\alpha(\lambda)=0,$ for all constant functions $h(t)=\lambda.$

vi. If h differentiable then $L_\alpha(h)(t)=t^{1-\alpha}\frac{dh}{dt}(t).$

Theorem (Chain Rule): Consider $h,g:(a,\infty)\rightarrow R$ be α-differentiable functions, here $0<\alpha\le 1$. Whether $k(t)=h(g(t))$. At the time $k(t)$ is α-differentiable, for all t with $t\neq a$ and $g(t)\neq 0$, we have [21]

$$\left(L_{\alpha}^{a}k\right)(t)=\left(L_{\alpha}^{a}h\right)\left(g(t)\right)\cdot\left(L_{\alpha}^{a}g\right)(t)\,g(t)^{\alpha-1}.$$

If $t=a$ we have

$$\left(L_{\alpha}^{a}k\right)(t)=\lim_{t\to a^{+}}\left(L_{\alpha}^{a}h\right)\left(g(t)\right)\cdot\left(L_{\alpha}^{a}g\right)(t)\,g(t)^{\alpha-1}.$$

Conformable Derivatives for Some Special Functions

1. $L_{\alpha}(1)=0.$
2. $L_{\alpha}\left(e^{cx}\right)=cx^{1-\alpha}e^{cx}, c\in\mathbb{R}.$
3. $L_{\alpha}(\sin bx)=bx^{1-\alpha}\cos bx, b\in\mathbb{R}.$
4. $L_{\alpha}(\cos bx)=-bx^{1-\alpha}\sin bx, b\in\mathbb{R}.$
5. $L_{\alpha}\left(\frac{t^{\alpha}}{\alpha}\right)=1.$

3. The Description of the sine-Gordon Expansion Method

We will give basic steps of the SGEM in this section.

Suppose that the solution of the following nonlinear partial differential equation;

$$P\left(u,u_{x},u_{t},u_{xx},u_{tt},u_{xt},u_{xxx},\ldots\right)=0, \tag{5}$$

where $u=u(x,t)$ is a function depends on x and t. Using the wave transform $u=u(x,t)=U(\xi),\ \xi=\mu(x-ct)$ into the Eq.(5), gives the nonlinear ordinary (NODE) differential equation as,

$$N\left(U,U',U'',U''',\ldots\right)=0, \tag{6}$$

where N is a nonlinear polynomial including U and its ordinary derivatives with respect to ξ.

To obtain the solutions of Eq.(5), we suppose the following expressions

$$U(\xi)=\sum_{i=1}^{n}\tanh^{i-1}(\xi)\left[B_{i}\operatorname{sech}(\xi)+A_{i}\tanh(\xi)\right]+A_{0}. \tag{7}$$

According to two significant equations as below,

$$\sin\left(w(\xi)\right) = \sec h(\xi), \tag{8}$$

$$\cos\left(w(\xi)\right) = \tan h(\xi), \tag{9}$$

Eq. (7) can be rewritten according to Eqs. (8) and (9) as follows;

$$U\left(w\right) = \sum_{i=1}^{n} \cos^{i-1}\left(w\right)\left[B_i \sin\left(w\right) + A_i \cos\left(w\right)\right] + A_0. \tag{10}$$

According to the balance principle, n is found between the highest order derivative and the nonlinear term with the highest power in the nonlinear ordinary differential equation. Putting Eq.(10) and its sequential derivatives into the NODE, we obtain a polynomial equation with $\sin^i\left(w\right)\cos^j\left(w\right)$. Using some trigonometric properties to the polynomial equation, it is obtained an algebraic equation system by equating to zero the same power summation of coefficients. With help of the calculation program, we solve the equation system to obtain the A_i, B_i and c values. Substituting the A_i, B_i, c values into Eq.(10), we get the new travelling wave solutions to the Eq. (5).

4. Application of the Method

We will give implementation the proposed method to the conformable (2+1)-dimensional Calogero–Bogoyavlenskii–Schiff equation in this section.

The conformable (2+1)-dimensional Calogero–Bogoyavlenskii–Schiff equation is given as,

$$4u_{txx}^{\theta} + 6u_{xx}u_{xy} + 4u_x u_{xxy} + 2u_{xxx}u_y + u_{xxxxy} + u_{yyy} + 4\beta u_{xxy} = 0,$$

where $0 < \theta \le 1$ is order of conformable derivative, β is an arbitrary constant.

By using wave transfomation,

$$u\left(x, y, t\right) = U\left(\xi\right), \xi = \left(x + y - c\frac{t^{\theta}}{\theta}\right),$$

where c wave speed, after then doing some mathematical operations, Eq.(4) turns to following nonlinear ordinary differential equation

$$U'' + \left(4\beta - 4c + 1\right)U + 3U^2 = 0. \tag{11}$$

Homogeneous balance principle gives $n = 2$.

For the value $n = 2$, Eq.(10) takes the form,

$$U\left(w\right) = B_1 \sin\left(w\right) + A_1 \cos(w) + B_2 \cos(w)\sin\left(w\right) + A_2 \cos^2(w) + A_0 \tag{12}$$

Differentiating Eq.(12) twice, yields

$$U''(w) = -2A_1\cos(w)\sin^2(w) - 4A_2\cos^2(w)\sin^2(w) + 2A_2\sin^4(w) + B_1\cos^2(w)\sin(w) - B_1\sin^3(w) + B_2\cos^3(w)\sin(w) - 5B_2\cos(w)\sin^3(w) \tag{13}$$

Substituting Eq. (12) and Eq. (13) into Eq. (11), we obtain an algebraic system of equations by collecting the coefficients of all the trigonometric term of the same power and equating the sum of each collection to zero. By solving the algebraic equations system, we find some cases which can be seen below.

Case-1: $A_0 = \frac{2}{3}, A_1 = 0, A_2 = -1, B_1 = 0, B_2 = -i, c = \beta,$

By using above coefficients, we get the following hyperbolic function solution

$$u_1(x,y,t) = \frac{1}{3}\left(-x - y + \frac{t^\theta \beta}{\theta}\right) + i\,\mathrm{sech}\left(x + y - \frac{t^\theta \beta}{\theta}\right) + \tanh\left(x + y - \frac{t^\theta \beta}{\theta}\right). \tag{14}$$

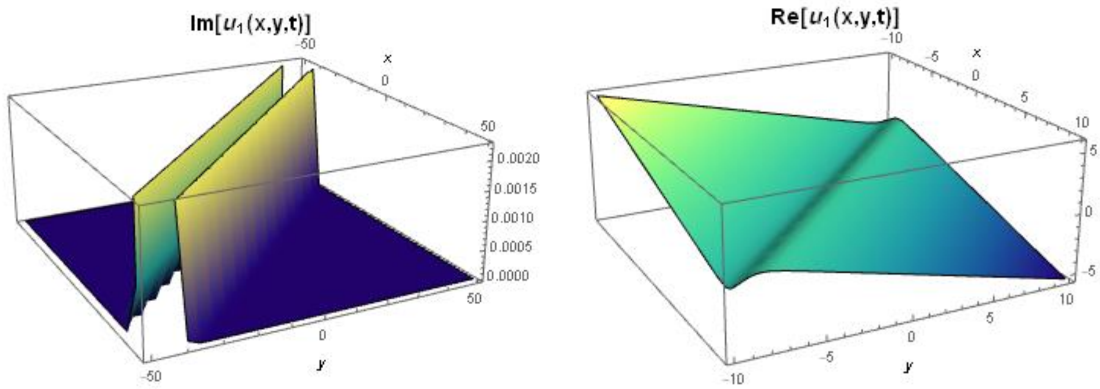

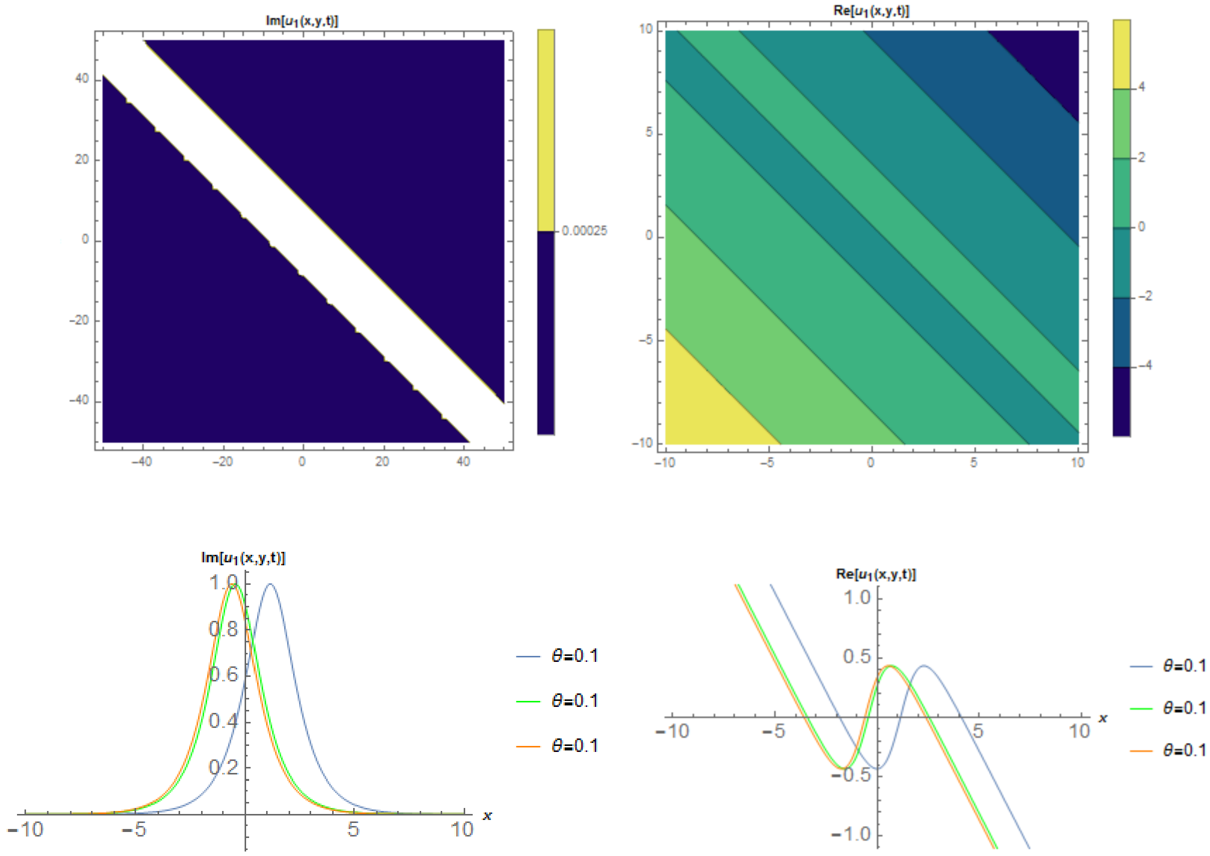

Figure-1: For the values 3D and contour shape $\theta = 0.5, \beta = 0.2$, 2D shapes for $t = 2$.

Case-2: $A_0 = 1, A_1 = 0, A_2 = -1, B_1 = 0, B_2 = i, c = \dfrac{1}{2} + \beta,$

By using above coefficients, we get another the following hyperbolic function solution

$$u_2(x,y,t) = -i\,\mathrm{sech}\left(x + y - \frac{t^{\theta}\left(\frac{1}{2} + \beta\right)}{\theta}\right) + \tanh\left(x + y - \frac{t^{\theta}\left(\frac{1}{2} + \beta\right)}{\theta}\right), \tag{15}$$

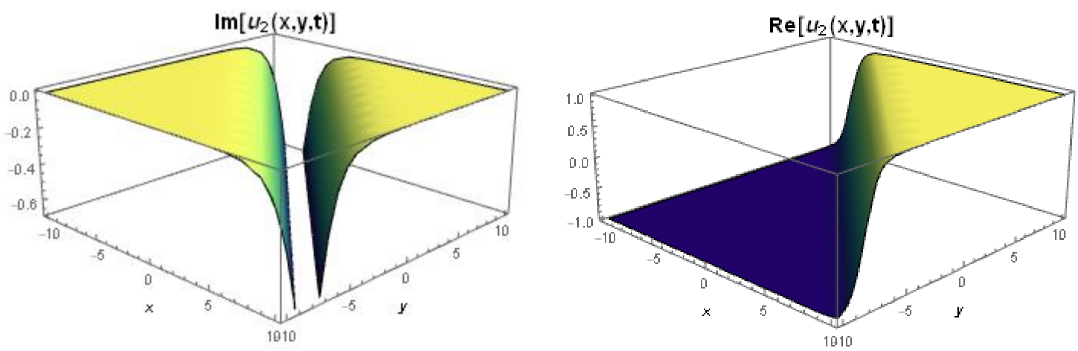

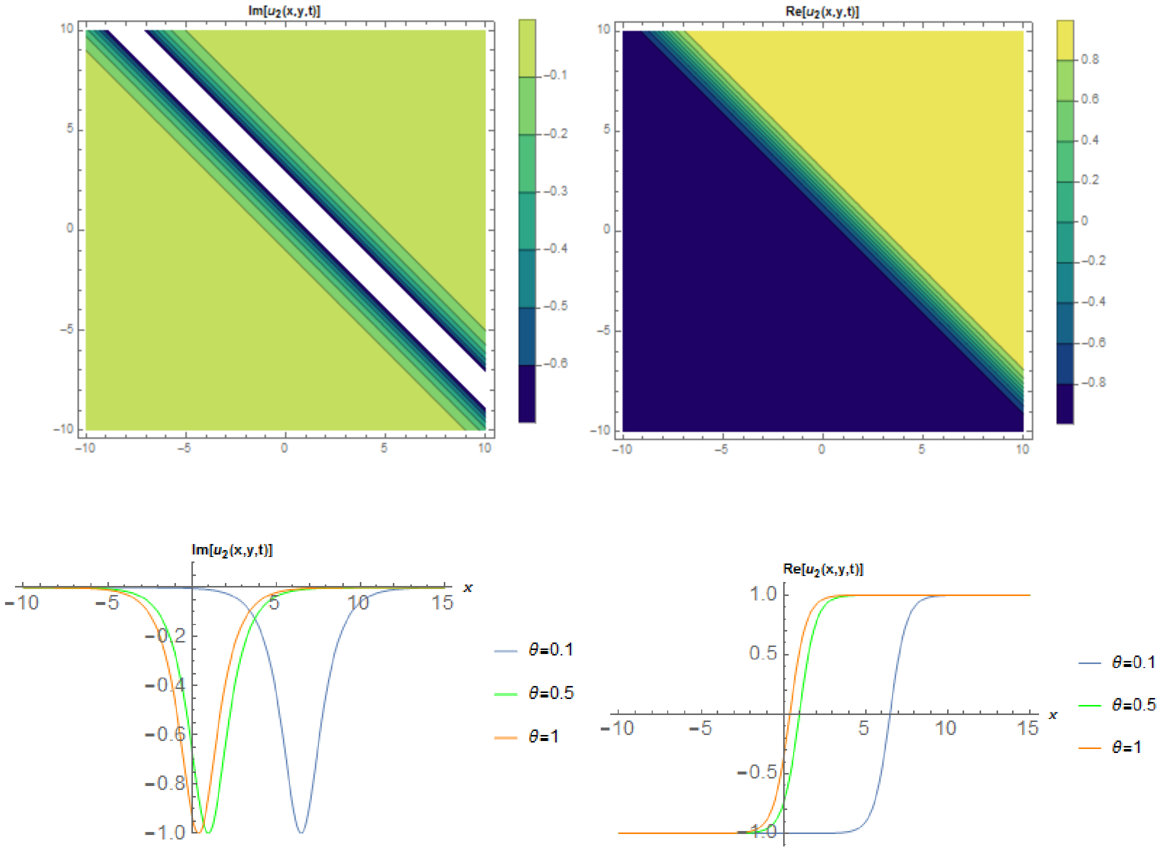

Figure-2: For the values 3D and contour shape $\theta = 0.5, \beta = 0.2$, 2D shapes for $t = 2$.

Case-3: $A_0 = \frac{2}{3}, A_1 = 0, A_2 = -, 2B_1 = 0, B_2 = 0, c = -\frac{3}{4} + \beta,$

By using above coefficients, we get the following hyperbolic function solution

$$u_3(x,y,t) = -\frac{4}{3}\left(x + y - \frac{t^{\theta}\left(-\frac{3}{4}+\beta\right)}{\theta} \right) + 2\tanh\left(x + y - \frac{t^{\theta}\left(-\frac{3}{4}+\beta\right)}{\theta} \right). \quad (16)$$

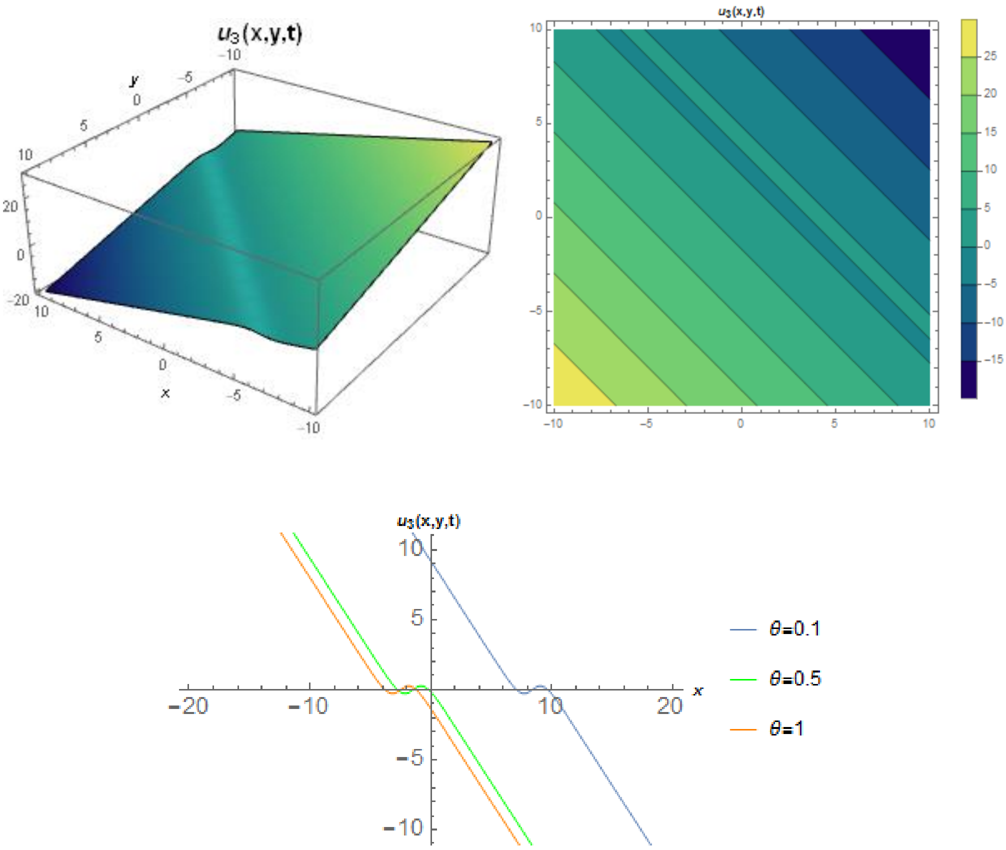

Figure 3: For the values 3D and contour shape $\theta = 0.5, \beta = 0.2$ and 2D shape for $t = 2$.

Case-4: $A_0 = \dfrac{2}{3}, A_1 = 0, A_2 = -1, B_1 = 0, B_2 = i, c = \beta,$

By using above coefficients, we obtain the following hyperbolic function solution

$$u_4(x,y,t) = \frac{1}{3}\left(-x - y + \frac{t^{\theta}\beta}{\theta}\right) - i\,\mathrm{sech}\left(x + y - \frac{t^{\theta}\beta}{\theta}\right) + \tanh\left(x + y - \frac{t^{\theta}\beta}{\theta}\right), \tag{17}$$

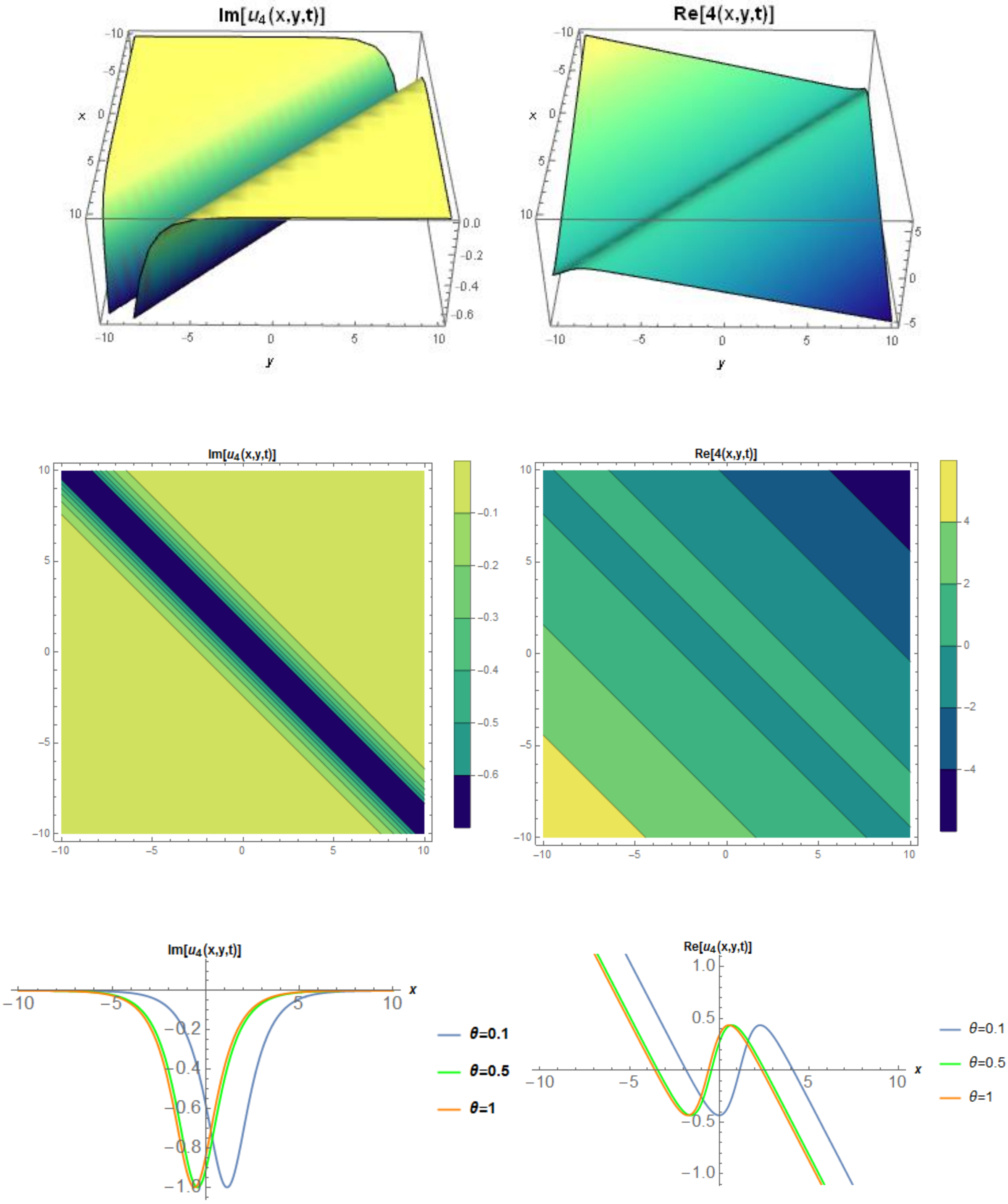

Figure 4: For the values 3D and contour shape $\theta = 0.5, \beta = 0.2$, 2D shapes for $t = 2$.

5. Conclusions

In this study, we derived four analytical soliton solution of the conformable (2+1)-dimensional Calogero–Bogoyavlenskii–Schiff equation by using the sine-Gordon expansion method. Obtained all solutions include dark soliton, kink soliton, bright soliton solutions which can be seen in Figures 1-4. We plotted 2D figures under the different conformable derivative order

$\theta = 0.1, 0.5$ and 1. We think that the presented soliton solutions that are useful, especially in plasma physics, ocean engineering, and electromagnetic engineering, will help researchers.

REFERENCES

[1] J. Manafian, Application of the ITEM for the system of equations for the ion sound and Langmuir waves, Opt Quant Electron, 49:17, 2017.

[2] H.F. Ismael, A. Seadawy, and H. Bulut, Multiple soliton, fusion, breather, lump, mixed kink-lump and periodic solutions to the extended shallow water wave model in (2 + 1)-dimensions, Mod. Phys. Lett. B, 2020, Article ID: 2150138, 2020.

[3] C. Qian, J. Rao, D. Mihalache, and J. He, Rational and semi-rational solutions of the y-nonlocal Davey–Stewartson I equation, Comput. Math. Appl. 75(9), pp. 3317–3330, 2018.

[4] C.M. Khalique and I.E. Mhlanga, Travelling waves and conservation laws of a (2 + 1)-dimensional coupling system with Korteweg–de Vries equation, Appl. Math. Nonlinear Sci. 3(1), pp. 241–254, 2018.

[5] J. Zheng, of a Nonlinear Fokker-Planck Equation Describing Cell Population Growth, Advances in Mathematical Physics, vol. 2020, Article ID 4975943, 2020.

[6] M. S. Hashemi, D. Baleanu, Lie Symmetry Analysis of Fractional Differential Equations, 1st Ed., Chapman and Hall/CRC, 2020.

[7] G. Yel , C. Cattani, , H.M. Baskonus, W. Gao, On the Complex Simulations with Dark-Bright to the Hirota-Maccari System, Journal of Computational and Nonlinear Dynamics, 6(16), 061005, 2021.

[8] A. Jhangeer, H. M. Baskonus, G. Yel, W. Gao, New exact solitary wave solutions, bifurcation analysis and first order conserved quantities of resonance nonlinear Shrödinger's equation with Kerr law nonlinearity, Journal of King Saud University - Science, 33(1), 101180, 2020.

[9] Eskitascıoglu, E. I., Aktas, M. B., and Baskonus, H. M., 2019, New Complex and Hyperbolic Forms for Ablowitz-Kaup-Newell-Segur Wave Equation With Fourth Order, Appl. Math. Nonlinear Sci., 4(1), pp. 93–112.

[10] R. Hirota, The Direct Method in Soliton Theory, Cambridge University Press, New York, 2004.

[11] Y. Zhang, H.H. Dong, X.E. Zhang, H.W. Yang, Rational solutions and lump solutions to the generalized (3 +1)- dimensional shallow water-like equation, Comput. Math. Appl. 73 (2017) 246–252.

[12] A.M. Wazwaz, The (2+1) and (3+1)-dimensional CBS equations: multiple soliton solutions and multiple singular soliton solutions, Z. Naturforsch. 65A (2010) 173–181.

[13] H. Roshid, M. F. Hoque, and M. A. Akbar, New extended (G′/G)-expansion method for traveling wave solutions of nonlinear partial differential equations (NPDEs) in mathematical physics, Ita. J. Pure Appl. Math. 33 (2014), 175–190

[14] Y. Gu and Y. Kong, Two different systematic techniques to seek analytical solutions of the higher-order modified Boussinesq equation, IEEE Access 7 (2019), 96818–96826.

[15] Z.X. Zhou, Darboux transformations and global solutions for a nonlocal derivative nonlinear Schrödinger equation, Communications in Nonlinear Science and Numerical Simulation, 62 (2018) 480-488.

[16] A. Yokus, H. Durur, Discussions on diffraction and the dispersion for traveling wave solutions of the (2+ 1)-dimensional paraxial wave equation. Mathematical Sciences, 1-11, 2021.

[17] Yokus, H. Durur, H. Ahmad, P. Thounthong, Construction of exact traveling wave solutions of the Bogoyavlenskii equation by (G′/G, 1/G)-expansion and (1/G′)-expansion techniques. Results in Physics, 19, 103409, 2020.
[18] H. Durur, O. Tasbozan, A. Kurt, New analytical solutions of conformable time fractional bad and good modified Boussinesq equations. Applied Mathematics and Nonlinear Sciences, 5(1), 447-454, 2020.
[19] R Khalila, M Al Horania, A Yousefa and M Sababheh, A new definition of fractional derivative, J. Comput. Appl. Math. 264, 65 (2014)
[20] A. Atangana, D. Baleanu, A. Alsaedi, New properties of conformable derivative, Open Math, 13, 889–898, 2015.
[21] T. Abdeljawad, (2015). On conformable fractional calulus, J. Computational Applied Mathematics, 279, 57-66.
[22] Bogoyavlenskii OI. Overturning solitons in new two-dimensional integrable equations. Math USSR Izv 1990;34:245.
[23] O.I. Bogoyavlenskii, Breaking solitons in 2+1-dimensional integrable equations, Russian Mathematical Surveys, 45 (1990) 1-86.
[24] S. Yu, K. Toda, T. Fukuyama, N-Soliton Solutions to a New (2 + 1) Dimensional Integrable Equation, 1998.
[25] A. M. Wazwaz, A study on two extensions of the Bogoyavlenskii– Schieff equation, Communications in Nonlinear Science and Numerical Simulation, 17 (2012) 1500-1505.
[26] L. Han, S. Bilige, R. Zhang, M. Li, Study on exact solutions of a generalized Calogero–Bogoyavlenskii–Schiff equation, Partial Differential Equations in Applied Mathematics, 2, 100010, 2020.
[27] Z. Hammouch, T. Mekkaoui, and P. Agarwal, Optical solitons for the Calogero-Bogoyavlenskii-Schiff equation in (2 + 1) dimensions with time-fractional conformable derivative, Eur. Phys. J. Plus, 133: 248, 2018.
[28] S. M. Mabrouk, Traveling Wave Solutions of the Extended Calogero-Bogoyavlenskii-Schiff Equation, International Journal of Engineering Research & Technology, 8(6), 2019.
[29] C. M. Khalique, A. Mehmood, On the solutions and conserved vectors for the two-dimensional second extended Calogero-Bogoyavlenskii-Schiff equation, Results in Physics 25 (2021) 104194.

Improving the Mortality Prediction in Intensive Care Unit: Feature Contribution Approach with SuperLearner Algorithm

İsmail GÜR [1,2] **, Mustafa Asım ÖZALP** [1] **,Kasırga YILDIRAK** [1] **,Necmettin ÜNAL** [3]

[1] Department of Actuarial Sciences, Hacettepe University, Ankara, Turkey

[2] Department of Actuary, Firat University, Elazig, Turkey

[3] Department of Anesthesiology&Intensive Care, Ankara University, Ankara, Turkey

m.asim.ozalp@hacettepe.edu.tr, ismail.gur@hacettepe.edu.tr, kasirga@hacettepe.edu.tr, mnunal@ankara.edu.tr,

Abstract

Mortality prediction is highly important issue on the actuarial perspective. For the mortality prediction, MIMIC-III database is examined. This dataset has various information about patients in intensive care units at Beth Israel Hospitals. The most crucial cause of deaths in the hospital is considered as Sepsis. Sepsis is defined as a serious condition resulting from the presence of harmful microorganisms in the blood or other tissues and the body's response to their presence, potentially leading to the malfunctioning of various organs, shock, and death [1].

In medical literature, many measures such as SOFA, SIPS, LODS, SIRS are examined for the sepsis-based organ failure assessment scores which are used to track patients' status in an intensive care unit. These measures are used with different variables as well as common variables. Statistically, the main difference between these measures is the variables used.

In this study, all variables in predetermined measures, and some additional variables, which are frequently discussed in the medical literature on explaining sepsis, are included in the analysis. The contribution of additional variables for improving the model accuracy is shown. In addition, a comparison with the SOFA criterion is performed. The life / death status of patients in intensive care unit is considered as a data mining problem and modeled with the SuperLearner algorithm.

Keywords: Machine learning, SuperLearner Algorithm, MIMIC-III, Sepsis, Sepsis severity scores, Statistical learning

1. Introduction

Systemic illness caused by the presence of harmful microorganisms in blood or tissue and the response of ill-body for recovering from these microorganisms that potentially, results as malfunction of the various, organs. These situations sometimes induce serious conditions like shocks or deaths, refers "sepsis". The one of four deaths of patients are caused by severe sepsis and septic shock. If illness progress severely, severe sepsis concludes as organ dysfunction. Hypotension persistency that affects blood pressure proceeds and patient enters into septic shock. Both severe sepsis and septic shock has vital results that resulted in permanent organ damage, physical or mental disability, morbidity, and lastly mortality. Recovering from all these results can be possible by back-breaking and highly costly treatments for healthcare systems [1,2,3,4].

In this study we use Multi-parameter Intelligent Monitoring in Intensive Care (MIMIC) data for analyzing the patient situations due to data reliability and ease of handling of patient database. MIMIC-III contains of more than 60000 admissions in Beth Israel Hospitals. In this datasets, the demographics, vital signs, necessary laboratory tests and used medications for each critical care patients are stored in this database. In medical literature, rule-based sepsis severity scores which are SOFA, SIPS, LODS, SIRS etc. are examined for sepsis based organ failure process. These scores mainly used to diagnose and track patients' status in stay on intensive care unit (ICU) [5,6].

By the technological progress on both medical and computational sciences, electronic health records have been stored in relevant database as MIMIC III. Therefore, detection and prediction of sepsis using machine learning and statistical learning methods have been proposed. Some of these studies are given below. Artificial neural networks [7] and dynamic Bayesian networks [8] , Survival-analytic models [9,10], and feature engineering [11,12] methods are proposed. The aim of these studies is to model and develop rule based systems, to unveil patients' responses in intensive care period and identify correlations between variables as much as possible.

In literature, deep learning algorithms are used besides SuperLearner algorithms for mortality, length of stay, ICD-9 code predictions [13,17]. SuperLearner algorithms are used for modelling different illnesses and social issues like HIV [14,22], prison violence [15], prostate cancer [16], colorectal cancer [18], osteoporotic hip fracture [19], tumor motion [20].

This study uses a dataset which consists 3216 adult ICU patients' records from MIMIC-III. Firstly, existed score models are executed in this study. After then, candidate variables that is not included in SOFA scores are added in models and the response of the models are calculated. MIMIC-III data set is analyzed by embedded models in Super-Learner algorithm. The accuracy of diagnosis in candidate models are determined by ROC curve values and the contribution of each variable in models can be calculated by the difference in AUC values.

2. Super-Learner Algorithm

For constructing prediction models for health-datasets, the most important issue is selecting or defining the best prediction models. By this purpose, Super Learner algorithm, presented by Polley et al. [23], aims to compare the performance of candidate machine learning algorithms by using cross-validation structure. Besides, it works as "ensemble models" that creates a linear combination of those models. By this approach, the best prediction model can be found by combination of embedded models.

The key measure of this algorithm, risk is the measure of model performance or accuracy. Basic purpose of using this embedded model is minimizing the estimated risk. Unless this model works well, prediction errors become fewer. This definition behaves in a same role like, Mean Square Error in regression models.

The weight of each individual learner in ensemble models shows us the relative importance of each models in ensemble. Theoretically, sum of weights equal 1 and each weights are greater than 0. If one model is wanted to execute, the weight has to be 1, and if it is happened, ensemble models can't be used for prediction improvement.

Each model in this ensemble models has its own hyper parameters which can be customized by users, or fitted by after data-driven testing. Data can be splitted two components, training, testing basically. By these stages, parameters of models can be fitted and models can become comparable. The impact or significance of each parameter for candidate models can be tested.

After preprocessing of MIMIC dataset, 10 mutually exclusive data-groups are separated randomly. By utilizing each candidate models, nine groups are used as training set for estimating the parameters of these candidate models. Our aim to predict the survival probability of patients in this datasets. After that remained one group as testing set, is used for calculating loss of modelling. This calculation is repeated for each mutually-exclusive group and cross-validation risk can be obtained. The least cross-validation risk for candidate models, the best candidate algorithm is selected.

Our aim in this study, calculating the effects of adding different features in the candidate models, when patient's survival probabilities become target for prediction. Selecting the best candidate models is the keypoint of the study. SuperLearner has many different type candidate models like, Random Forest, Decision Tree, Generalized Additive Models(GAM), Gradient Boosting Machines(GBM), Generalized Linear Models(GLM), K-Nearest Neighbors(KNN), Support Vector Machines(SVM), Logistic Regression, Basic Neural Networks(NN), XGBoost etc.. These candidate models can be compared with different model evaluation methods, like loss values for cross-validated data or AIC-BIC values for parametric model fitting, or AUC values for results on classification of dead or alive patients in cross-validated data [21]. If we get minimum loss values/minimum AIC or BIC/ maximum AUC values, the best candidate model can be determined. In our problem, AUC values are behold for comparison of models in Table 3.

$$AIC = -2\log L(\hat{\theta}) + 2k$$

where,θ,$L(\widehat{\theta}), k$ represents the vector of parameters, the likelihood of the model which executed with $\hat{\theta}$ and the number of parameters in the model successively.

$$BIC = -2\log L(\hat{\theta}) + klog(n)$$

Additionally ,n, the number of observations, used in BIC computation.

ROC (Receiver Operating Characteristics) Curve

For diagnosing the binary predictor, sensivity and specificity terms need to be evaluated. ROC curse, simply shows us, a plot of sensivity vs 1- specifity values of a diagnostic test. For interpretation, we have to pay attention to the area under curve in this plot. AUC value is computed by trapezoid rule.It takes values from [0,1] and if it takes nearly 0, it shows inaccurate prediction or diagnosis, whereas, if it takes nearly 1, model shows us accurate prediction results. If it takes 0.5 values, it shows us that assignment or diagnosis of patients become randomly, so it can't be acceptable. As a result, if AUC takes values between [0.5,1], our model can become candidate for comparison.

3. Model Implementation

In this study, intensive care patients aged between 18 and 65, available in the MIMIC III database, were examined. Mortality in the first 24 hours was estimated by examining the laboratory results and vital signs on the first day in intensive care. In the Mimic III data set, although there were 18809 patients with a SOFA score greater than 1 in the 18-65 age range are existed, missing status is encountered in the laboratory results and vital signs of 15593 patients. Patients with these missing observations were excluded from the analysis. Therefore, the observations of 3216 patients were examined. Statistical information about death rates and ages of 3216 patients within 24 hours is given in Table 1.

Table 1:Descriptive Statistics for MIMIC III database

	Total	Female	Male
n	3216	1228	1988
Death Rate	0.058	0.059	0.058
Minimum(Age)	18.09	18.09	18.26
Median (Age)	53.55	53.53	53.58
Mean (Age)	50.64	50.50	50.73
Variance (Age)	127.36	128.76	126.54
Maximum (Age)	64.98	64.98	64.97

The aim of this study is to investigate the effects of vital signs, glucose, hemoglobin and lactate variables on mortality within 24 hours as well as biliribin_max, creatinine_max, platelet_min, urineoutput, pao2fio2_min and mingcs variables used in SOFA score calculation. The variables used in the analysis are given in Table 2.

Table 2:Used Variables in Mortality Prediction Model

1	heartrate_min	2	heartrate_max	3	sysbp_min	4	sysbp_max
5	diasbp_min	6	diasbp_max	7	meanbp_min	8	meanbp_max
9	resprate_min	10	resprate_max	11	tempc_min	12	tempc_max
13	glucose_max	14	bilirubin_max	15	creatinine_max	16	hemoglobin_max
17	lactate_min	18	platelet_min	19	Urineoutput	20	pao2fio2_novent_min
21	pao2fio2_vent_min	22	Mingcs				

4. Results

Machine learning methods are used to predict mortality in intensive care patients within the first 24 hours. However, there are many machine learning algorithms in the literature, like Random Forests, Decision Trees, Artificial Neural Networks, Naive Bayes etc. It is important to choose the best method to achieve optimal results. For this reason, the SuperLearner algorithm has been reached by hosting the best performing methods that apply multiple machine learning methods with ensemble techniques. (Performance criterion: NNLS (The Lawson-Hanson algorithm for non-negative least squares). Multiple performance criteria have been tried, but the best results have been obtained with NNLS.) Mortality status in 24-hour is modeled with SuperLearner algorithm. Model results are given in Table 3.

Table 3:AUC and Sensitivity Results of Models

	Variables in Model	AUC	Sensitivity
SuperLearner Algorithm	Sofa variables, Heartrate, Sysbp and Lactate	0.922	0.886-0.957
	Sofa variables and Heartrate	0.895	0.853-0.938
	Sofa variables and Sysbp	0.888	0.838-0.938
	Sofa variables and meanbp	0.879	0.838-0.917
	Sofa variables and Daisbp	0.864	0.811-0.917
	Sofa variables and Lactate	0.86	0.799-0.920
	Sofa variables and Hemog	0.848	0.791-0.905
	Sofa variables and Resprate	0.847	0.794-0.899
	Sofa variables and Temp	0.847	0.792-0.802
	Sofa variables and Glucose	0.845	0.788-0.902
	Sofa variables and Age	0.836	0.78-0.893
	Sofa variables	0.843	0.794-0.894
Default Sepsis Scores	ApsIII	0.817	0.769-0.866
	Lods	0.823	0.823-0.881
	Mlods	0.781	0.714-0.849
	Saps	0.835	0.785-0.884
	Sofa	0.787	0.724-0.851
*Sofa Variables:biliribin_max, creatinine_max, platelet_min, urineoutput, pao2fio2_min ve mingcs			

When the AUCs obtained were compared;

• For Sofa variables, it can be determined that the SuperLearning algorithm is 5.6% better than its current scores.

• In the modeling based on mortality within 24 hours, vital signs showed an average increase of 5% in AUC.

• In the modeling based on mortality within 24 hours, Lactate provided an increase of approximately 2% in AUC.

• In the modeling based on mortality within 24 hours, the effect of age, hemoglobin and glaucous variables on the increase in AUC is less than 0.5%.

5. Conclusion

According to these results, it can be suggested that vital signs and lactate variables are effective in explaining mortality within 24 hours. As a result of the analysis made with the sofa variables, heartrate_min, sysbp_min and lactate variables, AUC was determined to be 92.2%. In addition to the variables used in sofa scoring, heartrate_min, sysbp_min and lactate provided a 7.9% increase in the explanation of 24-hour mortality.

6. References

[1] Angus, Derek C., et al. "Epidemiology of severe sepsis in the United States: analysis of incidence, outcome, and associated costs of care." Read Online: Critical Care Medicine| Society of Critical Care Medicine 29.7 (2001): 1303-1310.

[2] Healthcare Cost and Utilization Project (HCUP. "HCUP Facts and Figures: Statistics on Hospital-Based Care in the United States, 2009 [Internet]." (2011).

[3] Levy, Mitchell M., et al. "2001 sccm/esicm/accp/ats/sis international sepsis definitions conference." Intensive care medicine 29.4 (2003): 530-538.

[4] Dellinger, R. Phillip, et al. "Surviving Sepsis Campaign: international guidelines for management of severe sepsis and septic shock, 2012." Intensive care medicine 39.2 (2013): 165-228.

[5] Vincent, Jean-Louis, et al. "Use of the SOFA score to assess the incidence of organ dysfunction/failure in intensive care units: results of a multicenter, prospective study." Critical care medicine26.11 (1998): 1793-1800.

[6] Churpek, Matthew M., et al. "Incidence and prognostic value of the systemic inflammatory response syndrome and organ dysfunctions in ward patients." American journal of respiratory and critical care medicine 192.8 (2015): 958-964.

[7] Lipton, Zachary C., et al. "Learning to diagnose with LSTM recurrent neural networks." arXiv preprint arXiv:1511.03677(2015).

[8] Nachimuthu, Senthil K., and Peter J. Haug. "Early detection of sepsis in the emergency department using Dynamic Bayesian Networks." AMIA Annual Symposium Proceedings. Vol. 2012. American Medical Informatics Association, 2012.

[9] Henry, Katharine E., et al. "A targeted real-time early warning score (TREWScore) for septic shock." Science translational medicine 7.299 (2015): 299ra122-299ra122.

[10] Nemati, Shamim, et al. "An interpretable machine learning model for accurate prediction of sepsis in the ICU." Critical care medicine 46.4 (2018): 547-553.

[11] Mao, Qingqing, et al. "Multicentre validation of a sepsis prediction algorithm using only vital sign data in the emergency department, general ward and ICU." BMJ open 8.1 (2018): e017833.

[12] Calvert, Jacob S., et al. "A computational approach to early sepsis detection." Computers in biology and medicine 74 (2016): 69-73.

[13] Purushotham, Sanjay, et al. "Benchmark of deep learning models on large healthcare mimic datasets." arXiv preprint arXiv:1710.08531 (2017).

[14] Houssaïni, Allal, et al. "Investigation of Super Learner methodology on HIV-1 small sample: application on Jaguar Trial Data." AIDS research and treatment 2012 (2012).

[15] Baćak, Valerio, and Edward H. Kennedy. "Principled machine learning using the super learner: an application to predicting prison violence." Sociological Methods & Research 48.3 (2019): 698-721.

[16] Essilfie-Amoah, Ebo. "Application of SuperLearner Algorithm on Prostate Cancer Data." (2018).

[17] Golmakani, Marzieh K., and Eric C. Polley. "Super Learner for Survival Data Prediction." The International Journal of Biostatistics (2020).

[18] Li, Jiqing, et al. "Development and validation of a Super learner-based model for predicting survival in Chinese Han patients with resected colorectal cancer." Japanese Journal of Clinical Oncology 50.10 (2020): 1133-1140.

[19] Engels, Alexander, et al. "Osteoporotic hip fracture prediction from risk factors available in administrative claims data–A machine learning approach." PloS one 15.5 (2020): e0232969.

[20] Lin, Hui, et al. "A Super-Learner Model for tumor Motion prediction and Management in Radiation therapy: Development and feasibility evaluation." Scientific reports 9.1 (2019): 1-11.

[21] Kabir, Md Faisal, and Simone A. Ludwig. "Enhancing the performance of classification using Super Learning." Data-Enabled Discovery and Applications 3.1 (2019): 5.

[22] Petersen, Maya L., et al. "Super learner analysis of electronic adherence data improves viral prediction and may provide strategies for selective HIV RNA monitoring." Journal of acquired immune deficiency syndromes (1999) 69.1 (2015): 109.

[23] Polley, Eric C., and Mark J. Van der Laan. "Super learner in prediction." (2010).

A Novel Analytical Method to the Equation System of Ion-acoustic and Langmuir Waves in Plasmas Physics

Gülnur Yel[1*], Beyhan Kemaloğlu[2], Hasan Bulut[2]
[1]Faculty of Education, Final International University, Kyrenia, Mersin 10, Turkey
[2]Department of Mathematics, Firat University, Elazig, Turkey
gulnur.yel@final.edu.tr, beyhanozturk1980@gmail.com, hbulut@firat.edu.tr

Abstract
In this research, we apply a newly developed analytical scheme which is the rational sine-Gordon expansion method to construct novel solutions of a governing model for the ion-acoustic and Langmuir waves. All the solutions achieved have been analyzed graphically to reveal their physical properties. We concluded that the proposed method is an efficient method that gives more general analytical solutions to powerfully nonlinear partial differential models.

Keywords: The rational sine-Gordon expansion method; ion-acoustic wave; Langmuir wave; plasma physics; solitary wave solutions

1. Introduction

The nonlinear models have been arisen to describe natural phenomena in many fields such as optics, fluid dynamics, biology, chemistry, engineering, physics and many others describing nonlinear dynamical systems. These governing models have more difficulties to find analytical solutions than linear models. Mathematicians have developed so many analytical techniques to overcome these problems in recent years [1-11]. Every technique has some complications and not suitable to every governing models in application. This research study proposes an analytical method that has easy application to even high-nonlinear differential models and gives more general implicit analytical solutions. The proposed method, the rational sine-Gordon expansion method (RSGEM), is based on well-known the sine- Gordon expansion method.

Waves, acoustic waves, shallow-water waves, electromagnetic waves, seismic waves, help us to understand the behaviours of nonlinear dynamics in nature. Ion-acoustic waves are a type of longitudinal wave which oscillate in the direction of propagation. Langmuir waves, are also longitudinal wave, are speedy oscillations of the electron density in plasmas. The ion acoustic waves were firstly predicted based on the fluid dynamics in 1929 [13] and the first experimental observation was reported in 1933 [14]. After that time, researchers have submitted various studies on ion-acoustic and Langmuir waves in mathematics and physics. Ion-sound waves emissions by Langmuir soliton are investigated and formulated [15]. The properties of non-linear Langmuir waves in a multi-ion component plasma were investigated and it was concluded that the presence of more than one ion species in a plasma has significant effects on localized structures for non-linear Langmuir waves [16]. The ion acoustic and Langmuir waves equations system is analysed by the modulation instability analysis technique which has the standard linear stability analysis and the modulation instability gain spectrum analysis [17]. The three analytical shemes which are the extended simple equation, modified F-expansion and $\exp(-(\xi))$ expansion methods, have been used to find out wave solutions the equations system [18]. Using the improved $\tan\left(\phi(\xi)/2\right)$ -expansion method, kinks, singular kink-type and periodic solutions are obtained by Manafian [19]. Many other studies can be seen in detail [20-28].

This paper is organised as: In 2nd section, we give fundamental steps of the proposed method. The implementations of the analytical method to governing model and 2D, 3D and contour plots corresponding to all wave solutions are submitted in 3th section. Finally, we present some conclusions of this framework in last section 4.

2. Fundamental Structure of the RSGEM

In this section, we explain fundamental steps of the RSGEM.

Let's consider the nonlinear partial differential equation (NPDE) of the form below, for which the solution is searched ;

$$P\left(\varphi,\varphi_x,\varphi_t,\varphi_{xx},\varphi_{tt},\varphi_{xt},\varphi_{xxx},\varphi_{xxt},\ldots\right)=0, \tag{1}$$

$$N\left(\Phi,\Phi',\Phi'',\ldots\right)=0, \tag{2}$$

here N is a nonlinear ordinary equation (NODE) which has partial derivatives of Φ depends on ξ .

We suppose that the solution of Eq. (1) is considered in the following form [12],

$$\Phi\left(\xi\right)=\frac{\sum_{i=1}^{M}\tanh^{i-1}\left(\xi\right)\left[A_i\sec h\left(\xi\right)+C_i\tanh\left(\xi\right)\right]+A_0}{\sum_{i=1}^{M}\tanh^{i-1}\left(\xi\right)\left[B_i\sec h\left(\xi\right)+D_i\tanh\left(\xi\right)\right]+B_0.}, \tag{3}$$

which is also written as

$$\Phi\left(\varpi\right)=\frac{\sum_{i=1}^{M}\cos^{i-1}\left(\varpi\right)\left[A_i\sin\left(\varpi\right)+C_i\cos\left(\varpi\right)\right]+A_0}{\sum_{i=1}^{M}\cos^{i-1}\left(\varpi\right)\left[B_i\sin\left(\varpi\right)+D_i\cos\left(\varpi\right)\right]+B_0}. \tag{4}$$

A_i,B_i,C_i,D_i,A_0,B_0 are constants to be determined later.

By using $\varpi\left(\xi\right)=\frac{\Phi}{2}$ and $\varpi'\left(\xi\right)=\sin\varpi$, we get significant properties that are given as follows;

$\sin\left(\varpi\right)=\sec h\left(\xi\right)$ and $\cos\left(\varpi\right)=\tanh\left(\xi\right)$.

The values of A_i, B_i, C_i, D_i are not zero at the same time. Applying the homogeneous balance principle between the highest power nonlinear term and highest derivative in NODE the value of M is identified. Reduction the expression that corresponds to the same denominator and taking the coefficients of $\sin^i(\varpi)\cos^j(\varpi)$ to zero, this results in a set of algebraic equation $A_i, B_i, C_i, D_i, A_0, B_0$ values are found solving the set of algebraic equations by software. We substitute these values into Eq.(3) and get the new travelling wave solutions to the Eq.(1).

3. Application of the RSGEM

The equation model for Langmuir waves and ion sound waves [32,33]

$$\begin{aligned} &iE_t + \frac{1}{2}E_{xx} - nE = 0, \\ &n_{tt} - n_{xx} - 2\left(|E|^2\right)_{xx} = 0, \end{aligned} \tag{5}$$

where E represents electric field of the Langmuir oscillation and n represents density perturbation in the normalized form.

Let suppose that the wave transforms as follows;

$$\begin{aligned} &E(x,t) = U(\xi)e^{i\phi}, n(x,t) = V(\xi), \\ &\xi = rx + st, \phi = px + qt, \end{aligned} \tag{6}$$

where r, s, p, q are constants and will be determine later, $e^{i\phi}$ is an exponential function of $i\phi$.

Using wave transforms we find first and second partial derivatives of E and n with respect to x and t. We put them into Eq.(5) and integrate twice with respect to ξ getting integration constant zero, the followings are obtained.

$$V(\xi) = \frac{2U^2(\xi)}{p^2 - 1}, s = -rp. \tag{7}$$

After some mathematical operations, we have non-linear ordinary differential equation as,

$$r^2\left(p^2 - 1\right)U'' - \left(p^2 - 1\right)\left(2q + p^2\right)U - 4U^3 = 0. \tag{8}$$

According to homogeneous balance principle, it yields $M = 1$. For $M = 1$, Eq. (4) turns to

$$U(\xi) = \frac{A_1\sin(\zeta) + C_1\cos(\zeta) + A_0}{B_1\sin(\zeta) + D_1\cos(\zeta) + B_0}. \tag{9}$$

We put Eq.(9) and its second-order derivative into Eq.(8), which yields a polynomial in powers of $\sin^i(\xi)\cos^j(\xi)$ functions. Collecting the coefficients of similar powers of $\sin^i(\xi)\cos^j(\xi)$ and equate all summation to zero, we can obtain a system of algebraic equations. By using a software program, $A_1, B_1, C_1, D_1,\ A_0, B_0$ and the other parameters can be found. Finally, we put these coefficients into Eq.(3) and obtain new travelling wave solutions of the Eq.(5).

CASE 1: For

$$A_1 = \frac{1}{2}\sqrt{\left(-1+p^2\right)\left(p^2+2q\right)\left(B_0^2-D_1^2\right)}, A_0 = \frac{1}{2}i\sqrt{\left(-1+p^2\right)\left(p^2+2q\right)}D_1, B_1 = 0,$$

$$C_1 = \frac{1}{2}i\sqrt{\left(-1+p^2\right)\left(p^2+2q\right)}B_0, r = \sqrt{2\left(-p^2-2q\right)},$$

where $i^2 = -1$, putting these values into Eq.(3), it yields

$$n_1(x,t) = \frac{\left(p^2+2q\right)\left(iD_1 + \mathrm{Sech}[prt-rx]\sqrt{B_0{}^2-D_1{}^2} - iB_0\,\mathrm{Tanh}[prt-rx]\right)^2}{2\left(B_0 - D_1\,\mathrm{Tanh}[prt-rx]\right)^2},$$

$$E_1(x,t) = \frac{e^{i(qt+px)}\sqrt{-1+p^2}\sqrt{p^2+2q}\left(iD_1 + \mathrm{Sech}[prt-rx]\sqrt{B_0{}^2-D_1{}^2} - iB_0\,\mathrm{Tanh}[prt-rx]\right)}{2\left(B_0 - D_1\,\mathrm{Tanh}[prt-rx]\right)}.$$

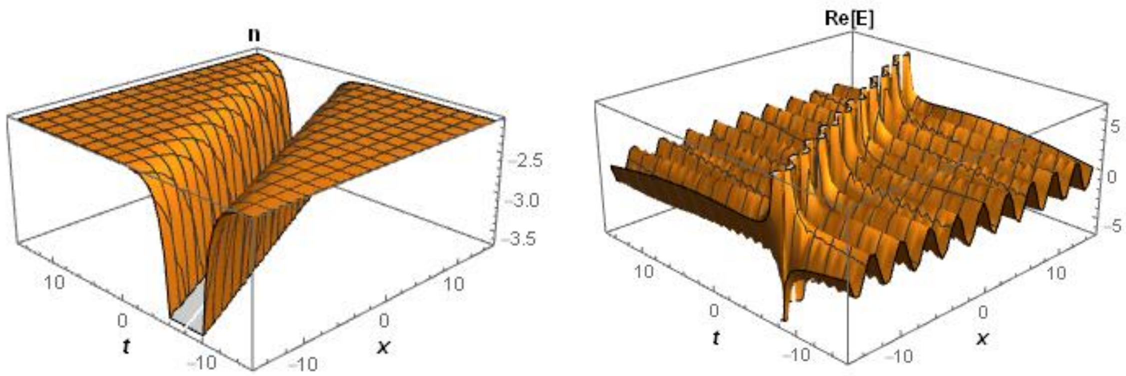

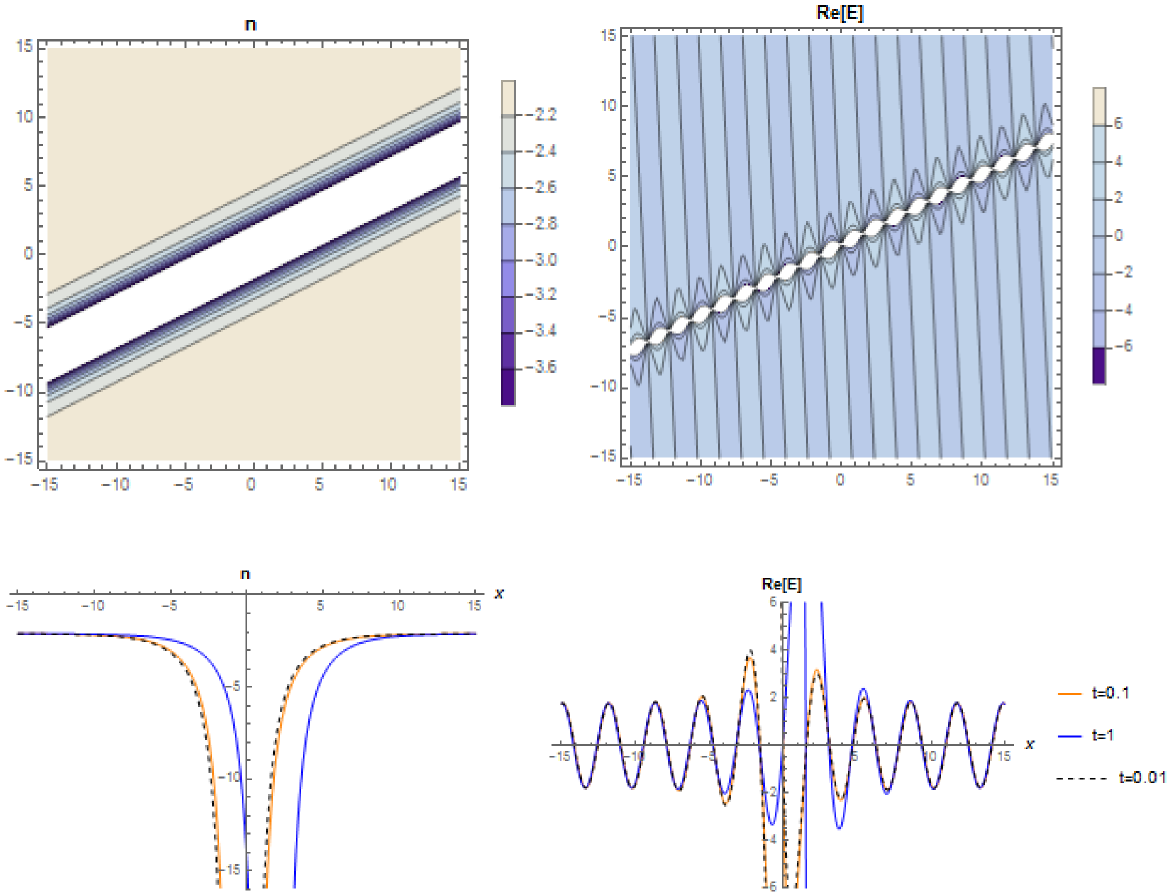

Figure 1: 3D, contour surfaces of $E_1(x,t)$ and $n_1(x,t)$ for the values $p=2, q=0.1, r=0.5, B_0=0.2, D_1=1$ and 2D views under the different values of t.

CASE 2: For

$$A_1=\frac{1}{2}\sqrt{4A_0^{\,2}+\frac{1}{2}\left(-1+p^2\right)r^2B_1^{\,2}},\ B_0=0,\ C_1=0,\ D_1=\frac{2\sqrt{2}A_0}{\sqrt{\left(-1+p^2\right)r^2}},\ q=\frac{1}{4}\left(-2p^2-r^2\right),$$

putting these values into Eq.(3), it yields

$$n_2(x,t)=\frac{2\left(A_0+\frac{1}{2}\mathrm{Sech}[prt-rx]\sqrt{4A_0^{\,2}+\frac{1}{2}\left(-1+p^2\right)r^2B_1^{\,2}}\right)^2}{\left(-1+p^2\right)\left(\mathrm{Sech}[prt-rx]B_1-\frac{2\sqrt{2}A_0\,\mathrm{Tanh}[prt-rx]}{\sqrt{\left(-1+p^2\right)r^2}}\right)^2},$$

$$E_2(x,t)=\frac{e^{i\left(\frac{1}{4}\left(-2p^2-r^2\right)t+px\right)}\left(A_0+\frac{1}{2}\mathrm{Sech}[prt-rx]\sqrt{4A_0^{\,2}+\frac{1}{2}\left(-1+p^2\right)r^2B_1^{\,2}}\right)}{\mathrm{Sech}[prt-rx]B_1-\frac{2\sqrt{2}a_0\,\mathrm{Tanh}[prt-rx]}{\sqrt{\left(-1+p^2\right)r^2}}}.$$

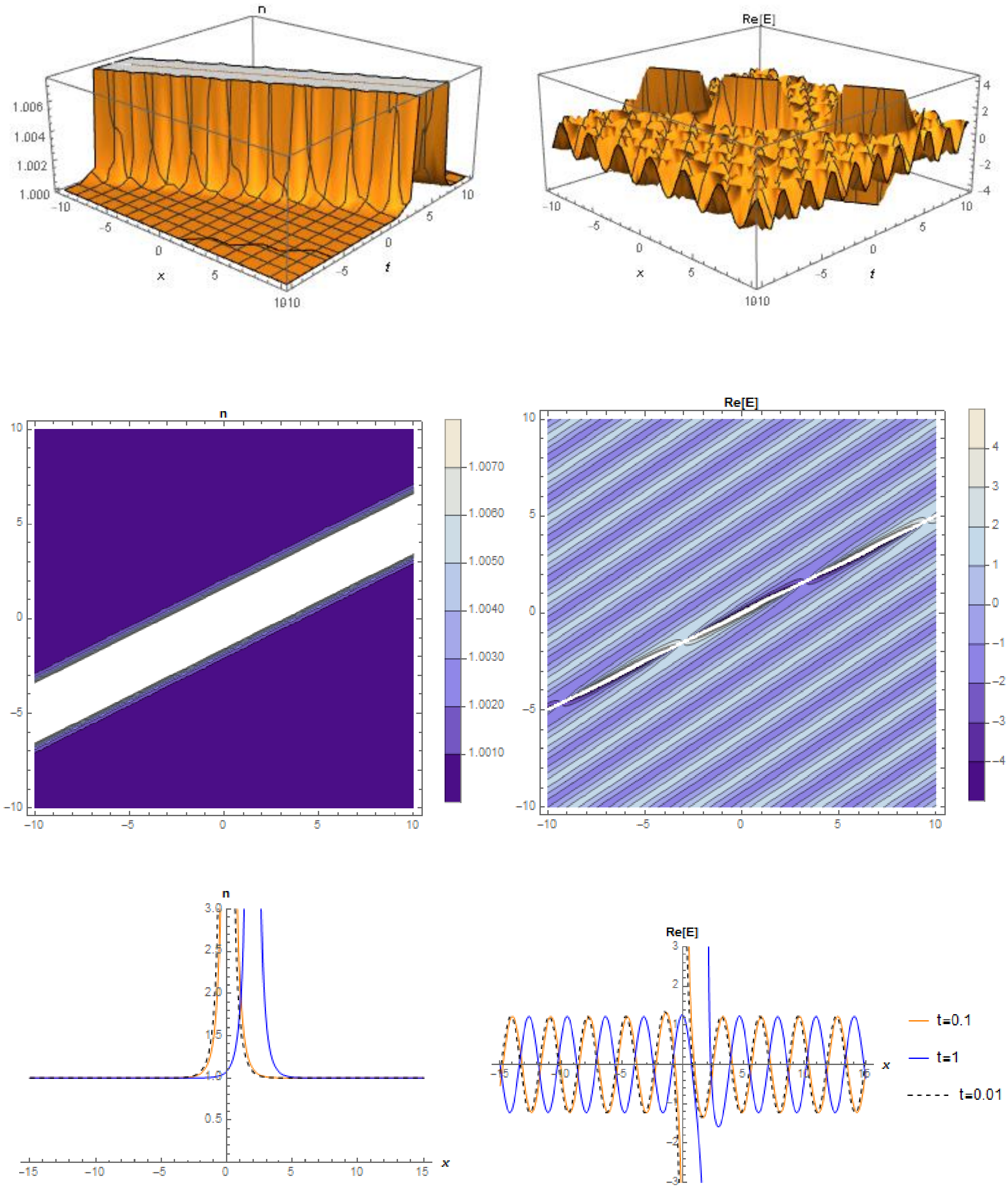

Figure 2: 3D, contour surfaces of $E_2(x,t)$ and $n_2(x,t)$ for the values $p=2, q=0.5, r=2, A_0=2, B_1=0.1$ and 2D views under the different values of t.

CASE 3: For

$$A_1=\frac{1}{2}\sqrt{4A_0^{\ 2}-\frac{1}{2}(-1+p^2)r^2\left(b_0^{\ 2}-b_1^{\ 2}\right)},\ C_1=-\frac{\sqrt{(-1+p^2)r^2}B_0}{2\sqrt{2}},\ D_1=-\frac{2\sqrt{2}A_0}{\sqrt{(-1+p^2)r^2}},\ q=\frac{1}{4}\left(-2p^2-r^2\right),$$

putting these values into Eq.(3), it yields

$$n_3\left(x,t\right)=\frac{2\left(A_0+\dfrac{\operatorname{Sech}[prt-rx]\left(\sqrt{\left(-1+p^2\right)r^2}\operatorname{Sinh}[prt-rx]B_0+\sqrt{8A_0^{\ 2}+\left(-1+p^2\right)r^2\left(-B_0^{\ 2}+B_1^{\ 2}\right)}\right)}{2\sqrt{2}}\right)^2}{\left(-1+p^2\right)\left(B_0+\operatorname{Sech}[prt-rx]B_1+\dfrac{2\sqrt{2}A_0\operatorname{Tanh}[prt-rx]}{\sqrt{\left(-1+p^2\right)r^2}}\right)^2},$$

$$E_3\left(x,t\right)=\frac{e^{i\left(\frac{1}{4}\left(-2p^2-r^2\right)t+px\right)}\left(A_0+\dfrac{\operatorname{Sech}[prt-rx]\left(\sqrt{\left(-1+p^2\right)r^2}\operatorname{Sinh}[prt-rx]B_0+\sqrt{8A_0^{\ 2}+\left(-1+p^2\right)r^2\left(-B_0^{\ 2}+B_1^{\ 2}\right)}\right)}{2\sqrt{2}}\right)}{B_0+\operatorname{Sech}[prt-rx]B_1+\dfrac{2\sqrt{2}A_0\operatorname{Tanh}[prt-rx]}{\sqrt{\left(-1+p^2\right)r^2}}}.$$

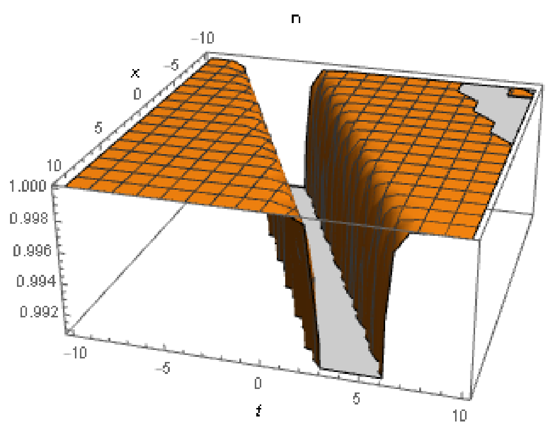

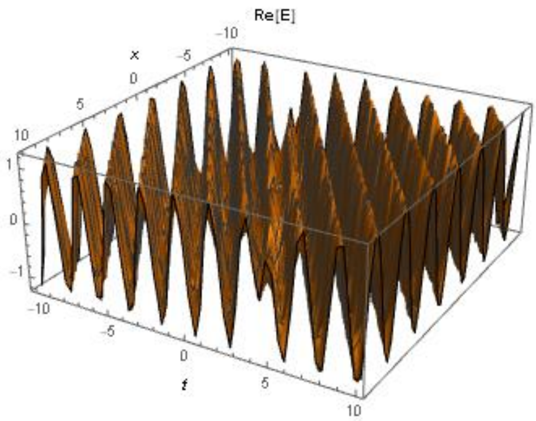

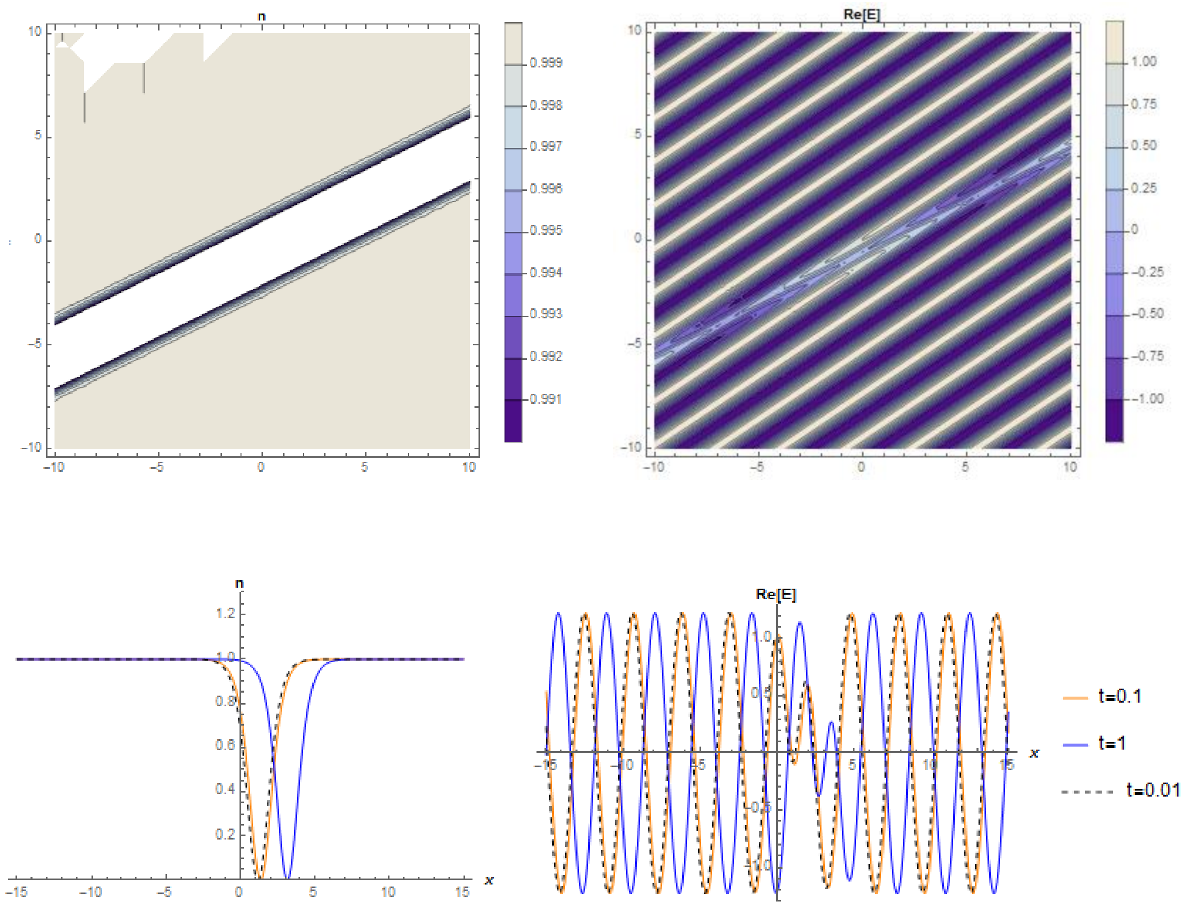

Figure 3: 3D, contour surfaces of $E_3(x,t)$ and $n_3(x,t)$ for the values $p=2, q=0.5, r=2, B_0=2, B_1=2$ and 2D views under the different values of t.

CASE 4: For

$$B_0=-\frac{\sqrt{A_0^2-A_1^2}D_1}{A_0},\ B_1=0,\ C_1=-\sqrt{A_0^2-A_1^2},\ r=-\frac{2\sqrt{2}A_0}{\sqrt{(-1+p^2)D_1^2}},\ q=-\frac{p^2}{2}-\frac{2A_0^2}{(-1+p^2)D_1^2},$$

putting these values into Eq.(3), it yields

$$n_4(x,t)=\frac{2\left(A_0+\mathrm{Sech}[\psi(x,t)]A_1-\sqrt{A_0^2-A_1^2}\,\mathrm{Tanh}[\psi(x,t)]\right)^2}{(-1+p^2)D_1^2\left(-\frac{\sqrt{A_0^2-A_1^2}}{A_0}+\mathrm{Tanh}[\psi(x,t)]\right)^2},$$

$$E_4(x,t) = \frac{e^{i\left(px+t\left(-\frac{p^2}{2}-\frac{2A_0^2}{\left(-1+p^2\right)D_1^2}\right)\right)}\left(A_0+\mathrm{Sech}[\psi(x,t)]A_1-\sqrt{A_0^2-A_1^2}\,\mathrm{Tanh}[\psi(x,t)]\right)}{D_1\left(-\frac{\sqrt{A_0^2-A_1^2}}{A_0}+\mathrm{Tanh}[\psi(x,t)]\right)},$$

where $\psi(x,t)=\frac{2\sqrt{2}pA_0t}{\sqrt{\left(-1+p^2\right)D_1^2}}-\frac{2\sqrt{2}A_0x}{\sqrt{\left(-1+p^2\right)D_1^2}}$.

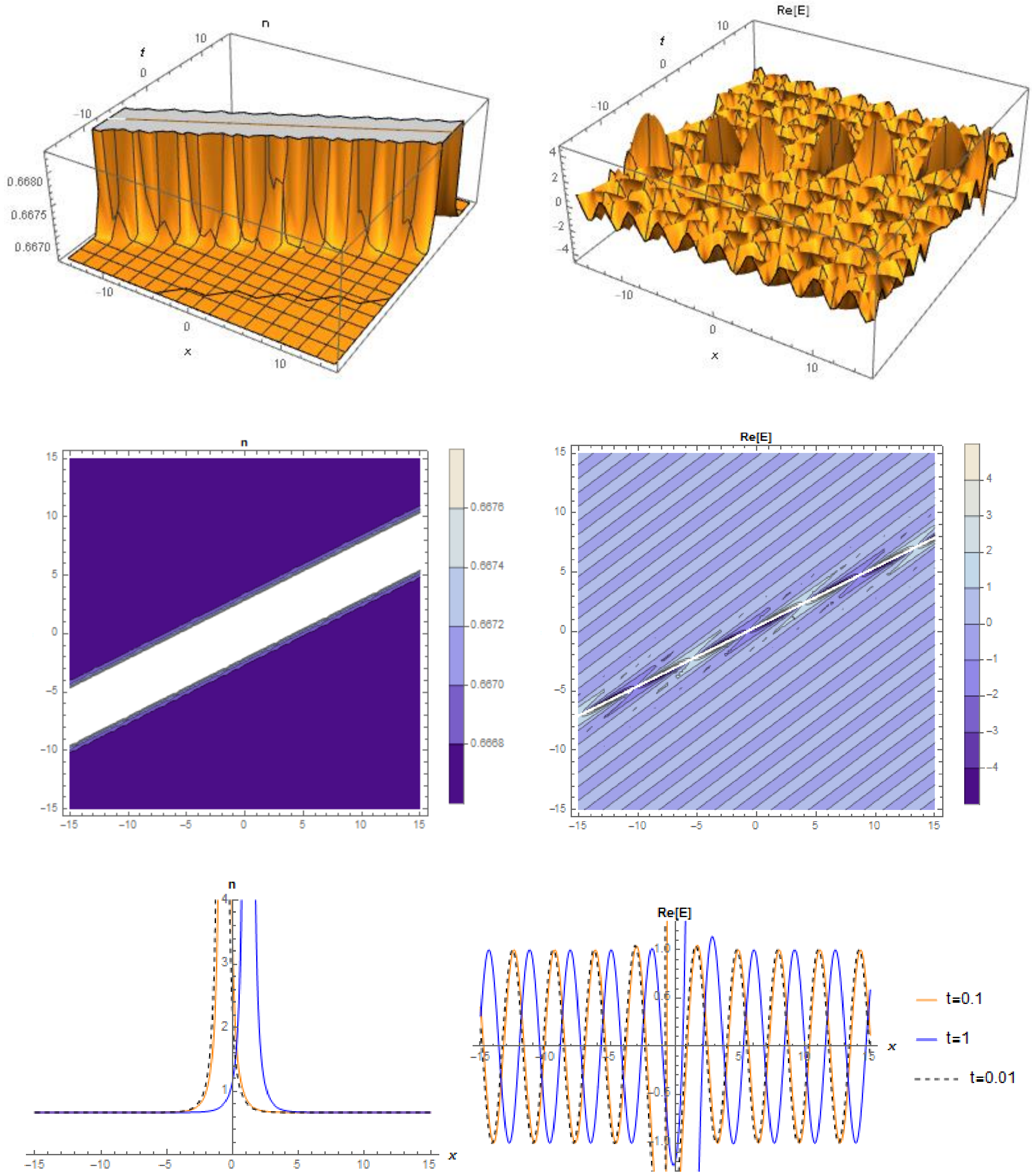

Figure 4: 3D, contour surfaces of $E_4(x,t)$ and $n_4(x,t)$ for the values $p=2, q=0.5, r=2, A_0=2, A_1=1, D_1=2$ and 2D views under the different values of t.

CASE 5: For

$$B_0=-\frac{\sqrt{-A_1^2D_1^2+A_0^2\left(B_1^2+D_1^2\right)}}{A_0},\; C_1=-\frac{\sqrt{-A_1^2D_1^2+A_0^2\left(B_1^2+D_1^2\right)}}{D_1}, r=\frac{2\sqrt{2}A_0}{\sqrt{\left(-1+p^2\right)D_1^2}},$$

$$q=-\frac{p^2}{2}-\frac{2A_0^2}{\left(-1+p^2\right)D_1^2},$$

putting these values into Eq.(3), it yields

$$n_5(x,t)=\frac{2\left(A_0+\mathrm{Sech}[\psi(x,t)]A_1+\frac{\sqrt{-A_1^2D_1^2+A_0^2\left(B_1^2+D_1^2\right)}\,\mathrm{Tanh}[\psi(x,t)]}{d_1}\right)^2}{\left(-1+p^2\right)\left(\mathrm{Sech}[\psi(x,t)]B_1-\frac{\sqrt{-A_1^2D_1^2+A_0^2\left(B_1^2+D_1^2\right)}}{A_0}-D_1\,\mathrm{Tanh}[\psi(x,t)]\right)^2},$$

$$E_5(x,t)=\frac{e^{i\left(px+t\left(-\frac{p^2}{2}-\frac{2A_0^2}{\left(-1+p^2\right)D_1^2}\right)\right)}\left(A_0+\mathrm{Sech}[\psi(x,t)]A_1+\frac{\sqrt{-A_1^2D_1^2+A_0^2\left(B_1^2+D_1^2\right)}\,\mathrm{Tanh}[\psi(x,t)]}{D_1}\right)}{\mathrm{Sech}[\psi(x,t)]B_1-\frac{\sqrt{-A_1^2D_1^2+A_0^2\left(B_1^2+D_1^2\right)}}{A_0}-D_1\,\mathrm{Tanh}[\psi(x,t)]},$$

where $\psi(x,t)=\frac{2\sqrt{2}pA_0t}{\sqrt{\left(-1+p^2\right)D_1^2}}-\frac{2\sqrt{2}A_0x}{\sqrt{\left(-1+p^2\right)D_1^2}}$.

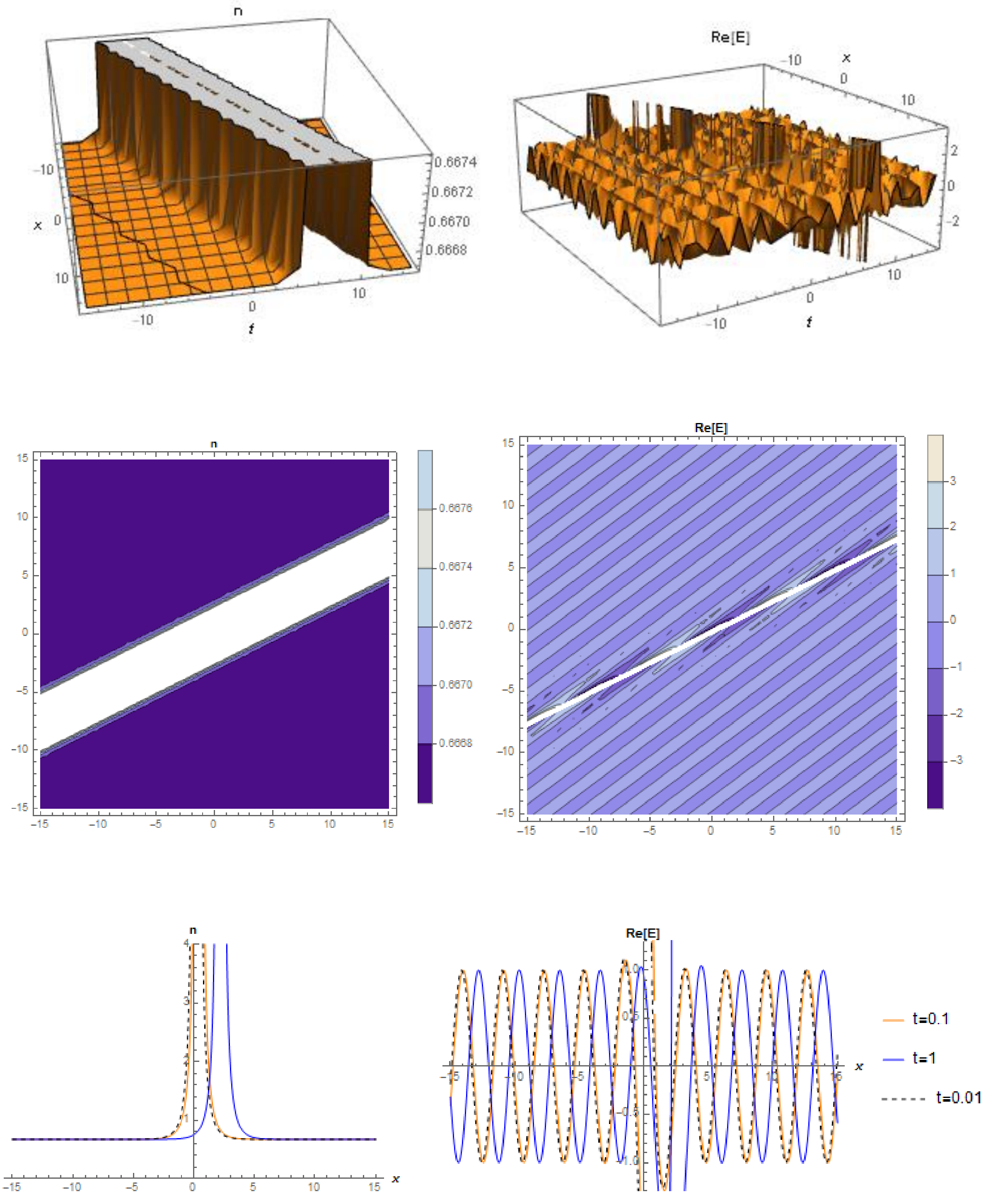

Figure 5: 3D, contour surfaces of $E_5(x,t)$ and $n_5(x,t)$ for the values $p=2, q=0.5, r=2, a_0=2, A_1=1, D_1=2, B_1=3$ and 2D views under the different values of t.

CASE 6: For

$$A_0 = \frac{-\sqrt{\left(-1+p^2\right)r^2\left(B_0^{\ 2}-D_1^{\ 2}\right)^2}-\sqrt{-1+p^2}\,r\left(B_0^{\ 2}-D_1^{\ 2}\right)}{2\sqrt{2}D_1},\ A_1=0,\ B_1=0,\ C_1=-\frac{\sqrt{-1+p^2}\,rB_0}{\sqrt{2}},$$

$$q=-\frac{r^2B_0^{\ 2}+\left(p^2+r^2\right)D_1^{\ 2}+\dfrac{r\sqrt{\left(-1+p^2\right)r^2\left(B_0^{\ 2}-D_1^{\ 2}\right)^2}}{\sqrt{-1+p^2}}}{2D_1^{\ 2}},$$

putting these values into Eq.(3), it yields

$$n_6\left(x,t\right)=\frac{\left(-\sqrt{\left(-1+p^2\right)r^2\left(B_0^{\ 2}-D_1^{\ 2}\right)^2}-\sqrt{-1+p^2}\,r\left(B_0^{\ 2}+D_1^{\ 2}-2B_0D_1\,\text{Tanh}[prt-rx]\right)\right)^2}{4(-1+p^2)D_1^{\ 2}\left(B_0-D_1\,\text{Tanh}[prt-rx]\right)^2},$$

$$E_6\left(x,t\right)=e^{i\left(px-\frac{t\left(r^2B_0^{\ 2}+\left(p^2+r^2\right)D_1^{\ 2}+\Psi\right)}{2D_1^{\ 2}}\right)}\times$$

$$\frac{\left(-\sqrt{\left(-1+p^2\right)r^2\left(B_0^{\ 2}-D_1^{\ 2}\right)^2}-\sqrt{-1+p^2}\,r\left(B_0^{\ 2}+D_1^{\ 2}-2B_0D_1\,\text{Tanh}[prt-rx]\right)\right)}{2\sqrt{2}D_1\left(B_0-D_1\,\text{Tanh}[prt-rx]\right)}.$$

where $\Psi=\dfrac{r\sqrt{\left(-1+p^2\right)r^2\left(B_0^{\ 2}-D_1^{\ 2}\right)^2}}{\sqrt{-1+p^2}}$.

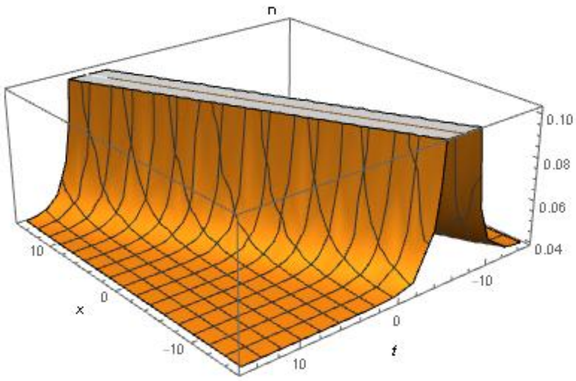

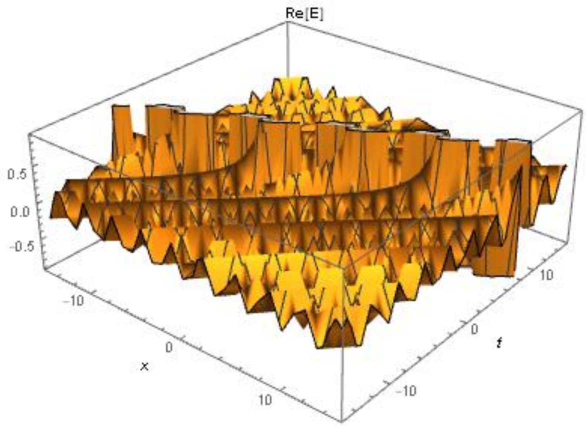

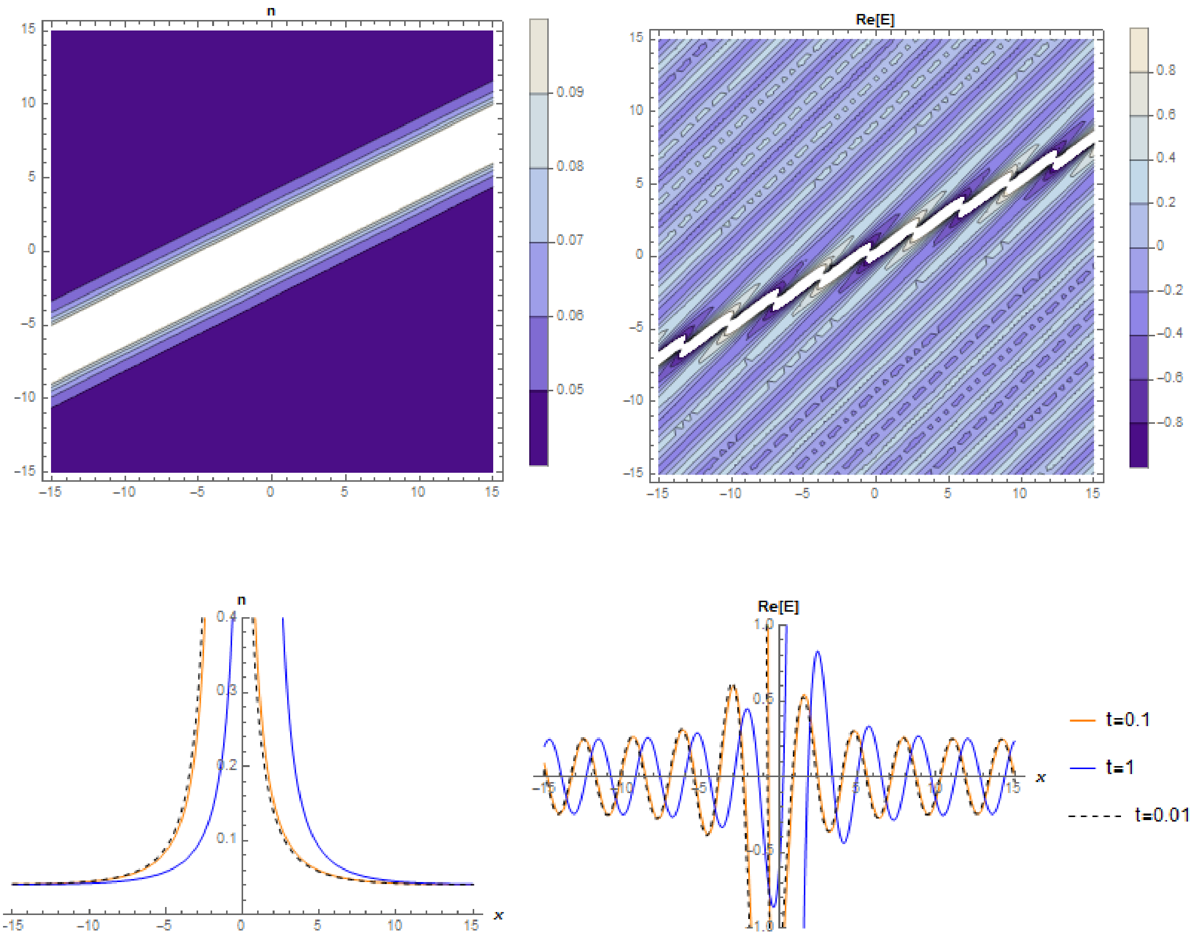

Figure 6: 3D, contour surfaces of $E_6(x,t)$ and $n_6(x,t)$ for the values $p=2, q=0.1, r=0.2, B_0=0.2, D_1=1$ and 2D views under the different values of t.

4. Conclusion

In this paper, we proposed a newly developed analytical method which is the rational sine-Gordon expansion method. By this way, we have found more general implicit analytical solutions to the ion-acoustic and Langmuir waves model, which have hyperbolic function, exponential function solutions. We illustrate the 3D and contour simulations of the travelling wave solutions of the governing model on Figures 1-6 for validity values of parameters and 2D views under the different values of $t=1, 0.1$ and 0.01.

When we compare our results, the all obtained solutions are more general and different from submitted in [24, 29-33].

While we solve the differential equation, due to the Eq.(9) has a rational function format, we can find more coefficients from the denominator. From this reason, the proposed method may be used make a contribution to scientific fields.

The analyzed model describing wave oscillation of ions and electrons in plasma physics. This models' analytical solutions may have noticeable effect in many fields such as plasma physics, space plasmas, electron waves, acoustic waves, magnetic fields. In future, plasmas will have more important practical applications in power produces fields such as nuclear fusion, solar energy. We hope that the conclusions obtained will be beneficial both theoretical and experimental studies in plasma physics. Finally, we reached that the new developed method is both easy and efficient technique to obtain general wave forms of nonlinear differential models arising in theoretical physics and engineering fields.

References

[1] Gao, W., Silambarasan, R., Baskonus, H. M., Anand, R. V., Rezazadeh, H. Periodic waves of the non dissipative double dispersive micro strain wave in the micro structured solids. Physica A: Statistical Mechanics and its Applications, 545, 123772, 2020.

[2] Darvishi, M. T., Najafi, M., Wazwaz, A. M. (2020). Construction of exact solutions in a magneto-electro-elastic circular rod. Waves in Random and Complex Media, 30(2), 340-353.

[3] Baskonus, H. M., Bulut, H., Atangana, A. (2016). On the complex and hyperbolic structures of the longitudinal wave equation in a magneto-electro-elastic circular rod. Smart Materials and Structures, 25(3), 035022.

[4] N.A.Kudryashov, The Radhakrishnan–Kundu–Lakshmanan equation with arbitrary refractive index and its exact solutions, Optik, 238, 166738, 2021.

[5] G. Yel, H.M. Baskonus, H. Bulut, Regarding some novel exponential travelling wave solutions to the Wu–Zhang system arising in nonlinear water wave model. Indian Journal of Physics, 93(8), 1031-1039, 2019.

[6] Yel, G., New wave patterns to the doubly dispersive equation in nonlinear dynamic elasticity, Pramana – J. Phys. 94(1):79, 2020.

[7] H. F Ismael, H. Bulut, H.M. Baskonus, Optical soliton solutions to the Fokas–Lenells equation via sine-Gordon expansion method and (m+G'/G)- expansion method, Pramana, 94(1), 35, 2020.

[8] H. F. Ismael, A. Seadawy and H. Bulut, Construction of breather solutions and N-soliton for the higher order dimensional Caudrey-Dodd-Gibbon-Sawada-Kotera equation arising from wave patterns, International Journal of Nonlinear Sciences & Numerical Simulation (2021).

[9] H.M. Baskonus, C. Cattani, A. Ciancio, New Contour Surfaces to the (2+ 1)-Dimensional Boussinesq Dynamical Equation, Special Functions and Analysis of Differential Equations, 1st Edition, 2020.

[10] Abdelrahman, M.A.E., Alshreef, G. Closed-form solutions to the new coupled Konno–Oono equation and the Kaup–Newell model equation in magnetic field with novel statistic application. Eur. Phys. J. Plus 136, 455, 2021.

[11] G. Yel , C. Cattani, , H.M. Baskonus, W. Gao, On the Complex Simulations with DarkBright to the Hirota-Maccari System, Journal of Computational and Nonlinear Dynamics, 6(16), 061005,2021.

[12] S.B. Yamgoue G.R. Deffo and F.B. Pelap, (2019). A new rational sine-Gordon expansion method and its application to nonlinear wave equations arising in mathematical physics Eur. Phys. J. Plus 134(380).

[13] L. Tonks and I. Langmuir, Oscillations in Ionized Gases, Phys. Rev. 33 (1929)195.

[14] R.W. Revans, The Transmission of Waves Through an Ionized Gas, Phys. Rev. 44(1933)798.

[15] M.Y. El-Ashry, Ion-sound emission by Langmuir Soliton Reflected at Density Barrier, International Atomic Energy Agency, IC/89/172,1989.

[16] Y.H., Chen, W. Lu and W.H. Wang, The Nonlinear Langmuir Waves in a Multi-ion-Component Plasma, Commun. Theor. Phys. 35, pp. 223–228, (2001)

[17] Karmina K Ali, R Yilmazer , H M Baskonus and H Bulut, Modulation instability analysis and analytical solutions to the system of equations for the ion sound and Langmuir waves, Physica Scripta, 95(6), 2020.

[18] A. R.Seadawy, A. Ali, D. Lu, Structure of system solutions of ion sound and Langmuir dynamical models and their applications, Pramana – J. Phys., 92:88, (2019).

[19] J. Manafian, Application of the ITEM for the system of equations for the ion sound and Langmuir waves, Opt Quant Electron (2017) 49:17.

[20] B. N. Breizman, V. E. Zakharov, and S. L. Musher, Kinetics of stimulated scattering of Langmuir waves by plasma ions, Zh. Eksp. Tear. Fiz. 64,1297-1313, 1973.

[21] A.Tripathy, S.Sahoo, Exact solutions for the ion sound Langmuir wave model by using two novel analytical methods, Results in Physics, 19, 103494, 2020

[22] A. R.Seadawy, D.Kumar, K.Hosseini, F.Samadani, The system of equations for the ion sound and Langmuir waves and its new exact solutions, Results in Physics, 9, 1631-1634, 2018.

[23] H. Ratcliffe, C.S. Brady, M. B. Che Rozenan, and V.M Nakariakov, A comparison of weak-turbulence and PIC simulations of weak electron-beam plasma interaction, arXiv:1410.4046v2, 2014.

[24] A. R.Seadawy, D. Lu, M. Iqbal, Application of mathematical methods on the system of dynamical equations for the ion sound and Langmuir waves, Pramana -J Phys, 93 (1), pp. 1-12, 2019.

[25] S. Duran, A. Yokuş, H. Durur and D. Kaya, Refraction simulation of internal solitary waves for the fractional Benjamin–Ono equation in fluid dynamics, Modern Physics Letters B, Vol. 35, No. 26, 2150363, 2021.

[26] A. Yokus,K. K Ali, R. Yılmazer, H. Bulut, On exact solutions of the generalized Pochhammer-Chree equation, *Computational Methods for Differential Equations*, doi: 10.22034/cmde.2021.45176.1903, 2021.

[27] K. K Ali, A. R. Seadawy, A. Yokus, R. Yilmazer and H. Bulut, Propagation of dispersive wave solutions for (3+1)- dimensional nonlinear modified Zakharov–Kuznetsov equation in plasma physics, International Journal of Modern Physics B, Vol. 34, No. 25, 2050227, 2020).

[28] A. Yokuş and D. Kaya, Comparison exact and numerical simulation of the traveling wave solution in nonlinear dynamics, International Journal of Modern Physics B, Vol. 34, No. 29, 2050282, 2020.

[29] Md N. Alam and M. S. Osman, New structures for closed-form wave solutions for the dynamical equations model related to the ion sound and Langmuir waves, Communications in Theoretical Physics, 73, 035001, 2021.

[30] Q. Zhou and M. Mirzazadeh, Analytical Solitons for Langmuir Waves in Plasma Physics with Cubic Nonlinearity and Perturbations, Zeitschrift Für Naturforschung A, 71(9), 2016.

[31] H.M. Baskonus, and H. Bulut, New wave behaviors of the system of equations for the ion sound and Langmuir Waves, Waves in Random and Complex Media 26(4), 2016.

[32] U. Younas , Aly R. Seadawy , M. Younis and S.T.R. Rizvi, Construction of analytical wave solutions to the conformable fractional dynamical system of ion sound and Langmuir waves, Waves in Random and Complex Media, DOI: 10.1080/17455030.2020.1857463, 2020.

[33] Yajima N, Oikawa M. Formation and interaction of sonic-Langmuir solitons: inverse scattering method. Progress of Theor Phys. 1976;56(6):1719–1739.

THE EFFECT OF SMOKING AND ALCOHOL CONSUMPTION ON HEALTH EXPENDITURES: THE TURKISH CASE FOR THE 1990-2019 PERIOD

Kerem ÖZEN[1]

M. Akif ARVAS[2]

[1] Ph.D. Student, Van Yüzüncü Yıl University, FEAS, Department of Economics keremozen5@gmail.com/Orcid ID: 0000-0003-2264-2787

[2] Prof. Dr. Van Yüzüncü Yıl University, FEAS, Department of Economics, aarvas@yyu.edu.tr /Orcid ID: 0000-0002-0866-8860

ABSTRACT

It is a well-known fact all over the world that smoking and alcohol consumption are the cause of serious diseases that can lead to death, and that their harm not only affects health but also the economy and the environment. Health problems caused by smoking and alcohol use and the resulting public expenditures bring an important responsibility especially to social security institutions. Therefore, there is an important alternative cost to the expenditures to eliminate the existing health problems. From this point of view, the main purpose of the study is to determine the effects of smoking and alcohol consumption on health expenditures. For this purpose, granger causality method was used to calculate the effects of these two variables on health expenditures. In the study, the data set for the period 1990 and 2019 were obtained from OECD STAT.

Keywords: Smoking, Alcohol, Health expenditures, Granger Causality

1. INTRODUCTION

Alcohol is defined as a sedative, pleasurable, narcotic substance with an ongoing definition from ancient times. As we approach today, it is thought that alcohol is an important factor in reducing stress. Considering the studies on the subject, it is supported by most authors that alcohol has a significant effect on stress. Due to this effect of alcohol, the demand for alcohol is increasing day by day. Therefore, in the following periods, the body becomes completely dependent on alcohol, which is called alcoholism.

The gradual increase in alcohol and tobacco use has become a problem that all countries in the world place emphasis on. On the other hand, many studies have been carried out by the World Health Organization to prevent the harms of alcohol and tobacco use. The first of these studies was a conference held in 1967 and this study was published in 1970. Later, the World Health Organization developed a project called smoking and health. Smokers cannot get rid of smoking behavior unless they get rid of nicotine addiction. At the same time, it is one of the effective studies to reduce these consumption rates with certain legal regulations in the use of products such as alcohol and tobacco. Cigarette and tobacco consumption have direct damages as well as costs. On the other hand, states are in close struggle with this issue because it threatens public health. Raising public awareness of states in reducing these damages is a policy at the forefront of the struggle.

Health expenditures are made by the states to reduce tobacco addiction due to diseases caused by tobacco consumption and to reduce mortality rates for this purpose. At the same time, tobacco products have a tax-increasing effect. Health expenditures related to tobacco consumption are made by the state due to both the diseases caused by the consumption of tobacco products and the reduction of tobacco addiction in the society. On the other hand, tobacco products have an increasing effect on tax revenue. Another effective intervention of the World Health Organization has also prevented the passive interaction of non-smokers in areas that people usually use in common. Ultimately, alcohol and tobacco control studies produce effective results for smokers as well as non-smokers.

2. SMOKING AND ALCOHOL CONSUMPTION

Those who use alcohol and cigarettes not only harm themselves, but also their environment. Such damages not only prevent the welfare of the society from reaching the highest level, but also disrupt the market mechanism. It seems impossible to achieve effective resource use because it disrupts the market mechanism. (Dinler,2008:552).

From a health point of view, people exposed to cigarette smoke are more likely to get the same diseases as smokers. In this respect, alcohol differs from cigarettes. In this respect, the damage caused by cigarettes to the environment is much more than alcohol, and it also causes pollution of nature in the butts thrown into the environment (Uğur, A., Akdemir E., Gürsel, E, 2010).

In these cases, there is a negative externality resulting from cigarette consumption. It also has a cost. Governments therefore use a certain percentage of taxes on alcohol and tobacco consumption from resource allocation to maintain efficiency and to ameliorate negative externalities from alcohol and cigarette consumption. Therefore, governments have to allocate a share from the budget to health expenditures. In case of market failures, the government implements both monetary and fiscal policies when necessary to eliminate macroeconomic instability (Dinler,2008:553-567).

It is known that smoking causes lung diseases, decreased blood circulation, skin aging, heart attacks and premature death (Ergüder, 2008:14). At the same time, it is known that smoking causes diseases such as asthma and COPD in pregnant women (Karlıkaya et al. 2006: 51). Due to the deterioration of the air quality in smoking environments, it is possible for non-smokers inside to be harmed by these airless environments. In addition, the duration of treatment of diseases caused by alcohol and cigarette use is a very costly and time-consuming process.

It is stated that in addition to the damages caused by the use of cigarettes and alcohol, the money spent to provide them will be much more beneficial for human health if the money spent is spent on other products rather than alcohol and cigarettes. For this purpose, at the same time, the share spent for the treatment of diseases caused by the consumption of these goods will cease to be an economic burden for a country (Uğur, A., Akdemir E., Gürsel, E, 2010). In this case, the states charge a certain amount of tax on the sale of alcohol and cigarettes in order to alleviate this burden a bit (Çapar:122). The distribution of such negative externalities to all taxpayers with increased health insurance and high taxes creates significant financial results (Sissosko, 2009: 90).

3. LITERATURE REVIEW

Uğur, Akdemir, Gürsel tried to determine the effect of indirect taxes on cigarettes and alcohol on consumption and thus on health expenditures in their 2010 study. For this purpose, regression analysis was used to determine the effect of cigarette consumption on health expenditures. As a result, it has been determined that there is a same-sided relationship between per capita health expenditures and tobacco consumption in Turkey. Same time; the effect of past tobacco consumption on per capita health expenditure is greater than the effect of current tobacco consumption on per capita health expenditure. We can explain this by the fact that the detrimental effects of tobacco appear after a certain period of time.

Mercan, İlbak et al., in their 2017 study, aimed to determine the views of people who have never used, used and quit alcoholic beverages in the past, and still use alcohol consumption culture, alcohol research and alcohol control policies. For this purpose, the qualitative method was preferred, the data were collected through semi-structured interviews and evaluated with thematic framework analysis. According to the results obtained, alcohol is a relaxation and socialization tool by the users; A conclusion has been reached which is described as unhappiness, restlessness, collapse and sin by those who do not use it.

In his 2014 study, Hayrullahoğlu examined whether the special consumption tax on tobacco products and alcoholic beverages is effective in reducing consumption by using tax rates, sales amounts and smuggling amounts. According to the findings, he stated that the increase in tax rates did not have the expected effect in reducing demand, as it led individuals to illegal consumption.

Beşer, Aşkan 2019 studies focused on the importance of combating cigarette addiction and examined the fight against addiction by increasing tax rates in reducing tobacco use. Qualitative method was used in the study and according to the findings; It has been stated that increasing the practical sanctions in order to increase social awareness can be effective.

Ögel, Tamar et al., in their 2000 study, investigated the frequency of alcohol use and accompanying socio-demographic characteristics in an Istanbul sample. In the study, a survey was conducted with 707 adults living in 24 different districts of Istanbul through face-to-face interviews at their homes. According to the findings, alcohol use rates were similar to previous household studies. However, the study revealed that the rate of alcohol consumption was more common among women. At the same time, although the rate of frequent alcohol use among women was the same, this rate was significantly higher among men.

Mercan, Altunay, and Arı (2013) investigated whether alcohol use increased in different skin diseases and whether it reached the level of addiction. For this purpose, 100 patients with psychiatric comorbidities and diagnosed with psychodermatological diseases were contacted. As the control group, 60 patients with chronic dermatosis and 74 healthy individuals without psychiatric comorbidity, except psychodermatological disease, were included in the study, and all participants were filled with a questionnaire that aimed to question their sociodemographic characteristics, disease history, duration of alcohol use and the relationship between use. According to the findings, patients with dermatological disease associated with psychosocial morbidity did not use alcohol more than patients with other chronic dermatosis and healthy individuals. In addition, it has been stated that large studies are needed for more decisive results due to different socio-cultural effects.

4. DATA SET, METHODOLOGY AND EMPIRICAL MODEL

The definition of variables in the study is as follow: HE stands for health expenditures measured in per capita expenditures in Turkish Liras. AC stands for alcohol consumption per person and finally TC is a proxy for per person tobacco consumption in TL. The data set for the period 1990-2019 were obtained from OECD STAT.

4.1. Granger Causality

By causality we mean causality in the Granger (1969) sense. That is, we would like to know if one variable precedes the other variable or if they are contemporaneous. The Granger approach to the question whether Alcohol and tobacco consumption cause health expenditure is to see how much of the current value of the second variables can be explained by past values the first two variables. For example, health expenditure (HE) is said to be Granger-caused by alcohol consumtion (AC) if AC helps in the prediction of HE, or, equivalently, if the coefficients of the lagged AC are statistically significant in a regression of AC on HE. Empirically, one can test for causality in Granger sense by means of the following vector autoregressive (VAR) model:

$$HE_t = \alpha_0 + \sum_{i=1}^{k} a_i HE_{t-i} + \sum_{i=1}^{k} a_i AC_{t-i} + e_{1t} \tag{1}$$

$$HE_t = \alpha_0 + \sum_{i=1}^{k} a_i HE_{t-i} + \sum_{i=1}^{k} a_i TC_{t-i} + e_{1t} \tag{2}$$

4.2. Estimation Results

Table 1. Unit Root Test

Variable	ADF Test Statistics	Critical Values 1%	5%	10%
Level				
Health (fixed)	-1.717	-3.723	-2.989	-2.625
Health (stable+trend)	-0.792	-4.343	-3.584	-3.230
Alcohol (fixed)	-4.274***	-3.723	-2.989	-2.626
Alcohol (fixed+trend)	-3.820**	-4.343	-3.584	-3.230
Tobacco (fixed)	-2.315	-3.723	-2.989	-2.625
Tobacco (stable +trend)	-0.614	-4.343	-3.584	-3.230
First Difference				
Health (fixed)	-3.531***	-3.730	-2.992	-2.626
Health (constant + trend)	-3.592**	-4.352	-3.588	-3.233
Alcohol (fixed)	-6.492***	-3.730	-2.992	-2.626
Alcohol (fixed+trend)	*-6.799****	-4.352	-3.588	-3.233
Tobacco (fixed)	-4.341***	-3.730	-2.992	-2.626
Tobacco (constant + trend)	-4.960***	-4.352	-3.588	-3.233

Note: ***,** represent 1% and 5% statistical significance levels, respectively. Schwarz information criterion was used in the selection of the lag length.

According to Table 1, except for the alcohol variable, all series became stationary only when the first difference was taken. After the series become stationary, we can move on to the determination of the lag length for the Vector Autoregressive (VAR) model.

Table 2. Granger Causality Wald Test

Equation	Excluded	Chi2	Df	Prob
Health	*Alcohol*	19.532	4	0.001
Health	*Tobacco*	2.0395	4	0.728
Health	*ALL*	21.926	8	0.005
Alcohol	*Health*	7.4923	4	0.112
Alcohol	*Tobacco*	6.333	4	0.176
Alcohol	*ALL*	16.361	8	0.037
Tobacco	*Health*	49.803	4	0.000
Tobacco	*Alcohol*	22.252	4	0.000
Tobacco	*ALL*	53.056	8	0.000

According to the test results in Table 2, while there was a unidirectional causality from alcohol to health variable (significant in 1%), no causality relationship was found from health to alcohol (coefficient insignificant, probe = 0.112). On the other hand, while the causality relationship from tobacco variable to health expenditures could not be found significant, it was observed that health expenditures were the granger cause of tobacco consumption (the coefficient was significant at 1%). Another interesting finding is that alcohol is a one-way granger cause of tobacco consumption.

5. Conclusion

In this study, the effects of alcohol and tobacco consumption on health expenditures in Turkey between 1990-2019 were examined. According to the applied Granger causality test results; while there was a unidirectional causality from alcohol to health variable (significant in 1%), no causal relationship was found from health to alcohol. Except for the alcohol variable, all series became after first difference. There has been a decrease in alcohol and tobacco consumption between the related years. In addition, it has been determined that the effect of tobacco consumption in the past periods on health expenditures is greater than the effect in the current period. This can be explained by the effect of tobacco consumption on human health after a certain period of time.

REFERENCES

MERCAN, S., İLBAK, A. and Others (2018), Views on Alcohol Consumption Culture and Alcohol Research and Alcohol Control Policies: A Qualitative Research, Turkish Green Crescent Society ISSN 2148-7286 eISSN 2149-1305

HAYRULLAHOĞLU, B. (2014), Success of Special Consumption Tax on Tobacco Products and Alcoholic Beverages in Turkey, ournal of Life Economics (JLE)

BEŞER, B., AŞKAN, H. (2019), The Effect of Cigarette Taxes on Reducing Cigarette Addiction in Turkey, Strategic Public Management Journal ISSN 2149-9543

ÖZKAN, E. (2017) The Case of Turkey in the Framework of Special Consumption Taxes Applied on Alcohol and Tobacco Products and Consumption Relationship, Yüksel Undergraduate Thesis

Bilir, N., Özcebe H. (2014), Tobacco Addiction and Control: Individual, Social and Social Marketing Approaches, Eurasian J Pulmonol 2014; 16:63-8

Ögel, K., Tamar, D. et al., (2000), Prevalence of Alcohol Use in Istanbul, Psychiatric Research and Training Center (PAREM)

BUZRUL, S. (2016), Alcoholic Beverage Consumption in Turkey, Journal of Food and Health Science, E-ISSN 2149-0473

Koca, B., Oğuzöncü, A. (2010), İnönü University Health School Students' Cigarette, Alcohol, Substance Use, Factors Affecting Substance Use and the Effect of Social Support from the Family, Kocaeli Medical Journal 2015; 4;2:4-13

UĞUR, A., AKDEMİR E., GÜRSEL, E. (2010), The Effect of Indirect Taxes on Cigarettes and Alcohol on Health Expenditures, Journal of Economic Sciences Volume 2, Issue 1, 2010 ISSN: 1309-8020 (Online)

Ari, S., Kivanc, I., Altunay, Mercan, S. (2013), The relationship between alcohol consumption and skin diseases: A cross-sectional controlled study, DOI: 10.5350/SEMB2013470408

Aydın, K., (2011), Alcoholic Beverage Culture and Household Alcohol Expenditures in Turkey, Electronic Journal of Social Sciences Electronic Journal of Social Sciences Electronic Journal of Social Sciences, Fall-2011 Vol:10 Issue:38 (335-347)

Başol, B., Can, S. (2015), A Study on the Economic Effects of Tobacco Consumption and Tobacco Control Policies, Balkan Journal of Social Sciences Vol/Volume: 4, No/Issue:7, 2015

Dinler Zeynel, Micro Economy, Ekin Publications 19th Edition, Bursa 2008.

Erguder Toker . The Who Framework Convention On Tobacco Control, Ministry of Health Ankara 2008.

Sissosko Macki, Cigarette Consumption in Different U.S. States, 1955–1998: An Empirical Analysis of the Potential Use of Excise Taxation to Reduce Smoking, Journal of Consumer Policy 25: 89–106, 2002 Kluwer Academic Publishers. Printed in the Netherlands 2002

Capar Mustafa, Special Consumption Tax and its Application in Turkey, Journal of TCA Issue: 52

Convergence Theorems for Multivalued Nonexpansive Mapping in Kohlenbach Hyperbolic Space

Makbule Kaplan [1]

[1] Faculty of Education, University of Sinop, Sinop, Turkey

mkaplan@sinop.edu.tr,

Abstract

In this paper, we introduce a new modified iteration process for multivalued mappings in Kohlenbach hyperbolic space. Under appropriate conditions, we prove some strong and Δ-convergence theorems for approximating a fixed point of nonexpansive multivalued mapping by the proposed process.Our results generalize some previous works results in literature.

Keywords: Multivalued nonexpansive mapings; Strong and Δ-convergence; Hyperbolic space

I. INTRODUCTİON

Fixed point theory contributes significantly to the theory of nonlinear functional analysis. The theory of iterative construction of fixed points of a nonlinear mapping under suitable set of control conditions is coined as metric fixed point theory. So, it has been study fixed point problems associated with a class of mappings in a suitable nonlinear structure.The term nonlinear structure in the Fixed point theory is referred as a metric space embedded with a "convex structure".The metric spaces dont have a such structure. Hence, there is need to introduce convex structure in the metric space. The notion of convex metric spaces was first studied by Takahashi [18].

Shimizu and Takahashi [17] generalized results of Lim [12] given above from uniformly convex Banach spaces to convex metric spaces. Many authors have studied to a great extent the Banach spaces with convex structures[2,6,7,9,10,15].

We work in the setting of hyperbolic spaces introduced by Kohlenbach [11], the hyperbolic space is an example of a metric space with convex structure.The hyperbolic space introduced by Kohlenbach is more restrictive than the type by Goebel and Kirk [5] but more general than the type by Reich and Shafrir [14].Non-positively curved hyperbolic space introduced by Kohlenbach provides rich geometrical structures suitable for metric fixed point theoryof various classes of mappings.

Definiton 1: A space (X, d) coupled with $W: X^2 \times [0,1] \to X$ fulfilling the following conditions :

i. $d(\nu, W(\varkappa, \omega, \beta)) \leq (1-\beta)d(\nu, \varkappa) + \beta d(\nu, \omega)$;
ii. $d(W(\varkappa, \omega, \beta), W(\varkappa, \omega, \gamma)) = |\beta - \gamma| d(\varkappa, \omega)$;
iii. $W(\varkappa, \omega, \beta) = W(\omega, \varkappa, 1-\beta)$;

iv. $d(W(\varkappa,\nu,\beta),W(\omega,w,\beta)) \le \beta d(\varkappa,\omega) + (1-\beta)d(\nu,w)$,

for all $\varkappa,\omega,\nu,w \in X$ and $\beta,\gamma \in [0,1]$ is called a hyperbolic space.

Definition 2: Let X be a hyperbolic space with a mapping $W: X^2 \times [0,1] \to X$.

i. A nonempty subse$t\ E \subseteq X\ is$ convex if $W(\varkappa,\omega,\beta) \in E$ for all $\varkappa,\omega \in E$ and $\beta \in [0,1]$

ii. A hyperbolic space $(X,d,W)\ is$ uniformly convex if for any $k > 0\ and\ \varepsilon \in (0,2]$, there exists a $\delta \in (0,1]$ such that for all $t,\varkappa,\omega \in X$,
$$d(W(\varkappa,\omega,(1/2)),t) \le (1-\delta)k,$$
whenewer $d(\varkappa,t) \le k, d(\omega,t) \le k\ and\ d(\varkappa,\omega) \ge \varepsilon k$.

iii. A map $\eta: (0,\infty) \times (0,2] \to (0,1]$ which provides such a $\delta = \eta(k,\varepsilon)$ for given $k > 0$ and $\varepsilon \in (0,2]$, is known as the modulus of uniform convexity.

Throught this paper, we will represent a complete uniformly convex hyperbolic space unless otherwise stated.

Definition 3: Let X be a metric space. For a bounded sequence $\{\varkappa_n\} \subseteq X$ e and $\varkappa \in X$, define $r(.,\{\varkappa_n\}): X \to [0,\infty)$ by

$$r(\varkappa,\{\varkappa_n\}) = limsup_{n\to\infty} d(\varkappa_n,\varkappa).$$

a) The asymptotic radius of $\{\varkappa_n\}$ relative $to\ E \subset X$ is $r(E,\{\varkappa_n\} = inf\{r(\varkappa,\{\varkappa_n\}): \varkappa \in X\}$.

b) for any $\omega \in E \subset X$, the asymptotic center of $\{\varkappa_n\}$ in relation to E is the set $A_E(\{\varkappa_n\}) = \{\varkappa \in X: r(\varkappa,\{\varkappa_n\}) \le r(\omega,\{\varkappa_n\})\}$.

Definition 4: If every subsequenc $\{\varkappa_{n_i}\}$ of $\{\varkappa_n\} \subseteq X$ has a unique asymptotic center $\varkappa \in X$, then we say $\varkappa_n$ Δ-converges to $\varkappa$. It be writen $\Delta - lim\varkappa_n = \varkappa$.

Let X be a metric space. A subset $E \subset X$ is a proximinal set if there is a point $\omega \in E$ such that $d(\varkappa,\omega) = dist(\varkappa,E) := \{inf\ d(\varkappa,z): z \in E\}\ for\ all\ \varkappa \in X$.

It is denoted by $P(E)$ the family of nonempty proximinal bounded subets of E. The Hausdorff metric H on $P(E)$ is defined by

$H(A,C) := max\{sup_{\varkappa\in A} d(\varkappa,C), sup_{\omega\in C} d(\omega,A)\}$ for all $A,C \in P(E)$. A multivalued map $T: E \to P(E)$ is nonexpansive if $H(T\varkappa,T\omega) \le d(\varkappa,\omega)$ for $all\ \varkappa,\omega \in E$. A point $\varkappa \in E$ is a fixed point of a map T if $\varkappa \in T\varkappa$. Denote the set of all fixed points of by $F(T)$ or F and $P_T(\varkappa) = \{\omega \in T\varkappa: d(\varkappa,\omega) = d(\varkappa,T\varkappa)\}$.

Lemma 1: Let E be a nonmepty closed convex subset of X. The asymptotic center of every bounded sequence $\{\varkappa_n\}$ in X is unique. Suppose $A(E,\{\varkappa_n\}) = \{\varkappa\}$ and $\{\omega_n\}$ is a subsequence of $\{\varkappa_n\}$ with $A(E,\{\omega_n\}) = \{\omega\}$. If $\{d(\varkappa_n,\omega)\}$ is convergent, then $x = \omega$.

Lemma 2: Let (X,d,W) be a uniformly convex hypebolic space and $\varkappa \in X$. Let $\{\alpha_n\} \in [b,c]$ for some $b,c \in (0,1)$ and $\{\varkappa_n\},\{\omega_n\} \subseteq X$. If for some $l>0$, $limsup_{n\to\infty} d(\varkappa_n,\varkappa) \leq l$, $limsup_{n\to\infty} d(\omega_n,\varkappa) \leq l$ and $lim_{n\to\infty} d(W(\varkappa_n,\omega_n,\alpha_n),\varkappa) = l$. Then $lim_{n\to\infty} d(\varkappa_n,\omega_n) = 0$.

Lemma 3: Let a mapping $T: E \to P(E)$ be multivalued and $P_T(\varkappa) = \{\omega \in T(\varkappa): d(\varkappa,\omega) = d(\varkappa,T(\varkappa))\}$. Then the following are equivalent:

i. $F(T) = F(P_T)$,
ii. $P_T(\varkappa) = \{\varkappa\}$ for each $\varkappa \in F(T)$,
iii. For each $\varkappa \in E, P_T(\varkappa)$ is closed subset of $T(\varkappa)$ and so it is compact,
iv. $d(\varkappa,T(\varkappa)) = d(\varkappa, P\_\{T\}(\varkappa))$ for each $\varkappa \in E$,
v. P_T is a multivalued mapping from E to $P(E)$.

The normal Mann iteration schme [13] have played a very helpful role in approximating the fixed point of a nonexpansive mapping in Banach space. Ishikawa [8] introduced a new iterative process which performs better than the Mann iteration for approximating the fixed points of same mapping in Hilbert space. Sastry and Babu [16] restated the Ishikawa iteration for multivalued nappings in Hilbert spaces. Phuengrattana and Suntai [19] introduced SP-iteration as a generalization of the Mann, Ishikawa and Noor iterations.Glowonski and Le Tallec [4] showed the three steps iteration yield better numerical results than the one or two steps iterations. Haubruge et al. [3] showed that three steps iteration process lead to highly parallel iterations in certain situations.

In this work, we introduce a multivalued version of iteration process which is defined by Atalan et al [1] hyperbolic space and use $P_T(\varkappa) = \{y \in T\varkappa: \|\varkappa - y\| = d(\varkappa,T\varkappa)\}$ instead of a stronger condition $T\varkappa = \{\varkappa\}$ for any $\varkappa \in F(T)$ to approximate fixed point of multivaled nonexpansive mapping for proposed process under some conditions hyperbolic space. Our algortihm is defined as follows:

Let E be a nonempty convex subset of X and $T: E \to P(E)$ multivalued mapping. Select $\varkappa_0 \in E$ and define $\{\varkappa_n\}$ as follows:

$$\left\{\begin{aligned} \varkappa_{n+1} &= u_n \\ y_n &= W\left(v_n, z_n, \tfrac{\beta_n}{1-\alpha_n}\right) \\ z_n &= W(x_n, w_n, \alpha_n) \end{aligned}\right. \tag{1.1}$$

where $w_n \in P_T(x_n), v_n \in P_T(z_n),\ u_n \in P_T(y_n)$ and $\alpha_n, \beta_n \in (0,1)$ such that $0 < \alpha_n + \beta_n < 1$.

We shall prove that iterative algorithm (1.1) can be used the aproximation of fixed points of a nonexpansive multivalued mapping in hyperbolic spaces.

Assume that P_T is nonexpansive multivalued mapping on E. From definition of P_T we can write $d(\varkappa,T\varkappa) \leq d(\varkappa,P_T(\varkappa))$for any x in E. Let a map $f: E \to E$ by $f(\varkappa) = u$ for some $u \in P_T(y) = P_T(W(v,z,\beta_1/1-\alpha_1))$, $v \in P_T(z) = P_T(W(x,w,\alpha_1))$ and $w \in P_T(\varkappa_n)$. For any $\varkappa_1,\varkappa_2 \in E$, let $w_1 \in P_T(\varkappa_1)$, $w_2 \in P_T(\varkappa_2)$ such that $d(w_1,w_2) = d(w_1,T\varkappa_2)$, $v_1 \in P_T(z_1) =$

$W(\varkappa_0, w_1, \alpha_1)$, $v_2 \in P_T(z_2) = W(\varkappa_0, w_2, \alpha_1)$ such that $d(v_1, v_2) = d(v_1, T(z_2))$, $u_1 \in P_T(y_1) = P_T\left(W(v_1, z_1, \frac{\beta_1}{1-\alpha_1})\right)$, $u_2 \in P_T(y_2) = P_T\left(W(v_2, z_2, \frac{\beta_1}{1-\alpha_1})\right)$ such that $d(u_1, u_2) = d(u_1, T(y_2))$.

Using (iv) of Definition 1, we have

$$d(f(\varkappa_1), f(\varkappa_2)) = d(u_1, u_2) = d(u_1, T(y_2)) = d(u_1, P_T(y_2)) \leq d(u_1, P_T(y_2)) \leq H(P_T(y_1), P_T(y_2))$$

$$\leq H\left(P_T(W(v_1, z_1, \tfrac{\beta_1}{1-\alpha_1})), P_T(W(v_2, z_2, \tfrac{\beta_1}{1-\alpha_1}))\right)$$

$$\leq d\left(W(v_1, z_1, \tfrac{\beta_1}{1-\alpha_1})), W(v_2, z_2, \tfrac{\beta_1}{1-\alpha_1})\right) \leq (1 - \tfrac{\beta_1}{1-\alpha_1}) d(v_1, v_2) + \tfrac{\beta_1}{1-\alpha_1} d(z_1, z_2)$$

$$\leq \frac{\beta_1}{1-\alpha_1} d(W(\varkappa_0, w_1, \alpha_1), W(\varkappa_0, w_2, \alpha_1)) + (1 - \frac{\beta_1}{1-\alpha_1}) d(v_1, T(z_2))$$

$$\leq \frac{\beta_1 \alpha_1}{1-\alpha_1} d(w_1, w_2) + (1 - \frac{\beta_1}{1-\alpha_1}) d(v_1, P_T(z_2))$$

$$\leq \frac{\beta_1 \alpha_1}{1-\alpha_1} d(w_1, w_2) + (1 - \frac{\beta_1}{1-\alpha_1}) H(P_T(z_1), P_T(z_2))$$

$$\leq \frac{\beta_1 \alpha_1}{1-\alpha_1} d(w_1, w_2) + (1 - \frac{\beta_1}{1-\alpha_1}) d(z_1, z_2)$$

$$\leq \frac{\beta_1 \alpha_1}{1-\alpha_1} d(w_1, w_2) + (1 - \frac{\beta_1}{1-\alpha_1}) H(P_T(W(\varkappa_0, w_1, \alpha_1)), P_T(W(\varkappa_0, w_2, \alpha_1)))$$

$$\leq \frac{\beta_1 \alpha_1}{1-\alpha_1} d(w_1, w_2) + (1 - \frac{\beta_1}{1-\alpha_1}) d(W(\varkappa_0, w_1, \alpha_1), W(\varkappa_0, w_2, \alpha_1))$$

$$\leq \frac{\beta_1 \alpha_1}{1-\alpha_1} d(w_1, w_2) + (1 - \frac{\beta_1}{1-\alpha_1}) \alpha_1 d(w_1, w_2)$$

$$= \alpha_1 d(w_1, w_2) = \alpha_1 d(w_1, T(\varkappa_2))$$

$$\leq \alpha_1 d(w_1, P_T(\varkappa_2))$$

$$\leq \alpha_1 H(P_T(\varkappa_1), P_T(\varkappa_2))$$

$$\leq \alpha_1 d(\varkappa_1, \varkappa_2).$$

$\alpha_1 < 1$, the mapping f is contraction, therefore f has a unique fixed point in E. Hence ıt be established the existence of $\varkappa_1$. Continuing this way, the existence of $\varkappa_2, \varkappa_3, \cdots$ and thus $\varkappa_n$ is guaranteed. So, our algorithm is well-defined.

II. Main results

Lemma 2.1: Let E be a nonempty closed convex subset of a uniformly convex hyperbolic space X and $T: E \to P(E)$ be a multivaled mapping such that P_T is nonexpansive mapping and with $F \neq \emptyset$. Let $\{\varkappa_n\}$ be the sequence define by algorithm (1.1). Then $lim_{n\to\infty} d(\varkappa_n, \varkappa)$ exists for each $\varkappa \in F$.

Proof: Let $\varkappa \in F. Then\ \varkappa \in P_T(\varkappa) = \{\varkappa\}$ by Lemma 3 and from (1.1), we have

$$
\begin{aligned}
d(y_n, p) &= d(W(v_n, z_n, \tfrac{\beta_n}{1-\alpha_n}), \varkappa) \\
&\leq (1 - \frac{\beta_n}{1-\alpha_n}) d(v_n, \varkappa) + \frac{\beta_n}{1-\alpha_n} d(z_n, \varkappa) \\
&\leq (1 - \frac{\beta_n}{1-\alpha_n}) H(P_T(z_n), P_T(\varkappa)) + \frac{\beta_n}{1-\alpha_n} d(W(x_n, w_n, \alpha_n), \varkappa) \\
&\leq (1 - \frac{\beta_n}{1-\alpha_n}) d(z_n, \varkappa) + \frac{\beta_n}{1-\alpha_n} [(1-\alpha_n) d(x_n, \varkappa) + \alpha_n d(w_n, \varkappa)] \\
&\leq (1 - \frac{\beta_n}{1-\alpha_n}) d(W(x_n, w_n, \alpha_n), \varkappa) + \frac{\beta_n}{1-\alpha_n} [(1-\alpha_n) d(x_n, \varkappa) + \alpha_n d(w_n, \varkappa)] \\
&\leq (1 - \frac{\beta_n}{1-\alpha_n}) [(1-\alpha_n) d(x_n, \varkappa) + \alpha_n d(w_n, \varkappa)] + \frac{\beta_n}{1-\alpha_n} [(1-\alpha_n) d(x_n, \varkappa) + \alpha_n d(w_n, \varkappa)] \\
&= (1-\alpha_n) d(x_n, \varkappa) + \alpha_n d(w_n, \varkappa) \\
&\leq (1-\alpha_n) d(x_n, \varkappa) + \alpha_n H(P_T(x_n), P_T(\varkappa)) \\
&\leq (1-\alpha_n) d(x_n, \varkappa) + \alpha_n d(x_n, \varkappa) = d(x_n, \varkappa).
\end{aligned}
$$

That is,

$$d(y_n, \varkappa) \leq d(x_n, \varkappa). \qquad (2.1)$$

Also,

$$
\begin{aligned}
d(x_{n+1}, \varkappa) = d(u_n, \varkappa) \leq d\big(u_n, P_T(\varkappa)\big) \leq H\big(P_T(y_n), P_T(\varkappa)\big) \\
\leq d(y_n, \varkappa)
\end{aligned}
$$

In this case,

$$d(x_{n+1}, \varkappa) \leq d(x_n, \varkappa). \qquad (2.2)$$

This means that $lim_{n\to\infty\}}\, d(x_n, \varkappa)$ exists for each $\varkappa \in F$.

Lemma 2.2: Let E be a nonempty closed convex subset of X and T, P_T, F and $\{x_n\}$ be as in Lemma 2.1. Let $\{\alpha_n\}, \{\beta_n\}, \{\gamma_n\}$ satisfy $0 < a \leq \alpha_n, \beta_n, \gamma_n \leq b < 1$. For sequence $\{x_n\}$ in (1.1), then we have $llim_{n\to\infty\}}\, d(x_n, P_T(x_n)) = 0$.

Proof: By Lemma 2.1 $lim_{n\to\infty\}}\, d(x_n, \varkappa)$ exists for each $\varkappa \in F$. Assume that $lim_{n\to\infty\}}\, d(x_n, \varkappa) = c$ for some $c \geq 0$.The case $c = 0$ is trivial. Suppose that $c > 0$. Now, $lim_{n\to\infty\}}\, d(x_{n+1}, \varkappa) = c$ can be written as $lim_{n\to\infty\}}\, d(u_n, \varkappa) = c$. As P_T is nonexpansive, we write

$$d(w_n, \varkappa) \leq d\big(w_n, P_T(\varkappa)\big) \leq H\big(P_T(x_n), P_T(\varkappa)\big) \leq d(x_n, \varkappa).$$

Taking lim $sup_{n\to\infty}$ to the both sides, we get

$$limsup_{n\to\infty} d(w_n, \varkappa) \le c \tag{2.3}$$

Next,

$$d(z_n, \varkappa) = d(W(x_n, w_n, \alpha_n), \varkappa)$$

$$\le (1-\alpha_n) d(x_n, \varkappa) + \alpha_n d(w_n, \varkappa)$$

$$\le (1-\alpha_n) d(x_n, \varkappa) + \alpha_n H\big(P_T(x_n), P_T(\varkappa)\big)$$

$$\le (1-\alpha_n) d(x_n, \varkappa) + \alpha_n d(x_n, \varkappa) = d(x_n, \varkappa).$$

Taking lim $sup_{n\to\infty}$ to the both sides, we obtain

$$lim\ sup_{n\to\infty} d(z_n, \varkappa) \le c \ \text{ and lim } sup_{n\to\infty}\ W(x_n, w_n, \alpha_n), \varkappa) \le c \tag{2.4}$$

Also,

$$d(v_n, \varkappa) \le d\big(v_n, P_T(\varkappa)\big) \le H\big(P_T(z), P_T(\varkappa)\big) \le d(z_n, \varkappa),$$

hence

$$\lim\ sup_{n\to\infty} d(v_n, \varkappa) \le c.$$

Again, by (1.1) can be rewritten as

$$d(x_{n+1}, \varkappa) = d(u_n, \varkappa) \le d\big(u_n, P_T(\varkappa)\big) \le H\big(P_T(y_n), P_T(\varkappa)\big)$$

$$\le d(y_n, \varkappa) = \mathrm{d}(\ W(v_n, z_n, \tfrac{\beta_n}{1-\alpha_n}), \varkappa)$$

$$\le \left(1 - \tfrac{\beta_n}{1-\alpha_n}\right)\ d(v_n, \varkappa) + \tfrac{\beta_n}{1-\alpha_n} d(z_n, \varkappa)$$

$$\le \left(1 - \tfrac{\beta_n}{1-\alpha_n}\right) H\big(P_T(z_n), P_T(\varkappa)\big) + \tfrac{\beta_n}{1-\alpha_n} d(z_n, \varkappa)$$

$$\le \left(1 - \tfrac{\beta_n}{1-\alpha_n}\right) d(z_n, \varkappa) + \tfrac{\beta_n}{1-\alpha_n} d(z_n, \varkappa) = d(z_n, \varkappa).$$

Taking lim $inf_{n\to\infty}$ to the both sides,

$$c \le lim\ inf_{n\to\infty}\ d(z_n, \varkappa) \tag{2.5}$$

From (4) and (5), we have

$$lim_{n\to\infty}\ d(z_n, \varkappa) = c = lim_{n\to\infty} d(W(x_n, w_n, \alpha_n), \varkappa) \tag{2.6}$$

Moreover, we obtain from $lim_{n\to\infty}\ d(x_n, \varkappa) = c$, (2.3), (2.6) and Lemma 2 that

$$lim_{n\to\infty}\ d(x_n, w_n) = 0.$$

Also, from (1.1) and (2.2), we can write

$$d(x_n, u_n) \leq d(x_n, x_{n+1}) + d(x_{n+1}, u_n) \to 0 \ as \ n \to \infty.$$

Since $d(\varkappa, P_T(\varkappa)) = inf_{z \in P_T(\varkappa)} d(\varkappa, z)$, therefore

$$d(x_n, P_T(x_n)) \leq \ d(x_n, w_n) \to 0 \ \ as \, n \to \infty$$

and

$$d\big(x_n, P_T(y_n)\big) \leq \ d(x_n, w_n) \to 0 \ \ as \, n \to \infty.$$

So, the proof completes.

Theorem 2.3: Let E be a nonempty closed convex subset of X and T, P_T and $\{x_n\}$ be as in Lemma 2.1. Then $\{x_n\}$ Δ-converges to a point in F.

Proof: Let $\varkappa \in F(T) = F(P_T)$. By the proof of Lemma 2.1, $\{ x_n \}$ is bounded and therefore $A(\{ \varkappa_n \}) = \{\varkappa\}$. Let $\{ \varkappa_{n_k} \}$ be any subsequence of $\{x_n\}$ such that $A\big(\{ \varkappa_{n_k} \}\big) = \{\varkappa^*\}$. By Lemma 2.2, $lim_{n\to\infty} d(x_n, P_T(x_n)) = 0$. We will show that $\varkappa^*$ is a fixed point of P_T. For this, take $\{\omega_m\}$ in $P_T \ (\varkappa^*)$. Then

$$\begin{aligned} r(\omega_n, \{ \varkappa_{n_k} \}) &= lim \ sup_{n\to\infty} \ d\big(\omega_m, \varkappa_{n_k} \big) \\ &\leq \lim \ sup_{n\to\infty} \Big\{ d\left(\omega_m, P_T\big(\varkappa_{n_k}\big)\right) + d\big(P_T\big(\varkappa_{n_k}\big), \varkappa_{n_k}\big) \Big\} \\ &\leq lim \ sup_{n\to\infty} \ H\big(P_T \ (\varkappa^*), P_T\big(\varkappa_{n_k}\big) \big) \\ &\leq lim \ sup_{n\to\infty} \ d\big(\varkappa^*, \varkappa_{n_k} \big) \\ &= r\big(\varkappa^*, \{\varkappa_{n_k}\}\big). \end{aligned}$$

This yields $|r(\omega_m, \{ \varkappa_{n_k} \}) - r\big(\varkappa^*, \{\varkappa_{n_k}\}\big)| \to 0 \ as \ m \to \infty.$ Lemma 1, we get $lim_{m\to\infty} \omega_m = \varkappa^*$. Note that $T\varkappa^* \in P(E)$ being proximinial is closed, hence $P_T \ (\varkappa^*)$ is closed and bounded. Hence $lim_{m\to\infty} \omega_m = \varkappa^* \in P_T \ (\varkappa^*)$. Consequently $\varkappa^* \in F(P_T)$. From the uniqueness of the asymptotic center, we get

$$\begin{aligned} lim \ sup_{n\to\infty} \ d\big(\varkappa_{n_k}, \varkappa^* \big) &\leq lim \ sup_{k\to\infty} \ d\big(\varkappa_{n_k}, \varkappa \big) \\ &\leq lim \ sup_{n\to\infty} \ d(\varkappa_n, \varkappa) \\ &\leq lim \ sup_{n\to\infty} \ d(\varkappa_n, \varkappa^*) \\ &= lim \ sup_{k\to\infty} \ d\big(\varkappa_{n_k}, \varkappa^* \big) \end{aligned}$$

contradiction and hence, $\varkappa = \varkappa^*$. Therefore $A\big(\{ \varkappa_{n_k} \}\big) = \{\varkappa^*\}$. Hence this show that $\{\varkappa_n\}$ Δ-converges to a fixed point of F.

A map $T: E \to P(E)$ is semicompact if any bounded sequence $\{\varkappa_n \}$ satisfying $lim_{n\to\infty} \ d(x_n, T(x_n)) = 0$ has a convergent subsequence.

Let $h: [0, \infty) \to [0, \infty)$be a nondecreasing function with $f(0) = 0, f(r) > 0$ for $r \in (0, \infty)$ and $T: E \to P(E)$ be a multivalued map. Then a map T is said to satisfy condition (I) if $d(\varkappa, T\varkappa) \geq f(d(\varkappa, F)$ for all $\varkappa \in E$.

Theorem 2.4: Let E be a nonempty closed convex subset of X and T, P_T and $\{\varkappa_n\}$ be as in Lemma 2.1. Then $\{\varkappa_n\}$ converges stongly to a fixed point $\varkappa \in F$ if and only if $liminf_{n\to\infty} d(x_n, T(x_n)) = 0$.

Proof: If $\{\varkappa_n\}$ converges to $\varkappa \in F$, then $lim_{n\to\infty} d(\varkappa_n, \varkappa) = 0$. Since $0 \leq d(x_n, F) \leq d(\varkappa_n, \varkappa)$ it follows that $\lim inf_{n\to\infty} d(x_n, F) = 0$. Conversely, suppose that $\lim inf_{n\to\infty} d(x_n, F) = 0$. From Lemma 2.1, we write

$$d(\varkappa_{n+1}, \varkappa) \leq d(\varkappa_n, F),$$

which implies that

$$d(\varkappa_{n+1}, F) \leq d(\varkappa_n, F).$$

So, $\lim_{n\to\infty} d(\varkappa_n, F)$ exists. From statement of Theorem $\lim inf_{n\to\infty} d(\varkappa_n, F) = 0$, thus $lim_{n\to\infty} d(\varkappa_n, F) = 0$. Next, we show that $\{\varkappa_n\}$ is a Cauchy sequence in E. For $k, n \in N$ and $k > n$, we can write

$$d(\varkappa_k, \varkappa_n) \leq d(\varkappa_k, \varkappa) + d(\varkappa, \varkappa_n) \leq 2d(\varkappa_n, \varkappa).$$

Taking inf on the set F, we get $d(\varkappa_k, \varkappa_n) \leq d(\varkappa_n, F)$.Letting $m, n \to \infty$ in the inequality $d(\varkappa_k, \varkappa_n) \leq d(\varkappa_n, F)$ shows that $\{\varkappa_n\}$ is a Cauchy sequence in E and therefore $\{\varkappa_n\} \to \varkappa^* \in E$. Next, we prove that $\varkappa^* \in F$. By $d\big(\varkappa_n, F(P_T)\big) = inf_{\varkappa^* \in F(P_T)} d(\varkappa_n, \varkappa^*)$ and for each $\epsilon > 0$ there exists ${z_n}^{(\epsilon)} \in F(P_T)$ such that

$$d\big(\varkappa_n, {z_n}^{(\epsilon)}\big) < d\big(\varkappa_n, F(T)\big) + \frac{\epsilon}{2}.$$

This means that $d\big(\varkappa_n, {z_n}^{(\epsilon)}\big) < \left(\frac{\epsilon}{2}\right)$. From $d\big({z_n}^{(\epsilon)}, \varkappa^*\big) \leq d\big(\varkappa_n, {z_n}^{(\epsilon)}\big) + d(\varkappa_n, \varkappa^*)$, we obtain

$$lim_{n\to\infty} d\big({z_n}^{(\epsilon)}, \varkappa^*\big) \leq \frac{\epsilon}{2}.$$

Finally, $d(P_T(\varkappa^*), \varkappa^*) \leq d\big(\varkappa^*, {z_n}^{(\epsilon)}\big) + d\big({z_n}^{(\epsilon)}, P_T(\varkappa^*)\big)$

$$\leq d\big(\varkappa^*, {z_n}^{(\epsilon)}\big) + H\big(P_T({z_n}^{(\epsilon)}), P_T(\varkappa^*)\big) \leq 2d\big(\varkappa^*, {z_n}^{(\epsilon)}\big)$$

which yields that $d(P_T(\varkappa^*), \varkappa^*) < \varepsilon$. Since ε is arbitrary, so $d(P_T(\varkappa^*), \varkappa^*) = 0$. F is closed , then $\varkappa^* \in F$.

Theorem 2.5: Let E be a nonempty closed convex subset of X and T, P_T and $\{\varkappa_n\}$be as in Lemma 2.1. Suppose P_T satisfy $condition$ (I), then the sequence $\{\varkappa_n\}$ converges strongly to $\varkappa \in F$.

Proof: For all $\varkappa \in F$, $\lim_{n\to\infty} d(\varkappa_n, \varkappa)$ exists. We call it c for some $c \geq 0$. If $c = 0$, then results follows directly. Assume that $c > 0$. By (2.2), we can write

$$inf_{\varkappa \in F(T)} d(\varkappa_{n+1}, \varkappa) \leq inf_{\varkappa \in F(T)} d(\varkappa_n, \varkappa),$$

implies that $d(\varkappa_{n+1}, F(T)) \leq d(\varkappa_n, F(T))$. Therefore $\lim_{n\to\infty} d(\varkappa_n, F)$ exists. With the help of Lemma 2.2. and $condition\ (I)$ and , we can write follows that

$$lim_{n\to\infty} f\left(d(\varkappa_n, F(T))\right) \leq lim_{n\to\infty} d(\varkappa_n, T(\varkappa_n)) = 0.$$

Thus

$$lim_{n\to\infty} f(d(\varkappa_n, F)) = 0.$$

By definition of f, ıt follows that $lim_{n\to\infty} d(\varkappa_n, F) = 0$. From proof of Theorem 2.4, we get the desired results.

Theorem 2.6: Let E be a nonempty closed convex subset of X and T, P_T and $\{\varkappa_n\}$ be as in Lemma 2.1. Suppose that P_T is semicompact, then sequence $\{\varkappa_n\}$ converges strongly to $\varkappa \in F$.

Proof: From Lemma 2.1, $\{\varkappa_n\}$ is bounded and by Lemma 2.2. $lim_{n\to\infty} d(\varkappa_n, P_T(\varkappa_n)) = 0$.. Since P_T is semi-compact, there exists a subsequence $\{\varkappa_{n_k}\}$of $\{\varkappa_n\}$ which converges to $\varkappa$. ıt follows from $lim_{n\to\infty} d(\varkappa_n, P_T(\varkappa_n)) = 0$ and Lemma 2.1 that $\varkappa \in F$. Since Lemma 2.1, $\lim_{n\to\infty} d(\varkappa_n, \varkappa)$ exists and therefore $\varkappa_n \to \varkappa$.

REFERENCES

1. Atalan Y., Karakaya V., (2019) Investigation of some fixed point theorems in hyperbolic spaces for a three step iteration process, Korean J. Math. Vol: 27, No: 4, 929—947, 2019.
2. Chang S. S., Wang G., Wang L., Tang Y. K. and Ma Z. L., Δ-convergence theorems for multi-valued nonexpansive mappings in hyperbolic spaces, Appl. Math. Comp., 249, 535-540, 2014.
3. Haubruge S., Nguyen V. H. and Strodiot J., Convergence analysis and applications of the glowinski-le tallec splitting method for finding a zero of the sum of two maximal monotone operators, J. Optim. Theory Appl., 97 (3), 645-673, 1998.
4. Glowinski R. and Le Tallec P., Augmented Lagrangian and operator-splitting methods in non linear mechanics, 9, SIAM, 1989.
5. Goebel K. and Kirk W. A., Iteration processes for nonexpansive mappings, Contemp. Math., 115-123, 1983.
6. Gunduz B., Karahan I., Convergence of SP iterative scheme for three multivalued mappings in hyperbolic space, J. Comput. Analy. Appl., 24, 815-827, 2018.

7. Karahan I., Jolaoso L.O., A Three steps iterative process for approximating the fixed points of multivalued generalized alpha-Nonexpansive mappings in uniformly convex hyperbolic spaces, Sigma J Eng & Nat Sci , Vol:38, No:2, 1031-1050, 2020.
8. Ishikawa S., Fixed points by a new iteration method, Proc. Amer. Math. Soc. 44, 147- 150, 1974.
9. Khan S.H., Agbebaku D., Abbas D., Three Step Iteration Process for Two Multivalued Nonexpansive Maps in Hyperbolic Spaces, Journal of Mathematical Extension,Vol:10, No: 4, 87-109, 2016.
10. Khan S.H., Abbas M., Common fixed points of two multi-valued nonexpansive maps in Kohlenbach hyperbolic spaces, Fixed Point Theory Appl., Article ID 181 (2014), 11 pages.
11. Kohlenbach U., Some logical metathorems with applications in functional analysis, Trans. Amer. Math. Soc.,Vol:357 No:1, 89-128, 2005.
12. Lim T.C., A fixed point theorem for multivalued nonexpansive mappings in a uniformly convex Banach space. Bull. Amer. Math. Soc., Vol:80,1123-1126, 1974.
13. Mann W.R., Mean value methods in iteration, Proc. Amer. Math. Soc., Vol:4, 506-510, 1953.
14. Reich S. and Shafrir I., Nonexpansive iterations in hyperbolic spaces, Nonlinear Anal. 15, 537-558, 1990.
15. Saluja G.S., Common fixed points for four multivalued nonexpansive mappings in Kohlenbach hyperbolic spaces,U.P.B. Sci. Bull., Series A, Vol:82, No:2, 2020
16. Sastry K.P.R, Babu G.V.R., Convergence of Ishikawa iterates for a multivalued mapping with a fixed point. Czechoslovak Math. J. Vol:55,817-826, 2005.
17. Shimizu T. and Takahashi W., Fixed points of multivalued mappings in certain convex metric spaces,Topol. Methods Nonlinear Anal, Vol:8,197-203, 1996.
18. Takahashi W.A., A convexity in metric space and nonexpansive mappings, I.Kodai Math. Sem. Rep., Vol:22, 142-149, 1970.
19. Phuengrattana W. and Suantai S., On the rate of convergence of Mann, Ishikawa, Noor and SP-iterations for continuous functions on an arbitrary interval, J. Comput. Appl. Math., 235, 3006-3014, 2011.

Development of an Integrated Supplier Portal for Procurement and Supplier Management

Ayşe İrem Özmen[1], Sera Özkıvanç[2], M. Fatih Akay[3]

[1]MDP Group, Department of Research and Development, Istanbul, Turkey
irem.ozmen@mdpgroup.com

[2]MDP Group, Department of Information Technologies, Istanbul, Turkey
[2]Mimar Sinan Fine Arts University, Institute of Sciences and Technology, Istanbul, Turkey
sera.ozkivanc@mdpgroup.com

[3]Çukurova University, Department of Computer Engineering, Adana, Turkey
mfakay@cu.edu.tr

ABSTRACT

An efficient supply chain relies on efficient communication channels between businesses and their suppliers. Manufacturing operations are dictated by the effectiveness of procurement and delivery activities. These include but are not limited to various procurement management tiers like supplier selection, auctions, stock orders, deliveries, and reconciliation activities. This paper presents the development and implications of an integrated web supplier portal. The aim of the Supplier Portal is to streamline and standardize supply chain processes. Current modules of the portal include supplier selection, procurement auctioning, order management, communication, supplier evaluation, and reconciliations management. Overall, the portal standardizes and simplifies supplier selection operations, resulting in higher quality materials and reduced manufacturing costs. The portal was tested, produced, and developed using PostgreSQL. Backend and frontend developments were realized with JavaScript in compliance with ES6 standards.

Keywords: Procurement Management, Supplier Portal, Supply Chain

1. INTRODUCTION

Procurement and supply chain management directly influence enterprises' profitability. A lack of timely and accurate acquirement of goods causes delays in business operations, which translate to long-term financial loss. Conversely, an optimized procurement strategy leads to decreased cost, reduced risk, and enhanced supplier quality. A digitally integrated procurement strategy can transform this mundane operation into a strategic and competitive move for increasing profit generation [1].

A significant number of companies administer procurement activities through outdated technologies like emails, text messaging or phone calls. These inefficient methods no longer hold a place in a rapidly evolving technological landscape. Organizations still employing these methods must urgently transition to smart systems. The widespread adoption of Industry 4.0 technologies in the manufacturing sector gives enterprises another incentive for matching competitors' performances [2]. Succeeding in a changing competitive environment requires strong relationships with suppliers; using a supplier portal is the most advantageous strategy for maintaining these relations.

A supplier portal is a platform that digitalizes procurement and supply chain operations. Supplier portals are an integral part of the digital supply chain and can improve supply chain performance. They minimize manual data entry, increase visibility and accessibility of information, and strengthen communication between businesses and suppliers. However, 60% of Turkish enterprises do not employ a supplier portal application. Only 58% of Turkish enterprises have up-to-date lists of approved suppliers [3].

As the selection of suppliers becomes more diverse and the supply chain environment more complex, the risks of ineffective procurement management strategies proliferate. Main short-term issues stemming from poor procurement processes include the following: redundant spending due to misinterpretation of contracts, poor quality purchases due to lack of supplier evaluation, and costly delays due to miscommunication between parties. The reoccurrence of these problems leads to long-term issues such as loss of profitability and mistrust from clients.

Furthermore, the COVID-19 pandemic has led to significant changes in enterprises' procurement strategies. Nationally, over 60% of procurement units have reassessed their priorities since the beginning of the pandemic. Cost reduction and risk management have become urgent concerns. A recent national report found that 43% of procurement units have cost reduction as their main strategic priority, while 24% are focusing on supplier research and management. The third most prevalent priority is digitizing of processes, accounting for 12% of procurement units [4]. Research shows that enterprises' operational performance heavily relies on supplier selection and management, providing ample reason to invest in web portal solutions [5, 6].

This paper presents the development of an integrated supplier portal that digitizes supplier selection and procurement processes. The Supplier Portal enables procurement auctioning, communication with suppliers, order management, quality evaluation, and reconciliation processes through a single platform. Thus, this product addresses an important gap in the industry, with a market potential that encompasses no less than 60% of enterprises nationwide.

Section 2 provides explanation on the portal's modules and features; Section 3 presents development methodology; Section 4 delves into the implications of this product. Finally, Section 5 presents future plans for the product's subsequent phases.

2. PROPOSED PRODUCT

The Supplier Portal is a platform that enables effective management of procurement and digital supply chain activities in a digital medium. Procurement refers to the purchasing of all goods and services acquired for maintaining an enterprise's activities. This portal facilitates a reliable and secure flow of information between buyer and supplier, significantly improving business processes across six key areas:

- Supplier selection
- Procurement auctioning
- Order management
- Communication
- Supplier evaluation
- Reconciliations management

Supplier selection

Once the enterprise has the Supplier Portal set up, they must inform their suppliers that procurement activities will henceforth be conducted via the portal. Suppliers wishing to engage in transactions with the enterprise must apply to register as business partners through the portal. The enterprise can view the applicants' past orders, certificates, and contracts. Following a vetting process, suppliers that are accepted as business partners gain access to the portal.

Procurement auctioning

When the enterprise wants to place an order, they advertise this need with a procurement auction. Suppliers get notified of the auction and can compete to provide the product or service. The enterprise's procurement department can compare the bidders' certificates, past orders, evaluations, ratings, and other relevant information as seen in Figure 1. Once a supplier is selected, the order process may begin.

Order management

Suppliers who win an auction get notified and can begin preparing their order. Enterprises can use the Supplier Portal to access critical information throughout the delivery process, as seen in Figure 1. Details like order number, order date, delivery stage, product details, and documentation are easily accessible.

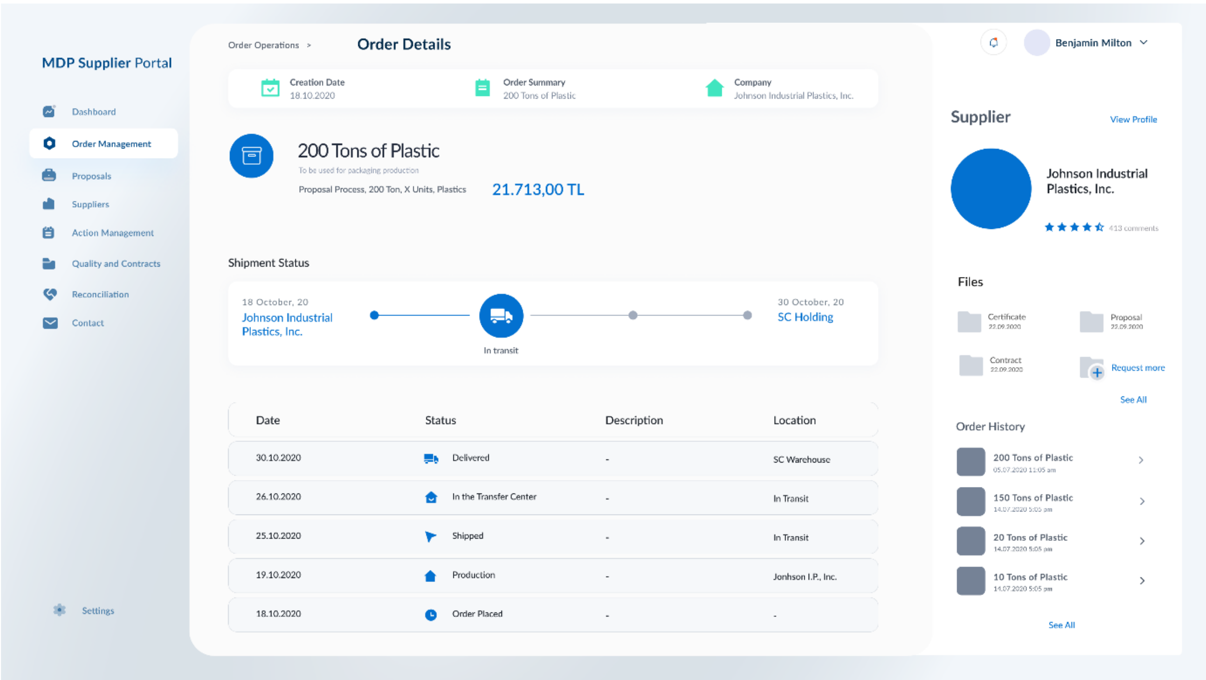

Figure 1. The Supplier Portal Order Management page

Communication

The Supplier Portal provides a communication channel between the enterprise and its suppliers. The enterprise shares announcements, while the supplier provides status notifications. Automatic alerts of critical dates and bidding schedules keep both parties informed of developments. This prevents the miscommunication that results from disparate correspondence methods (i.e., emails, SMS, and phone calls). Furthermore, it reduces the administrative workload required to follow up on orders.

Supplier evaluation

The enterprise evaluates its suppliers based on aspects like delivery performance, price stability, and availability of after-sales support, technical integrity, and any other factor it deems important. The evaluation screen can be seen in Figure 2. The portal calculates an average score for suppliers based on these inputs. Procurement can then refer to these evaluations for future auctions.

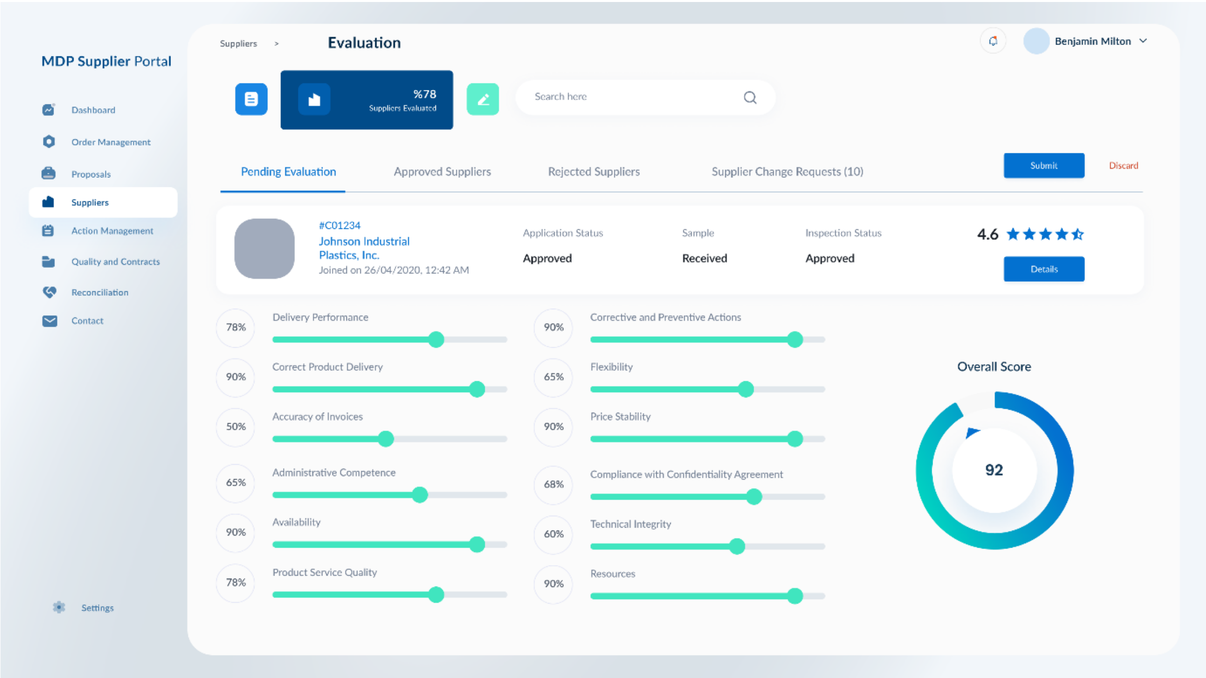

Figure 2. The Supplier Portal Supplier Evaluation page

Reconciliations management

The enterprise and its suppliers can perform reconciliation via the portal at the end of accounting periods. The enterprise fills in a form and sends it to the relevant supplier for approval; the supplier is only required to check and approve the balance. This feature significantly reduces administrative workload and minimizes the margin for human error.

3. METHODS

PostgreSQL was used for testing, production, and development. The database architecture was developed based on relational database rules. All normalization standards were tracked and designed using 4NF.

Backend and frontend developments were realized with JavaScript, following ES6 standards. Compliance with code writing standards was ensured by referring to the ESlint Library. Frontend development was realized with React.js. A combination of Redux and React technologies were utilized. Backend development was realized with Node.js. In the context of Node.js, codes were written using the Express framework.

RabbitMQ was used for the control of all mailing systems, creating a queue structure. This structure prevents potential timeout issues that may occur in request operations. The Amqlib Library was used for enabling communication with RabbitMQ. For the control of all mail systems, the micro service structure has been used with RabbitMQ and a queue structure has been created. The queue structure prevents timeout problems that may occur in request operations. A library called amqplib has been used to communicate with RabbitMQ.

Socket.IO was used for enabling instant transmission of notifications in the portal. The query and update processes in the backend section were coded using Sequelize; these allow the user to create new records, update and delete existing records with ease.

Unit tests were coded with Jest library. The code blocks that failed the unit tests were not transferred to the server. Thus, the error percentage is minimized in the live environment.

The order of operations for developing the product is illustrated in Figure 3. In the Version Control System, every branch goes through an automatized control system and an administrator review before going into the main branch. Modifications made in the development stage are compiled in the test server. End user tests are conducted before transferring to the main server.

When end user tests are successful, the developments are transferred to master branch with continuous integration.

The potential for errors in the main server is minimized by separating the servers from each other and automatizing the system with TravisCI and Bitbucket. This also ensures that any errors are reported.

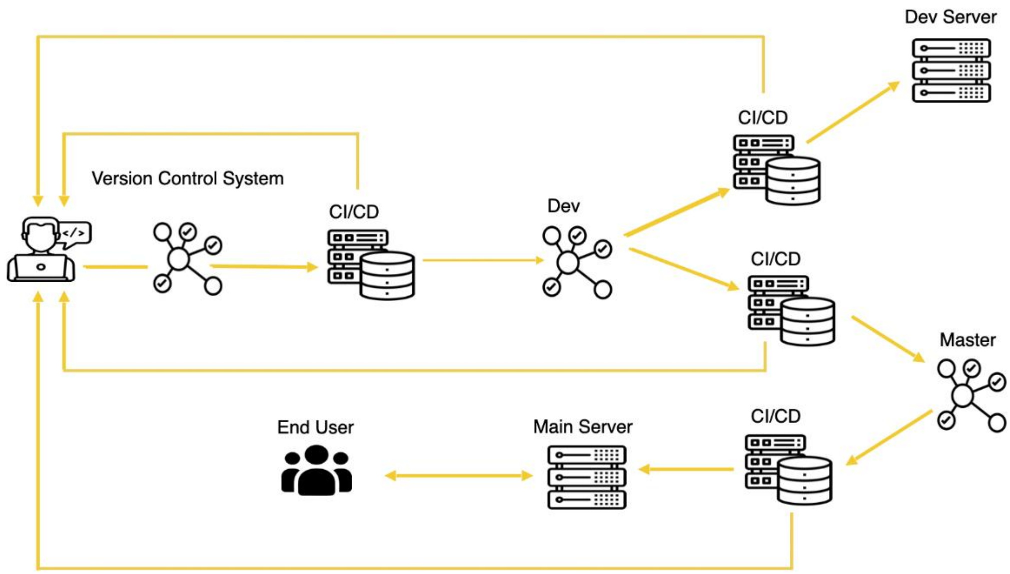

Figure 3. CI /CD

4. IMPLICATIONS OF THE PRODUCT

Supplier management practices heavily influence enterprises' operational performance. As more suppliers enter the market, acquiring quality materials at reasonable prices becomes more challenging. Procurement personnel may habitually lean towards the cheapest price or present positive bias towards suppliers with longstanding relationships [7]. The Supplier Portal prevents such subjectivities by providing a systematic approach to selecting bids. The portal enables enterprises to compare prices, predicted delivery dates, order histories, supplier ratings, payment terms, and more. Additional parameters can be added to the portal depending on enterprise priorities. Enterprises can request product samples at the click of a button.

Furthermore, the portal makes it easier for enterprises to expand their supplier portfolio. New suppliers register to the portal, fill in their information and upload the required documentation. This also leads to the standardization of submitted information from suppliers, which creates a more formal and neutral medium for assessing applicants [8]. Traditionally, procurement departments would have to undertake this administrative workload. Additionally, more suppliers lead to a wider selection of quality products and services.

Finally, the Supplier Portal enhances communication between business partners. Order delays lead to operational errors and costly downtime for enterprises. Research shows that active cooperation with suppliers reduces these risks. The portal's action alert and order tracking features ensure that suppliers provide the right product at the arranged time. By providing a fast and organized environment to evaluate and communicate with suppliers, the portal streamlines procurement and helps achieve more favorable deals.

5. CONCLUSION AND FUTURE WORK

Procurement departments have two main priorities: reducing cost and increasing operational efficiency. The COVID-19 pandemic has increased the urgency in enterprise efforts to cut spending where possible. As a result, many businesses want to minimize inventory stocking or shift to a just-in-time (JIT) strategy.

JIT is a production technique that involves acquiring the right amount of materials at the right time for manufacturing. Time lapse between material delivery and production is minimal. JIT eliminates the need for stocking, allows a reduction in raw material, and prevents waste. A critical factor for implementing JIT is material procurement; this relies on supplier selection and demand forecasting.

The Supplier Portal streamlines supplier selection in several ways. Enterprises can increase their supplier portfolio without effort, compare attributes, and refer to detailed performance evaluation. The next phase of product development will entail a demand forecasting module. This module will prevent bottlenecks by predicting supply needs and providing preemptive procurement recommendations.

Demand forecasting is a regression problem. Regression problems require a statistical, AI-based, or simulation approach. Current scientific research suggests that common methods for demand forecasting include Machine Learning (ML) and Deep Learning (DL). Therefore, future work will be actualized using the following solutions:

- Machine Learning/Deep Learning based time series
- Time-Delay Integration (TDI) and optimization
- Supervised Machine Learning
- Feature selection algorithms

The shift toward Industry 4.0 in production will further evolve the digital supply chain, giving way to technologies that anticipate enterprise needs. To survive in a competitive global market, businesses must leverage innovative solutions for streamlining procurement activities and maximizing profitability.

REFERENCES

[1] Seyedghorban, Zahra, Danny Samson, and Hossein Tahernejad. 2020. "Digitalization Opportunities For The Procurement Function: Pathways To Maturity". *International Journal Of Operations & Production Management 40 (11): 1685-1693. doi:10.1108/ijopm-04-2020-0214.*

[2] Sharma, Manu, and Sudhanshu Joshi. 2020. "Digital Supplier Selection Reinforcing Supply Chain Quality Management Systems to Enhance Firm's Performance". *The TQM Journal*. Published ahead of print, October 9, 2020. *doi:10.1108/TQM-07-2020-0160.*

[3] Erdal, Murat. 2019. "Türkiye Satınalma Raporu 2019, Satınalma Departmanlarının Mevcut Durumunu Ortaya Koyuyor." *Satın Alma Dergisi*, May 2019, 14.

[4] Dijital Satınalma Araştırması [Digital Procurement Research]. 2020. Ebook. PwC EMEA.

[5] Truong, Huy Quang, Maria Sameiro, Ana Cristina Fernandes, Paulo Sampaio, Binh An Thi Duong, Hiep Hoang Duong, and Estela Vilhenac. 2021. "Supply Chain Management Practices And Firms' Operational Performance". *International Journal Of Quality & Reliability Management 34 (2).*

[6] Garcia, Fabienne, Bernard Grabot, and Gilles Paché. 2019. "Adoption Mechanisms Of A Supplier Portal: A Case Study In The European Aerospace Industry". Computers & Industrial Engineering 137: 106105. doi:10.1016/j.cie.2019.106105.

[7] Truong, Huy Quang, Maria Sameiro, Ana Cristina Fernandes, Paulo Sampaio, Binh An Thi Duong, Hiep Hoang Duong, and Estela Vilhenac. 2021. "Supply Chain Management Practices And Firms' Operational Performance". *International Journal Of Quality & Reliability Management 34 (2).*

[8] Cheng, T.C.E., and S. Podolsky. 1996. *Just-in-Time Manufacturing: An Introduction.* 2nd. London: Chapman & Hall.

Antispiral Resonator Ground Plane Loaded Gamma (Γ) Shaped Microstrip Antenna Design

Emre Selçuk DEMİR[1], **Merih PALANDÖKEN**[1]

[1] Department of Electrical and Electronics Engineering, Katip Çelebi University, Çiğli, Izmir, Turkey

[1] Department of Electrical and Electronics Engineering, Katip Çelebi University, Çiğli, Izmir, Turkey

e.selcuk.demir@gmail.com

Abstract

Nowadays as a result of the rapid change and development of technology from day to day, there have been significant improvements in biomedical systems. As a result of these developments, biotelemetry systems, which is an important sub-branch of biomedical systems, have also been highly affected by these technological developments and changes. Biotelemetry systems is a type of biomedical system that allows remote monitoring of health data belonging to a patient. Therefore, antennas play an important role and application specifically designed for remote and wireless monitoring of patient's health data. In accordance with this scope, the frequently addressed antennas called Bioimplantable antennas are used in biotelemetry systems. Bioimplantable antennas should be designed to be as small as possible, as they are going to be placed inside the patient's body. Considering all these circumstances, small physical size, low loss, low cost, low power consumption and ease of fabrication are the important requirements to be fulfilled for the biotelemetry systems. Low profile microstrip antennas are a highly efficient type to be dedicated for the utilization in bioimplantable antenna design. In this paper, compact bioimplantable microstrip antenna consisting of Gamma(Γ) shaped microstrip lines loaded split ring resonator on antispiral resonator loaded ground plane is introduced for medical applications in MICS (402-405 MHz Medical Implant Communication System) frequency bandwith numerical computation results on tissue layers and properties included in the literature. Rogers RT/duroid 6010LM material with high dielectric constant $(\varepsilon_0 = 10.2)$ has been used in the antenna design. Numerical computations of the designed antenna have been carried out in CST Microwave Studio. The proposed bioimplantable antenna operates in the frequency range of 388-405 MHz with 4.9% bandwidth covering MICS band with S_{11} parameter of $-26.85dB$ at 395 MHz.

Keywords: *Antispiral Resonator, Implantable Antenna, Implantable Medical Devices, Medical Implant Communication System (MICS) Band, Biomedical Telemetry Systems, Microstrip Patch Antennas*

Introduction

As a result of rapid development in technology, many science and technology areas have been positively affected by these developments. One of the areas most affected by these developments is undoubtedly the field of Health Sciences. As a result of all these developments, a system called “Biotelemetry Systems” has been developed. These Biotelemetry systems, aiming to improve the patient's comfort of life while ensuring remote monitoring of the patient's health data in order to facilitate the diagnosis from the doctor's point of view. One of the most important parts used in Biotelemetry systems is the antenna topological geometry determining the physical size of the implantable system to be placed in the patient’s body. While biosensing system units monitoring the patient's health data can be fabricated in chip size the bioimplantable antennas providing the wireless communication in the system cannot be produced in micron size. The structural design and fabrication of bioimplantable antennas in compact sizes are very difficult since the decreased physical size results into the increment in the resonance frequency. Therefore, the overall size of the whole system usually is determined by the antenna physical dimensions. For this reason, microstrip antennas, which are easy to manufacture, have good radiation performance, are designed to obtain the reliable operation at low voltage and power levels where high data rates are provided. Such type of application specific antennas used in biotelemetry systems is termed as “bioimplantable antennas”. The operation frequency range of bioimplantable antennas used for medical therapy and diagnosis in biotelemetry systems has been determined by FCC (U.S. Federal Communications Commission) and ETSI (European Telecommunications Standards Institute). The operation band covering 402-405 MHz frequency range is called as MICS (Medical Implant Communication System) frequency band. The MICS frequency band is different from one country to another country covering the frequency ranges of 413-419 MHz, 426-432 MHz, 438-444 MHz, 451-457 MHz frequencies. 2360-2400 MHz, 2400-2500 MHz ISM (Industrial Scientific Medical) bands may also be preferred for bioimplantable antenna frequencies [1].

In the scope of bioimplantable antennas, A. Basir et al. designed an implantable antenna with a square spiral resonator structure. Rogers RT/duroid 6010 material has been used in the antenna design. While this material is not harmful to human health, it also positively affects antenna performance with a high dielectric constant (10.2). The antenna used in the article is designed to glow in the MICS (403 MHz) and ISM (2450 MHz) bands [2].

Rongqiang Li et al created an antenna design by creating cuts of various sizes on the copper surface. They used Rogers RT/duroid 6010 material in the antenna design. In the article, it is seen that the antenna designed to cover the MICS frequency band has radiation performance in the frequency range from 378 to 427 MHz [3].

Fanpeng Kong et al created their design by placing two antispiral resonator structures side by side, combining them with a feed line. For this antenna design, Rogers RT / duroid 6010 and PDMS were used together. PDMS is a kind of silicone-like coating used to cover the antenna. It has been concluded that this antenna, which radiates at the frequencies of 433 and 915 MHz, covers the MICS band [4].

Rongqiang Li et al referenced the semicircular shape for their design. Creating slot structures of various sizes on this semicircle, the team used the Rogers RT/duroid 6010 dielectric material for the antenna. Through the design they created, the antenna radiates in the 402 MHz MICS band [5].

Zhu Duan et al preferred the spiral resonator structure for antenna designs. They used the Rogers RT/duroid 6010 dielectric material in the design, in which they connected 2 spiral resonators in the antenna to be parallel to each other. The antenna they designed radiates in the 433 and 542 MHz frequency bands. 433 MHz since the MICS band is accepted by some countries, it is accepted that the antenna works in the MICS band [6].

Y. Cho et al examined the design he created by opening slots in various ways (such as Γ, E, l, -) to copper on the dielectric material and creating an antenna. They completed the design of the antenna by opening a slot in the form of "Γ" to the ground plane of the antenna. They used the Rogers RT/duroid 6010 dielectric material in the antenna they designed. Studying the operating frequency of the antenna, it was concluded that it radiates in both the MICS and ISM bands with 402 and 2450 MHz [7].

Imran Gani et al [7] used a similar design, but changed the antenna's ground plane by using a slot with a hook structure. They used the Rogers RT / duroid 6010 dielectric material in the antenna. Studying the operating frequency of the antenna, it was concluded that it radiates in the MICS band with 402 MHz [8].

Method

In order for Bioimplantable antennas to be used inside the body, the three basic design parameters to be considered are very important. The first design parameter to be considered is that the dielectric material to be used in the Bioimplantable antenna does not pose a danger to the health of the patient, and the dielectric material to be used should be selected as a material that does not interact chemically with tissues, that is, biocompatible material. The second important point is that both surfaces of the dielectric substance used contain copper, and because human tissue is conductive, the Bioimplantable antenna may short-circuit and damage the patient. A biocompatible Rogers RT/duroid 6010LM dielectric material was preferred and used in the antenna designed to solve the biocompatibility problem. Another reason for using the Rogers RT/duroid 6010LM dielectric material is that it is necessary to use a material with a high dielectric constant for the design of a Bioimplantable antenna. The properties of the Rogers RT/duroid 6010LM dielectric material used in the antenna designed for this purpose are as follows; the dielectric constant (ε_0) is 10.2, The Lost tangent is 0.0023, the copper thickness is 35µm and the dielectric thickness is 0.64 mm. Rogers RT/duroid 6010LM dielectric material is the most accurate choice for this antenna when looking at the literature. In order to eliminate the problem of causing damage to the patient by short-circuiting the Bioimplantable antenna, which is a second problem, the copper surfaces of the antenna must be insulated from the tissues. While providing this textural insulation, biocompatibility needs to be paid attention to again. For this reason, Rogers RT/duroid 6010LM dielectric material was added to the antenna, but substrate and superstrate materials without copper surface were added to the Bioimplantable antenna sandwich format. The third and most important point is the size of the Bioimplantable antennas designed. The smaller the dimensions, the greater the patient's comfort. Because of its dimensional advantage, the most commonly used design geometry in the literature is resonator structures. For this paper, the antispiral resonator structure was preferred and the antenna design was created. The main reason for using the Antispiral resonator structure is that it allows you to get a large glow surface in a small area.

Taking into account all these criteria, the design of "Antispiral Resonator Ground Plane Loaded Gamma (Γ) Shaped Microstrip Antenna Design" was made to glow in the MICS band (402-405 MHz) in human tissue. The designed antenna while the antenna design has a different and original than in the literature of the antennas in the literature and compared with the relevant working to have a smaller size band (MICS band S_{11}<-10 dB) and adequate performance throughout radiation have come to the fore. The patch plane of the designed antenna is shown in Figure 1 and the ground plane is shown in Figure 2, and the physical measurements of the antenna are as in Table 1.

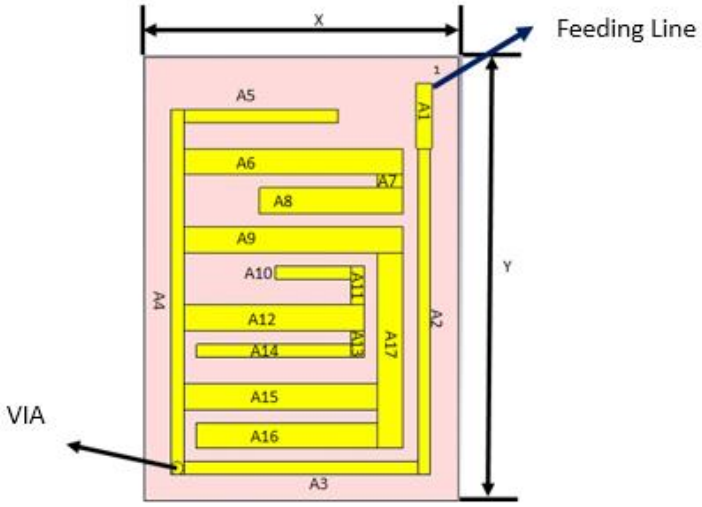

Figure 1. Antispiral Resonator Ground Plane Loaded Gamma (Γ) Shaped Microstrip Antenna's Patch Plane

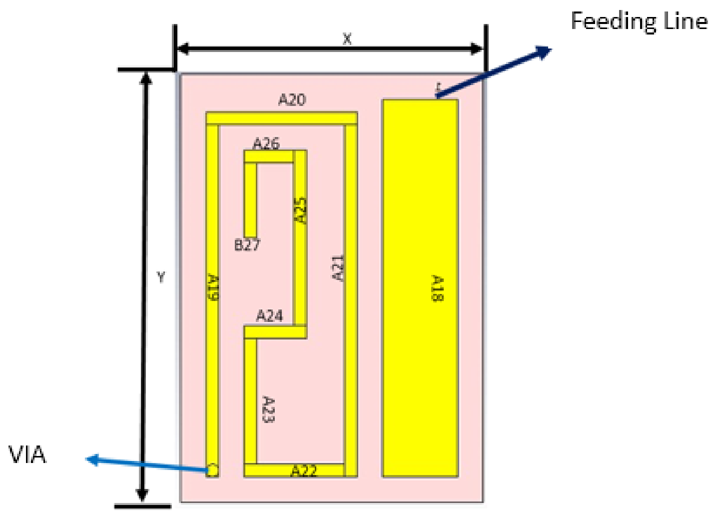

Figure 2. Antispiral Resonator Ground Plane Loaded Gamma (Γ) Shaped Microstrip Antenna's Ground Plane

Table 1. Antispiral Resonator Ground Plane Loaded Gamma (Γ) Shaped Microstrip Antenna's Physical Measurements

Parameters	Length (mm)	Width (mm)	Parameters	Length (mm)	Width (mm)
A1	2.5	0.59	**A15**	1	7.40
A2	12.5	0.5	**A16**	1	6.90
A3	0.5	8.95	**A17**	7.5	1
A4	14	0.5	**A18(Ground)**	15	3
A5	0.5	5.90	**A19**	14	0.5
A6	1	8.40	**A20**	0.5	6
A7	0.5	1	**A21**	14	0.5
A8	1	5.5	**A22**	0.5	4
A9	1	8.40	**A23**	5	0.5
A10	0.5	2.90	**A24**	0.5	2.5
A11	1.5	0.5	**A25**	7	0.5
A12	1	6.90	**A26**	0.5	2
A13	1	0.5	**A27**	3	0.5
A14	0.5	5.90	**X, Y**	17	12

The dimensions of the designed antenna are determined as 17 * 12 mm. By adding an antispiral resonator structure to the ground plane of the antenna, connecting it to each other with the patch plane (VIA), the radiation surface is increased without increasing the size of the antenna, reducing the radiation frequency to even lower levels, that is, to the frequency bands that will cover the MICS band.

Numerical Calculations of The Designed Antenna

The design parameters of the proposed antenna for this paper are given in Table 1. Numerical calculation results of the proposed antenna were made with the help of a program called CST Microwave Studio, and the resulting S parameter result is shown in Figure 3. Figure 4 shows the placement of the antenna inside the body, the position in which the antenna is located, and Table 2 shows the electrical properties and dimensional values of body tissues.

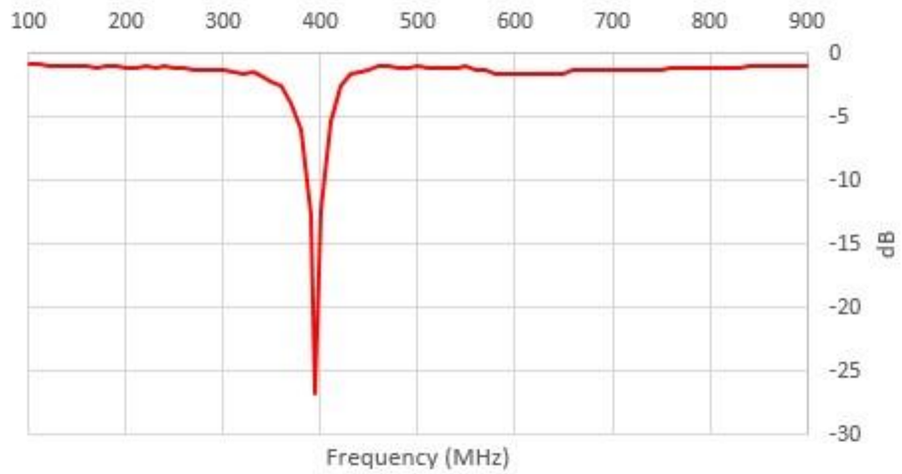

Figure 3. Antispiral Resonator Ground Plane Loaded Gamma (Γ) Shaped Microstrip Antenna's S parameter result

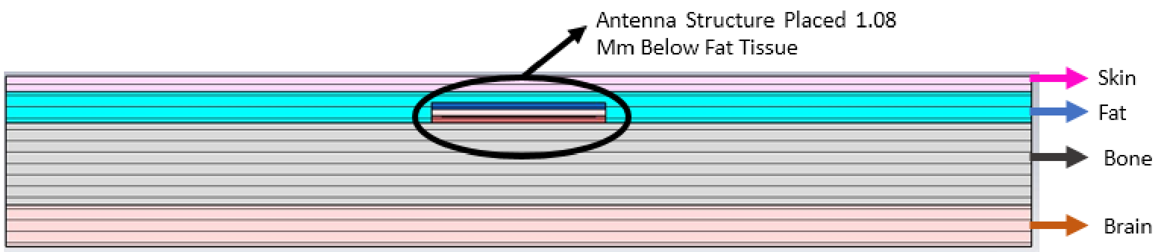

Figure 4. Position of Antenna Inside Body

Table 2. Electrical Properties and Dimensional Values of Body Tissues [9]

Tissue	Dielectric Constant (ε_0)	Conductivity (S/m)	Density (kg/m^3)	Tissue Size
Skin	46.7	0.69	1.01	100*100*1.5
Fat	11.6	11.6	0.92	100*100*3
Bone	17.8	17.8	0.16	100*100*8
Brain	49.7	49.4	0.59	100*100*4

As shown in Figure 4, when the antenna was placed inside the tissues and calculations were made using the values in Table 2, the result of the antenna's s parameter was formed as shown in Figure 3. In Figure 3, it was calculated that the antenna s parameter is in the frequency range of 388-405 MHz(S_{11}<-10dB), at 395 MHz, the minimum S_{11}=-26.85 and has a bandwidth of 2.13%.

One of the undesirable effects that Bioimplantable antennas can cause in the region where they are placed due to their placement in the body is the increase in temperature that they will cause in the relevant region. This value, known as the specific absorption rate (SAR), is a measure of whether the temperature increase is at an acceptable level, defining the average electromagnetic power value lost in a unit mass of tissue that will turn into heat due to conductivity in the tissue. The average SAR for 1 gram of body tissue is projected to be $1.6\,W/kg$. CST Microwave Studio performs calculations by applying 1W power while performing the calculation. In this direction, if the 1.6 value is divided by the calculated SAR value, the power to be applied to the antenna can be calculated as W. Because the resulting result is a small value, the W value can be converted to mW by multiplying by 1000. The result is that a maximum power of 9.2 MW can be applied when the necessary calculations are made for the Antispiral Resonator Ground Plane Loaded Gamma (Γ) Shaped Microstrip Antenna's.

Result

In this paper, the design of the antispiral resonator ground plane gamma (Γ) loaded slots ring microstrip antenna, which radiates in the mics frequency band and has small dimensions, is explained. The numerical calculation results of the designed antenna and the parameters used in these calculations are discussed in detail. For this antenna design, the gamma(Γ) shaped charged slots ring model on the patch plane was connected with the antispiral resonator located in the ground plane via connection and the numerical calculations were completed by the antenna transmission line supply method. The designed antenna is optimized according to the model in which skin, fat, bone and brain tissues are used, and the designed antenna radiates in the MICS frequency band. Antenna dimensions 17*12*0.64 two insulators of 0.64 mm were added to the bottom and top of this antenna structure, designated in mm. In addition, as a result of the SAR analysis, the maximum amount of power to be applied to the antenna was 9.2 mW. As a result, the S parameter is in the 388-405 MHz frequency range, minimum S_{11}=-26.85dB at 395 MHz and radiates in the MICS frequency band determined by 402-405 MHz with a 4.9% bandwidth, and the study showed that it can technically be used as an implantable antenna in biotelemetry systems.

REFERENCES

1. Ferdous, N., Nainee, N.T., Hoque, R., "Design and performance of Miniaturized Meandered patch antenna for implantable biomedical applications", 2nd International Conference on Electrical Engineering and Information Communication Technology (ICEEICT), pp. 1-4, 2015
2. A. Basir, A. Bouazizi, M. Zada, A. Iqbal, S. Ullah, U. Naeem, 'A Dual-band Implantable Antenna with Wide-band Characteristics at MICS and ISM Bands', Microwave and Optical Technology Letters, 24 October 2018
3. Rongqiang Li, Bo Li, Guohong Du, Xiaofeng Sun, Haoran Sun, 'A Compact Broadband Antenna with Dual-Resonance for Implantable Devices', Micromachines (Basel), 16 January 2019
4. Fanpeng Kong, Muhammad Zada, Hyoungsuk Yoo, Maysam Ghovanloo, 'Adaptive Matching Transmitter with Dual-Band Antenna for Intraoral Tongue Drive System', IEEE Transactions on Biomedical Circuits and Systems, December 2018
5. Rongqiang Li, Shaoqiu Xiao, 'Compact Slotted Semi-circular Antenna for Implantable Medical Devices', Electronics Letters, 01 November 2014
6. Zhu Duan, Yong-Xin Guo, Rui-Feng Xue, Minkyu Je, Dim-Lee Kwong, 'Differentially Fed Dual-Band Implantable Antenna for Biomedical Applications', IEEE Transactions on Antennas and Propagation, 17 July 2012
7. Y. Cho, H. Yoo, 'Miniaturised Dual-band Implantable Antenna for Wireless Biotelemetry', Electronics Letters, April 2016
8. Imran Gani, Hyoungsuk Yoo, 'Miniaturized Scalp-Implantable Antenna for Wireless Biotelemetry', International Workshop on Antenna Technology (iWAT), March 2015
9. Nizam Uddin, Raja Rashidul Hasan, Abdur Rahman, Shantanu Kumar Nath, Palash Sarkar, "Bio-implantable Antenna at Human Head Model", International Conference on Robotics, Electrical and Signal Processing Techniques (ICREST), 10-12 Jan. 2019

THE INFLUENCE OF VARIOUS SUPPORT SCHEMES ON THE ECONOMICAL FEASIBILITY OF VARIOUS SCALE WIND TURBINE SYSTEM IN DELTA STATE, NIGERIA

Taiwo Temitayo Ijaoye [1]

[1] Department of Electrical & Electronics Engineering, Cyprus International University, Nicosia, Cyprus

İjaoyetaiwo080@gmail.com

Mehmet Senol [2]

[2] Department of Electrical & Electronics Engineering, Cyprus International University, Nicosia, Cyprus

msenol@ciu.edu.tr

Abstract

The electricity demand of Nigeria is increasing rapidly with very little contribution from the renewable energy. The major source of the energy supply of the country is the fossil fuels that creates pollution. Additionally, it is a finite source in nature. As a result, there is a quick need to search for different opportunities to satisfy up with the strength requirement of the country. Energy resources have always remained as important power assets in Nigeria for several years. This research consequently examines on the various scale of wind turbine size in Federal Republic of Nigeria (FRN) and the influence of various support schemes, which can urge the wind power installations. Homer software is used to run simulations based on various support schemes in this project. Four support scheme is applied with four rated capacity of wind turbine of 80 kW, 100 kW, 250 kW, and 500 kW. Also, the average daily load is kept varying from 1000 kWh to 3000 kWh, in 1000 kWh steps so that to study, the effect of the aforementioned support schemes on the viability of wind power in a special state in FRN. The result shows that as the rated capacity of wind turbine (WT) increases from 80 kW through 500 kW, the gradual decrease in simple payback increases the present worth. Additionally, the research reveals that out of the entire support scheme, feed in tariff is selected to be the most feasible one. This eventually makes the setup of wind turbine in FRN to be notably viable.

Keywords: Capacity factor; Energy differences; IRR; O&M; Present worth; Simple payback.

1. BACKGROUND

The use of the wind energy is attractive because it is environmental friendly and economically feasible in many regions of the world [1]. For this cause, many countries nowadays has shown efforts for utilizing renewable energy (RE) such as wind energy [2]. Despite increase of fuel resources in FRN, the electricity demand per capita remains high [3]. However, the threat of predicted fuel depletion, climate change, pollution and oil value volatility, urge the country to develop various approaches for the electricity generations. These alternatives approaches are mainly renewables because they provide a solution for energy supply security issues [3].

There is an increment rate of fossil resources for the power generation in FRN. Therefore, collaborate with others power generation company to sustain the requirements of the country [4]. Electricity situation of FRN reflected that power request seem extremely rise, due to growing of geopolitical zones. However, makes the provision of the electricity to be insufficient, uncertain, and infrequent, as a result of nonrenewable resources that are quick to exhaust [5]. Circumstances requires the deviation of the energy by improve the huge renewable energy capita in FRN. Most of the zones in FRN endued with robust wind environments, especially in the seaside zones.

The Nigeria government proposed to increase hydropower generation to 5690 MW, thermal power to 2000 MW along with RE of about 1000 MW, and dissemination capacity of about thirty three thousand megawatt by 2020. This goal invented purposely to reduce FRN power mix of nonrenewable dependency and to increase the wind power generation (WPG) in the country. Additionally, because of this substitute resolution, several electricity delivery firms through freelance independent power purchasing system and States are presently financed to construct medium scale of WPG of 2000 MW transmitted to the FRN grid [6].

The wind power within FRN at ten meter altitude is studied for 10 wind locations around six geopolitical zones in the country displays that some locations have wind power between 1.0m/s and 6.3m/s that ratified FRN have reasonable wind energy [7]. Along with their drawn chart, is confirmed that off seashore in the southern regions of FRN have capacities for generating durable wind power [7]. However, wind speed capacities in seaside regions of FRN have demonstrated excellent wind prospective to implement the WPG. Also, reveals the wind power density evaluation at twenty five meter height that confirmed north central of FRN to be highly viable for yearly WPG of wind turbine load in kilowatt-hour [7].

The financial analysis of wind power generation is demonstrated in FRN [8]. The technical and economical study of six WPG are categorized in small, medium and large with their wind turbine size rated from 20 KW- 2 MW is studied [8]. However, electricity cost value together with the present value cost of electricity is estimated for all the six selected geopolitical zones of FRN. Therefore, this is done by using wind speed data between twenty-five years to thirty-seven years scale at hub height of 10m. Additionally, six models are used to evaluate the analysis for all the six geopolitical zones with their various hub height range from 36.6m through 70m. The result demonstrated that, Uyo has a least average total production energy output with P10-20 WT, whereas Kano using Vesta V80 WT given the highest average total production of energy output [8].

2. METHODOLOGY

The method that is used in this study specially deals with the feasibility evaluation of wind power by supplying energy for electrical loads of various sizes at a precise location in Federal Republic of Nigeria. Homer micro grid software is used to run the simulation on the way to validate the techno economics of wind energy installations. The average daily load used varies from 1000 to 3000 kWh, in 1000 kWh steps. The wind energy system is designed to operate throughout the year from January to December, whereas July offers the highest yield. Four-support schemes are used in the simulations. These are; self consumption, feed in tariff, monthly net metering, and annually net metering. Additionally, different wind turbine capacities such as 80 kW, 100 kW, 250 kW, and 500 kW are used. The optimum investment method is analyzed by changing the support scheme, daily load and the wind turbine size. In this context, simple payback period (SPB), internal rate of return (IRR), and net present worth (NPV) parameters are used.

Table 1: The basic simulation parameters for all the support schemes in homer software

ITEMS	Cost per kW	Selling price (FiT)	Power price (FiT)	Selling price (SEC)	Power price (SEC)	Selling price (MNM)	Power price (MNM)	Selling price (ANM)	Power price (ANM)	Fuel cost
PRICE/US$	1000	0.09	0.05	0.00	0.05	0.05	0.05	0.05	0.05	0.64

From [9]

Table 1 shows the basic simulation parameters for all the support schemes that is used for the technical analysis. Similarly, the set-up and repairs estimate of the WT is 2% [10], whereas cost per kW that is used for the simulation is US$1000 [10]. The daily load set up in the electrical load is; 1000 kWh, 2000 kWh, 3000 kWh respectively. Additionally, all these parameters is entered one after the other into the load and design program in the homer micro grid software. Hence, by clicking on the calculate button, the software would calculate it automatically. However, in this study wind resources location is determined by HOMER report considered the wind direction at 30m, 40m, 50m, and 60m. Homer micro grid software recognize as durable tool for modelling renewable energy technologies. The wind turbines designed to operate for one year, and the average wind speed of a selected region is 10m/s.

3. MATHEMATICAL ANALYSIS

3.1 Simple Payback (SPB)

This is represent a first approximation, required years to meet the initial investment cost, considering only the total annual saving.

$$SPB = \frac{I_c}{A_r - A_c} \tag{1}$$

where I_c is the installation cost of the wind turbine, A_r is the annual revenue of the wind turbine, and A_c is the annual cost of operation and maintenance (O&M) kWh of the electricity generated.

$$I_c = T_c \times R_c \tag{2}$$

Where T_c is the turbine cost per kilowatt, and R_c is the rated capacity of the wind turbine.

$$A_r = R_c \times N_d \times N_h \times M_c \times E_p \tag{3}$$

where A_r is the annual revenue of the wind turbine, N_d is the number of days in a year, N_h is the number of hours in a day, M_c (maintenance cost) is the O&M kWh of the electricity generated, and E_p is the electricity price in either FiT or net metering.

3.2 Net Present Worth (NPV)

This is the subtraction of the present worth of cash inflow and present worth of cash outflows within a period of time, whereas is given as;

$$NPV = PV\left(\frac{P}{A}, i, n\right) - PV(cost) \tag{4}$$

Or

$$NPV = PV\,(1 \div (1+i)^n) - PV_{cost} \tag{5}$$

$$NPV = PV\,(1 \div (1+0.05)^{20}) - PV_{cost} \tag{6}$$

where i is interest rate (reduction percentage) of the wind turbine and it is equal to 5% [11], whereas n is useful life of the wind turbine that is equal to 20 years. However, NPV is used for economic planning in power generation [9].

3.3 Internal Rate of Return (IRR)

This is the ratio of the total present rate of an installation cost equals to total present rate of the expected revenue of the project, and is given as;

$$IRR = \frac{r^a + NPV^a}{(NPV^a - NPV^b) \times r2^a - r2^b} \tag{7}$$

where r^a is discount rate, however, IRR is used to evaluate the viability of the project of the power generation. Take for example; if the goal IRR of a project is five percent and the IRR generated fifteen percent, hence, the enterprise should accept the undertaking.

4. RESULTS AND DISCUSSION

The homer software shows the simulation result of all the support schemes depending on the capacity of each wind turbine (WT) and the daily load in kWh. The useful life of the WT of various size is taken as 20 years. The result of all the four support schemes such as; Feed in tariff (FiT), Self consumption (SEC), Monthly net metering (MNM), and Annually net metering (ANM) in the simulation demonstrated throughout the entire tables and figures below. However, these entire figures shown below is design to illustrate the simulation output variation between the simple payback (SPB) and present worth (PW) for all the support schemes. Similarly, the simulation result shows that as the hub height increases simple payback period decreases more worth is produced [8].

Table 2: FiT/SEC (SPB & PW) simulation output in homer software

		FiT						SEC					
HUBE	RATED	SPB	PW	SPB	PW	SPB	PW	SPB	PW	SPB	PW	SPB	PW
HEIGHT	SIZE	1000 kWh	1000 kWh	2000 kWh	2000 kWh	3000 kWh	3000 kWh	1000 kWh	1000 kWh	2000 kWh	2000 kWh	3000 kWh	3000 kWh
30m	80 kW	1.69	$454,532	1.79	$400,015	1.89	$363,666	2.9	$113,716	2.8	$175,927	2.75	$221,365
40m	100 kW	1.31	$1,061,461	1.42	$932,615	1.52	$868,092	2.45	$144,041	2.4	$234,947	2.36	$315,590
50m	250 kW	0.88	$1,376,679	0.93	$1,304,472	0.97	$1,248,564	2.4	$150,646	2.32	$240,160	1.69	$340,054
60m	500 kW	0.42	$1,426,670	0.43	$1,402,470	0.44	$1,350,562	1.8	$215,728	1.65	$340,456	1.5	$447,317

Table 2 shows the output of all the four WT sizes of FiT & SEC from 80 kW to 500 kW and hub height from 30m to 60m. It shows that 80 kW operates at 30m, 100 kW at 40m, 250 kW at 50m and 500 kW at 60m. By keeping daily load of each WT capacity constant from 80 kW to 500 kW in FiT, there is decrease in SPB and increase in PW and as the daily load of each WT size increases from 1000 kWh to 3000 kWh, there is increase in SPB and decrease in PW, whereas in SEC by keeping the daily load constant of each WT size from 80 kW to 500 kW, there is decrease in SPB and increase in PW. Additionally, as daily load of each WT size increases from 1000 kWh to 3000 kWh, there is decrease in SPB and increase in PW.

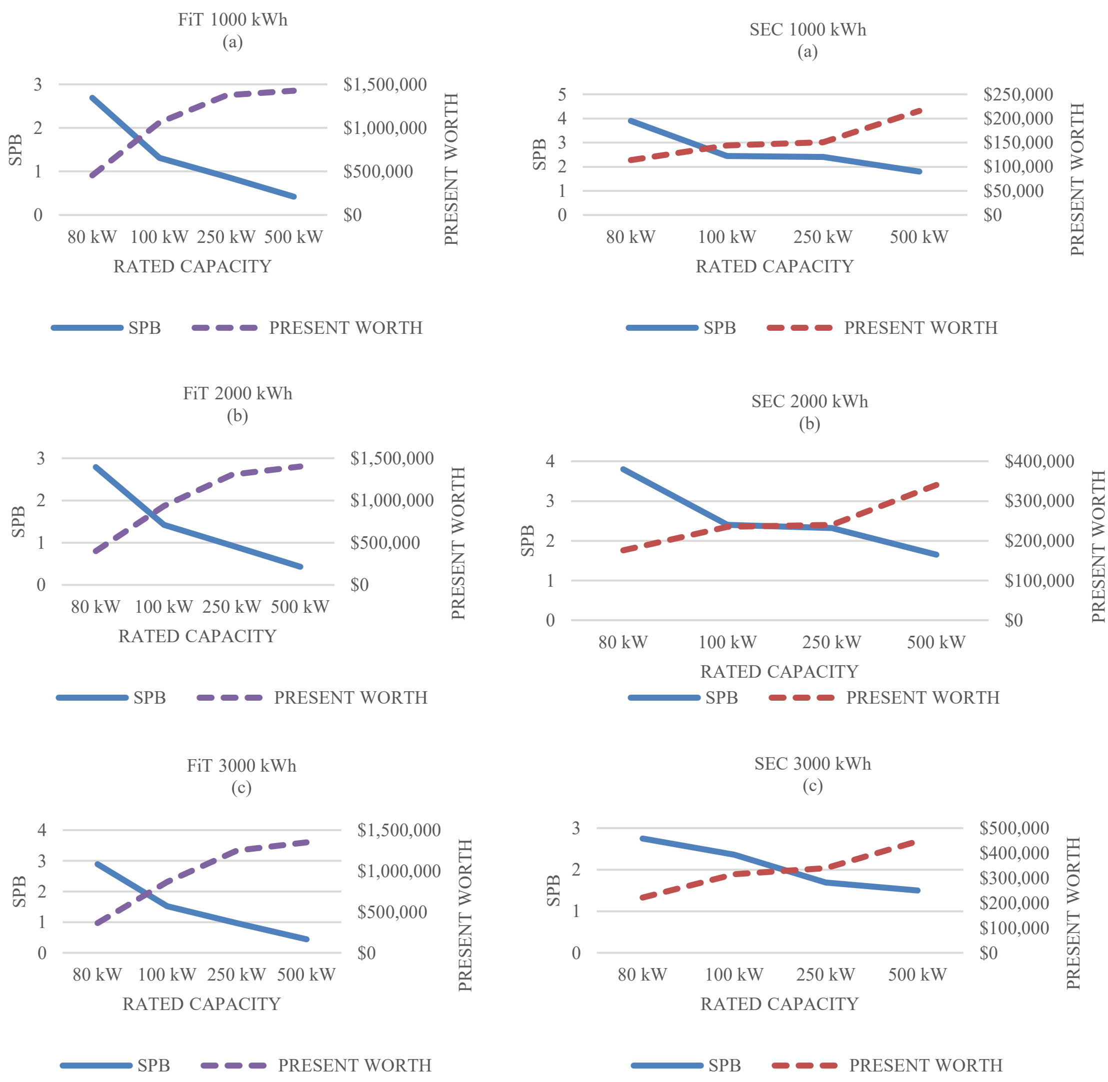

Figure 1: The trend in SPB and PW for FiT & SEC support scheme.

Figure 1 shows the trend in SPB along with PW for FiT & SEC support scheme. In FiT support scheme, as daily load increases from 1000 kWh to 3000 kWh for each wind turbine size from 80 kW to 500 kW as illustrated in the figure 1, there is gradual increase in SPB and decrease in PW of each wind turbine capacity, whereas in SEC support scheme, there is gradual decrease in SPB and increase in PW of each WT capacity.

Table 3: FiT/SEC (O&M & IRR) simulation output in homer software

		FiT						SEC					
HUBE	RATED	O&M	IRR	O&M	IRR	O&M	IRR	O&M	IRR	O&M	IRR	O&M	IRR
HEIGHT	SIZE	1000 kWh	1000 kWh	2000 kWh	2000 kWh	3000 kWh	3000 kWh	1000 kWh	1000 kWh	2000 kWh	2000 kWh	3000 kWh	3000 kWh
30m	80 kW	$23,277	38.10%	$17,277	32.70%	$2,447	31.60%	$10,756	6.20%	$21,563	10.80%	$34,020	14.20%
40m	100 kW	$56,328	81.30%	$35,104	73.50%	$12,276	68.70%	$11,330	9.10%	$22,803	15.80%	$36,095	21.90%
50m	250 kW	$59,303	119.20%	$36,776	113.30%	$17,277	108.70%	$12,387	9.40%	$25,442	15.90%	$40,468	22.80%
60m	500 kW	$84,387	120.80%	$61,014	119.20%	$38,797	117.20%	$16,941	45.40%	$33,862	45.40%	$50,852	50.10%

Table 3 shows the increase in O&M and IRR of FiT of each WT size from 80 kW to 500 kW by keeping daily load constant, and as daily load increases from 1000 kWh to 3000 kWh there is decrease in O&M along with IRR, whereas in SEC, shows increase in O&M and IRR from 80 kW to 500 kW by keeping daily load constant, and as the daily load of each WT size increases from 1000 kWh to 3000 kWh in 1000 kWh step. However, It is studied that, as the SPB increases, the PW decreases. Therefore, it affects the O&M and IRR. [8].

Table 4: MNM/ANM (SPB & PW) simulation output in homer sofware

		MNM						ANM					
HUBE	RATED	SPB	PW	SPB	PW	SPB	PW	SPB	PW	SPB	PW	SPB	PW
HEIGHT	SIZE	1000 kWh	1000 kWh	2000 kWh	2000 kWh	3000 kWh	3000 kWh	1000 kWh	1000 kWh	2000 kWh	2000 kWh	3000 kWh	3000 kWh
30m	80 kW	2.68	$346,411	2.68	$346,411	2.68	$346,411	2.68	$346,411	2.68	$346,411	2.68	$346,411
40m	100 kW	2.22	$578,091	2.22	$578,091	2.22	$578,091	2.22	$578,091	2.22	$578,091	2.22	$578,091
50m	250 kW	1.52	$779,444	1.52	$779,444	1.52	$779,444	1.52	$779,444	1.52	$779,444	1.52	$779,444
60m	500 kW	0.75	$798,648	0.75	$798,648	0.75	$798,648	0.75	$798,648	0.75	$798,648	0.75	$798,648

Table 4 shows the result of all the four WT sizes of MNM & ANM from 80 kW to 500 kW. However, by keeping daily load constant of each wind turbine size in MNM & ANM, there is decrease in SPB from 2.68 years at 80 kW to 0.75 year at 500 kW, whereas there is increase in PW from $346,411 to $798,648. Additionally, as daily load increases from 1000 kWh to 3000 kWh as illustrated in Table 5.6, all the WT sizes from 80 kW to 500 kW remain constant.

Table 5: FiT, SEC, MNM, ANM (Capacity factor (CF) & Total production (TP)

HUBE HEIGHT	RATED SIZE	CF 1000 kWh	TP 1000 kWh	CF 2000 kWh	TP 2000 kWh	CF 3000 kWh	TP 3000 kWh
30m	80 kW	22	157,219	22	157,219	28	198,220
40m	100 kW	28	252,017	28	252,017	30	265,225
50m	250 kW	30	658,017	30	658,017	35	768,230
60m	500 kW	35	1,554,193	35	1,554,193	40	1,768,250

Table 5 shows that the tendency of high production is possible as hub height increases. However, capacity factor (CF) reveals how efficient the turbine could connect the availability of energy within the wind ranges. Similarly, the CF for a realistic effectiveness WT at a prospective location may range between 15% and 40% [12].

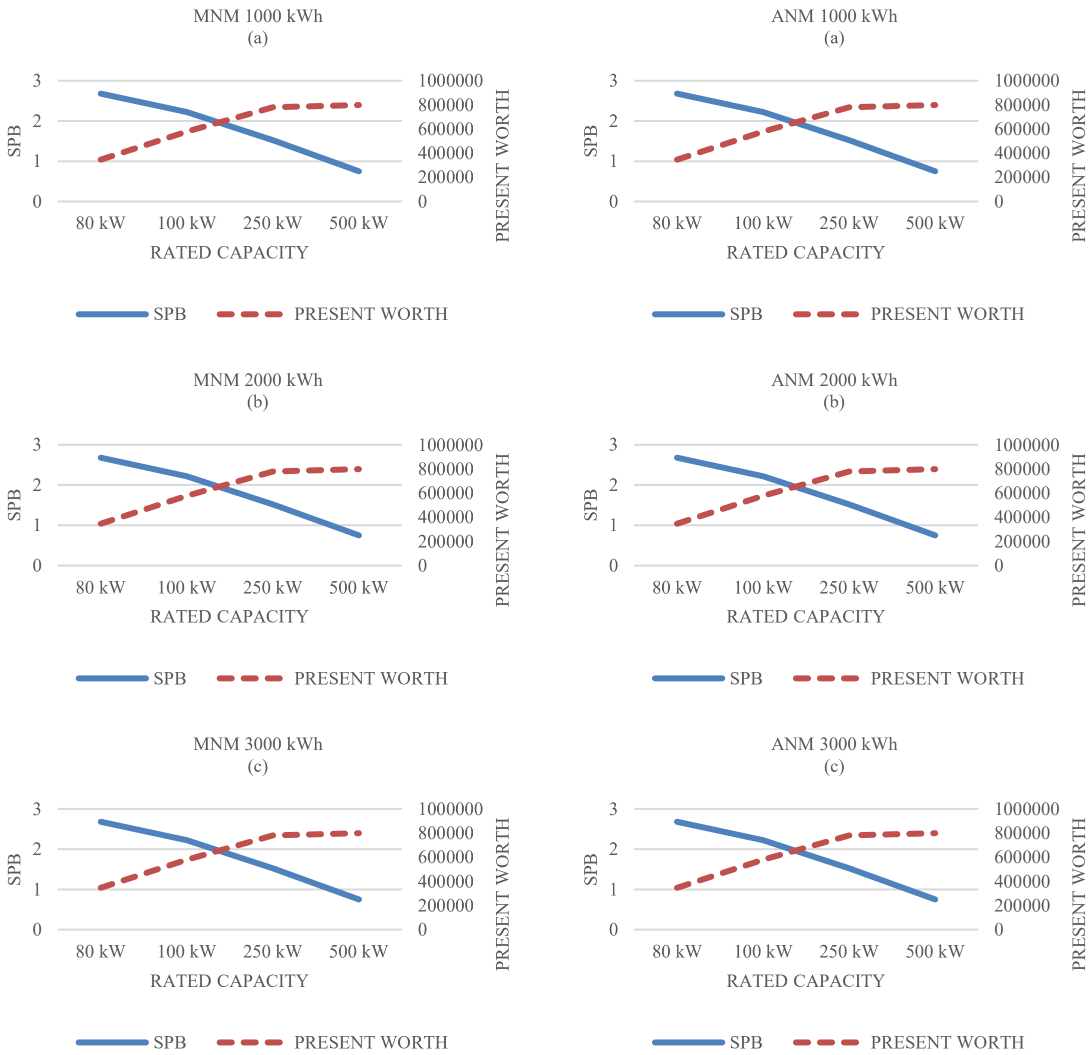

Figure 2: The trend in SPB and PW for MNM & ANM support scheme.

Figure 2 shows the trend in SPB along with PW for MNM & ANM support scheme, such that as daily load increases from 1000 kWh to 3000 kWh for each wind turbine size from 80 kW to 500 kW as illustrated in the figure 2, the SPB and PW remain constant.

Table 6: MNM/ANM (O&M & IRR) simulation output in homer software

		MNM						ANM					
HUBE HEIGHT	RATED SIZE	O&M 1000 kWh	IRR 1000 kWh	O&M 2000 kWh	IRR 2000 kWh	O&M 3000 kWh	IRR 3000 kWh	O&M 1000 kWh	IRR 1000 kWh	O&M 2000 kWh	IRR 2000 kWh	O&M 3000 kWh	IRR 3000 kWh
30m	80 kW	$23,476	30.40%	$9,950	30.40%	$5,153	30.40%	$23,476	30.40%	$9,950	30.40%	$5,153	30.40%
40m	100 kW	$28,200	48.80%	$12,991	48.80%	$5,259	48.80%	$28,200	48.80%	$12,991	48.80%	$5,259	48.80%
50m	250 kW	$41,653	70.20%	$23,403	70.20%	$5,512	70.20%	$41,653	70.20%	$23,403	70.20%	$5,512	70.20%
60m	500 kW	$42,012	72.10%	$23,509	72.10%	$8,300	72.10%	$42,012	72.10%	$23,509	72.10%	$8,300	72.10%

Table 6 shows increase in O&M and IRR from 80 kW to 500 kW at daily load of each WT sizes of MNM & ANM. Moreover, as the daily load of each WT size increases from 1000 kWh to 3000 kWh, there is decrease in O&M at each WT size, but IRR remain constant.

5. CONCLUSION

In this research, various support schemes on the financial viability of various wind turbine sizes from 80 kW to 500 kW are studied in FRN. The highest total production of wind energy generation is viable with 500 kW wind turbine, because of its highest rated wind speed amongst all the selected WT sizes. In all the support schemes such as; FiT, SEC, MNM, and ANM, 80 kW WT size produces the lowest energy output at 30m hub height, whereas the highest energy output is given by 500 kW wind turbine at 60m hub height with the FiT scheme. The capacity factor has the least value in 80 kW, WT size, 28% at 30m hub height, whereas the highest is 500 kW WT size, 40% at 60m hub height for all the support schemes. In the optimum investment; 80 kW of wind turbine has the highest SPB, the lowest PW and the lowest IRR, whereas 500 kW wind turbine has the lowest SPB, the highest PW and the highest IRR. The support scheme that has highest SPB and lowest PW is SEC. Moreover, the support scheme that has the lowest SPB and highest PW is FiT.

Therefore, FiT is considered the best type of support scheme for wind power generation in FRN. Additionally, it shows that FiT with 500 kW wind turbine capacity is the best among the entire support schemes, and can supplies the primary goal for renewable electricity at the FRN energy, which is a kind of immature market in terms of renewables. Besides, it stands the threat of combating the greenhouse gas emission that would have been discharged through a fossil fuel to pollute the environment. On the prevailing tariff conditions in FRN, this challenge might be considered as being financially possible due to its maximum present worth amongst the entire support schemes within the simulation. Similarly, FiT in this analysis considered outstanding as a way of selling renewable power development. The selling fee is higher than the power-purchasing fee unlike in net metering wherein it selling fee is not always greater than the retails fee. It implies cannot produce power beyond what you buy, and self-power consumption in this scheme most effective keep in mind the power rate by ingesting increasingly more power without promoting it back to the nationwide grid.

ACKNOWLEDGMENTS

İ am grateful to God almighty that make my research and paper work to be realistic.

REFERENCES

1. Ali Mostafaeipour, Productivity and development issues of global wind turbine industry, Renewable and Sustainable Energy Reviews, Vol:14, No:3, 1048-1058, (2010).

2. Majid Jamil, Sheeraz Kirmani, Himanshu Chatterjee, Technoeconomic viability of three different energy-supplying options for remote area electrification in India, International Journal of Sustainable Energy, Vol:33, No:2, 470-482, (2013).
3. Sunday Olayinka Oyedepo, Energy and sustainable development in Nigeria: the way forward, Energy, Sustainability and Society, Vol:15, No:2, 1-17, (2012).
4. Ohunakin Olayinka, Energy utilization and renewable energy sources in Nigeria, Applied Science, Vol:5, No:2, 171-177, (2010).
5. Ibitoye, Adenikinju, Future Demand for Electricity in Nigeria, Applied Energy, Vol:84, No:5, 492-504, (2007).
6. Geoffrey Hammond, Alternative Energy Strategies for the United Kingdom Revisited: Market Competition and Sustainability, Technological Forecasting and Social Change, Vol:59, No:2, 131-151, (1998).
7. Ohunakin Olayinka, Energy utilization and renewable energy sources in Nigeria, Applied Science, Vol:5, No:2, 171-177, (2010).
8. Olayinka S Ohunakin, Olanrewaju M Oyewola, Muyiwa S Adaramola, Economic analysis of wind energy conversion systems using levelised cost of electricity and present value method in Nigeria, International Journal of Energy and Environmental Engineering, Vol:4, No:2, 1-8, (2013).
9. Roche *et al.*, True cost of electricity: comparison of cost electricity generation in Nigeria, 5-34, https://ng.boell.org/sites/default/files/true_cost_of_power_technical_report_final.pdf [20/05/2019], (2017).
10. IRENA, Renewable Power Generation Cost, pp. 96, 104-108, (2017). 'file:///C:/Users/Markama/Downloads/IRENA_2017_Power_Costs_2018.pdf [11/8/2019].
11. Thornton Grant, Africa renewable discount rate survey, pp. 1-16, https://www.grantthornton.co.uk/globalassets/1.-member-firms/united-kingdom/pdf/documents/africa-renewable-energy-discount-rate-survey-2018.pdf [31/05/2019], (2018).
12. O.S. Ohunakin, M.S. Adaramola, O.M. Oyewola, Wind energy evaluation for electricity generation using WECS in seven selected locations in Nigeria, Applied Energy, Vol:88, No:9, 3197-3206, (2011).

MULTI-OBJECTIVE FUZZY-STOCHASTIC GOAL PROGRAMMING MODEL FOR FLEXIBLE JOB SHOP SCHEDULING WITH SEQUENCE-DEPENDENT SETUP TIMES

Bilge Varol, Kemal Subulan

Dokuz Eylül University, Engineering Faculty, Department of Industrial Engineering, Izmir, Turkey

bilgeevarol@gmail.com; kemal.subulan@deu.edu.tr

Abstract

This study addresses a multi-objective Flexible Job-Shop Scheduling Problem with Sequence-Dependent Setup Times (SDST-FJSSP) under a mixed fuzzy and stochastic types of uncertainties. Different types of uncertainties such as randomness and fuzziness are handled simultaneously to deal with the stochastic due dates, fuzzy processing and set-up times. In fact, the proposed mathematical model is an extended version of the original model that was first developed by Mousakhani (2013) for SDST-FJSSP. In this research, the proposed model aims to minimize total tardiness and maximum completion time concurrently. To do this, a non-preemptive goal programming approach is applied as a multi-objective optimization technique. Additionally, probabilistic uncertainty is handled by a chance-constrained stochastic program and a fuzzy mathematical programming approach is employed to cope with the possibilistic uncertainties. In detail, fuzzy processing and setup times are represented by triangular fuzzy numbers (TFNs). The proposed fuzzy-stochastic MIP model is converted to its crisp equivalent form by well-known transformation approaches in the literature. Finally, in order to show validity and practicality of the proposed fuzzy-stochastic MIP model, an illustrative example is presented and its optimization results via LINGO 18 are also reported.

Keywords: Flexible job-shop scheduling, sequence-dependent setup times and fuzzy-stochastic mixed-integer programming.

1. INTRODUCTION

The job-shop manufacturing is one of the well-known production systems in the literature. Additionally, job-shop scheduling problem is a popular combinatorial optimization problem known as NP-hard one. Since this problem is frequently encountered in real-life production systems, this paper addresses a flexible job-shop scheduling problem with sequence-dependent setup times. In fact, several extensions of the classical job-shop scheduling problem were presented by many researchers. In the classical job-shop scheduling problem, each job is processed on m machines to follow a pre-determined production route. However, flexible job-shop scheduling problem (FJSSP) is its extended version in which jobs can be processed on more than one machine instead of a single machine. In other words, production routes of the jobs are defined in a flexible manner. This expansion makes this problem much more difficult due to the increases in the number of possible schedules. In detail, two important decisions should be made while solving this problem. The first one is assigning the manufacturing operations to the machines and the other one is related to the sequence of these operations. The FJSSP is first handled by Bruker & Schlie (1990) in the literature. They considered generalization of the classical job-shop scheduling problem in which a set of machines are associated with each manufacturing operation of a job. They focused on the makespan objective while solving the problem by making use of heuristic algorithms. In fact, if the due dates are not considered in a JSSP, objective of the problem will be defined as makespan minimization in general. When these due dates are taken into consideration, objective function may be described as minimum total tardiness, number of tardy jobs and weighted total tardiness etc. In addition to these objectives, effectiveness of the generated schedules with higher customer satisfaction should also be taken into account according to the manufacturing company's long-term objectives. Moreover, these objectives can also be handled simultaneously in order to generate compromise production schedules. Coping with the sequence-dependent setup times is another important issue in FJSSPs. For instance, Bagheri & Zandieh (2011) addressed bi-criteria SDST-FJSSP to minimize makespan and mean tardiness instantaneously. They applied variable neighborhood search algorithm for solution of the examined problem.

In addition to multi-objectivity and sequence-dependent setup times, uncertainty in some parameters/inputs may result in other extensions in the JSSPs. Some researchers attempt to use fuzzy set theory which was first presented by Zadeh (1965) to handle uncertain parameters in JSSPs. Itoh & Ishii (1999) focused on fuzzy processing times and due-dates of a scheduling problem on one machine. They also aimed at minimum number of tardy jobs. On the other hand, some other researchers focused on stochastic job-shop scheduling problems (SJSSPs) which is an important aspect of manufacturing systems and the extended version of the classical JSSPs. Ebrahimi et al. (2014) focused on a hybrid flow shop scheduling with sequence dependent family setup time and stochastic due dates. They concerned with minimization of both makespan and total tardiness.

In this research, a hybrid fuzzy-stochastic mathematical programming approach is proposed to solve a multi-objective FJSSP with fuzzy processing and sequence-dependent setup times and stochastic due-dates. A non-pre-emptive goal programming technique is used to produce compromise schedules when minimizing the total tardiness and maximum completion time concurrently. While dealing with the stochastic due-dates, chance-constrained optimization method is employed. Moreover, a well-known transformation approach is also applied to convert the proposed fuzzy-stochastic program into its crisp equivalent form. Finally, it is tested on a numerical example and optimization results are reported.

2. A BRIEF LITERATURE REVIEW ON JSSP UNDER UNCERTAINTY

Although many studies are available on deterministic FJSSPs in the literature, there is a lack of papers on FJSSP under uncertain environments. Therefore, this section presents a brief literature survey on this research topic. Neumann & Schneider (1999) have discussed JSSP with stochastic precedence constraints. They applied different heuristic algorithms like shifting bottleneck to this problem so as to minimize expected value of makespan. A non-linear mathematical programming model was developed by Tavakkoli-Moghaddam et al. (2005) for a SJSSP. They targeted to minimize the sum of variation of actual processing time and planned process time, operational costs, and idle costs for each machine in a planning horizon. Lei

(2011) proposed an effective ordered operation-based genetic algorithm for stochastic JSSP with exponential processing times, random breakdown and non-resumable jobs. Also, he aimed at minimizing makespan and the total tardiness ratio. In addition, random processing times are also considered in that study.

Apart from the stochastic type of uncertainty, Lei (2010) applied a genetic algorithm to an FJSSP with fuzzy processing times which represented by TFNs. They aimed at minimizing the maximum fuzzy completion time. Petrovic et al. (2008) applied a genetic algorithm for solving the JSSP with lot-sizing problem so as to minimize average tardiness, the number of tardy jobs, setup times, idle times of machines and the flow times of jobs. In their model, processing times and the due dates are represented by fuzzy numbers. Lin (2001) applied a transformation approach to convert the JSSP with fuzzy processing times into its crisp equivalent form. Johnson's algorithm was also applied in the solution phase of the problem.

Table 1. A brief literature review on JSSPs under uncertain environments.

Article	Problem Type	Methodology	Objective	Type of uncertainty	
				Fuzzy	Stochastic
Neumann & Schneider (1999)	JSSP	Heuristic	$E(C_{max})$		√
Lin (2001)	JSSP	Heuristic	C_{max}	√	
Tavakkoli-Moghaddam et al. (2005)	JSSP	Math.Model & Neural Network+SA	$Cost + Time$		√
Petrovic et al. (2008)	JSSP	GA	$\overline{T}_j, number\ of\ T_j, S_j,$ F, idle time	√	
Lei (2010)	FJSSP	GA	C_{max}	√	
Lei (2011)	FJSSP	GA	$C_{max}, \sum T_j$	√	

3. PROBLEM DESCRIPTION & THE MATHEMATICAL FORMULATION

The FJSSP consists of a set of *n* jobs and *m* machines. However, each job includes different operations with its own processing routes and durations. Moreover, each machine is eligible for different job operations and eligibilities may be partially or fully different from each other. Each operation's processing times on each machine can also be partially or fully different from each other. The first objective of the mathematical model is to assign operations of jobs to machines and then, sequencing these operations on each machine so as to minimize total tardiness $\left(\sum_{j=1}^{n} T_j \text{ where } T_j = max\{C_{jt_j} - d_j, 0\}\right)$. In detail, T_j, d_j and C_{jt_j} are defined for the tardiness, due-date and completion time of job j, respectively. The second objective aims to minimize maximum completion time$\left(C_{max} = max\{C_{jt_j}\}\right)$. Furthermore, there are sequence-dependent setup times between each consecutive operations to be processed on the same machine. Based on these information, Mousakhani (2013) developed an effective mathematical programming model which reduces the model dimension and complexity when compared to the previous model of Saidi-Mehrabad & Fattahi (2007). For that reason, mathematical model which was proposed by Mousakhani (2013) requires less computational time to solve small- and medium-sized problems optimally. Therefore, our fuzzy-stochastic model is based on this original model. Unlike the original model of Mousakhani (2013), an additional objective, i.e., makespan minimization, is also incorporated in this research. After this revision, the proposed fuzzy-stochastic MIP model is designed as a multi-objective goal program. Briefly, objective functions of the fuzzy-stochastic SDST-FJSSP can be formulated as in Eqs. (1) – (2):

$$Minimize \quad C_{max} \tag{1}$$

$$Minimize \quad \sum_{j=1}^{n} T_j \tag{2}$$

This multi-objective nature of the problem is handled by a non-preemptive goal programming approach. To do this, objective weights are first determined by the decision maker according to his/her preferences. In this non-preemptive goal programming model, the objective function of the model can be reformulated as in the following Eq. (3):

$$Minimize \quad w_1.C_{max} + w_2.\sum_{j=1}^{n} T_j \tag{3}$$

where w_1 and w_2 are the weights of the first and second objectives, respectively. In addition, in the stated problem, it should be noted here that each machine has a setup time before its first operation. Thus, a dummy job is also defined in that model for implementing the starting setup times of machines. To do this, job "0" is assigned as the dummy job and it represents the first operation or job of all the machines.

A. Modelling assumptions

While developing the mathematical model, following assumptions are made: Each job has its own operations. Each job can be assigned to at least one machine. However, some of them can have alternative machines. The operations of each job have precedence processes. In other words, each job has a production route to follow. Processing times and sequence-dependent setup times of the job operations are not known certainly. Therefore, they are considered as ambiguous parameters and represented by TFNs. Due dates of the jobs are not known precisely. Since the examined production system is handled as a customer-oriented system in this study, they may have randomness in nature. Therefore, these random due dates which fitted to a Poisson distribution are incorporated into a chance-constrained stochastic program.

In most of the real-life applications, parameters/inputs of the SDST-FJSSP are not known precisely. However, the majority of the previous researches on JSSPs suppose that all of the scheduling parameters are deterministic. Actually, this assumption is not realistic and therefore, cannot reflect the real-life applications well. Based on this motivation, stochastic due dates and fuzzy processing and sequence-dependent setup times of the jobs are handled in an integrated manner. In the light of these facts, a fuzzy-stochastic MIP model can be formulated as in Eqs. (4) - (16) by using the mathematical nomenclature in Table 2.

Table 2. Mathematical nomenclature for the fuzzy-stochastic SDST-FJSSP.

Indices & sets	
N	The number of jobs ($j, h = 1,2, \dots, N$)
M	The number of machines ($i = 1, 2, \dots , M$)
j, h	Indexes for jobs where $j = \{1, 2, \dots , N\}$ and $h = \{0, 1, \dots , N\}$
i	Index for machines where $i = \{1, 2, \dots , M\}$
R_j	Subset including operations of job j where $\lvert R_j \rvert = r_j$
l, z	Indexes for operations of job j where $l, z = \{1,2, \dots, r_j\}$

Table 2. Mathematical nomenclature for the fuzzy-stochastic SDST-FJSSP (continued).

Deterministic parameters	
e_{jli}	*Binary parameter takes value of 1; if machine i is eligible lth operation of job j, and 0 otherwise*
w_1	*Weight of first objective (makespan)*
w_2	*Weight of second objective (total tardiness)*
M	*A huge positive number*
Fuzzy parameters	
$\tilde{p}_{jli}$	*Fuzzy processing time of lth operation of job j if it is processed by machine i*
$\tilde{S}_{jhi}$	*Fuzzy setup time of job j immediately after job h on machine i*
Stochastic parameters	
d_j	*Stochastic due-date for job j*
Decision variables	
X_{jlhzi}	*1 if O_{jl} is processed immediately after O_{hz} on machine i; 0 otherwise where $O_{ji} \neq O_{hz}$*
C_{jl}	*Continuous variable for the completion time of O_{jl}*
T_j	*Continuous variable for the tardiness of job j*
C_{max}	*Maximum completion time over all jobs (makespan)*

B. Mathematical formulation

In this research, it is aimed to minimize total tardiness and maximum completion time jointly. Formulation of the fuzzy-stochastic MIP model for the SDST-FJSSP can be given as in the following Eqs. (4) - (16):

$$Minimize \quad w_1 . C_{max} + w_2 . \sum_{j=1}^{n} T_j \tag{4}$$

Subject to:

$$\sum_{h=0}^{N} \sum_{z=1}^{r_h} \sum_{i=1}^{M} X_{jlhzi} = 1 \qquad \forall j, \forall l \in R_j \tag{5}$$

$$\sum_{h=0}^{N} \sum_{z=1}^{r_h} X_{jlhzi} \leq e_{jli} \qquad \forall j, l \in R_j, \forall i \tag{6}$$

$$\sum_{j=1}^{N} \sum_{l=1}^{r_j} \sum_{i=1}^{M} X_{jlhzi} \leq 1 \qquad \forall h| \geq 1, z \in r_h \tag{7}$$

$$\sum_{j=1}^{N} \sum_{l=1}^{r_h} X_{jl01i} \leq 1 \qquad \forall\, i \tag{8}$$

$$\sum_{j=1}^{N} \sum_{l=1}^{r_j} X_{jlhzi} \leq \sum_{j=0}^{N} \sum_{l=1}^{r_j} X_{hzjli} \qquad \forall\, h| \geq 1, z \in r_h, \forall i \tag{9}$$

$$C_{jl} \geq C_{jl-1} + \sum_{h=0}^{N} \sum_{z=1}^{r_h} \sum_{i=1}^{M} X_{jlhzi} . (\tilde{p}_{jli} + \tilde{S}_{jhi}) \qquad \forall j, l \in R_j \tag{10}$$

$$C_{jl} \geq C_{hz} + \sum_{i=1}^{M} X_{jlhzi} . (\tilde{p}_{jli} + \tilde{S}_{jhi}) - M. \left(1 - \sum_{i=1}^{M} X_{jlhzi} \right) \qquad \forall j, \forall l \in R_j, \forall h, z \in R_h \tag{11}$$

$$\Pr\left\{T_j \geq C_{jt_j} - d_j\right\} \geq \beta \quad \forall j,\ d_j \sim Poisson(\lambda_j) \tag{12}$$

$$C_{max} \geq C_{jl} \quad \forall j, \forall l \in R_j \tag{13}$$

$$T_j, C_{jl} \geq 0 \quad \forall j, \forall l \in R_j \tag{14}$$

$$X_{jlhzi} \in \{0,1\} \quad \forall i, \forall j, \forall l \in R_j, \forall h, z \in R_h \tag{15}$$

$$C_{j0} = C_{01} = 0 \tag{16}$$

In Eq. (4), weighted additive goal programming formulation is given for the objective functions which aim to minimize total tardiness and maximum completion time with respect to their weights. The constraint set in Eq. (5) ensures that each operation of jobs should be assigned at once and it also ensures that each operation has one preceding operation. According to Eq. (6), each operation can be assigned if it is eligible in that machine. Constraint set in Eq. (7) maintains that every operation may have at most one succeeding operation since the operation in the last position of each machine has no succeeding operation (Mousakhani, 2013). Constraint set in Eq. (8) guarantees that dummy job is defined for the first operation of each machine. According to constraint set in Eq. (9), jobs are sequential only, if they are on the same machine. Constraint set in Eq. (10) makes sure that a job cannot be processed on two different machines at the same time. Therefore, completion time of the l^{th} operation of a job should be greater than the sum of the completion time of its previous $(l-1)^{\text{th}}$operation, fuzzy sequence-dependent setup time and its fuzzy processing time. According to Eq. (11), a machine cannot process two different operations simultaneously. In other words, the difference between the completion times of two consecutive operations on a machine should be greater than the sum of setup time and the processing time of the operation processed later (Mousakhani, 2013). In Eq. (12), the tardiness of each job is calculated based on a chance constraint set. In this equation, stochastic due dates which have Poisson distribution are also included. It should also be highlighted here that this probabilistic constraint set can be satisfied under a pre-specified percentage, i.e. 90 or 95% of the time according to the value of β. Furthermore, due-date of the dummy "Job 0" is set to zero and also excluded from uncertainty. This chance constraint set and random variables are defined by making use of primary functions in LINGO 18.0 optimization software. Based on the constraint set in Eq. (13), makespan for the all jobs is calculated. Finally, continuous and binary variables of the mathematical model are defined in Eqs. (14) - (16).

C. The crisp equivalent formulations of the fuzzy constraints

In the above mathematical model, only the right hand sides of some constraints are represented by fuzzy numbers. These types of fuzzy mathematical programs are classified as Type-2 fuzzy mathematical programs by Baykasoğlu & Göçken (2008). Gen et al. (1992) proposed a transformation approach for solving Type-2 fuzzy mathematical models with TFNs. In that transformation approach, the joint conditional possibility distribution of the constraints with fuzzy right-hand side terms is defined by using the min-operator (Bellman & Zadeh, 1970) since the minimum of possibility may correspond to the feasibility of the constraints (Mula, Peidro, & Poler, 2010). In this approach, a fuzzy right-hand side parameter, i.e., $\tilde{b}$ can be represented by a TFN $\tilde{b} = (b_1, b_2, b_3)$ and its membership function is also given in Eq. (17) and demonstrated by Figure 1. In addition, this transformation approach is also a parametric method which depends on $\alpha - cuts$ where α can take a value between 0 and 1 $(0 \leq \alpha \leq 1)$.

$$\mu_{\tilde{b}}(\text{x}) = \begin{cases} \frac{1}{b_2 - b_1} . (x - b_2) + 1 & if \ (b_1 \leq x \leq b_2) \\ \frac{1}{b_2 - b_3} . (x - b_2) + 1 & if \ (b_2 \leq x \leq b_3) \\ 0 & if \ (x \leq b_1, b_3 \leq x) \end{cases} \tag{17}$$

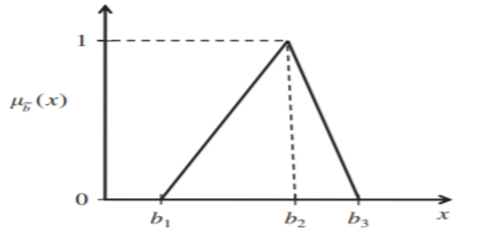

Figure 1. Membership function of a TFN (Mula, Peidro, & Poler, 2010).

When this transformation approach is applied to convert fuzzy constraints in Eqs. (10) - (11) into their crisp equivalent forms, the following reformulations in Eqs. (18) – (19) are provided.

$$C_{jl} \geq C_{jl-1} + \sum_{h=0}^{N} \sum_{z=1}^{r_h} \sum_{i=1}^{M} X_{jlhzi}. \left(\left((1-\alpha).p_{jli1} + \alpha.p_{jli2} \right) + \left((1-\alpha) * S_{jhi1} + \alpha.S_{jhi2} \right) \right) \quad \forall j, \forall l \in R_j \quad (18)$$

$$C_{jl} \geq C_{hz} + \sum_{i=1}^{M} X_{jlhzi} . \sum_{h=0}^{N} \sum_{z=1}^{r_h} \sum_{i=1}^{M} X_{jlhzi} . \left(\left((1-\alpha).p_{jli1} + \alpha.p_{jli2} \right) + \left((1-\alpha).S_{jhi1} + \alpha.S_{jhi2} \right) \right) - M. \left(1 - \sum_{i=1}^{M} X_{jlhzi} \right) \quad \forall j, \forall l \in R_j, \forall h, z \in R_h \quad (19)$$

where α represents the feasibility degree of constraints with fuzzy right-hand side parameters.

4. AN ILLUSTRATIVE EXAMPLE

In order to test performance of the proposed fuzzy-stochastic MIP model and demonstrate its validity and practicality, a trivial illustrative example which is revised based on the data of Mousakhani (2013) is presented in this section. There are four jobs and three machines in the example problem. As highlighted before, “Job 0” is defined as a dummy job in the examined problem. Thus, setup times of this dummy job are described as the initial setup times of the machines. Due dates of the jobs (except the dummy job) are fitted to a particular distribution, i.e., Poisson according to the input analysis performed in Arena simulation software. In detail, the best fitted probability distribution is determined as Poisson distribution with a mean value of 22.5 for these random due dates. As shown in Table 3, Jobs 1 and 4 involve three operations and jobs 2 and 3 include two operations. The processing route and fuzzy processing times of each job are presented in Table 3.

Table 3. Fuzzy processing times of the instance.

			Machines		
Jobs	Operations	Type	1	2	3
1	$O_{1,1}$	2	(7, 8, 9)	(6, 7, 8)	(0, 0, 0)
	$O_{1,2}$	3	(0, 0, 0)	(0, 0, 0)	(4, 5, 6)
	$O_{1,3}$	1	(5, 6, 7)	(0, 0, 0)	(5, 6, 7)
2	$O_{2,1}$	2	(5, 6, 7)	(9, 10, 11)	(0, 0, 0)
	$O_{2,2}$	1	(7, 8, 9)	(0, 0, 0)	(3, 4, 5)
3	$O_{3,1}$	1	(3, 4, 5)	(0, 0, 0)	(2, 3, 4)
	$O_{3,2}$	3	(0, 0, 0)	(0, 0, 0)	(3, 4, 5)
4	$O_{4,1}$	3	(0, 0, 0)	(0, 0, 0)	(3, 4, 5)
	$O_{4,2}$	1	(1, 2, 3)	(0, 0, 0)	(6, 7, 8)
	$O_{4,3}$	2	(7, 8, 9)	(8, 9, 10)	(0, 0, 0)

According to Table 3, $O_{1,1} = 2$ means that the first operation of job 1 is operation type 2. The eligible set of each operation type can be explained as follows: Operation type 1 can be processed by machines 1 and 3. Similarly, operation type 2 can be performed by machines 1 and 2. Lastly, operation type 3 can be processed only by machine 3. Finally, setup times which are also represented by TFNs are also presented in Table 4.

Table 4. Fuzzy setup times of the instance.

	Machine 1				Machine 2				Machine 3			
Jobs	1	2	3	4	1	2	3	4	1	2	3	4
0	(1,2,3)	(1,2,3)	(2,3,4)	(1,2,3)	(2,3,4)	(1,2,3)	(0,0,0)	(2,3,4)	(1,2,3)	(2,3,4)	(1,2,3)	(1,2,3)
1	(0,0,0)	(1,2,3)	(1,2,3)	(2,3,4)	(5,6,7)	(2,3,4)	(0,0,0)	(1,2,3)	(2,3,4)	(1,2,3)	(4,5,6)	(1,2,3)
2	(1,2,3)	(1,2,3)	(4,5,6)	(1,2,3)	(1,2,3)	(0,0,0)	(0,0,0)	(3,4,5)	(3,4,5)	(0,0,0)	(1,2,3)	(2,3,4)
3	(1,2,3)	(1,2,3)	(0,0,0)	(1,2,3)	(0,0,0)	(0,0,0)	(0,0,0)	(0,0,0)	(1,2,3)	(3,4,5)	(1,2,3)	(1,2,3)
4	(2,3,4)	(3,4,5)	(5,6,7)	(2,3,4)	(4,5,6)	(2,3,4)	(0,0,0)	(0,0,0)	(1,2,3)	(1,2,3)	(2,3,4)	(1,2,3)

5. COMPUTATIONAL RESULTS & WHAT-IF ANALYSIS

When the proposed fuzzy-stochastic MIP model is solved by stochastic programming solver of LINGO 18.0 optimization software under these data, computational results with different feasibility degrees are provided as given in Table 5.

Table 5. Multi-objective optimization results.

Feasibility degree ($\boldsymbol{\alpha}$)	Objective value	Makespan	Total tardiness	Actual Probability	Computational time (sec.)
0.0	30.5	30	31	0.95	67.11
0.2	34.90	31.6	37	0.95	51.79
0.4	39.30	34.2	44.4	0.95	87.31
0.6	44.2	37.2	51.2	0.95	79.01
0.8	47.7	42.6	52.8	0.95	60.12
1.0	51.5	45	58	0.95	81.98

It should be mentioned here that, sample size/the number of scenarios is set to 20 in the chance constraint set. Since due dates are determined as a stochastic parameters, tardiness values vary as can be seen in Table 5. Because, tardiness is directly affected by the due dates. When the satisfaction degree of fuzzy constraints are increased, objective values, i.e., makespan and total tardiness will also deteriorate. Because, $\alpha = 1$ means that the constraint satisfaction degree is 100% whereas $\alpha = 0$ corresponds to the maximum tolerance in fuzzy constraints. It should also be emphasized here that actual probabilities regarding the chance constraint set is equal to 95% for all feasibility degrees.

As mentioned previously, we applied a non-preemptive goal programming approach in order to obtain compromise or balanced solutions. Actually, when the values of objective weights are altered, different compromise solutions can be acquired. For that reason, we also performed what-if analysis so as to investigate the effects of these objective weights. To do this, the proposed fuzzy-stochastic model is run under different feasibility degrees $\alpha =${0, 0.2, 0.4, 0.6, 0.8, 1.0} and various objective weights {w_1=1, w_2=0; w_1=0.8, w_2=0.2; w_1=0.6, w_2=0.4; w_1=0.4, w_2=0.6; w_1=0.2, w_2=0.8; w_1=0, w_2=1}. The results of what-if analysis are depicted in Figure 2. According to the results, makespan objective will take values between 29 and 52 while total tardiness will take between 29 and 76 under different uncertainty levels and importance weights of the objectives.

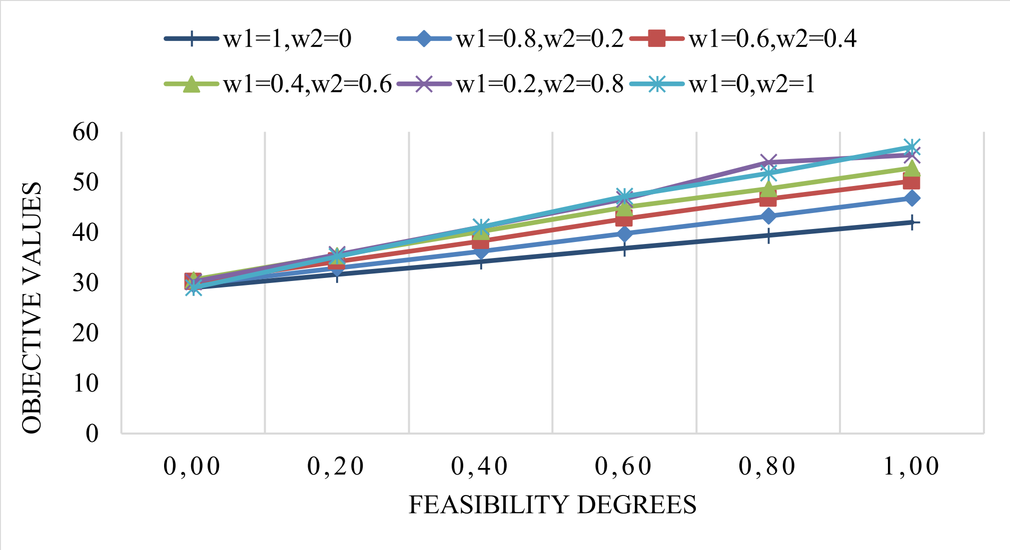

Figure 2. Results of what-if analysis on importance weights of the objectives.

6. CONCLUSIONS & FUTURE WORKS

In this research, a multi-objective fuzzy-stochastic MIP model is developed for SDST-FJSSP with multiple objectives. Actually, the proposed model is an extended version of the original model which was first proposed by Mousakhani (2013). Apart from this original model, total tardiness and makespan/maximum completion time objectives are handled simultaneously. In order to provide compromise or balanced schedules, a non-preemptive goal programming approach is employed. Furthermore, fuzzy processing times and sequence-dependent setup times that are represented by TFNs and stochastic due dates are handled simultaneously in the proposed model. To cope with Poisson distributed due dates, a chance-constrained stochastic program is utilized. Moreover, fuzzy processing and setup times in the model constraints are converted into their crisp equivalent forms by making use of a parametric transformation approach. The proposed fuzzy-stochastic MIP model is tested on a numerical example. Additionally, what-if analysis are also conducted to investigate the effects of objective weights on the compromise solutions. It can be concluded that the proposed fuzzy-stochastic model is able to present different applicable solutions under various uncertainty levels and scenarios. On the other hand, since the proposed solution approach is based on a mathematical programming based exact method, its application is very limited in case of larger scaled problem instances of SDST-FJSSP. For that reason, development of a metaheuristic or matheuristic based solution approach can be scheduled as a future work in order to obtain good quality solutions for large sized problem instances in reasonable computation times.

REFERENCES

1. Bagheri, A., & Zandieh, M. (2011). Bi-criteria flexible job-shop scheduling with sequence-dependent setup times - Variable neighbourhood search approach. Journal of Manufacturing Systems, 30, 8-15.
2. Baykasoğlu, A., & Göçken, T. (2008). A review and classification of fuzzy mathematical programs. Journal of Intelligent & Fuzzy Systems, 19, 205-229.

3. Bellman, R., & Zadeh, L. (1970). Decision-making in a fuzzy environment. Management Science, 17, 141-164.
4. Mousakhani, M. (2013). Sequence-dependent setup time flexible job shop scheduling problem to minimise total tardiness. International Journal of Production Research, 3476-3487.
5. Mula, J., Peidro, D., & Poler, R. (2010). The effectiveness of a fuzzy mathematical programming approach for supply chain production planning with fuzzy demand. International Journal of Production Economics, 128, 136-143.
6. Bellman, R., & Zadeh, L. (1970). Decision-making in a fuzzy environment. Management Science, 17, 141-164.
7. Brucker, P., & Schlie, R. (1990). Job-Shop Scheduling with Multi-Purpose Machines. Computing, 45, 369-375.
8. Ebrahimi, M., Fatemi Ghomi, S., & Karimi, B. (2014). Hybrid flow shop scheduling with sequence dependent family setup time and uncertain due dates. Applied Mathematical Modeling, 38, 2490-2504.
9. Fattahi, P., Mehrabad, M. S., & Jolai, F. (2007). Mathematical modeling and heuristic approaches to flexible job shp scheduling problems. Journal of Intelligent Manufacturing, 18, 331-342.
10. Gen, M., Tsujimura, Y., & Ida, K. (1992). Method for Solving Multi-objective Aggregate Production Planning Problem with Fuzzy Parameters. Computers and Industrial Engineering, 23, 117-120.
11. Itoh, T., & Ishii, H. (1999). Fuzzy due-date scheduling problem with fuzzy processing time. International Transactions in Operational Research, 6, 639-647.
12. Ku, W.-Y., & Beck, J. (2016). Mixed Integer Programming models for job shop scheduling: A computational analysis. Computers & Operations Research, 165-173.
13. Lei, D. (2010). A genetic algorithm for flexible job shop scheduling with fuzzy processing time. International Journal of Production Research, 48, 2995-3013.
14. Lei, D. (2011). Scheduling stochastic job shop subject to random breakdown to minimise makespan. The International Journal of Advanced Manufacturing Technology, 55, 1183-1192.
15. Lin, F.-T. (2001). A Job-Shop Scheduling Problem with Fuzzy Processing. International Conference on Computational Science-ICCS 2001 (pp. 409-418). San Francisco, CA, USA: Springer, Berlin, Heidelberg.
16. Mula, J., Peidro, D., & Poler, R. (2010). The effectiveness of a fuzzy mathematical programming approach for supply chain production planning with fuzzy demand. International Journal of Production Economics, 128, 136-143.
17. Neumann, K., & Schneider, W. G. (1999). Heuristic algorithms for job-shop scheduling problems with stochastic precedence constraints. Annals of Operations Research, 92, 45-63.
18. Petrovic, S., Fayad, C., Petrovic, D., Burke, E., & Kendall, G. (2008). Fuzzy job shop scheduling with lot-sizing. Annals of Operations Research, 159, 275-292.
19. Tavakkoli-Moghaddam, R., Jolai, F., Vaziri, F., Ahmed, P., & Azaron, A. (2005). A hybrid method for solving stochastic job shop scheduling problems. Applied Mathematics and Computation, 170, 185-206.
20. Zadeh, L. A. (1965). Fuzzy Sets. Information and Control, 8, 338-353.

TAYLOR COLLOCATION METHOD FOR SOLVING HIGH ORDER DIFFERENTIAL EQUATIONS AND DELAY DIFFERENTIAL EQUATIONS

H. LAIB[1], A. BELLOUR[2] AND A. BOULMERKA[1]

ABSTRACT. Taylor collocation method in the space of piecewise polynomials is applied to obtain the approximate solution for kth-order linear differential equations and delay differential equations (DDEs) with variable coefficients. An algorithm based on Taylor polynomials is developed to estimate the numerical solution of high-order linear DDEs. Numerical tests are included to prove the validity of the presented algorithm.

Key Words: High-order delay differential equation, Collocation method, Taylor polynomials.

2010 AMS Subject Classification: 34A35, 34K28, 34K40, 45L05.

1. Introduction

In this paper, we study a numerical method for the solution of kth-order delay differential equations with constant delay $\tau > 0$ and variable coefficients of the form:

$$x^{(k)}(t) = g(t) + \sum_{v=0}^{k-1} L_v(t)x^{(v)}(t) + \sum_{v=0}^{k-1} M_v(t)x^{(v)}(t-\tau), \tag{1.1}$$

for $t \in [0,T]$ and $x(t) = \Phi(t)$ for $t \in [-\tau, 0)$.

[1]Laboratory of Mathematics and their interactions, University Center of Mila, Algeria.

[2]Laboratory of Applied Mathematics and Didactics Ecole Normale Supérieure de Constantine, Constantine, Algeria.

The functions $g, \{L_v\}_{v=0}^{k-1}, \{M_v\}_{v=0}^{k-1} : [0,T] \to \mathbb{R}$ are sufficiently smooth. Furthermore, we suppose that

$\Phi^{(k)}(0) = g(0) + \sum_{v=0}^{k-1} L_v(0)\Phi^{(v)}(0) + \sum_{v=0}^{k-1} M_v(0)\Phi(-\tau).$

The existence and uniqueness of the smooth solution can be found in [4] and [7].

Delay differential equations (DDEs) have become crucial in the mathematical modelling of several sciences and engineering fields (see, e.g., [1, 8]). As a particular case in the epidemic model, Ghosh et al. [11] developed a model in the presence of vaccination to the newly entering individuals and considering a delay for the infected individuals to become infectious. Moreover, Liu et al. [20] developed two mathematical models describing the COVID-19 epidemics. The first one is an ODEs model, whilst the second one is a DDEs model with a time delay in newly infected individuals before they become infectious. Laib et al. [17] proposed a method for the solution of this model. In addition, Krasznai et al. [14] proposed a method to solve DDEs arising in the theory of neural networks. In population dynamics studying, Lenburya and Giang [19] proposed a model to simulate population growth of blowflies and baleen whales using nonlinear DDEs. On the other hand, Palumbo et al. [23] introduced a family of delay differential models of the glucose-insulin system for diabetological interest.

Several numerical methods have been proposed to approximate the solution of DDEs, including homotopy methods [2, 24], spectral and pseudospectral methods [6, 16], finite difference methods [15, 21], finite element methods [9, 25], Bernstein method [3], Taylor Collocation Method [5], and Hermite interpolation method [22].

We propose to use the Taylor collocation method (TCM), which is marked by the following main advantages: (i) the TCM method is direct, and the approximate solution is given by using explicit formulas. (ii) this method has a convergence order; (iii) moreover, no algebraic system needs to be solved, making the proposed algorithm very effective and easy to implement.

The outline of this paper follows; in section 2, we divide the interval $[0,T]$ into subintervals, and we approximate the solution of (1.1) in each interval by a Taylor polynomial. Numerical tests are provided in section 3. Finally, the paper is finished with a conclusion and some perspectives.

2. Description of the Method

We suppose that $T = r\tau$, where $r \in \{1, 2, 3, ...\}$. Let Π_N be a uniform partition of the interval $I = [0, T]$ defined by $t_n^i = i\tau + nh$, $n = 0, 1, .., N$, $i = 0, 1, .., r-1$, where the stepsize is given by $h = \frac{\tau}{N}$. Define the subintervals $\sigma_n^i = [t_n^i; t_{n+1}^i), n = 0, 1, .., N-1$, $i = 0, 1, .., r-1$ and $\sigma_{N-1}^{r-1} = [t_{N-1}^{r-1}, t_N^{r-1}]$. Moreover, denote by π_{m+k-1} the set of all real polynomials of degree not exceeding $m+k-1$, with $m > 1$. The real polynomial spline space of degree $m+k-1$ is defined as follows:

$$S_{m+k-1}^{(k-1)}(\Pi_N) = \{u \in C^{k-1}(I, \mathbb{R}) : u_n^i = u|_{\sigma_n^i} \in \pi_{m+k-1}, n = 0, ..., N-1, \ i = 0, 1, .., r-1\}.$$

This is the space of piecewise polynomials of degree (at most) $m+k-1$, such that $m+k > k \geq 1$. Its dimension is $rNm + k$, i.e., the same as the total number of the coefficients of the polynomials $u_n^i, n = 0, ..., N-1, i = 0, 1, .., r-1$. To find these coefficients, we use Taylor polynomial on each subinterval.

First, suppose that the approximation of x in the interval σ_0^0 is the polynomial

$$u_0^0(t) = \sum_{j=0}^{m+k-1} \frac{x^{(j)}(0)}{j!} t^j \ ; \quad t \in \sigma_0^0, \tag{2.1}$$

where $x^{(j)}(0), j = 0, ..., m+k-1$ is the exact value of $x^{(j)}$ at 0.

By differentiate equation (1.1) j-times, we get for $j = 0, 1, ..., m-1$,

$$x^{(j+k)}(0) = g^{(j)}(0) + \sum_{v=0}^{k-1}\sum_{l=0}^{j} \binom{j}{l} L_v^{(j-l)}(0) x^{(l+v)}(0) + \sum_{v=0}^{k-1}\sum_{l=0}^{j} \binom{j}{l} M_v^{(j-l)}(0) \Phi^{(l+v)}(-\tau),$$

such that $x^{(v)}(0) = \Phi^{(v)}(0)$ for all $v = 0, 1, ..., k-1$.

Second, the approximation of x is u_n^0 $(n \in \{1, 2, ..., N-1\})$ on the interval σ_n^0, such that

$$u_n^0(t) = \sum_{j=0}^{m+k-1} \frac{\hat{u}_{n,0}^{(j)}(t_n^0)}{j!} (t - t_n^0)^j; \quad t \in \sigma_n^0, \tag{2.2}$$

where $\hat{u}_{n,0}$ is the exact solution of the integro-differential equation, for $t \in \sigma_n^0$:

$$\hat{u}_{n,0}^{(k)}(t) = g(t) + \sum_{v=0}^{k-1} L_v(t)\hat{u}_{n,0}^{(v)}(t) + \sum_{v=0}^{k-1} M_v(t)\Phi^{(v)}(t-\tau), \tag{2.3}$$

such that $\hat{u}_{n,0}^{(v)}(t_n^0) = u_{n-1}^{0^{(v)}}(t_n^0)$ for all $v = 0, 1, ..., k-1$.

Now, for all $j = 0, 1, ..., m+k-1$ the formula for computing the values of the coefficients $\hat{u}_{n,0}^{(j)}(t_n^0)$ can be obtained by employing similar arguments to those used for obtaining the values of $x^{(j)}(0)$ above, we get the following formula:

$$\begin{aligned}\hat{u}_{n,0}^{(j+k)}(t_n^0) = g^{(j)}(t_n^0) &+ \sum_{v=0}^{k-1}\sum_{l=0}^{j}\binom{j}{l} L_v^{(j-l)}(t_n^0)\hat{u}_{n,0}^{(l+v)}(t_n^0) \\ &+ \sum_{v=0}^{k-1}\sum_{l=0}^{j}\binom{j}{l} M_v^{(j-l)}(t_n^0)\phi^{(l+v)}(t_n^0-\tau),\end{aligned} \tag{2.4}$$

for $j = 0, ..., m-1$ such that $\hat{u}_{n,0}^{(v)}(t_n^0) = u_{n-1}^{0^{(v)}}(t_n^0)$ for all $v = 0, 1, ..., k-1$.

Third, for x to be approximated by u_n^p ($n \in \{0, ..., N-1\}$ and $p \in \{1, 2, ..., r-1\}$) on the interval σ_n^p, x must be approximated by u_k^j ($0 \le k < n$ and $0 \le j \le p$) on each interval σ_k^j such that,

$$u_n^p(t) = \sum_{j=0}^{m+k-1} \frac{\hat{u}_{n,p}^{(j)}(t_n^p)}{j!}(t-t_n^p)^j; \quad t \in \sigma_n^p, \tag{2.5}$$

where $\hat{u}_{n,p}$ is the exact solution of the integro-differential equation:

$$\hat{u}_{n,p}^{(k)}(t) = g(t) + \sum_{v=0}^{k-1} L_v(t)\hat{u}_{n,p}^{(v)}(t) + \sum_{v=0}^{k-1} M_v(t)u_n^{p-1^{(v)}}(t-\tau), \tag{2.6}$$

for $t \in \sigma_n^p$, $\hat{u}_{0,p}^{(v)}(t_0^p) = u_{N-1}^{p-1^{(v)}}(t_0^p)$ and $\hat{u}_{n,p}^{(v)}(t_n^p) = u_{n-1}^{p^{(v)}}(t_n^p)$ for all $v = 0, 1, ..., k-1$.

The coefficients $\hat{u}_{n,p}^{(j)}(t_n^p)$ for $j = 0, ..., m-1$, is given by the following formula:

$$\begin{aligned}\hat{u}_{n,p}^{(j+k)}(t_n^p) = g^{(j)}(t_n^p) &+ \sum_{v=0}^{k-1}\sum_{l=0}^{j}\binom{j}{l} L_v^{(j-l)}(t_n^p)\hat{u}_{n,p}^{(l+v)}(t_n^p) \\ &+ \sum_{v=0}^{k-1}\sum_{l=0}^{j}\binom{j}{l} M_v^{(j-l)}(t_n^p)\hat{u}_{n,p-1}^{(l+v)}(t_n^{p-1}),\end{aligned} \tag{2.7}$$

such that $\hat{u}_{0,p}^{(v)}(t_0^p) = u_{N-1}^{p-1^{(v)}}(t_0^p)$ and $\hat{u}_{n,p}^{(v)}(t_n^p) = u_{n-1}^{p^{(v)}}(t_n^p)$ for all $v = 0, 1, ..., k-1$.

3. Analysis of Convergence

The following three lemmas will be used in this section.

Lemma 3.1. *(Discrete Gronwall-type inequality* [7]*) Let $\{k_j\}_{j=0}^{n}$ be a given non-negative sequence and the sequence $\{\varepsilon_n\}$ satisfies $\varepsilon_0 \leq p_0$ and*

$$\varepsilon_n \leq p_0 + \sum_{i=0}^{n-1} k_i \varepsilon_i, \quad n \geq 1,$$

with $p_0 \geq 0$. Then ε_n can be bounded by

$$\varepsilon_n \leq p_0 \exp\left(\sum_{j=0}^{n-1} k_j\right), \quad n \geq 1.$$

Lemma 3.2. [12] *Assume that the sequence $\{\varepsilon_n\}_{n\geq 0}$ of nonnegative numbers satisfies*

$$\varepsilon_n \leq A\varepsilon_{n-1} + B\sum_{i=0}^{n-1} \varepsilon_i + K, \quad n \geq 1,$$

where $A,\ B$ and K are nonnegative constants, then

$$\varepsilon_n \leq \frac{\varepsilon_0}{R_2 - R_1}[(R_2 - 1)R_2^n + (1 - R_1)R_1^n] + \frac{K}{R_2 - R_1}[R_2^n - R_1^n],$$

where, $R_1 = (1 + A + B - C)/2,\ R_2 = (1 + A + B + C)/2,$
therefore, $C = \sqrt{(1 - A)^2 + B^2 + 2AB + 2B}$ and $0 \leq R_1 \leq 1 \leq R_2$.

Before starting the main result, the following lemma is needed:

Lemma 3.3. *Let $g, \{L_v\}_{v=0}^{k-1}$ and $\{M_v\}_{v=0}^{k-1}$ be m-times continuously differentiable and Φ be $m+k$ times continuously differentiable on their respective domains. Then, there exists a positive number $\alpha(m)$ such that for all $n = 0, 1, ..., N-1,\ p = 0, 1, ..., r-1,$ and $j = 0, 1, ..., m+k,$ we have,*

$$\|\hat{u}_{n,p}^{(j)}\|_{L^\infty(\sigma_n^p)} \leq \alpha(m)$$

provided that h is sufficiently small, where $\hat{u}_{0,0}(t) = x(t)$ for $t \in \sigma_0^0$.

The following theorem describes the order of convergence of the method.

Theorem 3.4. *Let* g, $\{L_v\}_{v=0}^{k-1}$ *and* $\{M_v\}_{v=0}^{k-1}$ *be* m*-times continuously differentiable on their respective domains. Assume that* $u \in S_{m+k-1}^{(k-1)}(\Pi_N)$ *in the equations* (2.1), ..., (2.7) *define a unique approximate solution* u. *Then the resulting error function* $e := x - u$ *satisfy:*

$$\|e\|_{L^\infty(I)} \leq Ch^m,$$

C *is a finite constant independent of* h.

Proof. Using a more straightforward generalization of techniques employed in the case of high-order linear integro-differential equations by using the Taylor collocation method (see, for example, [5, 18]).

4. Numerical Examples

Numerical examples are given to illustrate the theoretical results obtained in the previous section. In each example, we calculate the error between x and the Taylor collocation solution u. We compare our results with other well-known methods: Multistep method[13], Spline method given in [10]. The results in these examples confirm the theoretical results obtained in section 3.

Example 4.1. *(*[13]*) Consider the linear ODE for the instantaneous charge* $q(t)$ *at time* t *on the capacitor in an LRC series circuit given by*

$$Lq'' + Rq' + \frac{1}{C}q = E(t),\ q(0) = 0,\ i(0) = q'(0) = 0,\ \ t > 0$$

The exact solution $q(t) = \frac{3}{4}\left(1 - e^{-10t}\left(cos(10t) + sin(10t)\right)\right)$ *and L, C, R, E(t), i(t) are the inductance, capacitance, resistance, the impressed voltage and the current, respectively. We solve the problem for* $L = 1$, $R = 20$, $C = 0.005$ *and* $E(t) = 150$. *The absolute errors for* $m = 7$, $m = 10$ *and* $h = 0,1$ *are compared with the absolute error of Multistep method* [13] *in Table 1.*

Table 1. Comparison of the absolute errors of Example 4.1

t	*Multistep method*[13]	*Present method* $m=7$	*Present method* $m=10$
0.0	0.0	0.0	0.0
0.1	1.61×10^{-3}	2.92×10^{-4}	1.10×10^{-6}
0.2	1.11×10^{-3}	1.00×10^{-3}	4.48×10^{-6}
0.3	3.52×10^{-4}	7.05×10^{-4}	2.22×10^{-6}
0.4	2.25×10^{-3}	1.62×10^{-4}	3.31×10^{-8}
0.5	2.81×10^{-3}	7.12×10^{-5}	5.20×10^{-7}
0.6	7.93×10^{-4}	6.86×10^{-5}	2.52×10^{-7}
0.7	1.50×10^{-5}	1.94×10^{-5}	7.57×10^{-9}
0.8	2.92×10^{-4}	3.35×10^{-6}	9.15×10^{-8}
0.9	2.43×10^{-4}	4.92×10^{-6}	4.54×10^{-8}
1.0	5.71×10^{-5}	1.63×10^{-6}	8.09×10^{-8}
1.1	9.21×10^{-6}	9.39×10^{-8}	4.59×10^{-8}
1.2	1.48×10^{-5}	3.09×10^{-7}	3.81×10^{-8}

Example 4.2. *([10]) Consider the second order linear delay differential equation*

$$\begin{aligned} x''(t) =& -5sin(t)e^{cos(t)} - (cos(t)+sin(t))\,x(t) - (6+sin(t))\,x'(t) \\ &+ sin(t-\frac{\pi}{4})x(t-\frac{\pi}{4}) + x'(t-\frac{\pi}{4}),\ t\in[0,2], \end{aligned}$$

and $\Phi(t)=e^{cos(t)}$ *for* $t\in[-\frac{\pi}{4},0)$. *The exact solution* $x(t)=e^{cos(t)}$. *The absolute errors for* $m=11,\ h=0,1$ *and* $h=0,2$ *are compared with the absolute error of Spline method* [10] *in Table 2.*

Table 2. Comparison of the absolute errors of Example 4.2

t	$h=0,2$		t	$h=0,1$	
	Spline method [10]	*Present method*		*Spline method* [10]	*Present method*
0.2	1.15×10^{-9}	3.47×10^{-12}	0.1	2.32×10^{-12}	8.51×10^{-16}
0.4	5.80×10^{-10}	1.92×10^{-11}	0.2	5.07×10^{-12}	2.95×10^{-12}
0.6	4.78×10^{-10}	9.18×10^{-11}	0.3	1.24×10^{-12}	2.10×10^{-11}
0.8	1.76×10^{-9}	8.08×10^{-11}	0.4	2.25×10^{-11}	5.70×10^{-11}
1.0	4.42×10^{-9}	6.76×10^{-11}	0.5	7.68×10^{-11}	6.21×10^{-11}
1.2	2.29×10^{-8}	5.96×10^{-11}	0.6	1.97×10^{-10}	5.80×10^{-11}
1.4	5.37×10^{-9}	4.15×10^{-11}	0.7	1.12×10^{-10}	4.58×10^{-11}
1.6	1.93×10^{-9}	1.83×10^{-10}	0.8	6.16×10^{-11}	2.90×10^{-11}
1.8	2.57×10^{-10}	9.85×10^{-9}	0.9	5.44×10^{-11}	3.22×10^{-11}
2.0	1.25×10^{-9}	7.82×10^{-9}	1.0	9.26×10^{-11}	5.90×10^{-11}

Example 4.3. *Consider the 7-th order DDE*

$$x^{(7)}(t) = g(t) + x(t) + t^2x'(t) + sin(t)x^{(6)}(t) + tx''(t - \frac{1}{2})$$
$$+ (t^2 - 1)x^{(5)}(t - \frac{1}{2}) + tx^{(6)}(t - \frac{1}{2}),\ t \in [0, 4].$$

g is chosen so that the exact solution is

$x(t) = \frac{1+t}{2e^t}$ *and the errors e for* $(m, N) = \{(3, 3), (4, 4), (5, 5), (7, 7)\}$ *at* $t = 0, 0.5, ..., 4$ *are presented In Table 3.*

Table 3. The absolute errors of Example4.3

t	$m = 3, N = 3$	$m = 4, N = 4$	$m = 5, N = 5$	$m = 7, N = 7$
0.0	0.0	0.0	0.0	0.0
0.5	5.37×10^{-10}	1.55×10^{-11}	2.14×10^{-12}	1.83×10^{-12}
1.0	1.09×10^{-7}	1.51×10^{-9}	9.34×10^{-11}	6.12×10^{-11}
1.5	2.11×10^{-6}	2.66×10^{-8}	5.79×10^{-10}	4.90×10^{-15}
2.0	1.70×10^{-5}	2.08×10^{-7}	7.06×10^{-10}	5.35×10^{-10}
2.5	8.81×10^{-5}	1.06×10^{-6}	2.61×10^{-9}	2.12×10^{-9}
3.0	3.50×10^{-4}	4.20×10^{-6}	2.12×10^{-8}	4.53×10^{-9}
3.5	1.19×10^{-3}	1.42×10^{-5}	9.35×10^{-8}	3.58×10^{-9}
4.0	3.69×10^{-3}	4.41×10^{-5}	3.26×10^{-7}	2.46×10^{-9}

5. Conclusion

In this paper, we have used a Taylor polynomials method to construct the numerical solution of the high-order differential equation and delay differential equation (1.1). The main novelty of this method is the study of the convergence of the approximate solution. The implementation of the proposed Taylor collocation method is straightforward. Numerical examples showed that the method is convergent with competitive accuracy compared to state-of-the-art techniques, and the obtained numerical results confirmed the theoretical estimates. Further researches on this kind of problems will be conducted by generalizing the proposed work to a system of kth-order DDEs.

References

[1] R. P. Agarwal, Difference Equations and Inequalities: Theory, Methods, and Applications. Second edition. Marcel Dekker, Inc.: New York, (2000).

[2] A. K. Alomari, M. S. M. Noorani and R. Nazar, Solution of delay differential equation by means of homotopy analysis method. Acta Applicandae Mathematicae, 108(2) (2009), 395-412.

[3] A. Bataineh, O. Isik, N. Aloushoush and N. Shawagfeh, Bernstein operational matrix with error analysis for solving high order delay differential equations. International Journal of Applied and Computational Mathematics, 3(3) (2017), 1749-1762.

[4] A. Bellen, M. Zennaro, Numerical Methods for Delay Differential Equations, Oxford, New York (2003).

[5] A. Bellour, M. Bousselsal and H. Laib, Numerical Solution of Second-Order Linear Delay Differential and Integro-Differential Equations by Using Taylor Collocation Method. International Journal of Computational Methods, 17(09) (2020), 1950070.

[6] D. Breda, S. Maset and R. Vermiglio, Pseudospectral differencing methods for characteristic roots of delay differential equations. SIAM Journal on Scientific Computing, 27(2) (2005), 482-495.

[7] H. Brunner, Collocation methods for Volterra integral and related functional differential equations, Cambridge university press, Cambridge, (2004).

[8] T.A. Burton, Volterra Integral and Differential Equations. Academic Press, New York (1983).

[9] K.Deng, Z. Xiong and Y. Huang, The Galerkin continuous finite element method for delay-differential equation with a variable term. Applied mathematics and computation, 186(2) (2007), 1488-1496.

[10] H. M. El-Hawary, A. El-ShamiK, Spline collocation methods for solving second order neutral delay differential equations. Int. J. Open Problems Compt. Math. 2(4), (2009) 536–545.

[11] U. Ghosh, S. Chowdhury and D.K. Khan, Mathematical modelling of epidemiology in presence of vaccination and delay. Comput. Sci. Inform. Technol. 3 (2013), 91-98.

[12] E. Hairer, C. Lubich and S. P. Norsett, Order of convergence of one-step methods for Volterra integral equations of the second kind, SIAM J. Numer. Anal. 20 (1983), 569-579.

[13] S. N. Jator, J. Li, A self starting linear multistep method for a direct solution of the general second order initial value problems. Intern J. Comp. Math. 86(5), (2009) 827-836.

[14] B. Krasznai, I. Győri and M. Pituk, The modified chain method for a class of delay differential equations arising in neural networks. Mathematical and computer modelling, 51(5-6) (2010), 452-460.

[15] M. K. Kadalbajoo and K. K. Sharma, A numerical method based on finite difference for boundary value problems for singularly perturbed delay differential equations. Applied Mathematics and Computation, 197(2) (2008), 692-707.

[16] M. M. Khader, The use of generalized Laguerre polynomials in spectral methods for solving fractional delay differential equations. Journal of computational and Nonlinear Dynamics, 8(4) (2013).

[17] H. Laib, A. Bellour and A. Boulmerka, Taylor collocation method for a system of nonlinear Volterra delay integro-differential equations with application to COVID-19 epidemic. International Journal of Computer Mathematics, (2021) 1-25.

[18] H. Laib, A. Bellour and M. Bousselsal, Numerical solution of high-order linear Volterra integro-differential equations by using Taylor collocation method. International Journal of Computer Mathematics, 96(5) (2019), 1066-1085.

[19] Y. Lenburya, D.V. Giang, Nonlinear delay differential equations involving population growth, Math. Comput. Modelling 40 (2004), 5–6. 583–590.

[20] Z. Liu, P. Magal, O. Seydi, and G. Webb, A COVID-19 epidemic model with latency period, Infect. Dis. Model. 5 (2020), 323–337.

[21] B. P. Moghaddam and Z. S. Mostaghim, A numerical method based on finite difference for solving fractional delay differential equations. Journal of Taibah University for Science, 7(3) (2013), 120-127.

[22] H. J. Oberle and H. J. Pesch, Numerical treatment of delay differential equations by Hermite interpolation. Numerische Mathematik, 37(2) (1981), 235-255.

[23] P. Palumbo, S. Panunzi and A. De Gaetano, Qualitative behavior of a family of delay-differential models of the glucose-insulin system. Discrete and Continuous Dynamical Systems-B, 7(2) (2007), 399.

[24] F. Shakeri and M. Dehghan, Solution of delay differential equations via a homotopy perturbation method. Mathematical and computer Modelling, 48(3-4) (2008), 486-498.

[25] H. Zarin, On discontinuous Galerkin finite element method for singularly perturbed delay differential equations. Applied Mathematics Letters, 38 (2014), 27-32.

WEIGHTED APPROXIMATION FOR KANTOROVICH TYPE q-BALAZS-SZABADOS OPERATORS

Hayatem Hamal, Pembe Sabancıgil

Department of Mathematics, Eastern Mediterranean University, Gazimagusa, North Cyprus

hafraj@yahoo.com, pembe.sabancigil@emu.edu.tr

Abstract

Balázs and Szabados studied approximation properties of the Bernstein type rational functions called the Balázs-Szabados operators. Different q-analogues of Balázs-Szabados operators are recently studied by several authors. New Kantorovich type q-analogue of the Balázs-Szabados operators are defined by Hamal and Sabancigil as follows:

$$R_{n,q}^{*}(f,x)=\sum_{k=0}^{n} r_{n,k}(q,x)\int_{0}^{1} f\left(\frac{[k]_q+q^k t}{b_n}\right)d_q t, \text{ where } f:[0,\infty)\to\mathbb{R},\ q\in(0,1),\ a_n=[n]_q^{\beta-1},$$

$$b_n=[n]_q^{\beta},\ 0<\beta\le\frac{2}{3},\ n\in\mathbb{N}, x\ge 0,\ r_{n,k}(q,x)=\frac{1}{(1+a_n x)^n}\begin{bmatrix} n\\ k\end{bmatrix}_q (a_n x)^k \prod_{s=0}^{n-k-1}\left(1+(1-q)[s]_q a_n x\right)$$

In this paper, we study weighted approximation properties of the new Kantorovich type q-Balázs-Szabados operators.

Let $B_2[0,\infty)=\left\{f:[0,\infty)\to R:|f(x)|\le M_f(1+x^2)\right\}$, where M_f is a constant depending on f, $C_2[0,\infty)=B_2[0,\infty)\cap C[0,\infty)$ and $C_2^{*}[0,\infty)=\left\{f\in C_2[0,\infty):\lim\limits_{x\to\infty}\frac{f(x)}{1+x^2}<\infty\right\}$.

The norm on the space $C_2^{*}[0,\infty)$ is shown as $\|f(x)\|_2=\sup\limits_{x\in[0,\infty)}\frac{f(x)}{1+x^2}$.

We have the following Korovkin type theorem.

Theorem 1 Assume that $q=q_n$ satisfies $0<q_n<1$ and $q_n\to 1$ as $n\to\infty$. Then for each $f\in C_2^{*}[0,\infty)$ we have $\lim\limits_{n\to\infty}\left\|R_{n,q_n}^{*}(f,x)-f(x)\right\|_2=0$.

Proof. By using the Korovkin theorem for weighted approximation (see [9],[10]), it is sufficient to show that

$$\lim_{n\to\infty}\left\|R_{n,q_n}^{*}(t^m;x)-x^m\right\|_2=0, \text{ for } m=0,\ 1,\ 2. \tag{1}$$

since $R_{n,q_n}^{*}(1;x)=1$, (1) holds true for $m=0$. Now by Lemma 5 in [3], we have

$$R_{n,q_n}^{*}(t;x)-x=\frac{1}{[2]_{q_n} b_{n,q_n}}+\frac{2q_n}{[2]_{q_n}}\frac{x}{1+a_{n,q_n}x}-x$$

$$=\frac{1}{[2]_{q_n} b_{n,q_n}}+\frac{(q_n-1)x}{[2]_{q_n}(1+a_{n,q_n}x)}-\frac{a_{n,q_n}x^2}{(1+a_{n,q_n}x)}$$

By applying triangle inequality, we have

$$\left|R^*_{n,q_n}(t;x)-x\right|\leq\frac{1}{[2]_{q_n} b_{n,q_n}}+\frac{(1-q_n)x}{[2]_{q_n}(1+a_{n,q_n}x)}+\frac{a_{n,q_n}x^2}{(1+a_{n,q_n}x)}.$$

Then, we obtain

$$\left\|R^*_{n,q_n}(t;x)-x\right\|_2\leq\sup_{0\leq x<\infty}\frac{1}{1+x^2}\left\{\frac{1}{[2]_{q_n} b_{n,q_n}}+\frac{(1-q_n)x}{[2]_{q_n}(1+a_{n,q_n}x)}+\frac{a_{n,q_n}x^2}{(1+a_{n,q_n}x)}\right\}$$

$$\leq\frac{1}{[2]_{q_n} b_{n,q_n}}\sup_{0\leq x<\infty}\frac{1}{1+x^2}+\frac{(1-q_n)}{[2]_{q_n}}\sup_{0\leq x<\infty}\frac{x}{1+x^2(1+a_{n,q_n}x)}+a_{n,q_n}\sup_{0\leq x<\infty}\frac{x^2}{1+x^2(1+a_{n,q_n}x)},$$

now by taking limit over all the last inequality, we have

$$\lim_{n\to\infty}\left\|R^*_{n,q_n}(t;x)-x\right\|_2\leq\lim_{n\to\infty}\frac{1}{[2]_{q_n} b_{n,q_n}}+\lim_{n\to\infty}\frac{(1-q_n)}{[2]_{q_n}}+\lim_{n\to\infty}a_{n,q_n}=0.$$

Again by using Lemma 5 in [3], we have

$$R^*_{n,q_n}(t^2;x)-x^2=\frac{1}{[3]_{q_n} b^2_{n,q_n}}+\frac{4q_n^3+5q_n^2+3q_n}{b_n[2]_{q_n}[3]_{q_n}}\frac{x}{1+a_{n,q_n}x}$$
$$+\frac{q_n[n-1]_{q_n}}{[n]_{q_n}}\frac{4q_n^3+q_n^2+q_n}{[2]_{q_n}[3]_{q_n}}\frac{x^2}{(1+a_{n,q_n}x)^2}-x^2$$

$$=\frac{1}{[3]_{q_n} b^2_{n,q_n}}+\frac{4q_n^3+5q_n^2+3q_n}{b_n[2]_{q_n}[3]_{q_n}}\frac{x}{1+a_{n,q_n}x}+\left\{\frac{q_n[n-1]_{q_n}}{[n]_{q_n}}\frac{4q_n^3+q_n^2+q_n}{[2]_{q_n}[3]_{q_n}}\frac{1}{(1+a_{n,q_n}x)^2}-1\right\}x^2.$$

Therefore,

$$\left|R^*_{n,q_n}(t^2;x)-x^2\right|\leq\frac{1}{[3]_{q_n} b^2_{n,q_n}}+\frac{4q_n^3+5q_n^2+3q_n}{b_n[2]_{q_n}[3]_{q_n}}\frac{x}{1+a_{n,q_n}x}+\frac{4q_n^3+q_n^2+q_n}{[n]_{q_n}[2]_{q_n}[3]_{q_n}}\frac{x^2}{(1+a_{n,q_n}x)^2}$$
$$+\left\{1-\frac{4q_n^3+q_n^2+q_n}{[2]_{q_n}[3]_{q_n}}\frac{1}{(1+a_{n,q_n}x)^2}\right\}x^2.$$

Then, we have

$$\left\|R^*_{n,q_n}\left(t^2;x\right)-x^2\right\|_2 \le \frac{1}{[3]_{q_n} b^2_{n,q_n}} \sup_{0\le x<\infty} \frac{1}{1+x^2} + \frac{4q_n^3+5q_n^2+3q_n}{b_n[2]_{q_n}[3]_{q_n}} \sup_{0\le x<\infty} \frac{x}{\left(1+a_{n,q_n}x\right)\left(1+x^2\right)}$$

$$+\frac{4q_n^3+q_n^2+q_n}{[n]_{q_n}[2]_{q_n}[3]_{q_n}} \sup_{0\le x<\infty} \frac{x^2}{\left(1+a_{n,q_n}x\right)^2\left(1+x^2\right)} + \sup_{0\le x<\infty} \frac{x^2}{\left(1+a_{n,q_n}x\right)^2\left(1+x^2\right)}$$

$$-\frac{4q_n^3+q_n^2+q_n}{[2]_{q_n}[3]_{q_n}} \sup_{0\le x<\infty} \frac{x^2}{\left(1+a_{n,q_n}x\right)^2\left(1+x^2\right)}.$$

Now by taking limit over all the last inequality, we have

$$\lim_{n\to\infty}\left\|R^*_{n,q_n}\left(t^2;x\right)-x^2\right\|_2 \le \lim_{n\to\infty}\frac{1}{[3]_{q_n} b^2_{n,q_n}} + \lim_{n\to\infty}\frac{4q_n^3+5q_n^2+3q_n}{b_n[2]_{q_n}[3]_{q_n}} + \lim_{n\to\infty}\frac{4q_n^3+q_n^2+q_n}{[n]_{q_n}[2]_{q_n}[3]_{q_n}} + 1 - \lim_{n\to\infty}\frac{4q_n^3+q_n^2+q_n}{[2]_{q_n}[3]_{q_n}}.$$

Hence,

$$\lim_{n\to\infty}\left\|R^*_{n,q_n}\left(t^2;x\right)-x^2\right\|_2 = 0.$$

Now, we present the next theorem to approximate all functions in $C_2^*[0,\infty)$. This type of results are given in [11] for locally integrable functions.

Theorem 2 Let $0<q_n<1$, $q_n \to 1$ as $n\to\infty$. Then for each $f\in C_2^*[0,\infty)$ and all $\upsilon>0$, we have $\lim_{n\to\infty}\sup_{x\in[0,\infty)} \frac{\left|R^*_{n,q_n}(f,x)-f(x)\right|}{\left(1+x^2\right)^{1+\upsilon}} = 0$.

Proof. Let $x_0\in[0,\infty)$. Then

$$\sup_{x\in[0,\infty)} \frac{\left|R^*_{n,q_n}(f;x)-f(x)\right|}{\left(1+x^2\right)^{1+\upsilon}} = \sup_{x\le x_0} \frac{\left|R^*_{n,q_n}(f;x)-f(x)\right|}{\left(1+x^2\right)^{1+\upsilon}} + \sup_{x>x_0} \frac{\left|R^*_{n,q_n}(f;x)-f(x)\right|}{\left(1+x^2\right)^{1+\upsilon}}$$

$$\le \left\|R^*_{n,q_n}(f;x)-f(x)\right\|_{C[0,x_0]} + \sup_{x\in[0,\infty)} \frac{\left|R^*_{n,q_n}\left(\left(1+t^2\right)f;x\right)-f(x)\right|}{\left(1+x^2\right)^{1+\upsilon}}$$

$$\le \left\|R^*_{n,q_n}(f;x)-f(x)\right\|_{C[0,x_0]} + \|f\|_2 \sup_{x>x_0} \frac{\left|R^*_{n,q_n}\left(\left(1+t^2\right);x\right)\right|}{\left(1+x^2\right)^{1+\upsilon}} + \sup_{x>x_0} \frac{|f(x)|}{\left(1+x^2\right)^{1+\upsilon}}. \tag{2}$$

Now, by definition of the norm of each function in $C_2^*[0,\infty)$, we have

$\left|f(x)\right| \le \|f\|_2\left(1+x^2\right)$, also we have $\sup_{x>x_0} \frac{|f(x)|}{\left(1+x^2\right)^{1+\upsilon}} \le \frac{\|f\|_2}{\left(1+x^2\right)^{\upsilon}} \le \frac{\|f\|_2}{\left(1+x_0^2\right)^{\upsilon}}$.

Let $\varepsilon > 0$. We can choose x_0 such that $\dfrac{\|f\|_2}{\left(1+x_0^2\right)^{\upsilon}} < \dfrac{\varepsilon}{3}$. (3)

By Theorem 1 , we get

$$\|f\|_2 \lim_{n\to\infty} \frac{\left|R^*_{n,q_n}\left(\left(1+t^2\right);x\right)\right|}{\left(1+x^2\right)^{1+\upsilon}} = \frac{1+x^2}{\left(1+x^2\right)^{1+\upsilon}}\|f\|_2 \le \frac{\|f\|_2}{\left(1+x^2\right)^{\upsilon}} \le \frac{\|f\|_2}{\left(1+x_0^2\right)^{\upsilon}} < \frac{\varepsilon}{3}.$$

By using Theorem 5.7 in [12], we can see that the first term of the inequality (2) implies that

$$\left\|R^*_{n,q_n}\left(f;x\right) - f\left(x\right)\right\|_{C[0,x_0]} < \frac{\varepsilon}{3}, \quad \text{as } n \to \infty \tag{4}$$

Taking the limit over inequality (2) and combining (3) and (4), we get the desired result.

Keywords: q-calculus, q-Balazs-Szabados operators, weighted approximation.

References

1. Balázs, K, Approximation by Bernstein type rational function. Acta Math. Acad. Sci. Hungar. Vol: 26, No:1-2, 123-134, 1975.
2. Balázs, K. and Szabados J, Approximation by Bernstein type rational function II. Acta Math. Acad. Sci. Hungar.Vol: 40, No:3-4, 331-337, 1982.
3. Hamal, H. and Sabancigil, P, Some Approximation properties of new Kantorovich type q-analogue of Balazs-Szabados Operators, Journal of Inequalities and Applications, Vol: 159, 2020.
4. Özkan, E. Y, Statistical Approximation Properties of Balázs-Szabados-Stancu Operators, Vol:28, No:9, 1943–1952, 2014.
5. Özkan, E. Y, Approximation Properties of Kantorovich type Balázs-Szabados operators. Demonstr. Math, Vol:52, 10–19, 2019.
6. Mahmudov, N. I, Approximation Properties of the Balázs-Szabados Complex Operators in the case . Comput. Methods Funct. Theory, Vol:16, 567 –583, 2016.
7. Kac, V., Cheung, P, Quantum Calculus. Springer-Verlag, Newyork, 2002.
8. Gadzhiev, A. D, P. P. Korovkin type theorems, Mathem. Zametki, Vol:20, No:5, Engl. Transl. Math Notes, Vol: 20, No:5-6, 995-998, 1976.
9. Gadzhiev, A. D, The convergence problem for a sequence of positive linear operators on unbounded sets and theores analogous to that of P.P Korovkin; Sov. Math. Dokl, Vol:15**,** No:5, 1433-1436, 1974.
10. Gupta. V, Some approximation properties on q-Durrmeyer operators. Appl. Math. Comput, Vol:197, No:1, 172-178, 2008.
11. Gadzhiev, A. D, Efendiyev, E.Ibikli, On Korovkin type theorem in the space of locally integrable functions. Czech. Math.J**,** Vol:53, No:128-1, 45-53, 2003.
12. Aral. A, Gupta. v, Agarwal. R. P, Applications of Calculus in Operator Theory. Springer, Chapters: 1, 4, 5, 2013.

Blockchain for Foreign Trade

Serkan AYVERDİ

Ünsped Gümrük Müşavirliği
ve Lojistik Hizmetler A.Ş.
Istanbul – Türkiye
serkanayverdi@ugm.com.tr

Eşref ADALI
Istanbul Technical University
Computer and Informatic Faculty
Istanbul – Türkiye
adali@itu.edu.tr

***Abstract**: There is a long history of studies conducted for correspondence in import and export transactions in accordance with certain standards. For example, countries in the EU economic group, including Turkey, prepare their customs declaration in accordance with EDIFACT which enabled documents to be shared between relevant organizations and directly transferred to information systems.*

Blockchain offers new possibilities for import and export transactions. The blockchain will provide document sharing among partners and provide significant credibility by keeping a record of the shared documents. As the leading customs consultancy firm (UGM) in Turkey, we have started to work to carry out customs clearance transactions on the blockchain. To establish the blockchain, the necessary technical infrastructure must be established, as well as the partners to participate in the blockchain. For this purpose, a bank, a logistics firm, an insurance company and an IT firm were brought together by UGM. The team created works on the determination of documents as customs clearance, work flow, processes, standards, information security, time stamp, electronic signature and infrastructure. The results of this collaboration will be presented in this paper.

***Keywords**: Blockchain, Foreign Trade, Information Security, Smart Contract, Time Stamp*

1. Introduction

The history of international trade can be traced back to the Silk Road. The Silk Road trade style, which was carried out by barter at the borders, has been maintained until recent times. Silk Road trade taught us three things:

1. Trade can only be done in safe environments.
2. The shopping parties should be able to trust each other.
3. At the end of the shopping, both parties should gain.

The development of trade over time has led to the emergence of a tool of change called money. We learn from Heradot that the first coin was used in Sardis, the capital of Lydia, around 1200 BC. Due to the heavy weight of coins, silk weaving first and then banknotes began to be used.

A safe environment for trade has been tried to be provided by the security forces of the countries. In this context, it can be said that caravanserais and inns built on the Silk Road fulfill an important task.

In the 20th century, it is witnessed that bankers and banks took charge to ensure the security of shopping. Documents issued by bankers or banks (which will later become banknotes) have started to be used as a means of payment in international shopping. Towards the end of the 20th century, because of the developments in the field of informatics, the "Value Added Network" (VAN) was started to be established. The companies that are connected to this trade network have started to maintain all their communication securely and registered through this network. The most important features provided by VAN can be explained as follows:

- Time independent but time stamped communication.
- Communication where the identities of the parties are unambiguous.
- Registration system that the parties cannot deny correspondence.

While these developments were taking place in the 1970s, we witness the development of standards for correspondence between organizations. The purpose of these studies can be explained as follows:

- Documents will be prepared in the information system in accordance with the format determined for that document type.
- The party receiving this prepared document will be able to directly transfer the information to its own information system. Thus, there will be no need for documents to be read and evaluated by human beings.
- A common alphabet (ASCII) will be used in the preparation of documents.
- The information system used by the party that prepares and sends and receives the documents will not have to have the same hardware and software.
- Algorithms that will ensure data communication security will be used against the corruption that may occur during the transmission of documents.

This application, whose features we explained, was introduced as "Electronic Data Interchange" (EDI), later it became United Nations (UN) services. The scope of EDI was later expanded and changed to UN-EDIFACT (Electronic Data Interchange for Administration, Commerce and Transport)). EDIFACT document templates are currently used by countries participating in the European Union customs (Turkey is in this cluster) in customs transactions.

With the introduction of Internet in the 1990s, commerce has gained a different dimension: a new form of commerce called e-commerce has emerged. E-commerce formats are classified as follows:

- Business - Customer (B-C): A firm selling a product or service to an individual.
- Business - Business (B-B): It is the act of selling goods and services between two firms.
- Business - Administration (B-A): Sales of goods and services made by a firm to a public institution.
- Customer - Administration (C-A): It is the act of selling goods and services made by an individual to a public institution.
- Customer - Customer (C-C): It is the sale of goods and services between two individuals.
- Customer - Business (C-B): It is the act of selling goods and services made by an individual to a firm.
- Customer - Administration (C-A): Sales of goods and services made by an individual to a public institution.
- Administration - Business (A-B): The sale of goods made by a public institution to a firm.
- Administration - Customer (A-C): The sale or service of a public agency to individuals.
- Direct Customer (D-C): Providing a manufacturer firm's goods and services directly to the customer.
- Government - Government (G-G): Includes the trade of a state with a state.

A group working in the field of security made a study in 1991 that documents could be shared between stakeholders with a time stamp. The result of this work, which was not considered important before, was presented by Satoshi Nakamoto with a paper named "Bitcoin: A Peer-to-Peer Electronic Cash System"[1]. This method, which is considered as a game changing technology, put bitcoin and blockchain issues on the trade agenda in 2009. In this method, bitcoin defines a new form of payment (money), and the blockchain defines the infrastructure [2].

Blockchain is an immutable ledger that records transactions in a business network, facilitates the asset tracking process, and shares this information. It can be an asset, a physical asset, or a digital value record. In the field of international trade, a blockchain can be used to exchange data and documents as digital assets or for documents related to payments, fees and charges. The main features and elements of the blockchain are briefly explained below:

- Increases productivity and decreases processing time by reducing repetitive processes.
- Minimizes the use of paper documents between institutions.
- Ensures the immutability of documents. Data cannot be changed, especially after smart contracts are operated. This feature prevents possible conflicts between partners.

The basic elements of the blockchain are [3,4]:

Distributed Ledger (Record): A record produced on the blockchain is written to the databases of all stakeholders connected to the network; Thus, the records are written to the distributed database. These records cannot be changed. The entries in the distributed ledger are written once; thus, unnecessary repetition is prevented.

Immutability of Records: Once a record is shared with stakeholders, no stakeholder can tamper with the registry and change the records. If it is understood that a transaction record was made incorrectly, a correction record is prepared and distributed. However, the old wrong record is not deleted and kept being seen.

Smart Contracts: Smart contracts are created to fulfill certain actions when the time comes and when conditions are met. Smart contracts take certain actions spontaneously when conditions are met and when the time comes. For example, payments, sending documents, insurance transactions can be carried out with smart contracts.

Usage areas and capabilities of the blockchain are explained in Figure-1.

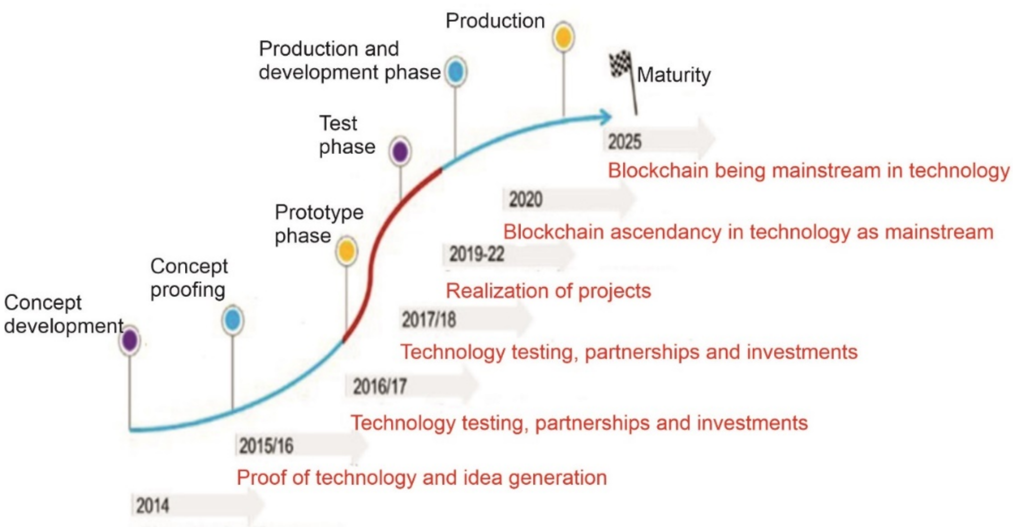

Figure-1: Development of blockchain

As can be understood from what is explained in the introduction, infrastructures and opportunities that provide trade and commerce have mutually influenced and directed each other over time. Within the scope of this declaration, an exemplary study on the use of blockchain in international trade is presented.

2. Infrastructure

The blockchain that will be introduced in this paper is related to international trade; It covers import and export transactions. The current import and export operations and the relations between stakeholders can be shown as in Figure-2. As seen in Figure-2, there are multidimensional relationships between stakeholders. These relationships naturally require many document flows. Naturally, we need to include bank, insurance and customs brokers in these relationships. It is clear that with these additions the shape will become more complex. Blockchain will make this complex structure in foreign trade uniform. In Figure-3, the main stakeholders of the foreign trade formed by the blockchain application are shown simply. Blockchain, by its very nature, a document created at the source reaches all stakeholders on the blockchain. The actions to be taken on each document received will be carried out in accordance with smart contracts.

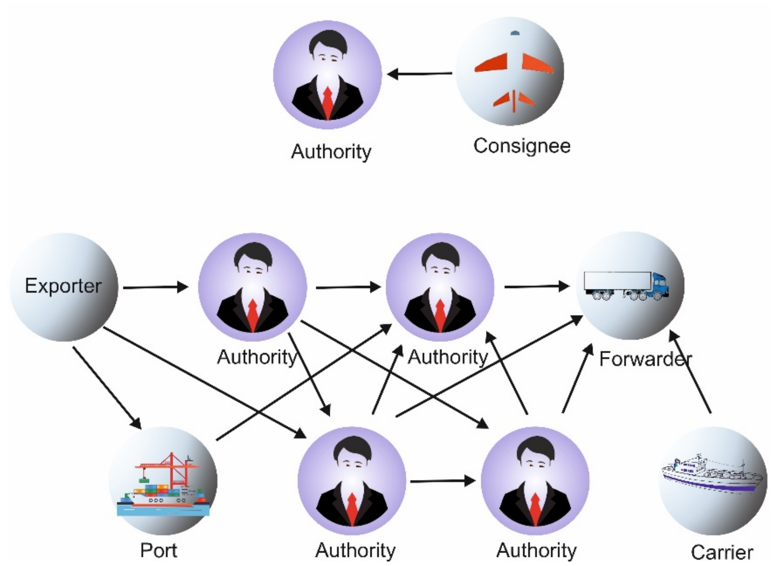

Figure-2: International Trade of today

The study was determined as a preliminary project, since it will be difficult at the first stage to create a blockchain that should include all stakeholders involved in import and export operations. Therefore, at least one of the stakeholders that should be in the foreign trade cluster has participated in the project. Stakeholders participating in the project are:

- Foreign trade firm (importer and exporter)
- Customs brokerage
- Bank (two banks)
- Carrier
- Insurer

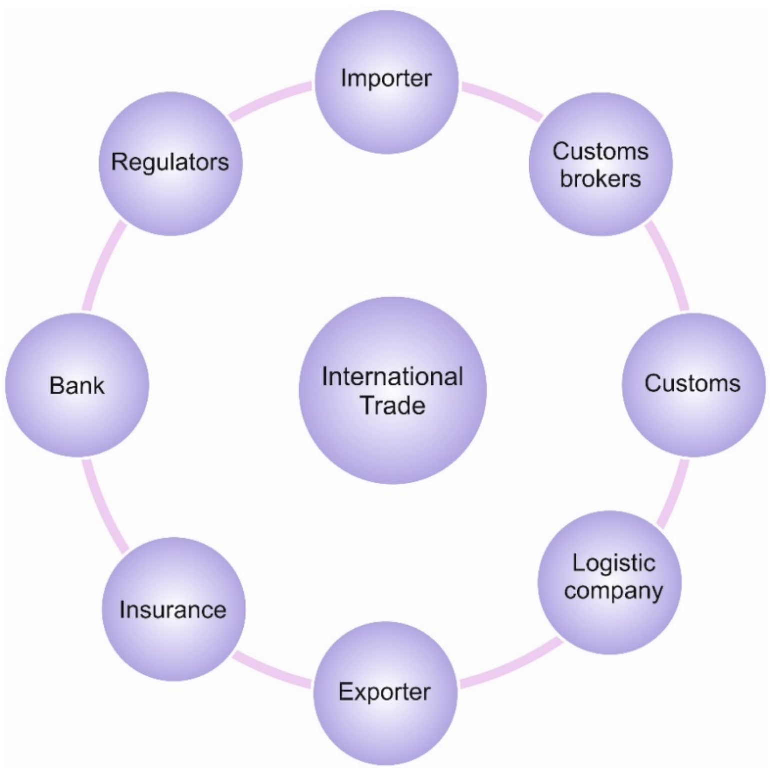

Figure-3: Main stakeholders of international trade

As can be understood from Figure-3, the preliminary project includes at least one example of the stakeholders that should be included. In the future, the following institutions are expected to join this blockchain.

- Ministry of Agriculture and Forestry
- Ministry of Commerce
- Ministry of Health
- Turkish Standardization Institute
- Environment and urban ministry
- Ministry of Transport and Infrastructure
- Chamber of Industry and Commerce (TİM, TOBB)
- Ministry of Treasury and Finance
- National Defense Department

- Borsa İstanbul
- Exporters' Associations
- Ministry of Science, Industry and Technology
- Culture and Tourism Ministry
- Ministry of Interior
- Nuclear Regulatory Authority
- Turkish Atomic Energy Authority
- Turkish Standard Institute (TSE)
- Energy and Natural Resources Ministry
- Energy Markets Regulatory Authority
- Ministry of Family Labor and Social Services
- Capital Market Authority
- General Directorate of Food and Control
- General Directorate of Eti Mining Operations
- Special Operations Directorate (Egm)

The blockchain to be established can be considered as a private blockchain. Because only permitted organizations will be able to participate in this network. The organizations described above will be able to connect to this network, which we call the Foreign Trade Blockchain (FTB). For an organization to start FTB, permission must be given by the blockchain administrator.

Within the scope of this paper, it will be assumed that the blockchain works, how to ensure its security and technical issues such as smart contracts are known.

3. Documents to be Shared

The blockchain is basically defined as a database established in a distributed structure. Therefore, a document created in a resource reaches other stakeholders as well. Issues related to foreign trade that may arise from this distributed structure and because problems are listed below [6]:

- **Document Fraud**: Forged documents or documents are fraudulent in international trade.
- **Production of the Same Document**: There is a possibility that some documents will be produced in more than one source. In such cases, some operations have to be done more than once and this may cause delays.
- **Compliance Obligation**: There must be harmony between the documents to be prepared by the parties. Processing documents that are incompatible with each other can cause problems.
- **Standard Documents**: All documents to be used in foreign trade must comply with national and international standards prepared on these issues.
- **Security**: It is extremely important to ensure the security of the documents that will circulate in the FTB.
- **Process Transparency**: All transactions circulating and processed on the FTB should be visible to the relevant stakeholders. However, some documents related to a company may not be required to be seen by competitors. In such cases, the document to be hidden is encrypted and can only be viewed by those who are permitted.
- **Cross-Border Cooperation**: Lack of digital channels to cooperate between domestic and international customs or ports may cause problems.
- **Trust and Reliability**: Hand-delivery of commercial documents to government agencies may result in falsification of documents and delays in transactions.

Considering the above-mentioned basic constraints, the documents that should be in the FTB's distributed data base have been determined by the stakeholders as follows:

- Customs declaration
- Receipt

4. FTB's Requirements

Periodical meetings are held and held with stakeholders to improve the targeted FTB. In these meetings, besides determining the documents to be used in the FTB, the requirements of the project are also tried to be determined. The features that emerged within the scope of these studies and provided by the FTB and determined as requirements for the project are explained below [5]:

- **Uniform Format of Documents**: It is important and required that each data to be distributed in the FTB have a single format. It would be appropriate to use international formats for documents, if any. Having a document prepared in a uniform format will make it easier for other stakeholders to understand and use this document.
- **Data / Document Ownership and Control**: There may be losses in traditional international trade in the process of finding and tracking who owns documents and data. On the other hand, it is possible to determine and monitor who produced a data or document in the blockchain. For this purpose, it will be necessary to clearly indicate the owner of each document and data distributed on the blockchain.
- **Single Workflow**: A single workflow refers to a network workflow that is not point-to-point between stakeholders but includes all stakeholders. Blockchain solution allows a seamless single workflow with the integration between stakeholders. Thus, it provides frictionless interactions between stakeholders and an overall improvement. This feature of the blockchain should be used.
- **Data Privacy**: Data privacy is an indispensable requirement in international trade. Confidentiality of user information, confidential business information, personally identifiable information and the like must be ensured. The blockchain can provide a suitable environment to ensure the confidentiality of such information, and this feature should be utilized.
- **Domestic Trade Process**: Due to the feature of the blockchain of distributed database, it should be arranged in a way to provide the automation processes necessary for trade with domestic organizations.
- **Foreign Trade Process**: Automation of the foreign trade process largely depends on the consolidation and modernization of domestic trade. Compliance with standards, data privacy, fulfillment of international documents and payments are important. These requirements can be met using blockchain technology.
- **Fulfillment of Transactions**: An international trade network is a system that includes the fulfillment of fees, fees, penalties, service-related costs and payments. Smart contracts can be used in the blockchain to perform such transactions, so smart contracts need to be prepared.
- **Immutability**: The reliability and transparency of a system depends on the controllability of the system. The immutability of data and documents on the blockchain is essential. It is known that a document or data written on a blockchain cannot be deleted or tampered with. It is also known that if the wrong record is entered, a correction record must be entered for it. Meanwhile, the wrong record is kept in the system without being deleted. This invariance feature of the blockchain should be utilized.
- **Analytical and Cognitive Skills**: The blockchain solution can provide analytical and cognitive solutions for risk and risk management. These solutions should be used.
- **Effective Fund Management**: Distributed ledger facilitates the movement of ownership of assets and documents. Fund movements between stakeholders can be monitored instantaneously by using the blockchain. The fund management feature of the blockchain should be utilized.

- **Faster Resolution of Disputes**: The blockchain maintains a ledger where the records of each transaction or event are shared. This data is added to the ledger only after stakeholder consensus has been reached. When disputes arise, they can be resolved by looking at the records. This feature of the blockchain should be utilized.
- **Risk management**: A blockchain creates a functional and legal structure. The legal structure obliges each stakeholder to take responsibility for the data and documents uploaded to the distributed ledger. An accountability principle applies to documents and data shared in the blockchain. The stakeholder who uploads the documents and data to the blockchain is responsible. This feature of the blockchain reduces the risk of fraud or data tampering, thus providing better risk management. The risk management feature of the blockchain must be used.
- **Origin of Goods**: The origin of the goods is very important in international trade. This feature greatly increases the transparency and confidence in the system. Products whose source is known to importers can be accurately priced and documented by customs officials. This feature must be used.
- **Automatic Reconciliations**: Documents and data are only written to the blockchain ledger after smart contracts are operated. These documents and data are called "*gold measure data*". This greatly reduces the need to run reconciliation programs to synchronize data across multiple systems. Data in the blockchain can be regarded as correct data. The automatic reconciliation feature must be used.
- **Data Recovery and Backup:** A distributed system, such as a blockchain, provides functions for data backup on multiple nodes and automatic backups. Data always stays in sync between distributed ledgers and data is never lost. This feature is an absolute requirement.

5 Conclusion

A study was initiated by UGM on the use of blockchain in international trade. Bank, insurance, transport and technology companies participated in this study. Participation is expected to increase. These blockchain efforts for foreign trade are expected to reach a certain maturity by the end of 2021.

References

[1] S. Nakamoto**,** *Bitcoin: A Peer-to-Peer Electronic Cash System*, Satoshi Nakamoto Institute, 2008

[2] M. Crosby, Nachiappan, P. Pattanayak, S. Verma, V. Kalyanaraman, *BlockChain Technology; Beyond Bitcoin, Sutardja Center for Entrepreneurship & Technology* Technical Report, 2015

[3] *Blockchain White Paper*, China Academy of Information and Communication Technology Trusted Blockchain Initiatives, 2018

[4] S. Voshmgir, V. Kalinov, *Blockchain*, BlockchainHub Berlin, 2017

[5] B*lockchain Technology for Paperless Trade Facilitation in Maldives*, Asian Development Bank, 2020

[6] E. Ganne, Can Blockchain Revolutionize International Trade?, World Trade Organization 2018

[7] A. Sahani, P. Singh, A. Kumar, *Introduction to Blockchain*, Journal of Informatics Electrical and Electronics Engineering, 2020, Vol. 01, Iss. 01, S. No. 004, pp. 1-9

[8] Y. Okazaki, *Unveiling the Potential of Blockchain for Customs*, World Customs Organization, 2018

THE INFLUENCE OF VARIOUS SUPPORT SCHEMES ON THE ECONOMICAL FEASIBILITY OF VARIOUS SCALE WIND TURBINE SYSTEM IN DELTA STATE, NIGERIA

Taiwo Temitayo Ijaoye [1]

[1] Department of Electrical & Electronics Engineering, Cyprus International University, Nicosia, Cyprus

İjaoyetaiwo080@gmail.com

Abstract

The electricity demand of Nigeria is increasing rapidly with very little contribution from the renewable energy. The major source of the energy supply of the country is the fossil fuels that creates pollution. Additionally, it is a finite source in nature. As a result, there is a quick need to search for different opportunities to satisfy up with the strength requirement of the country. Energy resources have always remained as important power assets in Nigeria for several years. This research consequently examines on the various scale of wind turbine size in Federal Republic of Nigeria (FRN) and the influence of various support schemes, which can urge the wind power (WP) installations. Homer software is used to run simulations based on various support schemes in this project. Four support scheme such as; feed in tariff, self-power consumption, month-to-month net metering and annually net metering is applied with four rated capacity of wind turbine of 80 kW, 100 kW, 250 kW, and 500 kW. Also, the average daily load is kept varying from 1000 kWh to 3000 kWh, in 1000 kWh steps so that to study, the effect of the aforementioned support schemes on the viability of WP in a special state in FRN. The result shows that as the rated capacity of wind turbine (WT) increases from 80 kW through 500 kW, the gradual decrease in simple payback increases the present worth. Additionally, the research reveals that out of the entire support scheme, feed in tariff is selected to be the most feasible one. This eventually makes the setup of wind turbine in FRN to be notably viable. The technical and economic analyses of the simulation confirmed that if the project is implemented it will be helpful to increase the energy mix of FRN.

Keywords: Energy differences; IRR; O&M; Present worth; Simple payback.

1. BACKGROUND

The use of the wind energy (WE) is attractive because it is environmental friendly and economically feasible in many regions of the world [1]. For this cause, many countries nowadays has shown efforts for utilizing renewable energy (RE) such as WE [5]. Despite increase of fuel resources in FRN, the electricity demand per capita remains high [9]. However, the threat of predicted fuel depletion, climate change, pollution and oil value volatility, urge the country to develop various approaches for the electricity generations. These alternatives approaches are mainly renewables because they provide a solution for energy supply security issues [9].

There is an increment rate of fossil resources for the power generation in FRN. Therefore, collaborate with others power generation company to sustain the requirements of the country [7]. Electricity situation of FRN reflected that power request seem extremely rise, due to growing of geopolitical zones. However, makes the provision of the electricity to be insufficient, uncertain, and infrequent, as a result of nonrenewable resources that are quick to exhaust [3]. Circumstances requires the deviation of the energy by improve the huge renewable energy (RE) capita in FRN. Most of the zones in FRN endued with robust wind environments, especially in the seaside zones.

The Nigeria government proposed to increase hydropower generation to 5690 MW, thermal power to 2000 MW along with RE of about 1000 MW, and dissemination capacity of about thirty three thousand megawatt by 2020. This goal invented purposely to reduce FRN power mix of nonrenewable dependency and to increase the wind power generation (WPG) in the country. Additionally, because of this substitute resolution, several electricity delivery firms through freelance independent power purchasing system (IPPs) and States are presently financed to construct medium scale of wind power generation (WPG) of 2000 MW transmitted to the FRN grid [2].

The WP within FRN at ten meter altitude is studied for 10 wind locations around six geopolitical zones in the country displays that some locations have wind power (WP) between 1.0m/s and 6.3m/s that ratified FRN have reasonable WE [12]. Along with their drawn chart, is confirmed that off seashore in the southern regions of FRN have capacities for generating durable WP [12]. However, wind speed capacities in seaside regions of FRN have demonstrated excellent wind prospective to implement the WPG. Also, reveals the WP density evaluation at twenty five meter height that confirmed north central of FRN to be highly viable for yearly WPG of WT load in kilowatt-hour [12].

The financial analysis of wind power generation (WPG) is demonstrated in FRN [6]. The technical and economical study of six WPG are categorized in small, medium and large with their wind turbine (WT) size rated from 20 KW- 2 MW is studied [6]. However, electricity cost value together with the present value cost of electricity is estimated for all the six selected geopolitical zones of FRN. Therefore, this is done by using wind speed (WS) data between twenty-five years to thirty-seven years scale at hub height of 10m. Additionally, six models are used to evaluate the analysis for all the six geopolitical zones with their various hub height range from 36.6m through 70m. The result demonstrated that, Uyo has a least average total production energy output with P10-20 WT, whereas Kano using Vesta V80 WT given the highest average total production of energy output [6].

2. METHODOLOGY

The method that is used in this study specially deals with the feasibility evaluation of wind power by supplying energy for electrical loads of various sizes at a precise location in Federal Republic of Nigeria. Homer micro grid software is used to run the simulation on the way to validate the techno economics of wind energy installations. The average daily load used varies from 1000 to 3000 kWh, in 1000 kWh steps. The wind energy system is designed to operate throughout the year from January to December, whereas July offers the highest yield. Four-support schemes are used in the simulations. These are; self consumption, feed in tariff, monthly net metering, and annually net metering. Additionally, different wind turbine capacities such as 80 kW, 100 kW, 250 kW, and 500 kW are used. The optimum investment method is analyzed by changing the support scheme, daily load and the wind turbine size. In this context, simple payback period (SPB), internal rate of return (IRR), and net present worth (NPV) parameters are used.

Table 1: The basic simulation parameters for all the support schemes in homer software

ITEMS	Cost per kW	Selling price (FiT)	Power price (FiT)	Selling price (SEC)	Power price (SEC)	Selling price (MNM)	Power price (MNM)	Selling price (ANM)	Power price (ANM)	Fuel cost
PRICE/US$	1000	0.09	0.05	0.00	0.05	0.05	0.05	0.05	0.05	0.64

From [10]

Table 1 shows the basic simulation parameters for all the support schemes that is used for the technical analysis. Similarly, the set-up and repairs estimate of the WT is 2% [4], whereas cost per kW that is used for the simulation is US$1000 [4]. The daily load set up in the electrical load is; 1000 kWh, 2000 kWh, 3000 kWh respectively. Additionally, all these parameters is entered one after the other into the load and design program in the homer software. Hence, by clicking on the calculate button, the software would calculate it automatically as illustrated in figure 1. However, in this study wind resources location is determined by HOMER report considered the wind direction at 30m, 40m, 50m, and 60m.

The wind turbines designed to operate for one year, and the average wind speed of a selected region is 10m/s.

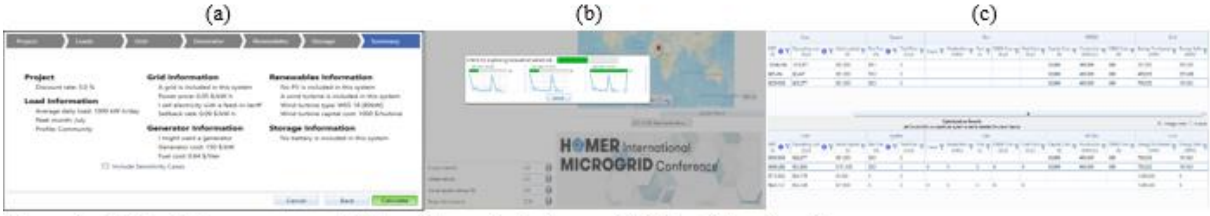

Figure 1: (a) Simulation summary, (b) Simulation calculation, and (c) Simulation Result

The simulation summary is concluded in figure 1. It shows the summary for all the simulation information. After this screen, the simulation gets ready to be launched to get results.

3. MATHEMATICAL ANALYSIS

3.1 Simple Payback (SPB)

This is represent a first approximation, required years to meet the initial investment cost, considering only the total annual saving.

$$SPB = \frac{I_c}{A_r - A_c} \tag{1}$$

where I_c is the installation cost of the wind turbine, A_r is the annual revenue of the wind turbine, and A_c is the annual cost of operation and maintenance (O&M) kWh of the electricity generated.

$$I_c = T_c \times R_c \tag{2}$$

Where T_c is the turbine cost per kilowatt, and R_c is the rated capacity of the wind turbine.

$$A_r = R_c \times N_d \times N_h \times M_c \times E_p \tag{3}$$

where A_r is the annual revenue of the wind turbine, N_d is the number of days in a year, N_h is the number of hours in a day, M_c (maintenance cost) is the O&M kWh of the electricity generated, and E_p is the electricity price in either FiT or net metering.

3.2 Net Present Worth (NPV)

This is the subtraction of the present worth of cash inflow and present worth of cash outflows within a period of time, whereas is given as;

$$NPV = PV\left(\frac{P}{A}, i, n\right) - PV(cost) \tag{4}$$

Or

$$NPV = PV\ (1 \div (1+i)^n\ ) - PV_{cost} \tag{5}$$

$$NPV = PV\ (1 \div (1+0.05)^{20}\ ) - PV_{cost} \tag{6}$$

where i is interest rate (reduction percentage) of the wind turbine and it is equal to 5% [13], whereas n is useful life of the wind turbine that is equal to 20 years. However, NPV is used for economic planning in power generation [10].

3.3 Internal Rate of Return (IRR)

This is the ratio of the total present rate of an installation cost equals to total present rate of the expected revenue of the project, and is given as;

$$IRR = \frac{r^a\ + NPV^a}{(NPV^a - NPV^b) \times r2^a - r2^b} \tag{7}$$

where r^a is discount rate, however, IRR is used to evaluate the viability of the project of the power generation. Take for example; if the goal IRR of a project is five percent and the IRR generated fifteen percent, hence, the enterprise should accept the undertaking.

4. RESULTS AND DISCUSSION

The homer software shows the simulation result of all the support schemes depending on the capacity of each wind turbine (WT) and the daily load in kWh. The useful life of the WT of various size is taken as 20 years. The result of all the four support schemes such as; Feed in tariff (FiT), Self consumption (SEC), Monthly net metering (MNM), and Annually net metering (ANM) in the simulation demonstrated throughout the entire tables and figures below. However, these entire figures shown below is design to illustrate the simulation output variation between the simple payback (SPB) and present worth (PW) for all the support schemes. Similarly, the simulation result shows that as the hub height increases simple payback period decreases more worth is produced [6].

Table 2: FiT/SEC (SPB & PW) simulation output in homer software

		FiT						SEC					
HUBE HEIGHT	RATED SIZE	SPB 1000 kWh	PW 1000 kWh	SPB 2000 kWh	PW 2000 kWh	SPB 3000 kWh	PW 3000 kWh	SPB 1000 kWh	PW 1000 kWh	SPB 2000 kWh	PW 2000 kWh	SPB 3000 kWh	PW 3000 kWh
30m	80 kW	1.69	$454,532	1.79	$400,015	1.89	$363,666	2.9	$113,716	2.8	$175,927	2.75	$221,365
40m	100 kW	1.31	$1,061,461	1.42	$932,615	1.52	$868,092	2.45	$144,041	2.4	$234,947	2.36	$315,590
50m	250 kW	0.88	$1,376,679	0.93	$1,304,472	0.97	$1,248,564	2.4	$150,646	2.32	$240,160	1.69	$340,054
60m	500 kW	0.42	$1,426,670	0.43	$1,402,470	0.44	$1,350,562	1.8	$215,728	1.65	$340,456	1.5	$447,317

Table 2 shows the output of all the four WT sizes of FiT & SEC from 80 kW to 500 kW and hub height from 30m to 60m. It shows that 80 kW operates at 30m, 100 kW at 40m, 250 kW at 50m and 500 kW at 60m. By keeping daily load of each WT capacity constant from 80 kW to 500 kW in FiT, there is decrease in SPB and increase in PW and as the daily load of each WT size increases from 1000 kWh to 3000 kWh, there is increase in SPB and decrease in PW, whereas in SEC by keeping the daily load constant of each WT size from 80 kW to 500 kW, there is decrease in SPB and increase in PW. Additionally, as daily load of each WT size increases from 1000 kWh to 3000 kWh, there is decrease in SPB and increase in PW.

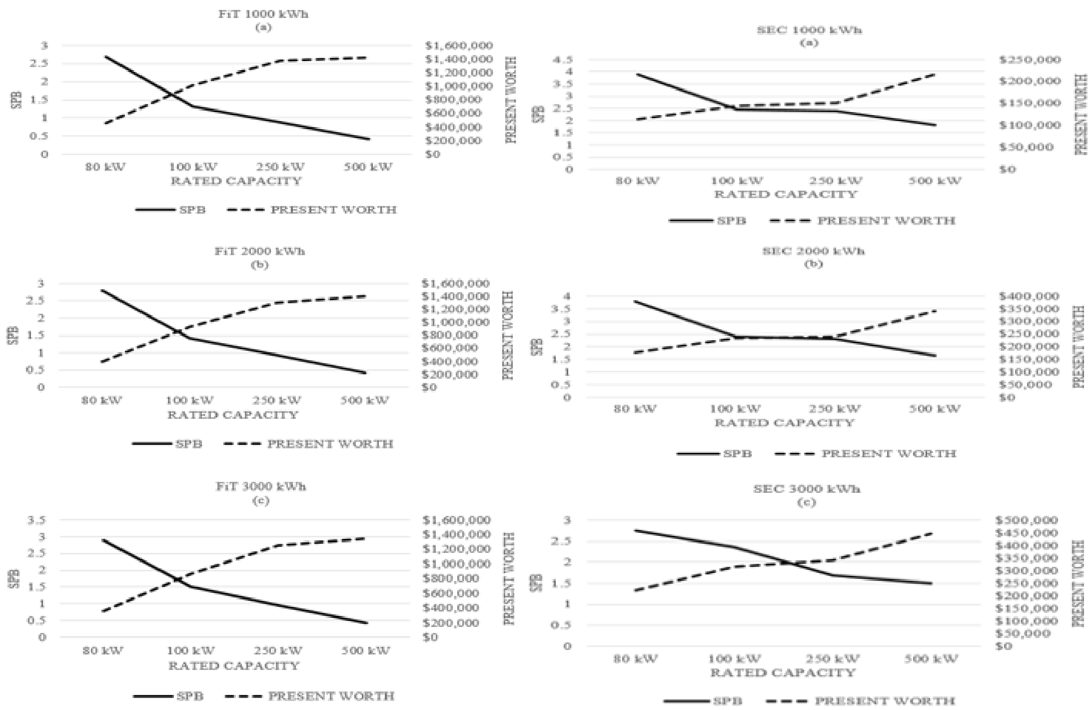

Figure 2: The trend in SPB and PW for FiT & SEC support scheme.

Figure 2 shows the trend in SPB along with PW for FiT & SEC support scheme. In FiT support scheme, as daily load increases from 1000 kWh to 3000 kWh for each wind turbine size from 80 kW to 500 kW as illustrated in the figure 2, there is gradual increase in SPB and decrease in PW of each wind turbine capacity, whereas in SEC support scheme, there is gradual decrease in SPB and increase in PW of each WT capacity.

Table 3: FiT/SEC (O&M & IRR) simulation output in homer software

		FiT						SEC					
HUBE HEIGHT	RATED SIZE	O&M 1000 kWh	IRR 1000 kWh	O&M 2000 kWh	IRR 2000 kWh	O&M 3000 kWh	IRR 3000 kWh	O&M 1000 kWh	IRR 1000 kWh	O&M 2000 kWh	IRR 2000 kWh	O&M 3000 kWh	IRR 3000 kWh
30m	80 kW	$23,277	38.10%	$17,277	32.70%	$2,447	31.60%	$10,756	6.20%	$21,563	10.80%	$34,020	14.20%
40m	100 kW	$56,328	81.30%	$35,104	73.50%	$12,276	68.70%	$11,330	9.10%	$22,803	15.80%	$36,095	21.90%
50m	250 kW	$59,303	119.20%	$36,776	113.30%	$17,277	108.70%	$12,387	9.40%	$25,442	15.90%	$40,468	22.80%
60m	500 kW	$84,387	120.80%	$61,014	119.20%	$38,797	117.20%	$16,941	45.40%	$33,862	45.40%	$50,852	50.10%

Table 3 shows the increase in O&M and IRR of FiT of each WT size from 80 kW to 500 kW by keeping daily load constant, and as daily load increases from 1000 kWh to 3000 kWh there is decrease in O&M along with IRR, whereas in SEC, shows increase in O&M and IRR from 80 kW to 500 kW by keeping daily load constant, and as the daily load of each WT size increases from 1000 kWh to 3000 kWh in 1000 kWh step. However, It is studied that, as the SPB increases, the PW decreases. Therefore, it affects the O&M and IRR. [6].

Table 4: MNM/ANM (SPB & PW) simulation output in homer software

		MNM						ANM					
HUBE HEIGHT	RATED SIZE	SPB 1000 kWh	PW 1000 kWh	SPB 2000 kWh	PW 2000 kWh	SPB 3000 kWh	PW 3000 kWh	SPB 1000 kWh	PW 1000 kWh	SPB 2000 kWh	PW 2000 kWh	SPB 3000 kWh	PW 3000 kWh
30m	80 kW	2.68	$346,411	2.68	$346,411	2.68	$346,411	2.68	$346,411	2.68	$346,411	2.68	$346,411
40m	100 kW	2.22	$578,091	2.22	$578,091	2.22	$578,091	2.22	$578,091	2.22	$578,091	2.22	$578,091
50m	250 kW	1.52	$779,444	1.52	$779,444	1.52	$779,444	1.52	$779,444	1.52	$779,444	1.52	$779,444
60m	500 kW	0.75	$798,648	0.75	$798,648	0.75	$798,648	0.75	$798,648	0.75	$798,648	0.75	$798,648

Table 4 shows the result of all the four WT sizes of MNM & ANM from 80 kW to 500 kW. However, by keeping daily load constant of each wind turbine size in MNM & ANM, there is decrease in SPB from 2.68 years at 80 kW to 0.75 year at 500 kW, whereas there is increase in PW from $346,411 to $798,648. Additionally, as daily load increases from 1000 kWh to 3000 kWh as illustrated in Table 5.6, all the WT sizes from 80 kW to 500 kW remain constant.

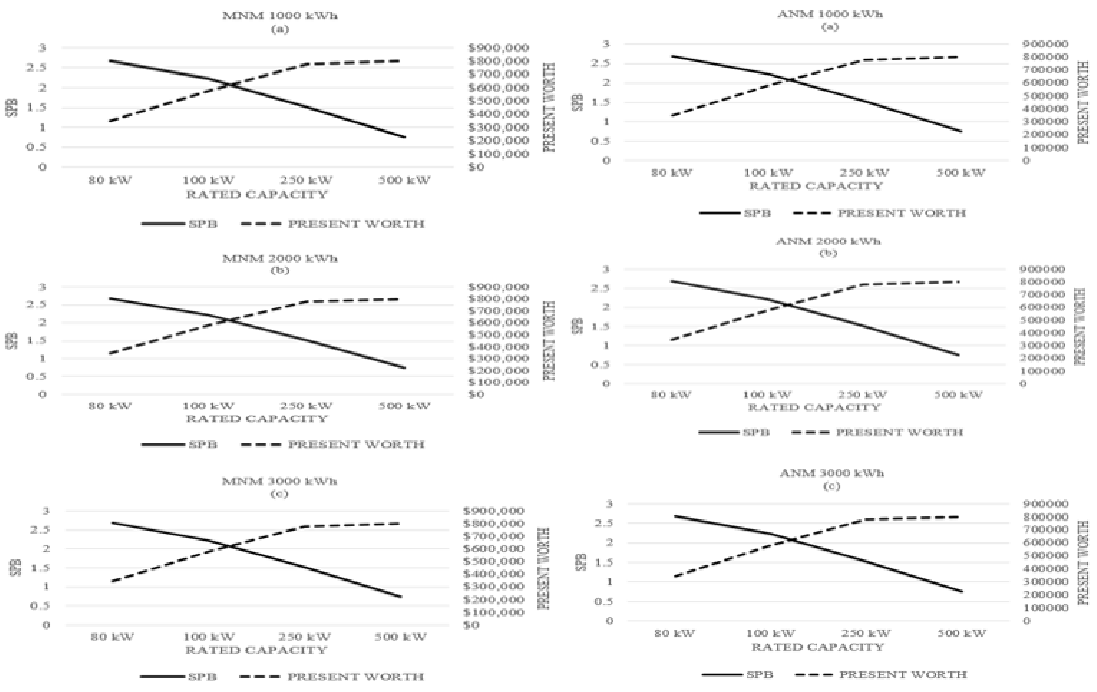

Figure 3: The trend in SPB and PW for MNM & ANM support scheme.

Figure 3 shows the trend in SPB along with PW for MNM & ANM support scheme, such that as daily load increases from 1000 kWh to 3000 kWh for each wind turbine size from 80 kW to 500 kW as illustrated in the figure 3, the SPB and PW remain constant.

Table 5: MNM/ANM (O&M & IRR) simulation output in homer software

		MNM						ANM					
HUBE HEIGHT	RATED SIZE	O&M 1000 kWh	IRR 1000 kWh	O&M 2000 kWh	IRR 2000 kWh	O&M 3000 kWh	IRR 3000 kWh	O&M 1000 kWh	IRR 1000 kWh	O&M 2000 kWh	IRR 2000 kWh	O&M 3000 kWh	IRR 3000 kWh
30m	80 kW	$23,476	30.40%	$9,950	30.40%	$5,153	30.40%	$23,476	30.40%	$9,950	30.40%	$5,153	30.40%
40m	100 kW	$28,200	48.80%	$12,991	48.80%	$5,259	48.80%	$28,200	48.80%	$12,991	48.80%	$5,259	48.80%
50m	250 kW	$41,653	70.20%	$23,403	70.20%	$5,512	70.20%	$41,653	70.20%	$23,403	70.20%	$5,512	70.20%
60m	500 kW	$42,012	72.10%	$23,509	72.10%	$8,300	72.10%	$42,012	72.10%	$23,509	72.10%	$8,300	72.10%

Table 5 shows increase in O&M and IRR from 80 kW to 500 kW at daily load of each WT sizes of MNM & ANM. Moreover, as the daily load of each WT size increases from 1000 kWh to 3000 kWh, there is decrease in O&M at each WT size, but IRR remain constant.

Table 6: FiT, SEC, MNM, ANM (Capacity factor (CF) & Total production (TP)

HUBE HEIGHT	RATED SIZE	CF 1000 KWh	TP 1000 KWh	CF 2000 KWh	TP 2000 KWh	CF 3000 KWh	TP 3000 KWh
30m	80 kW	22	157,219	22	157,219	28	198,220
40m	100 kW	28	252,017	28	252,017	30	265,225
50m	250 kW	30	658,017	30	658,017	35	768,230
60m	500 kW	35	1,554,193	35	1,554,193	40	1,768,250

Table 6 shows that the tendency of high production is possible as hub height increases. However, capacity factor (CF) reveals how efficient the turbine could connect the availability of energy within the wind ranges. Similarly, the CF for a realistic effectiveness WT at a prospective location may range between 15% and 40% [8].

5. CONCLUSION

In this research, various support schemes on the financial viability of various wind turbine sizes from 80 kW to 500 kW are studied in FRN. The highest total production of wind energy generation is viable with 500 kW wind turbine, because of its highest rated wind speed amongst all the selected WT sizes. In all the support schemes such as; FiT, SEC, MNM, and ANM, 80 kW WT size produces the lowest energy output at 30m hub height, whereas the highest energy output is given by 500 kW wind turbine at 60m hub height with the FiT scheme. The capacity factor has the least value in 80 kW, WT size, 28% at 30m hub height, whereas the highest is 500 kW WT size, 40% at 60m hub height for all the support schemes. In the optimum investment; 80 kW of wind turbine has the highest SPB, the lowest PW and the lowest IRR, whereas 500 kW wind turbine has the lowest SPB, the highest PW and the highest IRR. The support scheme that has highest SPB and lowest PW is SEC. Moreover, the support scheme that has the lowest SPB and highest PW is FiT.

Therefore, FiT is considered the best type of support scheme for wind power generation in FRN. Additionally, it shows that FiT with 500 kW wind turbine capacity is the best among the entire support schemes, and can supplies the primary goal for renewable electricity at the FRN energy, which is a kind of immature market in terms of renewables. Besides, it stands the threat of combating the greenhouse gas emission that would have been discharged through a fossil fuel to pollute the environment. On the prevailing tariff conditions in FRN, this challenge might be considered as being financially possible due to its maximum present worth amongst the entire support schemes within the simulation. Similarly, FiT in this analysis considered outstanding as a way of selling renewable power development. The selling fee is higher than the power-purchasing fee unlike in net metering wherein it selling fee is not always greater than the retails fee. It implies cannot produce power beyond what you buy, and self-power consumption in this scheme most effective keep in mind the power rate by ingesting increasingly more power without promoting it back to the nationwide grid.

REFERENCES

1. Ali Mostafaeipour, Productivity and development issues of global wind turbine industry, Renewable and Sustainable Energy Reviews, Vol:14, No:3, 1048-1058, (2010).
2. Geoffrey Hammond, Alternative Energy Strategies for the United Kingdom Revisited: Market Competition and Sustainability, Technological Forecasting and Social Change, Vol:59, No:2, 131-151, (1998).
3. Ibitoye, Adenikinju, Future Demand for Electricity in Nigeria, Applied Energy, Vol:84, No:5, 492-504, (2007).
4. IRENA, Renewable Power Generation Cost, pp. 96, 104-108, (2017). 'file:///C:/Users/Markama/Downloads/IRENA_2017_Power_Costs_2018.pdf [11/8/2019].
5. Majid Jamil, Sheeraz Kirmani, Himanshu Chatterjee, Technoeconomic viability of three different energy-supplying options for remote area electrification in India, International Journal of Sustainable Energy, Vol:33, No:2, 470-482, (2013).
6. Olayinka S Ohunakin, Olanrewaju M Oyewola, Muyiwa S Adaramola, Economic analysis of wind energy conversion systems using levelised cost of electricity and present value method in Nigeria, International Journal of Energy and Environmental Engineering, Vol:4, No:2, 1-8, (2013).

7. Ohunakin Olayinka, Energy utilization and renewable energy sources in Nigeria, Applied Science, Vol:5, No:2, 171-177, (2010).
8. O.S. Ohunakin, M.S. Adaramola, O.M. Oyewola, Wind energy evaluation for electricity generation using WECS in seven selected locations in Nigeria, Applied Energy, Vol:88, No:9, 3197-3206, (2011).
9. Sunday Olayinka Oyedepo, Energy and sustainable development in Nigeria: the way forward, Energy, Sustainability and Society, Vol:15, No:2, 1-17, (2012).
10. Roche *et al.*, True cost of electricity: comparison of cost electricity generation in Nigeria, 5-34, https://ng.boell.org/sites/default/files/true_cost_of_power_technical_report_final.pdf [20/05/2019], (2017).
11. Rupesh Thakre DuttSubroto, Sensitivity Analysis and Feasibility Analysis of Renewable Energy Project, International Journal of Engineering and Innovative Technology, Vol:4, No:6, 2277-3754, (2014).
12. Shoaib Muhammad, Saif Ur Rehman, Imran Siddiqui, Shafiqur Rehman, Shamim Khan, Aref Lashin, Comparison of Wind Energy Generation Using the Maximum Entropy Principle and the Weibull Distribution Function, Energies, Vol:9, No:10, 842, (2016).
13. Thornton Grant, Africa renewable discount rate survey, pp. 1-16, https://www.grantthornton.co.uk/globalassets/1.-member-firms/united-kingdom/pdf/documents/africa-renewable-energy-discount-rate-survey-2018.pdf [31/05/2019], (2018).

ACKNOWLEDGMENTS

İ am grateful to God almighty, and Asst. Prof. Dr. Mehmet Senol, Cyprus International University, Nicosia, Cyprus that make my research and paper work to be realistic.

ABBREVIATION

FRN	Federal Republic of Nigeria
O&M	Operation and Maintenance
RE	Renewable Energy
WE	Wind Energy
WP	Wind Power
WPG	Wind Power Generation
WR	Wind Resources
WS	Wind Speed
WT	Wind Turbine

Machine Learning Approaches to Sentiment Analysis Using Tweets About AstraZeneca COVID-19 Vaccine

Caglar Gurkan[1,*] **and Merih Palandoken**[2,3]

[1] Electrical and Electronics Engineering, Graduate School of Natural and Applied Sciences, Izmir Katip Celebi University, Izmir, Turkey

[2] Department of Electrical and Electronics Engineering, Faculty of Engineering and Architecture, Izmir Katip Celebi University, Izmir, Turkey

[3] Artificial Intelligence and Data Science Application and Research Center, Izmir Katip Çelebi University, Izmir, Turkey

caglar.gurkan@outlook.com

merih.palandoken@ikcu.edu.tr

Abstract

The novel coronavirus disease 2019 (COVID-19) has appeared in the city of Wuhan, China in December 2019. The coronavirus has caused huge damage to the health and life of people. The damages of COVID-19 have caused people to post a lot on Twitter. As a result, analysis of tweets sent during the COVID-19 pandemic has become an important text mining research subject. Tweets about AstraZeneca, the COVID-19 vaccine, have been used in this study. The dataset consists of a total of 10000 tweets in three classes as positive, neutral, and negative. Six mostly addressed machine learning algorithms, Naïve Bayes, Support Vector Machines, K-nearest Neighbor, Decision Trees, Logistic Regression, and Random Forest, have been investigated to determine the most suitable machine learning algorithm to classify sentiment in tweets. The highest classification performance, with an accuracy of 96.00% and F1-score of 95.52% has been achieved by SVM.

Keywords: Coronavirus; COVID-19; Vaccine; Sentiment analysis; Twitter; Tweets; Text mining; Machine learning

1. Introduction

With the increase of text data, a lot of research has been done in the area of natural language processing (NLP). NLP is used in several sub-research fields such as text classification, sentiment analysis, and information retrieval [1-3]. Text data in the NLP research is generally obtained from social media networks such as Twitter, Facebook, and Instagram. Especially Twitter is known that 186 million daily active users are writing 500 million tweets per day as of 2020 [4]. However, the analysis of tweets is difficult because the written text contains less than 280 characters, furthermore, Twitter users are getting involved in writing tweets in an informal way with emojis and abbreviations [5]. In addition to these difficulties, tweets are generally used in sentiment analysis studies on politics, health, and economics [6-8].

One hundred thirty-seven million people have infected worldwide on April 14, 2021 [9]. In order to reduce the number of cases and deaths, several companies such as BioNTech, AstraZeneca, and Moderna have developed vaccines. However, people's opinions about the vaccine differ from one another and these opinions are shared on Twitter, the social media network. As a result, analyzing these shared tweets has become the text mining research object. Thus, in this paper, in order to perform sentiment analysis (positive, neutral, and negative), tweets sent by Twitter users about the vaccine produced by AstraZeneca have been analysed. Machine learning-based algorithms, Naïve Bayes, Support Vector Machines (SVM), k-Nearest Neighbor (KNN), Decision Tree, Logistic Regression, Random Forest have been used together with Term Frequency-Inverse Document Frequency (TF-IDF) feature extraction technique for the classification of sentiments in tweets.

The rest of this paper is organised as follows. In Section 2, the related works on natural language processing have been reviewed. Section 3 has presented the utilized methodologies. In Section 4, the experimental analysis and the results have been reported. Lastly, in Section 5 concluding remarks have been presented.

2. Related Works

In this section, the studies providing the analysis of the tweets posted by Twitter users during the COVID-19 pandemic have been pointed out with the indication on research using machine learning for sentiment analysis.

Al-Rakha et al. proposed an ensemble model for the detection of misinformation in two classes as credible and non-credible using 400.000 Tweets. C4.5+Random Forest, SVM+ Random Forest, C4.5+KNN, SVM+KNN, SVM+BayesNet+KNN, C4.5+BayesNet+KNN, have been used together. In the study, the SVM+RF model has achieved the highest predictive performance with an accuracy of 97.80% [10]. Alhajji et al. used Naïve Bayes machine learning model for the sentiment analysis in two classes as positive and negative using 53.127 Tweets. The Naïve Bayes model has achieved with an accuracy of 89.00% [11]. Khanday et al. used machine learning models such as Logistic Regression, Naïve Bayes, SVM, and Decision Tree for the topic classification in two classes as propaganda and non-propaganda using 5000 tweets. The Decision Tree model has achieved the highest predictive performance with an accuracy of 98.53% [12]. Samuel et al. used machine learning models such as Linear Regression, Naïve Bayes, Logistic Regression, and KNN for the sentiment analysis in two classes as positive and negative using 4556 tweets. The Naïve Bayes model has achieved the highest predictive performance with an accuracy of 91.00% [13].

3. Methodology

In this section, the features of data, data preprocessing techniques, and utilized models have been presented for the sentiment analysis task.

3.1. Data and Preprocessing

The dataset consisting of 10000 tweets in English is related with AstraZeneca, the COVID-19 vaccine [14]. The dataset has been used for the purpose of sentiment analysis for the AstraZeneca vaccine. Tweets in the dataset are not labeled by the researchers. They have been labeled by using the TextBlob library which is widely used in NLP tasks [15]. The labeling process of tweets has been done in the following manner. Firstly, the subjectivity and polarity values have been found for all texts in the dataset. The values of polarity obtained have been labeled as positive if it is greater than 0, as neutral if it is equal to 0, and as negative if it is less than 0. When Figure 1 is examined, it can be deduced from tweets sent by Twitter users that most tweets are negative, the number of positive and neutral tweets is very close to each other. As a result, three labels (i.e. positive, neutral, and negative) have been created for the sentiment analysis using a dataset consisting of 10000 tweets. Also, 80% of the dataset has been used for the training process, while 20% has been used to test the trained model.

Several data preprocessing methods have been used in this paper. All letters in the corpus have been converted to lowercase letters. URLs, irrelevant words, numbers, sparse terms, punctuation, undefined characters, and English stop words (is, a, the, etc.) have been eliminated. In addition, the suffix of words has been removed using lemmatization. A natural language toolkit has been used in the data preprocessing stage [16].

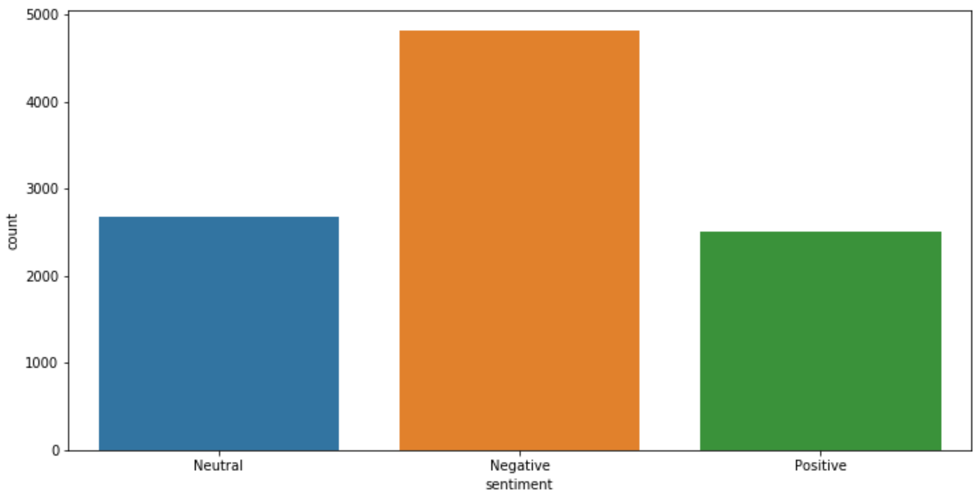

Figure 1. Number of tweets in each sentiment.

3.2. Models

Machine learning-based classifiers (Naïve Bayes, SVM, KNN, Decision Trees, Logistic Regression, Random Forest) have been used with the TF-IDF feature extraction scheme. This scheme has included three different word based N-gram models such as unigram (N = 1), bigram (N = 2), and trigram (N = 3). Consequently, eighteen different configurations of machine learning models have been used on the dataset. In the experimental analysis on Python, Scikit-learn library and GridSearchCV for hyperparameter optimization have been used. The results obtained in the experimental analysis are shown in section 4.

4. Results and Discussion

In the experimental analysis, the accuracy and F1-score values have been achieved by machine learning-based classifiers and are shown in Table 1 and Table 2, respectively.

Table 1. Accuracy values obtained by machine learning algorithms.

Classifiers	Unigram	Bigram	Trigram
NB	0.7875	0.7840	0.7645
SVM	**0.9600**	**<u>0.9450</u>**	0.9355
KNN	0.9075	0.8720	0.8750
DT	0.9155	0.9190	0.9265
LR	<u>0.9540</u>	0.9395	0.9350
RF	0.9115	0.9190	0.9240

Abbreviations: NB, Naïve Bayes; SVM, Support Vector Machines; KNN, k-Nearest Neighbor; DT, Decision Tree; LR, Logistic Regression; RF, Random Forest.

Note: The highest values have been indicated by bold, the second highest values have been indicated by underlined, and the third highest values have been indicated by bold-underlined.

Table 2. F1-score values obtained by machine learning algorithms.

Classifiers	Unigram	Bigram	Trigram
NB	0.7676	0.7614	0.7421
SVM	**0.9552**	**<u>0.9354</u>**	0.9235
KNN	0.8925	0.8530	0.8557
DT	0.9041	0.9062	0.9144
LR	<u>0.9473</u>	0.9288	0.9231
RF	0.8985	0.9066	0.9122

Abbreviations: NB, Naïve Bayes; SVM, Support Vector Machines; KNN, k-Nearest Neighbor; DT, Decision Tree; LR, Logistic Regression; RF, Random Forest.

Note: The highest values have been indicated by bold, the second highest values have been indicated by underlined, and the third highest values have been indicated by bold-underlined.

The accuracy values of 78.75%, 96.00%, 90.75%, 91.55%, 95.40%, and 91.15% have been achieved by Naïve Bayes, SVM, KNN, Decision Trees, Logistic Regression, and Random Forest, respectively using unigram TF-IDF feature extraction. The accuracy values of 78.40%, 94.50%, 87.20%, 91.90%, 93.95%, and 91.90% have been achieved by Naïve Bayes, SVM, KNN, Decision Trees, Logistic Regression, and Random Forest, respectively using bigram TF-IDF feature extraction. The accuracy values of 76.45%, 93.55%, 87.50%, 92.65%, 93.50%, and 92.40% have been achieved by Naïve Bayes, SVM, KNN, Decision Trees, Logistic Regression, and Random Forest, respectively using trigram TF-IDF feature extraction.

The F1-score values of 76.76%, 95.52%, 89.25%, 90.41%, 94.73%, and 89.85% have been achieved by Naïve Bayes, SVM, KNN, Decision Trees, Logistic Regression, and Random Forest, respectively using unigram TF-IDF feature extraction. The accuracy values of 76.14%, 93.54%, 85.30%, 90.62%, 92.88%, and 90.66% have been achieved by Naïve Bayes, SVM, KNN, Decision Trees, Logistic Regression, and Random Forest, respectively using bigram TF-IDF feature extraction. The accuracy values of 74.21%, 92.35%, 85.57%, 91.44%, 92.31%, and 91.22% have been achieved by Naïve Bayes, SVM, KNN, Decision Trees, Logistic Regression, and Random Forest, respectively using trigram TF-IDF feature extraction.

The best classification performance among six classification algorithms using TF-IDF feature extraction with the highest classification performance in the accuracy of 96.00% and F1-score of 95.52% has been achieved by SVM using unigram TF-IDF feature extraction technique. The second best classification performance with an accuracy of 95.40% and F1-score of 94.73% has been achieved by Logistic Regression using unigram TF-IDF feature extraction technique. The third best classification performance with an accuracy of 94.50% and F1-score of 93.54% has been achieved by SVM using the bigram TF-IDF feature extraction technique. Considering all results, the unigram TF-IDF feature extraction has more predictive performance than bigram and trigram TF-IDF feature extraction.

5. Conclusion

In this paper, sentiment classification analysis on tweets about the AstraZeneca COVID-19 vaccine has been conducted with the basis on six mostly addressed machine learning algorithms to determine the most suitable machine learning algorithm. The dataset including 10000 tweets in English is therefore related with AstraZeneca, the COVID-19 vaccine, and has been used for the sentiment analysis in three classes (i.e. positive, neutral, and negative). Among the three best predictive performances of machine learning-based classifiers using TF-IDF feature extraction, SVM with unigram TF-IDF feature extraction technique has obtained the highest predictive performance with the accuracy of 96.00% and F1-score of 95.52% in comparison to the second best Logistic Regression with unigram TF-IDF feature extraction technique with the accuracy of 95.40% and F1-score of 94.73% and third SVM with bigram TF-IDF feature extraction technique with the accuracy of 94.50% and F1-score of 93.54%. Also considering the classification performance of the developed NLP models, in this study a decision support system has been developed about to people's thoughts relating to the COVID-19 vaccine. Thus, governments and health organizations can more easily plan their vaccination policies.

References

1. M. Jiang et al., Text classification based on deep belief network and softmax regression, Neural Comput. Appl., Vol: 29, No: 1, 61-70, 2018.
2. C. C. Aggarwal and C. X. Zhai, A survey of text classification algorithms, in Mining Text Data, Springer US, 163–222, 2012.
3. M. Kaytan and D. Hanbay, Effective Classification of Phishing Web Pages Based on New Rules by Using Extreme Learning Machines, Anatol. J. Comput. Sci., Vol: 2, No: 1, 15–36, 2017.

4. S. Aslam, Twitter by the numbers: Stats , demographics & fun facts, Omnicore, 2017.
5. D. Ramage, S. Dumais, and D. Liebling, Characterizing microblogs with topic models, in ICWSM 2010 - Proceedings of the 4th International AAAI Conference on Weblogs and Social Media, 130-137, 2010.
6. D. Vilares, M. Thelwall, and M. A. Alonso, The megaphone of the people? Spanish SentiStrength for real-time analysis of political tweets, J. Inf. Sci., Vol: 41, No: 6, 799–813, 2015.
7. E. H. J. Kim, Y. K. Jeong, Y. Kim, K. Y. Kang, and M. Song, Topic-based content and sentiment analysis of Ebola virus on Twitter and in the news, J. Inf. Sci., Vol. 42, No. 6, 763–781, 2016.
8. M. D. P. Salas-Zárate, R. Valencia-García, A. Ruiz-Martínez, and R. Colomo-Palacios, Feature-based opinion mining in financial news: An ontology-driven approach, J. Inf. Sci., Vol: 43, No: 4, 458–479, 2017.
9. WHO Coronavirus (COVID-19) Dashboard | WHO Coronavirus (COVID-19) Dashboard With Vaccination Data, https://covid19.who.int/ (accessed Apr. 15, 2021).
10. M. S. Al-Rakhami and A. M. Al-Amri, Lies Kill, Facts Save: Detecting COVID-19 Misinformation in Twitter, IEEE Access, Vol: 8, 155961–155970, 2020.
11. M. Alhajji, A. Al Khalifah, M. Jawad, A. Msc, and M. Alkhalifah, Sentiment analysis of tweets in Saudi Arabia regarding governmental preventive measures to contain COVID-19, 2020.
12. A. M. U. D. Khanday, Q. R. Khan, and S. T. Rabani, Identifying propaganda from online social networks during COVID-19 using machine learning techniques, Int. J. Inf. Technol., Vol: 13, No: 1, 115–122, 2021.
13. J. Samuel, G. G. M. N. Ali, M. M. Rahman, E. Esawi, and Y. Samuel, COVID-19 public sentiment insights and machine learning for tweets classification, Inf., Vol: 11, No: 6, 314, 2020.
14. Coronavirus Vaccine Tweets (Covishield) | Kaggle, https://www.kaggle.com/chaitanyahivlekar/covishield-vaccine-tweets (accessed Apr. 15, 2021).
15. F. Å. Nielsen, A new ANEW: Evaluation of a word list for sentiment analysis in microblogs, CEUR Workshop Proc., Vol: 718, 93–98, 2011.
16. E. Loper and S. Bird, NLTK: The Natural Language Toolkit, Proc. ACL-02 Work. Eff. tools Methodol. Teach. Nat. Lang. Process. Comput. Linguist., 2002.

Heat and Mass Transportation of Different Shaped Porous Moist Object in a Channel

Fatih SELİMEFENDİGİL [1], Seda ÖZCAN ÇOBAN [1], Hakan F. ÖZTOP [2]

[1] Department of Mechanical Engineering, Celal Bayar University, Manisa, TURKEY

[2] Department of Mechanical Engineering, Technology Faculty, Fırat University, Elazığ, TURKEY

sedaozcan82@hotmail.com, fthsel@yahoo.com, hfoztop1@gmail.com

Abstract

Heat and mass transfer were investigated for convective drying of two different shaped porous food samples numerically. A 2D transient model was developed and laminar flow conditions were valid for drying air with constant channel inlet velocity and temperature. Effects of the arrangement of the triangular and rectangular porous objects in the channel on heat and moisture transfer were investigated. Average Nusselt number values and reduction in moisture content for different drying times were evaluated for two objects separately and results totally showed that convection is an important factor for evaporation of food samples and it is an efficient method for drying processes.

Keywords: Convective drying, Heat and mass transfer, porous matrix, CFD

1. Introduction

Evaporation of water vapor from porous moist objects is a very important issue used in many processes for a wide range of products that are mainly foods like fresh vegetables or fruits, meat and grains for preservation; or medicines and biomedical products for decreasing the volume; or bricks, concrete and ceramics for durability and strength [1]. Drying technologies are convenient methods for water removal from moist products and there are various kind of drying techniques like convective drying, infrared drying, freeze drying, microwave drying, solar drying, and combined drying processes [2-10].

One of the most common drying technique is convective drying because of its simplicity and practicality. Hot dry air flows through the moist object in order to transfer water vapor from product to air and this method also can be used as an auxiliary operation with other drying processes. Mathematical modelling is an applicable way of assuming drying kinematics with acceptable costs and time of computing. Governing equations of mass, momentum and energy converted from Fourier, Fick and Darcy's laws are used to calculate heat and moisture transfer in porous moist objects. Nasrallah et al. [11], made a comprehensive numerical study of heat and mass transfer of two different porous mediums (wood and brick) in forced convection drying. Results indicated that, temperature of the surface increased with time while saturation in the same place decreased for both of the samples. Kim et al. [12], developed convective drying of a 2D turbulent model of a moving moist object numerically. The results showed that the comparison between heat and mass transfer for the convective drying is valid only when the temperature of the object is close to the equilibrium temperature. Ponkham et al. [13], developed a mathematical model of combined far-infrared radiation and air drying of a ring-shaped pineapple. The drying model based on the solution of Fick's law was used to estimate moisture diffusion coefficient (D). The D values with shrinkage consideration were lower than the D values without shrinkage consideration for all drying conditions. There are wide range of numerical studies in literature investigating heat and moisture transportation in order to find optimum drying parameters.

2. Problem Definition

A schematic description of the problem is shown in Figure 1. Two-dimensional porous objects are located at the bottom of channel. Laminar flow of hot dry air at temperature 333 K through a channel with two porous domains including liquid water and water vapor is described. Multi-phase transport of water happens by means of evaporation so saturation of the porous medium changes due to the transport of water vapor from sample to air.

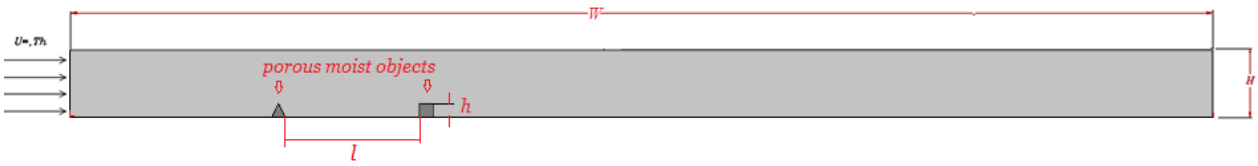

Figure 1. Mathematical model of problem

2.1.Governing Equations

Hot dry air flow through the channel initially. After a period of time, air gets humidified because of moisture transportation from porous object. Conservation of Mass and momentum equations for air-water vapor mixture in channel is given as follows [14, 15]:

$$\frac{\partial \rho_a}{\partial t} + \nabla . \rho_a \vec{u} = 0 \qquad (1)$$

$$\rho_a \frac{\partial \mathrm{u}}{\partial t} + \rho_a \vec{u} . \nabla \vec{u} = -\nabla . \left[p\vec{I} + (\mu_a)\left((\nabla . \vec{u}) + (\nabla . \vec{u})^T\right) - (2/3)(\nabla . \vec{u})\vec{I} \right] \qquad (2)$$

$$\rho_a c_{p,a} \frac{\partial \mathrm{T}}{\partial t} - \nabla . (k_a \nabla \mathrm{T}) + \rho_a c_{p,a} \vec{u} . \nabla \mathrm{T} = 0 \qquad (3)$$

Total volume of each porous object is constituted of three phases which are the solid part, pores filled with gas and pores filled with water and it is the sum of these three phases. Porosity is the fraction of space filled with two phases of water to the total volume of the medium as written below:

$$\varepsilon = \frac{\Delta V_{g+} \Delta V_w}{\Delta V} \qquad (4)$$

where ΔV is the total volume of porous medium and described as follows:

$$\Delta V = \Delta V_g + \Delta V_w + \Delta V_s \tag{5}$$

where *g*, *l* and *s* indicate gas, liquid and solid phases respectively. Saturation is related to the pore volume filled with water and gas, and it can be defined as the fraction of pore volume of water (or gas) to the total pore volume [16]

$$S_w = \frac{\Delta V_w}{\Delta V_g + \Delta V_w} = \frac{\Delta V_w}{\varepsilon \Delta V} \tag{6}$$

$$S_g = \frac{\Delta g}{\Delta V_g + \Delta V_w} = \frac{\Delta V_g}{\varepsilon \Delta V} \tag{7}$$

than it means; $S_l + S_g = 1$

Concentration of water (c_w) is a variable in order to describe the liquid water saturation Sl:

$$S_l = \frac{c_w M_w}{\rho_w \varepsilon} \tag{8}$$

where M_w is the molar mass of water (mol /kg) and ρ_w is the density of water (kg/m^3).

Transport of mass equations of liquid water, water vapor and air are described by a non-isothermal formulation of strong distributed evaporation from porous objects:

$$\frac{\partial c_g}{\partial t} + \nabla.(\overrightarrow{n_g}) = R_{evap} \tag{9}$$

$$\frac{\partial c_l}{\partial t} + \nabla.(\overrightarrow{n_l}) = -R_{evap} \tag{10}$$

$$\frac{\partial c_a}{\partial t} + \nabla.(\overrightarrow{n_a}) = 0 \tag{11}$$

In these equations, R_{evap} is the evaporation rate, $\vec{n}$ is the total flux vector due pressure gradients which is described by Darcy's law and molecular diffusion of vapor in pores which is described by Fick's law [37].

Energy balance equation assuming each of the phases are in thermal equilibrium including energy transport due to convection, conduction and evaporation is given as follows;

$$(\rho c_p)_{eff} \frac{\partial T}{\partial t} + \nabla.\vec{n}_g h_g + \vec{n}_w h_w = \nabla.\left(k_{eff} \nabla T\right) - h_{fg} R_{evap} + \dot{q} \tag{12}$$

The last term of the equation $\dot{q}$ is the heat source which means heat of evaporation in this problem described as follows:

$$\dot{q} = H_{evap}.m_{evap} \tag{13}$$

where, H_{evap} is the latent heat of evaporation with the unit (J/mol).

Effective thermal and physical properties of porous objects with the combinations of liquid water, water vapor phases and the solid part are given as follows:

Thermal conductivity;

$$keff = k_s(1-\varepsilon) + k_w\varepsilon S_l S + k_g\varepsilon(1-S_l)$$

Density;

$$\rho_{eff} = \varepsilon\left(S_g\rho_g + S_w\rho_w\right) + (1-\varepsilon)\rho_s$$

Specific heat;

$$c_{p,eff} = \frac{S_g\rho_{ma}c_{p,ma}+S_l\rho_w c_{p,w}}{\rho_{eff}}$$

Diffusivity;

$$D_{eff} = D_{va}\varepsilon^{3/4}S_g{}^{10/3} \tag{14}$$

D_{va} is the vapor-air diffusivity and $D_{va} = 2.6\cdot 10^{-5}\ m^2/s$.

Fully developed flow conditions are used at the outlet while no slip conditions on the top and bottom walls of the channel are valid. For the air in channel, boundary and initial conditions are given as below:

$c_v(0) = 0,\ P(0) = P_{atm}$

Inflow temperature of drying air: $T = T_h$

Inlet velocity: $U=U_0$

Initial conditions of porous matrix are given as follows:

$T(0) = 293\ K,\ S_l(0) = 0.5$

Initial concentrations of liquid and gas phases of water are described as follows;

$$c_l(o) = \frac{S_l(0)\rho_l\varepsilon}{M_l}$$

$$\boldsymbol{c_v(o)} = \frac{610.7*10^{7.5\frac{(T-273.15)}{(T-35.15)}}}{R}$$

Initial concentration of vapor saturation, $c_{v,sat}(0)=0.95914\ mol/m^3$ (15)

Thermal and physical properties of air, liquid water, vapor and solid matrix and dimensional parameter of the geometry for the problem are given in Table 1

Table 1. Thermal and physical properties of phases

Thermophysical properties		
Property	Phase	Value
Thermal conductivity, k	Air	0.025 W/mK
	Liquid water	0.59 W/mK
	Water vapor	0.026 W/mK
Specific heat, c_p	Air	1006 J/kgK
	Liquid water	4182J/kgK
	Water vapor	2062 J/kgK
Density, ρ	Air	1.205 kg/m^3
	Liquid water	998.2 kg/m^3
	Porous matrix	1528 kg/m^3
Dynamic viscosity, μ	Air	1.81.10^{-5} kg/ms
	Liquid water	1.002.10^{-3} kg/ms
	Water vapor	1.8.10^{-5} kg/ms
Molar mass	Air	0.028 kg/mol
	Liquid water	0.018 kg/mol
	Water vapor	0.018 kg/mol
Porosity, ε	Porous matrix	0.8
Permeability, κ	Porous matrix	1.10^{-14}
Dimensional Parameters		
H		0.05 m
W		0.85 m
h		0.2*H
l		1.5*h,7.5*h
Constant of evaporation (K)		1000 1/s

Relative permeability of each phase is related to saturation and properties of the phases. In this problem the functions describing κ_r are defined such that they are always positive [14]:

$$\kappa_{r,g} = \begin{cases} 1 - 1.1S_l, S_l < 1/1.1 \\ 0 \quad ,S_l \geq 1/1.1 \end{cases}$$

$$\kappa_{r,g} = \begin{cases} \left(\frac{S_l - S_{li}}{1 - S_{li}}\right)^3, S_l > S_{li} \\ 0 \quad , S_l > S_{li} \end{cases} \tag{16}$$

S_{li} is the irreducible liquid phase saturation, which is the remained liquid saturation inside the porous domains.

3. Solution methodology

Finite element method was used to solve governing equations along the boundary conditions and weak forms of the equations were obtained from Galerkin weighted residual method. Flow variables within the domain were approximated by Lagrange polynomials of different orders. Mesh generation of the geometry was made from triangular elements. Weak form of the governing equations was established and residuals were set to zero in a weighted average sense. The weight function was chosen from the same set of functions as that of trial function. The convergence of the solution is assumed when the relative error for each of the variables satisfy the convergence criteria of 10^{-6}.

4. Results and discussion

The convective drying of triangular and rectangular shaped porous moist objects in a channel investigated numerically. Temperature and velocity of drying air was fixed at $T_h=333\ K$ and $u_0= 0.5\ m/s$ respectively in laminar and fully-developed flow conditions. Interspacing distance between two porous objects had two different values of $l=1.5*h,\ 7.5*h$. Heat and moisture transport from porous domains to air in the channel computed for those conditions. Non-equilibrium mass conservation equations for the 2D model were used.

Figure 2 shows streamline distributions of varying configurations of porous objects. As it can be seen from the figures, a recirculation area is developed in the interspacing area between the objects and also a big vortex can be seen behind the second domain for all configurations. Saturation of liquid water with time evolution is shown in Figure 3 for the middle intersection line of the porous objects. Graphic of S_l values for rectangular domain located in the front of the channel is in Figure 3a and for triangular domain behind the channel is in Figure 3b. Because of the shape factor, evaporation of triangle object is more than rectangular object so the saturation content is less for rectangular domain. For the rectangle-rectangle configuration, saturation of the domain in front of the channel was less than the domain behind as it can be seen on Fig.4.

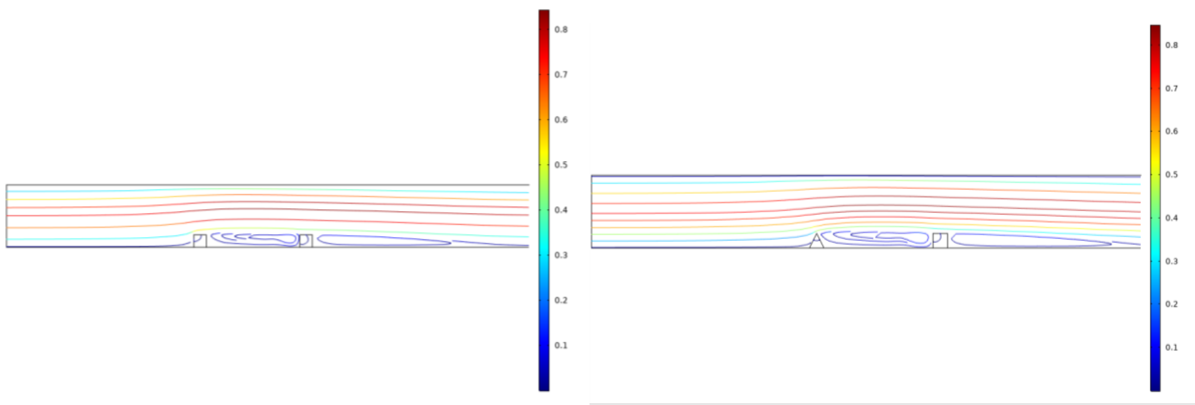

(a) l=7.5*h, RR (b) l=7.5*h, TR

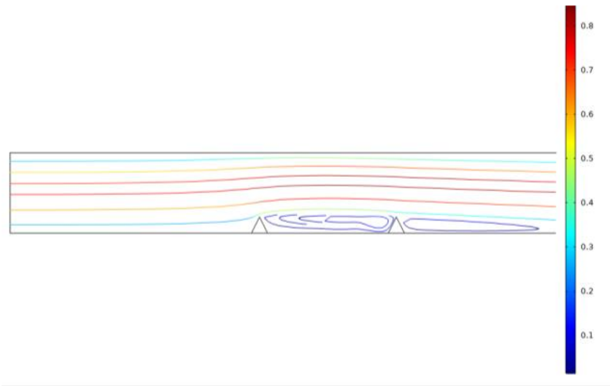

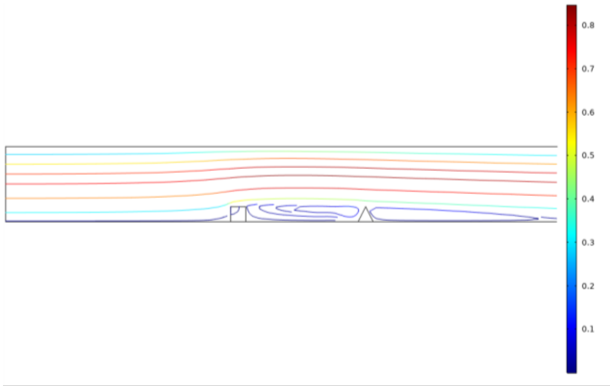

(c)l=7.5*h, TT (d) l=7.5*h, RT

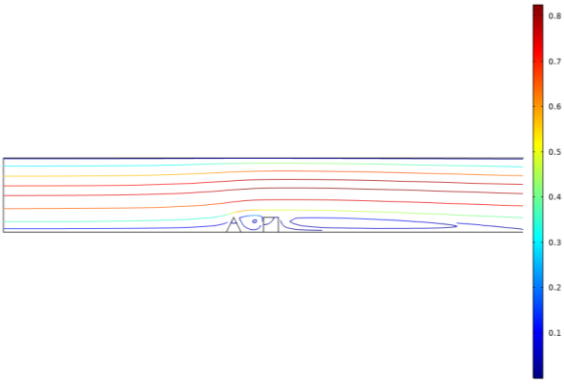

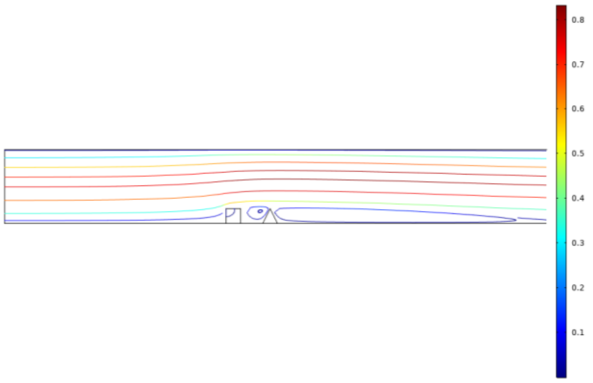

(e) l=1.5*h, TR (f) l=1.5*h, RT

Figure 2. Streamline distributions for different configurations of porous domains

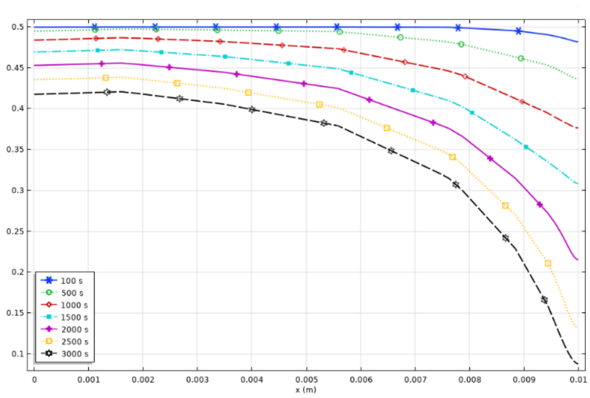

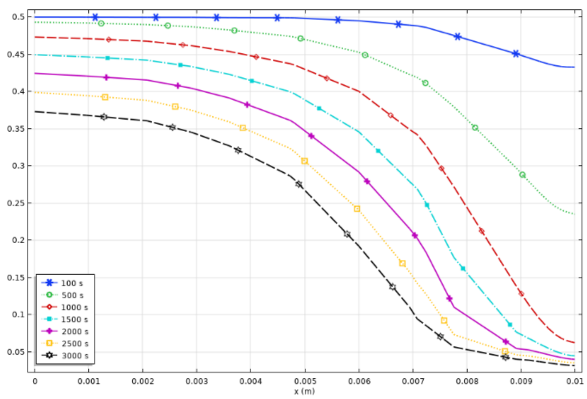

(a)Domain 1 (b) Domain 2

Figure 3. Liquid water saturation of each domain for rectangle-triangle configuration (l=7.5*h)

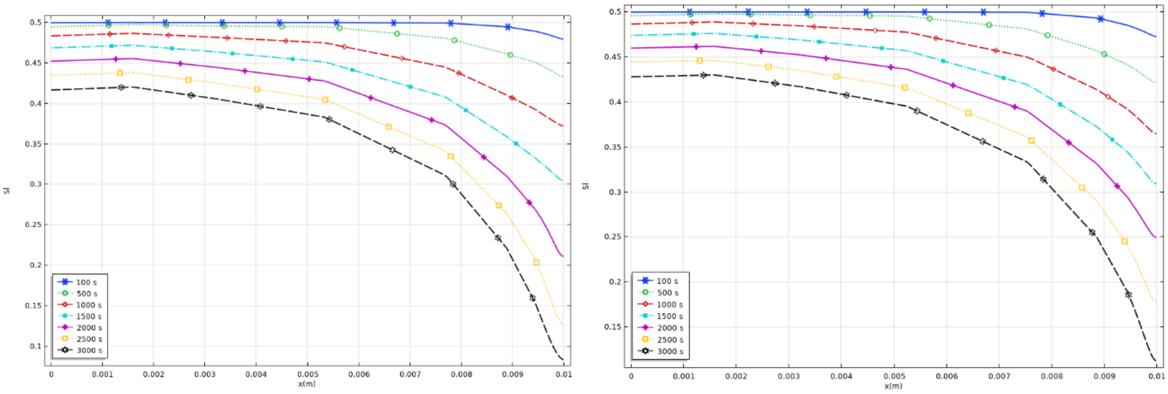

(a)Domain 1 (b) Domain 2

Figure 4. Liquid water saturation of each domain for rectangle-rectangle configuration (l=7.5*h)

Reduce in moisture content for all configurations for two interspacing distances of porous objects in channel at the drying time of 3000 s is shown in table 2. Most evaporation is seen at the triangle-triangle configuration with 51.8 % reduce for the object at the front, and 48.9% reduce for the object behind of the channel. When the distance between the objects is closer (l=1.5*h), it makes a blockage effect for the second object and diminishes the drying effects especially when rectangular objects is at the frontside of the channel. Such as for RT configuration when the distance between the objects is 1.5*h, percentage of evaporation is 29.26% for domain 2 while it is 44.88% when the distance is 7.5*h. Average Nusselt number values of porous objects for all configurations are shown in table 3 at the time of drying t=3000s. For distance of l=7.5*h at the triangle-rectangle configuration, heat transfer is at the biggest value for the rectangle object. Also, at rectangular-rectangular configuration, the values of Nusselt numbers are higher compared to other configurations. The blockage effect is seen also on heat transfer when the distance between the objects is 1.5*h, looking that most of the Nusselt number values are lower for the objects in the back than the objects at the front.

Table 2. Reduce in moisture content for different configurations at t=3000 s for D1 and D2 for two interspacing distances

	Reduce in Moisture content (%)		
Configuration	***l***	***D1***	***D2***
TT	1.5*h	48.972	39.636
	7.5*h	51.756	48.87
TR	1.5*h	49.668	29.048
	7.5*h	51.688	34.996
RT	1.5*h	34.474	29.256
	7.5*h	35.84	44.376
RR	1.5*h	34.612	21.652
	7.5*h	36.218	32.652

Table 3. Average Nusselt number values for different configurations at t=3000 s for D1 and D2 for two interspacing distances

	Average Nusselt Number		
Configuration	***l***	***D1***	***D2***
TT	1.5*h	14.144	14.017
	7.5*h	14.911	15.829
TR	1.5*h	14.259	16.211
	7.5*h	14.849	18.509
RT	1.5*h	16.29	10.854
	7.5*h	16.862	14.758
RR	1.5*h	16.176	12.519
	7.5*h	17.157	17.509

5. Conclusions

Heat and moisture transport at convective drying of two different shaped porous moist objects are investigated numerically. Moisture transport at the triangular shaped porous objects was more than rectangular shaped objects for all configurations. Besides, the distance between the porous domains is an important effect for evaporation of moisture from object. This study shows that, shape and arrangement of the porous objects are effective on convective drying processes.

Acknowledgements

This study is supported from the (THE SCIENTIFIC AND TECHNOLOGICAL RESEARCH COUNCIL OF TURKEY- TUBİTAK) under the grant no: 119M050 which is gratefully acknowledged.

REFERENCES

1. Sreeyuth Lal, Francesco Lucci, Thijs Defraeye, Lily D. Poulikakos, Manfred N. Partl, Dominique Derome, Jan Carmeliet, CFD modeling of convective scalar transport in a macroporous material for drying applications, International Journal of Thermal Sciences, No:123, 86-98, 2018.

2. Oztop, H.F., Akpinar, E.K., Numerical and experimental analysis of moisture transfer for convective drying of some products. International Communication of Heat and Mass Transfer, No:35, 169-177, 2008.

3. Nu~nez Vega, A.-M., Sturm, B., Hofacker, W., Simulation of the convective drying process with automatic control of surface temperature. Journal of Food Engineering, No:170, 16-23,2016.

4. Thanimkarn, S., Cheevitsopon, E., & Jongyingcharoen, J. S, Effects of vibration, vacuum, and material thickness on infrared drying of Cissus quadrangularis, Linn. Heliyon, Vol:5, No:6, 2019.

5. Onwude, D. I., Hashim, N., Abdan, K., Janius, R., & Chen, G, The effectiveness of combined infrared and hot-air drying strategies for sweet potato, Journal of Food Engineering, No: 241, 75–87, 2019.

6. Chengdeng Chi, Xiaoxi Li, Yiping Zhang, Song Miao, Ling Chen, Lin Li, Yi Liang, Understanding the effect of freeze-drying on microstructures of starch hydrogels, Food Hydrocolloids, Vol:101, 105509, 2020.

7. Piazza, R. D., Pelizaro, T. A. G., Rodriguez-Chanfrau, J. E., La Serna, A. A., Veranes-Pantoja, Y., & Guastaldi, A. C., Calcium phosphates nanoparticles: The effect of freeze-drying on particle size reduction. Materials Chemistry and Physics, Vol:239, 122004, 2020.

8. Abbasi Souraki, B., & Mowla, D, Experimental and theoretical investigation of drying behaviour of garlic in an inert medium fluidized bed assisted by microwave. Journal of Food Engineering, Vol: 88, No: 4, 438–449, 2008.

9. Djebli, A., Hanini, S., Badaoui, O., Haddad, B., & Benhamou, A., Modeling and comparative analysis of solar drying behavior of potatoes, Renewable Energy. Vol:145, 1494-1506, 2020.

10. Wang, Q., Li, S., Han, X., Ni, Y., Zhao, D., & Hao, J, Quality evaluation and drying kinetics of shitake mushrooms dried by hot air, infrared and intermittent microwave–assisted drying methods, LWT, Vol:107, 236-242, 2019.

11. Nasrallah, S.B., Perre, P. Detailed study of a model of heat and mass transfer during convective drying of porous media. Int. J. Heat Mass Transfer, Vol:31, No: 5, 957- 967, 1995.

12. Kim, D., Son, D., Kim, S., Numerical analysis of convective drying of a moving moist object. International Journal of Heat and Mass Transfer, Vol: 99: 86–94, 2016.

13. Ponkham, K., Meeso, N., Soponronnarit, S., Siriamornpun, S, Modeling of combined far-infrared radiation and air drying of a ring shaped-pineapple with/without shrinkage. Food and Bioproducts Processing, Vol: 90, No: 2, 155–164, 2012.

14. Bird, R. B., Stewart, E. W., Lightfoot, N. E. Transport phenomena. John Wiley & Sons. 2007.

15. Verboven, P., Scheerlinck, N., De Baerdemaeker, J., Nicolaı, B.M. Sensitivity of the food centre temperature with respect to the air velocity and the turbulence kinetic energy. Journal of Food Engineering, Vol: 48: 53–60, 2001.

16. Kumar, C., Joardder, M.U.H., Farrell, T.W., Millar, G.J., Karim, A. A porous media transport model for apple drying. Biosystems Engineering, Vol: 176: 12-25, 2018.

Indoor and Outdoor Navigation Application Development with Augmented Reality Technology

Esin KARAN[1], Muhammed Eren MORKOÇ[1], Ahmet Erdoğan ŞİRECİ[1], Prof. Dr. Kemal FİDANBOYLU[1]

[1] Department of Computer Engineering, Bursa Uludag University, Bursa, Turkey
esinkarann@gmail.com, eren.morkoc@gmail.com, aesireci@gmail.com, kfidan@uludag.edu.tr

Abstract

Augmented Reality (AR) technology is a technology that eliminates computer interfaces, allowing the real and virtual to be displayed in the same environment, thus increasing the interaction with the real world. In recent years, there has been great advances in AR technology, making it easier to use and develop. AR technology is used in many fields such as education, medicine, transportation, industry, tourism and advertising. Widely used 2D maps and navigation systems, combined with AR technology, have added a different dimension to navigation applications by increasing the user experience. Today, there are many indoor and outdoor navigation applications that have adopted this approach. However, due to its complex structure and applicability, there are very few applications that offer indoor and outdoor navigation services together. In this paper, the results obtained from the indoor and outdoor navigation application developed using AR technologies are presented.

Keywords: Augmented Reality, Indoor Navigation, Outdoor Navigation, Unity, ARCore

1 Introduction

Augmented reality (AR) technology is a technology that increases the user experience where virtual objects are shown in the real environment without interrupting the interaction with the real world. The environment, which is a combination of the virtual and the reality, provides the user with a sensory experience, not a physical one. This technology, whose foundations are based on the book named "The Master Key" published by L. Frank Braum in 1901, is now used in areas such as tourism, advertising, education, industry, transportation, and medicine, where rapid information transfer is critical [1].

Navigation is a route-finding guide that guides from a location to a target location and determines many parameters such as direction, speed, location during this process. The concept of navigation emerged in 3500 BC when ships were used for commercial purposes [2]. As a result of advances in technology, primitive navigation systems were replaced by modern navigation systems with an error rate of close to zero. With the navigation systems used today, the user has to follow the physical path and the route suggested by the navigation at the same time. In this case, the probability of making an error increases due to the splitting of the user focus. In order to minimize these errors, AR technology has begun to be applied in navigation systems developed for both indoor and outdoor use.

Several application techniques are used in AR technology. Techniques such as location-based AR, marker-based AR, and markerless AR are preferred according to the purpose, requirements and constraints of the application. Indoor and outdoor navigation systems use different AR methods due to their structures, requirements and functions. For this reason, a complex architecture is required in order to use AR technology in a single indoor and outdoor navigation application. Therefore, navigation applications that use AR technology for both indoors and outdoors at the same time are very few.

In the application presented in this paper, marker-based AR technologies are used in indoor navigation system and location-based AR technologies are used in outdoor navigation system. The application architecture, development process, used technologies and algorithms are explained in detail and supported with diagrams. In addition, results related to the developed application are presented.

2 AR Technology

AR technology is a technology that allows the user to experience the physical world and the virtual world in an integrated manner simultaneously. The virtual object created by the computer is combined with the real-world image and displayed to the user simultaneously with tools such as cameras and smart glasses, increasing the perception of reality. Therefore, AR technology is also referred to as "increased reality perception". Almost all kinds of digital objects such as video, 2D and 3D images can be produced with AR technology. These generated virtual objects are activated when they collect image or location information associated with them [3]. There are different Software Development Kits (SDK) such as ARCore, ARKit, Wikitude, Kudan for the application of AR technology. These SDKs are selected according to the requirements of the project to be developed, such as platform, software language, application method [4]. Commonly used application methods of AR technology are: marker-based AR, markerless AR and location-based AR. The appropriate method is selected based on the user needs and constraints.

2.1 Marker-Based AR

Marker-based AR technology, which is based on image processing technology, is a method of registering the marker displayed by the camera with the image of the virtual object belonging to the marker after it has been processed by the image processor. The virtual object is placed on the marker by obtaining x, y, z axes [5]. In this way, the location information of the marker in the physical world can be transferred to the computer.

In the marker-based AR method, the marker in the camera image is scanned first. After the marker is captured, predefined markers are compared with the captured marker. Then the virtual object paired with the marker is placed in the image [6]. By tracking the marker, the virtual object is kept in a fixed position with simultaneous localization and mapping (SLAM) technology [7]. Thus, a rich image is obtained in which virtual and real objects are displayed together. QR codes are generally preferred for marker selection. In order to get good results from the AR experience, it is necessary to avoid situations that make the marker difficult to detect, such as the use of light-reflecting and low-colored markers, and insufficient light for imaging.

2.2 Location-Based AR

Location-based AR technology, as its name suggests, is an AR method applied by simultaneously displaying the virtual object assigned to the location obtained from tools such as GPS and digital compass [8]. The virtual object to be placed in the real world is placed exclusively on the location information obtained through the device hardware. After the virtual object is placed, the image tracking continues. Since location-based AR technology is based on data from vehicles such as GPS and digital compass, incorrect generation of these data leads to incorrect AR application. Therefore, the performance of sensor technologies plays a key role in location-based AR technology. As the sensor technologies develop, location-based AR technology will be able to give more stable results [6].

2.3 Markerless AR

Markerless AR is an AR method that does not need any reference node to place the virtual object. It does not need any information about the user's environment to view the virtual object. Instead, it is sufficient to have a smooth textured surface that can be detected by the camera [9]. The virtual object to be placed is not specifically defined for the surface on which it is located. The relevant virtual object is placed on the detected surface and displayed to the user simultaneously. For example, IKEA Place application, which is one of the applications made with markerless AR method, allows the furniture to be placed in the space virtually [10]. This method provides a wider application area and flexible usage compared to marker-based AR.

2.4 Navigation Systems

The navigation system is a route-finding system that guides the user along the specified route and helps him/her to reach the desired location. It also calculates information such as speed, location, and direction. The history of the concept of navigation goes back to 3500 BC, the beginning of the use of cargo boats [11]. Navigation methods using compass and map in ancient times are called primitive navigation systems when compared with today's technologies. As a result of advances in technology and science, systems such as artificial satellites, inertial navigation systems and global satellite systems are widely used today [12]. These systems, in which parameters such as location, speed and direction can be determined precisely, continue to be used in indoor and outdoor navigation systems.

Today, navigation systems have developed to a great extent in order to serve the navigation needs of increasingly complex city structures. GPS is generally used for determining the location in outdoor navigation applications. However, in environments such as tunnels where GPS data cannot be obtained, uninterrupted position determination can be performed by making a dead calculation or by using tools such as gyroscopes and accelerometers [13]. Thus, the navigation process can continue without interruption.

With the proliferation and complexity of places such as airports, shopping malls and plazas, navigation systems have become a necessity for interior spaces too. Today, there are many applications developed for indoor navigation. When developing indoor navigation, there are many different methods of location determination such as GPS, magnetic positioning, Wi-fi and Bluetooth. GPS data is generally not preferred for indoor applications because it causes a lot of deviation. Instead, Wi-fi and Bluetooth-based systems with less deviation values are used. Triangulation, circle intersection and fingerprint methods such as ToA, TDoA, AoA, and RSSI, may be preferred for positioning applications [14].

As location information with low deviation rate can be obtained with GPS when navigating outdoors, location-based AR is generally preferred. In indoor navigation applications, marker-based AR is generally preferred. Examples for the application of AR technology to navigation systems are shown in Figure 1 and Figure 2.

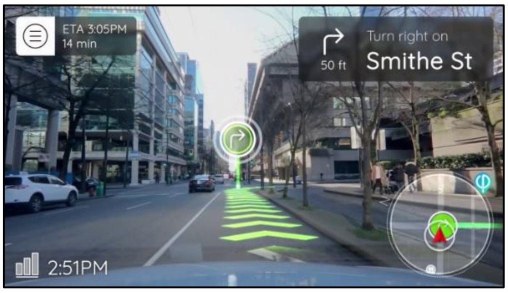

Fig. 1. Outdoor navigation with AR [15].

Fig. 2. Indoor navigation with AR [16].

3 AR Application Structures

In this section, methods and algorithms used in developing AR applications are discussed. Since different methods are used for indoor and outdoor navigation systems, their requirements are discussed separately.

3.1 Outdoor Navigation with AR

Many different issues have been taken into account when choosing the AR method, in which the external navigation of the application will be improved. Marker-based AR technology has not been preferred due to the limitations such as weather conditions can damage the markers over time, and the marker reading in large areas negatively affects the user experience. Location-based AR technology has been preferred due to the fact that GPS data can be obtained anywhere in the world and the accuracy rate is high in location determination in today's technology.

In order to provide the best AR experience in outdoor navigation, the deviation in GPS data must drop below 6 meters before starting. After waiting until the GPS data reaches the desired deviation value, the necessary calculations are made and the alignment of the Unity world with the real world is provided. The most important detail here is to align the virtual world with the real world and find out how many meters the person has traveled. In order to achieve this, it should be calculated how many meters the change in the coordinates taken from the GPS corresponds to on the earth. For this, the formulas in Equation (1) and Equation (2) have been developed. The values obtained as a result of the calculation are used to align the virtual world with the real world after finding how many meters the person has traveled.

$$X_1 = (Latitude_{Current} - Latitude_0) * A * B \quad (1)$$

$$X_2 = (Longitude_{Current} - Longitude_0) * A * C \quad (2)$$

The $Latitude_{Current}$ variable in Equation (1) contains the current latitude information received from the GPS, and the $Latitude_0$ variable contains the latitude information of the origin node selected on the world. $Longitude_{Current}$ and $Longitude_0$ variables in Equation (2) are designed similar to Equation (1) and they keep longitude information in them. X_1 and X_2 variables keep the calculation result in meters. Variables B and C are coefficients that convert the result of the operation to meters. These coefficients are used to find out how many meters the change in coordinates corresponds to and is determined specifically according to the selected origin node. In different devices, the precision of the decimal parts of the coordinates coming from the GPS differs. The variable A in both equations is used to convert these values from decimals to integers.

The formulas in Equation (1) and Equation (2) have been defined and used in the application as shown in Equations (3), (4), (5), (6) and (7).

$$Latitude_0 = 39.993534 \tag{3}$$

$$Longitude_0 = 32.847882 \tag{4}$$

$$A = 1000000 \tag{5}$$

$$B = 0.111111 \tag{6}$$

$$C = 0.083333 \tag{7}$$

After the necessary calculations and definitions are completed, the route is calculated using Dijkstra's algorithm, which calculates the shortest route [17]. For this purpose, the target nodes and turning nodes that can be visited have been introduced to the system beforehand and turned into a graph. The graph contains the distance information of each node to other nodes associated with it. Dijkstra's algorithm performs calculations on these nodes, determining the intermediate nodes on the shortest route to the target and these nodes are sent to the drawing algorithm to visualize the route.

In the Dijkstra algorithm, virtual objects are placed at each of the intermediate nodes and lines are drawn between both nodes. Then, the route created by starting the AR experience is presented to the user. Objects drawn should not shift from their current position as the user moves, and must remain stationary. This process is undertaken by ARCore and is performed by following certain reference nodes located in the real world. There are several ways to identify these reference nodes. One of them is to put markers and the other is to use surface detection. In the proposed application, the surface recognition system provided by ARCore SDK has been used to achieve this. The patterns on the ground in Figure 6 and Figure 10 are visualized versions of the surfaces found by ARCore. The flow chart of the described system is shown in Figure 3.

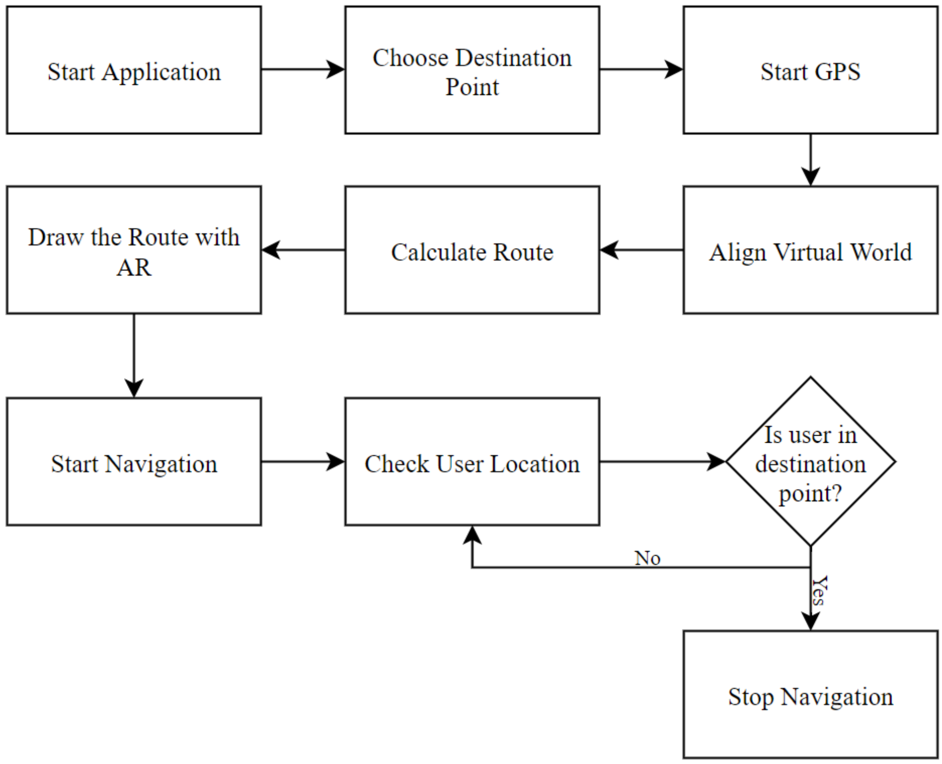

Fig. 3. AR Outdoor Navigation Algorithm.

3.2 Indoor Navigation with AR

The most important problem when implementing navigation systems is the ability to determine the location. The methods used for determining the position indoors cause deviations. Considering these constraints, the marker-based AR method, which does not require location determination, was preferred while developing the indoor navigation of the application. At the same time, it is among the most important advantages that the markers can be better viewed indoors and that they do not cause wear over time because they are not exposed to weather conditions. Indoor navigation application with AR is similar to outdoor navigation application. However, there are marker recognition steps instead of location determination steps in indoor navigation.

In practice, before starting indoor navigation, it is necessary to select the desired destination. In order to start the AR application, the marker closest to the user must be scanned. The detected marker is searched in the database that holds all the markers in the application, and the user is positioned using the information in which order the matching marker is in the database. Each of the markers kept in the database is unique and represents one of the destinations to go.

After the user is positioned, the virtual world and the real world are aligned according to the location of the person and the objects are created in the correct positions. After the alignment is completed, the node where the user is located is sent to the Dijkstra algorithm as the starting node and the target chosen as the destination node and the route is created. Virtual objects are placed at intermediate nodes on the specified route and lines are drawn between each node. Then, the route created by starting the AR application is presented to the user. Fixing objects around the world is the same as the system used in outdoor navigation, and a surface recognition system is used (Figure 6 and Figure 10). The flowchart of the described system is shown in Figure 4.

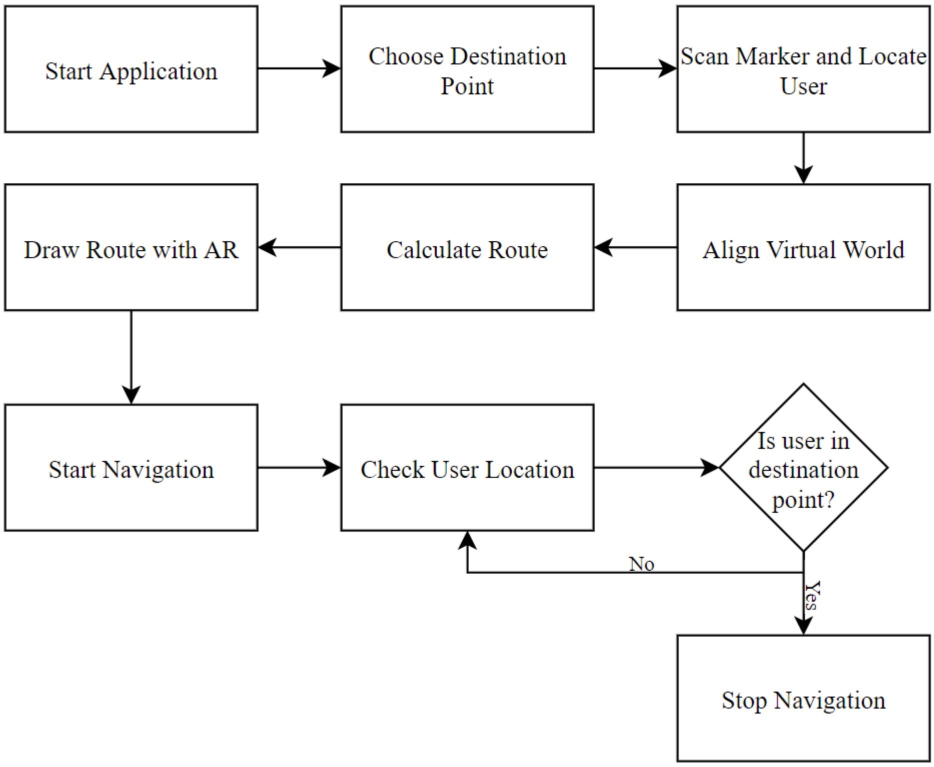

Fig. 4. AR Indoor Navigation Algorithm.

4 Results Obtained from the AR Application

Figure 5 shows the coordinates of the intermediate nodes selected to be used in the Dijkstra algorithm and the route produced by the navigation algorithm. The green nodes on the map show the locations that can be the target node, and the blue nodes indicate the intermediate nodes and returns that are selected to draw the route properly.

Figures 6, 7 and 8 show the screen view of the outdoor navigation in working condition. It is seen that the route plotted in Figure 8 deviates a few meters from the normal route shown in Figure 5. The reason for this is that the coordinate data coming from GPS has 2-10 m deviation in open areas [19, 20]. Before starting the navigation, this deviation level was expected to decrease to 6 m, thus the sensitivity was increased and a more accurate route was drawn.

In Figure 6 and Figure 7, the route created by the application in two different running situations is shown. Since the GPS deviation is lower in Figure 6, it is seen that the route was drawn as expected. In Figure 7, since the GPS deviation is greater, the target has shifted.

Fig. 5. Outdoor navigation graph map.

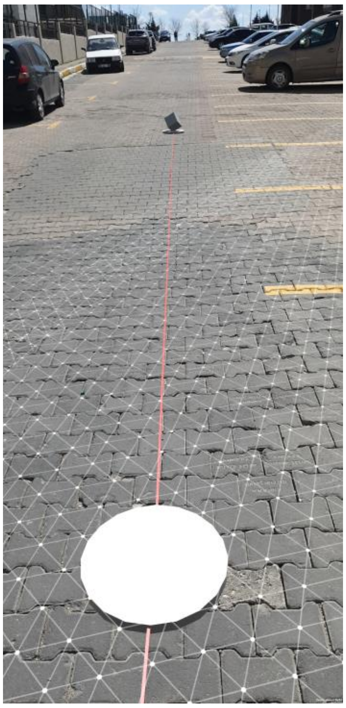

Fig. 6. Outdoor navigation screenshot 1.

Fig. 7. Outdoor navigation screenshot 2.

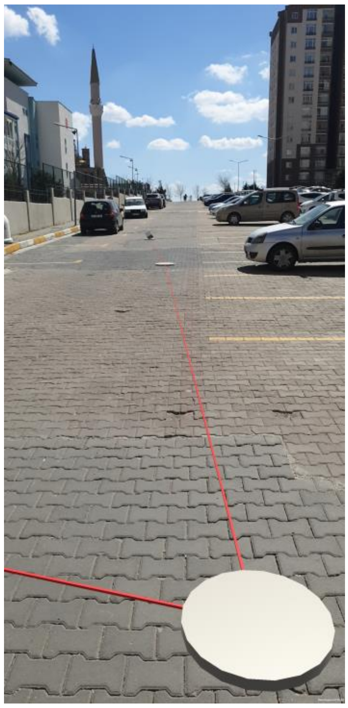

Fig. 8. Outdoor navigation screenshot 3.

Figure 9 shows the locations of the intermediate nodes and the route created by the navigation algorithm for the indoor navigation application. Green nodes on the map indicate locations that can be target, and blue nodes indicate intermediate nodes and returns that are determined to draw the route properly.

In Figures 10, 11 and 12, screenshots of indoor navigation running at different times are shown. As can be seen from these figures, each time the application is run, the entire route is drawn exactly as in Figure 9. Here, markers used for location determination give more precise results than GPS. In this way, the navigation system can be transferred to the AR environment with almost no deviation.

The biggest disadvantage of AR systems using marker is that a new marker must be read in order to be able to reposition. Until then, the user has to proceed without updating the location on the route drawn by the AR system. In addition, visual markers must be present everywhere for positioning on earth. Although this is applicable for indoor navigation, it is not realistic to apply to the whole world in outdoor navigation.

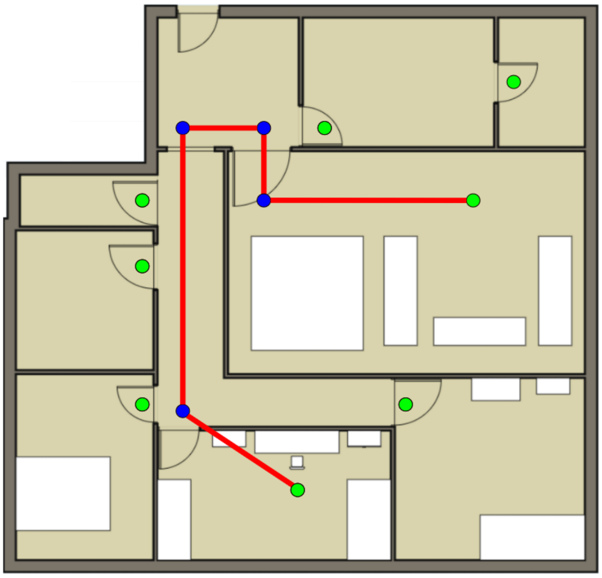

Fig. 9. Indoor navigation graph map.

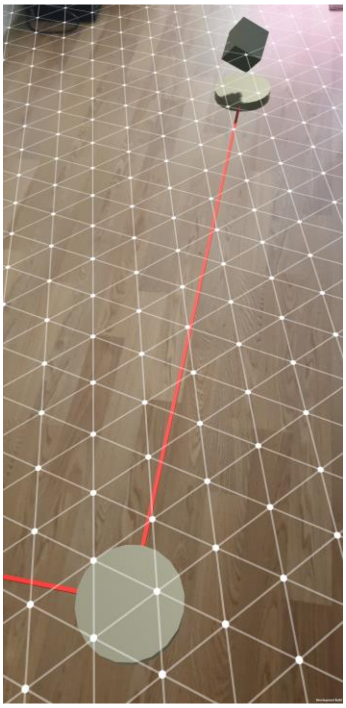

Fig. 10. Indoor navigation screenshot 1.

Fig. 11. Indoor navigation screenshot 2.

Fig. 12. Indoor navigation screenshot 3.

5 Conclusions

In this paper, the development of indoor and outdoor navigation systems with AR technology was explained with reference to the information available in the literature. Using the ARCore SDK, an Android-based application was developed over Unity and the results of the application were discussed. As a result of the study, it was determined that navigation systems can be used successfully with AR technology, but the correct technique should be selected according to the usage environment.

REFERENCES

[1] L.F. Baum, The Master Key an Electrical Fairy Tale, 1901.
[2] Ö. Bozal, Navigasyona Hazırlık ve Geleneksel Navigasyon Yöntemleri, 3* Yelkenci Makalesi, Bogazici University, Istanbul, August 2016.
[3] M. Mehdi, A. Lemieux, Augmented Reality: Applications, Challenges and Future Trends, Applied Computational Science, 205-214, 2014.
[4] D. Amin, S. Govilkar, Comparative Study Of Augmented Reality SDK's, International Journal on Computational Sciences & Applications (IJCSA), Vol. 5, No.1, 2015.
[5] F.M. Akbaş, C. Güngör, Arttırılmış Gerçeklikte İşaretçi Tabanlı Takip Sistemleri Üzerine Bir Literatür Çalışması ve Tasarlanan Çok Katmanlı İşaretçi Modeli, Fen ve Mühendislik Dergisi, Dokuz Eylul University, Izmir, 19(56), May 2017.
[6] R. Romli, A.F. Razali, N.H. Ghazali, N.A. Hanin, S.Z. Ibrahim, Mobile Augmented Reality (AR) Marker-based for Indoor Library Navigation, 1st International Symposium on Engineering and Technology (ISETech), Materials Science and Engineering Vol. 767(2020), 2019.
[7] J. Manhed, Investigating Simultaneous Localization and Mapping for an Automated Ground Vehicle, M.Sc. Thesis, Linköping University, Sweeden, 53s, 2019.
[8] G. Zyejnieks, "Marker-based vs Markerless Augmented Reality: Pros, Cons & Examples". https://overlyapp.com/blog/marker-based-vs-markerless-augmented-reality-pros-cons-examples (30.03.2021).
[9] S. Schechter, "What is Markerless Augmented Reality?". www.marxentlabs.com/what-is-markerless-augmented-reality-dead-reckoning (28.03.2021).
[10] "IKEA Place". https://www.ikea.com/au/en/customer-service/mobile-apps/say-hej-to-ikea-place-pub1f8af050 (28.03.2021).
[11] Lee, Junghyun, Introduction to Navigation Systems, In Multi-purposeful Application of Geospatial Data, IntechOpen, 2017.
[12] "Navigation". https://en.wikipedia.org/wiki/Navigation (03.01.2021).
[13] D.R.L. Güner, M.K. Özgören, B.E. Platin, Küresel Konumlama Sistemlerinin Kullanılamadığı Durumlarda Ataletsel Navigasyon Sistemlerinin Başarımının Korunması, EMO Bilimsel Dergi,3(5), 55-61, June 2013.
[14] H. Doughangi, Kapalı alanda konum belirleme sistemi, M.Sc. Thesis, Istanbul Ticaret University, 2017.
[15] "Phiar raises $3 million for an AR navigation app for drivers", https://laptrinhx.com/phiar-raises-3-million-for-an-ar-navigation-app-for-drivers-3509012289/ (13.03.2021).
[16] "AR Indoor Navigation", https://www.viewar.com/ar-indoor-navigation (13.03.2021).
[17] H. Ceylan, Comparison of Shortest Path and Least Risk Path According to the 2D and 3D Visualizations for Multilayered Indoor Spaces, M.Sc. Thesis, Department of Geomatics Engineering, Istanbul Technical University, January 2015.

COMPUTING THE DIFFERENTIAL OF SUNFLOWER GRAPHS

Akın Kanlı [1]

Zeynep Nihan Berberler [2]

[1] Department of Computer Science, Dokuz Eylul University, İzmir, Turkey

[2] Department of Computer Science, Dokuz Eylul University, İzmir, Turkey

akinkanli@yahoo.com, zeynep.berberler@deu.edu.tr

Abstract

In this article, we compute the differential of sunflower graphs and investigate the conditions under which the sunflower graphs are dominant differential.

Keywords: Differential; Domination; Graph invariant.

1. Introduction

In this paper, simple, finite and undirected graphs without loops and multiple edges are considered. Let $G=(V,E)$ be a graph with vertex set $V(G)$ and edge set $E(G)$. The *neighborhood* of a vertex $v \in V(G)$ is the set of vertices adjacent to v, denoted $N_G(v)$ or just $N(v)$. Thus, $N(v)=\{u \in V(G) | uv \in E(G)\}$ and $N(v)$ is referred to as the *open neighborhood* of v. The *degree* of a vertex $v \in V(G)$ is defined as $d(v)=|N(v)|$ where $|*|$ denotes the number of elements in the set (i.e. the cardinality). For $S \subseteq V(G)$, the subgraph of G induced by S is denoted by $G[S]$. [2].

For any real number x we define the *ceiling function* $\lceil x \rceil$ as the smallest integer greater than or equal to x and similarly we define the *floor function* $\lfloor x \rfloor$ as the largest integer smallest than or equal to x.

The differential in graphs is a subject of increasing interest, both in pure and applied mathematics. The research and application of the $\partial(G)$ appears mainly in computational mathematics. The differential of a graph was introduced in [6] in 2006, and studied by several authors [1,5,7-18,19], motivated by its applications to information diffusion in social networks. The study of the mathematical properties of the differential in graphs stated in [5-18]. This parameter has been studied by many authors, both from the viewpoint of combinatorics and from the viewpoint of the algorithmic complexity. We refer to the papers [5-18] and the literature quoted therein. Since computing the differential of a graph is NP-complete in general, it becomes an interesting question to calculate differential for some special classes of interesting or practically useful graphs.

Let $G=(V,E)$ be a graph of order n, for every set $D \subseteq V$ let $B(D)$ be the set of vertices in $V \setminus D$ that have a neighbor in the vertex set D. The *differential of* D is defined as $\partial(D)=|B(D)|-|D|$ and the *differential of a graph* G, written $\partial(G)$, is equal to $\max\{\partial(D): D \subseteq V\}$. We will say that $D \subseteq V$ is a *differential set* or ∂*-set* if $\partial(D)=\partial(G)$ is called a ∂*-set* or *differential set*. Note that the connectivity of G is not an important restriction, since if G has connected components $G_1,\ldots,G_k$, then $\partial(G)=\partial(G_1)+\ldots+\partial(G_k)$. Therefore, we will only consider connected graphs.

A set D of vertices of a graph G is said to be a *dominating set* if every vertex in $V(G) \setminus D$ is adjacent to a vertex in D. The *domination number* of G, denoted by $\gamma(G)$ is the minimum size of a dominating set of G [2]. We will say that G is a *dominant differential* graph if it contains a ∂-set which is also a dominating set [17].

In the following section, the differential of sunflower graphs is computed and exact formula is derived.

2. Differential of sunflower graphs

Sunflower graph SF_n consists of a wheel with central vertex c and an n-cycle $v_0, v_1, \ldots, v_{n-1}$ and additional n vertices $w_0, w_1, \ldots, w_{n-1}$ where w_i is joined by links to v_i, v_{i+1} for $i=0,1,\ldots n-1$ where $i+1$ is taken modulo n. SF_n has $2n+1$ vertices and $4n$ edges [4]. The central vertex c of SF_n has a vertex degree of n. There are two types of vertices in $SF_n \setminus \{c\}$ as vertices of degree five and two, respectively. The vertices of degree two and five are referred to as minor and major vertices, respectively [3].

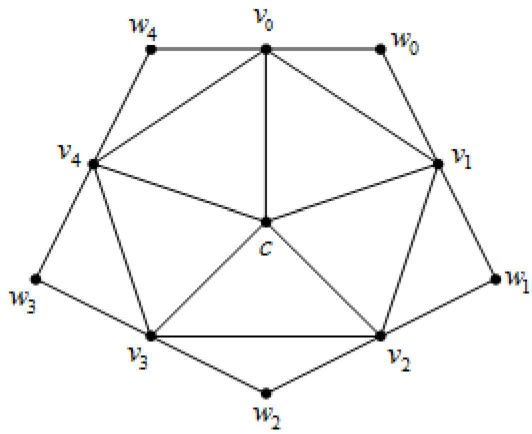

Figure 2.1. Sunflower graph SF_n for $n=5$ with 11 vertices and 20 edges

Theorem 2.1. *The differential of the sunflower graph* SF_n *with* $2n+1$ *vertices is* $\partial(SF_n)=n+1$.

Proof. If we take the central vertex c of SF_n to the set D_1, so $D_1 = \{c\}$, then we have that $B\{D_1\} = \{v_0,\ldots,v_{n-1}\}$ and so $\partial(D_1) = n-1$, and taking any other subset of $V(SF_n)$ to the set D_1 yields $\partial(D_1) \le n-1$.

For $n \ne 3k+1$ $(k \in \mathrm{Z}^+)$, if we take the maximal ∂-set of the n-cycle in SF_n consisting of the vertices $v_0,\ldots,v_{n-1}$ to the set D_2, then since $|D_2| = \left\lceil \frac{n}{3} \right\rceil$, we have $\partial(D_2) = n+1$, and taking any other subset of $V(SF_n)$ to the set D_2 yields $\partial(D_2) < n+1$.

For $n = 3k+1$ $(k \in \mathrm{Z}^+)$, if we take the maximal ∂-set of the n-cycle in SF_n consisting of the vertices $v_0,\ldots,v_{n-1}$ to the set D_2, then since $|D_2| = \left\lfloor \frac{n}{3} \right\rfloor$, we have $\partial(D_2) = n$. If we take the major vertex $v_t \in V(SF_n)$ $(0 \le t \le n-1, v_t \notin D_2, v_t \notin B(D_2))$ to the set D_2, then we have $|D_2| = \left\lceil \frac{n}{3} \right\rceil$ and so $\partial(D_2) = n+1$, and taking any other subset of $V(SF_n)$ to the set D_2 yields $\partial(D_2) < n+1$.

If we take a minor vertex w_i $(0 \le i \le n-1)$ of SF_n to the set D_3, that is $D_3 = \{w_i\}$, then we have $B(D_3) = \{v_i, v_{i+1}\}$ where $i+1$ is taken modulo n, yielding $\partial(D_3) = 1$.

For $n \ne 3k$ $(k \in \mathrm{Z}^+)$, let $S_1 = V(C_n) \setminus B(D_3)$ where C_n is the n-cycle in SF_n consisting of the vertices $v_0,\ldots,v_{n-1}$. Then, we have $C_n[S_1] = P_{n-2}$ where P_{n-2} is the path graph with $n-2$ vertices. If we take the maximal ∂-set of $C_n[S_1]$ to the set D_3 having the set D_4, then we receive $|D_4| = 1 + \left\lceil \frac{n-2}{3} \right\rceil$ and so $\partial(D_4) = n$, and taking any other subset of $V(SF_n)$ to the set D_4 yields $\partial(D_4) < n$.

For $n = 3k$ $(k \in \mathrm{Z}^+)$, let $S_2 = V(C_n) \setminus B(D_3)$ where C_n is the n-cycle in SF_n consisting of the vertices $v_0,\ldots,v_{n-1}$. Then, we have $C_n[S_2] = P_{n-2}$ where P_{n-2} is the path graph with $n-2$ vertices. If we take the maximal ∂-set of $C_n[S_2]$ to the set D_3 having the set D_4, then for $k > 1$ we have $|D_4| = 1 + \left\lfloor \frac{n-2}{3} \right\rfloor$ and so $\partial(D_4) = n-1$. For $\forall k \in \mathrm{Z}^+$, if we take the major vertex $v_p \in V(SF_n)$ $(0 \le p \le n-1, v_p \notin D_4, v_p \notin B(D_4))$ to the set D_4, we have $|D_4| = 2 + \left\lfloor \frac{n-2}{3} \right\rfloor$ and so $\partial(D_4) = n$, and taking any other subset of $V(SF_n)$ to the set D_4 yields $\partial(D_4) < n$.

By the definition of graph differential, we have

$\partial(SF_n) = \max\{D_j\} \ \ (1 \le j \le 4)$

$\partial(SF_n) = n+1$.

The theorem is thus proved. ■

Theorem 2.2. [18] *A graph G is dominant differential if and only if* $\partial(G) = n - 2\gamma(G)$.

Remark 2.1. We can easily observe that the domination number of the sunflower graph is $\gamma(SF_n) = \left\lceil \frac{n}{2} \right\rceil$ and by Theorem 2.2 we conclude that the sunflower graph SF_n with $2n+1$ vertices are dominant differential for $n = 2k \ \ (k \in Z^+, k > 1)$.

REFERENCES

1. Akın Kanlı, Zeynep Nihan Berberler, Differential in infrastructure networks, RAIRO-Operations Research, DOI: https://doi.org/10.1051/ro/2020032.
2. Douglas B. West, Introduction to Graph Theory, Prentice Hall, NJ, 2001.
3. Imran Javaid, Sara Shokat, On the partition dimension of some wheel related graphs, Journal of Prime Research in Mathematics, Vol:4, 154-164, 2008.
4. Joseph A. Gallian, A dynamic survey of graph labeling, Electronic Journal of Combinatorics, Vol:15, 2008.
5. Juan Carlos Hernández-Gómez, Differential and operations on graphs, International Journal of Mathematical Analysis, Vol:9, 341–349, 2015.
6. Jessica L. Mashburn, Teresa W. Haynes, Sandra M. Hedetniemi, Stephen T. Hedetniemi, Peter J. Slater, Differentials in graphs, Utilitas Mathematica, Vol:69, 43-54, 2006.
7. José M. Sigarreta, Differential in Cartesian Product Graphs, Ars Combinatoria, Vol:CXXVI, 259-267, 2016.
8. Jason Robert Lewis, Differentials of graphs, Master's Thesis, East Tennessee State University, 2004.
9. Ludwin Ali Hernández Basilio, Sergio Bermudo, José M. Sigarreta, Bounds on the differential of a graph, Utilitas Mathematica, Vol:103, 319-334, 2017.
10. P. Roushini Leely Pushpam, D. Yokesh, Differential in certain classes of graphs, Tamkang Journal of Mathematics, Vol:41, 129-138, 2010.
11. Sergio Bermudo, Henning Fernau, Combinatorics for smaller kernels: the differential of a graph, Theoretical Computer Science, Vol:562, 330–345, 2015.

12. Sergio Bermudo, Henning Fernau, Computing the differential of a graph: hardness, approximability and exact algorithms, Discrete Applied Mathematics, Vol:165, 69-82, 2014.
13. Sergio Bermudo, Henning Fernau, José M. Sigarreta, The differential and the Roman domination number of a graph, Applicable Analysis and Discrete Mathematics, Vol:8, 155–171, 2014.
14. Sergio Bermudo, Henning Fernau, Lower bounds on the differential of a graph, Discrete Mathematics, Vol:312, 3236–3250, 2012.
15. Sergio Bermudo, Juan Carlos Hernández-Gómez, José M. Rodríguez, José M. Sigarreta, Relations between the differential and parameters in graphs, Electronic Notes in Discrete Mathematics, Vol:46, 281-288, 2014.
16. Sergio Bermudo, José M. Rodríguez, José M. Sigarreta, On the differential in graphs, Utilitas Mathematica, Vol:97, 257-270, 2015.
17. Sergio Bermudo, L. De la Torre, Ana M. Martín-Caraballo, José M. Sigarreta, The differential of the strong product graphs, International Journal of Computer Mathematics, Vol:92, No:6, 1124–1134, 2015.
18. Sergio Bermudo, On the differential and Roman domination number of a graph with minimum degree two, Discrete Applied Mathematics, Vol:232, 64-72, 2017.
19. Zeynep Nihan Berberler, Akın Kanlı, Differential in complementary prisms, submitted.

WAVE SIMULATIONS IN LIQUIDS CONTAINING GAS BUBBLES

Gülnur Yel[1*], Miraç Kayhan[2] , Hasan Bulut[3]

[1]Faculty of Education, Final International University, Kyrenia, Mersin 10, Turkey

[2] Department of Mathematics, University of İnonu, Malatya, Turkey

[3]Department of Mathematics, Firat University, Elazig, Turkey

gulnur.yel@final.edu.tr, mirackayhan@yandex.com, hbulut@firat.edu.tr,

Abstract

In this paper, we apply an efficient method which is the sine-Gordon expansion method to present new wave simulations of a governing model. We consider the conformable (3+1)-dimensional Kudryashov-Sinelshchikov equation describing wave propagation in bubble gas liquid. We have various type solutions such as dark, bright and periodic wave. Finally, some figures are showed physical behaviours of obtained solutions with by 3D,2D and contour surfaces.

Keywords: The sine-Gordon expansion method; the conformable (3+1)-dimensional Kudryashov-Sinelshchikov equation; travelling wave solutions.

1. INTRODUCTION

Nonlinear differential equations (NLPDEs) in applied science plays an important role such as chemical physics, plasma physics, optical fibers, fluid mechanics etc. The wave solutions to the nonlinear partially differential equation have been used to describe some physical phenomena. In recent years, plenty of efficient analytical methods have been developed to find the wave solutions of NLPDEs. Some of these methods are, generalized exponential rational function method [4,5], the first integral method [8], Hirota bilinear method [9], the Sumudu transform method [10], the Bäcklund transform method [11], the exponential function method [12], the F-expansion method [13], the generalized Bernoulli sub-ODE method [14], the improved Bernoulli sub-ODE method [15], the Darboux transformations [16].

The (3+1) - dimensional Kudryashov-Sinelshchikov equation is given by [1,3]

$$\left(u_t+\alpha uu_x+\gamma u_{xxx}\right)_x+du_{yy}+eu_{zz}=0. \tag{1.1}$$

where $u(x,y,z,t)$ is a function of the spatial coordinates of x,y,z and t time. α and γ symbolize the nonlinearity and dispersion, respectively, when d and e describe transverse wave variation in $y-$ and $z-$ directions.

In 2010, Kudryashov and Sinelshchikov have introduced the evolution equation by using experimental and theoretical studies at first time [2]. Kudryashov- Sinelshchikov (KS) equation describes pressure waves in mixtures of liquid-gas bubbles subject to heat transfer and viscosity consideration. This equation, which is a generalized version of the Korteweg de-Vries equations (KdV) and Korteweg de-Vries-Burgers (KdVB) equations, was solved by S. Li and his team using the (G '/ G) method in 2013 and some exact solutions were obtained [27]. In this paper, we have obtained some exact solutions by applying the sine-Gordon expansion method [7] to the (3+1)-dimensional conformable Kudryashov-Sinelshchikov equation.

This paper is arranged as; some basic conformable derivative subjects are given in section 2. In section 3, the basic steps of the proposed procedure, the Sine-Gordon expansion method, are discussed. The governing model's implementation and 3D, 2D, and contour figures are given in section 4. Finally, there are some observations and discussions pertaining to all of the solutions found in conclusion section 5.

2. Preliminary remarks on conformable derivative

Definition: Let $h:[0,\infty)\rightarrow\mathbb{R}$ be a given function, the conformable derivative of h of order α is defined as,

$$L_\alpha(h)(t)=\lim_{\varepsilon\to\infty}\frac{h\left(t+\varepsilon t^{1-\alpha}\right)-h(t)}{\varepsilon},$$

for all $t>0,\ \alpha\in(0,1)$ [17].

Theorem: Let L_α be the derivative operator with order α and $\alpha\in(0,1)$ and h,k be $\alpha-$ differentiable at a point $t>0$. Then [17,18], we have the followings

i. $L_\alpha(ah+bk)=aL_\alpha(h)+bL_\alpha(k),\quad \forall a,b\in R.$

ii. $L_\alpha\left(t^p\right)=p.t^{p-\alpha},\quad \forall p\in R.$

iii. $L_\alpha(hk)=hL_\alpha(k)+kL_\alpha(h).$

iv. $L_\alpha\left(\frac{h}{k}\right)=\frac{kL_\alpha(h)-hL_\alpha(k)}{k^2}.$

v. $L_\alpha(\lambda)=0,$ for all constant functions $h(t)=\lambda.$

vi. If h differentiable then $L_\alpha(h)(t)=t^{1-\alpha}\frac{dh}{dt}(t).$

3. The sine-Gordon expansion method

We will give general structure of the SGEM in this section [19-26].

Suppose that the following nonlinear partial differential equation which is searched solution;

$$P\left(u,u_x,u_t,u_{xx},u_{tt},u_{xt},u_{xxx},\ldots\right)=0. \tag{3.1}$$

where $u=u(x,t)$ is a function depends on x and t . Using the wave transform $u=u(x,t)=U(\xi),\ \xi=\mu(x-ct)$ into the Eq (3.1), gives the nonlinear ordinary (NODE) differential equation as,

$$N\left(U,U',U'',U''',\ldots\right)=0, \tag{3.2}$$

where N is a nonlinear polynomial including U and its ordinary derivatives with respect to ξ.

To obtain the solutions of Eq.(3.1), we suppose the following trial solution form,

$$U(\xi)=\sum_{i=1}^{n}\tanh^{i-1}(\xi)\left[B_i\operatorname{sech}(\xi)+A_i\tanh(\xi)\right]+A_0. \tag{3.3}$$

According to two significant equations as below,

$$\sin\left(w(\xi)\right)=\sec h(\xi), \tag{3.4}$$

$$\cos\left(w(\xi)\right)=\tan h(\xi), \tag{3.5}$$

Eq. (3.3) can be rewritten follows;

$$U(w)=\sum_{i=1}^{n}\cos^{i-1}(w)\left[B_i\sin(w)+A_i\cos(w)\right]+A_0. \tag{3.6}$$

According to the balance principle, n is found between the highest order derivative and the nonlinear term with the highest power in the nonlinear ordinary differential equation. Putting Eq.(3.6) and its sequential derivatives into the NODE, we obtain a polynomial equation with $\sin^i(w)\cos^j(w)$. Using some trigonometric properties to the polynomial equation, it is obtained an algebraic equation system by equating to zero the same power summation of coefficients. With help of the calculation program, we solve the equation system to obtain the A_i, B_i and c values. Substituting the A_i, B_i, c values into Eq.(3.3), we get the new travelling wave solutions to the Eq. (3.1).

4. Application of SGEM

The generalised (3+1)-dimensional conformable Kudryashov-Sinelshchikov equation is given as

$$\left(u_t^{\theta}+\alpha u u_x+\gamma u_{xxx}\right)_x+du_{yy}+eu_{zz}=0, \tag{4.1}$$

where θ is order of conformable derivative between $0<\theta\leq 1$.

We use wave transformation as given below,

$$u(x,y,z,t)=U(\xi),\xi=\mu\left(x+y+z-c\frac{t^{\theta}}{\theta}\right). \tag{4.2}$$

where μ is wave number and c wave speed. Getting partial derivatives of $u(x,y,z,t)$ function with respect to x,y,z,t, we find a non-linear ordinary differential equation as,

$$\mu\left(-c\mu U'+\alpha\mu UU'+\gamma\mu^3 U'''\right)'+d\mu^2 U''+e\mu^2 U''=0. \tag{4.3}$$

We integrate Eq.(4.3) twice with respect to ξ and suppose the integration constant to be zero, by this way, we get

$$\left(-c+d+e\right)U+\frac{\alpha}{2}U^2+\gamma\mu^2U''=0. \tag{4.4}$$

According to homogeneous balance principle, we obtain a relationship between U'' and U^2 in Eq.(4.4), $n=2$.

For the value $n=2$ Eq.(3.6) take the form,

$$U(w)=B_1\sin(w)+A_1\cos(w)+B_2\cos(w)\sin(w)+A_2\cos^2(w)+A_0 \tag{4.5}$$

Differentiating Eq.(4.5) twice, yields

$$U''(w) = -2A_1\cos(w)\sin^2(w) - 4A_2\cos^2(w)\sin^2(w) + 2A_2\sin^4(w) + B_1\cos^2(w)\sin(w)$$
$$-B_1\sin^3(w) + B_2\cos^3(w)\sin(w) - 5B_2\cos(w)\sin^3(w) \quad (4.6)$$

Substituting Eqs. (4.5) and (4.6) into Eq.(4.4), we obtain the following an algebric system of equations by collecting the coefficients of all the trigonometric term of the same power and equating the sum of each collection to zero.

$$\text{constant: } -cA_0 + dA_0 + eA_0 + \frac{\alpha A_0^2}{2} + \frac{\alpha A_1^2}{4} - \frac{cA_2}{2} + \frac{dA_2}{2} + \frac{eA_2}{2} + \frac{1}{4}\gamma\mu^2 A_2 +$$
$$\frac{1}{2}\alpha A_0 A_2 + \frac{3\alpha A_2^2}{16} + \frac{\alpha B_1^2}{4} + \frac{\alpha B_2^2}{16} = 0$$
$$\sin(w): \frac{\alpha A_1^2}{4} - \frac{cA_2}{2} + \frac{dA_2}{2} + \frac{eA_2}{2} - \gamma\mu^2 A_2 + \frac{1}{2}\alpha A_0 A_2 - \frac{\alpha A_0^2}{4} - \frac{\alpha B_1^2}{4} = 0$$
$$\cos(w): \frac{1}{2}\gamma\mu^2 B_1 + \frac{1}{4}\alpha A_2 B_1 + \frac{1}{4}\alpha A_1 B_2 = 0$$
$$\sin(w)\cos(w): -cB_1 + dB_1 + eB_1 - \frac{1}{2}\gamma\mu^2 B_1 + \alpha A_0 B_1 + \frac{1}{4}\alpha A_2 B_1 + \frac{1}{4}\alpha A_1 B_2 = 0$$
$$\cos^2(w): \frac{3}{4}\gamma\mu^2 B_2 + \frac{1}{8}\alpha A_2 B_2 = 0$$
$$\sin^2(w)\cos(w): \frac{1}{2}\alpha A_1 B_1 - \frac{cB_2}{2} + \frac{dB_2}{2} + \frac{eB_2}{2} - \gamma\mu^2 B_2 + \frac{1}{2}\alpha A_0 B_2 + \frac{1}{4}\alpha A_2 B_2 = 0$$
$$\cos^2(w)\sin(w): \frac{1}{2}\gamma\mu^2 A_1 + \frac{1}{4}\alpha A_1 A_2 - \frac{1}{4}\alpha B_1 B_2 = 0$$
$$\sin^2(w)\cos^2(w): -cA_1 + dA_1 + eA_1 - \frac{1}{2}\gamma\mu^2 A_1 + \alpha A_0 A_1 + \frac{3}{4}\alpha A_1 A_2 - \frac{1}{4}\alpha B_1 B_2 = 0$$
$$\cos^3(w)\sin(w): \frac{3}{4}\gamma\mu^2 A_2 + \frac{\alpha A_2^2}{16} - \frac{\alpha B_2^2}{16} = 0$$

To obtain the new solitary solution to Eq. (1.1) , we solve the above system of equations and substitute the obtained results of the coefficients in Eq. (3.3).

Case-1

$$A_0 = -A_2,\ A_1 = 0,\ B_1 = 0,\ B_2 = iA_2,\ e = c - d - \gamma\mu^2, \alpha = -\frac{6\gamma\mu^2}{A_2}$$

which gives:

$$u_1(x,y,z,t) = A_2\left(-1 + i\,\mathrm{sec}\,h\left[\mu\left(x+y+z-c\frac{t^{\theta}}{\theta}\right)\right]\tanh\left[\mu\left(x+y+z-c\frac{t^{\theta}}{\theta}\right)\right] + \tanh^2\left[\mu\left(x+y+z-c\frac{t^{\theta}}{\theta}\right)\right]\right) \quad (4.7)$$

When we consider the suitable values of parameters, we can find new wave simulations for Eq. (1.1) as following figures :

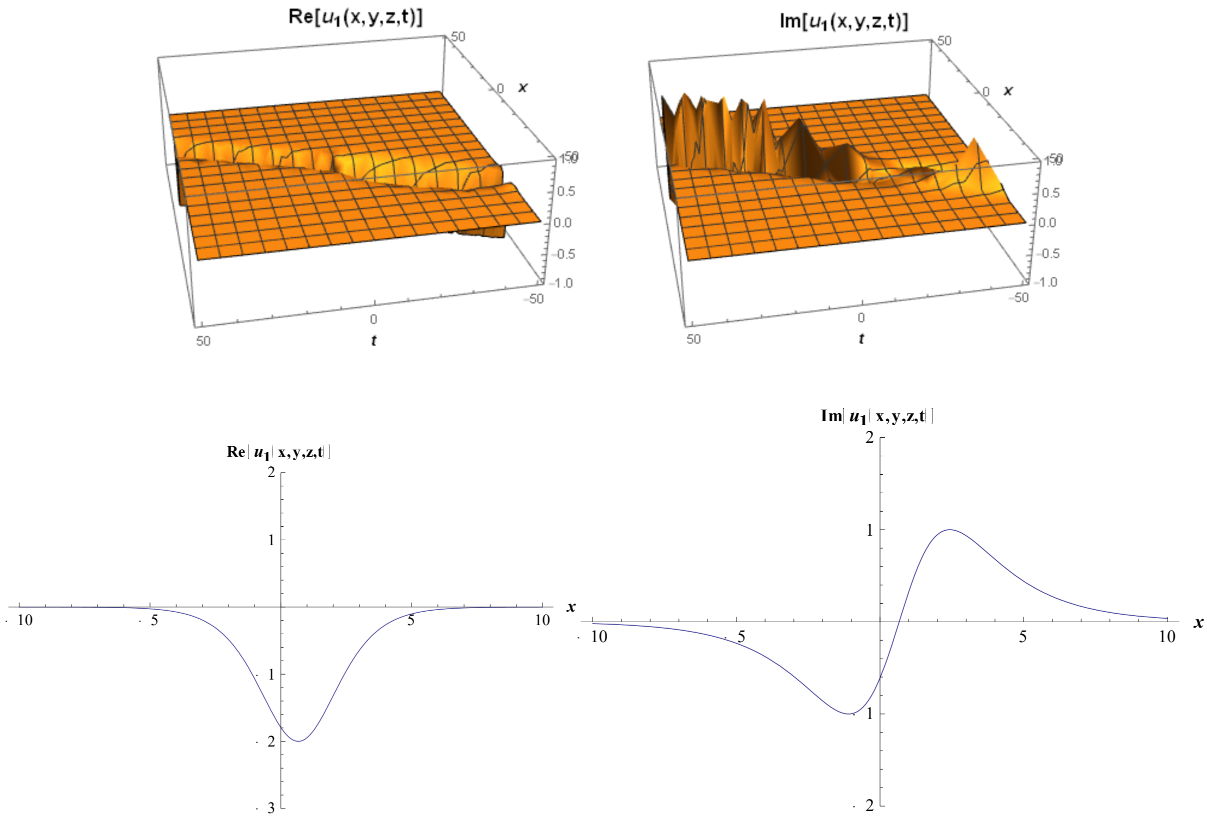

Figure-1 The 3D and 2D surfaces of the travelling wave solution Eq. (4.7) by considering the values $\theta = 0.9,\ A_2 = 2,\ \mu = 0.5,\ c = 0.6,\ z = 0, y = 0,\ t = 1.$

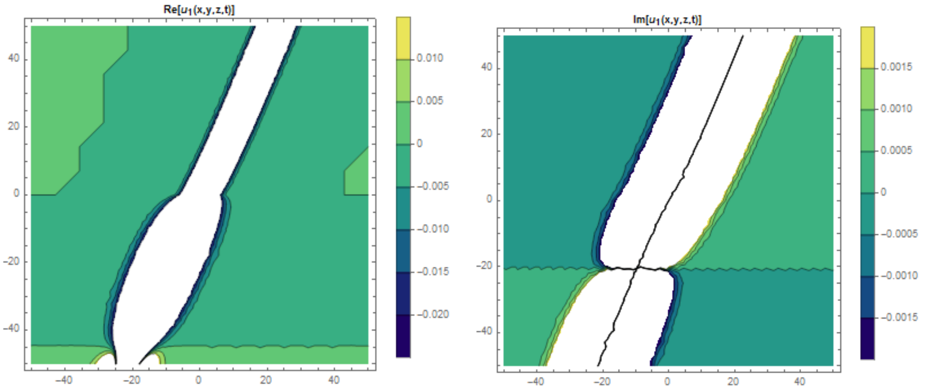

Figure-2 The contour plots surfaces of the travelling wave solution Eq. (4.7) by considering the values $\theta = 0.9,\ A_2 = 2,\ \mu = 0.5,\ c = 0.6,\ z = 0, y = 0,\ t = 1.$

Case-2

$$A_1 = 0,\ A_2 = -A_0,\ B_1 = 0,\ B_2 = iA_0,\ e = c - d - \frac{\alpha A_0}{6}, \gamma = \frac{\alpha A_0}{6\mu^2}$$

which gives:

$$u_2(x,y,z,t) = \operatorname{sec}h\left[\mu\left(x+y+z-c\frac{t^\theta}{\theta}\right)\right]A_0\left(\operatorname{sec}h\left[\mu\left(x+y+z-c\frac{t^\theta}{\theta}\right)\right] + i\tanh\left[\mu\left(x+y+z-c\frac{t^\theta}{\theta}\right)\right]\right)$$

(4.8)

When we consider the suitable values of parameters, we can find new wave simulations for Eq. (1.1) as following figures :

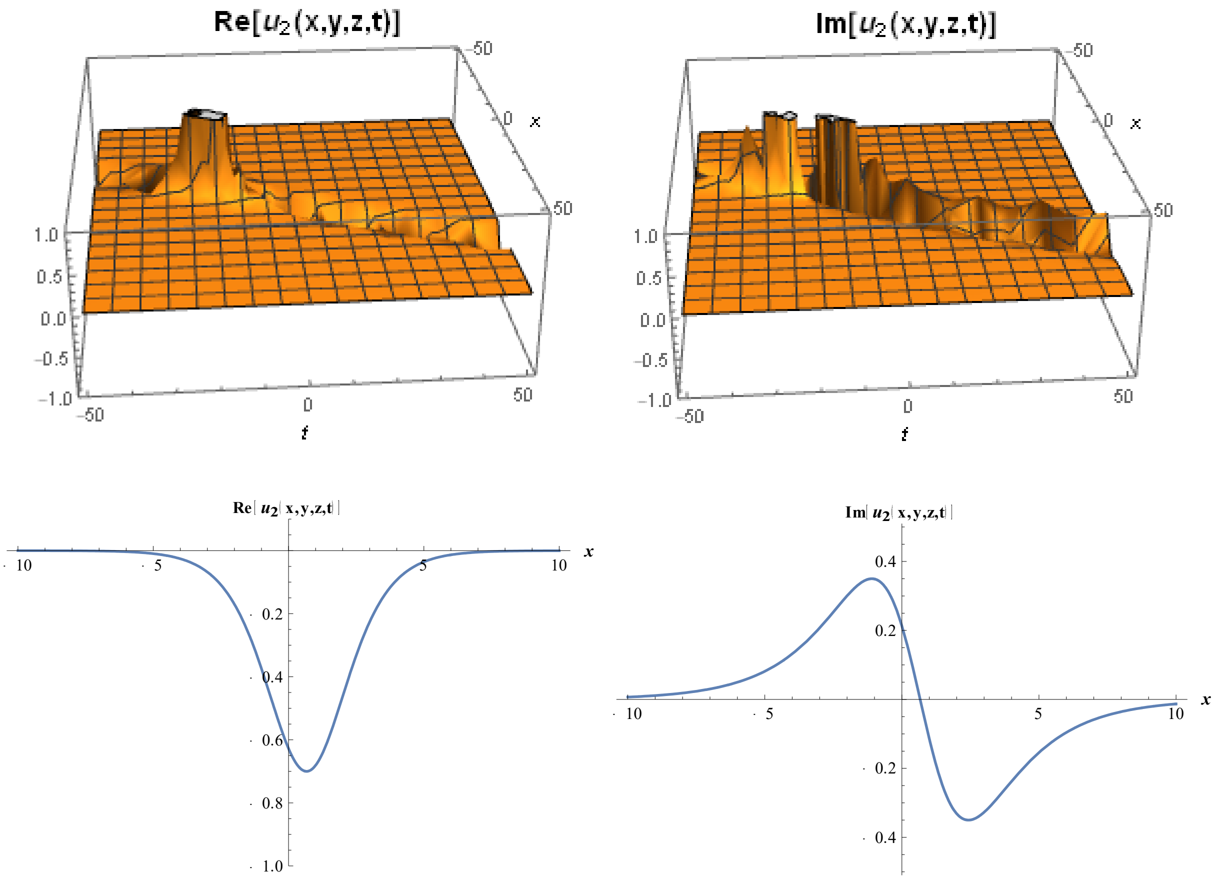

Figure-3 The 3D and 2D surfaces of the travelling wave solution Eq. (4.8) by considering the values $\theta = 0.9,\ A_0 = 2,\ \mu = 0.5,\ c = 0.6,\ z = 0, y = 0,\ t = 1.$

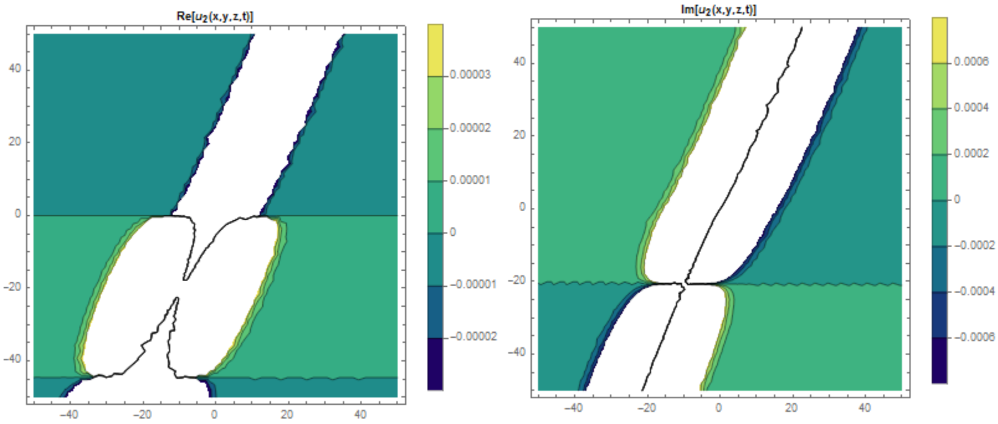

Figure-4 The contour surfaces of the travelling wave solution Eq. (4.8) by considering the values $\theta = 0.9,\ A_2 = 2,\ \mu = 0.5,\ c = 0.6,\ z = 0, y = 0,\ t = 1.$

Case-3

$$A_0 = \frac{6(c-d-e)}{\alpha}, A_1 = 0,\ A_2 = \frac{6(-c+d+e)}{\alpha},\ B_1 = 0,\ B_2 = -\frac{6i(c-d-e)}{\alpha}, \gamma = \frac{-c+d+e}{\mu^2}$$

which gives;

$$u_3(x,y,z,t) = \frac{6(c-d-e)}{\alpha + i\sinh\left[\mu\left(x+y+z-c\dfrac{t^\theta}{\theta}\right)\right]} \tag{4.9}$$

When we consider the suitable values of parameters, we can find new wave simulations for Eq. (4.9) as following figures :

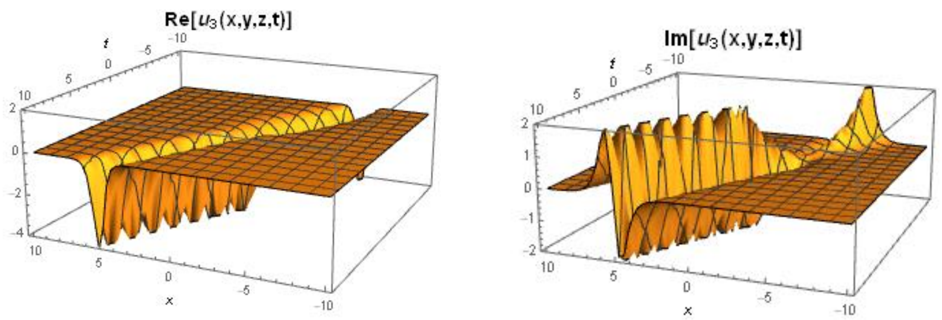

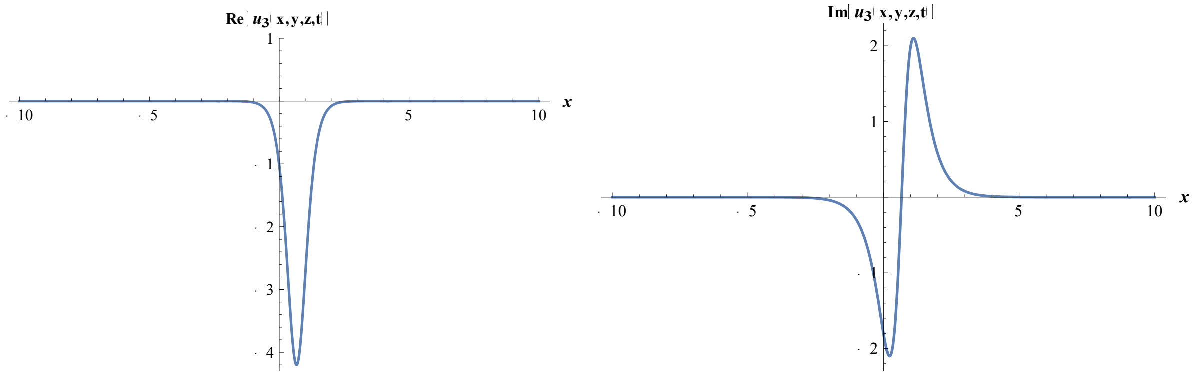

Figure-5 The 3D and 2D surfaces of the travelling wave solution Eq. (4.9) by considering the values $\theta=0.9,\ \mu=2,\ c=0.6,\ z=0,y=0,\ d=1.5,\ e=0.5,\ \alpha=2,\ t=1$

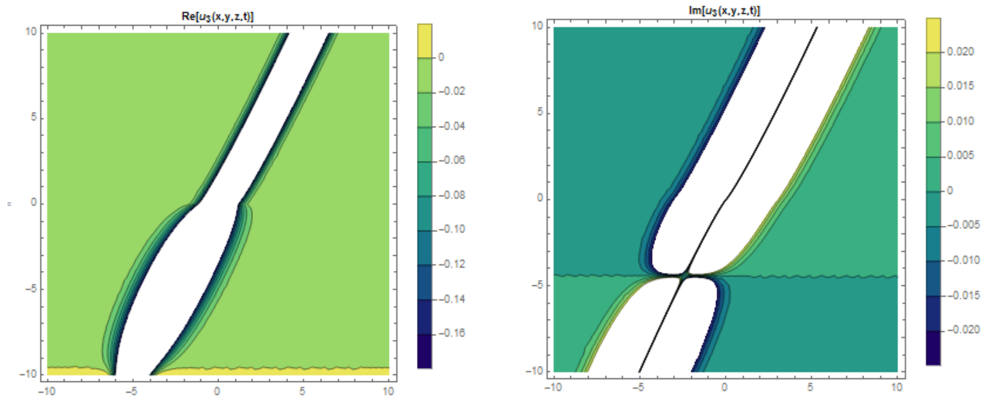

Figure-6 The contour surfaces of the travelling wave solution Eq. (4.9) by considering the values $\theta=0.9,\ \mu=2,\ c=0.6,\ z=0,y=0,\ d=1.5,\ e=0.5,\ \alpha=2,\ t=1$

Case-4

$$A_0=-\frac{2iB_2}{3},A_1=0,\ A_2=iB_2,\ B_1=0,\gamma=-\frac{i\alpha B_2}{6\mu^2},\ d=c-e-\frac{1}{6}i\alpha B_2$$

which gives;

$$u_4(x,y,z,t)=\frac{1}{3}B_2\left(-2i+3\left(\sec h\left[\mu\left(x+y+z-c\frac{t^\theta}{\theta}\right)\right]+i\tanh\left[\mu\left(x+y+z-c\frac{t^\theta}{\theta}\right)\right]\right)\tanh\left[\mu\left(x+y+z-c\frac{t^\theta}{\theta}\right)\right]\right) \tag{4.10}$$

When we consider the suitable values of parameters, we can find new wave simulations for Eq. (4.10) as following figures :

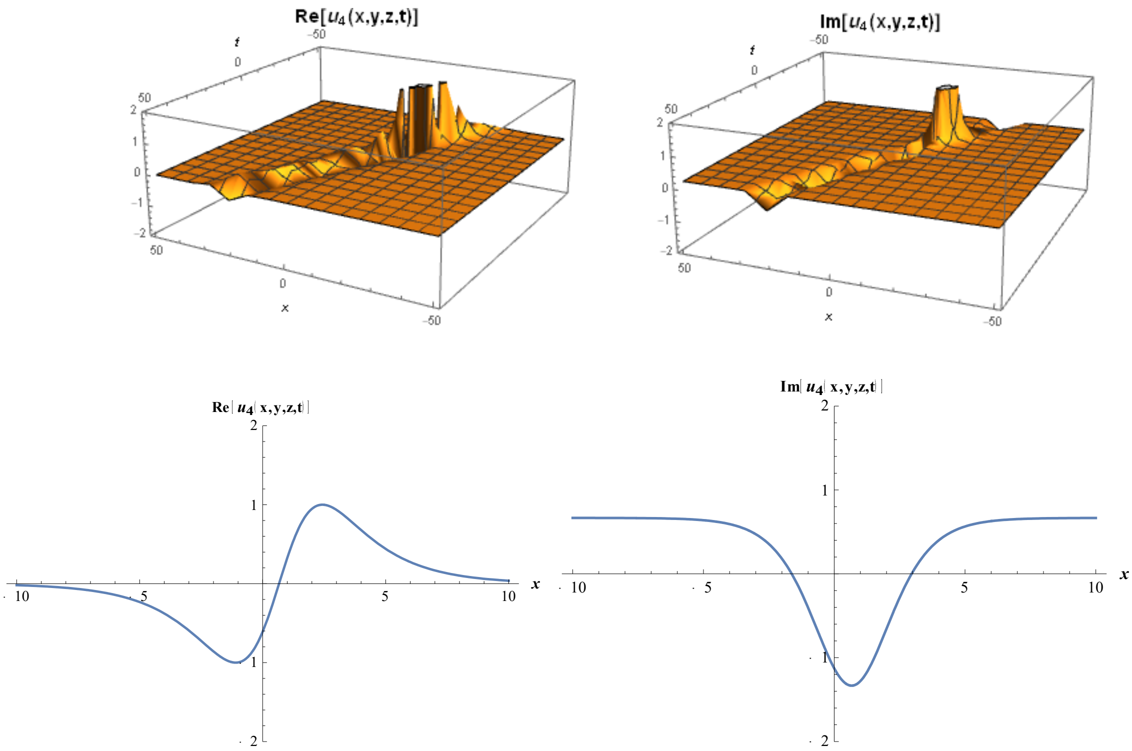

Figure-7 The 3D and 2D surfaces of the travelling wave solution Eq. (4.10) by considering the values $\theta = 0.9,\ \mu = 0.5,\ c = 0.6,\ z = 0, y = 0,\ B_2 = 2,\ t = 1$

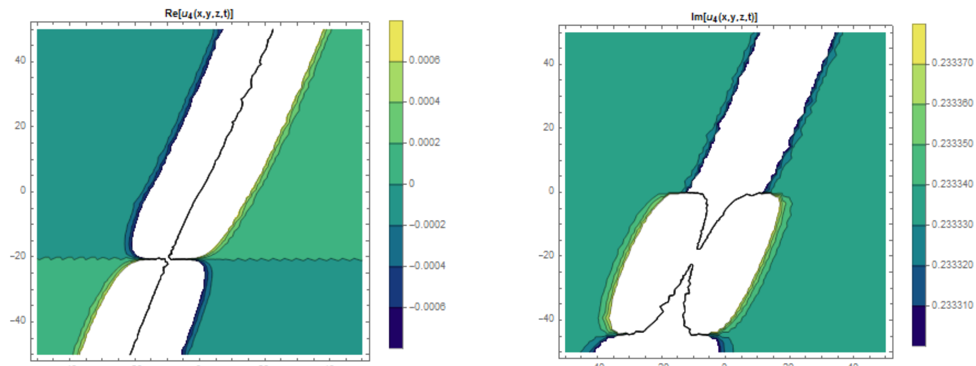

Figure-8 The contour surfaces of the travelling wave solution Eq. (4.10) by considering the values $\theta = 0.9,\ \mu = 0.5,\ c = 0.6,\ z = 0, y = 0,\ B_2 = 2,\ t = 1$

Case-5

$$A_0 = \frac{2iB_2}{3},\ A_1 = 0,\ A_2 = -iB_2,\ B_1 = 0, \alpha = -\frac{6i(c-d-e)}{B_2},\ \gamma = \frac{-c+d+e}{\mu^2}$$

which gives;

$$u_5(x,y,z,t)=\frac{1}{3}B_2\left(2i+3\left(\sec h\left[\mu\left(x+y+z-c\frac{t^\theta}{\theta}\right)\right]-i\tanh\left[\mu\left(x+y+z-c\frac{t^\theta}{\theta}\right)\right]\right)\tanh\left[\mu\left(x+y+z-c\frac{t^\theta}{\theta}\right)\right]\right) \tag{4.11}$$

When we consider the suitable values of parameters, we can find new wave simulations for Eq. (4.11) as following figures :

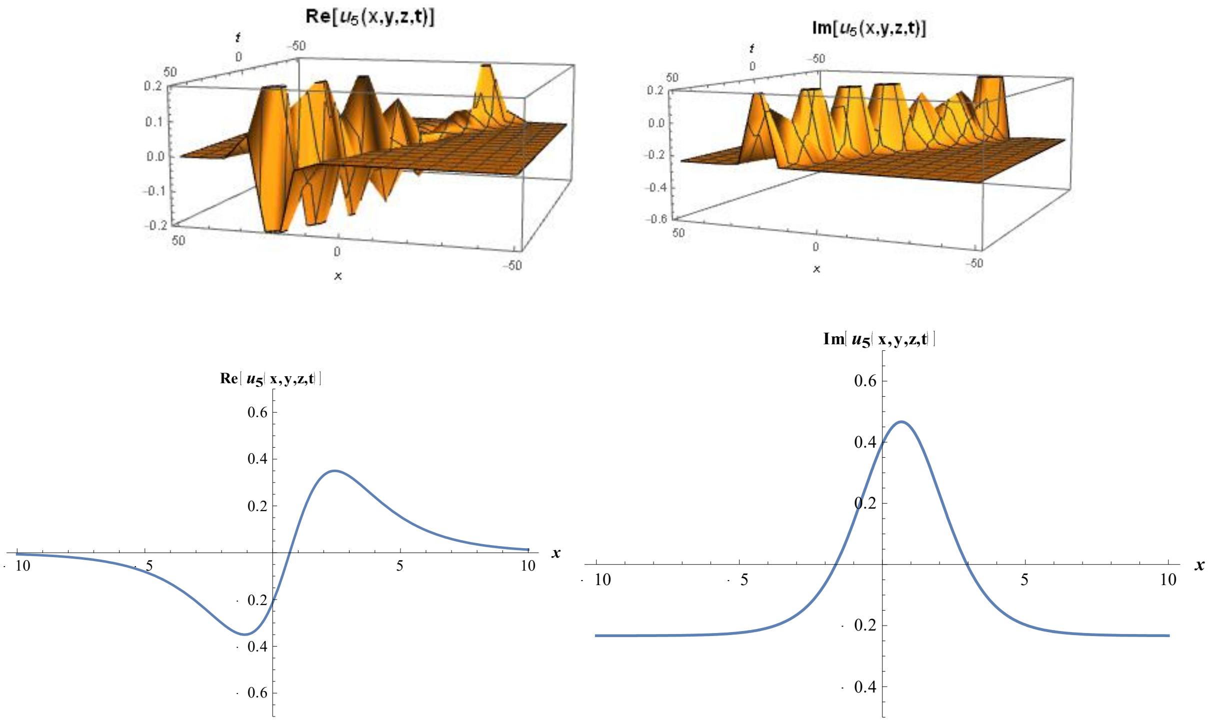

Figure-9 The 3D and 2D surfaces of the travelling wave solution Eq. (4.10) by considering the values $\theta=0.9,\ \mu=0.5,\ c=0.6,\ z=0, y=0,\ B_2=0.7,\ t=1$

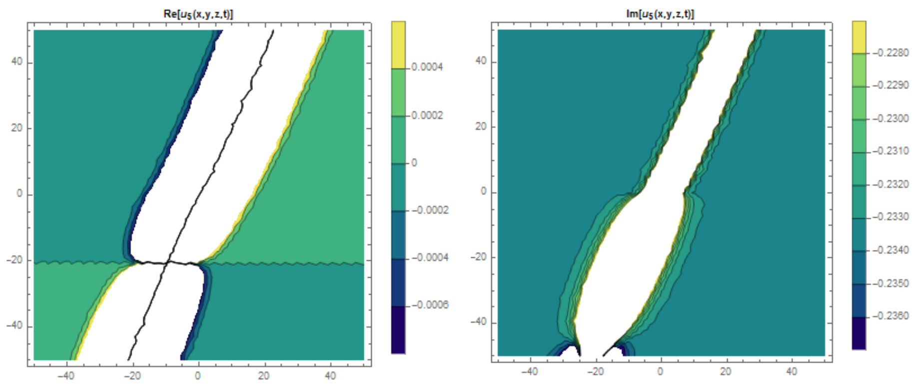

Figure-10 The contour surfaces of the travelling wave solution Eq. (4.10) by considering the values $\theta=0.9,\ \mu=0.5,\ c=0.6,\ z=0, y=0,\ B_2=0.7,\ t=1$.

5. Conclusion

In this paper, the sine-Gordon expansion method has been applied to the (3+1)-dimensional conformable Kudryashov-Sinelshchikov equation. We have obtained some new traveling wave solutions such as complex solutions. According to new results and all figures, it has been observed that this method is a powerful tool for solving such governing models.

REFERENCES

1. Y.B. Chukkol, M.N.B. Mohamad, M. Muminov, Explicit solutions to the (3+1) dimensional Kudryashov-Sinelshchikov equations in bubbly flow dynamics, Journal of Applied Mathematics, Vol:2018, 7452786, 2018.
2. N.A. Kudryashov, D.I. Sinelshchikov, Nonlinear wave in bubbly liquids with consideration for viscosity and heat transfer. Phys Lett A. 2010;374:2011–2016.
3. N. Kudryashov and D. I. Sinelshchikov, Equation for the three-dimensional nonlinear waves in liquid with gas bubbles, Physica Scripta, Vol:85, 025402, 2012.
4. G. Yel, H. M. Baskonus, Solitons in Conformable Time-Fractional Wu-Zhang System Arising in Coastal Design, Pramana- Journal of Physics, 93(4),2019.
5. K. Hosseini, A. Bekir, M. Kaplan, Ö. Güner, On a new technique for solving the nonlinear conformable time- fractional differantial equations, Opt. Quant. Electron., 343, 2017.
6. T. Kanagawa, M. Watanabe, T. Yano and S. Fujıkawa, Nonlinear Wave Equations for Pressure Wave Propagation in Liquids Containing Gas Bubbles, Journal of Fluid Science and Technology, 6(6), 2011.
7. H. Bulut, E. Aksan, M. Kayhan, T, Sulaiman, New solitary wave structures to the (3+1) dimensional Kadomtsev-Petviashvili and Schrödinger equation, Journal of Ocean Engineering and Science, 4(4), 373-378,2019.
8. M. Mirzazadeh, M. Eslami, Exact solutions of the Kudryashov-Sinelshchikov equation and nonlinear telegraph equation via the first integral method, Nonlinear Analysis:Modelling and Control, 17(4), 481–488, 2012.
9. O. Pashaev, G. Tanoglu, Vector shock soliton and the Hirota bilinear method, Chaos, Solitons and Fractals, 26, 95-105, 2005.
10. F.B.M., Belgacem, Sumudu transform applications to Bessel functions and equations, Applied Mathematical Sciences 4 (74), 3665–3686, 2010.

11. J.-M. Tu, S.-F. Tian, M.-J. Xu, X.-Q. Song, T.-T. Zhang, Backlund transformation, infinite conservation laws and periodic wave solutions of a generalized (3+1)-dimensional nonlinear wave in liquid with gas bubbles, Nonlinear Dynamics, 83(3), 1199–1215, 2016.
12. H. Bulut, S. Ateş, H.M. Baskonus, Some novel exponantial function structures to the Cahn-Allen equation, Cogent Physics, 3(1), 2016.
13. Ebaid ,E. H. Aly, Exact solutions for the transformed reduced Ostrovsky equation via the F-expansion method in terms of Weierstrass-elliptic and Jacobian-elliptic functions, Wave Motion, 49(2), 296–308, 2012.
14. B. Zheng, Application of a Generalized Bernoulli Sub-ODE Method for Finding Traveling Solutions of Some Nonlinear Equations, WSEAS transactions on Mathematics, 2012.
15. E. Aksan, H. Bulut, M. Kayhan, Some Wave simulation properties of the (2+1) dimensional Breaking Soliton equation, ITM Web of Conferance, 13, 2017.
16. Z. Ru-Guang , C. Jie, Two Hierarchies of New Differential-Difference Equations Related to the Darboux Transformations of the Kaup—Newell Hierarchy, Communications in Theoretical Physics, 63(1), 2015.
17. R. Khalil, M. Al Horani, A. Yousef, et al. A new definition of fractional derivative, J. Comput Appl. Math. , 264, 65–70, 2014.
18. A. Atangana, D. Baleanu, A. Alsaedi, New properties of conformable derivative, Open Math, 13, 889–898, 2015.
19. D. Kumar, K. Hosseini, F. Samadani, The sine-Gordon expansion method to look fort he travelling wave solutions of the Tzitzéica type equations in nonlinear optics, Optik, 149, 439-446, 2017.
20. H. M. Baskonus, New acoustic wave behaviors to the Davey–Stewartson equation with power-law nonlinearity arising in fluid dynamics, Nonlinear Dynam., 86,177–183, 2016.
21. C. Yan, A simple transformation for nonlinear waves, Phys. Lett. A, 224, 77–84, 1996.
22. H. F. Ismael, H. Bulut, H. M. Baskonus, Optical soliton solutions to the Fokas-Lenells equation via sine-Gordon expansion method and (m+G'/G,)-expansion method, Pramana, 35, 2020.
23. G. Yel, , H. M. Baskonus, H. Bulut, Novel archetypes of new coupled Konno-Oono equation by using sine-Gordon expansion method, Opt. Quant. Electron., 285, 2017.
24. Y. Zhen-Ya, Z. Hong-Oing, F. En-Gui, New explicit and travelling wave solutions for a class of nonlinear evolution equations, Acta. Phys. Sin, 48, 1–5, 1999.

25. Z. Yan, H. Zhang, New explicit and exact travelling wave solutions for a system of variant Boussinesq equations in mathematical physics, Phys. Lett. A, 252, 291–296, 1999.
26. S. B. Yamgoué, G. R. Deffo, F. B. Pelap, , A new rational sine-Gordon expansion method and application to nonlinear wave equations arising in mathematical physics, The European Physical J. Plus, 380, 2019.
27. Y.He, S. Li, and Y. Long, Exact Solutions of the Kudryashov-Sinelshchikov Equation Using the Multiple G'/G -Expansion Method, Hindawi, 708049, 7, 2013.

THE STRENGTH AND IMPORTANCE OF NUMBERS NAMES AND THEİR INFLUENCE ON OUR LİFE

Cemil İNAN[1], Fahim HUSSAINI[2]

[1] Department of Management, University of Artuklu, Mardin /Turkey,cinan@artuklu.edu.tr

[2] Department of Economy, University of Artuklu, Mardin /Turkey,fehims165@gmail.com

Abstract

This research sheds light on an essential aspect of how numerical science affects human names and characters at every point in human life. The expectations at every stage of life involve a change from one person to another. For example, life expectancy, education, and present individual income, these things and others have been created as a result of life and living needs. From picking exact character names, doing the chores of everyday life, preferring colors and types of clothes, performing religion that has embraced, everything in our life has a tremendous impact on people's choices. Accordingly, are there no other factors affecting our personality? Is it not connected with any concealed or revealed energy that appears to affect humanity? Hence, how does the name influence the person? If so, what is it? What kind of communication? In this paper, we will try to make some progress with settling the questions with evidence on how the influences of the names on human beings and their connection have not been undiscovered yet. Besides, what are the titles? What are their meanings, and how are they created? What is the numerical equivalent of letters? In the books, Al Futuhat Al Makkiyya (Ibn Arabi) and (Pythagoras) talked about the power of letters and their effect on names accompanied by numbers. Therefore, we will establish the continuation of its strength, the importance of figures and characters providing evidence from American leaders, how numbers and letters influence the power of authority and change behavior, in addition, how it affects human alphabets. In general, scientists have also provided information on many topics related to letters and numbers, even today, which all the materials gave references covering research.

Keywords Heesab al Abjad, name-number effect, name effect.

.

[1] Doç. Dr., Artuklu Üniversitesi, cemilinan@artuklu.edu.tr

[2] Ögr.Üyesi Artuklu Üniversitesi fahims1665@gmail.com

"This Numerology is the future of all counseling. It is the oldest system known to humanity, the most sacred and the most accurate. You can learn to change people's destiny." Yogi Bhajan

"Numbers are the highest degree of knowledge. It is knowledge itself." Plato

Introduction

In their number, the heavenly religions are based on the existence of a creative, "Creator" of this universe and all beings, including the human race. This great Creator wanted us to know his miracles in creating the universe with all it has and to know ourselves. In order to prove his existence by the keys, which he deposited in his holy books through knowledge of letters and numbers in the so-called Heesab al Jumal. Whether al-Zabouri, the Torah, or the Bible, and up to the Quranic alphabet in Arabic. So, we can say that these books are keys to reveal the vision of man around himself and his world in order to the unity of his creation and to unique it in the universe along with its number of algorithms and character traits. It has proven that the Arabic alphabet is the most established one because it is the most recent in terms of the teachings of all previous books in general, and it is more necessary for them. The truth-seeker discovers no contradiction between math and abstract science, but they are at the top of the agreement, which indicates the Arabic alphabet is the correct and last one. Otherwise, the rest of the previous "Heesab al Jumal" would not have ceased to exist.

HISTORICAL ANALYSIS OF THE CONCEPT

Before Islam, the Arabs used numerical equivalents for each letter, and the letters were in the alphabet sorted into words randomly. The same view that Abu Abdullah Ibn Musa Al Khwarizmi (780-847) briefly mentions in his book "Mafatih Aleulum." Semitic languages, including Arabic, have used this science in the past. People used to assign a particular number to each letter and identify these numbers with the letters. This number differs from one culture to another. The Jews used these numbers more than the Arabs used. Ibn Arabi says: "know that the letters have characteristics, which are on three, including digital, verbal and influential characters, and I mean by evoking up the letters that man evokes in his illusion and imagination and depicts them, either he evokes up digital letters or verbal letters, and then the letters have another rank, and it does so by evoking up as it does with writing or uttering."[3] Then he "adds, showing the ranks of these letters, and says: The verbal alphabets have positions in the work and some letters are more general than each other and more, as the letter (الواو) is more general because they have the power of all letters and (الهاء) the least practical ones."[4] A person's name affects their personality because each letter has a power that affects itself, behavior, health, and even the future. As Adam Alter says: "Adam's naming of the animals raises complex issues, including the deeper meanings of our

---

[3] *Manbae 'Usul Alhikmat*, p. 31

[4] The book *(Aldaraj)* a written copy in the Egyptian House of Books in the collection No. 202 of the volumes of M. p. 14 15 - quoting from the book "*The Philosophy of Ibn Sabeen" by Dr. / Abu Al-Wafa Al-Ghamy Al-Taftazani* Edition of the Dar Alkitab Allubnanii - Beirut, p. 140

names.” In adam and adamah there is an obvious play on words, a practice that the Bible shares with other ancient literature. This should not, however, be mistaken for mere punning. Names were regarded not only as labels. But also as symbols, magical keys, as it were, to the nature and essence of the given being or thing. Some scientists see that as the vibrating of letters that affect the body's power and that the power of these names is related to the universe's energy. It also affects the whole universe as these letters are symbols of sounds in existence. Each letter represents a particular sound, and the entirety of sounds produce all languages in the world. Additionally, each letter has a numeric value that communicates the related cosmic vibration that makes up the sound. The sum of the numbers derived from the letters in his name provides the connection to these cosmic vibrations. These figures show much in the individual's personality in order to ask him or her what the purpose of the life path and other effects such as career, interests, attitude, relationship compatibility, location, and business ventures are. In addition, motivation and the talents inherent in him. In the movie "Hidden Figures." Glenn said: "If she says the numbers are good, I'll be ready." According to Margot Lee Shetterly, citing Johnson in her book "Hidden Figures" (William Morrow, 2016). As you know, many letters that make the sounds are the source of languages that are identified for people around the world. The variations of words in the synthesis and their meanings make us feel in the language. It is divided into many languages and indicates the sub-languages with the possibilities and capabilities. All science has embraced its diversity worldwide, from ancient times until the present, and it will remain so. What is the truth about these letters? Did scientists have access to that fact? Or are they still searching for it, and they have not reached its end? The discovery of the letters is considered one of the most numerous discoveries in human history, and some attribute it to the Babylonian Arabs and others to the Phoenicians, following the different nations who took the alphabet and arithmetic sentences from them. Hence, we see that alphabetical order is the basis of Semitic and non-Semitic alphabets, and it has been taken from the Arabic alphabet, as in Hebrew and Greek. Scholars suggest that the alphabets have been obtained from Arabic, which is incomplete in the languages and letters of other countries that their root is in the Arabic alphabet and arithmetic then confirmed through historical and archaeological research. On the other hand, the arithmetic of sentences is an integral part of the Arabic language.

The science of letters and numbers is the foundation of the structure in the universe and humankind. As Ibn Arabi says: “each number and letter expresses the life path, owing a natural going through childhood, youth, and elderly. And its age is longer or shorter than the time of birth, having specific functions to perform and take into account, which means that the numbers and letters linked to the correct mathematical equations affect us positively or negatively and affect our fluctuations in our lives.” Also, there is no coincidence in life and nothing out of the cosmic system. So the importance of numbers and letters in people's names had been known from ancient times when Pythagorean was very interested in numerals. Also, it is the process of studying numbers, a mysterious method that reflects some of an individual's talents and tendencies as an integral part of the cosmic plan. Other psychologists believe that the capacity of names may look working and that it influences us negatively or positively because it is the first connection between the individual and society.

The dynamic vibrations of numerology have a profound effect on our lives. When we observe the numbers and numerical models, we can understand the world and universe's messages, and Ibn Khaldun has summarized it as “the nature and secrets of the letters are valid in the names; they are valid in the universes according to this system. And the universes from the first creativity move through its phases and express its secrets.” But also better understand our inner world and gain the ability to change our lives. Therefore, knowing the name of any object, its name, and its energy can provide control over it. And this is an application of "The Science of Letters," which is usually called "The Symphony." It is important to note that this is much deeper than mere "divination." There is no doubt that the science of numbers and letters depends on fixed, accurate foundations and calculations in contrast to astrology has found on the principle of predictions and occultism. Numerology focuses on calculating the number of letters and words, and it is possible to arrive at the inference of certain future events. However, this is only the first instance, which is the simplest of all. Then from the results of that calculation, it is possible to make transformations that will cause their impact to be appropriate to the events themselves. And the incidents take place in the universe where people learn about overlapping letters with numbers of this science. A person who realizes the meaning of his name and its effect can directly change his desires and behaviors, good or bad. Shakespeare said “that a rose by any other name would not smell as sweet. But there is evidence that suggests that he was wrong in this assertion.” One identifies that he has these characteristics and understands that the name is inappropriate and foreign, so he is less integrated into society and gradually isolates himself beyond the community.

Numerology experts identify the best times for changes and activities that will help them achieve their goals at certain times in their lives and have responsibilities regarding the specific functions performed and the correct mathematical equations that affect them. Names are associated with numbers, and numbers are the first and most important discoveries of the superior human mind since ancient times. They used numbers in their observations. For example, ancient Babylonians used numbers to predict the planets and priests of the pharaohs to divine a flood of the Nile. Life today is full of numbers like the devices you used to read this article. Among those who say we have the (Math) technology because we know some numbers, it started with simple calculators then ended with modern devices. So they claim that if we understand the science of numbers, we will know ourselves and everything around us. What is the validity of this statement as long as the numbers are listed in everything? Numerology was contemplated from the beginning by Pythagoras from BC 570 to BC. He is an Ionian philosopher who lived between 495 BC. Pythagoras, who wrote his name in world history with golden letters, is a famous mathematician. He is also the founder of the movement known as Pythagoreanism. Pythagoras is also commonly known as the Father of numbers, and he is the author of the famous theory of current triangles. Historians' belief in the mystery of what the numbers mean, they found several discoveries that showed there is no room for coincidence associated with numbers in mathematics.

EXAMINING THE CALCULATION METHOD

It is high time to prove the power of letters and numbers impressive that the letter was applied and stated in the universe system that it exists in numerology. It works within their framework and reveals their secrets with numbers. Humankind has arranged Arabic letters according to their own culture. The Arabic letters system is used in alphabetical order written by the Phoenicians, and learners use it as "أبجد هوز حطي كلمن سعفص قرشت" According to the ones mentioned in Semitic languages such as Persian and Urdu. While Arabic linguists increase the letter "ثخذ ضظغ" then the scientist Nasser bin Asim arranged the letters alphabetically as "أ. ب. ت". Arranged " these indexes and stereotypes were formed in this way while teaching. It is also the same system that applies to the Latin alphabet, in which "AB" Western languages adhere to alphabetical order and a numerical root method. For example, the Arabic language has twenty-eight letters, and the rest of the world's languages are believed to have similar numbers. Heesab al Jumal, in the science of multiple rules, has applied the interpretation of letters into different languages, and the first was Arabic.

AN EXPLANATION OF THE ARABIC ALPHABET OR ARABIC ABJAD IS THE SENSE OF EACH LETTER.		
Arabic alphabet	**Name and Transcription**	**The meaning**
أ	**alif**	Existence
ب	**ba: b**	Moving from one case to another, from one adjective to adjective.
ج	**jim: j**	Continuance.
د	**dal: d**	Is Absorption of each side.
هـ	**ha: h**	Perception.
و	**waw: w**	Is accompanied by assistance.
ز	**za:z**	Abundance.
ح	**ha: h**	Briefings all sides.
ط	**ta: t**	Is the power of the argument.
ي	**ya:y**	Perfection.
ك	**kaf: K**	Is the entire transition from one case to another, from one adjective to another.
ل	**lam:l**	Is full continuity.
م	**mim: m**	Is full of the attractiveness of a person or something.
ن	**nun: n**	Full of perception.
س	**sin: s**	Is Full accompaniment and assistance.
ع	**^{c} ayn: ^{c}**	Is full of abundance.
ف	**fa:f**	Is full encirclement.
ص	**sad**	Sultan or the power of the argument.
ق	**qaf: q**	Stability.
ر	**ra: r**	Is The severity of moving from one case to another, or from one point to another.
ش	**shin: sh**	Is density and continuity.
ت	**ta: t**	Is The self, the intensity of absorption, and the surround.
ث	**tha: th**	Is The end of the road or life.
خ	**kha: kh**	For example, an accompaniment, an interruption, or an interruption, then an accompaniment.
ذ	**dhal: dh**	Is intense abundance.

ض	**dad:d**	Is powerful inside, it cannot be broken out easily.
ظ	**.za: z.**	Is a great affair or a great argument.
غ	**ghayn: gh**	Cessation.

The table below describes alphabetic character equivalents such as "**Heesab al Jumal"** which are the same as those used by other sciences:

NUMERICAL VALUES FOR ARABIC ALPHABET							
Numerical Value	**Letter (Basic Form)**	**Numerical Value**	**Letter (Basic Form)**	**Numerical Value**	**Letter (Basic Form)**	**Numerical Value**	**Letter (Basic Form)**
400	ت	60	س	8	ح	1	ا
500	ث	70	ع	9	ط	2	ب
600	خ	80	ف	10	ي	3	ج
700	ذ	90	ص	20	ك	4	د
800	ض	100	ق	30	ل	5	هـ
900	ظ	200	ر	40	م	6	و
1000	غ	300	ش	50	ن	7	ز

Affiliated with the Arabic alphabet is an elaborate system of numerology through which each letter is assigned a numerical value, thus making possible the expression of any written statement by a corresponding number or set of numbers. This science is called "**abjad**." The use of numbers has several practical reasons, one of them to calculate your name. Thus, for the calculation numbers for the names, we take the personal names. Then we convert the letters into numbers, as shown in the attached table. Once converted to numbers, we add the sum of numbers to the number representing the personality. For example, the name of "داود" will become letters if we add numbers next to each letter. We convert the letters of "داود" into the numbers like this: (4 = د 6 = و 1 =ا 4 = د) the result is 15, we add the two numbers together (1+5), so the number is 6, after simplified. We check the numbers below in which each number has certain characteristics.

Number	**The meaning**
1	The Creator.
2	Intellect.
3	Soul.

4	Nature.
5	Creator in relation to what is below him.
6	Intellect in relation to what is below it.
7	Soul in relation to what is below it.
8	Nature in relation to what is below it.
9	The material world, having no relation to anything below it.

These figures have a unique language known to the ancients and are used yet, in their current research and writing. Some people believed that each number corresponded to a letter and had a meaning. Therefore, the language of numbers is the simplified concept of general understanding and brings them closer to the subconscious. Humans understood and came to the secret of creation, then sat on the throne of wisdom because knowledge is perfect, and the ray of the soul extends from the creator who contains this knowledge. We can say that the origin of science is the human in it. Socrates is famous for arguing "that we must Know Thyself to be wise, that the unexamined life is not worth living." A person begins to search for himself by deducing himself from the numbers, and the letters represent everything he wants to learn about numerology and how his name will guide him. The odd numbers (1-3-5-7) denote 9, and these numbers are the basic structure and functionality of life. For example, "every seven years of your life points to something new in your life happening" (7-14-21-28) according to Esoteric Science, which can prove success, illness, or superiority in life. These concepts are known to everyone in the world. However, while our universities in the Arab society do not take this issue very seriously and do not process it enough, the West researches and processes the science of numerology and takes it sufficiently. For example, in Germany, some universities treat numerology as a doctorate.

Researchers at American New York University have concluded that your name is the main factor in accepting your job, and attribute this to the fact that those people always prefer easy-to-pronounce names, as psychologist Adam Alter says: "The absorption of easy-to-understand information always keeps it in our mind, so it is closer to the self, and so names must be more appropriate, clear and well-established mind." In a similar study, researchers found that some companies involved in using "rationally" trading or similar names outperformed others on the stock market. According to the famous Greek mathematician (Pythagoras) who was so interested in numerology and how numbers came to be and cited, he said: "Nature is a book written in the language of numbers." While Plato's View says: numbers are the essence of things as a picture. Plato divides two types of numbers: Mathematical numbers and ideal numbers, "he says that numbers as units corresponding to sensory things are mathematical numbers, but numbers are according to the principles of things, and through which we can draw the rest of existence, they can be called the names of optimal numbers or numbers as images." And the difference between Pythagoras and Plato is that the numbers, in Plato, have a central place between sensory and mental presence, while, in Pythagoras, the presence of numbers is the perceived existence. In addition to the physicist, astronomer, and mathematician Galileo Galilei added, "this science is written in a mathematical language, and the letters are triangles, circles, and other geometrical figures, without which it is humanly impossible to comprehend a single word" (1564–1642).

Thus, it means that we can solve the mysteries of creation through numbers and equations. The seeker's book deals with this issue and says: "the Divine religions contain many references to numbers and their meanings." For instance, during (354 to 430 AD), the numbers cited by Saint Augustine when he said: “Numbers are the language of the universe and are the creator of human beings to confirm the truth.” Likewise, we find in the Torah of the Bible, specifically in the Book of Daniel and the Gospel of Revelation, that there are many symbolic numbers mentioned, for example, the number 666, it represents evil, the beast or the Antichrist, and the number 3 represents perfection and the Holy Trinity. As the number 7 in Hebrew is the word for perfection, spiritual perfection, then the number 10 symbolizes hierarchical completeness, and the number 12 expresses completion in judgment because there are 12 months in the year, 12 tribes of the sons of Jacob, and 12 messengers of Christ who conduct the sacred mission and so on. Numerology has explained the actuality of the spiritual relationship between numbers, living, and inanimate.

CONCLUSİON

We'll note that America's name with simple mathematical equations is in the number (2) according to the table of Heesab al Jumal. So the energy of the President *(Bill Clinton)* بيل كلينتون had won in the number (5). It added that there could be stability in America unless there is a governor named (3 – 5 – 7 - 9). It pointed out that Heesab al-Jumal may seem obvious and in accordance with the law on number energy.

And for President *(George Washington)* جورج واشنطن the first president of America was in number (7), He led the rebellion that ended with the declaration of the United States' separation from Britain on 4 July 1776. By adding the date (4+7+1+7+7+6), we reach an individual number from one to nine. These numbers become (5), in addition, the total number of *(George Washington)* جورج واشنطن number (7). Therefore, his name (*George Washington*) جورج واشنطن would bring stability to the rule of America.

To the effect that by applying this law to the former president *(Barack Obama)* باراك أوباما the sum of his name becomes (5). It would have stability in America's governance, which was the case, and by applying the same law to the former head of state *(Donald Trump)* دونالد ترامب number (9). So it has firmness in the rule of America, in addition to the new leader *(Joe Biden)* جو بايدن number (9), and to have stability in the authority of America.

In general, numerology proposes the reason you are here. Your name is an essential factor in developing your sense of self, thus helping you move forward in various life and career paths. It is another science that assists in understanding ourselves better. We comprehend that this research is not being accepted and known by many people, and we are aware that more research is needed on the subject as the ambiguity of the problem has not been fully resolved yet. Therefore, we must publicize this knowledge more so that numerology can go a long way and reach its true secrets. Finally, we must understand and express that letters and numbers affect 30% of human life and personality while 70% of the remaining influence environmental, economic, and educational conditions. It’s never too late to find out what makes your numbers resonate the best for you and have a successful life!

REFERENCES

1. Al-Khashshāb, Y. and al-‘Arīnī, B., ضبط وتحقيق الالفاظ الإستلهية التنحية الواردة في كتاب مفاتيح العلوم للخوارزمي / /ليحيى الخشاب، الباز العريني. [Ḍabṭ wa-taḥqīq al-alfāẓ al-istilahiyah al-tankhiyah al-wāridah fī kitāb Mafātīḥ al-‘ulūm lil-Khuwarizmi] Controlling and realizing the developmental vocabulary contained in the book of *Mufatih*, Cairo, 1958 (Arabic).

2 Ibn Arabi. *Manba' Ushul al-Hikmah*. Page 31.

3. The book *(Aldaraj)* a written copy in the Egyptian House of Books in the collection No. 202 of the volumes of M. p. 14 15 - quoting from the book “*The Philosophy of Ibn Sabeen” by Dr. / Abu Al-Wafa Al-Ghamy Al-Taftazani* Edition of the Dar Alkitab Allubnanii - Beirut, p. 140

4. Alter, Adam, 1980-, *Drunk Tank Pink: And Other Unexpected Forces That Shape How We Think, Feel, and Behave.* New York, N.Y.: Penguin Books, 2014.

5. "'Hidden Figures': When did John Glenn ask for 'the girl' to check the numbers?". *collectSPACE*. Retrieved January 31, 2017.

6. Speiser, E. A. Genesis: *A New Translation with Introduction and Commentary* (3rd ed.; AB 1; Garden City, New York: Doubleday, 1986, Anchor Bible, volume 1, 1964) xxii-lii, 3-33, 44-59 and 128-46.

7. Sonak, Sangeeta M. (2017), *Marine Shells of Goa: A Guide to Identification*. Panaji, India: Springer International Publishing.

8. Cf. J. Lougovaya, "A Perfect Pangram: *A Reconsideration of the Evidence,"* Greek, Roman, and Byzantine Studies 57, no. 1 (2017): 186.

9. Kahn, C., 2001, *Pythagoras and the Pythagoreans*, Indianapolis: Hackett.

10. Gregory Andrew (2015), *"The Pythagoreans: Number and Numerology,"* in Lawrence, Snezana; McCartney, Mark (eds.), *Mathematicians and their Gods: Interactions between Mathematics and ReligiouBeliefs,* Oxford, England: Oxford University Press, pp. 21–50, ISBN 978-0-19-870305-1

11. Steven Roger Fischer FRS is the author of many popular books, including *A History of Language* (1999) and *A History of Writing* (2001), both published by Reaktion.

12. Robinson, Andrew, (1995). *The Story of Writing: Alphabets, Hieroglyphs & Pictograms*, New York: Thames & Hudson Ltd. page 172.

13. Very true. https://www.youtube.com/channel/UCVbAr3fQsyDtExDd2CGSLAQ

14. https://ar.wikipedia.org/wiki/png

15. Hakim G. M. Chishti N.D.The Book of Sufi Healing.ISBN-13:9780892813247. Publisher: Inner Traditions/Bear & Company. Publication date: 04/01/1985.

16. Greek Philosophy - Famous Philosopher - Socrates (469 - 399 B.C.) 'Know Thyself' - Discussion of Quotes on the Philosophy & Metaphysics of Socrates. https://www.spaceandmotion.com/Philosophy-SocratesPhilosopher.htm

17. *Dictionary of mysticism and esoteric traditions,* edited by Nevill Drury. (Santa Barbara, Calif.: ABC-CLIO, 1992) Pub Cat 93-2934; available at the Information Desk. A revised edition of *the Dictionary of Mysticism and the occult,* 1985. Brief definitions or descriptions of occult terms, movements, personalities, gods, goddesses, etc. A good quick reference tool.

18. Peterson, p. 12. https://en.wikipedia.org/wiki/Mathematics

19. Gerard Watson, St. *Augustine's Theory of Language*, The Maynooth Review / Revieú Mhá Nuad Vol. 6, No. 2 (May 1982), pp. 4-20 (17 pages) Published By: Faculty of Arts, Celtic Studies & Philosophy NUIM

20. Frances Flannery, "666 in Popular Culture and History", n.p. [cited 31 May 2021]. Online: *https://www.bibleodyssey.org:443/en/passages/related-articles/666-in-popular-culture-and-history*

21. Mushegh Asatrian, *Ibn Khaldūn on Magic and the Occult,* Iran & the Caucasus, Vol. 7, No. 1/2 (2003), pp. 73- 123 (51 pages) Published By: Brill. Al Muqaddima Part 189**:** *The first section of chapter 29 The science of the secrets of the letters.*

22. Daniel J. Boorstin. *THE SEEKERS, The Story of Man's Continuing Quest to Understand His World.* 298 pp. New York: Random House. https://en.wikipedia.org/wiki/The_Seekers_(book)

23. Ahmed Mahmoud Abu Al-Rub, *The secrets of names in human life.* Section: Study of names. Publisher: Al-Mohtaseb Library. Release date: January 01, 2014.

Repdigits as Product of Lucas and Fibonacci numbers

Abdullah ÇAĞMAN[1]

[1] Department of Mathematics, Ağrı İbrahim Çeçen University, Ağrı, Turkey

acagman@agri.edu.tr,

Abstract

In this work, we find all repdigits which can be expressed as the product of a Lucas number and a Fibonacci number. That is, we solve the Diophantine Equation $L_n \cdot F_n = x \cdot \left(\frac{10^t-1}{9}\right)$.

Keywords: Repdigit, Lucas Number, Pell Number.

1. INTRODUCTION

Before proceeding with the proof of the main result in the article, let's remind some information for the readers:

Binet's formula for Fibonacci numbers is

$$F_n = \frac{\varphi^n - \psi^n}{\sqrt{5}}$$

where $\varphi = (1 + \sqrt{5})/2$ (the golden ratio) and $\psi = (1 - \sqrt{5})/2$. From this formula, one can easiliy get

$$\varphi^{n-2} \leq F_n \leq \varphi^{n-1}. \tag{1}$$

Also, we can write

$$F_n = \frac{\varphi^n}{\sqrt{5}} + \theta \tag{2}$$

where $|\theta| \leq 1/\sqrt{5}$.

Similarly, Binet's formula for Lucas numbers is

$$L_n = \varphi^n + \psi^n \tag{3}$$

and we can obtain that

$$\varphi^{n-1} \leq L_n \leq 2\varphi^n. \tag{4}$$

In this study, our main result is the following:

Theorem 1.1. There is no positive solution of the Diophantine equation

$$L_n \cdot F_n = x \cdot \left(\frac{10^t - 1}{9}\right) \tag{5}$$

for $1 \leq x \leq 9$.

2. PRELIMINARIES

The preliminary information given below will be used in the proof of the Theorem 1.1.

Definition 2.1. Let z be an algebraic number of degree d with minimal polynomial

$$a_0x^d + a_1x^{d-1} + \cdots + a_d = a_0 \cdot \prod_{i=1}^{d}(x - z_i)$$

where a_i's are relatively prime integers with $a_0 > 0$ and z_i's are conjugates of z. Then

$$h(z) = \frac{1}{d}\left(\log a_0 + \sum_{i=1}^{d} \log(\max\{|z_i|, 1\})\right)$$

is called the logarithmic height of z.

One can see this definition and some properties of the logarithmic height in [5].

We will use the following theorem (see [4] or Theorem 9.4 in [2]) and lemma (see [1] which is a variation of the result due to [3]) for proving our results.

Theorem 2.2. Let $z_1, z_2, \dots, z_s$ be nonzero elements of a real algebraic number field F of degree D and $b_1, b_2, \dots, b_s$ rational integers. Set

$$B \coloneqq \max\{|b_1|, |b_2|, \dots, |b_s|\}$$

and

$$\Lambda \coloneqq z_1^{b_1} \dots z_s^{b_s} - 1.$$

If Λ is nonzero, then

$$\log|\Lambda| > -3 \cdot 30^{s+4} \cdot (s+1)^{5.5} \cdot D^2 \cdot (1 + \log D) \cdot (1 + \log(sB). A_1 \dots A_s)$$

where

$$A_i \geq \max\{D \cdot h(z_i), |\log z_i|, 0.16\}$$

for all $1 \leq i \leq s$. If $\mathrm{F} = \mathbb{R}$, then

$$\log|\Lambda| > -1.4 \cdot 30^{s+3} \cdot (s)^{4.5} \cdot D^2 \cdot (1 + \log D) \cdot (1 + \log B . A_1 \ldots A_s).$$

Lemma 2.3. Let A, B, μ be some real numbers with $A > 0$ and $B > 1$ and let γ be an irrational number and M be a positive integer. Take p/q as a convergent of the continued fraction of γ such that $q > 6M$. Set $\varepsilon := \|\mu q\| - M\|\gamma q\| > 0$ where $\|\cdot\|$ denotes the distance from the nearest integer. Then there is no solution to the inequality

$$0 < |u\gamma - v + \mu| < AB^{-w}$$

in positive integers u, v and w with

$$u \leq M \text{ and } w \geq \frac{\log \frac{Aq}{\varepsilon}}{\log B}.$$

3. THE PROOF OF THEOREM 1.1

Let us write Equations (2) and (3) in Equation (5). We obtain

$$\left(\frac{\varphi^n}{\sqrt{5}} + \theta\right)(\varphi^n + \psi^n) = x \cdot \left(\frac{10^t - 1}{9}\right).$$

By using $|\theta| \leq 1/\sqrt{5}$ and $|\psi|^n \leq \psi$ we get

$$\left|\frac{(\varphi^2)^n}{\sqrt{5}} - \frac{x \cdot 10^t}{9}\right| < 0.8 \cdot \varphi^n.$$

If we divide both sides by $(\varphi^2)^n/\sqrt{5}$, we have

$$\left|1 - 10^t \cdot (\varphi^2)^{-n} \cdot (x \cdot \sqrt{5}/9)\right| < 1.79 \cdot \varphi^{-n} \qquad (6)$$

Applying Theorem 2.2 to this form we get

$$n < 4.36 \times 10^{15} \text{ and } t < 3.67 \times 10^{15} \qquad (7)$$

with the parameters

$$A_1 = 5, A_2 = 1, A_3 = 6 \text{ and } B = n.$$

Now, let us improve the bounds in (7). Set

$$\Omega := t\log 10 - n\log(\varphi^2) + \log\left(x \cdot \frac{\sqrt{5}}{9}\right).$$

Using the inequality (6) It is easy to see that

$$|\Omega| < 1.79\varphi^{-n+1}.$$

Hence, we get

$$0 < t\log 10 - n\log(\varphi^2) + \log\left(x \cdot \frac{\sqrt{5}}{9}\right) < 1.79\varphi^{-(n-1)}$$

which allows the application of the Lemma 2.3 by dividing both sides of the inequality with $\log(\varphi^2)$. The inequality becomes

$$0 < t\frac{\log 10}{\log(\varphi^2)} - n + \frac{\log\left(x \cdot \frac{\sqrt{5}}{9}\right)}{\log(\varphi^2)} < 1.86\varphi^{-(n-1)}.$$

From the application of Lemma 2.3, we get the result

$$n < 94 \text{ and } t < 80$$

to have a solution for the Equation (5).

Thus, searching for these bounds in Mathematica shows that there is no solution of the Equation (5). This completes our proof.

REFERENCES

1. Jhon J Bravo and Florian Luca. On a conjecture about repdigits in k-generalized fibonacci sequences. Publ. Math. Debrecen, 82(3-4):623–639, 2013.
2. Yann Bugeaud, Maurice Mignotte, and Samir Siksek. Classical and modular approaches to exponential diophantine equations i. fibonacci and lucas perfect powers. Annals of Mathematics, pages 969–1018, 2006.
3. Andrej Dujella and Attila Petho. A generalization of a theorem of baker and davenport. The Quarterly Journal of Mathematics, 49(195):291–306, 1998.
4. Eugene M Matveev. An explicit lower bound for a homogeneous rational linear form in the logarithms of algebraic numbers. ii. Izvestiya: Mathematics, 64(6):1217, 2000.
5. Nigel P Smart. The algorithmic resolution of Diophantine equations: a computational cookbook, volume 41. Cambridge University Press, 1998.

Analysis of Wave Solutions of The Nonlinear Model Equation with New Function Method

Tolga AKTÜRK[1]

[1]Department of Mathematics and Science Education, Faculty of Education, Ordu University, Turkey

[1]tolgaakturkk@gmail.com;

Abstract

In this study, the Sinh-Poisson equation's wave solution has been obtained by using the new function method. When the solution function of this nonlinear model equation is analyzed, it is seen that it is the function that includes the periodic behavior model. Two and three-dimensional density and contour graphs were obtained by determining the parameters suitable for the solution function visually of this periodic behavior model.

Keywords: The Sinh-Poisson equation; the new function method.

INTRODUCTION

It is essential to analyze events encountered in real life that concern science fields such as physics, chemistry, biology, engineering, and health. A well-defined mathematical model is needed to analyze such events. It is imperative to solve nonlinear partial differential equations, which are models representing such events. For this reason, various methods have been introduced to the literature to investigate the solutions to such equations [1-11]. The aim of this study is to define wave solutions to Sinh-Poisson equation by using new function method [12]

$$\omega_{xx} + \omega_{tt} = \beta^2 \, Sinh(\omega). \tag{1}$$

NEW FUNCTION METHOD

In this part of the article, the new function method used in the study is introduced. The general form of the Sinh-Poisson equation is as follows:

$$P\left(\omega_{xx}, \omega_{tt}, Sinh(\omega)\right) = 0. \tag{2}$$

Applying the wave transformation to the nonlinear partial differential equation (2) $\omega(x,t) = \omega(\eta)$, $\eta = k(x - ct)$, the general form of the following nonlinear ordinary differential equation is obtained,

$$N\left(\omega', \omega'' \ldots\right) = 0. \tag{3}$$

According to the method used in the study, the ω function provides the following relation:

$$F(\omega'') = G(g(\omega)), \tag{4}$$

where F, G and g are any functions. The derivative terms required in equation (3) are as follows:

$$\omega' = f(g(\omega)), \quad \omega'' = f(g(\omega))g'(\omega)f'(g(\omega)). \tag{5}$$

Substituting Eq. (5) into Eq. (4),

$$F(f(g(\omega))g'(\omega)f'(g(\omega))) = G(g(\omega)). \tag{6}$$

If $\psi = g(\omega)$ is taken as the following equation (6) can be written,

$$F(\psi' f(\psi) f'(\psi)) = G(\psi). \tag{7}$$

Equation (7) is reduced to an equation that can be separated into variables, and the following integral operation is written for the solution of this equation,

$$\frac{d\omega}{f(g(\omega))} = d\mu \Rightarrow \int \frac{du}{f(g(\omega))} = \int d\mu = \mu + P. \tag{8}$$

Where P is an integration constant.

SOLUTION FOR THE SINH-POISSON EQUATION

When wave transformation is applied to equation (1), the following nonlinear ordinary differential equation is obtained,

$$k^2(1+c^2)\omega'' = \beta^2\, Sinh(\omega). \tag{9}$$

Consider the transformation given below,

$$\omega' = f(Cosh(\omega)), \tag{10}$$

If the derivative term required in equation (9) is obtained from equation (10),

$$\omega'' = Sinh(\omega) f(Cosh(\omega)) f'(Cosh(\omega)). \tag{11}$$

Substituting Eq. (11) into Eq. (9),

$$k^2(1+c^2) f(Cosh(\omega)) f'(Cosh(\omega)) = \beta^2. \tag{12}$$

If ψ is substituted for $Cosh(\omega)$ in equation (12),

$$k^2(1+c^2) f(\psi) f'(\psi) = \beta^2. \tag{13}$$

If equation (13) is constructed by integrating according to ψ,

$$f^2(\psi) = \frac{\beta^2}{k^2\left(1+c^2\right)}\psi + P, \tag{14}$$

where P is a constant of integration. If equation (14) is constructed,

$$f(\psi) = \pm\sqrt{\frac{\beta^2}{k^2\left(1+c^2\right)}\psi + P}\,. \tag{15}$$

Let ω' is a function of $Cosh(\omega)$ and $Cosh(\omega) = \psi$. In this case, the following transformation can be written,

$$\omega = ArcCosh\psi \Rightarrow \omega' = \frac{\psi'}{\sqrt{\psi^2 - 1}} = f\left(Cosh(\omega)\right) = f(\psi). \tag{16}$$

If it is arranged using equation $\frac{\psi'}{\sqrt{\psi^2-1}} = f(\psi)$,

$$\psi' = \frac{d\psi}{d\eta} = f(\psi) = \sqrt{\left(\psi^2-1\right)\left(\frac{\beta^2}{k^2\left(1+c^2\right)}\psi + P\right)}. \tag{17}$$

If the roots depended to ψ in equation (17) are calculated using a package program,

$$\frac{2\beta^2}{k^2\left(1+c^2\right)}\left(\psi^3 + P\psi^2 - \psi - P\right) = 0,$$

$$\psi_1 = -P, \quad \psi_2 = -1, \quad \psi_3 = -1. \tag{18}$$

Where, $\psi_i\ (i = 1,\cdots,3)$ are roots of equation.

Considering the roots obtained from equation (18), equation (17) was solved using Mathematica packet program. In this way, the wave solution of equation (1) is obtained as follows.

$$\eta + Q = \frac{\sqrt{2}\sqrt{\left(1+c^2\right)}kArcTan\left[\frac{\sqrt{P+\psi}}{\sqrt{1-P}}\right]}{\sqrt{1-P}\beta}, \tag{19}$$

where Q is a constant of integration.

Replace ψ with $Cosh(\omega)$, η with $\eta = k(x-ct)$ in (19) and then the wave solutions for Eq. (1) can be get as follows:

$$\omega = ArcCosh[-P+\lambda] - P\lambda. \tag{20}$$

Where $\lambda = Tan\left[\frac{\sqrt{2}\sqrt{\left(1+c^2\right)}Q\sqrt{1-P}\beta + \sqrt{2}\sqrt{\left(1+c^2\right)}k\eta\sqrt{1-P}\beta}{\left(2+2c^2\right)k}\right]^2$.

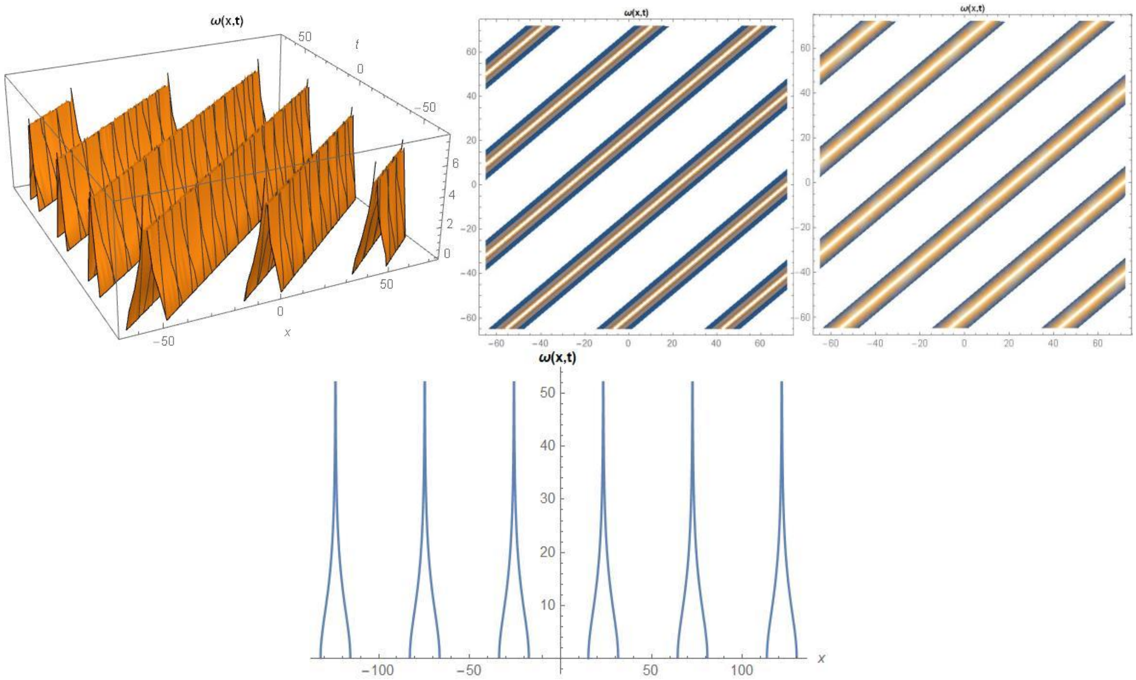

Figure 1. Three-dimensional, contour, density graphs of solution (20) at $c = 1.2,\ P = 0.5,\ Q = 2.5,\ k = 1.1, \beta = 0.2$ and two-dimensional graph for $t = 1$.

CONCLUSIONS

Using a new function method, the Sinh-Poisson equation was studied to obtain the wave solution. When the resulting solution function is analyzed, it is determined that the ArcCosh function, which has the character of a periodic function, is obtained. Obtaining this kind of solution function provides an advantage for commenting on the motion model of the Sinh-Poisson equation that we work within all ranges. In order to analysis the behaviors of the obtained solution function visually, two-three-dimensional contour and density graphs were obtained by determining the appropriate values for the parameters in the solution function. The results show that the new function technique is a highly effective mathematical technique for solving nonlinear partial differential equations.

REFERENCES

1. Liu, C.S., Trial equation method and its applications to nonlinear evolution equations Acta. Phys. Sin., 54, 2505- 2509, 2005.
2. Zaitsev, V. F., & Polyanin, A. D., Handbook of Nonlinear Partial Differential Equations, 2003.
3. Gurefe, Y., Misirli, E., Sonmezoglu, A., & Ekici, M. "Extended trial equation method to generalized nonlinear partial differential equations." Applied Mathematics and Computation 219.10 (2013): 5253-5260.
4. Shen, G., Sun, Y., and Xiong, Y., New travelling-wave solutions for Dodd-Bullough equation, *J. Appl. Math.*2013, pp. 5, 2013.
5. Sun, Y., New travelling wave solutions for Sine-Gordon equation, *J. Appl. Math.*2014, pp. 4, 2014.
6. Bulut, H., Akturk, T., and Gurefe, Y., Travelling wave solutions of the (N+1)-dimensional sine-cosine-Gordon equation, *AIP Conf. Proc.* pp. 5, 2014.
7. Kudryashov, N. A., One method for finding exact solutions of nonlinear differential equations, *Commun. Nonl. Sci. Numer. Simul.***17**, 2248-2253, 2012.
8. Aktürk, T, Gürefe, Y., and Bulut, H., New function method to the (N+1)-dimensional nonlinear problems, *An International Journal of Optimization and Control: Theories & Applications (IJOCTA)*, 7(3), 234-239, 2017.
9. Khan, K., Akbar, M. A., Application of exp-expansion method to find the exact solutions of modified Benjamin-Bona-Mahony equation, *World Applied Sciences Journal*, 24(10), 1373-1377, 2013.
10. Bulut, H., Aktürk, T., Yel G., An Application of the Modified Expansion Method to Nonlinear Partial Differential Equation, *Turkish Journal of Mathematics and Computer Science*, 10, 202–206, 2018.
11. Sakar, M. G., Saldır, O., Improving variational iteration method with auxiliary parameter for nonlinear time-fractional partial differential equations, *Journal of Optimization Theory and Applications*, 174(2), 530-549, 2017.
12. Kayum, Md Abdul, et al., Stable solutions to the nonlinear RLC transmission line equation and the Sinh–Poisson equation arising in mathematical physics, *Open Physics,* 18(1), 710-725, 2020.

New Generalizations of Srivastava Hypergeometric Functions and Their Integral Representations

Enes Ata, İ. Onur Kıymaz

Kırşehir Ahi Evran Uni., Dept. of Math., Turkey.

enesata.tr@gmail.com, iokiymaz@ahievran.edu.tr

Abstract

In this paper, we introduce a new extension of Srivastava's triple hypergeometric functions H_A, H_B and H_C, by using an extension of beta function, which given with a Fox-Wright function in its kernel. Also by using the same extended beta function, the new extension of Appell's hypergeometric function of the first kind is introduced. Furthermore, some integral representations of new extensions of Srivastava's triple hypergeometric functions are given.

Keywords: Beta function, Gauss hypergeometric function, Fox-Wright function, Srivastava's triple hypergeometric functions, Appell's hypergeometric function, Exton's function.

1. Introduction

In recent years, some expansions of special functions, which frequently used in applied mathematics, have been studied by many scientists [3, 6, 7, 18, 19, 20]. Particularly, for $Re(p) > 0$, $Re(x) > 0$, $Re(y) > 0$, $Re(c) > Re(b) > 0$ the following extension of beta function was introduced by Ata and Kıymaz in [6] as:

$$^{\Psi}\hat{B}_p(x,y) := {}^{\Psi}B_p\left[\begin{matrix}(\beta_i,\alpha_i)_{1,\xi}\\(\mu_j,\kappa_j)_{1,\eta}\end{matrix}\middle| x,y\right] = \int_0^1 t^{x-1}(1-t)^{y-1}{}_{\xi}\Psi_{\eta}\left(-\frac{p}{t(1-t)}\right)dt.$$

Later, by using this extension of beta function, Ata and Kıymaz [6] extended the hypergeometric function as follows:

$$^{\Psi}\hat{F}_p(a,b;c;z) := {}^{\Psi}F_p\left[\begin{matrix}(\beta_i,\alpha_i)_{1,\xi}\\(\mu_j,\kappa_j)_{1,\eta}\end{matrix}\middle| a,b;c;z\right] = \sum_{n=0}^{\infty}(a)_n\frac{^{\Psi}\hat{B}_p(b+n,c-b)}{B(b,c-b)}\frac{z^n}{n!}.$$

Respectively, they called them as ${}_{\xi}\Psi_{\eta}$-beta function and ${}_{\xi}\Psi_{\eta}$-Gauss hypergeometric function. Note that the function ${}_{\xi}\Psi_{\eta}$ used above is known as the Fox-Wright function [1] which defined as:

$${}_{\xi}\Psi_{\eta}(z) = {}_{\xi}\Psi_{\eta}\left[\begin{matrix}(\beta_i,\alpha_i)_{1,\xi}\\(\mu_j,\kappa_j)_{1,\eta}\end{matrix}\middle| z\right] = \sum_{n=0}^{\infty}\frac{\prod_{i=1}^{\xi}\Gamma(\alpha_i n+\beta_i)}{\prod_{j=1}^{\eta}\Gamma(\kappa_j n+\mu_j)}\frac{z^n}{n!}, \tag{1}$$

where $z, \beta_i, \mu_j \in \mathbb{C}, \alpha_i, \kappa_j \in \mathbb{R}, i = 1, \ldots, \xi$ and $j = 1, \ldots, \eta$. The asymptotic behaviour of the above function was studied by Fox [4, 5] and Wright [8, 9, 10] for the large values of z, considering the condition

$$\sum_{j=1}^{\eta}\kappa_j - \sum_{i=1}^{\xi}\alpha_i > -1.$$

If these conditions are met, for any $z \in \mathbb{C}$ the series (1) is convergent. For $\kappa, \mu, z \in \mathbb{C}$, $Re(\kappa) > -1$, the classic Wright function [1]

$${}_0\Psi_1(z) = {}_0\Psi_1\left[\begin{matrix}\overline{}\\(\mu,\kappa)\end{matrix}\middle| z\right] = \sum_{n=0}^{\infty}\frac{1}{\Gamma(\kappa n+\mu)}\frac{z^n}{n!}$$

can obtained by choosing $\xi = 0$ and $\eta = 1$ in equation (1). Also, Ata [7] defined some special functions that were generalized with the help of the classic Wright function. In this paper, we defined the extended Appell's hypergeometric function as:

$$\begin{aligned} {}^{\Psi}\hat{F}_{1,p}(a,b,c;d;x,y) &:= {}^{\Psi}F_{1,p}\left[\begin{matrix}(\beta_i,\alpha_i)_{1,\xi}\\ (\mu_j,\kappa_j)_{1,\eta}\end{matrix}\middle| a,b,c;d;x,y\right] \\ &= \sum_{m,n=0}^{\infty}(b)_m(c)_n\frac{{}^{\Psi}\hat{B}_p(a+m+n,d-a)}{B(a,d-a)}\frac{x^m}{m!}\frac{y^n}{n!} \end{aligned} \tag{2}$$

$$\left(p\geq 0, \max\{|x|,|y|\}<1, Re(d)>Re(a)>0\right),$$

which we called as ${}_{\xi}\Psi_{\eta}$-Appell F_1 function.

2. Extended Srivastava's triple hypergeometric functions

Srivastava defined triple hypergeometric functions H_A, H_B and H_C in [12, 13] and then many authors have studied some integral representations of these functions [2, 15, 16, 17].

This paper, we introduce the extensions of Srivastava's triple hypergeometric functions as follows:

$$\begin{aligned} {}^{\Psi}\hat{H}_{A,p}(\alpha,\beta_1,\beta_2;\gamma_1,\gamma_2;x,y,z) &:= {}^{\Psi}H_{A,p}\left[\begin{matrix}(\beta_i,\alpha_i)_{1,\xi}\\ (\mu_j,\kappa_j)_{1,\eta}\end{matrix}\middle| \alpha,\beta_1,\beta_2;\gamma_1,\gamma_2;x,y,z\right] \\ &= \sum_{m,n,k=0}^{\infty}\frac{(\alpha)_{m+k}(\beta_1)_{m+n}}{(\gamma_1)_m}\frac{{}^{\Psi}\hat{B}_p(\beta_2+n+k,\gamma_2-\beta_2)}{B(\beta_2,\gamma_2-\beta_2)}\frac{x^m}{m!}\frac{y^n}{n!}\frac{z^k}{k!} \end{aligned} \tag{3}$$

$$\big(p\geq 0, Re(\gamma_2)>Re(\beta_2)>0, r=|x|<1, s=|y|<1, t=|z|<(1-r)(1-s)\big),$$

$$\begin{aligned} {}^{\Psi}\hat{H}_{B,p}(\alpha,\beta_1,\beta_2;\gamma_1,\gamma_2,\gamma_3;x,y,z) &:= {}^{\Psi}H_{B,p}\left[\begin{matrix}(\beta_i,\alpha_i)_{1,\xi}\\ (\mu_j,\kappa_j)_{1,\eta}\end{matrix}\middle| \alpha,\beta_1,\beta_2;\gamma_1,\gamma_2,\gamma_3;x,y,z\right] \\ &= \sum_{m,n,k=0}^{\infty}\frac{(\alpha+\beta_1)_{2m+n+k}(\beta_2)_{n+k}}{(\gamma_1)_m(\gamma_2)_n(\gamma_3)_k}\frac{{}^{\Psi}\hat{B}_p(\alpha+m+k,\beta_1+m+n)}{B(\alpha,\beta_1)}\frac{x^m}{m!}\frac{y^n}{n!}\frac{z^k}{k!} \end{aligned}$$

$$\left(p\geq 0, r+s+t+2\sqrt{rst}<1\right),$$

$$\begin{aligned} {}^{\Psi}\hat{H}_{C,p}(\alpha,\beta_1,\beta_2;\gamma;x,y,z) &:= {}^{\Psi}H_{C,p}\left[\begin{matrix}(\beta_i,\alpha_i)_{1,\xi}\\ (\mu_j,\kappa_j)_{1,\eta}\end{matrix}\middle| \alpha,\beta_1,\beta_2;\gamma;x,y,z\right] \\ &= \sum_{m,n,k=0}^{\infty}\frac{(\beta_1)_{m+n}(\beta_2)_{n+k}}{(\gamma)_n}\frac{{}^{\Psi}\hat{B}_p(\alpha+m+k,\gamma+n-\alpha)}{B(\alpha,\gamma+n-\alpha)}\frac{x^m}{m!}\frac{y^n}{n!}\frac{z^k}{k!} \end{aligned} \tag{4}$$

$$\left(p\geq 0, r<1, s<1, t<1, r+s+t-2\sqrt{(1-r)(1-s)(1-t)}<2\right).$$

Respectively, we called them as ${}_{\xi}\Psi_{\eta}$-Srivastava H_A, ${}_{\xi}\Psi_{\eta}$-Srivastava H_B and ${}_{\xi}\Psi_{\eta}$-Srivastava H_C hypergeometric functions. The extended Srivastava's triple hypergeometric functions defined by (3) and (4) can also be given with the following series representations:

$${}^{\Psi}\hat{H}_{A,p}(\alpha,\beta_1,\beta_2;\gamma_1,\gamma_2;x,y,z) = \sum_{m=0}^{\infty}\frac{(\alpha)_m(\beta_1)_m}{(\gamma_1)_m}\,{}^{\Psi}\hat{F}_{1,p}(\beta_2,\beta_1+m,\alpha+m;\gamma_2;y,z)\frac{x^m}{m!},$$

$${}^{\Psi}\hat{H}_{C,p}(\alpha,\beta_1,\beta_2;\gamma;x,y,z) = \sum_{n=0}^{\infty}\frac{(\beta_1)_n(\beta_2)_n}{(\gamma)_n}\,{}^{\Psi}\hat{F}_{1,p}(\alpha,\beta_1+n,\beta_2+n;\gamma+n;x,z)\frac{y^n}{n!},$$

where ${}^{\Psi}\hat{F}_{1,p}$ is the extended Appell's hypergeometric function given by (2). Throughout this paper, we assume that p is any nonnegative real number.

3. Integral representations for ${}^{\Psi}\hat{H}_{A,p}$

Theorem 1. *For $Re(\gamma_2) > Re(\beta_2) > 0$, the following integral representation holds true:*

$$
\begin{aligned}
{}^{\Psi}\hat{H}_{A,p}(\alpha,\beta_1,\beta_2;\gamma_1,\gamma_2;x,y,z) &= \frac{\Gamma(\gamma_2)}{\Gamma(\beta_2)\Gamma(\gamma_2-\beta_2)}\int_0^1 t^{\beta_2-1}(1-t)^{\gamma_2-\beta_2-1}(1-yt)^{-\beta_1}(1-zt)^{-\alpha}\\
&\times {}_{\xi}\Psi_{\eta}\left(\frac{-p}{t(1-t)}\right){}_2F_1\left(\alpha,\beta_1;\gamma_1;\frac{x}{(1-yt)(1-zt)}\right)dt.
\end{aligned}
$$

Proof. Using the definition of ${}_{\xi}\Psi_{\eta}$-Srivastava H_A function

$$
\begin{aligned}
&{}^{\Psi}\hat{H}_{A,p}(\alpha,\beta_1,\beta_2;\gamma_1,\gamma_2;x,y,z)\\
&= \sum_{m,n,k=0}^{\infty}\frac{(\alpha)_{m+k}(\beta_1)_{m+n}}{(\gamma_1)_m}\frac{{}^{\Psi}\hat{B}_p(\beta_2+n+k,\gamma_2-\beta_2)}{B(\beta_2,\gamma_2-\beta_2)}\frac{x^m}{m!}\frac{y^n}{n!}\frac{z^k}{k!}\\
&= \sum_{m,n,k=0}^{\infty}\frac{(\alpha)_{m+k}(\beta_1)_{m+n}}{(\gamma_1)_m}\frac{1}{B(\beta_2,\gamma_2-\beta_2)}\int_0^1 t^{\beta_2+n+k-1}(1-t)^{\gamma_2-\beta_2-1}{}_{\xi}\Psi_{\eta}\left(\frac{-p}{t(1-t)}\right)\\
&\quad\times\frac{x^m}{m!}\frac{y^n}{n!}\frac{z^k}{k!}dt\\
&= \frac{\Gamma(\gamma_2)}{\Gamma(\beta_2)\Gamma(\gamma_2-\beta_2)}\int_0^1 t^{\beta_2-1}(1-t)^{\gamma_2-\beta_2-1}{}_{\xi}\Psi_{\eta}\left(\frac{-p}{t(1-t)}\right)\sum_{m,n,k=0}^{\infty}\frac{(\alpha)_m(\beta_1)_m}{(\gamma_1)_m}\\
&\quad\times(\beta_1+m)_n(\alpha+m)_k\frac{x^m}{m!}\frac{(yt)^n}{n!}\frac{(zt)^k}{k!}dt\\
&= \frac{\Gamma(\gamma_2)}{\Gamma(\beta_2)\Gamma(\gamma_2-\beta_2)}\int_0^1 t^{\beta_2-1}(1-t)^{\gamma_2-\beta_2-1}{}_{\xi}\Psi_{\eta}\left(\frac{-p}{t(1-t)}\right)\sum_{m=0}^{\infty}\frac{(\alpha)_m(\beta_1)_m}{(\gamma_1)_m}\frac{x^m}{m!}\\
&\quad\times\sum_{n=0}^{\infty}(\beta_1+m)_n\frac{(yt)^n}{n!}\sum_{k=0}^{\infty}(\alpha+m)_k\frac{(zt)^k}{k!}dt\\
&= \frac{\Gamma(\gamma_2)}{\Gamma(\beta_2)\Gamma(\gamma_2-\beta_2)}\int_0^1 t^{\beta_2-1}(1-t)^{\gamma_2-\beta_2-1}{}_{\xi}\Psi_{\eta}\left(\frac{-p}{t(1-t)}\right)\sum_{m=0}^{\infty}\frac{(\alpha)_m(\beta_1)_m}{(\gamma_1)_m}\frac{x^m}{m!}\\
&\quad\times(1-yt)^{-\beta_1-m}(1-zt)^{-\alpha-m}dt\\
&= \frac{\Gamma(\gamma_2)}{\Gamma(\beta_2)\Gamma(\gamma_2-\beta_2)}\int_0^1 t^{\beta_2-1}(1-t)^{\gamma_2-\beta_2-1}(1-yt)^{-\beta_1}(1-zt)^{-\alpha}{}_{\xi}\Psi_{\eta}\left(\frac{-p}{t(1-t)}\right)\\
&\quad\times{}_2F_1\left(\alpha,\beta_1;\gamma_1;\frac{x}{(1-yt)(1-zt)}\right)dt,
\end{aligned}
$$

which completes the proof. □

Theorem 2. *For $Re(\gamma_1)>Re(\beta_1)>0$ and $Re(\gamma_2)>Re(\beta_2)>0$, the following integral representation holds true:*

$$
\begin{aligned}
{}^{\Psi}\hat{H}_{A,p}(\alpha,\beta_1,\beta_2;\gamma_1,\gamma_2;x,y,z) &= \frac{\Gamma(\gamma_1)\Gamma(\gamma_2)}{\Gamma(\beta_1)\Gamma(\beta_2)\Gamma(\gamma_1-\beta_1)\Gamma(\gamma_2-\beta_2)}\int_0^1\int_0^1 u^{\beta_1-1}t^{\beta_2-1}\\
&\times(1-u)^{\gamma_1-\beta_1-1}(1-t)^{\gamma_2-\beta_2-1}(1-yt)^{\alpha-\beta_1}\left[(1-yt)(1-zt)-xu\right]^{-\alpha}\\
&\times{}_{\xi}\Psi_{\eta}\left(\frac{-p}{u(1-u)}\right){}_{\xi}\Psi_{\eta}\left(\frac{-p}{t(1-t)}\right)dudt.
\end{aligned}
$$

Proof. Using the integral representation of ${}_{\xi}\Psi_{\eta}$-beta function in the definition of ${}_{\xi}\Psi_{\eta}$-Srivastava H_A function and making similar calculations in the proof of Theorem 1, we get the desired result. $\square$

Theorem 3. *For $Re(\gamma_1) > Re(\beta_1) > 0$ and $Re(\gamma_2) > Re(\beta_2) > 0$, the following integral representation holds true:*

$$
\begin{aligned}
{}^{\Psi}\hat{H}_{A,p}(\alpha,\beta_1,\beta_2;\gamma_1,\gamma_2;x,y,z) &= \frac{\Gamma(\gamma_1)\Gamma(\gamma_2)}{\Gamma(\beta_1)\Gamma(\beta_2)\Gamma(\gamma_1-\beta_1)\Gamma(\gamma_2-\beta_2)} \int_0^1\int_0^1 u^{\beta_1-1}t^{\beta_2-1}(1-u)^{\gamma_1-\beta_1-1} \\
&\times (1-t)^{\gamma_2-\beta_2-1}(1-yt)^{-\beta_1}(1-xu-zt)^{-\alpha}\left[1-\frac{xyut}{(1-yt)(1-xu-zt)}\right]^{-\alpha} \\
&\times {}_{\xi}\Psi_{\eta}\left(\frac{-p}{u(1-u)}\right){}_{\xi}\Psi_{\eta}\left(\frac{-p}{t(1-t)}\right) dudt.
\end{aligned}
$$

Proof. Using the integral representation of ${}_{\xi}\Psi_{\eta}$-beta function in the definition of ${}_{\xi}\Psi_{\eta}$-Srivastava H_A function and making similar calculations in the proof of Theorem 1, we get the desired result. $\square$

Theorem 4. *For $Re(\gamma_2) > Re(\beta_2) > 0$, the following integral representation holds true:*

$$
\begin{aligned}
{}^{\Psi}\hat{H}_{A,p}(\alpha,\beta_1,\beta_2;\gamma_1,\gamma_2;x,y,z) &= \frac{\Gamma(\gamma_2)}{\Gamma(\beta_2)\Gamma(\gamma_2-\beta_2)} \int_0^{\infty} u^{\beta_2-1}(1+u)^{\alpha+\beta_1-\gamma_2}(1+u-yu)^{-\beta_1} \\
\times (1+u-zu)^{-\alpha}{}_{\xi}\Psi_{\eta}&\left(-2p-p\left(u+\frac{1}{u}\right)\right){}_2F_1\left(\alpha,\beta_1;\gamma_1;\frac{x(1+u)^2}{(1+u-yu)(1+u-zu)}\right)du.
\end{aligned}
$$

Proof. Using the integral representation of ${}_{\xi}\Psi_{\eta}$-beta function in the definition of ${}_{\xi}\Psi_{\eta}$-Srivastava H_A function and making similar calculations in the proof of Theorem 1, we get the desired result. $\square$

Theorem 5. *For $Re(\gamma_2) > Re(\beta_2) > 0$, the following integral representation holds true:*

$$
\begin{aligned}
{}^{\Psi}\hat{H}_{A,p}(\alpha,\beta_1,\beta_2;\gamma_1,\gamma_2;x,y,z) &= \frac{2\Gamma(\gamma_2)}{\Gamma(\beta_2)\Gamma(\gamma_2-\beta_2)}\int_0^{\frac{\pi}{2}}(\sin\theta)^{2\beta_2-1}(\cos\theta)^{2\gamma_2-2\beta_2-1}\left(1-y(\sin\theta)^2\right)^{-\beta_1} \\
\times \left(1-z(\sin\theta)^2\right)^{-\alpha}{}_{\xi}\Psi_{\eta}&\left(-p(\sec\theta)^2(\csc\theta)^2\right){}_2F_1\left(\alpha,\beta_1;\gamma_1;\frac{x}{\left(1-y(\sin\theta)^2\right)\left(1-z(\sin\theta)^2\right)}\right)d\theta.
\end{aligned}
$$

Proof. Using the integral representation of ${}_{\xi}\Psi_{\eta}$-beta function in the definition of ${}_{\xi}\Psi_{\eta}$-Srivastava H_A function and making similar calculations in the proof of Theorem 1, we get the desired result. $\square$

4. Integral representations for ${}^{\Psi}\hat{H}_{B,p}$

Theorem 6. *For $Re(\alpha) > 0$ and $Re(\beta_1) > 0$, the following integral representation holds true:*

$$
\begin{aligned}
{}^{\Psi}\hat{H}_{B,p}(\alpha,\beta_1,\beta_2;\gamma_1,\gamma_2,\gamma_3;x,y,z) &= \frac{\Gamma(\alpha+\beta_1)}{\Gamma(\alpha)\Gamma(\beta_1)}\int_0^1 t^{\alpha-1}(1-t)^{\beta_1-1}{}_{\xi}\Psi_{\eta}\left(\frac{-p}{t(1-t)}\right) \\
&\times X_4\left(\alpha+\beta_1,\beta_2;\gamma_1,\gamma_2,\gamma_3;xt(1-t),y(1-t),zt\right)dt.
\end{aligned}
$$

Proof. Using the definition of ${}_{\xi}\Psi_{\eta}$-Srivastava H_B function

$$\begin{aligned}
&{}^{\Psi}\hat{H}_{B,p}(\alpha,\beta_1,\beta_2;\gamma_1,\gamma_2,\gamma_3;x,y,z)\\
&\quad=\sum_{m,n,k=0}^{\infty}\frac{(\alpha+\beta_1)_{2m+n+k}(\beta_2)_{n+k}}{(\gamma_1)_m(\gamma_2)_n(\gamma_3)_k}\frac{{}^{\Psi}\hat{B}_p(\alpha+m+k,\beta_1+m+n)}{B(\alpha,\beta_1)}\frac{x^m}{m!}\frac{y^n}{n!}\frac{z^k}{k!}\\
&\quad=\frac{\Gamma(\alpha+\beta_1)}{\Gamma(\alpha)\Gamma(\beta_1)}\sum_{m,n,k=0}^{\infty}\frac{(\alpha+\beta_1)_{2m+n+k}(\beta_2)_{n+k}}{(\gamma_1)_m(\gamma_2)_n(\gamma_3)_k}\int_0^1 t^{\alpha+m+k-1}(1-t)^{\beta_1+m+n-1}\\
&\quad\quad\times{}_{\xi}\Psi_{\eta}\left(\frac{-p}{t(1-t)}\right)\frac{x^m}{m!}\frac{y^n}{n!}\frac{z^k}{k!}dt\\
&\quad=\frac{\Gamma(\alpha+\beta_1)}{\Gamma(\alpha)\Gamma(\beta_1)}\int_0^1 t^{\alpha-1}(1-t)^{\beta_1-1}{}_{\xi}\Psi_{\eta}\left(\frac{-p}{t(1-t)}\right)\sum_{m,n,k=0}^{\infty}\frac{(\alpha+\beta_1)_{2m+n+k}(\beta_2)_{n+k}}{(\gamma_1)_m(\gamma_2)_n(\gamma_3)_k}\\
&\quad\quad\times\frac{(xt(1-t))^m}{m!}\frac{(y(1-t))^n}{n!}\frac{(zt)^k}{k!}dt\\
&\quad=\frac{\Gamma(\alpha+\beta_1)}{\Gamma(\alpha)\Gamma(\beta_1)}\int_0^1 t^{\alpha-1}(1-t)^{\beta_1-1}{}_{\xi}\Psi_{\eta}\left(\frac{-p}{t(1-t)}\right)\\
&\quad\quad\times X_4\left(\alpha+\beta_1,\beta_2;\gamma_1,\gamma_2,\gamma_3;xt(1-t),y(1-t),zt\right)dt,
\end{aligned}$$

which completes the proof. □

Here, Exton's function X_4 is defined by [14]

$$X_4(a_1,a_2;c_1,c_2,c_3;x,y,z)=\sum_{m,n,k=0}^{\infty}\frac{(a_1)_{2m+n+k}(a_2)_{n+k}}{(c_1)_m(c_2)_n(c_3)_k}\frac{x^m}{m!}\frac{y^n}{n!}\frac{z^k}{k!},\quad\left(2\sqrt{r}+\left(\sqrt{s}+\sqrt{t}\right)^2<1\right).$$

Theorem 7. *For $Re(\alpha)>0$ and $Re(\beta_1)>0$, the following integral representation holds true:*

$$\begin{aligned}
{}^{\Psi}\hat{H}_{B,p}(\alpha,\beta_1,\beta_2;\gamma_1,\gamma_2,\gamma_3;x,y,z)&=\frac{2\Gamma(\alpha+\beta_1)}{\Gamma(\alpha)\Gamma(\beta_1)}\int_0^{\frac{\pi}{2}}(\sin\theta)^{2\alpha-1}(\cos\theta)^{2\beta_1-1}\\
\times{}_{\xi}\Psi_{\eta}\left(-p(\sec\theta)^2(\csc\theta)^2\right)&X_4\left(\alpha+\beta_1,\beta_2;\gamma_1,\gamma_2,\gamma_3;x(\sin\theta)^2(\cos\theta)^2,y(\cos\theta)^2,z(\sin\theta)^2\right)d\theta.
\end{aligned}$$

Proof. Using the integral representation of ${}_{\xi}\Psi_{\eta}$-beta function in the definition of ${}_{\xi}\Psi_{\eta}$-Srivastava H_B function and making similar calculations in the proof of Theorem 6, we get the desired result. □

Theorem 8. *For $Re(\alpha)>0$ and $Re(\beta_1)>0$, the following integral representation holds true:*

$$\begin{aligned}
{}^{\Psi}\hat{H}_{B,p}(\alpha,\beta_1,\beta_2;\gamma_1,\gamma_2,\gamma_3;x,y,z)&=\frac{\Gamma(\alpha+\beta_1)}{\Gamma(\alpha)\Gamma(\beta_1)}\int_0^{\infty}\frac{u^{\alpha-1}}{(1+u)^{\alpha+\beta_1}}{}_{\xi}\Psi_{\eta}\left(-2p-p\left(u+\frac{1}{u}\right)\right)\\
&\times X_4\left(\alpha+\beta_1,\beta_2;\gamma_1,\gamma_2,\gamma_3;\frac{xu}{(1+u)^2},\frac{y}{1+u},\frac{zu}{1+u}\right)du.
\end{aligned}$$

Proof. Using the integral representation of ${}_{\xi}\Psi_{\eta}$-beta function in the definition of ${}_{\xi}\Psi_{\eta}$-Srivastava H_B function and making similar calculations in the proof of Theorem 6, we get the desired result. □

Theorem 9. *For $Re(\alpha)>0$ and $Re(\beta_1)>0$, the following integral representation holds true:*

$$\begin{aligned}
{}^{\Psi}\hat{H}_{B,p}(\alpha,\beta_1,\beta_2;\gamma_1,\gamma_2,\gamma_3;x,y,z)&=\frac{\Gamma(\alpha+\beta_1)}{\Gamma(\alpha)\Gamma(\beta_1)}(b-a)^{1-(\alpha+\beta_1+2m+n+k)}\int_a^b(u-a)^{\alpha-1}(b-u)^{\beta_1-1}\\
\times{}_{\xi}\Psi_{\eta}\left(\frac{-p(b-a)^2}{(u-a)(b-u)}\right)&X_4\left(\alpha+\beta_1,\beta_2;\gamma_1,\gamma_2,\gamma_3;x(u-a)(b-u),y(b-u),z(u-a)\right)du.
\end{aligned}$$

Proof. Using the integral representation of ${}_\xi\Psi_\eta$-beta function in the definition of ${}_\xi\Psi_\eta$-Srivastava H_B function and making similar calculations in the proof of Theorem 6, we get the desired result. $\square$

5. Integral representations for ${}^{\Psi}\hat{H}_{C,p}$

Theorem 10. *For $Re(\gamma) > Re(\alpha) > 0$, the following integral representation holds true:*

$$
\begin{aligned}
{}^{\Psi}\hat{H}_{C,p}(\alpha,\beta_1,\beta_2;\gamma;x,y,z) = {} & \frac{\Gamma(\gamma)}{\Gamma(\alpha)\Gamma(\gamma-\alpha)}\int_0^1 t^{\alpha-1}(1-t)^{\gamma-\alpha-1}(1-xt)^{-\beta_1}(1-zt)^{-\beta_2} \\
& \times {}_\xi\Psi_\eta\left(\frac{-p}{t(1-t)}\right){}_2F_1\left(\beta_1,\beta_2;\gamma-\alpha;\frac{y(1-t)}{(1-xt)(1-zt)}\right)dt.
\end{aligned}
$$

Proof. Using the definition of ${}_\xi\Psi_\eta$-Srivastava H_C function

$$
\begin{aligned}
& {}^{\Psi}\hat{H}_{C,p}(\alpha,\beta_1,\beta_2;\gamma;x,y,z) \\
& = \sum_{m,n,k=0}^{\infty}\frac{(\beta_1)_{m+n}(\beta_2)_{n+k}}{(\gamma)_n}\frac{{}^{\Psi}\hat{B}_p(\alpha+m+k,\gamma+n-\alpha)}{B(\alpha,\gamma+n-\alpha)}\frac{x^m}{m!}\frac{y^n}{n!}\frac{z^k}{k!} \\
& = \sum_{m,n,k=0}^{\infty}\frac{(\beta_1)_{m+n}(\beta_2)_{n+k}}{(\gamma)_n}\frac{\Gamma(\gamma+n)}{\Gamma(\gamma)\Gamma(\gamma+n-\alpha)}\int_0^1 t^{\alpha+m+k-1}(1-t)^{\gamma+n-\alpha-1}{}_\xi\Psi_\eta\left(\frac{-p}{t(1-t)}\right) \\
& \quad \times \frac{x^m}{m!}\frac{y^n}{n!}\frac{z^k}{k!}dt \\
& = \frac{\Gamma(\gamma)}{\Gamma(\alpha)\Gamma(\gamma-\alpha)}\int_0^1 t^{\alpha-1}(1-t)^{\gamma-\alpha-1}{}_\xi\Psi_\eta\left(\frac{-p}{t(1-t)}\right)\sum_{m,n,k=0}^{\infty}\frac{(\gamma)_n}{(\gamma-\alpha)_n} \\
& \quad \times \frac{(\beta_1)_n(\beta_1+n)_m(\beta_2)_n(\beta_2+n)_k}{(\gamma)_n}\frac{(xt)^m}{m!}\frac{(y(1-t))^n}{n!}\frac{(zt)^k}{k!}dt \\
& = \frac{\Gamma(\gamma)}{\Gamma(\alpha)\Gamma(\gamma-\alpha)}\int_0^1 t^{\alpha-1}(1-t)^{\gamma-\alpha-1}{}_\xi\Psi_\eta\left(\frac{-p}{t(1-t)}\right)\sum_{n=0}^{\infty}\frac{(\beta_1)_n(\beta_2)_n}{(\gamma-\alpha)_n}\sum_{m=0}^{\infty}(\beta_1+n)_m\frac{(xt)^m}{m!} \\
& \quad \times \sum_{k=0}^{\infty}(\beta_2+n)_k\frac{(zt)^k}{k!}\frac{(y(1-t))^n}{n!}dt \\
& = \frac{\Gamma(\gamma)}{\Gamma(\alpha)\Gamma(\gamma-\alpha)}\int_0^1 t^{\alpha-1}(1-t)^{\gamma-\alpha-1}{}_\xi\Psi_\eta\left(\frac{-p}{t(1-t)}\right)\sum_{n=0}^{\infty}\frac{(\beta_1)_n(\beta_2)_n}{(\gamma-\alpha)_n}(1-xt)^{-\beta_1-n} \\
& \quad \times (1-zt)^{-\beta_2-n}\frac{(y(1-t))^n}{n!}dt \\
& = \frac{\Gamma(\gamma)}{\Gamma(\alpha)\Gamma(\gamma-\alpha)}\int_0^1 t^{\alpha-1}(1-t)^{\gamma-\alpha-1}(1-xt)^{-\beta_1}(1-zt)^{-\beta_2}{}_\xi\Psi_\eta\left(\frac{-p}{t(1-t)}\right) \\
& \quad \times {}_2F_1\left(\beta_1,\beta_2;\gamma-\alpha;\frac{y(1-t)}{(1-xt)(1-zt)}\right)dt,
\end{aligned}
$$

which completes the proof. $\square$

Theorem 11. *For* $Re(\gamma-\alpha-\beta_1)>0$*, the following integral representation holds true:*

$$
\begin{aligned}
{}^{\Psi}\hat{H}_{C,p}(\alpha,\beta_1,\beta_2;\gamma;x,y,z) = {} & \frac{\Gamma(\gamma)}{\Gamma(\alpha)\Gamma(\beta_1)\Gamma(\gamma-\alpha-\beta_1)}\int_0^1\int_0^1 t^{\alpha-1}u^{\beta_1-1}(1-t)^{\gamma-\alpha-1} \\
& \times (1-u)^{\gamma-\alpha-\beta_1-1}(1-xt)^{\beta_2-\beta_1}\left(1-xt-yu-zt+ytu+zxt^2\right)^{-\beta_2} \\
& \times {}_{\xi}\Psi_{\eta}\left(\frac{-p}{t(1-t)}\right){}_{\xi}\Psi_{\eta}\left(\frac{-p}{u(1-u)}\right)dtdu.
\end{aligned}
$$

Proof. Using the integral representation of ${}_{\xi}\Psi_{\eta}$-beta function in the definition of ${}_{\xi}\Psi_{\eta}$-Srivastava H_C function and making similar calculations in the proof of Theorem 10, we get the desired result. □

Theorem 12. *For* $Re(\gamma)>Re(\alpha)>0$*, the following integral representation holds true:*

$$
\begin{aligned}
{}^{\Psi}\hat{H}_{C,p}(\alpha,\beta_1,\beta_2;\gamma;x,y,z) = {} & \frac{\Gamma(\gamma)}{\Gamma(\alpha)\Gamma(\gamma-\alpha)}\int_0^{\infty} u^{\alpha-1}(1+u)^{\beta_1+\beta_2-\gamma}(1+u-xu)^{-\beta_1} \\
\times (1+u-zu)^{-\beta_2}{}_{\xi}\Psi_{\eta}\left(-2p-p\left(1+\frac{1}{u}\right)\right) & {}_2F_1\left(\beta_1,\beta_2;\gamma-\alpha;\frac{y(1+u)}{(1+u-xu)(1+u-zu)}\right)du.
\end{aligned}
$$

Proof. Using the integral representation of ${}_{\xi}\Psi_{\eta}$-beta function in the definition of ${}_{\xi}\Psi_{\eta}$-Srivastava H_C function and making similar calculations in the proof of Theorem 10, we get the desired result. □

Theorem 13. *For* $Re(\gamma)>Re(\alpha)>0$*, the following integral representation holds true:*

$$
\begin{aligned}
{}^{\Psi}\hat{H}_{C,p}(\alpha,\beta_1,\beta_2;\gamma;x,y,z) = {} & \frac{2\Gamma(\gamma)}{\Gamma(\alpha)\Gamma(\gamma-\alpha)}\int_0^{\frac{\pi}{2}}(\sin\theta)^{2\alpha-1}(\cos\theta)^{2\gamma-2\alpha-1}\left(1-x(\sin\theta)^2\right)^{-\beta_1} \\
& \times\left(1-z(\sin\theta)^2\right)^{-\beta_2}{}_{\xi}\Psi_{\eta}\left(-p(\sec\theta)^2(\csc\theta)^2\right) \\
& \times{}_2F_1\left(\beta_1,\beta_2;\gamma-\alpha;\frac{y(\cos\theta)^2}{(1-x(\sin\theta)^2)(1-z(\sin\theta)^2)}\right)d\theta.
\end{aligned}
$$

Proof. Using the integral representation of ${}_{\xi}\Psi_{\eta}$-beta function in the definition of ${}_{\xi}\Psi_{\eta}$-Srivastava H_C function and making similar calculations in the proof of Theorem 10, we get the desired result. □

Theorem 14. *For* $Re(\gamma)>Re(\alpha)>0$*, the following integral representation holds true:*

$$
\begin{aligned}
{}^{\Psi}\hat{H}_{C,p}(\alpha,\beta_1,\beta_2;\gamma;x,y,z) = {} & \frac{\Gamma(\gamma)}{\Gamma(\alpha)\Gamma(\gamma-\alpha)}(b-a)^{1-(\gamma+m+n+k)}\int_a^b(u-a)^{\alpha-1}(b-u)^{\gamma-\alpha-1} \\
\times\left(1-z(u-a)\right)^{-\beta_2}{}_{\xi}\Psi_{\eta} & \left(\frac{-p(b-a)^2}{(u-a)(b-u)}\right){}_2F_1\left(\beta_1,\beta_2;\gamma-\alpha;\frac{y(b-u)}{xz(u-a)^2}\right)du.
\end{aligned}
$$

Proof. Using the integral representation of ${}_{\xi}\Psi_{\eta}$-beta function in the definition of ${}_{\xi}\Psi_{\eta}$-Srivastava H_C function and making similar calculations in the proof of Theorem 10, we get the desired result. □

6. Conclusions

In this study, we defined the ${}_{\xi}\Psi_{\eta}$-Srivastava H_A, ${}_{\xi}\Psi_{\eta}$-Srivastava H_B and ${}_{\xi}\Psi_{\eta}$-Srivastava H_C hypergeometric functions with the help of the ${}_{\xi}\Psi_{\eta}$-beta function. Besides, the series representations of functions ${}_{\xi}\Psi_{\eta}$-Srivastava H_A and ${}_{\xi}\Psi_{\eta}$-Srivastava H_C are given in terms of ${}_{\xi}\Psi_{\eta}$-Appell F_1

function. Finally, some integral representations for each of the extended Srivastava's triple hypergeometric functions are presented. The closed-form expressions of the integrals presented here, are presumably not available in the existing literature.

References

[1] A.A. Kilbas, H.M. Srivastava, J.J. Trujillo, Theory and Applications of Fractional Differential, North-Holland Mathematics Studies 204, 2006.

[2] A. Çetinkaya, M.B. Yağbasan, İ.O. Kıymaz, The extended Srivastava's triple hypergeometric functions and their integral representations, J. Nonlinear Sci. Appl., 9, 4860-4866, 2016.

[3] A. Çetinkaya, İ.O. Kıymaz, P. Agarwal, R. Agarwal, A comparative study on generating function relations for generalized hypergeometric functions via generalized fractional operators, Advances in Difference Equations, 2018:156, 2018.

[4] C. Fox, The asymptotic expansion of generalized hypergeometric functions, Proceedings of the London Mathematical Society (Ser. 2), 27, 389-400, 1928.

[5] C. Fox, The G and H functions as symmetrical Fourier kernels, Transactions of the American Mathematical Society, 98, 395-429, 1961.

[6] E. Ata, İ.O. Kıymaz, A study on certain properties of generalized special functions defined by Fox-Wright function, Applied Mathematics and Nonlinear Sciences, 5(1), 147-162, 2020.

[7] E. Ata, Generalized beta function defined by Wright function, arXiv:1803.03121v3 [math.CA], 2021.

[8] E.M. Wright, The asymptotic expansion of the generalized hypergeometric function, Journal of the London Mathematical Society, 10, 286-293, 1935.

[9] E.M. Wright, The asymptotic expansion of integral functions defined by Taylor Series, Philosophical Transactions of the Royal Society of London, Series A., 238, 423-451, 1940.

[10] E.M. Wright, The asymptotic expansion of the generalized hypergeometric function II, Proceedings of the London Mathematical Society, 46(2), 389-408, 1940.

[11] G.E. Andrews, R. Askey, R. Roy, Special Functions, Cambridge University Press, Cambridge, 1999.

[12] H.M. Srivastava, Hypergeometric functions of three variables, Ganita, 15, 97-108, 1964.

[13] H.M. Srivastava, Some integrals representing triple hypergeometric functions, Rend. Circ. Mat. Palermo, 16, 99-115, 1967.

[14] H.M. Srivastava, P.W. Karlsson, Multiple Gaussian Hypergeometric Series, Ellis Horwood Series: Mathematics and its Applications, Ellis Horwood Ltd., Chichester, Halsted Press [John Wiley and Sons, Inc.], New York, 1985.

[15] J. Choi, A. Hasanov, M. Turaev, Integral representations for Srivastava's hypergeometric function H_A, Honam Math. J., 34, 113-124, 2012.

[16] J. Choi, A. Hasanov, M. Turaev, Integral representations for Srivastava's hypergeometric function H_B, J. Korean Soc. Math. Educ. Ser. B, Pure Appl. Math., 19, 137-145, 2012.

[17] J. Choi, A. Hasanov, M. Turaev, Integral representations for Srivastava's hypergeometric function H_C, Honam Math. J., 34, 473-482, 2012.

[18] M.A. Chaudhry and S.M. Zubair, Generalized incomplete gamma functions with applications, Journal of Computational and Applied Mathematics, 55, 99-124, 1994.

[19] M.A. Chaudhry, A. Qadir, M. Rafique, S.M. Zubair, Extension of Euler's beta function, Journal of Computational and Applied Mathematics, 78, 19-32, 1997.

[20] M.A. Chaudhry, A. Qadir, H.M. Srivastava, R.B. Paris, Extended hypergeometric and confluent hypergeometric functions, Applied Mathematics and Computation, 159, 589-602, 2004.

MATHEMATICS OF THE 2^{nd} LAW OF THERMODYNAMICS

MD. SHAFIQUL ISLAM[1]

Abstract. In this paper, I have shown the 2^{nd} law of thermodynamics as a consequence of the 1^{st} law of thermodynamics. It is not claimed that the 2^{nd} law of thermodynamics is a redundant of the 1^{st} law, rather I shown here how we can extract the 2^{nd} law from the mathematical formulation of the 1^{st} law of thermodynamics. The Clausius statement of the 2^{nd} law of thermodynamics is, it is impossible to construct a device whose sole effect is the transfer of heat from a cool reservoir to a hot reservoir. An alternative statement of the law is, "All spontaneous processes are irreversible" or, "the entropy of an isolated system always increases". Having strong experimental evidences, this empirical law is obvious, which tells us the arrow of time and the direction of spontaneous changes. I proved the statement in this paper using the mathematical formulation of the 1^{st} law of thermodynamics.

1. Introduction

The 1^{st} law of thermodynamics is often claimed as a version of the law of conservation of energy, adapted to the thermodynamic systems, which can be formulated as: $\delta Q_{\text{rev}} = dU - \delta W_{\text{rev}}$ Which states that the amount of heat accumulated by a closed system is spent to change its internal energy, and to do some work by the system on its surroundings. Here $\delta \mathrm{W}_{\text{rev}}$ is the differential work done by the surroundings on the system, so work done by the system on its surroundings is $(-\delta W_{\text{rev}})$. So, $\delta Q_{\text{rev}} = dU + p_{\text{ext}} dV$. This law is a very common-sense law, adapted to the thermodynamic system, which is the total energy of an isolated system e.g., the universe is conserved.

Key words and phrases: 2^{nd} law of thermodynamics; Entropy and Disorder; Irreversibility.

2. Preliminaries

In the mathematical formulation of the 1^{st} law of thermodynamics, the quantity of heat and work transfer are energies that depend on the process followed, whereas internal energy of a system is an extensive thermodynamic property of system, describes quantitatively an equilibrium state, irrespective of the process.
So, δQ_{rev}, δW_{rev} are non-exact differentials and dU is an exact differential. Let, $X(U, V)$ is the integrating factor, so that $X\delta Q_{\text{rev}}$ becomes exact. So, $X\delta Q_{\text{rev}} = XdU + Xp_{\text{ext}}dV$ is an exact differential equation.

2.1. **Definition.** $dZ = MdP + NdQ$ will be an exact differential equation provided that, $\left(\frac{\partial M}{\partial Q}\right)_P = \left(\frac{\partial N}{\partial P}\right)_Q$

2.2. **Assumption.** Let us assume that, X, the integrating factor, is a function of only internal energy U. Joule experimentally shown that the internal energy of an ideal gas is only the function of its temperature, independent of pressure or volume. So, $X = f(T)$.

As, $X\delta Q_{\text{rev}} = XdU + Xp_{\text{ext}}dV$ is an exact differential equation, from **Definition 2.1.**,

$$\left(\frac{\partial X}{\partial V}\right)_U = \left(\frac{\partial X p_{\text{ext}}}{\partial U}\right)_V$$

The above partial differential equation in general has more than one solution. The general solution can't be known as the Internal Energy as a function of temperature and the boundary conditions are not known. However, a particular solution for X can be obtained assuming X, the integrating factor as a function of only internal energy U. (2.2)
From **Assumption 2.2.**, $X = f(T)$, so, $\left(\frac{\partial X}{\partial V}\right)_U = 0$, i.e., $\left(\frac{\partial X}{\partial V}\right)_U = \left(\frac{\partial X p_{\text{ext}}}{\partial U}\right)_V = 0$, i.e. $Xp_{\text{ext}} =$ function of $V = g\left(\frac{T}{p_{\text{ext}}}\right)$ for ideal gas.
The functional equation $f(T)p_{\text{ext}} = g\left(\frac{T}{p_{\text{ext}}}\right)$ has a unique solution, i.e., $f(y) = g(y) = \frac{1}{y}$. So, the integrating factor $X = f(T) = \frac{1}{T}$
So, $\frac{\delta Q_{\text{rev}}}{T}$ is an exact differential. For reversible process, temperature of the system is same as the temperature of the surroundings at any particular instant of time.
So, $\frac{\delta Q_{\text{rev}}}{T_{\text{surr}}}$ is an exact differential and is known as differential change in entropy.
It can be shown that, maximum work delivered to surroundings for isothermal gas expansion can be obtained using a reversible path. (Atkins, 2001)

So, $(-W)_{\text{irrev}} < (-W)_{\text{rev}}$ i.e., $W_{\text{irrev}} > W_{\text{rev}}$
$\Delta U = Q_{\text{irrev}} + W_{\text{irrev}} = Q_{\text{rev}} + W_{\text{rev}}$ so, $Q_{\text{rev}} > Q_{\text{irrev}}$.
Being a state function,

$$\oint \frac{\delta Q_{\text{rev}}}{T_{\text{surr}}} = 0 \tag{2.1}$$

But, $Q_{\text{irrev}} < Q_{\text{rev}}$. So,

$$\oint \frac{\delta Q_{\text{irrev}}}{T_{\text{surr}}} < 0 \tag{2.2}$$

3. Existence on Global Systems

We proved the equation (2.1) and the inequality (2.2) using the fact for ideal gas laws, but they hold the same for any materials in the system. The fact behind this is, δQ_{rev} is the reversible heat accumulated by the system from its surroundings and T_{surr} is the temperature of surroundings. So, the surroundings can't see inside the system and provide the same heat irrespective of material in the system for its same temperature at the instant of heat exit. Similarly, δQ_{irrev} is the irreversible heat accumulated by the system from its surroundings and T_{surr} is the temperature of surroundings at that instant which are independent of the system provided that heat transfer occurs irreversibly. The accumulation rate of heat may be different for different systems but that is the kinetics of the systems, we will not deal with that here.

4. Proof

4.1. **Theorem.** *The 2nd Law of Thermodynamics is a consequence of the 1st Law of Thermodynamics.*

The above argument proves the existence of the equation

$$\oint \frac{\delta Q}{T_{\text{surr}}} \leq 0$$

for global systems. Where the equality holds for reversible cases, and for irreversible changes, the equality doesn't hold.

Let, a system (Figure 1) is isolated and spontaneously changes from A to B. The system is then brought into contact with a heat source of same temperature as B at that particular instant of time and reversibly brought back from B to A. (It would be necessary and sufficient to show

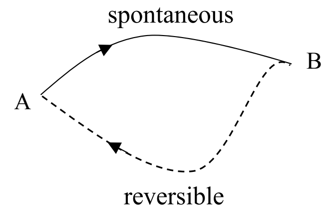

Figure 1

that, "changes from A to B is irreversible" to prove the above statement.)

4.2. **Proof by Contradiction.** Let us first assume that, spontaneous change from A to B is reversible. So, the total cyclic path is also reversible as all the elements of the path is reversible. (Silbey, 2004) Hence,

$$\oint \frac{\delta Q}{T_{\text{surr}}} = 0 \Rightarrow \oint_A^B \frac{\delta Q_{\text{spontaneous}}}{T_{\text{surr}}} + \oint_B^A \frac{\delta Q_{\text{rev}}}{T_{\text{surr}}} = 0$$

But,

$$\oint_A^B \frac{\delta Q_{\text{spontaneous}}}{T_{\text{surr}}} = 0$$

as, $Q_{\text{spontaneous}} = 0$ (isolated)

$$\therefore \oint \frac{\delta Q}{T_{\text{surr}}} = \oint_B^A \frac{\delta Q_{\text{rev}}}{T_{\text{surr}}} = 0$$

which is not true, because, $Q_{rev}(B \to A) \neq 0$ (not isolated). So,

$$\oint \frac{\delta Q}{T_{\text{surr}}} \neq 0.$$

That is a contradiction. So, our initial assumption was incorrect, i.e., spontaneous change from A to B must be irreversible. Consequently, the cycle of heating and cooling back to the same point A is an irreversible cycle, as, minimum a portion of this path is proved to be irreversible ($A \to B$). So,

$$\oint \frac{\delta Q}{T_{\text{surr}}} < 0 \Rightarrow \oint_A^B \frac{\delta Q_{\text{spontaneous}}}{T_{\text{surr}}} + \oint_B^A \frac{\delta Q_{\text{rev}}}{T_{\text{surr}}} < 0 \Rightarrow \oint_B^A \frac{\delta Q_{\text{rev}}}{T_{\text{surr}}} < 0$$

because,

$$\oint_A^B \frac{\delta Q_{\text{spontaneous}}}{T_{\text{surr}}} = 0$$

(isolated)

So,

$$\oint_A^B \frac{\delta Q_{\text{rev}}}{T_{\text{surr}}} > 0$$

which is the change in entropy for the spontaneous process, indicating that, entropy always increases in isolated system for spontaneous processes to occur. $\square$

From the above argument it is proved that, "All spontaneous processes are irreversible". Also, "the entropy of an isolated system always increases".

5. Efficiency of Heat Engines

Let us consider a heat engine, in the first cycle it gains ΔQ_1 amount of heat from a hot reservoir and releases ΔQ_2 amount of heat to a cold reservoir. So, the amount of heat energy converted into useful work by the heat engine is equal to: $\Delta Q_1 - |\Delta Q_2| = \Delta Q_1 + \Delta Q_2 > 0$

The engine is said to be reversible if in the reversed cycle it can work as a heat pump, i.e., it takes ΔQ_2 amount of heat from the cold reservoir and releases ΔQ_1 amount of heat to the hot reservoir, provided that it consumes the useful work converted in the first cycle. So, after completing two cycles, the engine is back to the old state, so, $\frac{\Delta Q_1}{T_1} + \frac{\Delta Q_2}{T_2} = 0$

But the equality doesn't hold for actual engines (irreversible). As we have proved that all spontaneous processes are irreversible. So, after completing the two cycles, the engine is not back to the old state, so, $\frac{\Delta Q_1}{T_1} + \frac{\Delta Q_2}{T_2} < 0 \Rightarrow 1 + \frac{T_1}{\Delta Q_1} \times \frac{\Delta Q_2}{T_2} < 0 \Rightarrow \frac{\Delta Q_2}{\Delta Q_1} < -\frac{T_2}{T_1}$

The efficiency of a heat engine is defined by the ratio of work done per cycle and the heat energy it gains per cycle, i.e., $\frac{\Delta Q_1 + \Delta Q_2}{\Delta Q_1} = 1 + \frac{\Delta Q_2}{\Delta Q_1} < 1 - \frac{T_2}{T_1}$, which is clearly less than 100% as we know $T_1, T_2 \nless 0$ from the 3^{rd} law of thermodynamics.

That is the evidence of the alternative formulation of the 2^{nd} law of thermodynamics used in the literature, "There does not exist any heat engine that does nothing but absorb heat energy from one single reservoir and convert it into work".

6. Conclusion

In this paper, we proved the 2^{nd} Law of Thermodynamics by Mathematical Arguments. Some familiar quotes used in the literature relevant to the 2^{nd} law of thermodynamics, "you can't unscramble an egg", "you can't take the cream out of the coffee" as these are irreversible processes. No matter how long you wait, the cream won't jump out of the coffee into the creamer or couldn't travel in time back to its old state. These seem to be just natural phenomena, but we have shown the mathematical validation of these natural phenomena. So, the 2^{nd} Law of Thermodynamics is not only a law of nature, but a law of mathematics also.

References

Atkins, P. (2001). *Physical chemistry.* W. H. Freeman.
Silbey, R. J. (2004). *Physical chemistry.* Wiley.

[1]Department of Materials and Metallurgical Engineering, Bangladesh University of Engineering and Technology, Dhaka-1000, Bangladesh
Email address: `mdshafiqulislam@ug.mme.buet.ac.bd`

A New Treatment of the Finite Difference Method for 2-Interval Sturm-Liouville Problems

S. Çavuşoğlu[1,*], O. Sh. Mukhtarov[2,3]

[1]Graduate School of Natural and Applied Sciences, Tokat Gaziosmanpasa University,Tokat, Turkey
[2]Department of Mathematics, Faculty of Science, Tokat Gaziosmanpaşa University, Tokat, Turkey
[3]Institute of Mathematics and Mechanics, Azerbaijan National Academy of Sciences, Baku, Azerbaijan.
* Corresponding author
e-mail: semihcavusoglu@gmail.com,omukhtarov@yahoo.com

Abstract :

Finite Difference Method (FDM) and its various genelalizaton are intended for 1-interval initial and/or boundary value problems for ordinary and partial differential equations.
In this study, we developed a new modification of FDM to solve not only 1-interval problems but also 2-interval differential equations with additional transmission conditions at one internal point of transition. In fact, we have two differential equations for left and right solutions. Additional transmission conditions are given in terms of limit values of the left and right solutions at the transition point.
The calculated numerical solutions are compared with the exact solutions. Graphical illustrations of the obtained numerical and exact solutions are also presented.

Keywords : Finite difference method, boundary value problems, transmission conditions, interior singular point

1 Introduction

The advent of FDM in physical applications began in the early 1950s. In the recent years many important theoretical results have been developed regarding the convergence, accuracy and stability of the FDM for Sturm-Liouville type boundary value problems, which are used extensively in solving of many problems in physics and engineering, such as fluid and solid mechanics, Newton's law of cooling, termodynamics, electrostatics and magnetostatics and etc. (see, for example [1]-[4] and references cited therein)
In this work we present a new modification of the classical FDM to solve 2-interval Sturm-Liouville problems, involving additional transmission conditions at an in-

ternal transition point.

2 MFDM applied to 2-interval Sturm-Liouville problems

In this section based on FDM we proposed a new technique for solving 2-interval Sturm-Liouville problems involving additional transmission conditions at an internal transition point . Consider the following 2-interval boundary value problem, consisting of the Sturm-Liouville equation

$$xy^{''} - y^{'} + 4x^3y = 0 \tag{2.1}$$

on two disjoint intervals $[-1, 1)$ and $(1, 3]$, separated boundary conditious at the end points $x = -1$ and $x = 3$, given by

$$y\,(-1) = 0, \quad y\,(3) = 2 \tag{2.2}$$

and transmission conditions at an internal transition point $x = 1$, given by

$$y(1-0) = 2y(1+0), \quad y'(1-0) = 3y'(1+0) \tag{2.3}$$

At first we will solve this problem without transmission conditions (2.3). By using an uniform cartesian grid $x_i = -1 + ih, \quad i = 0, 1, \quad \ldots, 40$, where $h = \frac{3-(-1)}{40} = 0,1$ and applying the central finite difference formulas at a typical grid point x_i we can replace the differential equation (2.1) at each internal grid point x_1, x_2,. . . ,and x_{39} by

$$x_i\frac{\Delta_+y_i - \Delta_-y_i}{h} - \frac{1}{2}(\Delta_+y_i + \Delta_-y_i) + 4x_i^3y(x_i) = 0, i = 0, 1, \ldots, 39 \tag{2.4}$$

where Δ_+y_i and $\Delta_-y_i)$ denotes the forward finite difference and backward finite difference of $y(x)$ at a grid point x_i respectively, that is

$$\Delta_+y_i = \frac{y(x_i + h) - y(x_i)}{h} \approx y'(x_i), \quad \Delta_-y_i = \frac{y(x_i) - y(x_i - h)}{h} \approx y'(x_i).$$

Applying boundary caonditions (2.2) we obtain

$$y(x_0) = 0, \quad y(x_{40}) = 2 \tag{2.5}$$

Defining the approximate finite difference solution (AFDS) for $y(x)$ at all grid points x_i as solution $y_i := y(x_i)$ and taking into account that $y_0 = 0, y_{40} = 2$ (see, (2.5)) we have the following system of linear algebraic equations with respect to the variables $y_1, y_2, \ldots, y_{39}$ given by

$$(2x_i + h)y_{i-1} + (-4x_i + 8h^2x_i^3)y_i + (2x_i - h)y_{i+1} = 0, \quad i = 1, 2, \ldots, 39 \tag{2.6}$$

Clearly, the system (2.6)can be written in a tridiagonal matrix-vector form

$$AY = b$$

where A is a tridiagonal matrix, given by

$$A = \begin{pmatrix} -4x_1+8h^2x_1^3 & 2x_1-h & \cdots & 0 & 0 & 0 \\ 2x_2+h & -4x_2+8h^2x_2^3 & \cdots & 0 & 0 & 0 \\ 0 & 2-h & \cdots & 0 & 0 & 0 \\ \vdots & \vdots & \ddots & \ddots & \vdots & \vdots \\ 0 & 0 & 0 & \cdots & -4x_{38}+8h^2x_{38}^3 & 2+h \\ 0 & 0 & 0 & \cdots & 2x_{39}+h & -4x_{39}+8h^2x_{39}^3 \end{pmatrix}$$

and Y and b are column vectors, given by

$$Y = \begin{pmatrix} y_1 \\ y_2 \\ \vdots \\ y_{38} \\ y_{39} \end{pmatrix}, \qquad b = \begin{pmatrix} 0 \\ 0 \\ \vdots \\ 0 \\ -2(2x_{39}-h) \end{pmatrix}.$$

The solution of this linear system of algebraic equations can be found by using Matlab/Octave. It is easy to check that the exact solution of the differential equation (2.1) satisfying the boundary conditions (2.2) is

$$y = -2csc(8)sin(1-x^2) \tag{2.7}$$

In the following table (see,Table.1) the finite difference solutions of the problem (2.1)-(2.2) are compared with the exact solution (2.7).

Table 1: Error analysis

		n=40				n=200	
x	Exact	FDM	EROR	x	Exact	FDM	EROR
1	-0,38178	-0,36601	0,01577	1	-0,08003	-0,07947	0,00056
2	-0,71213	-0,68227	0,02986	2	-0,15832	-0,15721	0,00111
3	-0,98686	-0,94487	0,04199	3	-0,65047	-0,64586	0,00461
5	-1,3779	-1,3178	0,06010	10	-0,71213	-0,70708	0,00505
10	-1,701	-1,6237	0,0773	100	0,00000	0,00000	0,00000
37	0.013776	0.10523	0,091454	197	1,97690	1,96540	0,01150
38	1,0683	1,1298	0,0615	198	2,01290	2,00060	0,01230
39	1,8255	1,8309	0,0054	199	2,02080	2,00790	0,01290

In the following figure (see,Fig.1) the finite difference solutions of the problem (2.1)-(2.2) are graphically compared with the exact solution (2.7).

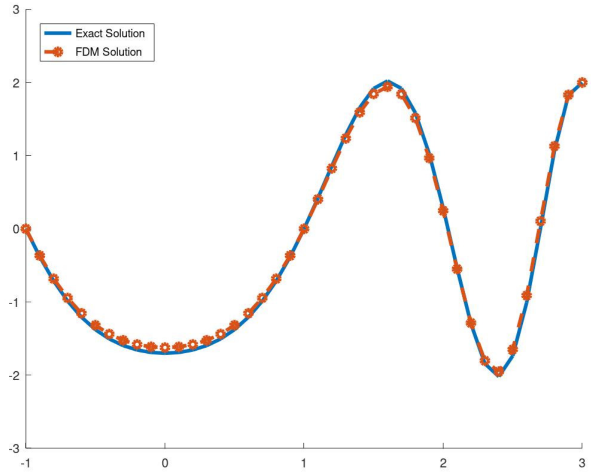

Figure 1: Graph of the FDM-solution and exact solution for the problem (2.1)-(2.2)

Now we are ready to find a finite difference solution of the main problem (2.1)-(2.3). By using an uniform cartesian grid $x_i = -1 + ih, \quad i = 0, 1, \ldots, 299$, where $h = \frac{3-(-1)}{299}$ and taking into account the transmission conditions (2.3) we have two additional linear equations

$$y_{149} - 2y_{150} = 0 \tag{2.8}$$

and

$$y_{148} - y_{149} - 3y_{150} + 3y_{151} = 0 \tag{2.9}$$

The solution of the system of linear algebraic equations (2.6), (2.8), (2.9) can be found by using MATLAB/Octave. Moreover, we can show that the boundary-value-transmission problem (2.1) has unique solution, given by

$$y = \begin{cases} -6sin(1)csc(8)cos(x^2) + 6cos(1)csc(8)sin(x^2)] & x \in [-1, 1) \\ 2sec(9)(1 - cos(1)cos(8)sin(9))cos(x^2) + 2cos(1)csc(8)sin(x^2), & x \in (1, 3] \end{cases} \tag{2.10}$$

In the Figure.2 the finite difference solution of the problem (2.1)-(2.3) is graphically compared with the exact solution (2.10).

4

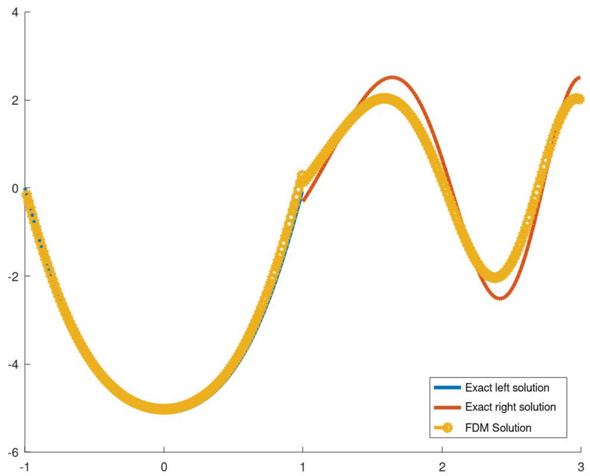

Figure 2: Graph of the FDM-solution and exact solution for the problem (2.1)-(2.3)

Remark 2.1. *As shown in Figure.1 and Figure.2 the error between the FDM and exact solution is decreases with increasing n.*

References

[1] K. E., Atkinson, W., Han , D., Stewart, (2011). Numerical Solution of Ordinary Differential Equations, In Numerical Solution of Ordinary Differential Equations.

[2] R.J., LeVeque, Finite difference methods for ordinary and partial differential equations, steady-state and time-dependent problems. Vol. 98. Siam, 2007.

[3] P. K., Pandey, Finite Difference Method for Numerical Solution of Two Point Boundary Value Problems with Non-uniform Mesh and Internal Boundary Condition, General Letters in Mathematics,(2018), 4(1), pp. 6–12.

[4] Roul, Pradip, VMK Prasad Goura, Numerical solution of doubly singular boundary value problems by finite difference method, Computational and Applied Mathematics 39.4 (2020): 1-25.

FREQUENCY ANALYZING WITH CLASSIC CAESAR CRYPTOGRAPHY METHOD

Yucel Inan[1]

[1] Department of Computer Engineering, Near East University, Nicosia, Cyprus

yucel.inant@neu.edu.tr,

Abstract

In this study, Cryptography systems are emphasized in order for the messages to be encrypted, transmitted and decoded according to the specific system. Caesar Cryptography is one of the easy to solve ciphers in Cryptography. For the frequency analysis of an encryption method, the basic operating principle of the encryption method is based on the frequency of use of letters in the alphabet to which the plain text to be encrypted belongs. In addition, the study aims to reveal the weaknesses and strengths of the software by examining the reliability of the letters against frequency analysis for the tests and the results are evaluated on the graphs and tables.

Keywords: Caesar Cipher, Cryptanalysis, Ciphered Text, Frequency Analysis Attacks, Letter weakness and strength of the Ciphered Text, Python.

1 Introduction

Security is a necessary element for human beings to survive [1]. Privacy is also a prerequisite for ensuring security. That is why security and privacy are two concepts that complement each other. The existence of a society is only proportional to the security it can provide. As security decreases, the threat and danger increase. The essence of security is based on “knowledge". In its broadest definition, it is called Cryptology, which is the combination of all the open and confidential messages made for the purpose of securing the security, the secure transmission of the messages and the deciphering of the transmitted messages, the **logos** which means secret in Greek, meaning **Cryptos** and science [2]. Information is becoming a more valuable issue today. The general problem of communication and informatics is information security. Virtual shopping, individual banking transactions and e-mail traffic over the Internet force the Internet to become a safer environment. This is to focus on how to achieve a high level of information and communication security. This is the Cryptography science that will provide. The aim here is to understand how to use letter frequency analysis to break certain ciphers. Monogram Frequency counts, Caesar ciphers type ciphers are more effective. The same plain letters are encoded in the same cipher letter. Although the letters have changed, the base letter frequencies do not change. If the plain letter is five frequencies, its cipher letter becomes 5 frequencies. This article aims to test Cryptographic reliability of the Caesar encryption algorithm. The Caesar cipher is easily solved by detecting the frequency of occurrence of each character and then comparing its own frequency to the frequency of the letter in the original message language, observing what it represents. The reliability of the comparisons between ciphers letter and plain letters were analyzed using the Python 2.7.15 language.

Cryptography is all of the techniques used to transform readable information into a form that cannot be read by undesired parties [3]. In Fig.1, the algorithm " **This is a secret message**" of the article is applied with the Cryptographic algorithm which is the subject of the article. The purpose of Cryptography is to ensure and protect the confidentiality of important information [4].

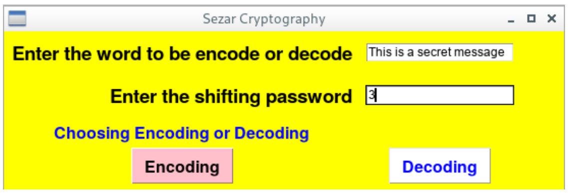

Fig.1. "Wklv lv d vhfuhw phvvdjh" cipher text is generating when the plain alphabet is shifted to 3 character left.

2 Related Works

Cryptanalysis has been the subject of many investigations. One of the studies published was that [5]. Emphasis is placed on the use of Genetic Algorithms in the Cryptanalysis of classical ciphers. Another publication in, Genetic Algorithm approach was applied for statistical analysis of English language documents in 2015 In [6] author. This publication has implemented encryption and decryption Caesar cipher using the Neural Network in 2014 [7]. This work Using Artificial Neural Network, it provides security for strength encryption against attacks[8].

3 Cryptanalysis

Cryptanalysis is the method of finding the correct text using some techniques from the encrypted, meaningless text[9]. Various methods have been tried to reach the hidden information. Some of these methods are attack techniques that are used against the Cryptographic methods, These are Known Plain text Attacks, Chosen Plain text Attacks, Chosen Cipher text Attacks, Brute Force Attacks, Letter Frequency Attacks, Man in the middle Attacks, Differential Attacks [10].

3.1 Cryptanalaysis of a Caesar Cipher Algorithm

Cryptanalysis, the science of deciphering the encrypted message, has emerged in an effort to break the simple ciphers. Simple cipher systems to solve all the cipher alphabets in an easier way to solve mathematics, statistics and linguistics should have sufficient knowledge of the fields. It is important to carry out important studies in these areas required for Cryptanalysis[11].The fact that these disciplines were developed led to the discovery of

Cryptanalysis by the famous Arab scientist and the first works in this field were written. The first of these is "*Manuscript on Deciphering Cryptographic Messages*" written by Al-Kindi, who lived in the 9th century and is known as the philosopher of Arabs. The first time on Cryptanalysis was the concept of frequency analysis. Al-Kindi technique to solve an encrypted message written in the same language long enough to find a text and calculate the frequency of each letter is necessary to use. The most commonly used letter in the text corresponds to the most commonly used letter in the encrypted message. The same is done for other letters in the order. After this is finished, the letters in the message will appear. Al-Kindi called this Cryptanalysis method frequency analysis [12].

3.2 Calculation of Letter Count

The algorithm was tested using the English text. The text used for the letter frequency consists of all the works of the cipher text. By using python language, this plain text is converted to cipher text by Caesar's cipher method. The spaces in cipher text are calculated without changing the punctuation marks. The count letter of Frequency and Analysis for Caesar Cipher Method has the following functions. Cipher Text Field, Letter Frequency and Letter Frequency Analysis, Delete button, Exit button. Fig.2 is shown Frequency letter count of cipher text.

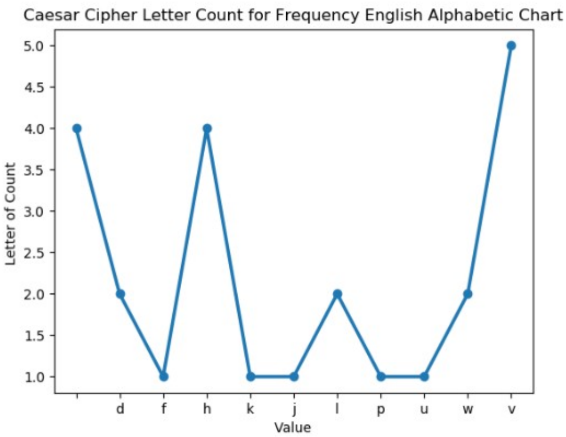

Fig.2. The relative number of letters in the y axis, the letters used in the x axis are shown.

Cipher text "Wklv lv d vhfuhw phvvdjh" is written in the top box. Clicking on the Letter Frequency button will generate a graph showing the letter frequency above. At this stage, the length of the cipher, the frequency of character formation, working time, interface are presented. This letter frequencies will help you to decode the cipher text. If the language of the message is known, the most common letter in that language and the cipher in the hand is replaced with the most common letter in the assumption that the cipher can be solved.

3.3 Letter Frequency Analysis

One of the Cryptanalysis methods is to detect the character frequency in the cipher text. Therefore, in order to test the cipher text, the results were analyzed. Frequency analysis is the process of counting the number of different encrypted text characters to decrypt the information. The English alphabet also has 26 letters. However, each one does not appear to be equal in the English text. E, T, A, O, I, N are the six most commonly used letters in English. V, K, J, X, Q, Z are rarely used in English text. As the different letters of the alphabet appear more or less often than others, we can perform some frequency analysis of an encrypted message to help us encrypt it. The English letters are in the frequency values expressed in Table1, the following frequency values are taken from Table1[1], the website and also the frequency result of the cipher text are shown on Table2.

Table1. Relative Frequencies of English alphabet letters values.

Letter	a	b	c	d	e	f	g	h	i	j	k	l	m	n	o	p	q	r	s	t	u	v	w	x	y	z
Freq %	8.1	1.4	2.7	4.2	12.7	2.2	2.0	6.0	6.9	0.1	3.8	4.0	2.4	6.7	7.5	1.9	0.1	5.9	6.3	9.2	2.7	1.0	5.3	0.2	4.0	0.1

Table2. Letter Frequencies values used in ciphered text.

Letter	a	b	c	d	e	f	g	h	i	j	k	l	m	n	o	p	q	r	s	t	u	v	w	x	y	z
Freq	0	0	0	2	0	1	0	4	0	1	1	2	0	0	0	1	0	0	0	0	1	5	2	0	0	0
Freq %	0.0	0.0	0.0	8.0	0.0	4.0	0.0	16.0	0.0	4.0	4.0	8.0	0.0	0.0	0.0	4.0	0.0	0.0	0.0	0.0	4.0	20.0	4.0	0.0	0.0	0.0

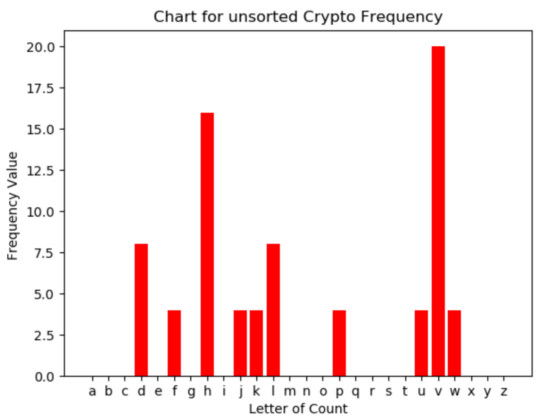

Fig.4. Ciphered text frequency analysis is shown in y axes, relative frequency percentage.

This designed ciphered text is calculated from frequency analysis on the graphical user interface. The graph is compiled by taking the English written text of the cipher.

1 http://pi.math.cornell.edu/~mec/2003-2004/cryptography/subs/frequencies.html

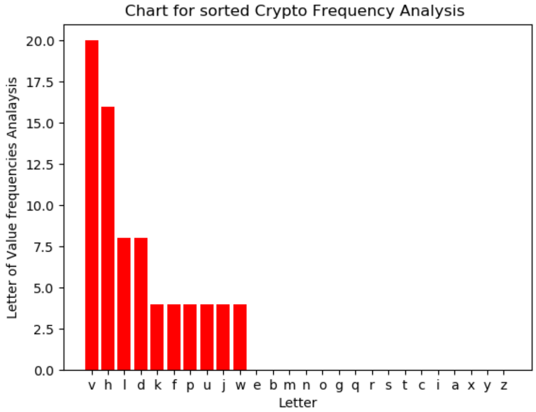

Fig.5. Ciphered text frequency analysis is shown in y axes, relative frequency percentage.

When “Frequency Analysis” button is clicked, there will be a graph showing the figure 5 frequency analysis of the above figure. This illustrates the graphical formation, the 24 characters of the cipher text, the length of the word, the frequency of the use of letters, the run time is presented in this graphical interface.At this stage, the formula = (f/n)*100 formula is used. f: Frequency of the letter, n: The total number of letters in the cipher text is n = 24. For example, the letter v is displayed 5 times, the frequency in the formula is the only visible number of the letter v, ie (5/24) * 100 = 20. The letter ‘E’ is the most common letter used in the English Language. The most common letter used in the ciphered text can also be matched with ’V' or not matched. Some predictions can do made and the text can be decoded by checking whether the letters v, h, l, d would create the most value according to how often the letters can be used, as shown in Table 4, Table 5, Table 6, Table 7, according to Fig.5. As a result, one or two trials can be obtained. The strengths and weaknesses of the algorithm are tested and the results are shown on graphic.

Table3. Letter Frequency Analysis Matching Estimation.

Matching1	e → v	t → h	a → d	o → l	i → f	n → j
Matching2	e → h	t → v	a → d	o → f	i → l	n → j

Table4. Matching1 Ciphered text is “Wklv lv d vhfuhw phvvdjh”

W	**k**	**l**	**v**		**l**	**v**		**d**		**v**	**h**	**f**	**u**	**h**	**w**		**p**	**h**	**v**	**v**	**d**	**j**	**h**
			e			e		a		e									e	e			
		i			i			a			e			e				e			a		e

Wk iv iv a v efuew pe v v aje

Maybe “is”? Maybe “s”?

Table5. Matching2

W	**k**	**l**	**v**		**l**	**v**		**d**		**v**	**h**	**f**	**u**	**h**	**w**		**p**	**h**	**v**	**v**	**d**	**j**	**h**
		i	s		i	s		a		s	e			e				e	s	s	a		e

W k i s is a se f u e t p essag e

Maybe “m”

Table6. Matching3

W	**k**	**l**	**v**		**l**	**v**		**d**		**v**	**h**	**f**	**u**	**h**	**w**		**p**	**h**	**v**	**v**	**d**	**j**	**h**
		i	s		i	s		a		s	e			e			m	e	s	s	a		e

??is is a se??e? Messa?e

Maybe “This”? Maybe “t”? Maybe “g”?

This is a se??et Message

Maybe “secret”?

This is a secret Message

3.4 Program Code

In the below Code, This code purpose of the given is to apply Letter Frequency Analysis. Python code, Analysing the Count Letter and Frequency of Encrypted Message.

```
Program Function letter_Frequency(event=None):
    k=""
    for i in message:
        if i.isupper():
            i=i.lower()
        if i.isdigit():
            k=k+str(i)
            continue
```

```
    if i<0:
        k=k+""
        continue
    k=k+i
d={}
for i in k:
    if i not in d:
        d[i]=1
    else:
        d[i]+=1
freq=[]
for i in range(26):
    freq.append(0)
for i in range(len(k)):
    if k[i] >='a' and k[i]<='z':
        sayi=ord(k[i])-ord('a')
        freq[sayi]=freq[sayi]+1

    alphabet=['a','b','c','d','e','f','g', 'h','i','j','k
        ,'n','o','p','q','r','s','t','u','v','w','x','y','z']
n=len(message)+0.0
freq_list=[]
for x in freq:
    freq_list.append((x/n)*100)

for i in range(len(freq_list)):
    for j in range(len(freq_list)):
        if freq_list[i]>freq_list[j]:
            temp=freq_list[i]
            freq_list[i]=freq_list[j]
            freq_list[j]=temp

            tempc=alphabet[i]
            alphabet[i]=alphabet[j]
            alphabet[j]=tempc
list1=[]
list2=[]
for i in range(len(alphabet)):
    list1.append(alphabet[i])
    list2.append(freq_list[i])
```

4 Conclusions

In this study, frequency analysis in the Caesar cipher method was examined. A letter frequency attack is applied to evaluate the encryption strength of the method. Longer cipher text give a better approximation to the letter frequency of the original language used, and as a result, each character of the cipher text is determined by comparing the frequencies of the letters in the cipher text and in the original language. For this reason, the encryption method can only guarantee the security of the data for a limited period of time.

References

1. Burman, S.: Cryptography and security - future challenges and issues, 15th International Conference on Advanced Computing and Communications (ADCOM 2007), pp. 547-551, Guwahati, Assam (2007).
2. Gunnels, P, E.: The mathematics of cryptology, http://people.math.umass.edu/~gunnells/talks/crypt.pdf, last accessed 2019/07/26.
3. Inan Y.: Comparing Image Distortion of LSB. In: Aliev R., Kacprzyk J., Pedrycz W., Jamshidi M., Sadikoglu F. (eds) 13th International Conference on Theory and Application of Fuzzy Systems and Soft Computing - ICAFS-2018. Advances in Intelligent Systems and Computing, vol. 896, Springer, Cham (2018).
4. Purnama B., Ah, H, R.: A new modified caesar cipher cryptography method with legible ciphertext from a message to be encrypted. Procedia Computer Science, 59, 195-204 (2015).
5. Al-Janabi, S, T., Al-Khateeb, B., Abd, A. J.: Intelligent techniques in Cryptanalaysis: Review and Future Directions, UHD Journal of Science and Technology, 1(1), 1-10 (2017).
6. Bhasin, H., Khan, A, B.: Cryptanalysis Using Soft Computing Techniques, Journal of Computer Sciences and Applications, 3(2), 52-55(2015).
7. Singh, J., Yadav, S, S.: Implementation of Caesar Cipher and Chaotic Neural network by using Matlab Simulator, International Journal of Recent Development in Engineering and Technology, 2(6), 16–20 (2014).
8. Volna, E., Kotyrba, M., Kocian, V., Janosek, M.: Cryptography based on Neural Network, In: Proceedings, 26th European Conference on Modelling and Simulation, pp. 386-391. European Council for Modeling and Simulation, Koblenz, Germany (2012).
9. Sun, Y., Chen, L., Xu, R., Kong, R..: An image encryption algorithm utilizing julia sets and hilbert curves, Plos One 9(1), 1-9 (2014).
10. Patni, P.: A poly alphabetic approach to ceasar cipher algorithm. International Journal of Computer Science and Information Technologies 4(6), 954-959(2013).
11. Mayur, T., Saraswat, L.: A review on common encryption techniques to brute force shielded technique: Honey encryption, International Journal for Scientific Research and Development 3(12), 203-204(2016).
12. Jothy, K, A., Sivakumar, K., Delsey, M, J.: Efficient cloud computing with secure data storage using aes and pgp algorithm, International of Computer Science and Information Technologies 8(6), 582-585(2017).

An Atomistic Investigation on the Thermodynamics of Indo-Cyanine-Green using DFT and Molecular Dynamics

Farid Alidoust[1], Ali Rostami[1, 2] and Hamit Mirtaghioglu[3]

[1]Photonics and Nanocrystals Research Lab (PNRL), University of Tabriz, Tabriz 5166614761, Iran

[2]SP-EPT Lab., ASEPE Company, Industrial Park of Advanced Technologies, Tabriz, 5364196795, Iran

[3]Faculty of Science and Literature, Department of Statistics, University of Bitlis Eren, Bitlis, Turkey

Abstract- Over recent years, photodynamic therapy and medical imaging techniques such as OCT and Photo-Acoustics have been instrumental in identifying and treating cancer patients. Among the methods proposed to increase the accuracy and depth of imaging, label-based methods have a special place. One of the well-known markers in this field is the ICG Dye. Despite years of use, there is still little data on some of its thermodynamic properties and its usage in the imagery of tumors is not accurate enough yet. Access to such physical parameters can help us identify cancer patients more quickly and accurately. In this research, we will first introduce and identify this marker and then, using numerical methods, density functional theory, and molecular dynamics, we will study its thermodynamic properties to obtain HOMO/LUMO orbitals energy, Dipole Moment which is a figure of merit for hydrophobicity, Polarizability, and most importantly its heat-capacity. To evaluate and validate employed numerical methods, we compared obtained results for the absorption spectrum with previous practical values. Finally, in this paper, we will present two mathematical models for the estimation of the temperature-dependent heat-capacity parameter of the ICG molecule.

Keywords: ICG, Photo-thermal, heat-capacity, DFT, MD.

Cancer is the principal reason for mankind's demise. That somehow can be managed with chemotherapy, surgery, and other techniques. Photo-dynamic-therapy, which requires the intake of photosensitizing medicines and sequential exposure of the body to electromagnetic irradiation, has appeared as a state-of-the-art therapy scheme for the cure of different tumors and more different diseases [1], [2]. Because of the selective nature of medicine-intake, together with the simple mechanism of light irradiation on the tissue involved with cancer, this method brings on the possibility of provoking sufficient cellular toxicity within cancerous cells and confined disturbance to the neighboring healthy tissues [3]. Hence, photo-dynamic-therapy has better characteristics against traditional tumor cures such as radiotherapy or chemotherapy. That is accurate, passive, light-activated, and has negligible secondary induced repercussions. Over the past decades, this method has been effectively utilized as a therapy for different varieties of cancers. However, quite a few photo-dynamic-therapy sensitizers have been recommended for severe medical applications up to date. Fluorescence imaging is an important way of detection and identifying tumor position. Fluorescent imaging will support the specialist to adequately envision the tumor so that tumor resection can be further adequate and flawless. This demands fluorophores that can absorb and then emit within the spectral region from 650 [nm] towards 1100 [nm]. The foremost intent behind imaging-based surgery is to determine all achievable tumors in the operating field. Fluorescent dyes that absorb and emit at higher wavelength closer to infra-red radiation can access deeper tissues, consequently enabling the surgeon to imagine the tumor beyond what can be observed on the outside [4]–[6]. Some of the fluorescent dyes can additionally develop reactive oxygen species (ROS) upon irradiation with light. Porphyrin has become a famous molecule employed for fluorescence imaging due to its absorption near 690 [nm]. Heptamethine cyanine dyes are a class of molecules with the capability to absorb in the NIR band. These dyes have aromatic and conjugated chromophores that support for long-wavelength absorption. Indocyanine green (ICG) is an instance of a heptamethine cyanine dye that is approved by the FDA and utilized in various medicinal examination methods (Figure 1) [7], [8]. Attaching various metallic nanoparticles into the porphyrin ring, the absorption spectrum can get redshift or create new absorption peaks providing more extensive tissue penetration or energy absorption in a wavelength of interest [9]. ICG absorbs near 790 [nm], making it a molecule of interest for the utilization of fluorescence imaging. The structure of ICG can directly be used as a template for the design of molecules with absorption wavelength around 800 [nm] or longer. Photodynamic therapy (PDT) is a therapeutic approach employed to heal several skin diseases and also recently cancer. The usage of PDT requires the presidency of a photosensitizer inside the blood flow, a photon emitting source, and the ubiquity of tissue oxygen at the position of interest. If the light source is employed, the photosensitizer is excited to a triplet state during absorption and inter-system exchange. Once in the triplet state, phosphorescence occurs. The energy from phosphorescence converts the tissue oxygen from the triplet to singlet state. Our intention here is to predict the thermomechanical properties of the so-called indo-cyanine-green molecule which is used as identification dye in biology and medical applications. ICG is a molecule identified to own the optical characteristics required in fluorescence imaging and PDT. It is well-known that nanoparticles smaller than one hundred nanometers can be better transported to tumor positions using the “enhanced permeability retention (EPR)” effect. [10]

1.1. Reasons for adopting ICG in photo-dynamic-therapy

ICG dye has a half-life of about five minutes in the body. ICG is usually at 1% of its infused concentration following 20 minutes, obtaining reiterated measurements on 20 minute period is possible. This presents ICG as an excellent tracer for employment in an operating room where the fluid administration of a subject may be essential. [11]–[13]. ICG molecule is a tri-carbo-cyanine dye with a molecular weight of 774. Its top optical absorption, when attached to plasma, is 805 NM, and prominent absorption is not existing at 820nm. ICG connects to plasma proteins with high affinity, causing it approximately only an intravascular material, solely being eliminated in the liver. It is owing to this lack of leakage that causes ICG spectroscopy such a decent method. The molecular conformation of ICG is presented in *Figure 1* [9], [11], [12], [14], [15]. ICG’s insignificant half-life time, while a great benefit, further restricts its precision. If inadequate perfusion exists in a patient, uniform mixing of ICG in the bloodstream may not occur before most of the tracer has been excluded by hepatic removal [16].

1.2. Photodynamic Therapy

Cellular destruction affected by the impact of electromagnetic irradiation and chemical compounds was introduced over fifty years ago [17]. A suggestion for the utilization of malignant-cell localizer and photo-toxic features of porphyrins varieties to be adopted in the therapy of tumors was reported in 1972 [18]. Three years later, the first example of the treatment was announced for experimental animal tumors employing PDT. A few months past, a report confirmed that PDT healing might eradicate tumor cells from human bladder relocated inside mice [3], [19]. After several years, effective therapy of a big group of patients with PDT was reported [20]. In the meantime, a vast amount of researches has been written in care of the preliminary efficacy of PDT for the medication of different cancers.

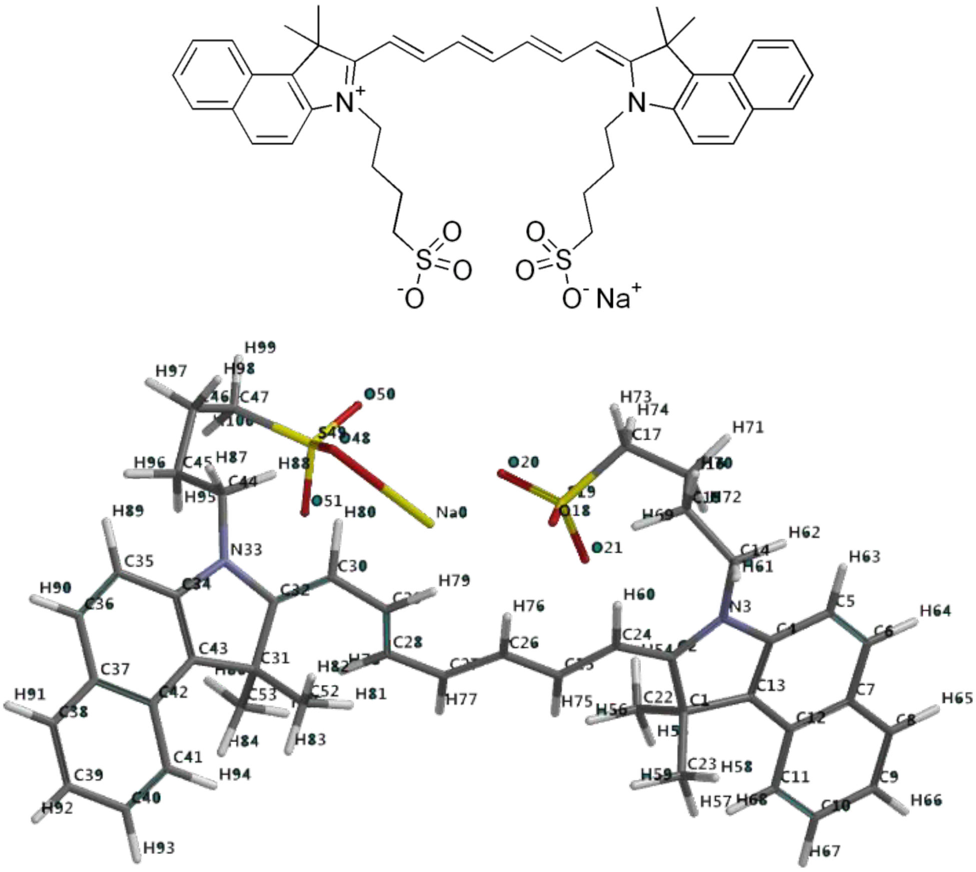

Figure 1. Indocyanine green (C43H47N2NaO6S2), 2D structure (a) and a 3D Conformer (b)

1.3. Recovering ICG to its ground-state

Assessing the quantum-yield (Φ) of any photo-sensitizer in the excited triplet state is essential in Photo-dynamic-therapy treatments. Various methods realized for that as well as triplet-sensitized isomerization [21], delayed fluorescence analyses [22], fluorescence extinction [23], time-resolved photo-thermal procedures [24], electron spin oscillation [25], and laser direct absorption and comparative actinometry [26]. Though, these approaches have their drawbacks as they usually rely on exact measures and conversely analyses conducted under proportional form such as the correlation of fluorescence amplitudes. A simplistic scheme toward the measurement of FT, which utilizes momentary dynamic forms of the molecule relaxation to its ground state has extended so as a result, circumvented the necessity of pertinent estimations [27]. Figure 2 explains a system of ground-state bleaching phases. In the absence of external stimulation, each molecule is within its ground state (Figure 2a). On the arrival of the pump pulse, specific molecules become excited and proceed on to excited singlet state ensuing a reduction of the particles within the ground state, which is shown in Figure 2b.

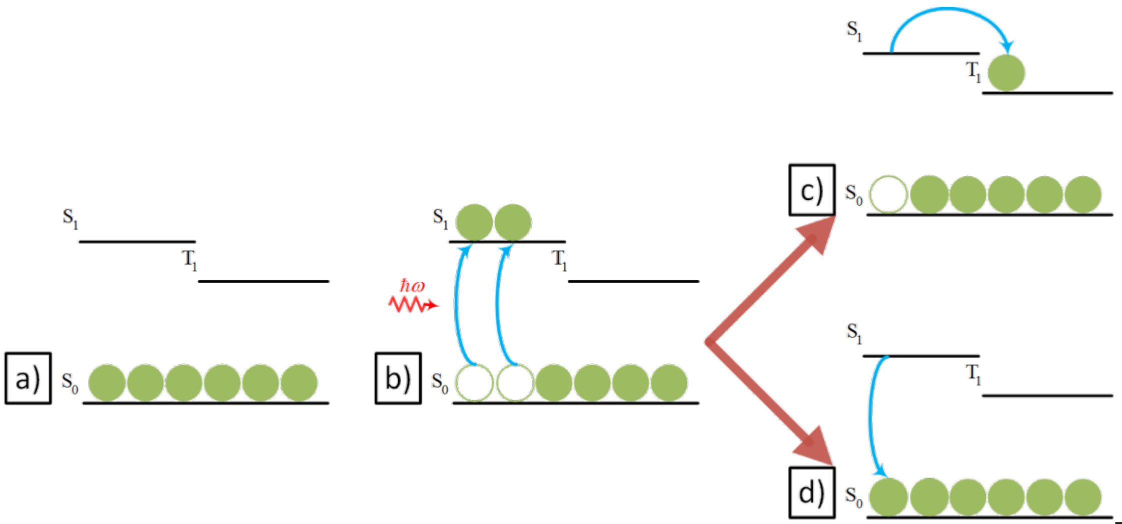

Figure 2. ICG Molecule interaction with its ground-state after excitation

That will cause acceleration to a drop in the absorption in particular frequencies wherein the molar quenching factor of the ground-state remains significantly more extensive concerning the excited one. Consequently, a rejecting force is formed. This restoration from the rejecting force concurs with the recovery of the stimulated molecules away into the ground state (Figure 2d). Full restoration will take place if each molecule goes to S0 state in the time of the evaluation. Nevertheless, full restoration cannot regularly be obtained if a considerable amount of molecules move into the long-lasting T1 phase throughout a radiationless action named intersystem crossing (Figure 2c).

1.4. Objectives of the research

Accurate imaging of cancerous tumors in the first stage requires precise hardware equipment. Also, in various cancers, various methods such as CT, ultrasound, and also in recent years, PhotoAcoustic imaging can be used. In photon-based imaging, the use of molecules such as ICG can increase the accuracy and resolution of the image. To increase the accuracy and depth of imaging, access to accurate thermodynamic characteristics of this molecule as well as its heat capacity is of special importance, because it can be used to perform finite element computer simulations and improve computer imaging from PhotoAcoustic signals. In this article; our goal is to quantitatively analyze the ICG molecule through DFT and molecular dynamics methods and obtain values related to the thermodynamic properties of this molecule. In the following sections of this paper, we will first deal with the mathematics behind heat capacity and then study the properties of molecules and extract heat capacity using DFT and MD. Finally, we will present two simple mathematical models, including a polynomial model and an exponential model to obtain the heat capacity of the ICG molecule relative to temperature.

Mathematics behind the Thermodynamics

In a system with constant N, V, during thermal-equilibrium, the least possible allowed energy of the system is the Helmholtz free energy (F) which may be represented as the partition-function Z in the form of $F = -k_B T \ln Z$ [28]–[30]. As a vibrational effect F_{vib}, it's better to initially analyze the partition-function intended for an individual harmonic-oscillator with a frequency of ω_i [29], [31].

$$Z_i = \sum_n^{\infty} e^{-\beta E_n} = \sum_i^{\infty} e^{-\beta\hbar\omega_i\left(n+\frac{1}{2}\right)} = \frac{e^{-\beta\hbar\omega_i/2}}{1-e^{-\beta\hbar\omega_i}} = \frac{1}{2\sinh\left(\frac{\beta\hbar\omega_i}{2}\right)} \tag{1}$$

Then within N lattice atoms, partition function could be as follows.

$$Z = \prod_i^{3N} Z_i = \prod_i^{3N} \frac{1}{2\sinh\left(\frac{\beta\hbar\omega_i}{2}\right)} \tag{2}$$

Where $\beta = 1 / k_B T$. Replacing that inside the mentioned relation F provides the subsequent equation for F_{vib} [29], [31].

$$F_{\mathrm{vib}} = k_B T \sum_i^{3N} \ln\left[2\sinh\left(\frac{\beta\hbar\omega_i}{2}\right)\right] \tag{3}$$

The Helmholtz energy, which acts as a function of heat and the volume of the system, could be represented as the addition of vibrational free energy $F_{vib}(T,V)$ and internal energy $U(V)$ [31].

$$F(T,V) = U(V) + k_B T \int_0^{\infty} d\omega \ln\left[2\sinh\left(\frac{\beta\hbar\omega}{2}\right)\right]\rho_V(\omega) \tag{4}$$

Where, $\rho_V(\omega)$ is the absolute VDOS for the system of volume V. As F decreases, if the system remains within its equilibrium form over constant volume and temperature, the thermal enlargement of the system $V(T)$ can be defined by decreasing F concerning V at a particular temperature T. The average value of pressure is linked with F as [30]:

$$P = -\left(\frac{\partial F}{\partial V}\right)_T \tag{5}$$

That indicates we may additionally ascertain the Gibbs free energy $G = F + PV$ after determining $V(T)$ and $F(V,T)$.

1.5. Calculating the heat capacity

Within a fixed volume, the heat capacity C_V is provided with:

$$C_V = \left(\frac{\partial U}{\partial T}\right)_V \tag{6}$$

Simulations usually compute the total internal energy U in a relaxed formation of a molecule's geometry, expressing the calculations are parameterized with dimension rather than temperature T. Still, for the vibrational free energy preceding, the heat-capacity may be re-declared as an integration of the VDOS derived from the dynamical-matrix computation. In a mechanical system with constant N and, V the total-internal-energy U will be as the equation below [30]:

$$U = \frac{\sum_n^{\infty} E_n e^{-\beta E_n}}{\sum_n^{\infty} e^{-\beta E_n}} = -\frac{\partial \ln Z}{\partial \beta} \tag{7}$$

Replacing the yields from equation (1), we acquire Eq. (8).

$$\ln Z = \ln \prod_i^{3N} \frac{1}{2\sinh\left(\frac{\beta\hbar\omega_i}{2}\right)} = -\sum_i^{3N} \ln\left[2\sinh\left(\frac{\beta\hbar\omega_i}{2}\right)\right] \tag{8}$$

That generates the latter formulation for the internal-energy

$$U = \sum_i^{3N} \frac{\hbar\omega_i}{2} \coth\left(\frac{\beta\hbar\omega_i}{2}\right) \tag{9}$$

Eventually, the temperature derivative returns the heat-capacity in a fixed volume.

$$C_V = \frac{\partial U}{\partial \beta}\frac{\partial \beta}{\partial T} = k_B \sum_i^{3N} \left(\frac{\beta\hbar\omega_i}{2}\right)^2 \operatorname{csch}^2\left(\frac{\beta\hbar\omega_i}{2}\right) \tag{10}$$

Eq. (10) conversely, can be represented in the integral mode of Eq. (11).

$$C_V(T,V) = k_B \int_0^{\infty} d\omega \left(\frac{\beta\hbar\omega_i}{2}\right)^2 \operatorname{csch}^2\left(\frac{\beta\hbar\omega_i}{2}\right) \rho_V(\omega) \tag{11}$$

Eq. (12) determines the heat-capacity in a constant pressure phase.

$$C_P = \left(\frac{\partial H}{\partial T}\right)_P \tag{12}$$

In equation (12), $H = U + PV$ denotes the total heat of the system, we alternately determine the residuum of $C_P - C_V$ and append the earlier result for C_V. Using the thermodynamic characteristics concerning internal-energy and total heat, we can write Eq. (13).

$$\begin{aligned} dH &= VdP + TdS + \mu dN \\ dU &= TdS - PdV - \mu dN \end{aligned} \tag{13}$$

With fixed pressure and volume in sequence (for constant N), Eq. (14) can be listed.

$$\begin{aligned} C_P &= \left(\frac{\partial H}{\partial T}\right)_P = T\left(\frac{\partial S}{\partial T}\right)_P \\ C_V &= \left(\frac{\partial U}{\partial T}\right)_V = T\left(\frac{\partial S}{\partial T}\right)_V \end{aligned} \tag{14}$$

Equation (15) represents the entropy as a function of volume and temperature.

$$S = \left(\frac{\partial S}{\partial V}\right)_T dV + \left(\frac{\partial S}{\partial T}\right)_V dT \tag{15}$$

Equation (16) calculates the volume as a function of pressure and temperature.

$$V = \left(\frac{\partial V}{\partial P}\right)_T dP + \left(\frac{\partial V}{\partial T}\right)_P dT \tag{16}$$

Therefore, by employing the Maxwell relation, Eqs. (17) and (18) will be derived [30].

$$\left(\frac{\partial P}{\partial T}\right)_V = \left(\frac{\partial S}{\partial V}\right)_T \tag{17}$$

$$S = \left(\frac{\partial P}{\partial T}\right)_V \left[\left(\frac{\partial V}{\partial T}\right)_P dT + \left(\frac{\partial V}{\partial P}\right)_T dP\right] + \frac{C_V}{T} dT \tag{18}$$

Which outcomes the Eq. (19).

$$C_P = T\left(\frac{\partial S}{\partial T}\right)_P = T\left(\frac{\partial P}{\partial T}\right)_V \left(\frac{\partial V}{\partial T}\right)_P + C_V \tag{19}$$

The partial derivative $(\partial P \,/\, \partial T)_V$ may be revised as Eq. (20) [30]

$$\left(\frac{\partial P}{\partial T}\right)_V = -\frac{(\partial V \,/\, \partial T)_P}{(\partial V \,/\, \partial P)_T} \tag{20}$$

Which can turn into Eq. (21).

$$C_P = C_V - T\frac{(\partial V \,/\, \partial T)_P^2}{(\partial V \,/\, \partial P)_T T} \tag{21}$$

The equation as mentioned earlier is generally formulated with the expression of the thermal-expansion factor α_V in Eq. (22).

$$\alpha_V = \frac{1}{V}\left(\frac{\partial V}{\partial T}\right)_P \tag{22}$$

From Eq. (23) one can calculate the isothermal bulk-modulus (B_T)

$$B_T = -V\left(\frac{\partial P}{\partial V}\right)_T \tag{23}$$

Equation (24) delivers the ultimate intended goal [28], [30].

$$C_P - C_V = VT\alpha_V^2 B_T \tag{24}$$

The heat capacity is described with representing the ICG molecule (system) being a combination of quantum harmonic oscillators, whose frequencies are defined employing the VDOS [32]. The specific heat-capacity is shown in Eq. (25, which is a function of temperature:

$$C_{\mathrm{v}}(T) = \frac{h^2}{mk_{\mathrm{B}}T^2}\int_0^\infty \frac{\nu^2 \exp\ h\nu \,/\, k_{\mathrm{B}}T}{\exp\ h\nu \,/\, k_{\mathrm{B}}T\ \ -1\ ^2} S(\nu)\mathrm{d}\nu \tag{25}$$

In Eq. (25, k_B, h , m are physical constants corresponding to Boltzmann's constant, Planck's constant and the collective mass of the atoms inside simulation area, T is the temperature, ν is the vibrational frequency, and $S(\nu)$ is the VDOS. The VDOS is computed by obtaining a Fourier transform of the atomic velocities [33].

$$S(\nu) = \frac{2}{k_B T}\sum_{i=1}^{N}\sum_{\alpha=x,y,z} m_i s_i^\alpha(\nu) \tag{26}$$

$$s_i^{\alpha}(\nu) = \frac{\left|\int_0^{t_{max}} dt' v_i^{\alpha}\ \ t'\ \ e^{-i2\pi\nu t}\right|^2}{t_{\max}}$$

To model any related vibrations, the system dimension needs to be taken big enough to accommodate vibrational modes with long wavelengths. The logging period for collecting snapshots of the MD-Trajectory needs to be arranged such that the sampling rate is two times higher than the most significant vibrational frequency that must be incorporated in the DOS. For example, if the time step is 1 femtosecond and the logging interval is 20 steps, then the sampling rate is 50 THz, and the highest frequency in the DOS is 25 THz.

DFT and MD Analysis

Over recent years, novel numerical approaches have increased the limit of scientific studies widely, and the events that may be examined in the guidelines of chemistry, physics, etc. are fulfilled. The root of all the characteristics of matters is not anything but the interaction among the electrons within the external shells of atoms, recognized as valence electrons. To obtain a more profound insight into these interactions, one must perform electronic structure computations to understand fluctuations of resistivity or thermal responses, such as heat-capacities, critical temperatures (melt point, boil point ...), etc. The main objective is the study of electronic structure, which is to answer the Schrodinger equation, $\hat{H}\Psi = E\Psi$ relating to the M-electron structure of concern. The $\hat{H}$ operator is a Hamiltonian applied to the Ψ wavefunction and E denotes the absolute energy of the structure. The answer to the aforementioned in the ICG Molecule is practically unachievable using the abinit technique as the structure is holding more than ten electrons. As the fundamental purpose of nearly all DFT studies intends to obtain the electrons density at the ground-state, the DFT approach remains restricted to the formations of several hundreds of particles in the calculation software. The ultimate plan in the DFT method signifies to solve the Schrodinger equation in a setting, and as a result, rather than determining the wavefunctions Ψ, the Schrodinger equation has to be solved about the electron-density n. This concept decreases the challenge of electron many-body synergies toward an efficient one electron formula determined using the exchange-correlation functional that is determined by just the electron-density [34]. Molecular-dynamics computations are a valuable mathematical mechanism in the study of the characteristics of materials. In most instances, MD analysis assesses the trajectory of all atoms, considering synergies with neighboring atoms through an inter-atomic potential. In our research, Parallel computing capabilities are used employing MPI libraries. All of the simulation regions are spatially distributed among processor cores.

1.6. DFT and MD packages and Basis Sets

Traditionally, the Kohn-Sham equations have to be solved repetitively, employing a supplement set of basis-functions. The basis-sets used in GAUSSIAN, Quantum-Espresso, or VASP DFT packages allow two leading benefits: (a) administration of basis-set converging; (b) the computation of the appearing forces going on the atoms and of the stresses on the unit-cell using the Hellmann-Feynman theory [35]. The latter presents an approach to quantum ab-initio and MD computations for determining the development of the atoms over time. In this research, we used a set of mentioned software to first achieve the optimal geometry of the ICG or conformer molecule, after calculating its zero-point energy or ZPE and other thermodynamic properties such as enthalpy and entropy, using the calculations in the second section to obtain the value of the heat capacity parameter, we obtained C_v for a wide temperature range from 1 to 1000 degrees Kelvin. The methods used in the calculations are DFT, HF, and a set of basic functions used in molecular dynamics calculations such as PM3, PM6, MMFF, and SYBYL.

1.7. Statistical view

Concerning the computations at a fixed temperature, NVT ensembles are frequently employed. The NVT indicates the value of temperature T, volume V, and the abundance of particles N. The mathematical averaging of samples taken of these ensembles represent a model of the actual system. To maintain the heat steady inside an NVT scheme, a heat controller is organized within the computation process. In this paper for molecular dynamics studies, the Nose-Hoover thermostat is applied. If someone needs to create a system among a fixed amount of particles at fixed temperature and pressure, the NPT is better employed. While toward the case of NVE, the number of particles, energy, plus volume endures steady.

1.8. Methods and Boundary Conditions

Calculation demands for a molecular dynamics analysis are linearly proportionate to an abundance of particles and to the number of time-steps within the computation. In each calculation, we accomplished handling a cell of 101 atoms. Geometry optimization and energy estimations of the ICG molecule structure were achieved by adopting Blöchl's all-electron projector-augmented-wave technique[36][37]. Toward the processing of particle exchange and correlation, the generalized gradient approximation (GGA) was employed[38]. Every relaxation in the geometry was performed by the tetrahedron scheme by Blöchl's improvement applying the conjugate gradient algorithm. The relaxation process on the geometry is done until the difference of energy within two consecutive optimizations is smaller than 10^{-4} eV.

2.1. Molecular orbitals of ICG

To investigate the HOMO/LUMO gap using Quantum Espresso (pw.x) computation, that is possible to depict the Density Of States (DOS) and then estimate the extent of vacant states nearby the Fermi level (E=0). Though, if we solely expect an accurate numerical value, that can be achieved rather promptly with the "pw2gap" script found on the Q-E website. The wrap as mentioned earlier, flows within all the eigenvalues after the output, including the state of spin-polarization (spin up/down) and k-points. It then instantly reprints the energies of the HOMO and LUMO orbitals as well as, of course, the separation between them. Computed HOMO/LUMO energies for ICG molecule adopting different calculation techniques are represented in Table 1.

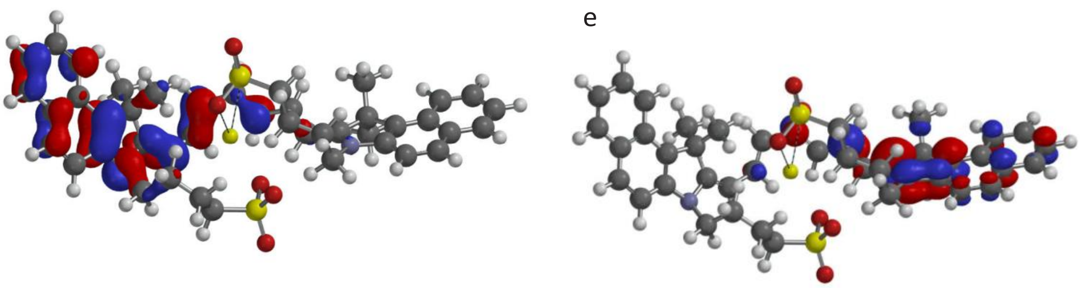

(a) (b)

Figure 3. HOMO(a) and LUMO(b) orbitals of ICG Molecule

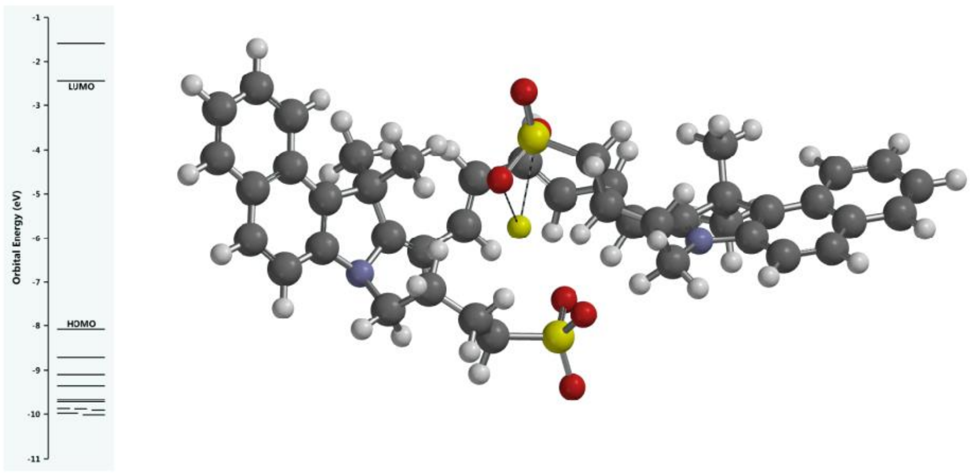

2.2. The Dipole Moment of ICG Molecule

Numerous particles have dipole moments because of the complex combination of negative and positive charge distributions on the different atoms. This phenomenon happens wherever the electron density is distributed unevenly among atoms. The first one to analyze molecular-dipoles widely was a physical chemist named *Peter J.W. Debye*. The electric dipole moment's unit is defined as (C·m) in the SI; though, a generally accepted unit in atomic physics is a unit called Debye (D) honoring Peter Debye's efforts. One Debye equals $3.34 \times 10^{-30}[C.m]$. Dipole moments happen if there is a separation of charge. Dipole moments result from diversity in electronegativity. A higher difference in electronegativity causes a larger value of the dipole moment. The dipole-moment is a postulate regarding the polarity of a molecule. Dipole moments in molecules are responsible for the behavior of a material in the existence of other molecules. Dipole moments can be seen in basic molecules such as water, and biomolecules such as proteins and also in our case ICG. Computed dipole moments for ICG molecule employing various calculation techniques are represented in Table 1.

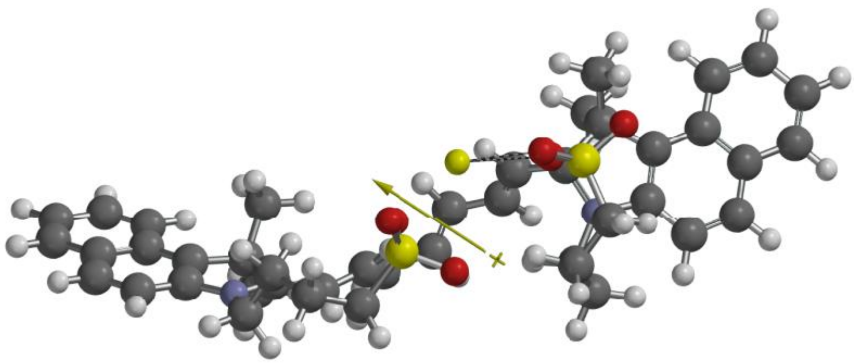

Figure 4. Electric Dipole Moment in ICG Molecule

Table 1. Computed thermo-dynamical properties of ICG using different Functional and computational methods

Computational Method	HOMO	LUMO	Dipole Moment	Polarizability	Thermodynamics				
					ZPE	S°	H° (au)	G°(au)	C_v
DFT/6-31G*	-8.2[eV]	-2.3[eV]	12.5D	101.42	2147.17 kJ/mol	925.75 J/mol°	0.5139	0.4085	585.69 J/mol°
H-F/6-31G*	-8.11[eV]	-2.4[eV]	12.27D	101.68	2310.53 kJ/mol	912.55 J/mol°	0.5073	0.3983	585.5 J/mol°
PM6	-8.09[eV]	-2.46[eV]	13.01D	102.24	2127.37 kJ/mol	939.25 J/mol°	0.5355	0.4289	601.72 J/mol°

PM3	-7.47[eV]	-0.53[eV]	14.15D	101.59	2016.10 kJ/mol	958.23 J/mol°	0.4904	0.3816	600.89 J/mol°
MMFF	-8.1[eV]	-2.36[eV]	12.06D	102.13	2049.58 kJ/mol	921.93 J/mol°	0.50468	0.3874	595.12
SYBYL	-8.4[eV]	-1.97[eV]	13.79D	102.49	2123.52 kJ/mol	976.56 J/mol°	0.5128	0.4085	603.01 J/mol°

2.3. ICG's Heat Capacity

DFT and Hartree-Fock calculations on the IGG molecule were performed using a basis set of 6-31G*; additionally, molecular-dynamics calculations have been conducted through PM3, PM6, MMFF, and SYBYL methods. The shown diagram of heat-capacity versus temperature (Figure 5) confirms the predictable limiting function between low and high temperatures. This is achieved, throughout determining the heat capacity, by representing the system as a group of quantum harmonic oscillators, whose frequencies are discovered from the vibrational density of states. Figure 6(a, b) exhibits the enthalpy and entropy of this molecule for a wide range of temperatures.

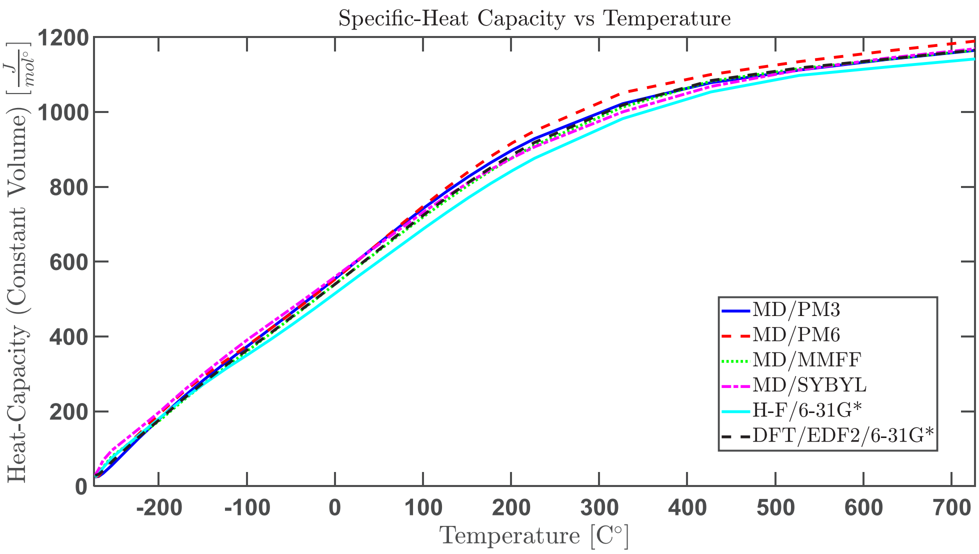

Figure 5. Temperature change and its effect on the specific heat capacity of ICG molecule

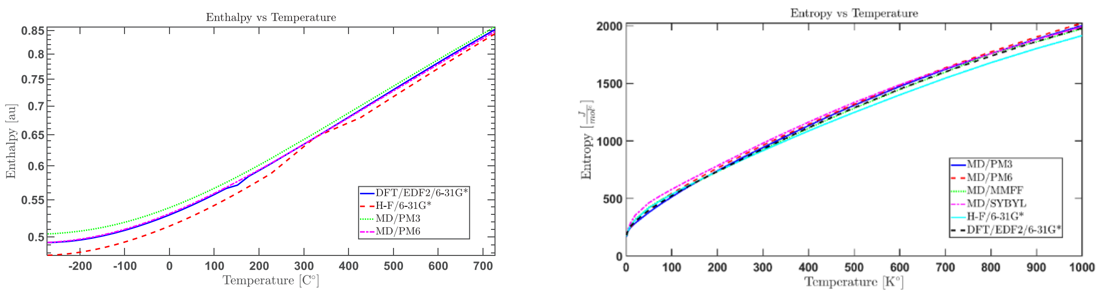

Figure 6. Enthalpy(a) and Entropy(b) of ICG molecule over the temperature

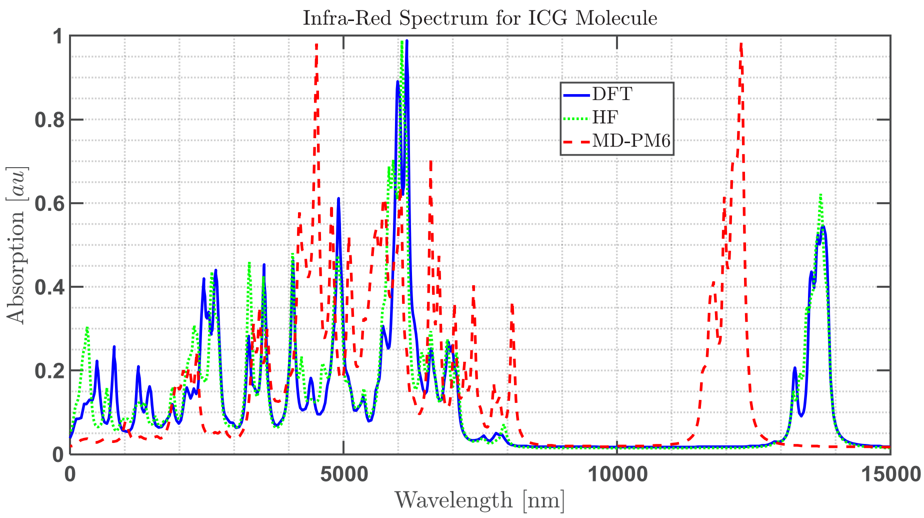

Figure 7. Calculated infrared spectrums using DFT, HF and MD-PM6 methods

We already know from previous works on the ICG molecule that it will have an absorption peak at around 800 nm.[9] To evaluate the accuracy of our simulations, we performed a numerical analysis of the absorption spectrum of the molecule using three methods: DFT, H-F, and PM6. The reason for choosing only three methods is due to the time-consuming nature of these calculations, and in the selection, we chose two accurate methods DFT and HF and a lighter and less accurate method PM6 which is a molecular dynamics method. As can be seen in Figure 7, the absorption spectrum of the DFT method shows an absorption peak of about 800 nm, while the HF and MD-PM6 methods did not perform well in pulling out this absorption peak. Therefore, due to the more accuracy of the DFT method in predicting the infrared absorption spectrum, we prefer the curve extracted from this method for the C_v parameter to the rest. Besides, by attending closely at the absorption spectra of Figure 7, we notice that this molecule has a higher absorption at longer wavelengths, such as 5 and 6 um in comparison to 800 nm. This feature can be used in medical imaging due to the possibility of a higher penetration depth of mentioned wavelengths in the body to improve the imaging depth of cancerous tumors. Based on the curve obtained for the heat capacity (C_v) parameter of the ICG molecule, we propose two simple mathematical models for extracting this parameter at different temperatures (

Table 2). The first model is a 6th order polynomial that fits well on the original curve. Given that the polynomial increases the complexity of the calculations, we propose a second model based on exponential functions, which has good accuracy too. A comparison of these proposed models and their absolute error relative to the original curve is shown in Figure 8. As can be seen, the error in both models is usually less than 1% in the temperature range and this shows their proper efficiency.

Table 2. Proposed models for heat capacity estimation over different temperatures

	Model-1	Model-2
Model	$C_v=p_1\times T^6+p_2\times T^5+p_3\times T^4+p_4\times T^3+p_5\times T^2+p_6\times T+p_7$	$C_v=ae^{bT}+ce^{dT}$

Coefficients	P_1=-2.67858573657377$\times 10^{-14}$ P_2=8.53753860483788$\times 10^{-11}$ P_3=-1.00441704317634$\times 10^{-7}$ P_4=5.26450777738992$\times 10^{-5}$ P_5=-0.0127731480010593 P_6=3.15511576144455 P_7=14.3914199490961, T[K°]	a=-2.679$\times 10^{8}$ b=-0.000782 c=2.679$\times 10^{8}$ d=-0.000782, T[K°]

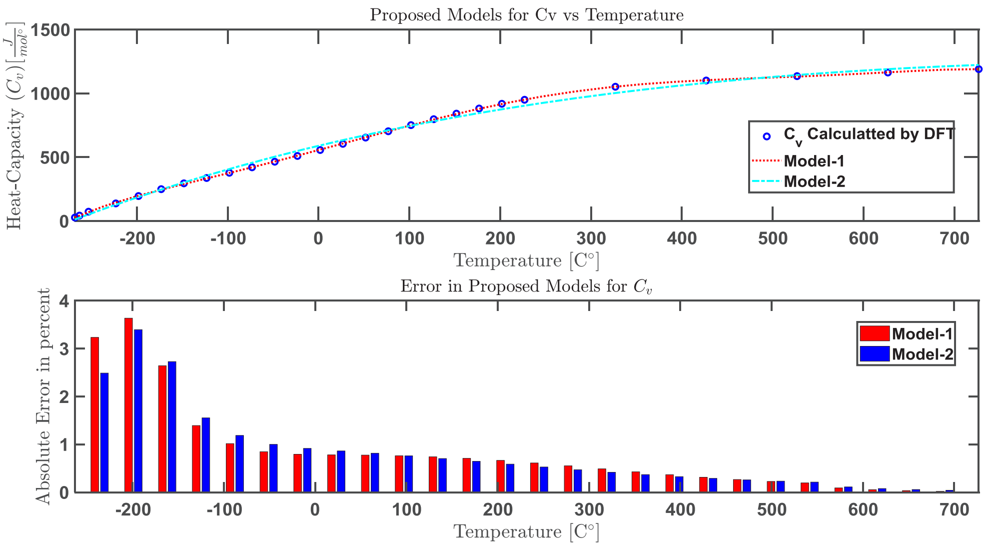

Figure 8. Proposed models for C_v estimation (a); Absolute error in percent in comparison with DFT values

It has previously been confirmed that DFT and MD methods provide a general method for standard atomistic analysis for an extensive variety of elements and their combinations. In this paper, we performed atomistic-level simulations employing the density-functional-theory and molecular dynamics technique to simulate the Thermodynamics process in an ICG molecule. We estimated HOMO/LUMO orbitals energy, Dipole Moment, and Polarizability of a single ICG molecule. We analyzed the heat-capacity of ICG at different temperatures. To validate results obtained for heat-capacity, we calculated the absorption spectrum over various wavelengths; and concerning that we found the DFT approach to be more accurate than others. Then we opt this method to get final results for heat-capacity and proposed two mathematical models for extraction of C_v over various temperatures. Furthermore, by simulating and analyzing the absorption spectrum for the ICG molecule, we found large absorption peaks at longer wavelengths than 800 nm which was reported in the previous works. This feature can be used to perform deeper medical imaging in methods such as OCT or PhotoAcoustic. Finally, it is important to mention that to examine atomistic aspects such as heat-capacity and dipole-moment, it is significant to have a reliable potential for the atoms forming an ICG molecule and choose multiple calculation methods and basis-sets to validate them.

References

[1] R. Ackroyd, C. Kelty, N. Brown, and M. Reed, "The history of photodetection and photodynamic therapy¶," *Photochem. Photobiol.*, vol. 74, no. 5, pp. 656–669, 2001.

[2] M. R. Detty, S. L. Gibson, and S. J. Wagner, “Current clinical and preclinical photosensitizers for use in photodynamic therapy,” *J. Med. Chem.*, vol. 47, no. 16, pp. 3897–3915, 2004.

[3] T. J. Dougherty, G. B. Grindey, R. Fiel, K. R. Weishaupt, and D. G. Boyle, “Photoradiation therapy. II. Cure of animal tumors with hematoporphyrin and light,” *J. Natl. Cancer Inst.*, vol. 55, no. 1, pp. 115–121, 1975.

[4] G. Kim *et al.*, “Indocyanine-green-embedded PEBBLEs as a contrast agent for photoacoustic imaging,” *J. Biomed. Opt.*, vol. 12, no. 4, p. 44020, 2007.

[5] M. A. Yaseen, J. Yu, M. S. Wong, and B. Anvari, “Stability assessment of indocyanine green within dextran-coated mesocapsules by absorbance spectroscopy,” *J. Biomed. Opt.*, vol. 12, no. 6, p. 64031, 2007.

[6] V. B. Rodriguez, S. M. Henry, A. S. Hoffman, P. S. Stayton, X. Li, and S. H. Pun, “Encapsulation and stabilization of indocyanine green within poly (styrene-alt-maleic anhydride) block-poly (styrene) micelles for near-infrared imaging,” *J. Biomed. Opt.*, vol. 13, no. 1, p. 14025, 2008.

[7] T. Hirata *et al.*, “Synthesis and reactivities of 3-indocyanine-green-acyl-1, 3-thiazolidine-2-thione (ICG-ATT) as a new near-infrared fluorescent-labeling reagent,” *Bioorg. Med. Chem.*, vol. 6, no. 11, pp. 2179–2184, 1998.

[8] D. E. Dolmans, D. Fukumura, and R. K. Jain, “Photodynamic therapy for cancer,” *Nat. Rev. Cancer*, vol. 3, no. 5, pp. 380–387, 2003.

[9] M. Dolatyari, F. A. Aghdam, G. Rostami, A. Rostami, and I. S. Amiri, “Introducing New Conjugated Quantum Dots for Photothermal Therapy in Biological Applications,” *PLASMONICS*, 2020.

[10] J. V Frangioni, “New technologies for human cancer imaging,” *J. Clin. Oncol.*, vol. 26, no. 24, p. 4012, 2008.

[11] Y.-L. He, H. Tanigami, H. Ueyama, T. Mashimo, and I. Yoshiya, “Measurement of blood volume using indocyanine green measured with pulse-spectrophotometry: its reproducibility and reliability,” *Crit. Care Med.*, vol. 26, no. 8, pp. 1446–1451, 1998.

[12] T. Iijima *et al.*, “Cardiac output and circulating blood volume analysis by pulse dye-densitometry,” *J. Clin. Monit.*, vol. 13, no. 2, pp. 81–89, 1997.

[13] T. Iijima, Y. Iwao, and H. Sankawa, “Circulating Blood Volume Measured by Pulse Dye-Densitometry Comparison with131I-HSA Analysis,” *Anesthesiol. J. Am. Soc. Anesthesiol.*, vol. 89, no. 6, pp. 1329–1335, 1998.

[14] M. Haller *et al.*, “Determination of plasma volume with indocyanine green in man,” *Life Sci.*, vol. 53, no. 21, pp. 1597–1604, 1993.

[15] J.-M. I. Maarek, D. P. Holschneider, and J. Harimoto, “Fluorescence of indocyanine green in blood: intensity dependence on concentration and stabilization with sodium poly aspartate,” *J. Photochem. Photobiol. B Biol.*, vol. 65, no. 2–3, pp. 157–164, 2001.

[16] O. Picker, G. Wietasch, T. W. L. Scheeren, and J. O. Arndt, “Determination of total blood volume by indicator dilution: a comparison of mean transit time and mass conservation principle,” *Intensive Care Med.*, vol. 27, no. 4, pp. 767–774, 2001.

[17] M. Keul, V. Soran, and G. Lazăr-Keul, “Über die chemische und photodynamische Wirkung von Neutralrot auf die Rotationsströmung beiHordeum vulgare L,” *Protoplasma*, vol. 67, no. 2–3, pp. 279–293, 1969.

[18] I. Diamond, A. Mcdonagh, C. Wilson, S. Granelli, S. Nielsen, and R. Jaenicke, “Photodynamic therapy of malignant tumors,” *Lancet*, vol. 300, no. 7788, pp. 1175–1177, 1972.

[19] J. F. Kelly, M. E. Snell, and M. C. Berenbaum, “Photodynamic destruction of human bladder carcinoma,” *Br. J. Cancer*, vol. 31, no. 2, pp. 237–244, 1975.

[20] T. J. Dougherty, J. E. Kaufman, A. Goldfarb, K. R. Weishaupt, D. Boyle, and A. Mittleman, “Photoradiation therapy for the treatment of malignant tumors,” *Cancer Res.*, vol. 38, no. 8, pp. 2628–2635, 1978.

[21] A. A. Lamola and G. S. Hammond, “Mechanisms of photochemical reactions in solution. XXXIII. Intersystem crossing efficiencies,” *J. Chem. Phys.*, vol. 43, no. 6, pp. 2129–2135, 1965.

[22] C. A. Parker and T. A. Joyce, “Triplet formation efficiencies from delayed fluorescence measurements,” *Chem. Commun.*, no. 8, pp. 234–235, 1966.

[23] A. R. Horrocks, T. Medinger, and F. Wilkinson, “A new accurate method for determining the quantum yields of triplet state production of aromatic molecules in solution,” *Chem. Commun.*, no. 19, p. 452, 1965.

[24] S. Nonell, P. F. Aramendia, K. Heihoff, R. M. Negri, and S. E. Braslavsky, “Laser-induced optoacoustic combined with near-infrared emission: an alternative approach for the determination of intersystem crossing quantum yields applied to porphycenes,” *J. Phys. Chem.*, vol. 94, no. 15, pp. 5879–5883, 1990.

[25] J. S. Brinen, “Application of electron spin resonance in the study of triplet states. III. Extinction coefficients of triplet-triplet transitions,” *J. Chem. Phys.*, vol. 49, no. 2, pp. 586–590, 1968.

[26] R. Bensasson, C. R. Goldschmidt, E. J. Land, and T. G. Truscott, “Laser intensity and the comparative method for determination of triplet quantum yields,” *Photochem. Photobiol.*, vol. 28, no. 2, pp. 277–281, 1978.

[27] B. Lament, J. Karpiuk, and J. Waluk, “Determination of triplet formation efficiency from kinetic profiles of the ground state recovery,” *Photochem. Photobiol. Sci.*, vol. 2, no. 3, pp. 267–272, 2003.

[28] R. Kubo and D. A. McQuarrie, “Statistical mechanics,” *PhT*, vol. 18, no. 10, p. 74, 1965.

[29] B. Fultz, “Vibrational thermodynamics of materials,” *Prog. Mater. Sci.*, vol. 55, no. 4, pp. 247–352, 2010.

[30] D. V Schroeder, “An introduction to thermal physics.” American Association of Physics Teachers, 1999.

[31] G. Grimvall, *Thermophysical properties of materials*. Elsevier, 1999.

[32] J. Horbach, W. Kob, and K. Binder, “Specific heat of amorphous silica within the harmonic approximation,” *J. Phys. Chem. B*, vol. 103, no. 20, pp. 4104–4108, 1999.

[33] S. Liu, “T., Blanco, M. & Goddard III, WA The two-phase model for calculating thermodynamic properties of liquids from molecular dynamics: Validation of the phase diagram of Lennard-Jones fluids,” *J. Chem. Phys*, vol. 119, pp. 11792–11805, 2003.

[34] J. Hafner, “Materials simulations using VASP—a quantum perspective to materials science,” *Comput. Phys. Commun.*, vol. 177, no. 1–2, pp. 6–13, 2007.

[35] R. P. Feynman, “Forces in molecules,” *Phys. Rev.*, vol. 56, no. 4, p. 340, 1939.

[36] P. E. Blöchl, “Projector augmented-wave method,” *Phys. Rev. B*, vol. 50, no. 24, p. 17953, 1994.

[37] G. Kresse and D. Joubert, “From ultrasoft pseudopotentials to the projector augmented-wave method,” *Phys. Rev. B*, vol. 59, no. 3, p. 1758, 1999.

[38] R. M. Nieminen, “Developments in the density-functional theory of electronic structure,” *Curr. Opin. Solid State Mater. Sci.*, vol. 4, no. 6, pp. 493–498, 1999.

New Generalizations of Lauricella Hypergeometric Functions and Their Integral Representations

Enes Ata, İ. Onur Kıymaz

Kırşehir Ahi Evran Uni., Dept. of Math.,Turkey.

enesata.tr@gmail.com, iokiymaz@ahievran.edu.tr

Abstract

In this paper, using generalized beta function including Fox-Wright function in its kernel, we described new generalizations for the Lauricella hypergeometric functions $F_A^{(r)}$, $F_B^{(r)}$, $F_C^{(r)}$ and $F_D^{(r)}$. Furthermore, we obtained various integral formulas for the newly defined Lauricella generalized hypergeometric functions.

Keywords: Beta function, Confluent hypergeometric function, Fox-Wright function, Lauricella's hypergeometric functions.

1. Introduction

In recent years, some expansions of special functions, which frequently used in applied mathematics, have been studied by many scientists [2, 6, 7, 13, 16, 17]. Particularly, for $Re(p) > 0$, $Re(x) > 0$, $Re(y) > 0$, $Re(c) > Re(b) > 0$ the following extension of beta function was introduced by Ata and Kıymaz in [6] as:

$$ {}^{\Psi}\hat{B}_p(x,y) := {}^{\Psi}B_p \left[\begin{matrix} (\beta_i,\alpha_i)_{1,\xi} \\ (\mu_j,\kappa_j)_{1,\eta} \end{matrix} \middle| x,y \right] = \int_0^1 t^{x-1}(1-t)^{y-1} {}_{\xi}\Psi_{\eta}\left(-\frac{p}{t(1-t)}\right) dt. $$

Later, by using this extension of beta function, Ata and Kıymaz [6] extended the hypergeometric function as follows:

$$ {}^{\Psi}\hat{\Phi}_p(b;c;z) := {}^{\Psi}\Phi_p \left[\begin{matrix} (\beta_i,\alpha_i)_{1,\xi} \\ (\mu_j,\kappa_j)_{1,\eta} \end{matrix} \middle| b;c;z \right] = \sum_{n=0}^{\infty} \frac{{}^{\Psi}\hat{B}_p(b+n,c-b)}{B(b,c-b)} \frac{z^n}{n!}. $$

Respectively, they called them as ${}_{\xi}\Psi_{\eta}$-beta function and ${}_{\xi}\Psi_{\eta}$-confluent hypergeometric function. Also, the following equation is provided for the ${}_{\xi}\Psi_{\eta}$-confluent hypergeometric function:

$$ {}^{\Psi}\hat{\Phi}_p(b;c;z) = e^z \, {}^{\Psi}\hat{\Phi}_p(c-b;c;-z). \tag{1} $$

Note that the function ${}_{\xi}\Psi_{\eta}$ used above is known as the Fox-Wright function [1] which defined as:

$$ {}_{\xi}\Psi_{\eta}(z) = {}_{\xi}\Psi_{\eta} \left[\begin{matrix} (\beta_i,\alpha_i)_{1,\xi} \\ (\mu_j,\kappa_j)_{1,\eta} \end{matrix} \middle| z \right] = \sum_{n=0}^{\infty} \frac{\prod_{i=1}^{\xi}\Gamma(\alpha_i n+\beta_i)}{\prod_{j=1}^{\eta}\Gamma(\kappa_j n+\mu_j)} \frac{z^n}{n!}, \tag{2} $$

where $z, \beta_i, \mu_j \in \mathbb{C}, \alpha_i, \kappa_j \in \mathbb{R}, i = 1, \ldots, \xi$ and $j = 1, \ldots, \eta$. The asymptotic behaviour of the above function was studied by Fox [4, 5] and Wright [8, 9, 10]. For $\kappa, \mu, z \in \mathbb{C}, Re(\kappa) > -1$, the classic Wright function [1]

$$ {}_0\Psi_1(z) = {}_0\Psi_1 \left[\begin{matrix} \overline{} \\ (\mu,\kappa) \end{matrix} \middle| z \right] = \sum_{n=0}^{\infty} \frac{1}{\Gamma(\kappa n+\mu)} \frac{z^n}{n!} $$

can obtained by choosing $\xi = 0$ and $\eta = 1$ in equation (2). Also, Ata [7] defined some special functions that were generalized with the help of the classic Wright function.

2. Generalized Lauricella's hypergeometric functions

Lauricella's hypergeometric functions $F_A^{(r)}$, $F_B^{(r)}$, $F_C^{(r)}$ and $F_D^{(r)}$ in [12, 14] and then many authors have studied on these functions [3, 18, 19, 20].

This paper, we introduce the generalized Lauricella's hypergeometric functions as follows:

$$
\begin{aligned}
{}^{\Psi}\hat{F}_{A,p}^{(r)}(a,b_1,\ldots,b_r;c_1,\ldots,c_r;x_1,\ldots,x_r) &:= {}^{\Psi}F_{A,p}^{(r)}\left[\begin{matrix}(\beta_i,\alpha_i)_{1,\xi}\\(\mu_j,\kappa_j)_{1,\eta}\end{matrix}\middle| a,b_1,\ldots,b_r;c_1,\ldots,c_r;x_1,\ldots,x_r\right]\\
&= \sum_{n_1,\ldots,n_r=0}^{\infty}(a)_{n_1+\ldots+n_r}\frac{{}^{\Psi}\hat{B}_p(b_1+n_1,c_1-b_1)}{B(b_1,c_1-b_1)}\cdots\frac{{}^{\Psi}\hat{B}_p(b_r+n_r,c_r-b_r)}{B(b_r,c_r-b_r)}\frac{x_1^{n_1}}{n_1!}\cdots\frac{x_r^{n_r}}{n_r!}
\end{aligned}
$$

$$
\left(|x_1|+\ldots+|x_r|<1, Re(c_i)>Re(b_i)>0 \text{ for } i=1,\ldots,r\right),
$$

$$
\begin{aligned}
{}^{\Psi}\hat{F}_{B,p}^{(r)}(a_1,\ldots,a_r,b_1,\ldots,b_r;c;x_1,\ldots,x_r;\lambda) &:= {}^{\Psi}F_{B,p}^{(r)}\left[\begin{matrix}(\beta_i,\alpha_i)_{1,\xi}\\(\mu_j,\kappa_j)_{1,\eta}\end{matrix}\middle| a_1,\ldots,a_r,b_1,\ldots,b_r;c;x_1,\ldots,x_r;\lambda\right]\\
&= \sum_{n_1,\ldots,n_r=0}^{\infty}\frac{(a_1)_{n_1}\ldots(a_r)_{n_r}(\lambda)_{n_1}(b_2)_{n_2}\ldots(b_r)_{n_r}}{(c)_{n_1+\ldots+n_r}}\frac{{}^{\Psi}\hat{B}_p(b_1+n_1,\lambda-b_1)}{B(b_1,\lambda-b_1)}\frac{x_1^{n_1}}{n_1!}\cdots\frac{x_r^{n_r}}{n_r!}
\end{aligned}
$$

$$
\left(\max\{|x_1|,\ldots,|x_n|\}<1, Re(\lambda)>Re(b_1)>0\right),
$$

$$
\begin{aligned}
{}^{\Psi}\hat{F}_{C,p}^{(r)}(a,b;c_1,\ldots,c_r;x_1,\ldots,x_r;\lambda) &:= {}^{\Psi}F_{C,p}^{(r)}\left[\begin{matrix}(\beta_i,\alpha_i)_{1,\xi}\\(\mu_j,\kappa_j)_{1,\eta}\end{matrix}\middle| a,b;c_1,\ldots,c_r;x_1,\ldots,x_r;\lambda\right]\\
&= \sum_{n_1,\ldots,n_r=0}^{\infty}\frac{(a)_{n_1+\ldots+n_r}(b)_{n_1+\ldots+n_r}}{(\lambda)_{n_1}(c_2)_{n_2}\ldots(c_r)_{n_r}}\frac{{}^{\Psi}\hat{B}_p(\lambda+n_1,c_1-\lambda)}{B(\lambda,c_1-\lambda)}\frac{x_1^{n_1}}{n_1!}\cdots\frac{x_r^{n_r}}{n_r!}
\end{aligned}
$$

$$
\left(\sqrt{|x_1|}+\ldots+\sqrt{|x_n|}<1, Re(c_1)>Re(\lambda)>0\right),
$$

$$
\begin{aligned}
{}^{\Psi}\hat{F}_{D,p}^{(r)}(a,b_1,\ldots,b_r;c;x_1,\ldots,x_r) &:= {}^{\Psi}F_{D,p}^{(r)}\left[\begin{matrix}(\beta_i,\alpha_i)_{1,\xi}\\(\mu_j,\kappa_j)_{1,\eta}\end{matrix}\middle| a,b_1,\ldots,b_r;c;x_1,\ldots,x_r\right]\\
&= \sum_{n_1,\ldots,n_r=0}^{\infty}(b_1)_{n_1}\ldots(b_r)_{n_r}\frac{{}^{\Psi}\hat{B}_p(a+n_1+\ldots+n_r,c-a)}{B(a,c-a)}\frac{x_1^{n_1}}{n_1!}\cdots\frac{x_r^{n_r}}{n_r!}
\end{aligned}
$$

$$
\left(\max\{|x_1|,\ldots,|x_r|\}<1, Re(c)>Re(a)>0\right).
$$

Respectively, we called them as ${}_{\xi}\Psi_{\eta}$-Lauricella $F_A^{(r)}$, ${}_{\xi}\Psi_{\eta}$-Lauricella $F_B^{(r)}$, ${}_{\xi}\Psi_{\eta}$-Lauricella $F_C^{(r)}$ and ${}_{\xi}\Psi_{\eta}$-Lauricella $F_D^{(r)}$ hypergeometric functions.

3. Integral representations for ${}^{\Psi}\hat{F}_{A,p}^{(r)}$

Theorem 1. *For $Re(c_i)>Re(b_i)>0, (i=1,\ldots,r)$, the following integral representation holds true:*

$$
\begin{aligned}
{}^{\Psi}\hat{F}_{A,p}^{(r)}(a,b_1,\ldots,b_r;c_1,\ldots,c_r;x_1,\ldots,x_r) &= \frac{1}{B(b_1,c_1-b_1)\ldots B(b_r,c_r-b_r)}\int_0^1\cdots\int_0^1 t_1^{b_1-1}\ldots t_r^{b_r-1}\\
&\times(1-t_1)^{c_1-b_1-1}\ldots(1-t_r)^{c_r-b_r-1}{}_{\xi}\Psi_{\eta}\left(\frac{-p}{t_1(1-t_1)}\right)\cdots{}_{\xi}\Psi_{\eta}\left(\frac{-p}{t_r(1-t_r)}\right)\\
&\times F_A^{(r)}(a,b_1,\ldots,b_r;b_1,\ldots,b_r;t_1x_1,\ldots,t_rx_r)dt_1\ldots dt_r.
\end{aligned}
$$

Proof. Using the definition of ${}_{\xi}\Psi_{\eta}$-Lauricella $F_A^{(r)}$ function

$$\begin{aligned}
&{}^{\Psi}\hat{F}^{(r)}_{A,p}(a, b_1, \dots, b_r; c_1, \dots, c_r; x_1, \dots, x_r)\\
&= \sum_{n_1,\dots,n_r=0}^{\infty} (a)_{n_1+\dots+n_r} \frac{{}^{\Psi}\hat{B}_p(b_1+n_1, c_1-b_1)}{B(b_1, c_1-b_1)} \dots \frac{{}^{\Psi}\hat{B}_p(b_r+n_r, c_r-b_r)}{B(b_r, c_r-b_r)} \frac{x_1^{n_1}}{n_1!} \dots \frac{x_r^{n_r}}{n_r!}\\
&= \frac{1}{B(b_1, c_1-b_1) \dots B(b_r, c_r-b_r)} \sum_{n_1,\dots,n_r=0}^{\infty} (a)_{n_1+\dots+n_r} \int_0^1 t_1^{b_1+n_1-1}(1-t_1)^{c_1-b_1-1}\\
&\quad \times {}_{\xi}\Psi_{\eta}\left(\frac{-p}{t_1(1-t_1)}\right) \dots \int_0^1 t_r^{b_r+n_r-1}(1-t_r)^{c_r-b_r-1} {}_{\xi}\Psi_{\eta}\left(\frac{-p}{t_r(1-t_r)}\right)\\
&\quad \times \frac{x_1^{n_1}}{n_1!} \dots \frac{x_r^{n_r}}{n_r!} dt_1 \dots dt_r\\
&= \frac{1}{B(b_1, c_1-b_1) \dots B(b_r, c_r-b_r)} \sum_{n_1,\dots,n_r=0}^{\infty} (a)_{n_1+\dots+n_r} \int_0^1 t_1^{b_1-1}(1-t_1)^{c_1-b_1-1}\\
&\quad \times {}_{\xi}\Psi_{\eta}\left(\frac{-p}{t_1(1-t_1)}\right) \dots \int_0^1 t_r^{b_r-1}(1-t_r)^{c_r-b_r-1} {}_{\xi}\Psi_{\eta}\left(\frac{-p}{t_r(1-t_r)}\right)\\
&\quad \times \frac{(x_1t_1)^{n_1}}{n_1!} \dots \frac{(x_rt_r)^{n_r}}{n_r!} dt_1 \dots dt_r\\
&= \frac{1}{B(b_1, c_1-b_1) \dots B(b_r, c_r-b_r)} \int_0^1 \dots \int_0^1 t_1^{b_1-1} \dots t_r^{b_r-1}\\
&\quad \times (1-t_1)^{c_1-b_1-1} \dots (1-t_r)^{c_r-b_r-1} {}_{\xi}\Psi_{\eta}\left(\frac{-p}{t_1(1-t_1)}\right) \dots {}_{\xi}\Psi_{\eta}\left(\frac{-p}{t_r(1-t_r)}\right)\\
&\quad \times F_A^{(r)}(a, b_1, \dots, b_r; b_1, \dots, b_r; t_1x_1, \dots, t_rx_r) dt_1 \dots dt_r,
\end{aligned}$$

which completes the proof. □

Theorem 2. *For* $Re(c_i) > Re(b_i) > 0, (i = 1, \dots, r)$*, the following equation holds true:*

$$ {}^{\Psi}\hat{F}^{(r)}_{A,p}(a, b_1, \dots, b_r; c_1, \dots, c_r; x_1, \dots, x_r) = \frac{1}{\Gamma(a)} \int_0^{\infty} t^{a-1} e^{-t}\, {}^{\Psi}\hat{\Phi}_p(b_1; c_1; tx_1) \dots {}^{\Psi}\hat{\Phi}_p(b_r; c_r; tx_r) dt.$$

Proof. Using the integral representation of ${}_{\xi}\Psi_{\eta}$-beta function in the definition of ${}_{\xi}\Psi_{\eta}$-Lauricella $F_A^{(r)}$ function and making similar calculations in the proof of Theorem 1, we get the desired result. □

Theorem 3. *For* $Re(c_i) > Re(b_i) > 0, (i = 1, \dots, r)$*, the following equation holds true:*

$$\begin{aligned}
&{}^{\Psi}\hat{F}^{(r)}_{A,p}(a, b_1, \dots, b_r; c_1, \dots, c_r; x_1, \dots, x_r)\\
&\quad = \frac{1}{\Gamma(a)} \int_0^{\infty} t^{a-1} e^{-t(1-x_1-\dots-x_r)}\, {}^{\Psi}\hat{\Phi}_p(c_1-b_1; c_1; -tx_1) \dots {}^{\Psi}\hat{\Phi}_p(c_r-b_r; c_r; -tx_r) dt.
\end{aligned}$$

Proof. Using the integral representation of ${}_{\xi}\Psi_{\eta}$-beta function in the definition of ${}_{\xi}\Psi_{\eta}$-Lauricella $F_A^{(r)}$ function and making similar calculations in the proof of Theorem 1, we get the desired result. □

Theorem 4. *For $Re(c_i) > Re(b_i) > 0, (i = 1, \dots, r)$, the following equation holds true:*

$$
\begin{aligned}
{}^{\Psi}\hat{F}^{(r)}_{A,p}(a, b_1, \dots, b_r; c_1, \dots, c_r; x_1, \dots, x_r) &= \frac{2^r}{B(b_1, c_1-b_1) \dots B(b_r, c_r-b_r)} \int_0^{\frac{\pi}{2}} \dots \int_0^{\frac{\pi}{2}} \\
&\times (\sin\theta_1)^{2b_1-1} \dots (\sin\theta_r)^{2b_r-1} (\cos\theta_1)^{2c_1-2b_1-1} \dots (\cos\theta_r)^{2c_r-2b_r-1} \\
&\times {}_{\xi}\Psi_{\eta}\left(-p(\sec\theta_1)^2(\csc\theta_1)^2\right) \dots {}_{\xi}\Psi_{\eta}\left(-p(\sec\theta_r)^2(\csc\theta_r)^2\right) \\
&\times F^{(r)}_A\left(a, b_1, \dots, b_r; b_1, \dots, b_r; x_1(\sin\theta_1)^2, \dots, x_r(\sin\theta_r)^2\right) d\theta_1 \dots d\theta_r.
\end{aligned}
$$

Proof. Using the integral representation of ${}_{\xi}\Psi_{\eta}$-beta function in the definition of ${}_{\xi}\Psi_{\eta}$-Lauricella $F^{(r)}_A$ function and making similar calculations in the proof of Theorem 1, we get the desired result. □

Theorem 5. *For $Re(c_i) > Re(b_i) > 0, (i = 1, \dots, r)$, the following equation holds true:*

$$
\begin{aligned}
{}^{\Psi}\hat{F}^{(r)}_{A,p}(a, b_1, \dots, b_r; c_1, \dots, c_r; x_1, \dots, x_r) &= \frac{1}{B(b_1, c_1 - b_1) \dots B(b_r, c_r - b_r)} \int_0^{\infty} \dots \int_0^{\infty} \\
\times \frac{u_1^{b_1-1}}{(1+u_1)^{c_1}} \dots \frac{u_r^{b_r-1}}{(1+u_r)^{c_r}} {}_{\xi}\Psi_{\eta}\left(-2p - p\left(u_1 + \frac{1}{u_1}\right)\right) &\dots {}_{\xi}\Psi_{\eta}\left(-2p - p\left(u_r + \frac{1}{u_r}\right)\right) \\
\times F^{(r)}_A\left(a, b_1, \dots, b_r; b_1, \dots, b_r; \frac{x_1 u_1}{1+u_1}, \dots, \frac{x_r u_r}{1+u_r}\right) du_1 \dots du_r.
\end{aligned}
$$

Proof. Using the integral representation of ${}_{\xi}\Psi_{\eta}$-beta function in the definition of ${}_{\xi}\Psi_{\eta}$-Lauricella $F^{(r)}_A$ function and making similar calculations in the proof of Theorem 1, we get the desired result. □

4. Integral representations for ${}^{\Psi}\hat{F}^{(r)}_{B,p}$

Theorem 6. *For $Re(\lambda) > Re(b_1) > 0$, the following integral representation holds true:*

$$
\begin{aligned}
{}^{\Psi}\hat{F}^{(r)}_{B,p}(a_1, \dots, a_r, b_1, \dots, b_r; c; x_1, \dots, x_r; \lambda) &= \frac{1}{B(b_1, \lambda-b_1)} \int_0^1 t^{b_1-1}(1-t)^{\lambda-b_1-1} {}_{\xi}\Psi_{\eta}\left(\frac{-p}{t(1-t)}\right) \\
&\times F^{(r)}_B(a_1, \dots, a_r, \lambda, b_2, \dots, b_r; c; tx_1, \dots, x_r) dt.
\end{aligned}
$$

Proof. Using the definition of ${}_{\xi}\Psi_{\eta}$-Lauricella $F^{(r)}_B$ function

$$
\begin{aligned}
&{}^{\Psi}\hat{F}^{(r)}_{B,p}(a_1, \dots, a_r, b_1, \dots, b_r; c; x_1, \dots, x_r; \lambda) \\
&= \sum_{n_1, \dots, n_r=0}^{\infty} \frac{(a_1)_{n_1} \dots (a_r)_{n_r} (\lambda)_{n_1} (b_2)_{n_2} \dots (b_r)_{n_r}}{(c)_{n_1+\dots+n_r}} \frac{{}^{\Psi}\hat{B}_p(b_1 + n_1, \lambda - b_1)}{B(b_1, \lambda - b_1)} \frac{x_1^{n_1}}{n_1!} \dots \frac{x_r^{n_r}}{n_r!} \\
&= \frac{1}{B(b_1, \lambda - b_1)} \sum_{n_1, \dots, n_r=0}^{\infty} \frac{(a_1)_{n_1} \dots (a_r)_{n_r} (\lambda)_{n_1} (b_2)_{n_2} \dots (b_r)_{n_r}}{(c)_{n_1+\dots+n_r}} \int_0^1 t^{b_1+n_1-1}(1-t)^{\lambda-b_1-1} \\
&\quad \times {}_{\xi}\Psi_{\eta}\left(\frac{-p}{t(1-t)}\right) \frac{x_1^{n_1}}{n_1!} \dots \frac{x_r^{n_r}}{n_r!} dt \\
&= \frac{1}{B(b_1, \lambda - b_1)} \int_0^1 t^{b_1-1}(1-t)^{\lambda-b_1-1} {}_{\xi}\Psi_{\eta}\left(\frac{-p}{t(1-t)}\right) \\
&\quad \times \sum_{n_1, \dots, n_r=0}^{\infty} \frac{(a_1)_{n_1} \dots (a_r)_{n_r} (\lambda)_{n_1} (b_2)_{n_2} \dots (b_r)_{n_r}}{(c)_{n_1+\dots+n_r}} \frac{(tx_1)^{n_1}}{n_1!} \dots \frac{x_r^{n_r}}{n_r!} dt \\
&= \frac{1}{B(b_1, \lambda - b_1)} \int_0^1 t^{b_1-1}(1-t)^{\lambda-b_1-1} {}_{\xi}\Psi_{\eta}\left(\frac{-p}{t(1-t)}\right) \\
&\quad \times F^{(r)}_B(a_1, \dots, a_r, \lambda, b_2, \dots, b_r; c; tx_1, \dots, x_r) dt,
\end{aligned}
$$

which completes the proof. □

Theorem 7. *For $Re(\lambda) > Re(b_1) > 0$, the following integral representation holds true:*

$$
{}^{\Psi}\hat{F}^{(r)}_{B,p}(a_1,\ldots,a_r,b_1,\ldots,b_r;c;x_1,\ldots,x_r;\lambda) = \frac{2}{B(b_1,\lambda-b_1)}\int_0^{\frac{\pi}{2}}(\sin\theta)^{2b_1-1}(\cos\theta)^{2\lambda-2b_1-1} \\
\times {}_{\xi}\Psi_{\eta}\left(-p(\sec\theta)^2(\csc\theta)^2\right) F^{(r)}_{B}(a_1,\ldots,a_r,\lambda,b_2,\ldots,b_r;c;x_1(\sin\theta)^2,\ldots,x_r)d\theta.
$$

Proof. Using the integral representation of ${}_{\xi}\Psi_{\eta}$-beta function in the definition of ${}_{\xi}\Psi_{\eta}$-Lauricella $F^{(r)}_{B}$ function and making similar calculations in the proof of Theorem 6, we get the desired result. □

Theorem 8. *For $Re(\lambda) > Re(b_1) > 0$, the following integral representation holds true:*

$$
{}^{\Psi}\hat{F}^{(r)}_{B,p}(a_1,\ldots,a_r,b_1,\ldots,b_r;c;x_1,\ldots,x_r;\lambda) = \frac{1}{B(b_1,\lambda-b_1)}\int_0^{\infty}\frac{u^{b_1-1}}{(1+u)^{\lambda}} \\
\times {}_{\xi}\Psi_{\eta}\left(-2p-p\left(u+\frac{1}{u}\right)\right) F^{(r)}_{B}\left(a_1,\ldots,a_r,\lambda,b_2,\ldots,b_r;c;\frac{x_1u}{1+u},\ldots,x_r\right)du.
$$

Proof. Using the integral representation of ${}_{\xi}\Psi_{\eta}$-beta function in the definition of ${}_{\xi}\Psi_{\eta}$-Lauricella $F^{(r)}_{B}$ function and making similar calculations in the proof of Theorem 6, we get the desired result. □

5. Integral representations for ${}^{\Psi}\hat{F}^{(r)}_{C,p}$

Theorem 9. *For $Re(c_1) > Re(\lambda) > 0$, the following integral representation holds true:*

$$
{}^{\Psi}\hat{F}^{(r)}_{C,p}(a,b;c_1,\ldots,c_r;x_1,\ldots,x_r;\lambda) = \frac{1}{B(\lambda,c_1-\lambda)}\int_0^1 t^{\lambda-1}(1-t)^{c_1-\lambda-1}{}_{\xi}\Psi_{\eta}\left(\frac{-p}{t(1-t)}\right) \\
\times F^{(r)}_{C}(a,b;\lambda,c_2,\ldots,c_r;tx_1,\ldots,x_r)dt.
$$

Proof. Using the definition of ${}_{\xi}\Psi_{\eta}$-Lauricella $F^{(r)}_{C}$ function

$$
\begin{aligned}
&{}^{\Psi}\hat{F}^{(r)}_{C,p}(a,b;c_1,\ldots,c_r;x_1,\ldots,x_r;\lambda) \\
&= \sum_{n_1,\ldots,n_r=0}^{\infty}\frac{(a)_{n_1+\ldots+n_r}(b)_{n_1+\ldots+n_r}}{(\lambda)_{n_1}(c_2)_{n_2}\ldots(c_r)_{n_r}}\frac{{}^{\Psi}\hat{B}_p(\lambda+n_1,c_1-\lambda)}{B(\lambda,c_1-\lambda)}\frac{x_1^{n_1}}{n_1!}\ldots\frac{x_r^{n_r}}{n_r!} \\
&= \frac{1}{B(\lambda,c_1-\lambda)}\sum_{n_1,\ldots,n_r=0}^{\infty}\frac{(a)_{n_1+\ldots+n_r}(b)_{n_1+\ldots+n_r}}{(\lambda)_{n_1}(c_2)_{n_2}\ldots(c_r)_{n_r}}\int_0^1 t^{\lambda+n_1-1}(1-t)^{c_1-\lambda-1}{}_{\xi}\Psi_{\eta}\left(\frac{-p}{t(1-t)}\right) \\
&\quad\times\frac{x_1^{n_1}}{n_1!}\ldots\frac{x_r^{n_r}}{n_r!}dt \\
&= \frac{1}{B(\lambda,c_1-\lambda)}\int_0^1 t^{\lambda-1}(1-t)^{c_1-\lambda-1}{}_{\xi}\Psi_{\eta}\left(\frac{-p}{t(1-t)}\right)\sum_{n_1,\ldots,n_r=0}^{\infty}\frac{(a)_{n_1+\ldots+n_r}(b)_{n_1+\ldots+n_r}}{(\lambda)_{n_1}(c_2)_{n_2}\ldots(c_r)_{n_r}} \\
&\quad\times\frac{(tx_1)^{n_1}}{n_1!}\ldots\frac{x_r^{n_r}}{n_r!}dt \\
&= \frac{1}{B(\lambda,c_1-\lambda)}\int_0^1 t^{\lambda-1}(1-t)^{c_1-\lambda-1}{}_{\xi}\Psi_{\eta}\left(\frac{-p}{t(1-t)}\right)F^{(r)}_{C}(a,b;\lambda,c_2,\ldots,c_r;tx_1,\ldots,x_r)dt,
\end{aligned}
$$

which completes the proof. □

Theorem 10. *For* $Re(c_1) > Re(\lambda) > 0$*, the following integral representation holds true:*

$$
{}^{\Psi}\hat{F}^{(r)}_{C,p}(a,b;c_1,\ldots,c_r;x_1,\ldots,x_r;\lambda) = \frac{2}{B(\lambda,c_1-\lambda)}\int_0^{\frac{\pi}{2}}(\sin\theta)^{2\lambda-1}(\cos\theta)^{2c_1-2\lambda-1}
$$
$$
\times\, {}_{\xi}\Psi_{\eta}\left(-p(\sec\theta)^2(\csc\theta)^2\right) F^{(r)}_{C}(a,b;\lambda,c_2,\ldots,c_r;x_1(\sin\theta)^2,\ldots,x_r)d\theta.
$$

Proof. Using the integral representation of ${}_{\xi}\Psi_{\eta}$-beta function in the definition of ${}_{\xi}\Psi_{\eta}$-Lauricella $F^{(r)}_{C}$ function and making similar calculations in the proof of Theorem 9, we get the desired result. □

Theorem 11. *For* $Re(c_1) > Re(\lambda) > 0$*, the following integral representation holds true:*

$$
{}^{\Psi}\hat{F}^{(r)}_{C,p}(a,b;c_1,\ldots,c_r;x_1,\ldots,x_r;\lambda) = \frac{1}{B(\lambda,c_1-\lambda)}\int_0^{\infty}\frac{u^{\lambda-1}}{(1+u)^{c_1}}\,{}_{\xi}\Psi_{\eta}\left(-2p-p\left(u+\frac{1}{u}\right)\right)
$$
$$
\times\, F^{(r)}_{C}\left(a,b;\lambda,c_2,\ldots,c_r;\frac{x_1u}{1+u},\ldots,x_r\right)du.
$$

Proof. Using the integral representation of ${}_{\xi}\Psi_{\eta}$-beta function in the definition of ${}_{\xi}\Psi_{\eta}$-Lauricella $F^{(r)}_{C}$ function and making similar calculations in the proof of Theorem 9, we get the desired result. □

6. Integral representations for ${}^{\Psi}\hat{F}^{(r)}_{D,p}$

Theorem 12. *For* $Re(c) > Re(a) > 0$*, the following integral representation holds true:*

$$
{}^{\Psi}\hat{F}^{(r)}_{D,p}(a,b_1,\ldots,b_r;c;x_1,\ldots,x_r) = \frac{1}{B(a,c-a)}\int_0^1 t^{a-1}(1-t)^{c-a-1}\,{}_{\xi}\Psi_{\eta}\left(\frac{-p}{t(1-t)}\right)
$$
$$
\times\, F^{(r)}_{D}(a,b_1,\ldots,b_r;a;tx_1,\ldots,tx_r)dt.
$$

Proof. Using the definition of ${}_{\xi}\Psi_{\eta}$-Lauricella $F^{(r)}_{D}$ function

$$
\begin{aligned}
&{}^{\Psi}\hat{F}^{(r)}_{D,p}(a,b_1,\ldots,b_r;c;x_1,\ldots,x_r)\\
&= \sum_{n_1,\ldots,n_r=0}^{\infty}(b_1)_{n_1}\ldots(b_r)_{n_r}\frac{{}^{\Psi}\hat{B}_p(a+n_1+\ldots+n_r,c-a)}{B(a,c-a)}\frac{x_1^{n_1}}{n_1!}\ldots\frac{x_r^{n_r}}{n_r!}\\
&= \frac{1}{B(a,c-a)}\sum_{n_1,\ldots,n_r=0}^{\infty}(b_1)_{n_1}\ldots(b_r)_{n_r}\int_0^1 t^{a+n_1+\ldots+n_r-1}(1-t)^{c-a-1}\,{}_{\xi}\Psi_{\eta}\left(\frac{-p}{t(1-t)}\right)\\
&\quad\times\frac{x_1^{n_1}}{n_1!}\ldots\frac{x_r^{n_r}}{n_r!}dt\\
&= \frac{1}{B(a,c-a)}\int_0^1 t^{a-1}(1-t)^{c-a-1}\,{}_{\xi}\Psi_{\eta}\left(\frac{-p}{t(1-t)}\right)\sum_{n_1,\ldots,n_r=0}^{\infty}(b_1)_{n_1}\ldots(b_r)_{n_r}\\
&\quad\times\frac{(tx_1)^{n_1}}{n_1!}\ldots\frac{(tx_r)^{n_r}}{n_r!}dt\\
&= \frac{1}{B(a,c-a)}\int_0^1 t^{a-1}(1-t)^{c-a-1}\,{}_{\xi}\Psi_{\eta}\left(\frac{-p}{t(1-t)}\right)\sum_{n_1,\ldots,n_r=0}^{\infty}\frac{(a)_{n_1+\ldots+n_r}(b_1)_{n_1}\ldots(b_r)_{n_r}}{(a)_{n_1+\ldots+n_r}}\\
&\quad\times\frac{(tx_1)^{n_1}}{n_1!}\ldots\frac{(tx_r)^{n_r}}{n_r!}dt\\
&= \frac{1}{B(a,c-a)}\int_0^1 t^{a-1}(1-t)^{c-a-1}\,{}_{\xi}\Psi_{\eta}\left(\frac{-p}{t(1-t)}\right)F^{(r)}_{D}(a,b_1,\ldots,b_r;a;tx_1,\ldots,tx_r)dt,
\end{aligned}
$$

which completes the proof. □

Theorem 13. *For* $Re(c) > Re(a) > 0$, *the following integral representation holds true:*

$$
\begin{aligned}
{}^{\Psi}\hat{F}^{(r)}_{D,p}(a, b_1, \ldots, b_r; c; x_1, \ldots, x_r) = &\frac{1}{B(a, c-a)} \int_0^1 t^{a-1}(1-t)^{c-a-1} {}_{\xi}\Psi_{\eta}\left(\frac{-p}{t(1-t)}\right) \\
&\times (1-tx_1)^{-b_1} \ldots (1-tx_r)^{-b_r} dt.
\end{aligned}
$$

Proof. Using the integral representation of ${}_{\xi}\Psi_{\eta}$-beta function in the definition of ${}_{\xi}\Psi_{\eta}$-Lauricella $F_D^{(r)}$ function and making similar calculations in the proof of Theorem 12, we get the desired result. $\square$

Theorem 14. *For* $Re(c) > Re(a) > 0$, *the following integral representation holds true:*

$$
\begin{aligned}
{}^{\Psi}\hat{F}^{(r)}_{D,p}(a, b_1, \ldots, b_r; c; x_1, \ldots, x_r) = &\frac{2}{B(a, c-a)} \int_0^{\frac{\pi}{2}} (\sin\theta)^{2a-1}(\cos\theta)^{2c-2a-1} \\
\times {}_{\xi}\Psi_{\eta}\left(-p(\sec\theta)^2(\csc\theta)^2\right) &F_D^{(r)}\left(a, b_1, \ldots, b_r; a; x_1(\sin\theta)^2, \ldots, x_r(\sin\theta)^2\right) d\theta.
\end{aligned}
$$

Proof. Using the integral representation of ${}_{\xi}\Psi_{\eta}$-beta function in the definition of ${}_{\xi}\Psi_{\eta}$-Lauricella $F_D^{(r)}$ function and making similar calculations in the proof of Theorem 12, we get the desired result. $\square$

Theorem 15. *For* $Re(c) > Re(a) > 0$, *the following integral representation holds true:*

$$
\begin{aligned}
{}^{\Psi}\hat{F}^{(r)}_{D,p}(a, b_1, \ldots, b_r; c; x_1, \ldots, x_r) = &\frac{1}{B(a, c-a)} \int_0^{\infty} \frac{u^{a-1}}{(1+u)^c} {}_{\xi}\Psi_{\eta}\left(-2p - p\left(u + \frac{1}{u}\right)\right) \\
&\times F_D^{(r)}\left(a, b_1, \ldots, b_r; a; \frac{x_1 u}{1+u}, \ldots, \frac{x_r u}{1+u}\right) du.
\end{aligned}
$$

Proof. Using the integral representation of ${}_{\xi}\Psi_{\eta}$-beta function in the definition of ${}_{\xi}\Psi_{\eta}$-Lauricella $F_D^{(r)}$ function and making similar calculations in the proof of Theorem 12, we get the desired result. $\square$

7. Conclusions

In this study, we defined the ${}_{\xi}\Psi_{\eta}$-Lauricella $F_A^{(r)}$, ${}_{\xi}\Psi_{\eta}$-Lauricella $F_B^{(r)}$, ${}_{\xi}\Psi_{\eta}$-Lauricella $F_C^{(r)}$ and ${}_{\xi}\Psi_{\eta}$-Lauricella $F_D^{(r)}$ hypergeometric functions with the help of the ${}_{\xi}\Psi_{\eta}$-beta function. Finally, some integral representations for each of the new generalizations of Lauricella's hypergeometric functions are presented. The closed-form expressions of the integrals presented here, are presumably not available in the existing literature.

References

[1] A.A. Kilbas, H.M. Srivastava, J.J. Trujillo, Theory and Applications of Fractional Differential, North-Holland Mathematics Studies 204, 2006.

[2] A. Çetinkaya, İ.O. Kıymaz, P. Agarwal, R. Agarwal, A comparative study on generating function relations for generalized hypergeometric functions via generalized fractional operators, Advances in Difference Equations, 2018:156, 2018.

[3] A. Hasanov, H.M. Srivastava, Some decomposition formulas associated with the Lauricella function $F_A^{(r)}$ and other multiple hypergeometric functions, Appl. Math. Lett., 19.2, 113-121, 2006.

[4] C. Fox, The asymptotic expansion of generalized hypergeometric functions, Proceedings of the London Mathematical Society (Ser. 2), 27, 389-400, 1928.

[5] C. Fox, The G and H functions as symmetrical Fourier kernels, Transactions of the American Mathematical Society, 98, 395-429, 1961.

[6] E. Ata, İ.O. Kıymaz, A study on certain properties of generalized special functions defined by Fox-Wright function, Applied Mathematics and Nonlinear Sciences, 5(1), 147-162, 2020.

[7] E. Ata, Generalized beta function defined by Wright function, arXiv:1803.03121v3 [math.CA], 2021.

[8] E.M. Wright, The asymptotic expansion of the generalized hypergeometric function, Journal of the London Mathematical Society, 10, 286-293, 1935.

[9] E.M. Wright, The asymptotic expansion of integral functions defined by Taylor Series, Philosophical Transactions of the Royal Society of London, Series A., 238, 423-451, 1940.

[10] E.M. Wright, The asymptotic expansion of the generalized hypergeometric function II, Proceedings of the London Mathematical Society, 46(2), 389-408, 1940.

[11] G.E. Andrews, R. Askey, R. Roy, Special Functions, Cambridge University Press, Cambridge, 1999.

[12] H.M. Srivastava, H.L. Manocha, A Treatise On Generating Functions. Halsted Press Wiley, New York, 1984.

[13] H.M. Srivastava, P. Agarwal, S. Jain, Generating functions for the generalized Gauss hypergeometric functions, Applied Mathematics and Computation, 247, 348-352, 2014.

[14] H.M. Srivastava, P.W. Karlsson, Multiple Gaussian Hypergeometric Series, Ellis Horwood Series: Mathematics and its Applications, Ellis Horwood Ltd., Chichester, Halsted Press [John Wiley and Sons, Inc.], New York, 1985.

[15] M.A. Chaudhry, S.M. Zubair, Generalized incomplete gamma functions with applications, Journal of Computational and Applied Mathematics, 55, 99-124, 1994.

[16] M.A. Chaudhry, A. Qadir, M. Rafique, S.M. Zubair, Extension of Euler's beta function, Journal of Computational and Applied Mathematics, 78, 19-32, 1997.

[17] M.A. Chaudhry, A. Qadir, H.M. Srivastava, R.B. Paris, Extended hypergeometric and confluent hypergeometric functions, Applied Mathematics and Computation, 159, 589-602, 2004.

[18] P.A. Padmanabham, H.M. Srivastava, Summation formulas associated with the Lauricella function $F_A^{(r)}$, Appl. Math. Lett., 13.1, 65-70, 2000.

[19] R.P. Agarwal, Min-Jie Luo, P. Agarwal, On the extended Appell-Lauricella hypergeometric functions and their applications, Filomat, 31(12), 3693-3713, 2017.

[20] S. Jain, P. Agarwal, İ.O. Kıymaz, Fractional integral and beta transform formulas for the extended Appell-Lauricella hypergeometric functions, Tamap Journal of Mathematics and Statistics, DOI:10.29371/2018.16.32, 2018.

Time Series Forecasting of Ethereum Prices Using Deep Learning Methods

Caglar Gurkan[1,*] **and Merih Palandoken**[2,3]

[1] Electrical and Electronics Engineering, Graduate School of Natural and Applied Sciences, Izmir Katip Celebi University, Izmir, Turkey

[2] Department of Electrical and Electronics Engineering, Faculty of Engineering and Architecture, Izmir Katip Celebi University, Izmir, Turkey

[3]Artificial Intelligence and Data Science Application and Research Center, Izmir Katip Çelebi University, Izmir, Turkey

caglar.gurkan@outlook.com

merih.palandoken@ikcu.edu.tr

Abstract

Cryptocurrencies have become popular with the development of blockchain technology. Hence, the cryptocurrencies are used in online payments system supported by several securing technologies. Since the cryptocurrencies are popular nowadays, their prices on the stock exchange often change quite rapidly. As a result, the time series forecasting of cryptocurrencies has become a vital research topic. In this paper, Ethereum prices have been studied. Recurrent Neural Networks models such as Simple RNN, Long Short Term Memory, Gated Recurrent Unit, Bidirectional Long Short Term Memory, and Bidirectional Gated Recurrent Unit have been used to analyse and predict Ethereum prices. The best forecasting performance among these models has been achieved by the BiGRU model using 15-time steps with MAPE value of 5.57651, RMSE value of 105.81920, MAE value of 72.15339, ME value of 363.47583, and R2 value of 0.97090. Consequently, the decision support system has been developed for the time series forecasting of Ethereum prices.

Keywords: Cryptocurrency; Ethereum; Blockchain; Time series; Price prediction; Deep learning; Recurrent neural network; Expert systems

1. Introduction

Digitalization has become an important issue with the development of technologies used in different sectors. Cryptocurrencies have become popular in the financial sector with these technological developments. The most popular cryptocurrency is Bitcoin (BTC), while the second one is Ethereum (ETH). Cryptocurrencies have started to be used as secure digital money with the introduction of these technologies. This secure structure is provided by blockchain technology developing each day continuously [1]. Hence, cryptocurrencies have recently started to be used in online payments. In this regard, the analysis and forecasting of cryptocurrencies have become an important research subject.

In this paper analysis and forecasting of ETH prices based on deep learning models have been focused. The cryptocurrency having the highest market capitalization after Bitcoin is ETH [2]. In this context, it is quite important to analyze ETH prices and forecasting future prices. For this reason, Recurrent Neural Network (RNN) based models, Simple RNN, Long Short Term Memory (LSTM), Gated Recurrent Unit (GRU), Bidirectional Long Short Term Memory (BiLSTM), Bidirectional Gated Recurrent Unit (BiGRU), have been used in the study for time series analysis. In addition, these models have been used with two different time-steps values as 15 and 30. The Mean Absolute Percentage Error (MAPE), Root Mean Square Error (RMSE), Mean Absolute Error (MAE), Maximum Error (ME) and R^2 metrics have been used to figure out the performance analysis and comparison. As a result, the best forecasting performance in MAPE value of 5.57651, RMSE value of 105.81920, MAE value of 72.15339, ME value of 363.47583, and R2 value of 0.97090 has been achieved by BiGRU model with 15-time steps.

The contributions of this proposed study are outlined as follows:

a) ETH prices by using RNN models, such as Simple RNN, LSTM, GRU, BiLSTM, and BiGRU have been analysed.

b) The results obtained by considering 15 and 30 time steps have been analysed by using the MAPE, RMSE, MAE, ME, and R^2 metrics.

c) A decision support system for the time series forecasting of ETH prices has been developed.

The submitted paper is organized as follows. In Section 2, the related works on time series forecasting for cryptocurrencies have been reviewed. Section 3 has presented the utilized methods. In Section 4, the experimental results have been reported. Lastly, in Section 5 concluding remarks have been presented.

2. Related Works

In this section, the studies providing the analysis of the cryptocurrencies have been pointed out with the indication on research using machine and deep learning for time series forecasting.

Zoumpekas et al. used Convolutional Neural Networks (CNN), LSTM, Stacked Long Short-Term Memory (sLSTM), BiLSTM, and GRU for ETH price analysis and prediction. In the study, the BiLSTM model has achieved the highest forecasting performance [3]. Yazdinejad et al. used machine and deep learning methods such as Random Forest, Support Vector Machine, Naive Bayes, Multilayer Perceptron, K-Nearest Neighbor, Ada Boost, Decision tree, and five different LSTM architecture designs for 500 cryptocurrency malware hunting. In the study, LSTM design-3 has achieved the highest predictive performance [4]. McNally et al. used Simple RNN, LSTM, and ARIMA models for BTC price prediction. In the study, the LSTM model has achieved the highest forecasting performance [5]. Ji et al. used Deep Neural Network (DNN), Simple RNN, LSTM, CNN, Deep Residual Networks and their combinations for BTC price prediction. In the study, LSTM has achieved the highest forecasting performance [6]. Livieris et al. used a multiple-input deep neural network based on LSTM for BTC, ETH, and Ripple (XRP) price prediction [7].

3. Methodology

The utilized methodology in the study is presented under the subtitles data and preprocessing and models.

3.1. Data and Preprocessing

The dataset consisting of 2079 samples between 07/08/2015 and 15/04/2021 has been used. The closing price samples of ETH are shown in Figure 1. 80%, 10%, and 10% of the data set have been used for the training, validation, and test process, respectively. The dataset includes five different features, such as date, open, high, low, and volume. These features have been used for forecasting of the closing price of ETH. Missing values have been replaced by mean values for each feature. Thereafter, the features have been scaled range in 0-1 using min-max scaling. In addition, the value of time steps has been used as 15 and 30 in the experimental analysis.

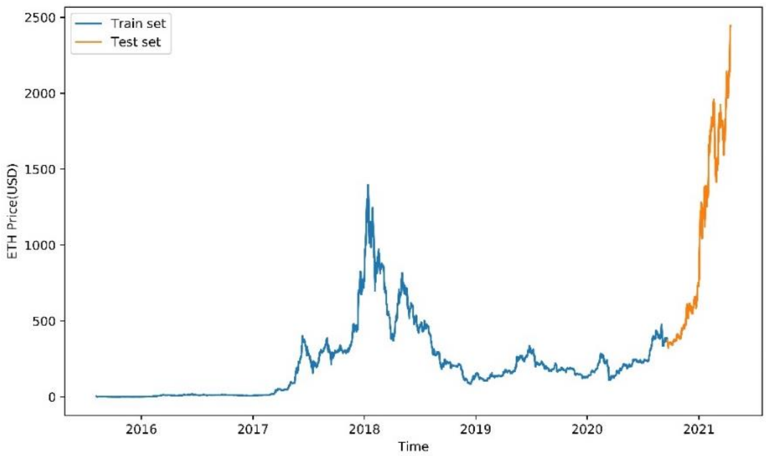

Figure 1. Bitcoin price between 07/08/2015 and 15/04/2021.

3.2. Models

RNN deep neural network architecture has been used to processing of sequential data. In this architecture design, the connections between several neurons form a directed graph [8]. RNN architecture design makes any length of input data to be processed possible. While processing data, past information on the processed data is also taken into account in the training phase. Generally, RNN has a great advantage when processing the time series data. On the other hand, in Simple RNN architecture design when the layers become deep, exploding or vanishing gradient problems occur, which is degraded the performance of Simple RNN [9]. LSTM and GRU are other deep neural network architecture designs based on Simple RNN. GRU architecture is a basic variant of the LSTM architecture design. LSTM and GRU have solved the problem of vanishing gradient [10]. LSTM architecture design consists of a cell and three gates as input, output, and forget. GRU architecture design consists of update and reset gates [11]. Subsequently to these architecture designs, BiLSTM and BiGRU architecture designs have been developed. BiLSTM and BiGRU architecture designs can take input in forward and backward directions. As a result, in this paper, five different RNN designs, which are Simple RNN, LSTM, GRU, BiLSTM, and BiGRU have been used in the deep learning models.

The proposed Simple RNN, LSTM, GRU, BiLSTM, and BiGRU architecture designs consist of dropout layer, dense layer, Simple RNN, LSTM, GRU, Bidirectional LSTM, and Bidirectional GRU layers. Firstly, three Simple RNN, LSTM, GRU, Bidirectional LSTM, and Bidirectional GRU layers for Simple RNN, LSTM, GRU, BiLSTM, and BiGRU architecture designs have been used, respectively. In addition, the dropout layers have been used with a threshold value of 0.2 between these layers. Dense layer has been used in the last layer of these designs. The same hyperparameters in Simple RNN, LSTM, GRU, BiLSTM, and BiGRU architecture designs have been used for an objective comparison. Hyperparameters for each layer are determined with the number of neurons as 128, 64, and 32, respectively. Activation function and recurrent dropout threshold value have been used as 'tanh' and '0.1', respectively. Furthermore, while excluding the last layer of RNNs part, return sequences have been used as 'true'. Other hyperparameters in the Keras library have been used as default. In the last layer of these presented architecture designs, a dense layer with the activation function of 'linear' and the number of 1 unit has been used.

In the training phase for all these architecture designs, loss function, optimizer, learning rate value, batch size value, and epoch value have been set as 'mean squared error', 'adam', 0.001, 128, and 100, respectively. Architecture design is demonstrated in Figure 2. Scikit-learn and Keras libraries have been used on Spyder Integrated Development Environment (IDE) in the experimental analysis procedure. The experimental results are demonstrated in section 4.

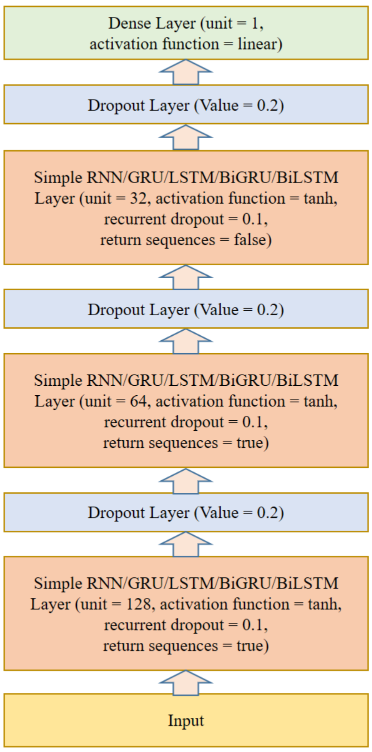

Figure 2. The architecture of the proposed RNNs based models.

4. Results and Discussion

In the experimental analysis, the MAPE, RMSE, MAE, ME, and R^2 values have been achieved by RNN based forecasting models using 15-time steps and 30-time steps. They are shown in Table 1 and Table 2, respectively.

The MAPE values of 9.89570, 7.62121, 7.49335, 7.67349, and 5.57651 have been obtained by Simple RNN, LSTM, GRU, BiLSTM, and BiGRU, respectively using 15-time steps. The RMSE values of 206.37288, 142.80177, 145.68867, 158.26411, and 105.81920 have been obtained by Simple RNN, LSTM, GRU, BiLSTM, and BiGRU, respectively using 15-time steps. The MAE values of 144.39049, 100.47967, 103.07377, 106.58208, and 72.15339 have been obtained by Simple RNN, LSTM, GRU, BiLSTM, and BiGRU, respectively using 15-time steps. The ME values of 682.65857, 510.06079, 475.12952, 606.73975, and 363.47583 have been obtained by Simple RNN, LSTM, GRU, BiLSTM, and BiGRU, respectively using 15-time steps. The R^2 values of 0.88933, 0.94701, 0.94484, 0.93491, and 0.97090 have been obtained by Simple RNN, LSTM, GRU, BiLSTM, and BiGRU, respectively using 15-time steps.

The MAPE values of 9.43851, 9.09959, 8.04758, 10.00580, and 5.92589 have been obtained by Simple RNN, LSTM, GRU, BiLSTM, and BiGRU, respectively using 30-time steps. The RMSE values of 179.52415, 175.20459, 147.95750, 209.32432, and 115.41735 have been obtained by Simple RNN, LSTM, GRU, BiLSTM, and BiGRU, respectively using 30-time steps. The MAE values of 133.35700, 124.50980, 109.93346, 147.30624, and 80.63772 have been obtained by Simple RNN, LSTM, GRU, BiLSTM, and BiGRU, respectively using 30-time steps. The ME values of 578.12439, 634.39209, 467.02515, 675.71265, 385.47656 have been obtained by Simple RNN, LSTM, GRU, BiLSTM, and BiGRU, respectively using 30-time steps. The R^2 values of 0.91199, 0.91617, 0.94022, 0.88035, and 0.96362 have been obtained by Simple RNN, LSTM, GRU, BiLSTM, and BiGRU, respectively using 30-time steps.

Table 1. Performance analysis of models for 15-time steps.

Models	MAPE	RMSE	MAE	ME	R^2
Simple RNN	9.89570	206.37288	144.39049	682.65857	0.88933
LSTM	<u>7.62121</u>	<u>142.80177</u>	<u>100.47967</u>	<u>510.06079</u>	<u>0.94701</u>
GRU	<u>**7.49335**</u>	<u>**145.68867**</u>	<u>**103.07377**</u>	<u>**475.12952**</u>	<u>**0.94484**</u>
BiLSTM	7.67349	158.26411	106.58208	606.73975	0.93491
BiGRU	**5.57651**	**105.81920**	**72.15339**	**363.47583**	**0.97090**

Note: The highest performance has been indicated by bold, the second highest performance has been indicated by underlined, and the third highest performance has been indicated by bold-underlined.

The best three forecasting performance among Simple RNN, LSTM, GRU, BiLSTM, BiGRU models for 15-time steps is achieved with MAPE value of 5.57651, RMSE value of

105.81920, MAE value of 72.15339, ME value of 363.47583, and R^2 value of 0.97090 in BiGRU model. The second top forecasting performance in MAPE value of 7.62121, RMSE value of 142.80177, MAE value of 100.47967, ME value of 510.06079, and R^2 value of 0.94701 has been achieved by the LSTM model. The third top forecasting performance in MAPE value of 7.49335, RMSE value of 145.68867, MAE value of 103.07377, ME value of 475.12952, and R^2 value of 0.94484 has been achieved by GRU model.

Table 2. Performance analysis of models for 30-time steps.

Models	MAPE	RMSE	MAE	ME	R^2
Simple RNN	9.43851	179.52415	133.35700	578.12439	0.91199
LSTM	**9.09959**	**175.20459**	**124.50980**	**634.39209**	**0.91617**
GRU	8.04758	147.95750	109.93346	467.02515	0.94022
BiLSTM	10.00580	209.32432	147.30624	675.71265	0.88035
BiGRU	**5.92589**	**115.41735**	**80.63772**	**385.47656**	**0.96362**

Note: The highest performance has been indicated by bold, the second highest performance has been indicated by underlined, and the third highest performance has been indicated by bold-underlined.

The best three forecasting performance among Simple RNN, LSTM, GRU, BiLSTM, BiGRU models for 30-time steps has been achieved with MAPE value of 5.92589, RMSE value of 115.41735, MAE value of 80.6372, ME value of 385.47656, and R2 value of 0.96362 in BiGRU model. The second top forecasting performance in MAPE value of 8.04758, RMSE value of 147.95750, MAE value of 109.93346, ME value of 467.02515, and R2 value of 0.94022 has been achieved by GRU model. The third top forecasting performance in MAPE value of 9.09959, RMSE value of 175.20459, MAE value of 124.50980, ME value of 634.39209, and R2 value of 0.91617 has been achieved by the LSTM model.

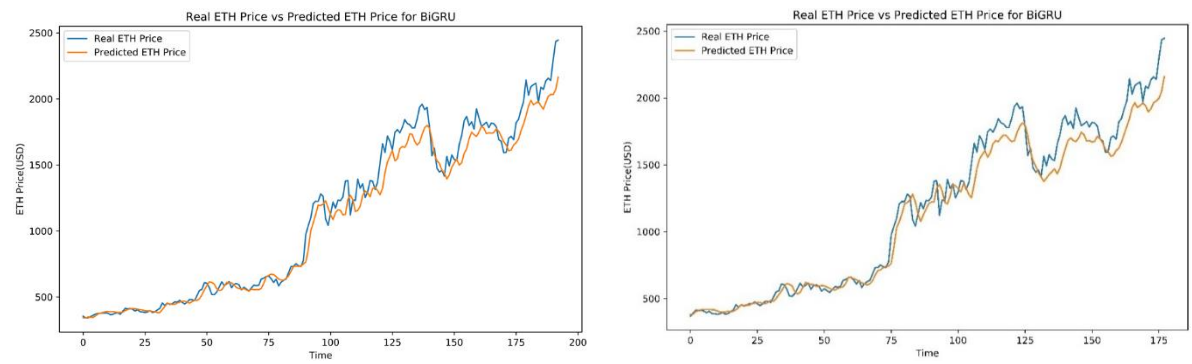

(a) **(b)**

Figure 3. (a) Real vs predicted ETH price for BiGRU using 15-time steps **(b)** Real vs predicted ETH price for BiGRU using 30-time steps.

In general analysis, 15-time steps have outperformed the 30-time steps. In considering the overall experimental analysis, the BiGRU model has outperformed other RNN based models while the Simple RNN model has the lowest forecasting performance. The best forecasting performances are shown in Figure 3 (a) and Figure 3 (b) for 15-time steps and 30-time steps, respectively.

5. Conclusion

In this paper, ETH prices analysis and prediction between 07/08/2015 and 15/04/2021 have been conducted with the RNN based models such as Simple RNN, LSTM, GRU, BiLSTM, and BiGRU. The data set includes 2079 samples with five different features, such as date, open, high, low, and volume. These features have been used to forecast the closing price of ETH with different time steps of 15 and 30. The best forecasting performance in MAPE value of 5.92589, RMSE value of 115.41735, MAE value of 80.6372, ME value of 385.47656, and R2 value of 0.96362 has been achieved by BiGRU model using 15-time steps. The second best forecasting performance in MAPE value of 5.92589, RMSE value of 115.41735, MAE value of 80.6372, ME value of 385.47656, and R2 value of 0.96362 has been achieved by BiGRU model 30-time steps. The third best forecasting performance in MAPE value of 7.62121, RMSE value of 142.80177, MAE value of 100.47967, ME value of 510.06079, and R^2 value of 0.94701 has been achieved by LSTM model using 15-time steps. Considering all results 15-time steps have outperformed the 30-time steps, additionally, the BiGRU model has outperformed the other RNN based models.

References

1. N. Gandal and H. Halaburda, Can we predict the winner in a market with network effects? Competition in cryptocurrency market, Games, Vol: 7, No: 3, 16, 2016.

2. Cryptocurrency Prices, Charts And Market Capitalizations | CoinMarketCap. https://coinmarketcap.com/ (accessed Apr. 16, 2021).

3. T. Zoumpekas, E. Houstis, and M. Vavalis, ETH analysis and predictions utilizing deep learning, Expert Syst. Appl., Vol: 162, 113866, 2020.

4. A. Yazdinejad, H. HaddadPajouh, A. Dehghantanha, R. M. Parizi, G. Srivastava, and M. Y. Chen, Cryptocurrency malware hunting: A deep Recurrent Neural Network approach, Appl. Soft Comput. J., Vol: 96, 106630, 2020.

5. S. McNally, J. Roche, and S. Caton, Predicting the Price of Bitcoin Using Machine Learning, in Proceedings - 26th Euromicro International Conference on Parallel, Distributed, and Network-Based Processing, PDP 2018, 339-343, 2018.

6. S. Ji, J. Kim, and H. Im, A comparative study of bitcoin price prediction using deep learning, Mathematics, Vol: 7, No: 10, 898, 2019.

7. I. E. Livieris, N. Kiriakidou, S. Stavroyiannis, and P. Pintelas, An advanced CNN-LSTM model for cryptocurrency forecasting, Electron., Vol: 10, No: 3, 1–16, 2021.

8. A. Onan, Mining opinions from instructor evaluation reviews: A deep learning approach, Comput. Appl. Eng. Educ., Vol: 28, No: 1, 117–138, 2020.

9. L. Zhang, S. Wang, and B. Liu, Deep learning for sentiment analysis: A survey, Wiley Interdiscip. Rev. Data Min. Knowl. Discov., Vol: 8, No: 4, 2018.

10. R. Pascanu, T. Mikolov, and Y. Bengio, On the difficulty of training recurrent neural networks, in 30th International Conference on Machine Learning, ICML 2013, 2347–2355, 2013.

11. K. Cho et al., Learning phrase representations using RNN encoder-decoder for statistical machine translation, in EMNLP 2014 - 2014 Conference on Empirical Methods in Natural Language Processing, Proceedings of the Conference, 1724-1734, 2014.

DECOMPOSITION AND DECOUPLING ANALYSIS OF CARBON DIOXIDE EMISSIONS FROM ECONOMIC GROWTH IN OECD OVER 1990-2018

Seher BODUR[1], İhsan ALP[2]

[1]Department of Statistics, University of Bitlis Eren, Bitlis, Turkey

[2]Department of Statistics, University of Gazi, Ankara, Turkey

skorkmaz@beu.edu.tr,

ihsanalp@gazi.edu.tr

Abstract

Global warming has serious impacts on natural ecosystems and human socioeconomic systems and requires urgent action. Decoupling analysis is an important tool to evaluate the relationship between economic growth and environmental issues. In this study, it is aimed to comprehensively understand the interdependence between the economy and CO_2 emissions of the Organization for Economic Co-operation and Development (OECD) countries from 1990 to 2018, and to ensure reference for developing countries. First, the driving forces of energy-related CO_2 emissions of OECD countries are determined using the Logarithmic Mean Divisia Index-II (LMDI-II) decomposition method. Moreover, to investigate the decoupling between economic growth and CO_2 emissions of the same countries, the results of the LMDI-II method are integrated into the Tapio decoupling method. The results of the LMDI-II decomposition method show that per capita Gross Domestic Product (GDP) plays an important role in the increase of CO_2 emissions, while energy intensity plays an important role in the reduction of CO_2 emissions. Finally, based on results of the combined Tapio method, the decoupling status of the OECD are determined and recommendations are presented.

Keywords: Decomposition method; Decoupling index; Index.

1. INTRODUCTION

Since the 1980s, global warming has been a cause for concern as it has caused a number of problems, such as melting glaciers and rising sea levels. According to the evidence provided by the Intergovernmental Panel on Climate Change (IPCC), among the six types of greenhouse gas emissions, CO_2 emissions account for more than half of the total greenhouse gas impact. For this reason, the main reason for global warming is due to the increase in CO_2 emissions. The Paris Agreement aims to keep the average increase in global temperature below at least 2 °C to avoid major damage to climate change. In 2019, United States (US) and Turkey's CO_2 emissions were 4.964 billion tons (mt), and 0.383 mt, respectively. Additionally, the US, accounted for 41.3% of the total CO_2 emissions of the Organization for Economic Cooperation and Development (OECD) countries (BP, 2020). Thus, due to the growing concern about global climate change, both the driving factors that affect CO_2 emissions and the subject how to decouple from economic growth of CO_2 emissions has become increasingly apparent.

In most countries shortly after the world oil crisis of 1973/1974, it was of great interest to measure the impact of structural change in industrial production on total industrial energy demand in order to better understand the mechanisms of change in energy use in industry (Ang, 2004b). Extensive efforts have been made to understand the mechanisms of change in industrial energy use through industry-wide analysis. In this context, many decomposition analyzes have been proposed. Decomposition analysis is an analytical tool designed to measure the driving forces affecting changes in the aggregate indicator, using principles taken from index value theory. For this purpose, the Logarithmic Mean Divisia Index (LMDI) decomposition analysis was proposed by Ang and Choi (1997). The LMDI decomposition method has found an important application in studies analyzing environmental pollution and energy consumption in some countries and regions. The LMDI decomposition method consists of two different methods: Logarithmic Mean Divisia Index-I (LODE-I) and Logarithmic Mean Divisia Index-II (LODE-II). The difference between them is due to the weight formulas used. The LODE-I method was introduced by Ang, Zhang and Choi (1998). The LODE-II method was introduced by Ang, Liu, and Chew (2003).

Sustaining economic growth and reducing CO_2 emissions at the same time pose a major challenge. Various indicators are available to track changes in the relationship between economic growth and CO_2 emissions. The term decoupling, introduced by Von (1989), was first used by Zhang (2000) to study environmental problems. It was later presented as an indicator by the OECD (2002). While this indicator is easy to calculate, it has not provided enough information to reveal the actions between economic growth and the environment. To overcome this weakness, another decoupling indicator presented by Tapio (2005) was defined to investigate the decoupling state of economic growth and energy-related CO_2 emissions from the transport sector of 15 European countries. In this decoupling indicator, eight logical possibilities are presented to differentiate the state of decoupling: recessive coupling, expansive coupling, weak negative decoupling, strong negative decoupling, expansive negative decoupling, weak decoupling, strong decoupling, and expansive decoupling.

Tapio decoupling analysis has attracted great attention in studies between economic growth and environmental issue (or energy) on recent years. Vehmas, Luukkanen and Kaivo-Oja (2007) redefined Tapio (2005) decoupling framework by extracting two decoupling states (expansive coupling and recessive coupling) while working on the decoupling of resource flow and economic development in the Euroepan Union (EU). Using the OECD indicator, De Freitas and Kaneko (2011) demonstrated the important decoupling between economic activity and CO_2 emissions from energy consumption in Brazil from 1980 to 2009. Conrad and Cassar (2014) calculated the OECD indicator for several extremes on the small island of Malta from 1995 to 2011 and revealed the weak (relative) decoupling for greenhouse gases. Using the Tapio method, Ren, Yin, and Chen (2014) state four differentiation states of China manufacturing industry as: strong negative decoupling (1996-1999), weak decoupling (2000-2001), expansive negative decoupling (2002-2004) and weak decoupling (2005-2010). Shuai, Chen, Wu, Zhang, and Tan (2019); They used the Tapio decoupling method to describe the decoupling states of economic growth resulting from carbon intensity, per capita carbon emissions, and total carbon emissions.

2. METHODOLOGY AND DATA

2.1.Data

In this study, firstly the LMDI-II method is used to determine the driving forces of energy-related CO_2 emissions in 35 OECD countries. Later, the results of the LMDI-II method are combined with the Tapio decoupling method to investigate the relationship between economic growth and CO_2 emissions of the same countries. Energy-related CO_2 emissions, fossil energy

consumption (oil, natural gas and coal consumption), primary energy consumption, per capita Gross Domestic Product (GDP) and population data are used in these analyzes.
GDP and population data were derived from World Development Indicators (WorldBank, 2020). Energy-related CO_2 emissions, fossil energy consumption (oil, natural gas and coal consumption) and primary energy consumption were obtained from BP Statistical Review of World Energy (BP, 2020). Missing data were estimated by regression method.

2.2.LMDI-II Decomposition Analysis

At the Intergovernmental Panel on Climate Change (IPSC) seminar, Professor Yoichi Kaya suggested Kaya identity for the first time. He associated CO_2 emissions with per capita GDP, energy policies, and population factors (Kaya, 1990). Thus, energy-related CO_2 emissions can be expressed using ideas from existing decomposition models, the extended Kaya identity and LMDI-II decomposition method:

$$C = \sum_i \frac{C_i}{F_i} \times \frac{F_i}{E_i} \times \frac{E_i}{GDP_i} \times \frac{GDP_i}{P_i} \times \frac{P_i}{P} \times PY \tag{1}$$

where, C is CO_2 emissions related with total energy; C_i is the CO_2 emissions of i-th unit; F_i is the total oil, natural gas and coal consumption of i-th unit; E_i is the primary energy consumption of i-th unit; GDP_i is the GDP of i-th unit; P_i is the population of i-th unit and PY represents the total population.

$$FE_i = \frac{C_i}{F_i}, ET_i = \frac{F_i}{E_i}, EY_i = \frac{E_i}{GDP_i}, GP_i = \frac{GDP_i}{P_i}, PD_i = \frac{P_i}{P}, PY = P \tag{2}$$

If written as above, equation (2) can be written as follows:

$$C = \sum_i FE_i \times ET_i \times EY_i \times GP_i \times PD_i \times P \tag{3}$$

where, FE_i is the CO_2 emission intensity of fossil energy of i-th unit; ET_i is the energy consumption structure of i-th unit; EY_i is the energy intensity of i-th unit; GP_i is per capita GDP of i-th unit; PD_i is the total population distribution of i-th unit and P denotes the total population (Chen, Wang, Cui, Huang ve Song, 2018).

Using the LMDI-II method, the factors contributing to the changes in CO_2 emission were analyzed. According to (Ang 2004a), changes in total CO_2 emission from year 0 to T, the difference change of CO_2 emission in additive decomposition could be calculated as:

$$\Delta C_{toplam} = C^T - C^0 = \Delta C_{FE} + \Delta C_{ET} + \Delta C_{EY} + \Delta C_{GP} + \Delta C_{PD} + \Delta C_P \tag{4}$$

where FE, ET, EY, GP, PD, P sub-indices, respectively, represent the changes in CO_2 emissions affected by changes in the CO_2 emission intensity of fossil energy, changes in CO_2 emissions affected by changes in energy consumption structure, changes in CO_2 emissions affected by changes in energy intensity, changes in CO_2 emissions affected by changes in per capita GDP, changes in CO_2 emissions affected by changes in population distribution and changes in CO_2 emissions affected by changes in population size.

In the above equation, the contribution of each factor is determined as follows:

$$\Delta C_{FE} = \sum_i \frac{L\left(\frac{C_i^T}{C^T}, \frac{C_i^0}{C^0}\right) L(C^T, C^0)}{\sum_j L\left(\frac{C_j^T}{C^T}, \frac{C_j^0}{C^0}\right)} \times ln\left(\frac{FE_i^T}{FE_i^0}\right) \tag{5}$$

$$\Delta C_{ET} = \sum_i \frac{L\left(\frac{C_i^T}{C^T}, \frac{C_i^0}{C^0}\right) L(C^T, C^0)}{\sum_j L\left(\frac{C_j^T}{C^T}, \frac{C_j^0}{C^0}\right)} \times ln\left(\frac{ET_i^T}{ET_i^0}\right) \tag{6}$$

$$\Delta C_{EY} = \sum_i \frac{L\left(\frac{C_i^T}{C^T}, \frac{C_i^0}{C^0}\right) L(C^T, C^0)}{\sum_j L\left(\frac{C_j^T}{C^T}, \frac{C_j^0}{C^0}\right)} \times ln\left(\frac{EY_i^T}{EY_i^0}\right) \tag{7}$$

$$\Delta C_{GP} = \sum_i \frac{L\left(\frac{C_i^T}{C^T}, \frac{C_i^0}{C^0}\right) L(C^T, C^0)}{\sum_j L\left(\frac{C_j^T}{C^T}, \frac{C_j^0}{C^0}\right)} \times ln\left(\frac{GP_i^T}{GP_i^0}\right) \tag{8}$$

$$\Delta C_{PD} = \sum_i \frac{L\left(\frac{C_i^T}{C^T}, \frac{C_i^0}{C^0}\right) L(C^T, C^0)}{\sum_j L\left(\frac{C_j^T}{C^T}, \frac{C_j^0}{C^0}\right)} \times ln\left(\frac{PD_i^T}{PD_i^0}\right) \tag{9}$$

$$\Delta C_{P} = \sum_i \frac{L\left(\frac{C_i^T}{C^T}, \frac{C_i^0}{C^0}\right) L(C^T, C^0)}{\sum_j L\left(\frac{C_j^T}{C^T}, \frac{C_j^0}{C^0}\right)} \times ln\left(\frac{PY_i^T}{PY_i^0}\right) \tag{10}$$

where, $\sum_i \frac{L\left(\frac{C_i^T}{C^T}, \frac{C_i^0}{C^0}\right) L(C^T, C^0)}{\sum_j L\left(\frac{C_j^T}{C^T}, \frac{C_j^0}{C^0}\right)}$ is the weight function. $L\left(\frac{C_i^T}{C^T}, \frac{C_i^0}{C^0}\right)$ as following:

$$L\left(\frac{C_i^T}{C^T}, \frac{C_i^0}{C^0}\right) = \sum_i \frac{\frac{C_i^T}{C^T} - \frac{C_i^0}{C^0}}{ln\frac{C_i^T}{C^T} - ln\frac{C_i^0}{C^0}}, \quad \frac{C_i^T}{C^T} \neq \frac{C_i^0}{C^0}$$

$$= \frac{C_i^T}{C^T} \quad , \quad \frac{C_i^T}{C^T} = \frac{C_i^0}{C^0}$$

$$= 0 \quad , \quad \frac{C_i^T}{C^T} = \frac{C_i^0}{C^0} = 0.$$

2.3. Decoupling Analysis

In physics, the term "decoupling" means to separate the relationship between certain physical variables. The decoupling indicator was used by OECD (2002) to eliminate the relationship between environmental bads and economic goods. The decoupling analysis has been used to determine whether there is a synergy for the relation between carbon emissions and economic growth or not. This method has been widely used in the literature as it is an effective tool used to analyze the relation between two different variables. According to the definition presented by Tapio (2005), the decoupling indicator ε between economic growth and CO_2 emissions from 0 to t year can be expressed as:

$$\varepsilon_{\text{CO2,GDP}} = \frac{\%\Delta C}{\%\Delta GDP} = \frac{\frac{C^t - C^0}{C^0}}{\frac{GDP^t - GDP^0}{GDP^0}} \tag{11}$$

where, ε shows the elastic coefficient of decoupling, t is time, ΔC represents the change in CO_2 emission between 0 years and t years; ΔGDP shows the change in GDP between 0 years and t years.

As shown in Table 1, according to the differences in Tapio elastic indices, the decoupling state was subdivided into decoupling, negative decoupling, and coupling, which were further subdivided as strong decoupling, weak decoupling, recessive decoupling, strong negative decoupling, weak negative decoupling, expansive negative decoupling, expansive coupling, and recessive coupling (Tapio, 2005).

Table 1. Classification of decomposition states

Classification	Decoupling state	ΔCO_2	ΔGDP	ε
Decoupling	Strong (absolute) decoupling	<0	>0	ε <0
	Weak (relative) decoupling	>0	>0	$0 \leq \varepsilon < 0.8$
	Recessive decoupling	<0	<0	$\varepsilon > 1.2$
Negative decoupling	Strong negative decoupling	>0	<0	$\varepsilon < 0$
	Weak negative decoupling	<0	<0	$0 \leq \varepsilon < 0.8$
	Expansive negative decoupling	>0	>0	$\varepsilon > 1.2$
Coupling	Expansive coupling	>0	>0	$0.8 \leq \varepsilon < 1.2$
	Recessive coupling	<0	<0	$0.8 \leq \varepsilon \leq 1.2$

3. APPLICATIONS AND RESULTS

3.1.Results of LMDI-II decomposition analysis

In this study change in energy-related CO_2 emissions in five periods 1990-2000, 2001-2006, 2007-2009, 2010-2015, and 2016-2018 for OECD countries is examined. The effects of driving factors affecting the change in CO_2 emissions during these five periods were calculated in Matlab and the results are shown in Table 2.

Table 2. Results of LMDI-II additive decomposition analysis

Period	ΔC	ΔCfe	ΔCet	ΔCey	ΔCgp	ΔCpd	ΔCp
1990-2000	1451.325	-338.802	-144.314	-1895.668	2726.660	73.446	1030.003
2001-2006	567.387	-30.906	-85.213	-1122.517	1320.869	3.817	481.336
2007-2009	-1126.456	-147.663	-210.189	-417.077	-551.525	4.777	195.222
2010-2015	-572.052	-218.833	-161.873	-1452.114	889.853	-6.008	376.924
2016-2018	91.530	-112.440	-110.577	-290.197	461.159	0.605	142.980

As seen in Table 2, the CO_2 emissions of OECD increased by 1.451 mt during 1990-2000. The increases in CO_2 emissions arising from per capita GDP, population distribution and population size were by 2.726 mt, 0.073 mt, and 1.030 mt, respectively. In addition, the reductions in CO_2 emissions owing to CO_2 emission intensity of fossil energy, energy consumption structure, and energy intensity were 0.338 mt, 0.144 mt, and 1.895 mt, respectively. Thus, in the period 1990-2000, per capita GDP and energy intensity were the main factors affecting the changes in CO_2 emissions.

From 2001 to 2006, the CO_2 emissions of OECD increased by 0.567 mt. The increases in CO_2 emissions from per capita GDP, population distribution, and population size were 1.320 mt, 0.003 mt and 0.481 mt, respectively. Additionally, the reductions in CO_2 emissions owing to CO_2 emission intensity of fossil energy, energy consumption structure, and energy intensity were 0.030, 0.085 mt, and 1.122 mt, respectively. Thus, the main factors affecting the changes in CO_2 emissions were per capita GDP and energy intensity during 2001-2006.

The CO_2 emissions of OECD decreased by 1.126 mt in the period 2007-2009. While per capita GDP was the main factor reducing CO_2 emissions during 2007-2009, it played an important role in the increase of CO_2 emissions in other periods. The reason for this, there was a brief decrease in the total amount of CO_2, because of a certain impact of the global economic crisis on per capita GDP. Additionally, the increases in CO_2 emissions owing to population distribution and population size were 0.004 mt and 0.195 mt, respectively.

Between 2010 and 2015, the CO_2 emissions of OECD decreased by 0.572 mt. The reductions in CO_2 emissions owing to CO_2 emission intensity of fossil energy, energy consumption structure, and energy intensity were 0.218 mt, 0.161 mt, and 1.452 mt, respectively. In addition, the increases in CO_2 emissions due to per capita GDP, population distribution and population size were 0.889 mt, 0.006 mt and 0.376 mt, respectively.

During 2016-2018, there was an increase by 0.091 mt in CO_2 emissions of OECD. The increases in CO_2 emissions due to per capita GDP, population distribution and population size were 0.461 mt, 0.0006 mt and 0.142 mt, respectively. In addition, the CO_2 emission intensity of fossil energy, energy consumption structure and energy intensity reduced CO_2 emissions by 0.112 mt, 0.110 and 0.290 mt, respectively. Thus, per capita GDP, population distribution and population size were the factors that increased the changes in CO_2 emissions in the 2016-2018 period.

Also, as shown in Figure 1, referring to the five periods studied, the factors affecting an increase in CO_2 emissions of OECD are per capita GDP, population distribution and population size. Among these driving factors, per capita GDP has the largest effect. The impact of population distribution is too small to be ignored. In addition, the factor that has the greatest impact on the reduction in CO_2 emissions is energy intensity.

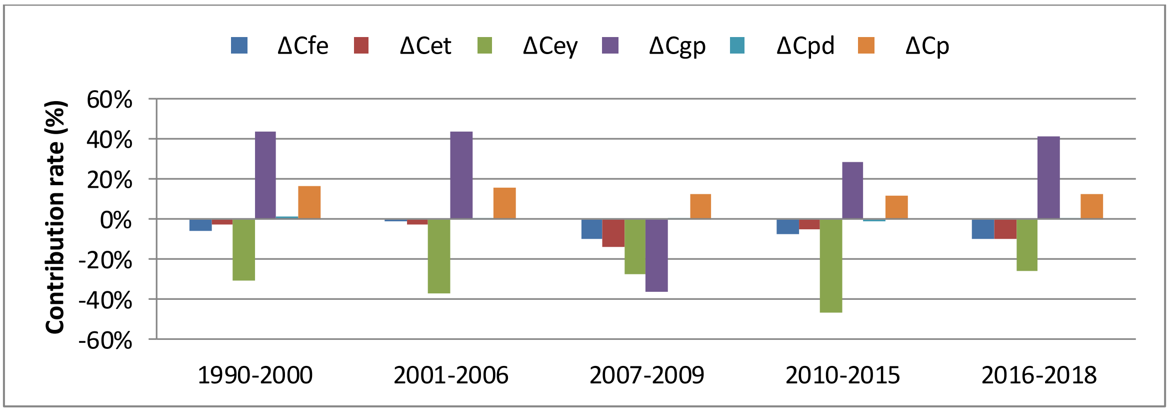

Figure 1. Contributions of driving factors to CO_2 emissions

28 time periods are calculated in order to understand the impact of driving factors affecting CO_2 emissions in consecutive years of OECD, as well as to evaluate the consistency with the results in the five periods mentioned above. The results are shown in Table 3.

Table 3. Results of LMDI-II additive decomposition analysis from 1990 to 2018

Period	ΔC	ΔCfe	ΔCet	ΔCey	ΔCgp	ΔCpd	ΔCp
1990-1991	-11,8634	-39,8514	-55,8182	-88,8756	56,4485	4,7263	111,5070
1991-1992	27,3505	-81,2235	12,2423	-219,2611	196,6868	7,4659	111,4401
1992-1993	83,3602	-18,8512	-68,2586	-63,1021	119,8880	7,5934	106,0907
1993-1994	185,4257	-48,6219	29,4000	-217,4612	314,8343	6,8298	100,4447
1994-1995	148,1891	-90,5757	-62,1884	-48,7097	243,9176	6,7485	98,9967
1995-1996	430,6136	-2,4082	1,8255	-9,0996	335,7566	7,0178	97,5214
1996-1997	142,7712	3,8698	10,6892	-360,8191	380,7747	8,5713	99,6854
1997-1998	30,9756	-14,7033	-1,0444	-347,9533	289,8909	8,1211	96,6646
1998-1999	115,1288	-53,3933	-22,6140	-286,3296	372,3872	8,1048	96,9737
1999-2000	300,0486	23,5579	13,0466	-275,2399	433,4503	8,9420	96,2918
2000-2001	-56,5310	12,1723	15,0322	-266,4610	80,9720	4,6720	97,0815
2001-2002	64,1146	-39,4169	-26,6034	-108,4476	140,8975	1,7240	95,9611
2002-2003	247,0906	37,4290	67,3133	-153,0093	203,2050	-1,0859	93,2385
2003-2004	161,9184	-23,3005	-66,3642	-201,9041	356,4047	0,5149	96,5677
2004-2005	112,6939	17,6906	-5,6787	-303,0407	304,8689	1,1439	97,7099
2005-2006	-17,4682	-23,5248	-55,3111	-366,6910	324,5134	2,4829	101,0625
2006-2007	119,9203	-27,0145	57,3572	-265,8583	255,6513	-0,2248	100,0094
2007-2008	-218,8328	-7,3512	-66,6167	-203,1321	-48,5884	2,1090	104,7465
2008-2009	-908,0362	-139,3336	-143,8698	-218,4872	-501,4237	2,2550	92,8231
2009-2010	459,2534	-12,8145	-10,7179	102,6680	294,9032	1,5646	83,6499
2010-2011	-131,8117	4,8368	-17,1956	-375,5858	193,1515	0,5355	62,4458
2011-2012	-167,6849	-73,8632	49,2701	-342,1928	122,0843	-0,3620	77,3787
2012-2013	33,8430	-29,5780	-67,6780	-75,6973	133,1783	-3,4793	77,0973
2013-2014	-183,2150	-18,7754	-72,5254	-370,5036	201,5597	-2,6087	79,6384
2014-2015	-123,7787	-96,8657	-53,4554	-288,0387	235,8576	-0,6888	79,4122
2015-2016	-74,4932	-99,2591	-64,8391	-133,9504	143,2077	0,0554	80,2923
2016-2017	39,0481	-41,3942	-48,9433	-180,7117	237,8955	0,1685	72,0334
2017-2018	52,3321	-70,6728	-61,6457	-109,6257	223,2329	0,2872	70,7562

In order to understand the percentage contributions of driving factors that affect the changes in CO_2 emissions of OECD in consecutive years, the content of Table 3 has been transformed into the graph in Figure 2.

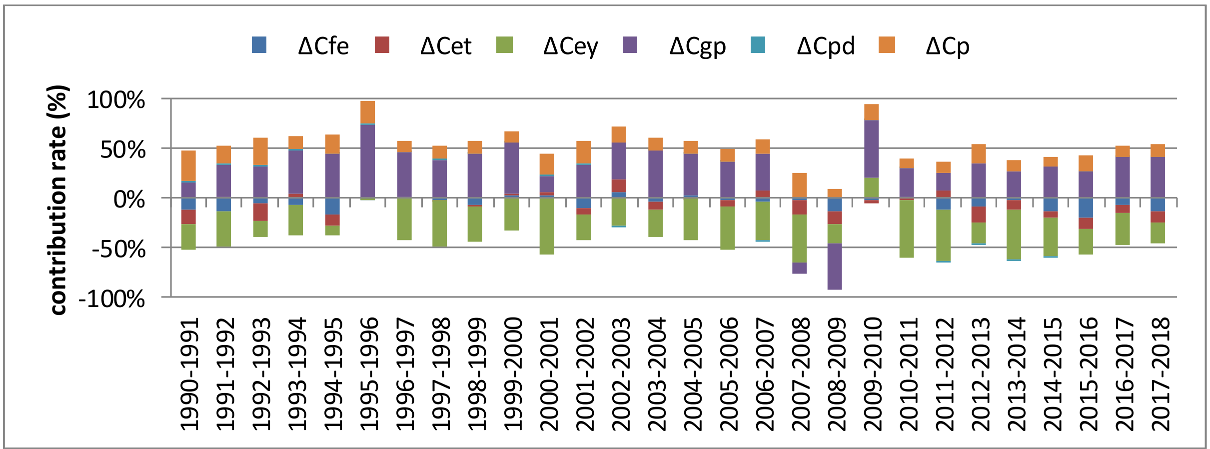

Figure 2. Contributions of driving factors to CO_2 emissions from 1990 to 2018

According to Table 3 and Figure 2, changes in CO_2 emissions are generally consistent with the five periods studied. Per capita GDP (except 2007-2008, and 2008-2009), population size are the factors that increase CO_2 emissions. Per capita GDP is the factor that affected the decrease in CO_2 emissions in the period of 2007-2009 due to the global economic crisis. Additionally, the main factors affecting the decrease of CO_2 emissions are energy intensity. As in the five periods studied, the effect of population distribution on the increase in CO_2 emissions is negligible from 1990 to 2018.

Results of the combined Tapio decoupling analysis

Table 4 shows the decoupling states between CO_2 emissions and economic growth of OECD in the periods 1990-2000, 2001-2006, 2007-2009, 2010-2015 and 2016-2018. 3 states of decoupling occurred during these periods: weak decoupling, recessive decoupling, and strong decoupling.

Table 4. Decoupling indices of OECD countries

Period	$\Delta C/C^0$	$\Delta GDP/GDP^0$	$\varepsilon_{CO2,GDP}$	Decoupling/Coupling State
1990-2000	0.1184	0.3077	0.3849	WD
2001-2006	0.0435	0.1311	0.3318	WD
2007-2009	-0.0830	-0.0323	2.5695	RD
2010-2015	-0.0437	0.0933	-0.4681	SD
2016-2018	0.0074	0.0469	0.1573	WD

WD: Weak decoupling, RD: Recessive decoupling, SD: Strong decoupling.

As seen in Table 4, strong decoupling between CO_2 emissions and economic growth in the period 2010-2015 is available. That is, it means that there is economic growth while CO_2 emissions are decreasing, and it is the most favorable situation to be achieved. Thus, economic growth and reduction in CO_2 emissions are achieved simultaneously. In addition, CO_2 emissions have decreased without compromising economic growth.

In the periods 1990-2000, 2001-2006 and 2016-2018, the decoupling state between CO_2 emissions and economic growth is weak decoupling. This situation indicates that the growth rate in CO_2 emissions is lower than the economic growth rate.

Between 2007 and 2009, the decoupling state between CO_2 emissions and economic growth is recessive decoupling. This case indicates that there is a decrease in both economic growth rate and CO_2 emissions. However, the reduction in CO_2 emissions is faster than the decline in the economic growth rate.

Table 5. Decoupling indexes of OECD counties from 1990 to 2018

Period	$\Delta C/C^0$	$\Delta GDP/GDP^0$	$\varepsilon_{CO2,GDP}$	Decoupling/Coupling State
1990-1991	-0.0014	0.0151	-0.0946	SD
1991-1992	0.0017	0.0209	0.0818	WD
1992-1993	0.0065	0.0122	0.5318	WD
1993-1994	0.0152	0.0308	0.4942	WD
1994-1995	0.0119	0.0269	0.4426	WD
1995-1996	0.0352	0.0310	1.1360	EC
1996-1997	0.0108	0.0346	0.3116	WD
1997-1998	0.0018	0.0282	0.0644	WD
1998-1999	0.0085	0.0325	0.2609	WD
1999-2000	0.0229	0.0400	0.5714	WD
2000-2001	-0.0047	0.0139	-0.3372	SD

2001-2002	0.0048	0.0156	0.3097	WD
2002-2003	0.0191	0.0198	0.9642	EC
2003-2004	0.0122	0.0318	0.3826	WD
2004-2005	0.0083	0.0276	0.3012	WD
2005-2006	-0.0015	0.0301	-0.0489	SD
2006-2007	0.0089	0.0256	0.3473	WD
2007-2008	-0.0162	0.0026	-6.3262	SD
2008-2009	-0.0679	-0.0348	1.9522	RD
2009-2010	0.0366	0.0289	1.2671	END
2010-2011	-0.0102	0.0179	-0.5710	SD
2011-2012	-0.0130	0.0127	-1.0262	SD
2012-2013	0.0029	0.0147	0.2002	WD
2013-2014	-0.0142	0.0205	-0.6929	SD
2014-2015	-0.0098	0.0242	-0.4063	SD
2015-2016	-0.0060	0.0173	-0.3469	SD
2016-2017	0.0032	0.0243	0.1300	WD
2017-2018	0.0042	0.0221	0.1905	WD

SD: Strong decoupling, WD: Weak decoupling, EC: Expansive coupling, RD: Recessive decoupling, END: Expansive negative decoupling.

According to Table 5, OECD countries achieved strong decoupling between CO_2 emissions and economic growth in the periods 1990-1991, 2000-2001, 2005-2006, 2007-2008, 2010-2011, 2011-2012, 2013-2014, 2014-2015 and 2015-2016. This means that per capita GDP is growthing while CO_2 emissions are decreasing.

CONCLUSION

The global warming that is being experienced at the present time is an important global environmental problem. The main results of this study taking into account this problem may be summarized as follows:

- LMDI-II additive decomposition method is used to investigate the driving factors affecting CO_2 emissions in OECD.
- In this paper is effectively combined with the decomposition results of LMDI-II method and the Tapio decoupling analysis method to explore the decoupling relationship between CO_2 emissions and economic growth from 1990 to 2018.

In light of these results, developing countries such as Turkey should focus on renewable energy sources and reduce the use of solid fuels to improve the energy efficiency performance. Particularly in the production department, the share of non-fossil fuels should be increased with financial incentives and tax advantages.
In short, using filters to increase the rate of renewable energy in the energy generation structure and to reduce air pollution will be the key to achieve strong decoupling.

REFERENCES

1. Ang, B. W. (2004a). Decomposition analysis for policymaking in energy: which is the preferred method?. *Energy policy*, *32*(9), 1131-1139.
2. Ang, B. W. (2004b). *Decomposition analysis applied to energy*. Holland: Elsevier, 761-769.

3. Ang, B. W., and Choi, K. H. (1997). Decomposition of aggregate energy and gas emission intensities for industry: a refined Divisia index method. *The Energy Journal*, *18*(3), 59-73.
4. Ang, B.W., Liu, F.L., Chew, E.P. (2003). Perfect decomposition techniques in energy and environmental analysis. *Energy Policy*, 31, 1561–1566.
5. Ang, B. W., Zhang, F. Q., & Choi, K. H. (1998). Factorizing changes in energy and environmental indicators through decomposition. *Energy*, *23*(6), 489-495.
6. BP (2020). BP statistical review of world energy. URL: https://www.bp.com/, Accessed on 1 July 2020.
7. Chen, J., Wang, P., Cui, L., Huang, S., and Song, M. (2018). Decomposition and decoupling analysis of CO2 emissions in OECD. *Applied energy*, *231*, 937-950.
8. Conrad, E., and Cassar, L. (2014). Decoupling economic growth and environmental degradation: Reviewing progress to date in the small island state of Malta. *Sustainability*, *6*(10), 6729-6750.
9. De Freitas, L. C. and Kaneko, S. (2011). Decomposing the decoupling of CO2 emissions and economic growth in Brazil. *Ecological Economics*, *70*(8), 1459-1469.
10. Kaya, Y. (1990). *Impact of carbon dioxide emission control on GNP growth: Interpretation of proposed scenarios*. Paper presented at the IPCC Energy and Industry Subgroup, Response Strategies Working Group, Paris, France.
11. Organisation for Economic Co-operation and Development (OECD). (2002). Indicators to measure decoupling of environmental pressure from economic growth.
12. Ren, S., Yin, H., and Chen, X. (2014). Using LMDI to analyze the decoupling of carbon dioxide emissions by China's manufacturing industry. *Environmental Development*, *9*, 61-75.
13. Shuai, C., Chen, X., Wu, Y., Zhang, Y., and Tan, Y. (2019). A three-step strategy for decoupling economic growth from carbon emission: empirical evidences from 133 countries. *Science of The Total Environment*, *646*, 524-543.
14. Tapio, P. (2005). Towards a theory of decoupling: degrees of decoupling in the EU and the case of road traffic in Finland between 1970 and 2001. *Transport policy*, *12*(2), 137-151.
15. Vehmas, J., Luukkanen, J., and Kaivo-Oja, J. (2007). Linking analyses and environmental Kuznets curves for aggregated material flows in the EU. *Journal of Cleaner Production*, *15*(17), 1662-1673.
16. Von Weizsacker, E. U. (1989). *Erdpolitik: ökologische Realpolitik an der Schwelle zum Jahrhundert der Umwelt*. Wissenschaftliche Buchgesellschaft.
17. World Bank. World Development Indicators. Available from: http://databank.worldbank.org/data/reports.aspx?source=world-development-indicators Accessed on 18 July 2020.
18. Zhang, Z. (2000). Decoupling China’s carbon emissions increase from economic growth: An economic analysis and policy implications. *World Development*, *28*(4), 739-752.

Coefficient Inequalities for A Subclass of Bi-Univalent Functions Defined by Pell-Lucas Polynomials

Onur SABUR, Murat ÇAĞLAR, Erhan DENİZ

Department of Mathematics, Faculty of Science and Letters, Kafkas University, Kars, Turkey

onursabur@gmail.com, mcaglar25@gmail.com, edeniz36@gmail.com

Abstract

In this study, we investigate a certain subclass of bi-univalent functions defined by Pell-Lucas polynomials. For functions belonging to the defined subclass, we then derive coefficient inequalities and Fekete-Szegö inequalities.

Keywords: Analytic functions, Bi-univalent functions, Coefficient inequalities, Fekete-Szegö inequality, Pell-Lucas polynomials.

1. INTRODUCTION

Let $\mathbb{R}$ be the set of real numbers, $\mathbb{C}$ be the set of complex numbers and

$$\mathbb{N} = \{1, 2, 3, ...\} \tag{1}$$

be the set of positive integers. Let A denote the class of functions of the form

$$f(z) = z + \sum_{n=2}^{\infty} a_n z^n \tag{2}$$

which are analytic in the open unit disk $\Delta = \{z : z \in \mathbb{C} \text{ and } |z| < 1\}$. Further, by S we shall denote the class of all functions in A which are univalent in Δ.

It is well known that every function $f \in S$ has an inverse f^{-1}, defined by

$$f^{-1}(f(z)) = z \qquad (z \in \Delta) \tag{3}$$

and

$$f^{-1}(f(w)) = w \qquad (|w| < r_0(f);\ r_0(f) \geq \frac{1}{4}) \tag{4}$$

where

$$f^{-1}(w) = w - a_2 w^2 + (2a_2^2 - a_3)w^3 - (5a_2^3 - 5a_2 a_3 + a_4)w^4 + \cdots. \tag{5}$$

A function $f \in A$ is said to be bi-univalent in Δ if both the function f and its inverse f^{-1} are univalent in Δ. Let σ denote the class of bi-univalent functions in Δ given by (2).

In 2010, Srivastava et al. [1] revived the study of bi-univalent functions by their pioneering work on the study of coefficient problems. Various subclasses of the bi-univalent function class σ were introduced and nonsharp estimates on the first two coefficients $|a_2|$ and $|a_3|$ in the Taylor-Maclaurin series expansion (2) were found in the recent investigations (see, for example, [2-23]) and including the references therein. The afore-cited all these papers on the subject were actually motivated by the work of Srivastava et al. [1]. However, the problem to find the coefficient bounds on $|a_n|$ $(n=3,4,\cdots)$ for functions $f\in\sigma$ is still open problem.

The following classical Fekete-Szegö inequality, which is investigated by means of Loewner's chain method, involves the Taylor-Maclaurin coefficient of $f\in S$ given by (2):

$$\left|a_3-\mu a_2^2\right|\leq 1+2\exp\left(-\frac{2\mu}{1-\mu}\right) \qquad (0\leq\mu<1).$$

For analytic functions f and g in Δ, f is said to be subordinate to g if there exists an analytic function w such that

$$w(0)=0,\ |w(z)|<1 \text{ and } f(z)=g(w(z))\ (z\in\Delta). \tag{6}$$

This subordination will be denoted here by

$$f\prec g\ (z\in\Delta) \tag{7}$$

or, conventionally, by

$$f(z)\prec g(z)\ (z\in\Delta) \tag{8}$$

In particular, when g is univalent in Δ,

$$f\prec g\ \ (z\in\Delta)\Leftrightarrow f(0)=g(0) \text{ and } f(\Delta)\subset g(\Delta). \tag{9}$$

Let $p(x)$ and $q(x)$ be polynomials with real coefficients. The (p,q)-Lucas polynomials $L_{p,q,n}(x)$ are established by the recurrence relation [22],

$$L_{p,q,n}(x)=p(x)L_{p,q,n-1}(x)+q(x)L_{p,q,n-2}(x) \quad (n\geq 2)$$

from which the first few Lucas polynomials can be found as

$$L_{p,q,0}(x)=2,\ L_{p,q,1}(x)=p(x),\ L_{p,q,2}(x)=p^2(x)+2q(x).$$

For the special cases of $p(x)=2x$ and $q(x)=1$, we can get the Pell-Lucas polynomials.

The first few Lucas polynomials can be found as

$$L_{2x,1,0}(x)=2,\ L_{2x,1,1}(x)=2x,\ L_{2x,1,2}(x)=4x^2+2. \tag{10}$$

The generating function of the Pell-Lucas polynomials $L_{2x,1,n}(x)$ (see [22]) is given by

$$G_{\{L_{2x,1,n}(x)\}}(z)=\frac{2-2xz}{1-2xz-z^2}=\sum_{n=0}^{\infty}L_{2x,1,n}(x)z^n \,. \tag{11}$$

In this paper, we obtain coefficient estimates and Fekete-Szegö inequality for subclass $\mathrm{R}_G(\beta,\gamma,\delta,x)$.

2. COEFFICIENT ESTIMATES AND FEKETE-SZEGÖ INEQUALITIES

A functions $f\in A$ of the form (2) belongs to the class $\mathrm{R}_G(\beta,\gamma,\delta,x)$ for $\gamma\geq 1,\ \delta\geq 0,\ \beta\in\mathbb{C}/\{0\}$ and $z,w\in\Delta$, if the following conditions are satisfied:

$$1+\frac{1}{\beta}\left[(1-\gamma)\frac{f(z)}{z}+\gamma f'(z)+\delta zf''(z)-1\right]\prec \mathrm{G}\{L_{2x,1,n}(x)\}(z)-1 \tag{12}$$

and for $g(w)=f^{-1}(w)$

$$1+\frac{1}{\beta}\left[(1-\gamma)\frac{g(w)}{w}+\gamma g'(w)+\delta zg''(w)-1\right]\prec \mathrm{G}\{L_{2x,1,n}(x)\}(w)-1\,. \tag{13}$$

Theorem 1. Let $f\in\mathrm{R}_G(\beta,\gamma,\delta,x)$. Then

$$|a_2|\leq\frac{2|x||\beta|\sqrt{2|x|}}{\sqrt{\left|4x^2\beta(1+2\gamma+6\delta)-\left(4x^2+2\right)(1+\gamma+2\delta)^2\right|}}\,,$$

(14)

$$|a_3|\leq\frac{2|x||\beta|}{1+2\gamma+6\delta}+\frac{4|x^2||\beta^2|}{(1+\gamma+2\delta)^2}$$

and for $\mu\in\mathbb{R}$

$$\left|a_3-\mu a_2^2\right|\leq\begin{cases}\dfrac{2|x||\beta|}{1+2\gamma+6\delta}, & 0\leq|F(\mu,\beta,\gamma,\delta,x)|\leq\dfrac{|\beta|}{2(1+2\gamma+6\delta)}\\[2ex] 4|x||F(\mu,\beta,\gamma,\delta,x)|, & |F(\mu,\beta,\gamma,\delta,x)|\geq\dfrac{|\beta|}{2(1+2\gamma+6\delta)}\end{cases} \tag{15}$$

where

$$F(\mu,\beta,\gamma,\delta,x)=\frac{2(1-\mu)x^2\beta}{4x^2\beta(1+2\gamma+6\delta)-\left(4x^2+2\right)(1+\gamma+2\delta)^2}\,.$$

Proof. Let $f \in \mathrm{R}_G(\beta,\gamma,\delta,x)$ be given by the Taylor-Maclaurin expansion (2). Then, there are analytic functions u and v such that

$$u(0)=0;\ \ v(0)=0,\ \ |u(z)|<1 \text{ and } |v(w)|<1\ \ (\forall z,w\in\Delta) \tag{16}$$

and we can write

$$1+\frac{1}{\beta}\left[(1-\gamma)\frac{f(z)}{z}+\gamma f'(z)+\delta z f''(z)-1\right]=G\left\{L_{2x,1,n}(x)\right\}u(z)-1 \tag{17}$$

and

$$1+\frac{1}{\beta}\left[(1-\gamma)\frac{g(w)}{w}+\gamma g'(w)+\delta w g''(w)-1\right]=G\left\{L_{2x,1,n}(x)\right\}v(w)-1 \tag{18}$$

Equivalently,

$$1+\frac{1}{\beta}\left[(1-\gamma)\frac{f(z)}{z}+\gamma f'(z)+\delta z f''(z)-1\right]=1+2xu_1 z+\left[2xu_2+(4x^2+2)u_1^2\right]z^2+\cdots \tag{19}$$

and

$$1+\frac{1}{\beta}\left[(1-\gamma)\frac{g(w)}{w}+\gamma g'(w)+\delta z g''(w)-1\right]=1+2xv_1 w+\left[2xv_2+(4x^2+2)v_1^2\right]w^2+\cdots. \tag{20}$$

From (19) and (20) and in view of (11), we obtain

$$1+\frac{1}{\beta}\left[(1-\gamma)\frac{f(z)}{z}+\gamma f'(z)+\delta z f''(z)-1\right]=1+2xt_1 z+\left[2xt_2+(4x^2+2)t_1^2\right]z^2+\cdots \tag{21}$$

and

$$1+\frac{1}{\beta}\left[(1-\gamma)\frac{g(w)}{w}+\gamma g'(w)+\delta z g''(w)-1\right]=1+2xs_1 w+\left[2xs_2+(4x^2+2)s_1^2\right]w^2+\cdots. \tag{22}$$

$$u(z)=\sum_{n=1}^{\infty}t_n z^n \qquad \text{and} \qquad v(w)=\sum_{n=1}^{\infty}s_n w^n \tag{23}$$

then it is well known that

$$|t_n|\le 1 \quad \text{and} \quad |s_n|\le 1 \qquad (n\in\mathbb{N}). \tag{24}$$

Thus upon comparing the corresponding coefficients in (21) and (22), we have

$$\left(\frac{1+\gamma+2\delta}{\beta}\right)a_2=2xt_1, \tag{25}$$

$$\left(\frac{1+2\gamma+6\delta}{\beta}\right)a_3=2xt_2+(4x^2+2)t_1^2, \tag{26}$$

$$\frac{-(1+\gamma+2\delta)}{\beta}a_2 = 2xs_1 \tag{27}$$

and

$$\frac{(1+2\gamma+6\delta)}{\beta}(2a_2^2-a_3) = 2xs_2+(4x^2+2)s_1^2. \tag{28}$$

From (25) and (27) we can easily see that

$$t_1 = -s_1 \tag{29}$$

and

$$a_2^2 = \frac{4x^2\beta^2}{2(1+\gamma+2\delta)^2}(t_1^2+s_1^2). \tag{30}$$

If we add (26) to (28), we get

$$\frac{2(1+2\gamma+6\delta)}{\beta}a_2^2 = 2x\left(t_2+s_2\right)+\left(4x^2+2\right)(t_1^2+s_1^2). \tag{31}$$

By substituting (30) in (31), we obtain

$$a_2^2 = \frac{8x^3\beta^2(t_2+s_2)}{8x^2\beta(1+2\gamma+6\delta)-2\left(4x^2+2\right)(1+\gamma+2\delta)^2} \tag{32}$$

and by taking $|t_n| \le 1,\ |s_n| \le 1$ and $|t_2+s_2| \le |t_2|+|s_2|$, we have

$$|a_2| \le \frac{2|\beta||x|\sqrt{2|x|}}{\sqrt{\left|4x^2\beta(1+2\gamma+6\delta)-\left(4x^2+2\right)(1+\gamma+2\delta)^2\right|}}. \tag{33}$$

By subtracting (28) from (26) and in view of (29), we obtain

$$2\left(\frac{1+2\gamma+6\delta}{\beta}\right)\left(a_3-a_2^2\right) = 2x(t_2-s_2)+\left(4x^2+2\right)(t_1^2-s_1^2),$$

$$a_3 = \frac{2x\beta(t_2-s_2)}{2(1+2\gamma+6\delta)}+a_2^2. \tag{34}$$

Then in view of (30), (34) becomes,

$$a_3 = \frac{2x\beta(t_2-s_2)}{2(1+2\gamma+6\delta)}+\frac{4x^2\beta^2(t_1^2+s_1^2)}{2(1+\gamma+2\delta)^2} \tag{35}$$

and so,

$$|a_3| \le \frac{2|x||\beta|}{1+2\gamma+6\delta} + \frac{4|x^2||\beta^2|}{(1+\gamma+2\delta)^2}. \tag{36}$$

From (35), for $\mu \in \mathbb{R}$, we write

$$a_3 - \mu a_2^2 = \frac{\beta p(x)(t_2 - s_2)}{2(1+2\gamma+6\delta)} + (1-\mu)a_2^2. \tag{37}$$

By substituting (32) in (37), we have

$$a_3 - \mu a_2^2 = \frac{2x\beta(t_2 - s_2)}{2(1+2\gamma+6\delta)} + \frac{8(1-\mu)x^3\beta^2(t_2+s_2)}{2\left[4x^2\beta(1+2\gamma+6\delta) - \left(4x^2+2\right)(1+\gamma+2\delta)^2\right]}$$

If we take the right side from here to t_2 and s_2

$$\begin{aligned} a_3 - \mu a_2^2 &= \left(\frac{2x\beta}{2(1+2\gamma+6\delta)} + \frac{8(1-\mu)x^3\beta^2}{2\left[4x^2\beta(1+2\gamma+6\delta) - \left(4x^2+2\right)(1+\gamma+2\delta)^2\right]} \right) t_2 \\ &\quad + \left(\frac{8(1-\mu)x^3\beta^2}{2\left[4x^2\beta(1+2\gamma+6\delta) - \left(4x^2+2\right)(1+\gamma+2\delta)^2\right]} - \frac{2x\beta}{2(1+2\gamma+6\delta)} \right) s_2 \\ &= p(x)\left\{ \left(F(\mu,\beta,\gamma,\delta,x) + \frac{\beta}{2(1+2\gamma+6\delta)} \right) t_2 + \left(F(\mu,\beta,\gamma,\delta,x) - \frac{\beta}{2(1+2\gamma+6\delta)} \right) s_2 \right\} \end{aligned} \tag{38}$$

where

$$F(\mu,\beta,\gamma,\delta,x) = \frac{2(1-\mu)x^2\beta}{4x^2\beta(1+2\gamma+6\delta) - \left(4x^2+2\right)(1+\gamma+2\delta)^2}. \tag{39}$$

Hence, we conclude that

$$|a_3 - \mu a_2^2| \le \begin{cases} \dfrac{2|x||\beta|}{1+2\gamma+6\delta}, & 0 \le |F(\mu,\beta,\gamma,\delta,x)| \le \dfrac{|\beta|}{2(1+2\gamma+6\delta)} \\ \\ 4|x||F(\mu,\beta,\gamma,\delta,x)|, & |F(\mu,\beta,\gamma,\delta,x)| \ge \dfrac{|\beta|}{2(1+2\gamma+6\delta)} \end{cases} \tag{40}$$

and it evidently completes the proof of Theorem 1.

Corollary 1. Let $f \in \mathrm{R}_G(1,0,\delta,x)$. Then

$$|a_2| \le \frac{2|x|\sqrt{2|x|}}{\sqrt{\left|4x^2(1+6\delta)-\left(4x^2+2\right)(1+2\delta)^2\right|}},$$

$$|a_3| \le \frac{2|x|}{1+6\delta}+\frac{4|x^2|}{(1+2\delta)^2}$$

and for $\mu \in \mathbb{R}$

$$\left|a_3-\mu a_2^2\right| \le \begin{cases} \dfrac{2|x|}{1+6\delta}, & 0 \le |F(\mu,1,0,\delta,x)| \le \dfrac{1}{2(1+6\delta)} \\ \\ 4|x||F(\mu,1,0,\delta,x)|, & |F(\mu,1,0,\delta,x)| \ge \dfrac{1}{2(1+6\delta)} \end{cases}$$

where

$$F(\mu,1,0,\delta,x)= \frac{2(1-\mu)x^2}{4x^2(1+6\delta)-\left(4x^2+2\right)(1+2\delta)^2}.$$

Corollary 2. Let $f \in \mathrm{R}_G(1,\gamma,0,x)$. Then

$$|a_2| \le \frac{2|x|\sqrt{2|x|}}{\sqrt{\left|4x^2(1+2\gamma)-\left(4x^2+2\right)(1+\gamma)^2\right|}},$$

$$|a_3| \le \frac{2|x|}{1+2\gamma}+\frac{4|x^2|}{(1+\gamma)^2}$$

and for $\mu \in \mathbb{R}$

$$\left|a_3-\mu a_2^2\right| \le \begin{cases} \dfrac{2|x|}{1+2\gamma}, & 0 \le |F(\mu,1,\gamma,0,x)| \le \dfrac{1}{2(1+2\gamma)} \\ \\ 4|x||F(\mu,1,\gamma,0,x)|, & |F(\mu,1,\gamma,0,x)| \ge \dfrac{1}{2(1+2\gamma)} \end{cases}$$

where

$$F(\mu,1,\gamma,0,x)= \frac{2(1-\mu)x^2}{4x^2(1+2\gamma)-\left(4x^2+2\right)(1+\gamma)^2}.$$

REFERENCES

1. Srivastava H. M., Mishra A. K., Gochhayat P., Certain subclasses of analytic and bi-univalent functions, Applied Mathematics Letters, vol.23, no. 10, pp. 1188-1192, 2010.
2. Ali R. M., Lee S. K., Ravichandran V., Supramanian S., Coefficient estimates for bi-univalent Ma-Minda starlike and convex funtions, Applied Mathematics Letters, vol. 25, no. 3, pp. 344-351, 2012.
3. Altınkaya S., Yalçin S., On the Chebyshev polynomial coefficient problem of some subclasses of bi- univalent functions, Gulf Journal of Mathematics, vol.5, no. 3, pp. 34-40, 2017.
4. Altınkaya S., Yalçin S., Chebyshev polynomial coefficient bounds for subclass of bi-univalent functions, pp. 1-7, 2017, https://arxiv.org/abs/1605.08224.
5. Çağlar M., Deniz E., Srivastava H. M., Second Hankel determinant for certain subclasses of bi-univalent fonctions. Turkish Journal of Mathematics, vol. 41, pp. 694-706, 2017.
6. Girgaonkar V. B., Joshi S. B., Coefficient estimates for certain subclass of bi-univalent functions associated with Chepyshev polynomial, Ganita, vol. 68, no. 1, pp. 79-85, 2018.
7. Güney H. O., Murugusundaramoorthy G., Sokol J., Subclasses of bi-univalent functions related to shell-like curves connected with Fibonacci numbers, Acta Universitatis Sapientiae, Mathematica, vol. 10, no. 1, pp. 70-84, 2018.
8. Jahangiri J. M., Hamidi S. G., Halim S. A., Coefficients of bi-univalent functions with positive real part derivatives, Bulletin of the Malaysian Matematical Sciences Society, vol. 37, no. 3, pp. 633-640, 2014.
9. Kanas S., Analouei Adegani E., Zireh A., An unified approach to second Hankel determinant of bi-subordinate functions, Mediterranean Journal of Mathematics, vol. 14, no. 6, Article ID 233, 2017.
10. Lee S. K., Ravichandran V., Supramaniam S., Initial coeffcient of bi-univalent functions, Abstract and Applied Analysis, vol. 2014, Article ID 640856, pp. 1–6, 2014.
11. Li X.-F., Wang A.-P., Two new subclasses of bi-univalent functions, International Mathematical Forum, vol. 7, no. 29-32, pp. 1495–1504, 2012.
12. Magesh N., Bulut S., Chebyshev polynomial coeffcient estimates for a class of analytic bi-univalent functions related to pseudo-starlike functions, Afrika Matematika, vol. 29, no. 1-2, pp. 203–209, 2018.
13. Orhan H., Magesh N., Balaji V. K., Second Hankel determinant for certain class of bi-univalent functions defined by Chebyshev polynomials, Asian-European Journal of Mathematics, vol. 12, no. 1, pp. 1–16, 2019.
14. Peng Z., Han Q., On the coeffcient of several classes of bi-univalent functions, Acta Mathematica Sinica Series B (English Edition), vol. 34, no. 1, pp. 228–240, 2014.
15. Srivastava H. M., Altınkaya S., Yalçin S., Certain subclasses of bi-univalent functions associated with the Horadam polynomials, Iranian Journal of Science and Technology, Transactions A: Science, pp. 1–7, 2018.
16. Srivastava H. M., Sakar F. M., Güney H. Ö., Some general coeffcient estimates for a new class of analytic and bi-univalent functions defined by a linear combination, Filomat, vol. 32, no. 4, pp. 1313–1322, 2018.
17. Srivastava H. M., Eker S. S., Hamidi S. G., Jahangiri J. M., Faber polynomial coeffcient estimates for bi-univalent functions defined by the Tremblay fractional derivative operator, Bulletin of the Iranian Mathematical Society, vol. 44, no. 1, pp. 149–157, 2018.

18. Srivastava H. M., Magesh N., Yamini J., Initial coeffcient estimates for bi-λ-convex and bi-μ-starlike functions connected with arithmetic and geometric means, Electronic Journal of Mathematical Analysis and Applications, vol. 2, no. 2, pp. 152–162, 2014.
19. Tu Z., Xiong C. L., Coeffcient problems for unified starlike and convex classes of m-fold symmetric bi-univalent functions, Journal of Mathematical Inequalities, vol. 12, no. 4, pp. 921–932, 2018.
20. Xiong L., Liu X., Some extensions of coeffcient problems for bi-univalent Ma-Minda starlike and convex functions, Filomat, vol. 29, no. 7, pp. 1645–1650, 2015.
21. Zaprawa P., On the Fekete–Szegö problem for classes of bi-univalent functions, Bulletin of the Belgian Mathematical Society - Simon Stevin, vol. 21, no. 1, pp. 169–178, 2014.
22. Horadam A. F., Mahon J. M., Pell and Pell-Lucas polynomials, Fibonacci Quarterly, vol. 23, pp. 7–20, 1985.
23. Hörçum T., Koçer E. Gökçen, On some properties of Horadam polynomials, International Mathematical Forum, vol. 4, pp. 1243–1252, 2009.

Fekete-Szegö Inequlity for A Subclass of Bi-Univalent Functions Defined by Horadam Polynomials

Ozan Ali ÇAĞRAŞAN, Murat ÇAĞLAR, Erhan DENİZ

Department of Mathematics, Faculty of Science and Letters, Kafkas University, Kars, Turkey

ozanalicagrasan@hotmail.com, mcaglar25@gmail.com, edeniz36@gmail.com

Abstract

In this study, we obtain coefficient inequalities and Fekete-Szegö inequalities for a certain subclass of bi-univalent functions defined by Horadam polynomials.

Keywords: Analytic functions, Bi-univalent functions, Coefficient inequalities, Fekete-Szegö inequality, Horadam polynomials.

1. INTRODUCTION

Let $\mathbb{R}$ be the set of real numbers, $\mathbb{C}$ be the set of complex numbers and

$$\mathbb{N} = \{1, 2, 3, \ldots\} \tag{1}$$

be the set of positive integers. Let A denote the class of functions of the form

$$f(z) = z + \sum_{n=2}^{\infty} a_n z^n \tag{2}$$

which are analytic in the open unit disk $\Delta = \{z : z \in \mathbb{C} \text{ and } |z| < 1\}$. Further by S we shall denote the class of all functions in A which are univalent in Δ.

It is well known that every function $f \in S$ has an inverse f^{-1}, defined by

$$f^{-1}(f(z)) = z \qquad (z \in \Delta) \tag{3}$$

and

$$f^{-1}(f(w)) = w \qquad (|w| < r_0(f);\ r_0(f) \geq \frac{1}{4}) \tag{4}$$

where

$$f^{-1}(w) = w - a_2 w^2 + (2a_2^2 - a_3)w^3 - (5a_2^3 - 5a_2 a_3 + a_4)w^4 + \cdots. \tag{5}$$

A function $f \in A$ is said to be bi-univalent in Δ if both the function f and its inverse f^{-1} are univalent in Δ. Let σ denote the class of bi-univalent functions in Δ given by (2).

In 2010, Srivastava et al. [1] revived the study of bi-univalent functions by their pioneering work on the study of coefficient problems. Various subclasses of the bi-univalent functions class σ were introduced and nonsharp estimates on the first two coefficients $|a_2|$ and $|a_3|$ in the Taylor-Maclaurin series expansion (2) were found in there recent investigations (see, for example, [2-23]) and including thereferences therein. The afore-cited all these papers on the subject were actually motivated by the work of Srivastava et al. [1]. However, the problem to find the coefficient bounds on $|a_n|$ $(n = 3, 4, \cdots)$ for functions $f \in \sigma$ is stil open problem.

The following classical Fekete-Szegö inequality, which is investigated by means of Loewner's chain method, involves the Taylor-Maclaurin coefficient of $f \in S$ given by (2):

$$\left|a_3 - \mu a_2^2\right| \le 1 + 2\exp\left(-\frac{2\mu}{1-\mu}\right) \qquad \left(0 \le \mu < 1\right).$$

For analytic functions f and g in Δ, f is said to be subordinate to g if there exists an analytic function w such that

$$w(0) = 0, \ |w(z)| < 1 \text{ and } f(z) = g(w(z)) \quad (z \in \Delta). \tag{6}$$

This subordination will be denoted here by

$$f \prec g \quad (z \in \Delta) \tag{7}$$

or, conventionally, by

$$f(z) \prec g(z) \quad (z \in \Delta). \tag{8}$$

In particular, when g is univalent in Δ,

$$f \prec g \ (z \in \Delta) \Leftrightarrow f(0) = g(0) \text{ and } f(\Delta) \subset g(\Delta). \tag{9}$$

The Horadam polynomials $h_n\left(x, a, b; p, q\right)$, or briefly $h_n(x)$ are given by the following recurrence relation (see [22,23]):

$$h_1(x) = a\,, \ h_2(x) = bx\,, \ h_3(x) = pbx^2 + aq \tag{10}$$

and

$$h_n(x) = pxh_{n-1}(x) + qh_{n-2}(x) \qquad (n \ge 3)$$

for some real constants a, b, p and q.

The generating function of the Horadam polynomials $h_n(x)$ (see [23]) is given by

$$\Pi(x,z)=\frac{a+(b-ap)xz}{1-pxz-qz^2}=\sum_{n=1}^{\infty}h_n(x)z^{n-1}. \tag{11}$$

Here, and in what follows, the argument $x\in\mathbb{R}$ is independent of the argument $z\in\mathbb{C}$; that is, $x\neq\Re(z)$.

Note that for particular values of a,b,p and q, the Horadam polynomial $h_n(x)$ leads to various polynomials, among those, we list a few cases here (see [22,23] for more details):

(1) For $a=b=p=q=1$, we have the Fibonacci polynomials $F_n(x)$.
(2) For $a=2$ and $b=p=q=1$, we obtain the Lucas polynomials $L_n(x)$.
(3) For $a=q=1$ and $b=p=2$, we get the Pell polynomials $P_n(x)$.
(4) For $a=b=p=2$ and $q=1$, we attain the Pell-Lucas polynomials $Q_n(x)$.
(5) For $a=b=1$, $p=2$ and $q=-1$, we have the Chebyshev polynomials $T_n(x)$ of the first kind.
(6) For $a=1$, $b=p=2$ and $q=-1$, we obtain the Chebyshev polynomials $U_n(x)$ of the second kind.

In this paper, we obtain coefficient estimates and Fekete-Szegö inequality for subclass $\mathrm{R}_{\Pi}(\beta,\gamma,\delta,x)$.

2. COEFFICIENT ESTIMATES AND FEKETE-SZEGÖ INEQUALITIES

A functions $f\in A$ of the form (2) belongs to the class $\mathrm{R}_{\Pi}(\beta,\gamma,\delta,x)$ for $\gamma\geq 1$, $\delta\geq 0$, $\beta\in\mathbb{C}/\{0\}$ and $z,w\in\Delta$, if the following conditions are satisfied:

$$1+\frac{1}{\beta}\left[(1-\gamma)\frac{f(z)}{z}+\gamma f'(z)+\delta zf''(z)-1\right]\prec\Pi(x,z)+1-a \tag{12}$$

and for $g(w)=f^{-1}(w)$

$$1+\frac{1}{\beta}\left[(1-\gamma)\frac{g(w)}{w}+\gamma g'(w)+\delta wg''(w)-1\right]\prec\Pi(x,w)+1-a \tag{13}$$

where the real constant a is as in (10).

Theorem 1. Let $f \in \mathrm{R}_{\Pi}(\beta,\gamma,\delta,x)$. Then

$$|a_2| \le \frac{|\beta||bx|\sqrt{|bx|}}{\sqrt{\left|\beta\left(1+2\gamma+6\delta\right)b^2x^2-\left(pbx^2+qa\right)\left(1+\gamma+2\delta\right)^2\right|}}, \tag{14}$$

$$|a_3| \le \frac{|\beta||bx|}{(1+2\gamma+6\delta)}+\frac{\beta^2b^2x^2}{(1+\gamma+2\delta)^2}$$

and for $\mu \in \mathbb{R}$

$$\left|a_3-\mu a_2^2\right| \le \begin{cases} \dfrac{|\beta||bx|}{(1+2\gamma+6\delta)}, & 0 \le |F(\mu,\beta,\gamma,\delta,x)| \le \dfrac{|\beta|}{2(1+2\gamma+6\delta)} \\ \\ 2|bx||F(\mu,\beta,\gamma,\delta,x)|, & |F(\mu,\beta,\gamma,\delta,x)| \ge \dfrac{|\beta|}{2(1+2\gamma+6\delta)} \end{cases} \tag{15}$$

where

$$F(\mu,\beta,\gamma,\delta,x)=\frac{(1-\mu)b^2x^2\beta^2}{2\left[\beta bx(1+2\gamma+6\delta)-pbx^2(1+\gamma+2\delta)^2\right]}.$$

Proof. Let $\mathrm{R}_{\Pi}(\beta,\gamma,\delta,x)$ be given by the Taylor-Maclaurin expansion (2). Then, there are analytic functions Φ and Ψ such that

$$\Phi(0)=0;\ \Psi(0)=0,\ |\Phi(z)|<1 \text{ and } |\Psi(1)|<1 \quad (\forall z,w\in\Delta) \tag{16}$$

and we can write

$$1+\frac{1}{\beta}\left[(1-\gamma)\frac{f(z)}{z}+\gamma f'(z)+\delta zf''(z)-1\right]=\prod\left(x,\Phi(z)\right)+1-a \tag{17}$$

and

$$1+\frac{1}{\beta}\left[(1-\gamma)\frac{g(w)}{w}+\gamma g'(w)+\delta wg''(w)-1\right]=\prod\left(x,\Psi(w)\right)+1-a. \tag{18}$$

Equivalently,

$$1+\frac{1}{\beta}\left[(1-\gamma)\frac{f(z)}{z}+\gamma f'(z)+\delta zf''(z)-1\right]=1+h_1(x)-a+h_2(x)\Phi(z)+h_3(x)\left[\Phi(z)\right]^2+\ldots \tag{19}$$

and

$$1+\frac{1}{\beta}\left[(1-\gamma)\frac{g(w)}{w}+\gamma g'(w)+\delta w g''(w)-1\right]=1+h_1(x)-a+h_2(x)\Psi(w)+h_3(x)\left[\Psi(w)\right]^2+\dots \quad (20)$$

From (19) and (20) and in view of (11), we obtain

$$1+\frac{1}{\beta}\left[(1-\gamma)\frac{f(z)}{z}+\gamma f'(z)+\delta z f''(z)-1\right]=1+h_2(x)p_1z+\left[h_2(x)p_2+h_3(x)p_1^2\right]z^2+\dots \quad (21)$$

and

$$1+\frac{1}{\beta}\left[(1-\gamma)\frac{g(w)}{w}+\gamma g'(w)+\delta w g''(w)-1\right]=1+h_2(x)q_1w+\left[h_2(x)q_2+h_3(x)q_1^2\right]w^2+\dots \quad (22)$$

If

$$\Phi(z)=\sum_{n=1}^{\infty}p_nz^n \qquad \text{and} \qquad \Psi(w)=\sum_{n=1}^{\infty}q_nw^n , \quad (23)$$

then it is well known that

$$|p_n|\le 1 \quad \text{and} \quad |q_n|\le 1 \quad (n\in\mathbb{N}). \quad (24)$$

Thus upon comparing the corresponding coefficients in (21) and (22), we have

$$\frac{1+\gamma+2\delta}{\beta}a_2=h_2(x)p_1, \quad (25)$$

$$\frac{1+2\gamma+6\delta}{\beta}a_3=h_2(x)p_2+h_3(x)p_1^2, \quad (26)$$

$$-\left(\frac{1+\gamma+2\delta}{\beta}\right)a_2=h_2(x)q_1, \quad (27)$$

and

$$\left(\frac{1+2\gamma+6\delta}{\beta}\right)\left(2a_2^2-a_3\right)=h_2(x)q_2+h_3(x)q_1^2. \quad (28)$$

From (25) and (27) we can easily see that

$$p_1=-q_1. \quad (29)$$

Provided $h_2(x)=bx\neq 0$ and

$$2\left(\frac{1+\gamma+2\delta}{\beta}\right)^2a_2^2=\beta^2\left[h_2(x)\right]^2\left(p_1^2+q_1^2\right),$$

$$a_2^2 = \frac{\beta^2 \left[h_2(x)\right]^2 \left(p_1^2 + q_1^2\right)}{2\left(1+\gamma+2\delta\right)^2}. \tag{30}$$

If we add (26) and (28), we get

$$2\left(\frac{1+\gamma+2\delta}{\beta}\right)a_2^2 = h_2(x)(p_2+q_2) + h_3(x)\left(p_1^2+q_1^2\right). \tag{31}$$

By substituting (30) in (31), we obtain

$$a_2^2 = \frac{\beta^2 \left[h_2(x)\right]^3 \left(p_2+q_2\right)}{2\beta\left[h_2(x)\right]^2 \left(1+2\gamma+6\delta\right) - 2h_3(x)\left(1+\gamma+2\delta\right)^2} \tag{32}$$

and by taking $h_2(x) = bx \neq 0$ and $h_3(x) = pbx^2 + qa$ in (32), it further yields

$$|a_2| \le \frac{|\beta||bx|\sqrt{|bx|}}{\sqrt{\left|\beta\left(1+2\gamma+6\delta\right)b^2x^2 - \left(pbx^2+qa\right)\left(1+\gamma+2\delta\right)^2\right|}}. \tag{33}$$

By subtracting (28) from (26) and in view of (29), we obtain

$$2\left(\frac{1+2\gamma+6\delta}{\beta}\right)a_3 - 2\left(\frac{1+2\gamma+6\delta}{\beta}\right)a_2^2 = h_2(x)(p_2-q_2) + h_3(x)\left(p_1^2-q_1^2\right),$$

$$a_3 = \frac{\beta h_2(x)(p_2-q_2)}{2\left(1+2\gamma+6\delta\right)} + a_2^2. \tag{34}$$

Then in view of (30), (34) becomes

$$a_3 = \frac{\beta h_2(x)(p_2-q_2)}{2\left(1+2\gamma+6\delta\right)} + \frac{\beta^2\left[h_2(x)\right]^2\left(p_1^2+q_1^2\right)}{2\left(1+\gamma+2\delta\right)^2}. \tag{35}$$

Applying (10), we deduce that

$$|a_3| \le \frac{|\beta||bx|}{1+2\gamma+6\delta} + \frac{\beta^2 b^2 x^2}{\left(1+\gamma+2\delta\right)^2}. \tag{36}$$

From (34), for $\mu \in \mathbb{R}$, we write

$$a_3 - \mu a_2^2 = \frac{\beta h_2(x)(p_2-q_2)}{2\left(1+2\gamma+6\delta\right)} + (1-\mu)a_2^2. \tag{37}$$

By substituting (32) in (37), we have

$$a_3-\mu a_2^2=\frac{\beta h_2(x)(p_2-q_2)}{2\left(1+2\gamma+6\delta\right)}+\left(\frac{(1-\mu)\beta^2\left[h_2(x)\right]^3\left(p_2+q_2\right)}{2\beta\left[h_2(x)\right]^2\left(1+2\gamma+6\delta\right)-2h_3(x)\left(1+\gamma+2\delta\right)^2}\right)$$

$$=h_2(x)\left\{\left(F(\mu,\beta,\gamma,\delta,x)+\frac{\beta}{2(1+2\gamma+6\delta)}\right)p_2+\left(F(\mu,\beta,\gamma,\delta,x)-\frac{\beta}{2(1+2\gamma+6\delta)}\right)q_2\right\} \tag{38}$$

where

$$F(\mu,\beta,\gamma,\delta,x)=\frac{(1-\mu)\beta^2\left[h_2(x)\right]^2}{2\left[\beta\left[h_2(x)\right]^2(1+2\gamma+6\delta)-h_3(x)(1+\gamma+2\delta)^2\right]}. \tag{39}$$

Hence, we conclude that

$$\left|a_3-\mu a_2^2\right|\le\begin{cases}\dfrac{|\beta||h_2(x)|}{1+2\gamma+6\delta}, & 0\le|F(\mu,\beta,\gamma,\delta,x)|\le\dfrac{|\beta|}{2(1+2\gamma+6\delta)}\\[2ex] 2|h_2(x)||F(\mu,\beta,\gamma,\delta,x)|, & |F(\mu,\beta,\gamma,\delta,x)|\ge\dfrac{|\beta|}{2(1+2\gamma+6\delta)}\end{cases} \tag{40}$$

and in view of (10), it evidently completes the proof of Theorem 1.

Corollary 1. Let $f\in R_{\Pi}(1,0,\delta,x)$. Then

$$|a_2|\le\frac{|bx|\sqrt{|bx|}}{\sqrt{\left|(1+6\delta)b^2x^2-\left(pbx^2+qa\right)(1+2\delta)^2\right|}},$$

$$|a_3|\le\frac{|bx|}{1+6\delta}+\frac{b^2x^2}{(1+2\delta)^2}$$

and for $\mu\in\mathbb{R}$

$$\left|a_3-\mu a_2^2\right|\le\begin{cases}\dfrac{|bx|}{1+6\delta}, & 0\le|F(\mu,1,0,\delta,x)|\le\dfrac{1}{2(1+6\delta)}\\[2ex] 2|bx||F(\mu,1,0,\delta,x)|, & |F(\mu,1,0,\delta,x)|\ge\dfrac{1}{2(1+6\delta)}\end{cases}$$

where $F(\mu,1,0,\delta,x)=\dfrac{(1-\mu)bx}{2\left[(1+6\delta)-px(1+2\delta)^2\right]}$.

Corollary 2. Let $f \in R_{\Pi}(1,\gamma,0,x)$. Then

$$|a_2| \le \frac{|bx|\sqrt{|bx|}}{\sqrt{\left|(1+2\gamma)b^2x^2-\left(pbx^2+qa\right)(1+\gamma)^2\right|}},$$

$$|a_3| \le \frac{|bx|}{1+2\gamma}+\frac{\beta^2b^2x^2}{(1+\gamma)^2}$$

and for $\mu \in \mathbb{R}$

$$|a_3-\mu a_2^2| \le \begin{cases} \dfrac{|bx|}{1+2\gamma}, & 0 \le |F(\mu,1,\gamma,0,x)| \le \dfrac{1}{2(1+2\gamma)} \\ \\ 2|bx||F(\mu,1,\gamma,0,x)|, & |F(\mu,1,\gamma,0,x)| \ge \dfrac{1}{2(1+2\gamma)} \end{cases}$$

where

$$F(\mu,1,\gamma,0,x)=\frac{(1-\mu)bx}{2\left[(1+2\gamma)-px(1+\gamma)^2\right]}.$$

REFERENCES

1. Srivastava H. M., Mishra A. K., Gochhayat P., Certain subclasses of analytic and bi-univalent functions, Applied Mathematics Letters, vol.23, no. 10, pp. 1188-1192, 2010.
2. Ali R. M., Lee S. K., Ravichandran V., Supramanian S., Coefficient estimates for bi-univalent Ma-Minda starlike and convex funtions, Applied Mathematics Letters, vol. 25, no. 3, pp. 344-351, 2012.
3. Altınkaya S., Yalçin S., On the Chebyshev polynomial coefficient problem of some subclasses of bi- univalent functions, Gulf Journal of Mathematics, vol.5, no. 3, pp. 34-40, 2017.
4. Altınkaya S., Yalçin S., Chebyshev polynomial coefficient bounds for subclass of bi-univalent functions, pp. 1-7, 2017, https://arxiv.org/abs/1605.08224.
5. Çağlar M., Deniz E., Srivastava H. M., Second Hankel determinant for certain subclasses of bi-univalent fonctions. Turkish Journal of Mathematics, vol. 41, pp. 694-706, 2017.
6. Girgaonkar V. B., Joshi S. B., Coefficient estimates for certain subclass of bi-univalent functions associated with Chepyshev polynomial, Ganita, vol. 68, no. 1, pp. 79-85, 2018.
7. Güney H. O., Murugusundaramoorthy G., Sokol J., Subclasses of bi-univalent functions related to shell-like curves connected with Fibonacci numbers, Acta Universitatis Sapientiae, Mathematica, vol. 10, no. 1, pp. 70-84, 2018.
8. Jahangiri J. M., Hamidi S. G., Halim S. A., Coefficients of bi-univalent functions with positive real part derivatives, Bulletin of the Malaysian Matematical Sciences Society, vol. 37, no. 3, pp. 633-640, 2014.

9. Kanas S., Analouei Adegani E., Zireh A., An unified approach to second Hankel determinant of bi-subordinate functions, Mediterranean Journal of Mathematics, vol. 14, no. 6, Article ID 233, 2017.
10. Lee S. K., Ravichandran V., Supramaniam S., Initial coeffcient of bi-univalent functions, Abstract and Applied Analysis, vol. 2014, Article ID 640856, pp. 1–6, 2014.
11. Li X.-F., Wang A.-P., Two new subclasses of bi-univalent functions, International Mathematical Forum, vol. 7, no. 29-32, pp. 1495–1504, 2012.
12. Magesh N., Bulut S., Chebyshev polynomial coeffcient estimates for a class of analytic bi-univalent functions related to pseudo-starlike functions, Afrika Matematika, vol. 29, no. 1-2, pp. 203–209, 2018.
13. Orhan H., Magesh N., Balaji V. K., Second Hankel determinant for certain class of bi-univalent functions defined by Chebyshev polynomials, Asian-European Journal of Mathematics, vol. 12, no. 1, pp. 1–16, 2019.
14. Peng Z., Han Q., On the coeffcient of several classes of bi-univalent functions, Acta Mathematica Sinica Series B (English Edition), vol. 34, no. 1, pp. 228–240, 2014.
15. Srivastava H. M., Altınkaya S., Yalçin S., Certain subclasses of bi-univalent functions associated with the Horadam polynomials, Iranian Journal of Science and Technology, Transactions A: Science, pp. 1–7, 2018.
16. Srivastava H. M., Sakar F. M., Güney H. Ö., Some general coeffcient estimates for a new class of analytic and bi-univalent functions defined by a linear combination, Filomat, vol. 32, no. 4, pp. 1313–1322, 2018.
17. Srivastava H. M., Eker S. S., Hamidi S. G., Jahangiri J. M., Faber polynomial coeffcient estimates for bi-univalent functions defined by the Tremblay fractional derivative operator, Bulletin of the Iranian Mathematical Society, vol. 44, no. 1, pp. 149–157, 2018.
18. Srivastava H. M., Magesh N., Yamini J., Initial coeffcient estimates for bi-λ-convex and bi-μ-starlike functions connected with arithmetic and geometric means, Electronic Journal of Mathematical Analysis and Applications, vol. 2, no. 2, pp. 152–162, 2014.
19. Tu Z., Xiong C. L., Coeffcient problems for unified starlike and convex classes of m-fold symmetric bi-univalent functions, Journal of Mathematical Inequalities, vol. 12, no. 4, pp. 921–932, 2018.
20. Xiong L., Liu X., Some extensions of coeffcient problems for bi-univalent Ma-Minda starlike and convex functions, Filomat, vol. 29, no. 7, pp. 1645–1650, 2015.
21. Zaprawa P., On the Fekete–Szegö problem for classes of bi-univalent functions, Bulletin of the Belgian Mathematical Society - Simon Stevin, vol. 21, no. 1, pp. 169–178, 2014.
22. Horadam A. F., Mahon J. M., Pell and Pell-Lucas polynomials, Fibonacci Quarterly, vol. 23, pp. 7–20, 1985.
23. Hörçum T., Koçer E. Gökçen, On some properties of Horadam polynomials, International Mathematical Forum, vol. 4, pp. 1243–1252, 2009.

A Unifying Computational Approach for Shallow Water Model of the Tsunami

P. Veeresha

Abstract

In this paper, the solution and corresponding consequences of the system exemplifying the shallow water model of the tsunami are analyzed within the frame of fractional calculus (FC) using the *q-homotopy analysis transform method* (*q*-HATM). The future method is an elegant blend of homotopy scheme with Laplace transform. Three examples are considered to validate and illustrate the efficiency of the future method in the present framework. The nature of obtained solution has been captured for distinct arbitrary order. The obtained results illuminate that, the considered method is easy to apply and more effective to examine the nature of multi-dimensional differential equations of fractional order arisen in related areas of science and technology.

Keywords: Homotopy analysis method; Caputo fractional derivative; Laplace transform; wave propagation; Tsunami.

Center for Mathematical Needs, Department of Mathematics, CHRIST (Deemed to be University), Bengaluru-560029, India

E-mail: pundikala.veeresha@christuniversity.in & viru0913@gmail.com (P. Veeresha)

1. Introduction

The notion of the fractional derivative has been manufacturing due to the convolutions connected with a heterogeneousness. Even though the classical calculus concept is an efficient tool to investigate stimulating properties of real-world problems, researchers pointed out some limitations related to history and hereditary consequences. Due to the rapid expansion of mathematical methods with computer package, numerous scholars began to work on FC to illustrate their physical behaviors through examining many complex and nonlinear models. Recently, several revolutionary definitions and notations are nurtured by senior researchers about the representation of both differential and integral operators of fractional order, and those programmed the groundwork [1-6]. The concept and theory of FC are related to applied projects, and it is widely hired in many areas [7-14]. In order to find the numerical and analytical solution for the corresponding systems, researchers considered efficient, novel, reliable schemes. Particularly, numerical, semi-analytical, and analytical algorithms area attracted researchers [15-34].

The study of nonlinear and system of differential equations is the hot topic in the present era due to their significant applications to illustrate real-world problems in an accurate manner. Particularly, partial differential equations are suitable tools for exemplifying the physical phenomena associated with both time and space consequences. In this paper, we consider the system of three partial differential equations illustrating the nonlinear shallow-water model of the tsunami. The large-scale underwater disturbances are generated due to gravity waves on the sea surface, called Tsunami [35]. Typical trigger mechanisms are earthquake-initiated landslides, volcanic eruptions, seabed displacements, the impact of large objects into underwater explosions. The surface waves generated by tsunami have a very long wavelength associated with the ocean basin's depth, where they propagate [36-39].

Here, we consider the system exemplifying the shallow water model of the tsunami with the velocity of cross-shore (V_c), the velocity of along-shore (V_a), surface elevation (E) as follows [36-39]

$$\begin{aligned} &\frac{\partial V_c(x,y,t)}{\partial t} + V_c\frac{\partial V_c}{\partial x} + V_a\frac{\partial V_c}{\partial y} = -2c^2\frac{\partial E}{\partial x}, \\ &\frac{\partial V_c(x,y,t)}{\partial t} + V_c\frac{\partial V_a}{\partial x} + V_a\frac{\partial V_a}{\partial y} + 2c^2\frac{\partial E}{\partial y} = 0, \end{aligned} \tag{1}$$

$$\frac{\partial E(x,y,t)}{\partial t} + +(V_c\, E)_x + (V_a\, E)_y = 0.$$

Here, Eq. (1) is the non-dimensional model with the gravity g and constant reference depth H and $c = \sqrt{gH}$. The essential physical properties of the nonlinear model can be captured by generalizing the classical concept, which helps to incorporate the hereditary consequences and memory effects in the model. Now, Eq. (1) is considered as

$$\begin{aligned} &D_t^\alpha V_c(x,y,t) + V_c \frac{\partial V_c}{\partial x} + V_a \frac{\partial V_c}{\partial y} = -2c^2 \frac{\partial E}{\partial x}, \\ &D_t^\alpha V_a(x,y,t) + V_c \frac{\partial V_a}{\partial x} + V_a \frac{\partial V_a}{\partial y} = -2c^2 \frac{\partial E}{\partial y},\ \ 0 < \alpha \le 1, \\ &D_t^\alpha E(x,y,t) + (V_c\, E)_x + (V_a\, E)_y = 0, \end{aligned} \tag{2}$$

where α is Caputo fractional order.

In the present work, we find the solution and examine behaviors of the system of equations demonstrating the shallow water model by using q-HATM. The projected technique is proposed by Singh et al. [40] using Laplace transform (LT) with the concept of homotopy analysis method [41, 42]. Recently, many researchers have been extremely employed due to its consistency and efficacy in finding the solution for diverse nonlinear models [43-52]. The hired scheme can lessen the time and computational work while maintaining great accuracy.

2. Preliminaries

Here, we present the notion of FC and LT.

Definition 1. The fractional Riemann-Liouville integral of a function $f(t) \in C_\delta (\delta \ge -1)$ is presented as

$$\begin{aligned} &J^\alpha f(t) = \frac{1}{\Gamma(\mu)} \int_0^t (t-\vartheta)^{\alpha-1} f(\vartheta) d\vartheta, \\ &J^0 f(t) = f(t). \end{aligned} \tag{5}$$

Definition 2. The fractional Caputo derivative of $f \in C_{-1}^n$ is defined as

$$D_t^\alpha f(t) = \begin{cases} \dfrac{d^n f(t)}{dt^n}, & \alpha = n \in \mathbb{N}\,, \\ \dfrac{1}{\Gamma(n-\alpha)} \displaystyle\int_0^t (t-\vartheta)^{n-\alpha-1} f^{(n)}(\vartheta) d\vartheta, & n-1 < \alpha < n\,, n \in \mathbb{N}. \end{cases} \tag{6}$$

Definition 3. Let $D_t^\alpha f(t)$ be a Caputo fractional derivative, then the LT is

$$L[D_t^\alpha f(t)] = s^\alpha F(s) - \sum_{r=0}^{n-1} s^{\alpha-r-1}\, f^{(r)}(0^+), (n-1 < \alpha \le n), \tag{7}$$

where $F(s)$ is LT of $f(t)$.

3. Fundamental idea proposed scheme

Here, we consider the arbitrary order differential equation with linear $\mathcal{R}$ and nonlinear $\mathcal{N}$ operators as follows

$$D_t^{\alpha} v(x,t) + \mathcal{R}\, v(x,t) + \mathcal{N}\, v(x,t) = f(x,t), \quad n-1 < \alpha \leq n. \tag{8}$$

On using the LT on Eq. (8), we have

$$s^{\alpha}\mathcal{L}[v(x,t)] - \sum_{k=0}^{n-1} s^{\alpha-k-1} v^{(k)}(x,0) + \mathcal{L}[\mathcal{R}v(x,t)] + \mathcal{L}[\mathcal{N}v(x,t)] = \mathcal{L}[f(x,t)]. \tag{9}$$

The above equation simplifies

$$\mathcal{L}[v(x,t)] - \frac{1}{s^{\alpha}}\sum_{k=0}^{n-1} s^{\alpha-k-1} v^{k}(x,0) + \frac{1}{s^{\alpha}}\{\mathcal{L}[\mathcal{R}v(x,t)] + \mathcal{L}[\mathcal{N}\, v(x,t)] - \mathcal{L}[f(x,t)]\} = 0. \tag{10}$$

with nonlinear operator

$$\begin{aligned}\mathcal{N}[\varphi(x,t;q)] = \mathcal{L}[\varphi(x,t;q)] - \tfrac{1}{s^{\alpha}}\textstyle\sum_{k=0}^{n-1} s^{\alpha-k-1}\varphi^{(k)}(x,t;q)(0^{+}) \\ + \tfrac{1}{s^{\alpha}}\{\mathcal{L}[\mathcal{R}\,\varphi(x,t;q)] + L[\mathcal{N}\varphi(x,t;q)] - L[f(x,t)]\},\ q \in \left[0, \tfrac{1}{n}\right],\end{aligned} \tag{11}$$

and homotopy

$$(1 - nq)\mathcal{L}[\varphi(x,t;q) - v_0(x,t)] = \hbar q \mathcal{N}[\varphi(x,t;q)], \tag{12}$$

where $\hbar \neq 0$ is an auxiliary parameter and L is LT. For $q = 0$ and $q = \frac{1}{n}$, we have

$$\varphi(x,t;0) = v_0(x,t),\ \varphi\left(x,t;\frac{1}{n}\right) = v(x,t), \tag{13}$$

Expanding $\varphi(x,t;q)$ in series form, one can get

$$\varphi(x,t;q) = v_0(x,t) + \sum_{m=1}^{\infty} v_m(x,t) q^m. \tag{14}$$

where

$$v_m(x,t) = \frac{1}{m!}\frac{\partial^m \varphi(x,\ t;q)}{\partial q^m}\Big|_{q=0}. \tag{15}$$

For Eq. (8)

$$v(x,t) = v_0(x,t) + \sum_{m=1}^{\infty} v_m(x,t)\left(\frac{1}{n}\right)^m. \tag{16}$$

Differentiating Eq. (12) with respect to q about m-times and then dividing by $m!$ and then considering $q = 0$, we have

$$\mathcal{L}[v_m(x,t) - k_m v_{m-1}(x,t)] = \hbar \Re_m(\vec{v}_{m-1}), \tag{17}$$

where

$$\vec{v}_m = \{v_0(x,t), v_1(x,t), \ldots, v_m(x,t)\}. \tag{18}$$

By applying the inverse LT on Eq. (17), we obtain

$$v_m(x,t) = k_m v_{m-1}(x,t) + \hbar \mathcal{L}^{-1}[\Re_m(\vec{v}_{m-1})], \tag{19}$$

where

$$\begin{aligned} \Re_m(\vec{v}_{m-1}) = L[v_{m-1}(x,t)] - \left(1 - \frac{k_m}{n}\right)\left(\sum_{k=0}^{n-1} s^{\alpha-k-1} v^{(k)}(x,0) + \frac{1}{s^\alpha} L[f(x,t)]\right) \\ + \frac{1}{s^\alpha} L[R v_{m-1} + \mathcal{H}_{m-1}], \end{aligned} \tag{20}$$

and

$$k_m = \begin{cases} 0, & m \leq 1, \\ n, & m > 1. \end{cases} \tag{21}$$

In Eq. (20), $\mathcal{H}_m$ signifies homotopy polynomial and defined as

$$\mathcal{H}_m = \frac{1}{m!}\left[\frac{\partial^m \varphi(x,t;q)}{\partial q^m}\right]_{q=0} \text{and } \varphi(x,t;q) = \varphi_0 + q\varphi_1 + q^2\varphi_2 + \cdots . \tag{22}$$

By the assist of Eqs. (19) and (20), we obtain

$$\begin{aligned} v_m(x,t) = (k_m + \hbar) v_{m-1}(x,t) - \left(1 - \frac{k_m}{n}\right) \mathcal{L}^{-1}\Big(\sum_{k=0}^{n-1} s^{\alpha-k-1} v^{(k)}(x,0) \\ + \frac{1}{s^\alpha} \mathcal{L}[f(x,t)]\Big) + \hbar \mathcal{L}^{-1}\left\{\frac{1}{s^\alpha} L[R v_{m-1} + \mathcal{H}_{m-1}]\right\}. \end{aligned} \tag{23}$$

4. Solution for Shallow Water Model

Here, we illustrated the hired scheme to find the solution for the fractional-order shallow water model. Now, consider Eq. (2)

$$\begin{aligned} & D_t^\alpha V_c(x,y,t) + V_c \frac{\partial V_c}{\partial x} + V_a \frac{\partial V_c}{\partial y} + 2c^2 \frac{\partial E}{\partial x} = 0, \\ & D_t^\alpha V_a(x,y,t) + V_c \frac{\partial V_a}{\partial x} + V_a \frac{\partial V_a}{\partial y} + 2c^2 \frac{\partial E}{\partial y} = 0, \qquad 0 < \alpha \leq 1, \\ & D_t^\alpha E(x,y,t) + \frac{\partial}{\partial x}(V_c\, E) + \frac{\partial}{\partial y}(V_a\, E) = 0, \end{aligned} \tag{24}$$

with

$$\begin{aligned} & V_c(x,y,0) = a^2 \frac{g}{d} \operatorname{sech}^2\left(\sqrt{\frac{3a}{4d^3}}\, x\right) \operatorname{sech}^2\left(\sqrt{\frac{3a}{4d^3}}\, y\right), \\ & V_a(x,y,0) = a^2 \frac{g}{d} \operatorname{sech}^2\left(\sqrt{\frac{3a}{4d^3}}\, x\right) \operatorname{sech}^2\left(\sqrt{\frac{3a}{4d^3}}\, y\right), \\ & E(x,y,0) = a^2 \operatorname{sech}^2\left(\sqrt{\frac{3a}{4d^3}}\, x\right) \operatorname{sech}^2\left(\sqrt{\frac{3a}{4d^3}}\, y\right), \end{aligned} \tag{25}$$

where $d = 20$ is the constant value of sea depth, g is the acceleration due to gravity, and $a = 2$ is the initial wave. Now, employing LT on Eq. (24), we get

$$L[V_c(x,y,t)] - \frac{1}{s}\left\{a^2 \frac{g}{d}\,\mathrm{sech}^2\left(\sqrt{\frac{3a}{4d^3}}x\right)\mathrm{sech}^2\left(\sqrt{\frac{3a}{4d^3}}y\right)\right\} + \frac{1}{s^\alpha}L\left\{V_c\frac{\partial V_c}{\partial x} + V_a\frac{\partial V_c}{\partial y} + 2c^2\frac{\partial E}{\partial x}\right\} = 0,$$

$$L[V_a(x,y,t)] - \frac{1}{s}\left\{a^2 \frac{g}{d}\,\mathrm{sech}^2\left(\sqrt{\frac{3a}{4d^3}}x\right)\mathrm{sech}^2\left(\sqrt{\frac{3a}{4d^3}}y\right)\right\} + \frac{1}{s^\alpha}L\left\{V_c\frac{\partial V_a}{\partial x} + V_a\frac{\partial V_a}{\partial y} + 2c^2\frac{\partial E}{\partial y}\right\} = 0, \quad (27)$$

$$L[E(x,y,t)] - \frac{1}{s}\left\{a^2\,\mathrm{sech}^2\left(\sqrt{\frac{3a}{4d^3}}x\right)\mathrm{sech}^2\left(\sqrt{\frac{3a}{4d^3}}y\right)\right\} + \frac{1}{s^\alpha}L\left\{\frac{\partial}{\partial x}(V_c\,E) + \frac{\partial}{\partial y}(V_a\,E)\right\} = 0.$$

Now, N is given by

$$N^1[\varphi_1,\varphi_2,\varphi_3] = L[\varphi_1(x,y,t;q)] - \frac{1}{s}\left\{a^2 \frac{g}{d}\,\mathrm{sech}^2\left(\sqrt{\frac{3a}{4d^3}}x\right)\mathrm{sech}^2\left(\sqrt{\frac{3a}{4d^3}}y\right)\right\} +$$
$$\frac{1}{s^\alpha}L\left\{\varphi_1(x,y,t;q)\frac{\partial\varphi_1(x,y,t;q)}{\partial x} + \varphi_2(x,y,t;q)\frac{\partial\varphi_1(x,y,t;q)}{\partial y} + 2c^2\frac{\partial\varphi_3(x,y,t;q)}{\partial x}\right\},$$

$$N^2[\varphi_1,\varphi_2,\varphi_3] = L[\varphi_2(x,y,t;q)] - \frac{1}{s}\left\{a^2 \frac{g}{d}\,\mathrm{sech}^2\left(\sqrt{\frac{3a}{4d^3}}x\right)\mathrm{sech}^2\left(\sqrt{\frac{3a}{4d^3}}y\right)\right\} + \quad (28)$$
$$\frac{1}{s^\alpha}L\left\{\varphi_1(x,y,t;q)\frac{\partial\varphi_2(x,y,t;q)}{\partial x} + \varphi_2(x,y,t;q)\frac{\partial\varphi_2(x,y,t;q)}{\partial y} + 2c^2\frac{\partial\varphi_3(x,y,t;q)}{\partial x}\right\},$$

$$N^3[\varphi_1,\varphi_2,\varphi_3] = L[\varphi_3(x,y,t;q)] - \frac{1}{s}\left\{a^2\,\mathrm{sech}^2\left(\sqrt{\frac{3a}{4d^3}}x\right)\mathrm{sech}^2\left(\sqrt{\frac{3a}{4d^3}}y\right)\right\} +$$
$$\frac{1}{s^\alpha}L\left\{\frac{\partial}{\partial x}\big(\varphi_1(x,y,t;q)\,\varphi_3(x,y,t;q)\big) + \frac{\partial}{\partial y}\big(\varphi_2(x,y,t;q)\varphi_3(x,y,t;q)\big)\right\}.$$

The deformation equation of m-th order at $\mathcal{H}(x,y,t) = 1$ is

$$L\big[V_{c_m}(x,y,t) - k_m V_{c_{m-1}}(x,y,t)\big] = \hbar\Re_{1,m}\big[\vec{V}_{c_{m-1}},\vec{V}_{a_{m-1}},\vec{E}_{m-1}\big],$$
$$L\big[V_{a_m}(x,y,t) - k_m V_{a_{m-1}}(x,y,t)\big] = \hbar\Re_{1,m}\big[\vec{V}_{c_{m-1}},\vec{V}_{a_{m-1}},\vec{E}_{m-1}\big], \quad (29)$$
$$L[E_m(x,y,t) - k_m E_{m-1}(x,y,t)] = \hbar\Re_{1,m}\big[\vec{V}_{c_{m-1}},\vec{V}_{a_{m-1}},\vec{E}_{m-1}\big],$$

where

$$\Re_{1,m}\big[\vec{V}_{c_{m-1}},\vec{V}_{a_{m-1}},\vec{E}_{m-1}\big]$$
$$= L\big[V_{c_{m-1}}(x,y,t)\big]$$
$$-\left(1-\frac{k_m}{n}\right)\frac{1}{s}\left\{a^2\frac{g}{d}\,\mathrm{sech}^2\left(\sqrt{\frac{3a}{4d^3}}x\right)\mathrm{sech}^2\left(\sqrt{\frac{3a}{4d^3}}y\right)\right\} \quad (30)$$
$$+\frac{1}{s^\alpha}L\left\{\sum_{j=0}^{i}V_{c_j}\frac{\partial V_{c_{m-1-i}}}{\partial x} + \sum_{j=0}^{i}V_{a_j}\frac{\partial V_{c_{m-1-i}}}{\partial y} + 2c^2\frac{\partial}{\partial x}\frac{\partial E_{m-1}}{\partial x}\right\},$$

$$
\begin{aligned}
&\Re_{2,m}\left[\overrightarrow{V_{c}}_{m-1}, \overrightarrow{V_{a}}_{m-1}, \vec{E}_{m-1}\right] \\
&\quad = L\left[V_{a_{m-1}}(x,y,t)\right] \\
&\quad - \left(1 - \frac{k_m}{n}\right)\frac{1}{s}\left\{a^2 \frac{g}{d}\operatorname{sech}^2\left(\sqrt{\frac{3a}{4d^3}}x\right)\operatorname{sech}^2\left(\sqrt{\frac{3a}{4d^3}}y\right)\right\} \\
&\quad + \frac{1}{s^\alpha}L\left\{\sum_{j=0}^{i} V_{c_j}\frac{\partial V_{a_{m-1-i}}}{\partial x} + \sum_{j=0}^{i} V_{a_j}\frac{\partial V_{a_{m-1-i}}}{\partial y} + 2c^2\frac{\partial}{\partial x}\frac{\partial E_{m-1}}{\partial x}\right\},
\end{aligned}
$$

$$
\begin{aligned}
&\Re_{3,m}\left[\overrightarrow{V_{c}}_{m-1}, \overrightarrow{V_{a}}_{m-1}, \vec{E}_{m-1}\right] \\
&\quad = L\left[E_{m-1}(x,y,t)\right] \\
&\quad - \left(1 - \frac{k_m}{n}\right)\frac{1}{s}\left\{a^2 \frac{g}{d}\operatorname{sech}^2\left(\sqrt{\frac{3a}{4d^3}}x\right)\operatorname{sech}^2\left(\sqrt{\frac{3a}{4d^3}}y\right)\right\} \\
&\quad + \frac{1}{s^\alpha}L\left\{\frac{\partial}{\partial x}\sum_{j=0}^{i} V_{c_j}E_{m-1-i} + \frac{\partial}{\partial y}\sum_{j=0}^{i} V_{a_j}E_{m-1-i}\right\}.
\end{aligned}
$$

By plugging inverse LT on Eq. (29), one can get

$$
\begin{aligned}
V_{c_m}(x,y,t) &= k_m V_{c_{m-1}}(x,y,t) + \hbar L^{-1}\left\{\Re_{1,m}\left[\overrightarrow{V_{c}}_{m-1}, \overrightarrow{V_{a}}_{m-1}, \vec{E}_{m-1}\right]\right\}, \\
V_{c_m}(x,y,t) &= k_m V_{c_{m-1}}(x,y,t) + \hbar L^{-1}\left\{\Re_{2,m}\left[\overrightarrow{V_{c}}_{m-1}, \overrightarrow{V_{a}}_{m-1}, \vec{E}_{m-1}\right]\right\}, \qquad (31) \\
E_m(x,y,t) &= k_m E_{m-1}(x,y,t) + \hbar L^{-1}\left\{\Re_{3,m}\left[\overrightarrow{V_{c}}_{m-1}, \overrightarrow{V_{a}}_{m-1}, \vec{E}_{m-1}\right]\right\},
\end{aligned}
$$

By the assist of above equation and using initial conditions

$$
V_{c_0}(x,y,t) = a^2\frac{g}{d}\operatorname{sech}^2\left(\sqrt{\frac{3a}{4d^3}}x\right)\operatorname{sech}^2\left(\sqrt{\frac{3a}{4d^3}}y\right), V_{a_0}(x,y,t) =
$$

$$
a^2\frac{g}{d}\operatorname{sech}^2\left(\sqrt{\frac{3a}{4d^3}}x\right)\operatorname{sech}^2\left(\sqrt{\frac{3a}{4d^3}}y\right), E_0(x,y,t) = a^2\operatorname{sech}^2\left(\sqrt{\frac{3a}{4d^3}}x\right)\operatorname{sech}^2\left(\sqrt{\frac{3a}{4d^3}}y\right),
$$

we evaluate the term series solution

$$
\begin{aligned}
V_c(x,y,t) &= V_{c0}(x,y,t) + \sum_{m=1}^{\infty} V_{c_m}(x,t)\left(\frac{1}{n}\right)^m, \\
V_a(x,y,t) &= V_{a0}(x,y,t) + \sum_{m=1}^{\infty} V_{a_m}(x,t)\left(\frac{1}{n}\right)^m, \qquad (32) \\
E(x,y,t) &= E_0(x,y,t) + \sum_{m=1}^{\infty} E_m(x,t)\left(\frac{1}{n}\right)^m,
\end{aligned}
$$

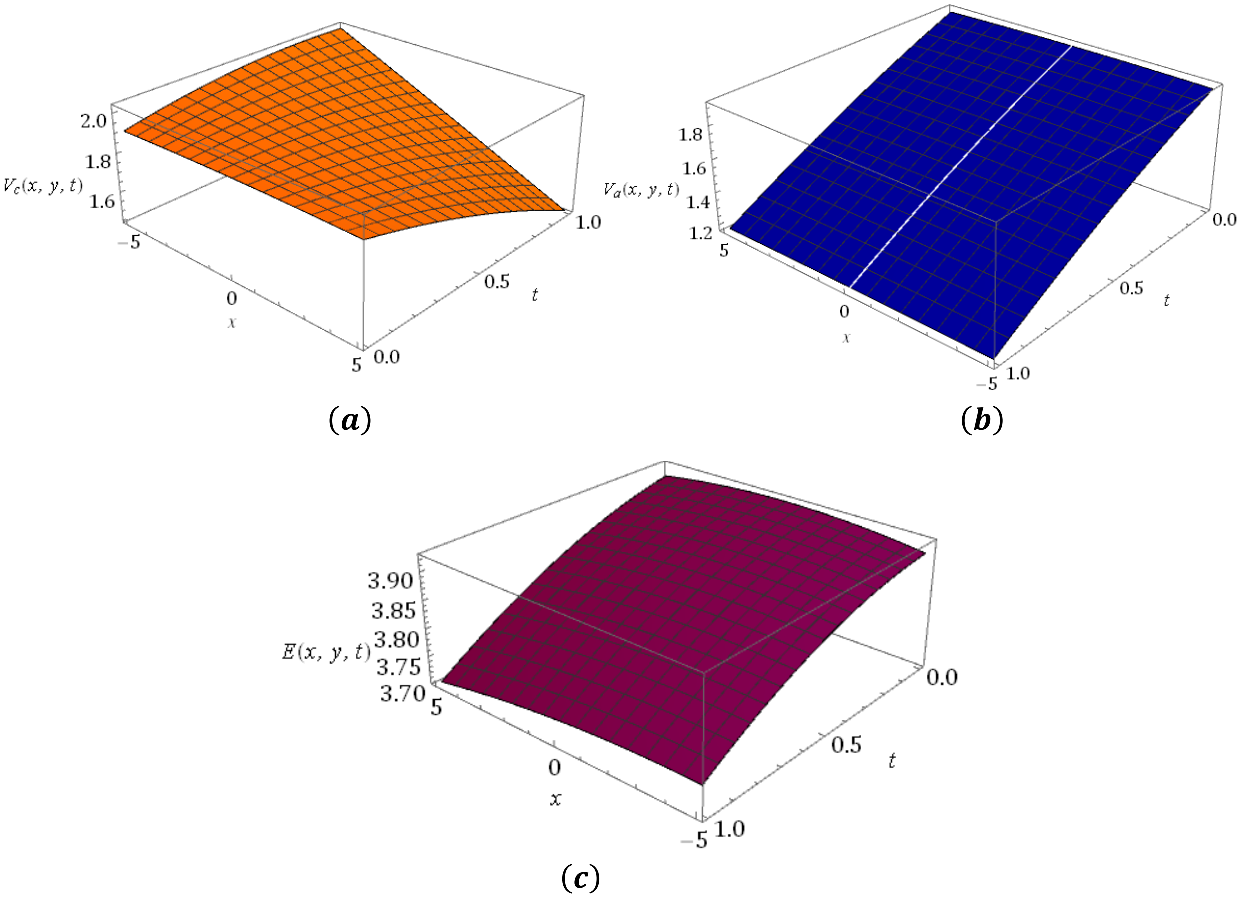

Figure 1 Surfaces of $(a) V_c(x,y,t)$, $(b) V_a(x,y,t)$ and $(c)\ E(x,y,t)$ for the obtained solution at $\hbar = -1, n = 1,\ y = 10$ and $\alpha = 1$.

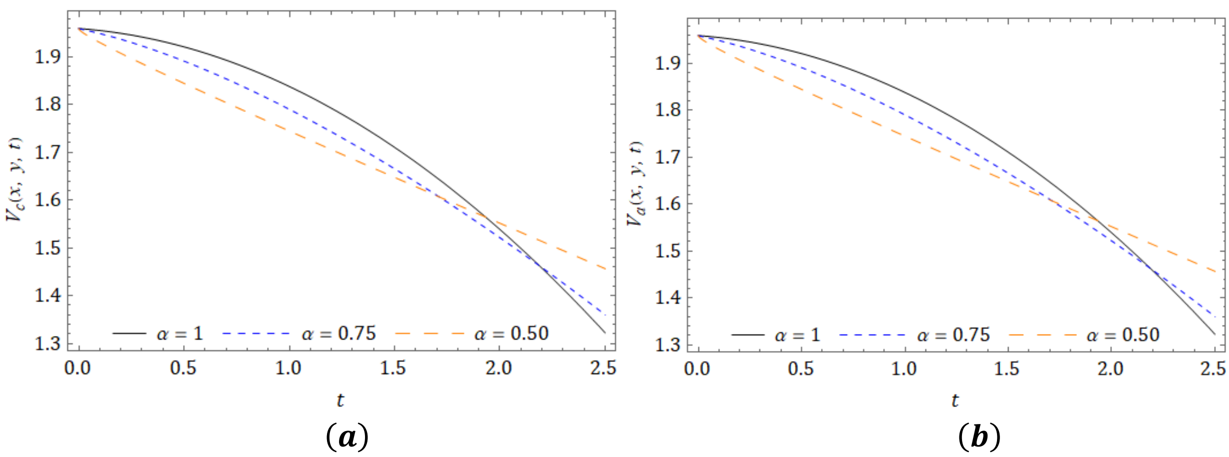

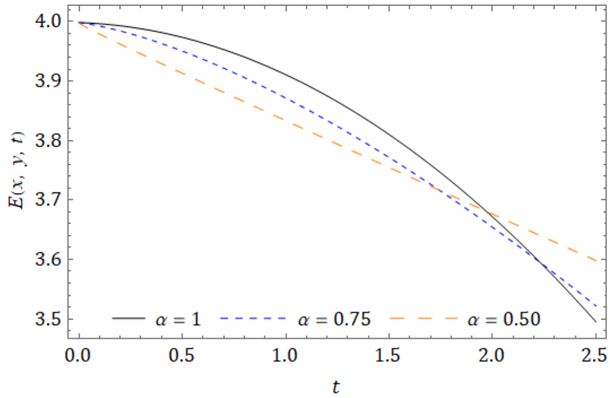

$(\boldsymbol{c})$

Figure 2 Nature of $(a) V_c(x, y, t)$, $(b) V_a(x, y, t)$ and (c) $E(x, y, t)$ for different order at $\hbar = -1, n = 1,\ y = 1$ and $x = 1$.

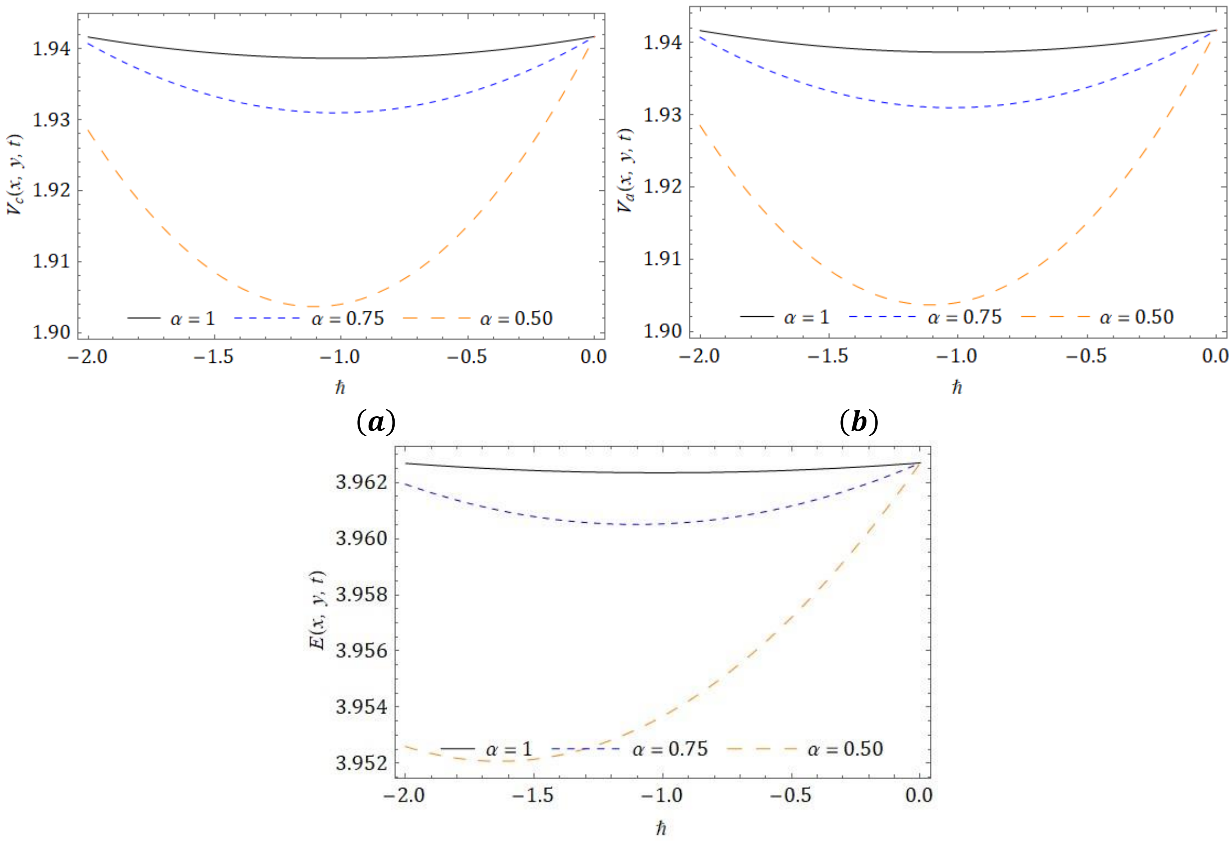

$(\boldsymbol{c})$

Figure 3 $\hbar$-curves q-HATM results for $(a) V_c(x, y, t)$, $(b) V_a(x, y, t)$ and (c) $E(x, y, t)$ with distinct α at $n = 1, x = 5, y = 5, t = 0.01$.

5. Results and Conclusion:

We analyzed the nature of results obtained for the system of equations exemplifying the shallow water model of the tsunami using an efficient and reliable scheme. The surface of the q-HATM results is captured in Figure 1 for all the compartments. The nature of the obtained results is illustrated with different fractional-order and presented in Figure 2. The hired method is associated with homotopy parameter ($\hbar$) and hence the corresponding nature is drowned with the $\hbar$-curves for different fractional-order and cited in Figure 3. These curves help to control and control the convergence region. For a proper choice of $\hbar$, the obtained results quickly tend to the analytical results. The present study confirms the hired nonlinear phenomena conspicuously depending on the time instant and the time history, which can be proficiently exemplified by using the concept of FC. This gives fascinating and helpful consequences. Lastly, we can conclude that the projected algorithm is more effective and highly methodical. It can be applied to scrutinize the various classes of complex models.

References

[1] J. Liouville, Memoire surquelques questions de geometrieet de mecanique, et sur un nouveau genre de calcul pour resoudreces questions, J. Ecole. Polytech. 13 (1832), 1-69.

[2] G.F.B. Riemann, Versucheinerallgemeinen Auffassung der Integration und Differentiation, Gesammelte Mathematische Werke, Leipzig, (1896).

[3] M. Caputo, Elasticita e Dissipazione, Zanichelli, Bologna, (1969).

[4] K. S. Miller, B. Ross, An introduction to fractional calculus and fractional differential equations, A Wiley, New York, (1993).

[5] I. Podlubny, Fractional Differential Equations, Academic Press, New York, (1999).

[6] A. A. Kilbas, H.M. Srivastava, J.J. Trujillo, Theory and applications of fractional differential equations, Elsevier, Amsterdam, (2006).

[7] H. F. Ismael, H. Bulut, H. M. Baskonus, W shaped surfaces to the nematic liquid crystals with three nonlinearity laws, Soft Comput., 25 (2021), 4513–4524.

[8] W Gao, et al., A new study of unreported cases of 2019-nCOV epidemic outbreaks, Chaos Solitons Fractals, 138 (2020), DOI: 10.1016/j.chaos.2020.109929.

[9] M. S. Kiran, et al., A mathematical analysis of ongoing outbreak COVID-19 in India through nonsingular derivative, Numer. Meth. Partial Diffe. Equa., 37 (2) (2021), 1282-1298.

[10] C. Baishya, S. J. Achar, P. Veeresha, D. G. Prakasha, Dynamics of a fractional epidemiological model with disease infection in both the populations, Chaos, 31 (043130) (2021), DOI: 10.1063/5.0028905.

[11] S. W. Yao, E. Ilhan, P. Veeresha, H. M. Baskonus, A powerful iterative approach for quintic complex Ginzburg-Landau equation within the frame of fractional operator, Fractals, 25 (5) (2021), DOI: 10.1142/S0218348X21400235.

[12] P. Veeresha, D.G. Prakasha, D. Baleanu, An efficient numerical technique for the nonlinear fractional Kolmogorov-Petrovskii-Piskunov equation, Mathematics 7 (3) (2019) 1-18. DOI:10.3390/math7030265.
[13] P. Veeresha, D. G. Prakasha, S. Kumar, A fractional model for propagation of classical optical solitons by using non-singular derivative, Math. Meth. Appl. Sci., (2020), DOI: 10.1002/mma.6335.
[14] H. Ismael, H. M. Baskonus, H. Bulut, Abundant novel solutions of the conformable Lakshmanan–Porsezian–Daniel model, Discrete Contin. Dyn. Syst. -S, 14 (7) (2021), 2311-2333.
[15] P. Veeresha, D. G. Prakasha, A.-H. Abdel-Aty, H. Singh, E. E. Mahmoud, S. Kumar, An efficient approach for fractional nonlinear chaotic model with Mittag-Leffler law, J. King Saud Univ. Sci., 33 (2) (2021), DOI: 10.1016/j.jksus.2021.101347.
[16] W. Gao, et al., New numerical simulation for fractional Benney-Lin equation arising in falling film problems using two novel techniques, Numerical Methods for Partial Differential Equations, 37 (1) (2021), 210-243.
[17] L. Akinyemi, P. Veeresha, Ajibola, Numerical solutions for coupled nonlinear Schrodinger-Korteweg-de Vries and Maccari's systems of equations, Modern Physics Letters B, 35 (20) (2021), DOI: 10.1142/S0217984921503395.
[18] C. Baishya, Dynamics of Fractional Holling Type-II Predator-Prey Model with Prey Refuge and Additional Food to Predator, J. Appl. Nonlinear Dyn., 10 (2) (2021), 315-328.
[19] P. Veeresha, D. G. Prakasha, D. Baleanu, An efficient technique for fractional coupled system arisen in magneto-thermoelasticity with rotation using Mittag-Leffler kernel, J. Comput. Nonlinear Dynam., 16(1) (2021), DOI: 10.1115/1.4048577.
[20] D. G. Prakasha, et al., An efficient computational technique for time-fractional Kaup-Kupershmidt equation, Numerical Methods for Partial Differential Equations, 37 (2) (2021), 1299-1316.
[21] T. A. Sulaiman, H. Bulut, H. M. Baskonus, On the exact solutions to some system of complex nonlinear models, Appl. Math. Nonlinear Sci., 6 (1) (2021), 29-42.
[22] E. I. Eskitasçıoglu, M. B. Aktas, H. M. Baskonus, New complex and hyperbolic forms for Ablowitz–Kaup–Newell–Segur wave equation with fourth order, Appl. Math. Nonlinear Sci., 4 (1) (2019), 105-112.
[23] L. Akinyemi, O. S. Iyiola, Analytical Study of (3+1)-Dimensional Fractional-Reaction Diffusion Trimolecular Models, Int. J. Appl. Comput. Math 7, 92 (2021). https://doi.org/10.1007/s40819-021-01039-w.
[24] P. Veeresha, D. G. Prakasha, Z. Hammouch, An efficient approach for the model of thrombin receptor activation mechanism with Mittag-Leffler function, Nonlinear Analysis: Problems, Applications and Computational Methods, 44-60, (2020).
[25] L. Akinyemi, M. Şenol, S. N. Huseen, Modified homotopy methods for generalized fractional perturbed Zakharov–Kuznetsov equation in dusty plasma, Adv. Differ. Equ., 45 (2021), DOI: 10.1186/s13662-020-03208-5.

[26] L. Akinyemi, O. S. Iyiola, Exact and approximate solutions of time-fractional models arising from physics via Shehu transform, Math. Meth. Appl. Sci., 43 (12) (2020), 7442-7464.

[27] W. Li, L. Akinyemi, D. Lu, M. M. A. Khater, Abundant Traveling Wave and Numerical Solutions of Weakly Dispersive Long Waves Model, Symmetry., 13 (6) (2021), DOI: 10.3390/sym13061085.

[28] M. Şenol, O. S. Iyiola, H. D. Kasmaei, L. Akinyemi, Efficient analytical techniques for solving time-fractional nonlinear coupled Jaulent–Miodek system with energy-dependent Schrödinger potential, Adv. Differ. Equ., 462 (2019), DOI: 10.1186/s13662-019-2397-5.

[29] P. Veeresha, D. G. Prakasha, D. Kumar, Fractional SIR epidemic model of childhood disease with Mittag-Leffler memory, Fractional Calculus in Medical and Health Science, (2020), 229-248, DOI: 10.1201/9780429340567-9.

[30] P. Veeresha, H. M. Baskonus, W. Gao, Strong interacting internal waves in rotating ocean: Novel fractional approach, Axioms 10 (2) (2021), 123.

[31] E. Ilhan, et al., Fractional approach for a mathematical model of atmospheric dynamics of CO2 gas with an efficient method, Chaos, Solitons and Fractals, (2021).

[32] P. Veeresha, A numerical approach to the coupled atmospheric ocean model using a fractional operator, Mathematical Modelling and Numerical Simulation with Applications 1 (1) (2021), 1-10.

[33] W. Gao, et al., New numerical simulation for fractional Benney–Lin equation arising in falling film problems using two novel techniques, Numer. Methods Partial Differ. Equ., 37 (1) (2021), 210-243.

[34] D. G. Prakasha, N. S. Malagi, P. Veeresha, New approach for fractional Schrödinger–Boussinesq equations with Mittag-Leffler kernel, Math. Meth. Appl. Sci., 43 (2020), 9654–9670.

[35] T. Jacobson, Vorticity on a Barred Beach, 2001.

[36] S. Waewcharoen, S. Boonyapibanwong, S. Koonprasert, Application of 2D-nonlinear shallow water model of tsunami by using Adomian decomposition method, In AIP Conference Proceedings, 1048 (1) (2008), 580-584.

[37] A. G. Marchuk, A. A. Anisimov, A method for numerical modeling of tsunami run-up on the coast of an arbitrary profile, In Proceedings of International Tsunami Symposium (ITS), (pp. 7-10), (2001).

[38] N. Gedik, E. Irtem, S. Kabdasli, Laboratory investigation on tsunami run-up, Ocean Eng., 32 (2001), 513-528.

[39] D. Younesiana, H. Askari, Z. Saadatnia, A. Yildirim, Analytical solution for nonlinear wave propagation in shallow media using the variational iteration method, Waves in Random and Complex Media, 22 (2) (2012), 133-142.

[40] J. Singh, D. Kumar, R. Swroop, Numerical solution of time- and space-fractional coupled Burgers' equations via homotopy algorithm, Alexandria Eng. J., 55 (2) (2016), 1753-1763.

[41] S.J. Liao, Homotopy analysis method and its applications in mathematics, J. Basic Sci. Eng., 5 (2) (1997), 111-125.

[42] S. J. Liao, Homotopy analysis method: a new analytic method for nonlinear problems, Appl. Math. Mech., 19 (1998), 957-962.
[43] H. M. Srivastava, D. Kumar, J. Singh, An efficient analytical technique for fractional model of vibration equation, Appl. Math. Model., 45 (2017), 192-204.
[44] P. Veeresha, D. G. Prakasha, H. M. Baskonus, New numerical surfaces to the mathematical model of cancer chemotherapy effect in Caputo fractional derivatives, Chaos 29 (013119) (2019), DOI: 10.1063/1.5074099.
[45] W. Gao, et al., New numerical results for the time-fractional Phi-four equation using a novel analytical approach, Symmetry, 12 (3) (2020), DOI: 10.3390/sym12030478.
[46] P. Veeresha, D. G. Prakasha, Solution for fractional Zakharov-Kuznetsov equations by using two reliable techniques, Chinese J. Phys., 60 (2019), 313-330.
[47] D. Kumar, R. P. Agarwal, J. Singh, A modified numerical scheme and convergence analysis for fractional model of Lienard's equation, J. Comput. Appl. Math. 399 (2018) 405-413.
[48] P. Veeresha, E. Ilhan, H. M. Baskonus, Fractional approach for analysis of the model describing wind-influenced projectile motion, Phys. Scr., 96 (2021), DOI: 10.1088/1402-4896/abf868.
[49] P. Veeresha, D.G. Prakasha, H.M. Baskonus, Novel simulations to the time-fractional Fisher's equation, Math. Sci., 13 (1) (2019), 33-42.
[50] N. S. Malagi, et al., A new computational technique for the analytic treatment of time fractional Emden Fowler equations, Mathematics and Computers in Simulation, 190 (2021), 362-376.
[51] P. Veeresha, D. G. Prakasha, J. Singh, D. Kumar, D. Baleanu, Fractional Klein-Gordon-Schrödinger equations with Mittag-Leffler memory, Chinese J. Phy., 68 (2020), 65-78.
[52] A. Prakash, P. Veeresha, D. G. Prakasha, M. Goyal, A new efficient technique for solving fractional coupled Navier-Stokes equations using q-homotopy analysis transform method. Pramana - J. Phys. 93 (6) (2019) 1-10. DOI: 10.1007/s12043-019-1763-x.

CHIRPED W-SHAPED OPTICAL SOLITONS OF THE RANGWALA-RAO EQUATION

Mustafa MIZRAK[1]

[1]Department of Computer Engineering, Faculty of Engineering, Şırnak University, Şırnak, Turkey

mmizrak@sirnak.edu.tr

Abstract

In this study, the exact nonlinearly chirped soliton solutions are derived from a special nonlinear Schrödinger equation known as Rangwala-Rao equation which are interest in describes plasma physics, wave propagation in nonlinear optical fibres and Ginzburg-Landau theory of superconductivity. Propogating chirped soliton solutions for Rangwala-Rao equation investigated by application of the ansatz method.

Keywords: Ansatz method, Chirped soliton, Exact solution

1.INTRODUCTION

The history of the soliton begins with the single-wave observation John Scott Russell accidentally observed in a canal near Edinburg in August 1834. This unusual single-wave, has more than 2 km long way with no changing height and shape. John Scott Russell called this phenomenon the *Wave of Translation*.

After this observation Russell performed numerous experiments in natural settings and in his laboratory, specially made small tank in his yard. In these studies, he achieved the following properties of the solitary wave:

1. A solitary wave has a constant velocity and retains its shape.

2. The velocity v on the canal depth h and height of the wave y_0, is defined by the equation

$$v=\sqrt{g\left(y_0+h\right)},$$

where g is the acceleration and under the condition $y_0 < h$.

3. A sufficiently high solitary wave turns into two or more small solitary waves.

4. Solitary waves preserves its shape and velocity after pass through each other.

Ten years later, Russell published an article called *Report on Waves*. But this article didn't make that impact on the continent. In 1871, the French scientist Joseph Valentine de Boussinesq (1842-1929) indicated that Russell's solitary wave may exist and calculated its shape and velocity to approximate. This was later confirmed by Rayleigh (1876) and Saint-Venant (1885). These three scientist establish a mathematical basis for the solitary wave. Finally, the Dutch scientist Diderik Johannes Korteweg (1848-1941) and his student Gustav de Vries came up with a new equation describing solitary waves that shortened to Korteweg-de Vries (KdV) equation. Korteweg and de Vries found a simpler equation for shallow water waves, derived their periodic solitions and showed how long waves could generate solitary waves. Korteweg and de Vries did not return to studying the KdV equation. It is not even mentioned in Korteweg's biography published in 1945.

After the paper by Korteweg and de Vries nothing happened until the Enrico Fermi, John Pasta, Stanislaw Ulam and Mary Tsingou paper in 1955 in which they numerically studied a one-dimensional inharmonic lattice of identical masses connected by nonlinear springs. The next step came a decade later when Norman J. Zabusky and Martin David Kruskal considered the same model in the continuum limit. They observed nonlinear interactions among solitary-wave pulses propagating in nonlinear dispersive media when searching the numerical solutions of the KdV equation. They reached a surprising conclusion that the interaction of the two solitary waves is the same as that of two colliding elementary particles. So, they called such waves *solitons*.

In fact, Zabusky and Kruskal incidentally chose the name soliton. They first chose the name solitron but this word registered name of a firm, for this reason they delete the "r" from the name and thus solitron became soliton[1-4].

Mathematicians usually prefer distinguish between solitons and solitary waves. They call solitons solitary waves that do not change shape aftes colliding with other solitons.

One of the wave phenomena that attracted attention recently is chirped solitons. The origin of the word chirp is derived from the chirping sound of birds. For instance, in optical transmission systems, ultrashort pulses may display chirp. Chirp utilized in spread spectrum communication and some devices as sonar and radar [5].

Among the many nonlinear evolution equations describing solitary wave processes, the most important is the nonlinear Schrödinger equation (NSL). In this study, we consider a class of nonlinear Schrödinger-type equation equation which are of interest in plasma phsics, wave propagation in optic fibers, Ginzburg-Landau theory of superconductivity

$$q_{xt} - \beta_1 q_{xx} + q + i\epsilon\beta_2 |q|^2 q_x = 0, \qquad \epsilon = \mp 1 \tag{1}$$

where β_1 and β_2 are real constants. This equation firstly introduced Abbas A. Rangwala and Jyoti A. Rao when they are studied the mixed derivative NSL equations. This equation was later named by Zhang as Rangwala-Rao (RR) equation [6-8].

2.MATHEMATICAL ANALYSIS

In this study we search exact chirped soliton solutions of RR equation. We try to find traveling wave solution of the Eq.(1) as [8-13]

$$q(x,t) = \rho(\xi) e^{i[\chi(\xi) - \omega t]} \tag{2}$$

where $\xi = kx - vt$, $\rho = \rho(\xi)$ is function of amplitude, $\chi = \chi(\xi)$ is function of phase, v is the wave velocity, and ω is the frequency of the wave oscillation. And, corresponding chirp is defined as

$$\delta\omega(x,t) = -\frac{\partial}{\partial t}[\chi(\xi) - \omega t] = -\chi'(\xi) \tag{3}$$

Inserting Eq.(2) in Eq.(1), the real and imaginary parts gives, respectively

$$\rho - k\epsilon\rho^3\beta_2\chi' + k\rho\omega\chi' + kv\rho(\chi')^2 + k^2\rho\beta_1(\chi')^2 - kv\rho'' - k^2\beta_1\rho'' = 0, \tag{4}$$

$$-k\omega\rho' - 2kv\rho'\chi' - 2k^2\beta_1\rho'\chi' - kv\rho\chi'' - k^2\rho\beta_1\chi'' + k\epsilon\rho^2\beta_2\rho' = 0, \tag{5}$$

where prime stands for differentiations with respect to ξ. Multiplying Eq.(5) by ρ and integrating once time gives the result

$$\chi' = \frac{A}{(v + k\beta_1)\rho^2} - \frac{\omega}{2(v + k\beta_1)} + \frac{\epsilon\beta_2\rho^2}{4(v + k\beta_1)}, \tag{6}$$

where A is an integration constant. So, the resultant chirp consisting of linear and nonlinear terms is obtained by

$$\delta\omega = -\frac{A}{(v+k\beta_1)\rho^2} + \frac{\omega}{2(v+k\beta_1)} - \frac{\epsilon\beta_2\rho^2}{4(v+k\beta_1)}. \tag{7}$$

On substituting Eq.(6) in Eq.(4) gives

$$-k(v+k\beta_1)\rho'' + \left(\frac{A^2k}{v+k\beta_1}\right)\frac{1}{\rho^3} + \left(\frac{4v-k\omega^2+4k\beta_1-2Ak\epsilon\beta_2}{4(v+k\beta_1)}\right)\rho$$
$$+\frac{k\epsilon\omega\beta_2}{2(v+k\beta_1)}\rho^3 - \frac{3k\beta_2^2}{16(v+k\beta_1)}\rho^5 = 0. \tag{8}$$

Multiplying Eq.(8) by ρ' and integrating gives

$$(\rho')^2 = -\frac{2B}{k(v+k\beta_1)} - \left(\frac{A^2}{(v+k\beta_1)^2}\right)\frac{1}{\rho^2} + \left(\frac{v}{k(v+k\beta_1)^2} - \frac{\omega^2}{4(v+k\beta_1)^2} + \frac{\beta_1}{(v+k\beta_1)^2} - \frac{A\epsilon\beta_2}{2(v+k\beta_1)^2}\right)\rho^2 +$$
$$\frac{\epsilon\omega\beta_2}{4(v+k\beta_1)^2}\rho^4 - \frac{\beta_2^2}{16(v+k\beta_1)^2}\rho^6, \tag{9}$$

where B is the second integration constant. Eq.(9) shows the evolution of the wave amplitude in a nonlinear medium governed by the RR equation.

Next, we search chirped soliton solutions of the Eq.(1). To this end, if variable change is made as

$$\rho^2(\xi) = U(\xi) \tag{10}$$

reduces Eq.(9) the following elliptic equation[14-18]:

$$(U')^2 = -a_0 + a_1U + a_2U^2 + a_3U^3 - a_4U^4, \tag{11}$$

where

$$a_0 = \frac{4A^2}{(v+k\beta_1)^2},\ a_1 = -\frac{8B}{k(v+k\beta_1)},\ a_2 = \frac{4v-k\omega^2+4k\beta_1-2Ak\epsilon\beta_2}{k(v+k\beta_1)^2},$$
$$a_3 = \frac{\epsilon\omega\beta_2}{(v+k\beta_1)^2},\ a_4 = \frac{\beta_2^2}{4(v+k\beta_1)^2}. \tag{12}$$

The elliptic Eq.(11) is known that admit different solutions such as bright, dark, periodic etc.

3. W-SHAPED SOLITONS

To obtain the nonlinear equation for the wave amplitude, we search soliton ansatz of the type

$$U(s) = \beta + g\,\mathrm{sech}(\mu s), \tag{13}$$

which allows for W-shaped solitons under the conditions $\beta g < 0$ and $|g| > \beta$ [18].

Inserting Eq.(13) into Eq.(11) and equating different powers of the sech functions, we get the following equations:

$$-a_0 + \beta a_1 + \beta^2 a_2 + \beta^3 a_3 - \beta^4 a_4 = 0, \tag{14}$$

$$g\left(a_1 + 2\beta a_2 + 3\beta^2 a_3 - 4\beta^3 a_4\right) = 0, \tag{15}$$

$$g^2\left(a_2 + 3\beta a_3 - 6\beta^2 a_4 - \mu^2\right) = 0, \tag{16}$$

$$g^3\left(a_3 - 4\beta a_4\right) = 0, \tag{17}$$

$$g^2\left(\mu^2 - a_4 g^2\right) = 0. \tag{18}$$

Solving these equations by aid of Mathematica programme, we get

$$\beta = \frac{a_3}{4a_4}\ , \tag{19}$$

$$g = \pm\frac{\sqrt{3a_3^2 + 8a_2 a_4}}{2\sqrt{2}a_4}, \tag{20}$$

$$\mu = \pm g\sqrt{a_4}, \tag{21}$$

and

$$a_0 = -\frac{a_3^2\left(5a_3^2 + 16a_3 a_4\right)}{256a_4^3},\quad a_1 = -\frac{a_3\left(4a_2 a_4 + a_3^2\right)}{8a_4^2}, \tag{22}$$

provided that $a_3 \neq 0$ and $a_4 \neq 0$.

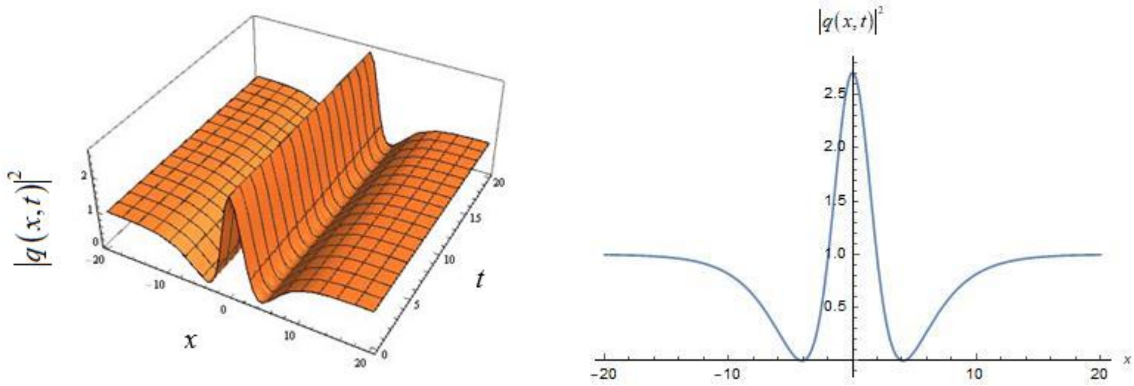

Figure 1. For the values $\beta = 1,\ \lambda = 1,\ \mu = 0.4$ and $v = 0.002$ the intensity $|q(x,t)|^2$ evolution of W-shaped soliton.

By using relations in Eq.(22), we get the integration constants as $A^2 = a_0 (v + k\beta_1)^2 / 4$ and $B = -a_1 k (v + k\beta_1)/8$. Also, using Eq.(19) and Eq.(20) we can determine amplitude g as

$$g = \pm\sqrt{6\beta^2 + \lambda^2}, \tag{23}$$

with $\lambda^2 = a_2 / a_4$. In light of this information, we can write the exact chirped soliton solution of Eq.(1) as

$$q(x,t) = \left[\beta \pm \sqrt{6\beta^2 + \lambda^2}\,\mathrm{sech}\left[\mu(kx - vt)\right]\right]^{1/2} e^{i\left[\chi(kx-vt)-\omega t\right]}. \tag{24}$$

Thus, corresponding chirping is found as

$$\delta\omega = -\frac{A}{(v + k\beta_1)\left(\beta \pm \sqrt{6\beta^2 + \lambda^2}\,\mathrm{sech}\left[\mu(kx - vt)\right]\right)} + \frac{\omega}{2(v + k\beta_1)} - \frac{\epsilon\beta_2\left(\beta \pm \sqrt{6\beta^2 + \lambda^2}\,\mathrm{sech}\left[\mu(kx - vt)\right]\right)}{4(v + k\beta_1)}. \tag{25}$$

Eq.(24) describes the evolution of two different type soliton pulses for the RR equation. In this type of solutions, the strength of the background is determined by the parameter β. Here, only the soliton solution in Eq.(24) considered as minus signed. The variation of the soliton intensity calculated from Eq.(24) is shown in Fig. 1. It can be clearly seen that the soliton intensity profile takes a W shape and remains unchanged over a significant propagation distance. This remarkable soliton shape is a result of the self-steepening effect. The W-shaped soliton structure was first found by Li et al. for a higher-order NSL equation with third order dispersion, self steepening and self-frequency effects [19-23].

4. CONCLUSIONS

Exact chirped soliton solutions for RR equation have obtained by this study. We used the coupled amplitude-phase method to derive a nonlinear differential equation for the evolution of the wave amplitude. The wave amplitude is shown to satisfy a nonlinear differential equation contains two integration constants which can be easily determined with the initial parameters of the wave. By using a proper ansatz, we get the exact W-shaped soliton solution with nonlinear chirp for RR equation. The nonlinear chirp associated with this interesting soliton structure has been shown a nontrivial form involving two intensity terms. Such chirped soliton solutions result from the balance between group velocity dispersion and self-steepening effects.

REFERENCES

1. Anjan Biswas, Swapan Konar, Introduction to non-Ker Law Optical Solitons , Chapman and Hall/CRC applied mathematics and nonlinear science series, 2007.
2. Alexandre T. Filippov, The Versatile Soliton, Springer Science +Business Media, 2010.
3. Enrico Fermi, John Pasta, Stanislaw Ulam and Mary Tsingou, Studies of Nonlinear Problems, Los Alamos Scientific Laboratory of the University of California, May 1955.
4. Norman J. Zabusky, Martin David Kruskal, Interaction of “Solitons” in a collisionless plasma and the recurrence of initial states, Physical Review Lettters, Volume 15, Number 6, 9 August 1965.
5. Mibaile Justin, Malwe Boudoue Hubert, Gambo Betchewe, Timoleon Crepin, Serge Yamigno Dokac, Kofane , Chirped solitons in derivative nonlinear Schrödinger equation, Chaos. Solitons and Fractals 9-54, 2018.
6. De-xing Kong, Explicit exact solutions for the Lienard equation and its applications, Physics Letters A 196 301-306, 1995.
7. Jin-Liang Zhang, Ming-Liang Wang, Exact solutions to a class of nonlinear Schrödinger type equations, PRAMANA journal of physics Vol. 67, No. 6 December pp. 1011-1022, 2006.
8. Zeid I. A. Al-Muhiameed, Emad A. B Abdel-Salam, Generalized Hyperbolic Function Solution to a Class of Nonlinear Schrödinger-Type Equations, Hindawi Publishing Corporation Journal of Applied Mathematics Volume 2012, Article ID 265348, 15 pages, 2012.

9. Serge Yamigno Dokac, Mibaile Justin, Gambo Betchewe, Kofane Timoleon Crepin, Optical chirped soliton in metamaterials, Nonlinear Dyn 90:13-18, 2017.
10. Houria Triki, Rubayyi Alqahtani, Qin Zhou, Anjan Biswas, New envelope solitons for Gerdjikov-Ivanov model in nonlinear fiber optics", Superlattices and Microstructures 111 326-334, 2017.
11. Anjan Biswas, Mehmet Ekici, Abdullah Sonmezoglu, Rubayyi T. Alqahtani, Sub-pico-second chirped optical solitons in mono-mode fibers with Kaup-Newell equation by extended trial function method, Optik 168 208-216, 2018.
12. Abdel Kader Daoui, Faiçal Azzouzi, Houria Triki, Anjan Biswas, Qin Zhou, Seithuti P. Moshokoa, Milivoj Belic, Propagation of chirped gray optical dips in nonlinear metamaterials, Optics Communications 430 461-466, 2019.
13. Houria Triki, Anjan Biswas, Qin Zhou, Seithuti P. Moshokoa, Milivoj Belic, Chirped envelope optical solitons for Kaup-Newell equation, Optik - International Journal for Light and Electron Optics 177 1-7, 2019.
14. Elsayed M.E. Zayed, Mohamed E.M. Alngar, Application of newly proposed sub-ODE method to Locate chirped optical solitons to Triki-Biswas equation, Optik - International Journal for Light and Electron Optics 207 164360, 2020.
15. Emmanuel Yomba, The sub-ODE method for finding exact travelling wave solutions of generalized nonlinear Camassa-Holm, and generalized nonlinear Schrödinger equations,Phys. Lett. A 372 215-222, 2008.
16. Li-Hua Zhang, Yin-Yu He, Sub-ODE's New Solutions and Their Applications to Two Nonlinear Partial Differential Equations with Higher-Order Nonlinear Terms, Commun. Theor. Phys. (Beijing, China) 52 pp. 773-778, 2009.
17. Zi-Liang Li, Periodic Wave Solutions of a Generalized KdV-mKdV Equation with Higher-Order Nonlinear Terms, Z. Naturforsch. 65a, 649-657, 2010.
18. Xuegang Hu, Yong Hong Wu, Ling Li, New Traveling Wave Solutions of the Boussinesq Equation Using a New Generalized Mapping Method, Journal of Basic and Applied Physics May 2013, Vol. 2 Iss. 2, PP. 68-77, 2013.
19. Zhonghao Li, Lu Li, Huiping Tian, Guosheng Zhou, New types of solitary wave solutions for the higher order nonlinear Schrödinger equation, Phys. Rev. Lett. 84 (18) 4096-4099, 2000.

20. Ur Rehman, H., Imran, M.A., Bibi,M., Riaz, M., Akgül, A., New soliton solutions of the 2D-chiral nonlinear Schrodinger equation using two integration schemes, Mathematical Methods in the Applied Sciences 44 (7), 5663-5682, 2020.
21. Inc, M., Akgül, A., Classifications of Soliton Solutions of the Generalized Benjamin-Bona-Mahony Equation with Power-Law Nonlinearity, Journal of Advanced Physics 7 (1), 130-134, March 2018.
22. Tchier, F., Inc, M., Bulent Kilic, B., Akgül, A., On soliton structures of generalized resonance equation with time dependent coefficients, Optik 128, 218-223,2016.
23. Hashemi, M. S., Inc, M., Kilic, B., Akgül, A., On solitons and invariant solutions of the Magneto-electro-elastic circular rod Waves in Random and Complex Media 26 (3), 259-271, 2016.

EXPRESSION OF THE LAW AS A MATHEMATICAL

Emrah YILMAZ[2] M.Tuncay GENÇOĞLU[1]

[1] Fırat University, Vocational School of Technical Sciences, Elazığ, Turkey

mt.gencoglu@firat.edu.tr

[2] Fırat University, Eco Informatics Department Graduate Student

emrahyilmaz3423@gmail.com

Abstract

Reaching an ideal order is the common goal of law and mathematics. However, the methods they use to achieve this goal are different. It is an indisputable fact that mathematics is a universal language. Therefore, legal laws can be expressed mathematically by making use of the universality of mathematics. Thus, developments in law find a place for themselves in the wider international arena, thanks to a common language. It is also thought that both the mathematical analysis of the events and the mathematical expression of the laws will contribute to the effective decision-making and deterrent sanctions of the judges in the British American Legal System and the Continental European Legal System. Even though it is thought that way, it is difficult to find the mathematical equivalent of every legal concept.

Keywords: Mathematical Statement of Law, Law and Mathematics, Mathematical Modeling, Law and Mathematics in Achieving Ideal Order, Universal Language in Law.

1. Introduction

The primary purpose of trying to express laws using mathematical terms is to create a universal language in law that can be understood by everyone and to contribute to the knowledge of the laws of different countries for everyone who knows mathematics without the need for translation. Nations have their own languages. The main language families found in the world are: Indo-European, Hami-Sami, Bantu, Sino-Tibetan and Ural-Altaic language families. According to the structure, the language is examined in three groups as monosyllabic, inflected and agglutinative languages[4]. Law, on the other hand, consists of three separate groups: Continental, Anglo-American and Islamic.

2. Relationship of Law and Mathematics

Galileo said that "nature is written in the language of mathematics". It can be said that mathematics is the product of the first people who try to make their daily life easier by acquiring new information and strive to make sense of what is happening around them. Mathematics was born from man's effort to find the unknown[5]. Especially in the early ages, the effort to find solutions to situations such as obtaining the livelihood from agriculture and animal husbandry and sharing the lands, suitable planting time for crops, grazing of animals without any attachments, etc., led to the emergence of mathematics. Like mathematics, natural law takes its source from nature. Cicero said that "true law is natural reason in harmony with nature"[6].

According to the view, the reason why a behavior is prohibited is not that the legislator prohibits that behavior; behavior is against natural reason, in other words, against natural law. According to natural law, for a rule to be a legal rule, it must first be just. Looking back at the history of humanity, it is seen that the concept of justice has changed throughout history. The concept of justice, which was based on nature in the first ages, left its place to a legal order whose source was divine will in the middle ages.

In the Age of Enlightenment, the scholastic and god-centered understanding of law left its place to the natural law understanding based on a secular and human-centered basis.

Mathematics is a tool used to validate and explain our everyday knowledge[1]. In addition to daily life, analyzes are made using mathematics, statistics and logic in both social sciences and positive sciences. Gauss says "mathematics is the queen of the sciences"[7]. So what is the opposite of science? Science is organized knowledge that chooses a part of the universe or events as a subject and tries to draw conclusions by using empirical methods and reality. It is the process of acquiring knowledge and methodical research, which starts from the desire to know a certain subject and is directed towards a certain purpose. When science is mentioned, rules that do not change according to time and place come to mind. On the other hand, law is fed by society and is constantly changing. Although we talk about universal concepts such as equality and justice when talking about law, the rules of law are not universal. It differs from society to society. The reason for this is that every society has its own traditions. However, mathematics is universal, not affected by language, religion and social values. While mathematics is based on numbers and formulas, law focuses on human behavior and tries to create a social ideal order by basing these behaviors on various norms. In doing so, it takes its source from experience or events that are likely to happen. Observation is in the foreground[3].

3. Mathematatıcal Modelıng Methods of Laws

The mathematical modeling method is a method used to solve problems encountered in both science and social sciences. In order to use this modeling technique, it is necessary to create the appropriate mathematical expression form from the connections that regulate the relationship between the data, namely verbal expressions. A mathematical expression can be created algebraically (formula and function), numerical (numerical results) and geometric (schema and graph). Especially in the field of economics, functions are used. E.g; production function, utility function, etc. The function corresponds exactly to each number in one array with the number in another array.

3.1. Mathematics of Crime

The purpose of the laws is not only to protect the victim, but also to create a deterrent against crimes. Because if the punishment received in the face of the crime committed is not more than the benefit obtained from that crime, it will be very difficult to prevent the crime and the criminal. In the book "Law and Economics" written by Cooter and Ulen, the behavior of a reasonable criminal is explained using mathematical concepts under the title of reasonable crime mathematics. Let's think this way, let the variable x represent the severity of the crime in terms of dollar amount, and the variable y represent the income earned through the crime committed by the criminal in terms of dollar amount. So

$y=y(x)$

is an increasing function. If we consider that f is a fine here, the function becomes

$f=f(x)$

when a crime of x severity is committed. The possibility of punishment after the crime has been committed.

If we say

$p=p(x);$

the expected penalty is equal to the product of the penalty amount and probability:

p(x)*f(x)

Here, the reasonable criminal's goal is to maximize his net payoff. The net gain is equal to the profit from the offense minus the expected penalty.

y=y(x) : profit from crime

max y(x)-p(x)*f(x) : highest net income

Here, the marginal values of the p(x) and f(x) functions are looked at to find the change in the probability and amount of the penalty if the x value changes by one unit. In an example of embezzlement by the criminal, his net gain is maximized when his marginal profit is equal to the expected marginal loss from the penalty[3]. Based on this analysis, necessary measures can be taken to reduce the crime rate of the reasonable criminal who does not consider the moral elements.

3.2. Deterrence Level and Mathematics

Simple mathematical methods can be used to find the appropriate deterrence level. For example, a person who smashes the window of a shop by throwing a stone will directly harm the shop owner. Therefore, it is an indirect loss for other shop owners to worry about breaking the windows of their own shops due to the commission of this crime. From this point of view, the direct loss is “d”, the indirect loss is “dz”, and the total loss is “d+dz”. If the criminal profits from the crime he committed (assuming he broke in and stole something) to find the net profit; The profit is subtracted from the total loss and d+dz-b is obtained. If we say the probability of the crime to occur “p”, the process of catching the criminal and the process after being caught “m”, the social damage; equals the sum of expected harm and deterrence [(d+dz-b)*p(m)+m]. From this equation, the higher the cost of deterrence, the less likely the optimal deterrent to be a perfect deterrent. In other words, this means that in the example we gave above, the criminal broke the glass, the law enforcement officers mobilized to catch the criminal, and in this process, the expenses incurred by the police, the minutes they kept, the processes in custody after being caught, the gathering of judges and prosecutor's offices, etc. The higher the cost, the lower the deterrence efficiency. If the net harm from crime increases, optimal deterrence decreases[3].

4. Application

We will talk about the method of expressing the laws mathematically.

1) Creating the link that organizes the relationship between the data to build the mathematical model
2) Establishment of the mathematical model
3) Creating a mathematical expression from a verbal expression;
a) Algebraic: analytical expression (formula, function construction)**
b) Numeric: get numeric result
c) Geometric: solving the solution with the help of diagrams, graphics

The purpose of this method; to express the laws with mathematics, which is a universal language, and to facilitate their learning around the world.

4.1. TMK 989

“A possessor whose movable is stolen, lost or disposed of in any other way against his will can file a movable lawsuit against anyone who holds that property within five years.”

t = movable property (let t be a value defined in the set f)
f(t)= real owner of the movable
From this point of view, with the help of the resultant function, h(f(t) actually belongs to f and becomes h(thief) who uses t for himself.
h(f(t)) → i(t) (transfer of movables taken/stolen from owner without consent of owner to i)
i(t): person who owns movables in good faith
e(t): duration of stay of the movable in one person
e: duration $0<e\leq5$
Pursuant to 989 of the TMK, the real owner of the movable has the right to file a lawsuit against the owner of the movable within 5 years. If the plaintiff (the real owner of the movable) proves that the movable belongs to him, he can take the movable back from the third party. The inverse function is used for the mathematical representation of this situation.
It is written as

$$x = f^{-1}(y).$$

$i^{-1}(t)$: Define the inverse of the i function. (It means that the real owner of the movable can take back the movable from the bona fide third party.)
e(t)>5
f(t)=f(i(t)), t≤5
i(t), t>5 i(t) : bona fide third person who will own the movable if the period exceeds 5 years. In this case, f loses his right to sue i.

4.2. CMK 247

"A public official whose possession has been transferred to him due to his duty or who embezzles the property for which he is responsible for the protection and supervision of himself or someone else is sentenced to imprisonment from five years to twelve years."
The algebraic method, which is one of the mathematical modeling methods used to express TMK 988 and 989, was used for the above-mentioned law article.
t^m: goods
k: public official
f(t^m):real owner of the property
k(f(t^m)): public official who embezzles property that actually belongs to f
b(f(t^m)): embezzlement of property
h^a : jail sentence
e: duration
e(h^a) :duration of prison sentence
k e(h^a)): the period of imprisonment of the public official who embezzled property
5≤ k e(h^a))≤12

"If the crime is committed with fraudulent acts to ensure that the embezzlement is not disclosed, the penalty to be imposed is increased by half."

k(f(t^m))+fraudulent behavior
5+2.5≤ k e(h^a))≤12+6

"In case the embezzlement crime is committed to be returned after the property has been used for a temporary period of time, the penalty to be imposed may be reduced by half."
k(e(t^m)): residence time of the good at k

$e(t^m) < \infty$ (time is finite, so let the symbol ∞ represent the return of the goods after some time)

It is understood that there is no definite statement that the penalty can be reduced by half as per TCK 247/3. In case of a discount, the minimum penalty is 5-5/2=2.5, and the maximum penalty is 12-12/6=6. If there is no reduction, it is punished with a penalty of 5 to 12 years. In this case, the penalty rate range is between $2.5 \leq$ k $e(h^a)) \leq 12$.

5. Result

The mathematical representation of laws has many advantages and disadvantages. The main purpose of this study is to appropriate legal laws, expressions and concepts to the society through a universal language that everyone can understand. In this context, when laws are expressed with mathematics, which is a universal language, everyone can understand the rules of law without the need for translation. Thus, laws become the focus of attention not only for lawyers but also for people from different walks of life. As a natural result of this, the same legal rules become understandable by societies with different languages, religions and cultures, and the development of law becomes faster. With the help of mathematical models, verbal expressions are converted into numerical expressions and the information is kept in the mind for a long time. The rote gets rid of logic. Thanks to the mathematical modeling, semantic differences due to the wrong use of punctuation marks in the written language are prevented.

As for the disadvantages of mathematical expression of laws, the fact that not every concept has a mathematical equivalent makes it necessary to express some concepts verbally. E.g; Although concepts such as truth, truth, and truth are often used to mean the same thing in daily life, their meanings are fundamentally different.

Therefore, it is difficult to express these meaning differences with mathematical symbols. Even if these concepts are used by giving symbols such as x, y, z, verbal explanation is needed when expressing them[2]. In addition, in the TMK, a gap is left in the rules for the judge to use his discretion, whereas the mathematics is precise and clear.

References

[1] Balkır, Z. & Apaydın, E. (2011). Hukuk Eğitimi ve Matematik. 2nd International Conference on New Trends in Education and Their Implications.

[2] Can, C. ,(2005). Hukuk ve Matematik.

[3] Cooter, R. & Ulen, T., (1997). Law and Economics (2nd ed.). USA: Addison- Educational Publisher Inc.

[4] Emiroğlu,H.: Kavimler Hukuku (ius gentium), Değişim Yayınları-2007

[5] Gözler, K. (2008). Tabii Hukuk ve Hukuki Pozitivizme Göre Adalet Kavramı.

[6] Gözler, K. (1998). Hukuka Giriş. Bursa: Ekin Kitabevi.

[7] Sertöz, S. (2003). Matematiğin Aydınlık Dünyası, Ankara.

A NEW SUBSTITUTION METHOD FOR NON-LINEAR BLOCK ENCRYPTION

Mehmet Vural[1] **Muharrem Tuncay GENÇOĞLU**[2]

[1] Bingöl University, Genç Vocational School, Bingöl, TÜRKİYE,

mehmet1vural@gmail.com

[2] Fırat University, Vocational School of Technical Sciences, Elazığ, TÜRKİYE,
mt.gencoglu@firat.edu.tr

Abstract

Information technologies have gained more importance, especially in the Covid 19 pandemic period. In this process, the rate of online shopping increases, and different models are preferred by providing education and business life remotely. There are major grievances due to cyber-attacks made due to the security weakness in the databases of websites and servers. sometimes related to each other, sometimes they operate independently. Block cipher algorithms are generally preferred for transactions requiring integrity checking. Also, Block encryption algorithms proposed by Shannon are based on diffusion and confusion methods. Scrambling is used to hide the relationship between the scrambled message and the public message while aiming to keep the traces in the spreading open message unnoticed in the encrypted message. Propagation and mixing occur by s-boxes displacement and linear transformation, respectively. In block cipher algorithms, more than one encryption step can be performed on the cycle of a block. Usually, the key to encrypt the message is used in each different step. The length of the key used in block encryption algorithms should be chosen to be stronger against the attacks to be made. The long preferred key makes it difficult to decipher the encrypted message against brute-force attacks. The number of steps performed in block cipher algorithms should be chosen appropriately. Thus, with the replacement processes, the encryption algorithm becomes both faster and stronger. Besides, the fact that the characters used in the password are different from each other is a very important factor in increasing the complexity. In this way, the clear message can be better protected against attacks.With a new substitution method for the non-linear block cipher developed, the message is made meaningless by replacing every information recorded in the database of the servers with the help of a key. Since the steps of the existing block cipher algorithms are more (DES 16, BLOWFISH 16), the processing time increases. In a new substitution method for nonlinear block cipher developed, the low number of steps shortens the encryption time. Security is provided by making the recorded information more complex. Even if the attacks on servers and databases are successful, real and meaningful information will not be accessible because the information is encrypted incomprehensibly.

Keywords: Block encryption, Database, Encryption

1. Introductıon

Especially during the Covid 19 pandemic period, the importance of information technologies has been well understood and many people are doing their jobs remotely through information technologies. In this process, the rate of people shopping online is increasing, different models are preferred by giving education and business life remotely. There are great victims of cyber-attacks due to the security weakness in the databases of websites and servers. Information is recorded in the databases of many e-commerce websites and servers without using any encryption algorithms. In cases where a web site with a security vulnerability is seized by malicious people, all the information recorded in the database is accessed. In this case, it is undesirable for the customer information to be accessed by third parties. In addition to providing services such as selling products to customers, it is also important to securely hide customer information. The integrity and confidentiality of the data is ensured by using some cryptographic protocols of government institutions or personal data[1]. While cryptographic protocols are sometimes made incomprehensible with the help of a key, sometimes they are used together with steganography techniques to ensure data security by embedding them in text, audio, video and image files[2,3,4,5,6]. While cryptography makes the data meaningless, steganography completely hides the data[9]. Steganography is done by hiding data in text, image, video, audio files[6,10,11,12]. Therefore, steganography is not an encryption method, but a supplementary element for encryption[13]. In some encryption algorithms, data is encrypted first and then the encrypted data is hidden in another file, that is, data security is ensured by using a hybrid model[7,8].

2. Proposed Method

Initially, eight-character block data is encrypted with an eight-character key, subjected to various rules, and the information is recorded in the database using the substitution process in the encryption algorithm. The encryption scheme is shown in Figure 1 and the decryption scheme in Figure 2.

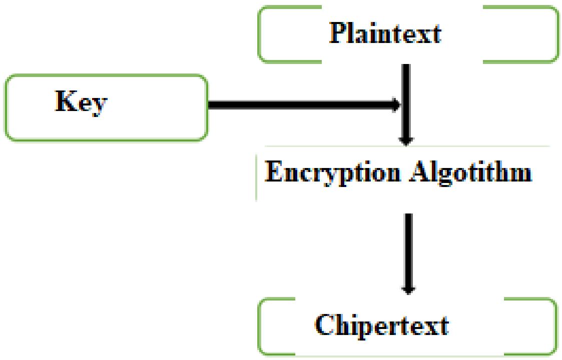

Figure 1. Encryption diagram of the proposed model.

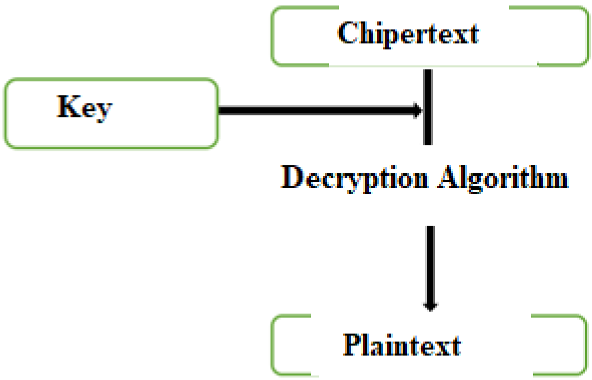

Figure 2. Decryption diagram of the proposed model.

2.1. Encryption Algorithm

First of all, in the encryption algorithm, after the data is encrypted with a key using a set of rules, the obtained data is recorded in the database. The working principle of the encryption algorithm is as follows.

- The data to be encrypted is processed in octal blocks with the key.
- The key to be used must consist of eight characters.
- Mode 256 is used in encryption calculations.
- All keys and data are processed by converting them to Binary in blocks of octal.

Steps;

- With the eight-character key, the first eight characters of the data are converted to Binary,
- A new key is created by combining the odd numbers of the key with the even numbers of the data.
- A new message is created by combining the odd numbers of the data with the even numbers of the key.
- The bits of the new key (0-31) are XORing the bits of the new data (32-63), and the bits of the new key (32-63) are XORing the bits of the new data (0-31),
- Then, the base two numbers are converted to decimal.
- The decimal number obtained in the next step is subtracted from 255.
- Whichever character the output value represents; this character is recorded in the database.

2.2. Decryption Algorithm

The decryption process is the decryption by applying the steps in the encryption algorithm in the opposite direction. The working principles of the decryption algorithm are as follows:

- Encrypted characters have a decimal equivalent.
- The value in decimal base is subtracted from 255.
- The entire key is accomplished by converting the encrypted data into Binary in blocks of octal.
- Encrypted data is processed by the key in octet blocks.
- The message is reached by performing the displacement operation in these octal blocks.

2.3. Application

		Anahtar=	Sim_2816					Mesaj=	ElifAsaf		
S	=	01010011	2	=	00110010	E	=	01000101	A	=	01000001
i	=	01101001	8	=	00111000	l	=	01101100	s	=	01110011
m	=	01101101	1	=	00110001	i	=	01101001	a	=	01100001
_	=	01011111	6	=	00110110	f	=	01100110	f	=	01100110

Figüre 3. Key and message binary conversion

S		i		m		_		2		8		1		6	
1	2	**3**	4	**5**	6	**7**	8	**9**	10	**11**	12	**13**	14	**15**	16
0101	0011	0110	1001	0110	1101	0101	1111	0011	0010	0011	1000	0011	0001	0011	0110

E		l		i		f		A		s		a		f	
1	**2**	3	**4**	5	**6**	7	**8**	9	**10**	11	**12**	13	**14**	15	**16**
0100	0101	0110	1100	0110	1001	0110	0110	0100	0001	0111	0011	0110	0001	0110	0110

Figüre 4. Separation process of key and message binary conversion

In Figures 3 and 4, a new key is obtained by bringing together the odd numbers of the key and the even numbers of the message obtained in the separation process of the binary conversion of the key and the message. The new message is obtained by bringing the odd numbers of the message and the even numbers of the key side by side.

yeni anahtar															
1 a	2 m	3 a	4 m	5 a	6 m	7 a	8 m	9 a	10 m	11 a	12 m	13 a	14 m	15 a	16 m
0101	0101	0110	1100	0110	1001	0101	0110	0011	0001	0011	0011	0011	0001	0011	0110

yeni mesaj															
1 m	2 a	3 m	4 a	5 m	6 a	7 m	8 a	9 m	10 a	11 m	12 a	13 m	14 a	15 m	16 a
0100	0011	0110	1001	0110	1101	0110	1111	0100	0010	0111	1000	0110	0001	0110	0110

Figure 5. Generated new key and new message

Figure 6 shows the process of XORing the bits of the new key (0-31) with the bits of the new message (32-63), then the bits of the new key (32-63) and the bits of the new message (0-31).

	0101	0101	0110	1100	0110	1001	0101	0110	yeni anahtarın 0-31 bitleri
XOR	0100	0010	0111	1000	0110	0001	0110	0110	yeni mesajın 32-63 bitleri
	0001	0111	0001	0100	0000	1000	0011	0000	

	0011	0001	0011	0011	0011	0001	0011	0110	yeni anahtarın 32-63 bitleri
XOR	0100	0011	0110	1001	0110	1101	0110	1111	yeni mesajın 0-31 bitleri
	0111	0010	0101	1010	0101	1100	0101	1001	

Figure 6.XOR'ing process

The binary data obtained in the next step is shown in figure 7 in decimal form.

0001 0111	0001 0100	0000 1000	0011 0000	0111 0010	0101 1010	0101 1100	0101 1001
23	20	8	48	114	90	92	89

Figure 7. Converting Binary to Decimal

The numbers in the next step are subtracted from 255. The operations performed are shown in Figure 8.

255	-	23	=	232
255	-	20	=	235
255	-	8	=	247
255	-	48	=	207
255	-	114	=	141
255	-	90	=	165
255	-	92	=	163
255	-	89	=	166

Figure 8. Transaction result

The characters (Ş Ù ¸ ¤ ì Ñ ú ª) corresponding to the ASCII code of these obtained numbers are recorded in the database. Figure 9 shows the unencrypted recorded form in the database, and figure 10 shows the registration information in encrypted form.

Tablo1 Tablo1

Numara	ad	soyad
1	Elif	Asaf

Figüre 9. Unencrypted information

Tablo1 Tablo1

Numara	ad	soyad
2	Ş Ù ¸ ¤	ì Ñ ú ª

Figure 10. encrypted information

2.4. Decryption

First, the ASCII equivalents of the characters are found and these values are subtracted from 255. The operations performed are shown in Figure 11.

255	-	232	=	23
255	-	235	=	20
255	-	247	=	8
255	-	207	=	48
255	-	141	=	114
255	-	165	=	90
255	-	163	=	92
255	-	166	=	89

Figure 11. Transaction result

The numbers obtained as a result of the operation are converted to Binary code. In the next step, the encrypted data with the key is subjected to XOR'ing.

	0101	0011	0110	1001	0110	1101	0101	1111	0011	0010	0011	1000	0011	0001	0011	0110	anahtar
XOR	0001	0010	0001	1010	0000	1100	0011	1001	0111	0111	0101	0100	0101	1000	0101	0000	şifreli veri
	0100	0001	0111	1101	0110	0001	0110	0110	0100	0101	0110	1100	0110	1001	0110	0110	

Figure 12. Decryption of data

The next step is to successfully decode the encrypted data by relocating the sequence of the new Binary code obtained according to the specified algorithm.

3. Conclusion

They are constantly attacking e-commerce websites, servers of public institutions and private companies by malicious people. Cyber-attacks on e-commerce websites have increased worldwide, especially during the pandemic process. As a result of these attacks, sometimes companies suffer financial damage, and sometimes companies cause loss of reputation.

From time to time, people are shopping on e-commerce sites that cannot be secured without realizing it. When a cyber-attack occurs on the e-commerce website where they shop, people stop shopping on this e-commerce website because they think that their information will be stolen and shared with others, even if they do not suffer any harm.

A new substitution method has been developed for non-linear block ciphers, and all information on e-commerce sites is encrypted in the database. Even if they capture all the information in the database as a result of such attacks, malicious people will not gain anything because the data is meaningless. In this case, it allows people to shop online safely. In addition, financial loss will not occur in companies and companies will not be discredited. In public institutions and private companies, there will be no chaos as there will be no service disruption. A new substitution method for non-linear block ciphers creates a secure trade area as well as secure education, secure communication, etc. It can be integrated into many fields.

References

[1]. Keliher L., Linear Cryptanalysis of Substitution-Permutation Networks, Ph.D. Thesis, 2002.

[2]. Lu, J., & Seo, H. (2020). A Key Selected S-Box Mechanism and Its Investigation in Modern Block Cipher Design. Security and Communication Networks, 2020.

[3]. Abood, O. G., Elsadd, M. A., & Guirguis, S. K. (2017, December). Investigation of cryptography algorithms used for security and privacy protection in smart grid. In 2017 Nineteenth International Middle East Power Systems Conference (MEPCON) (pp. 644-649). IEEE.

[4]. Gençoğlu, M. T. (2019). Importance of Cryptography in Information Security. IOSR J. Comput. Eng, 21(1), 65-68.

[5]. Petre, I., 2006, Cryptography and Network Security Lecture 3: Block ciphers and DES, [Online], Abo Akademi University, http://web.abo.fi/~ipetre/crypto/lecture3.pdf (Erişim Tarihi:15.11.2007)

[6]. Gençoğlu,, M. T. (2019). Embedded image coding using laplace transform for Turkish letters. Multimedia Tools and Applications, 78(13), 17521-17534.

[7]. Kumar, M. A., & Karthikeyan, S. (2012). Investigating the efficiency of Blowfish and Rejindael (AES) Algorithms. International Journal of Computer Network and Information Security, 4(2), 22.

[8]. Sharif, S. O., & Mansoor, S. P. (2010, August). Performance analysis of stream and block cipher algorithms. In 2010 3rd International Conference on Advanced Computer Theory and Engineering (ICACTE) (Vol. 1, pp. V1-522). IEEE.

[9]. Gençoğlu, M. T. (2017). Combining Cryptography with Steganography. In ITM web of Conferences (Vol. 13, p. 01010). EDP Sciences.

[10]. Gençoğlu, M. T. (2017). Cryptanalysis of a new method of cryptography using laplace transform hyperbolic functions. Communications in Mathematics and Applications, 8(2), 183-189.

[11]. Gençoğlu, M.T., Vural, M, Enhancing The Data Security by using Audio Steganography with Taylor Series Cryptosystem, Turkish Journal of Science & Technology 16(1), (2021) 47-64.

[12]. Schneier, B. (1993, December). Description of a new variable-length key, 64-bit block cipher (Blowfish). In International Workshop on Fast Software Encryption (pp. 191-204). Springer, Berlin, Heidelberg.

[13]. Gençoğlu, M. T. (2018). Kaotik Fonksiyonlar Ile EKG Sinyalleri Kullanarak Kişisel Bilgi Şifrelemenin Matematiksel Kriptoanalizi. Fırat Üniversitesi Mühendislik Bilimleri Dergisi, 32(2).

[14]. Gençoğlu, M. T. Cryptographic Defence With Embedded Audio Based on Bernoulli Numbers. International Journal of Engineering Science and Application, 3(4), 159-163.

[15]. Vural, M., Gençoğlu, M. T. (2018). Embedded audıo codıng usıng laplace transform for turkısh letters. Fundamental scıences and applıcatıons, 109.

[16]. Wang, X., Wang, X., Zhao, J., & Zhang, Z. (2011). Chaotic encryption algorithm based on alternant of stream cipher and block cipher. Nonlinear Dynamics, 63(4), 587-597.

[17]. Gençoğlu, M.T., Vural, M, Image Codıng Usıng Laplace Transform, ITM Web of Conferences 22, 01010 (2018), Doi: 10.1051/itmconf/20182201010

[18]. Daemen, J., & Rijmen, V. (1998, September). The block cipher Rijndael. In International Conference on Smart Card Research and Advanced Applications (pp. 277-284). Springer, Berlin, Heidelberg.

RANDOM NUMBER GENERATORBASED CASCADE FUNCTION

Tuncay Genç[1], Muharrem Tuncay Gençoğlu[2]

[1] Institute of Science, University of Firat, Elazig, Turkey,tncygnc@gmail.com

[2]Vocational School of Technical Sciences, University of Firat, Elazig, Turkey,mtgencoglu23@gmail.com

Abstract

cascade function is designed by combining two seed maps that resultantly have more parameters, high complexity, randomness, and more unpredictable behavior. In the paper, a cascade fractal function, i.e. cascade-PLMS is proposed by considering the phoenix and lambda fractal functions. The constructed cascade-PLMS exhibits the required fractal features such as fractional dimension, self-similar structure, and covering entire phase space by the data sequence in addition to the chaotic properties. Due to the chaotic behavior, the proposed function is utilized to generate a pseudo-random number sequence in both integer and binary format. This is the result of an extreme scalability feature of a fractal function that can be implemented on a large scale. A sequence generator is designed by performing the linear function operation to the real and imaginary part of a cascade-PLMS, cascade-PLJS separately, and the iteration number at which the cascade- LJS converges to the fixed point. The performance analysis results show that the given method has a large keyspace, fast key generation speed, high key sensitivity, and strong randomness. Therefore, the scheme can be efficiently used further to design a secure cryptosystem with the ability to withstand various attacks.

Keywords: Cascade phoenix lambda fractal, PRNG, Mandelbrot set, Dynamic behavior, Key security analysis.

1. Introduction

The Internet age has caused the need for network security to expand as a result of digital information flowing over an insecure environment. Cryptography is one of the most obvious ways to protect data from illegal users [1]. Since the last few years, a chaotic system has attracted researchers to use it in the field of cryptography. The dynamic properties of a nonlinear chaotic system such as unpredictability, randomness, sensitivity to a minute change in initial value, ergodicity, complexity and deterministic dynamics lead to the design of a secure encryption system. The above-mentioned features prepare for the construction of a chaotic system with increased security and high complexity [2, 3].

A fractal is a graphical representation of a chaotic function with a complex structure and infinite scaling in all directions. In addition to chaotic behavior, a fractal function has properties such as construction in a complex space, fractal dimension, and self-similarity [4, 5]. A hybrid fractal function includes a larger number of control parameters but has the characteristics of seed functions. Recently, the composite fractal function has been proposed by the authorities for image encryption systems [6]. Many hybrid chaotic maps and their applications have been studied by cryptography researchers and s-box design researchers [7-11]. In addition, it is widely used in user authentication for medical image analysis and image hashing [12, 13]. Unpredictable behavior and extreme sensitivity to change in initial values have led to the fractal function being preferred for designing a pseudo-random number generator (PRNG).

A so-called word denotes a random sequence calculated using a deterministic system. According to mathematical theory, a deterministic system can be predicted. A complex array producer whose seed value can be selected can help increase safety and reduce correlation in the produced sequence. A PRNG has a wide range of applications in various fields such as the gaming industry, artificial intelligence, cryptography, statistical simulation. On the other hand, by visualizing the spontaneous chaotic oscillation of the current, a real random number sequence with semiconductor advantages is generated [14].

Recently, Barnsley's chaos game rules have been used to generate a pseudo-random number generator [15]. A complex Newtonian fractal function was used to generate a safe PRNG due to strong statistical data and a random phase gap [16]. An additional advantage of the map is to have an integer and a PRNG in complex form. A modified logistic map was used to generate a two-stage PRNG, including the first pseudorandom number generator and the normal pseudorandom number generator, using the value obtained in the previous phase [17]. Another modified logistic map, XOR, has been successfully applied to generate random bit sequences by making a comparison between the inversion maps [11]. An original logistic map is combined with a piecewise map with a chaotic pseudorandom number generator [18]. To overcome the chaotic distortion due to computational accuracy, a self-perturbing hyperchaotic system-based PRN generator is proposed. The hyperchaotic map used was obtained using the classical Lorenz three-dimensional chaotic system [19]. A similar Lorenz-like Chen chaotic system was used in a study to construct a complex pseudorandom number generator [20,21]. Previously, a PRN generator was proposed using time series obtained from the generalized Lorenz chaotic map [10]. In another study, he proposed a method to extract about 8 bits per iteration from the decimal part of the chaotic map and generate a PRNG [11]. The method has been tested on various one-dimensional maps, including the logistic map, sine map, Renyi map, Chebyshev map, cubic map, cubic logistic map.

This study includes designing a pseudo-random number generator using a generalized cascade fractal function and the applicability of the function. The emergence of the chaotic features of the two maps provides a more complex environment for generating PRNG. A change in any single parameter creates an entirely new set of data, the most important requirement of a secure PRNG. The main contribution in the article can be summarized as follows:

1. The cascade structure of the fractal function is realized using the Phoenix and lambda fractal functions.

2. The dynamic behavior of the proposed cascade PLMS is analyzed and thoroughly investigated in terms of size, self-similar structure, trajectory and spider web diagram.

3. It is a cascade-PLMS, cascade-Phoenix Lambda Julia Set (cascade-PLJS) fractal function and a fixed point value specific cascade-PLJS method to generate a pseudo-random number generator.

4. Randomness and security of the generated PRNG, key gap key sensitivity, correlation value, autocorrelation analysis, information entropy, etc. verified by various tests such as

The remainder of the work is organized as follows. The proposed cascade-PLMS structure and cascade-PLJS and its dynamic properties are examined in Chapter 2. In section 3, the generated fractal functions are applied to generate a pseudo-random number generator. Randomness and security performance are used in the analysis of the PRNG produced in section 4. Finally, the article concludes with the direction of future work in Chapter 5.

2. Cascade Fractal Function and Dynamic Behavior Analysis

A cascade fractal function (Cascade-FF) is designed by considering two sequence-dependent core functions (For example F_1(x) and F_2(x)). For each iteration, the output of F_1(x) is put as input to F_2(x), and the output of F_2(x)is put as an input to F_1(x). If a repetitive output value is supplemented together, the number of iterations limit is exceeded [22]. Mathematically, for functions F_1(x) and F_2(x), a cascade-FF is defined as:

$$x_{n+1} = F_1(F_2(x_n)) \quad (1)$$

where F_1(x) andF_2(x) are two kernel functions that can be the same or different. Cascade function; Also known as function using cascade FF design. In this case, the function will be defined as:

$$x_{n+1} = F_1(F_1(x_n)) \quad (2)$$

Cascade FF has the ability to introduce different structures while changing the order of the contributing core functions.

$$x_{n+1} = F_1(F_2(x_n)) \quad (3)$$

and

$$x_{n+1} = F_2(F_1(x_n)) \quad (4)$$

This study focuses on one aspect of designing cascade FF using phoenix and lambda fractal function. If we recall the mathematical definition of Phoenix fractal and lambda fractal functions respectively [23]:

$$\begin{gathered} z_{n+1} = z_n^a + z_n^b * c + p * z_{n-1} \\ z_{n+1} = c * z_n * (1 - z_n)^{w-1} \end{gathered} \quad (5)$$

Here $c \in C$, and $-1<p<1$, $z_0 \neq 0$. The fractal images created by performing both functions are shown in Figure 1.

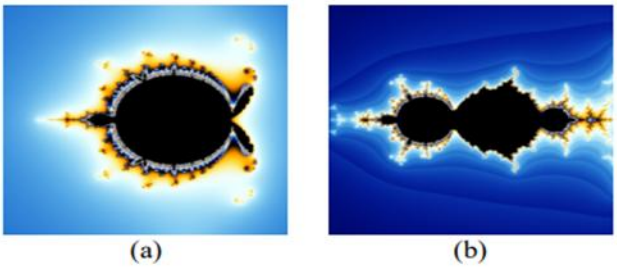

Figure 1. (a) Phoenix fraktal, (b) Lambda fraktal

2.1. Cascade-PLMS and Cascade-PLJS

It is stated that a cascade-PLMS function has a more complex and chaotic structure controlled by many parameters compared to a separate function. Too many parameters change their value, providing flexibility to have more randomness and unpredictable output sequences. Assuming the Phoenix fractal as $F_1(x)$ and lambda fractal $F_2(x)$, a cascade-PLMS is defined as follows:

All variables have normal meanings except temps. Phoenix function; Represents an intermediate value as an input supporting the lambda function. The cascade-PLMS function is a set of c values for the trajectory of the initial value, that is, z_n remains confined under the function iteration. The proposed cascade-PLMS function is used to generate a pseudo-random sequence of numbers with parameter values $z_0 = 0.09$, $p = -0.03$, a=2, b=1 and w=3.

Cascade-PLJS is nothing more than a fractal image for a fixed value c that starts with a nonzero z-value of the same function. This study showed a cascade-PLJS image for c = (0.7444196429, 0.6863839286). Both fractal images were drawn using UltraFractalTM for the parameter values given above and are shown in Figure 2. Repetitive execution of the function with a fixed value of c converges to an attractor with a fixed point or outside it, depending on whether the value c is inside the cascade PLMS image. The convergence rate of the function changes for different values of c. It will be used in the iteration number cascade-PLJS convergence pseudo-random number generation method.

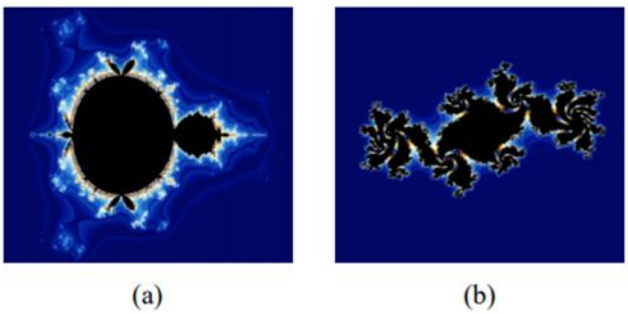

Figure 2. (a) Cascade-PLMS, (b) Cascade-PLJS

2.1.1. Dynamic Feature Analysis of Cascade-PLMS
2.1.1.1. Self Similar Structure

It is well known that a fractal image has a self-similar structure at a wide variety of different scales. The beauty of the Mandelbrot set is that it has endless knowledge about a small area of interest. As you zoom in on the set, newer fascinating images will be obtained. A new cascade PLMS is expected to generate artistically new examples and attractive fractal images after further research. Randomly selected fractal images obtained by zooming the cascade-PLMS function are shown in Figure 3.

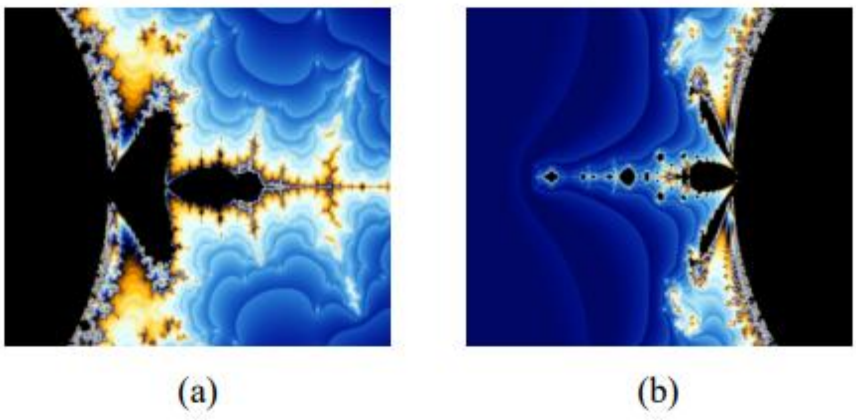

Figure 3. (a)-(b) Zoomed version of Cascade-PLMS

2.1.1.2. Fractal Dimension

According to Felix Hausdorff, rough and broken fractal images should have a dimension "between" [24]. This is a common way of measuring the complexity of the fractal image boundary.

An irregular two-dimensional fractal image is expected to have a dimension value between one and two.

Recently, the author developed a user interface to calculate the fractal dimension using the box-counting method [25]. If a fractal image is superimposed with a grid of N squares to occupy E number of sides, the fractal size can be calculated as:

$$dim = \frac{\text{Log}\,N}{\text{Log}\,E} \qquad (7)$$

The fractal dimension is a recommended system for several-digit PLMS. The results obtained were able to meet the requirement of a fractal function. The fractal dimension of the proposed stepped PLMS function for the parameters discussed above is 1.1535.

2.1.1.3. Trajectory and Cobweb Diagram

Orbital and spider web diagrams are used to successfully display successive iterations of a function The only difference is that a spider web diagram presents the function behavior of a one-dimensional map whereas an orbital diagram is used to show the path of the generated number array of the multidimensional map. The chaotic behavior of a function can be verified by spreading the generated sequence overtime over the entire phase space. A cascade PLMS fractal image is generated based on the number of iterations to constrain the first value in it. At the same time, a complex number array is generated in the execution of the function for each initial value. Therefore, Figure 4 below shows a trajectory diagram showing the occupancy of space with the recurrence values, as well as a spider web diagram showing the relationship between real and imaginary values. It can be said that the data covers the whole phase space in both diagrams.

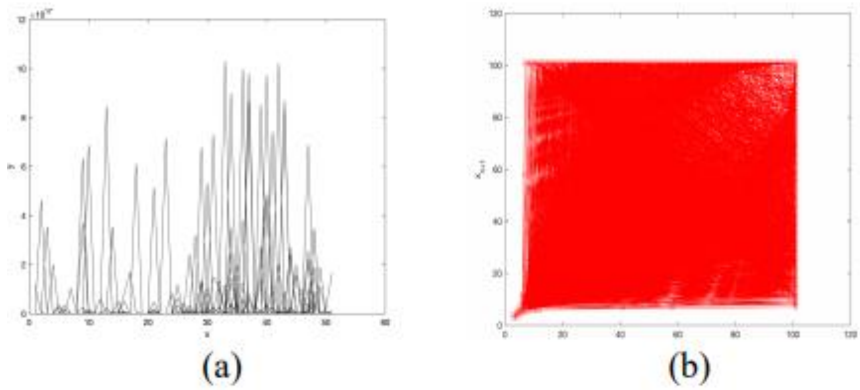

Figure 4. (a) Trajectory diagram, (b) Cobweb diagram

3. Pseudo-Random Number Generator Application

The pseudo-random number generator is implemented taking into account the cascade-PLMS and related cascade-PLJS functions suggested above. All randomness tests verify the proposed suitability for generating an unpredictable sequence of cascade functions. A pictorial representation of the proposed method can be seen in Figure 5.

Figure1. Block diagram of the proposed PRNG method

6

The process starts by executing both functions using the initial values set within their respective value ranges. Here, the cascading-PLMS function returns the initial values (z0, a, b, c, p, w) (0.09, 2, 1, 0, -0.03) while considering the c value (0.7444196429, 0.6863839286). , 3) Creates an array taking into account in Cascade-PLJS, which assumes other values as well as in Cascade-PLMS. The proposed detailed method technique is explained as follows:

Step 1: Calculate zdataMS and zdataJS as a complex set of numbers after running Cascade-PLMS and cascade-PLJS using the initial values mentioned above, respectively.

Step 2: Calculate the fixed point of the cascade-PLJS function for a given value of c and record the maximum number of iterations at which the fixed point is obtained.

Step 3: Split the real and imaginary parts of zdataMS into zdataMSreal and zdataMSimg, convert it to a one-dimensional array.

Step 4: Repeat step 3 using zdataJS and get the one-dimensional vector zdataJSreal and zdataJSimg.

Step 5: Perform the linear function operation on the real number array of both functions and Itr as follows:

$$updatedRealSeq = zdataMSreal * Itr + zdataJSreal \quad (8)$$

Step 6: Perform the same linear function operation on both the function and the imaginary number array of Itr as follows:

$$updatedImgSeq = zdataMSimg * Itr + zdataJSimg \quad (9)$$

Step 7: Convert the floating numbers to an integer by running the given function separately for the real array and the virtual array as follows:

$$IntRealSeq = round((updatedrealSeq * 2^{14}) \bmod 256) \quad (10)$$

$$IntImgSeq = round((updatedImgSeq * 2^{14}) \bmod 256)$$

Step 8: Finally, a pseudo-random sequence is calculated by combining both previously obtained sequences using the following function.

$$PRNG(2 * j) = IntRealSeq(i)$$

$$PRNG(2 * j + 1) = IntImgSeq(i) \quad (11)$$

where i = 1, 2,… starts 500000 and j = 0. . The result is an array of integers of length 106. After converting to binary form, 8 binary strings of length 8 * 106 are produced.

Thus, by combining the digits in a column, eight different binary random number sequences can be created. For a more random result, the array is combined to produce a pseudo-random sequence of numbers while considering the intermediate 500000 value of each real and virtual data.

3.1. Randomness and Security Analysis

3.1.1. Visual Description of PRN Sequence

The trajectory diagram is used to display the sequence created upon the execution of the function for a given set of initial values. A nonlinear pixel path distributed over the entire phase space represents the chaotic behavior of the map. Choosing an appropriate set of initial values can result in the generation of a random set of numbers that do not show periodic or closed curve motion.

Figure 6 shows a trajectory diagram of 500 randomly selected pixels.

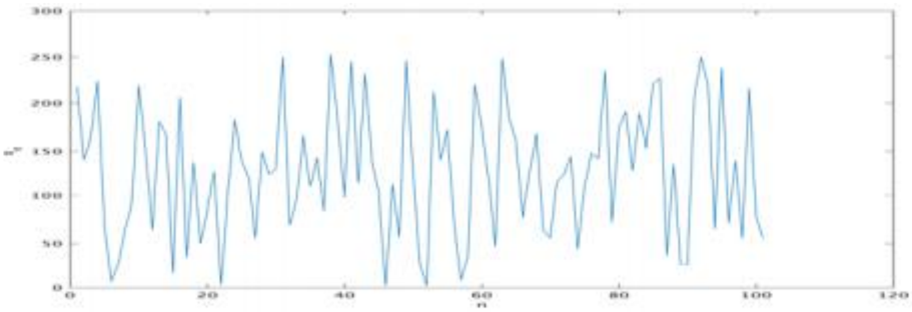

Figure2. Visual path of the generated sequence of numbers

3.1.2. Key Area

The key field is an important directory that represents a secure encryption system. The generator uses a cascade fractal function with a set of initial values and control parameters to generate a pseudo-random sequence. According to the function requirement, a set of values includes (z0, a, b, c, p, w) and a previous z value. According to the IEEE floating-point standard, the calculation precision of the double data type number is about 1015. Therefore, the possible keyspace is calculated as (1015)7=10105 ≈2320. Therefore, the 2100 predetermined key area required to resist force attack is large enough to the range [26].

3.1.2.1. Key Generation Speed

The proposed PRNG method is implemented on MATLABTM with a MacBook Pro with a 2.6 GHz 6 Core Intel Core i7 system configuration and 16 GB memory. The approximate time to generate a random key sequence of size 1000 * 1000 is 0.2084 seconds.

3.2.1.2. Key Sensitivity Using NBCR Analysis

A key sensitivity test analysis is performed to evaluate the effect of a small change in input value on the corresponding output value. The precision of the proposed pseudo-random number generator is tested by performing two tests: 1) visual criterion, 2) several digit change rate (NBCR).

To evaluate the visual effect of the two arrays, one control parameter value of the function is increased by 1014 and the others remain constant. Figure 7 shows the reaction of both the sequences formed with the initial values and the small mixed data set. The order is completely different even if a small change is made to the control parameter value of the generated number. The other test calculates the number of changed bits between two strings.

It is calculated as follows:

$$NBCR = \frac{Ham\_dis(x,y)}{bit\_len} \qquad (12)$$

It is expected that the digit change rate of two different number sequences will be close to 50%. The NBCR result in Table 1 shows that the pseudo-random sequence initially generated is different from the sequence generated after slightly increasing a control parameter value. Therefore, the generated sequences prove the key precision of the proposed pseudo-random number generator.

Table1. NBCR value of sequence produced using original values and modified values

Modified Parameter	NBCR Value
Change in initial value z (Seq1)	49.90
Change in distortion (Seq2)	49.95
Change in power"a" (Seq3)	50.01
Change in power"w" (Seq4)	50.04

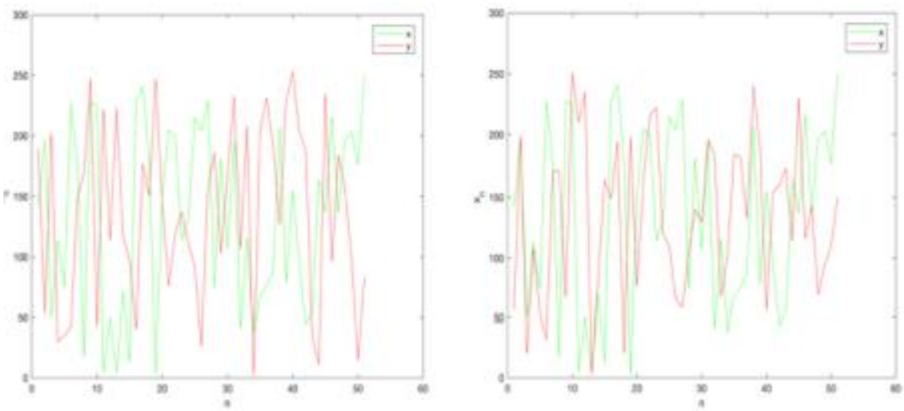

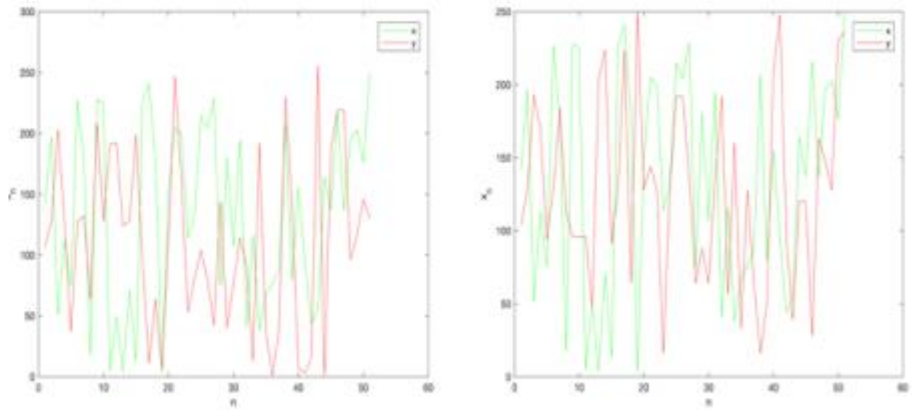

Figure 7. Graphical representation of key sentiment analysis of sequence generated using original values and modified values

3.2.1.3. Entropy Analyses

An information entropy concept was introduced by Shannon to describe the randomness and uncertainty in the information system [27]. It can be calculated using the given function:

$$H(s) = -\sum_{i=0}^{2^n-1} p(x_i) log_2[p(x_i)] \qquad (13)$$

Here, $p(x_i)$ specifies the probability of occurrence of a symbol xi in the pseudo-random sequence. If n digits are required to represent a symbol, the entropy of the information system is assumed to be close to n. A binary string requires only one bit to represent the symbol, i.e. zero or one. Therefore, the entropy value of a binary sequence is equal to one, considered the ideal value to demonstrate the randomness of the sequence.

3.2.1.4. Correlation Analyses

A correlation coefficient is calculated to analyze the relationship between two strings of pseudo-random numbers. A value close to zero indicates no relationship between the two sequences, while a value close to one strongly indicates the presence of a relationship. Because the two functions are cascaded, the pseudo-random number generator has many parameters. Therefore, correlation analysis is done by changing one key at a time and keeping other parameters constant. For the two arrays x and y, the correlation coefficient is calculated using the given equation:

$$CC(x,y) = \frac{N\sum_{i=1}^{N}(x_i y_i) - \sum_{i=1}^{N}(x_i)\sum_{i=1}^{N}(y_i)}{\sqrt{\left(N\sum_{i=1}^{N}(x_i)^2 - \left(\sum_{i=1}^{n}(x_i)^2\right)\right)\left(N\sum_{i=1}^{N}(y_i)^2 - \left(\sum_{i=1}^{n}(y_i)^2\right)\right)}} \qquad (14)$$

Table 2 below shows the effect of changing the parameters in terms of the correlation coefficient value. Each time a new array i.e. y is generated by adding e = $10^{-14}$to the previous parameter value and also keeping the others as before. The function is executed in the same way for each parameter and the corresponding correlation value is calculated. The obtained values indicate the high sensitivity of the array to the minute change in the parameter value.

Table2. Correlation coefficient values of the generated sequence, which are produced and modified using the original values.

Modified Parameter	Correlation coefficient
Change in initial value z (Seq1)	0.0034
Change in distortion (Seq2)	0.0024
Change in power"a" (Seq3)	-0.0003
Change in power"w" (Seq4)	0.0005

3.2.1.5. Autocorrelation Analyses

Autocorrelation analysis is performed to measure the similarity between a sequence of *0S* and its corresponding modified sequence of *0SS*. The formula for calculating the autocorrelation of an array with N dimensions is given as:

$$AC = \frac{M1 - M2}{N} \qquad (15)$$

M1 and M2 indicate the number of matches and mismatches between OS and OSS, respectively. A value falling in the range [-1, 1] indicates a highly random number sequence with little correlation with itself. A graphical view of the pixel autocorrelation can be seen in Figure 8.

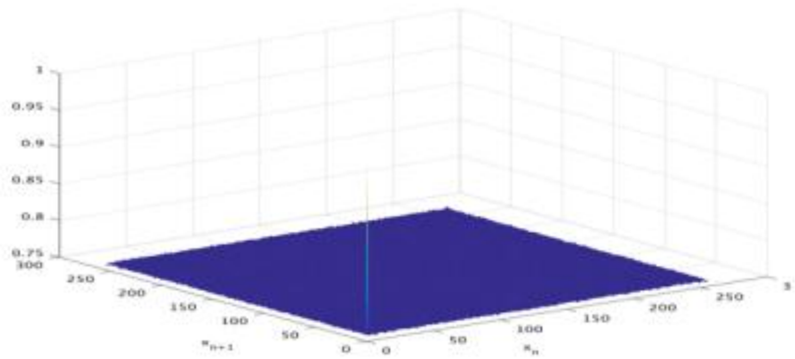

Figure 8. Autocorrelation analysis of the sequence of numbers

4. Conclusion

The function of a cascade fractal can be designed by combining any two available fractals. In this study, the dynamic motion of the cascade-PLMS function is analyzed by considering the phoenix and lambda fractals. The benefit of combining two nonlinear functions is to have a more complex structure that is used more to propose a random non-real number generator. Cascade-PLMS, a linear function operation was applied to the number of iterations obtained as a result of obtaining a fixed point of the cascade-PLJS. This is a view to generate PRNG, which is an integer and can be converted to an 8-bit binary string. Considering the column-by-bit arrangement of the data, a string of eight simultaneous binary numbers can be used in other applications. A small change in any system parameter aimed at the reliability of the generated PRNG results in the generation of a completely new non-real random number sequence. The proposed new concept of cascading fractal functions opens the door for researchers to analyze the feasibility of the model using other existing fractal functions. The choice of fractal definitely affects the complexity result based on the corresponding function combination. In addition, the resulting PRNG; It can be implemented in cryptographic application covering watermarks, encoding digital content and much more. It also aims to examine how quickly a bitstream can be generated so that it can be used in a hardware implementation.

References

[1] Stallings, W. (2006). Cryptography and network security: Principles and practice (4th ed), Pearson/Prentice Hall.

[2] Devaney, R., Devaney, RL. (2003). An Introduction to Chaotic Dynamical Systems, 2nd Edition, CRC Press.8

[3] Takens, F. (1988). An introduction to chaotic dynamical systems. *Acta Applicandae Mathematica*, C. 13(1), 221–226. doi:10.1007/BF00047506.

[4] Recknagel, F. (2006). Ecological Informatics–Scope, Technique and Applications. Springer, Berlin, Germany.

[5] Devaney, R., Keen, L. (Eds.). (1989). Chaos and Fractals: The Mathematics Behind the Computer Graphics (Vol. 39). *American Mathematical Society*. doi:10.1090/psapm/039.

[6] Mandelbrot, BB. (1982). The Fractal Geometry of Nature (2nd edition), Times Books.

[7] Agarwal, S. (2020). A new composite fractal function and its application in image encryption, *Journal of Imaging*, C. 6(7),70.

[8] Artuğer, F., Özkaynak, F. (2020). A novel method for performance improvement of chaos-based substitution boxes. *Symmetry*, C.12(4), 571. doi:10.3390/sym12040571.

[9] Bai, S., Zhou, L., Yan, M., Ji, X., Tao, X. (2020). Image cryptosystem for visually meaningful encryption based on fractal graph generating. *IETE Technical Review*, C. 0(0), 1–12. doi:10.1080/02564602.2020.1799875.

[10] Hua, Z., Jin, F., Xu, B., Huang, H. (2018). 2D Logistic-Sine-coupling map for image encryption. *Signal Processing*, C. 149, 148–161. doi:10.1016/j.sigpro.2018.03.010.

[11] Lynnyk, V., Sakamoto, N., Čelikovský, S. (2015). Pseudorandom number generator based on the generalized Lorenz chaotic system. *IFAC-PapersOnLine*, C. 48(18), 257–261. doi:10.1016/j.ifacol.2015.11.046.

[12] Moysis, L., Tutueva, A., Volos, C., Butusov, D., Munoz-Pacheco, JM., Nistazakis, H. (2020). A two-parameter modified logistic map and its application to random bit generation. *Symmetry*, C. 12(5), 829. doi:10.3390/sym12050829.

[13] Nayak, SR., Mishra, J. (2019). Analysis of Medical Images Using Fractal Geometry, Histopathological Image Analysis in Medical Decision Making. *IGI Global*. doi:10.4018/978-1-5225-6316-7.ch008.

[14] Khelaifi, F., He, H. (2020). Perceptual image hashing is based on structural fractal features of image coding and ring partition. *Multimedia Tools and Applications*, C. 79(27), 19025–19044. doi:10.1007/s11042-020-08619-w.

[15] Bonilla, LL., Alvaro, M., Carretero, M. (2016). Chaos-based true random number generators. *Journal of Mathematics in Industry*, C. 7(1), 1. doi:10.1186/s13362-016-0026-4.

[16] Ayubi, P., Setayeshi, S., Rahmani, AM. (2020). Deterministic chaos game: A new fractal-based pseudorandom number generator and its cryptographic application. *Journal of Information Security and Applications*, C.52, 102472. doi:10.1016/j.jisa.2020.102472.

[17] Jafari Barani, M., Ayubi, P., Yousefi Valandar, M., Irani, BY. (2020). A new Pseudo-random number generator based on a generalized Newton complex map with dynamic key. *Journal of Information Security and Applications*, C. 53, 102509. doi:10.1016/j.jisa.2020.102509.

[18] Wang, L., Cheng, H. (2019). Pseudo-random number generator based on a logistic chaotic system. *Entropy*, C. 21(10), 960.

[19] Sahari, ML., Boukemara, I. (2018). A pseudo-random numbers generator based on a novel 3D chaotic map with an application to color image encryption. *Nonlinear Dynamics*, C. 94(1), 723–744. doi:10.1007/s11071-018-4390-z.

[20] Zhao, Y., Gao, C., Liu, J., Dong, S. (2019). A self-perturbed pseudo-random sequence generator based on hyperchaos. *Chaos, Solitons & Fractals*, C. 10(4), 100023. doi:10.1016/j.csfx.2020.100023.

[21] Chen, G., Ueta, T. (1999). Yet another chaotic attractor. *International Journal of Bifurcation and Chaos*, C. 09(07), 1465–1466. doi:10.1142/S0218127499001024.

[22] Hamza, R. (2017). A novel pseudo-random sequence generator for image-cryptographic applications. *Journal of Information Security and Applications*, C. 35, 119–127. doi:10.1016/j.jisa.2017.06.005.

[23] Zhou, Y., Hua, Z., Pun, CM., Philip Chen, CL. (2015). Cascade chaotic system with applications. *IEEE Transactions on Cybernetics*, C. 45(9), 2001–2012. doi:10.1109/TCYB.2014.2363168.

[24] Peitgen, HO., Jürgens, H., Saupe, D. (1992). Chaos and fractals: new frontiers of science. *SpringerVerlag*. doi:10.1007/978-1-4757-4740-9.

[25] Czyz, J. (1994). The hausdorff measures, hausdorff dimensions and fractals. *Paradoxes of Measures and Dimensions Originating in Felix Hausdorff's Ideas*, C. 1–0, 219–413. doi:10.1142/9789814368193_0004

[26] Çimen, ME., Garip, Z., Boyraz, ÖF., Pehlivan, İ., Yildiz, MZ., Boz, AF. (2020). An interface design for calculation of fractal dimension. *Chaos Theory and Applications*, C. 2(1), 3–9.

[27] Alvarez, G., Li, S. (2006). Some basic cryptographic requirements for chaos-based cryptosystems. *International Journal of Bifurcation and Chaos*, C. 16(08), 2129–2151. doi:10.1142/s0218127406015970.

[28] Shannon, C. E. (1949). Communication Theory of Secrecy Systems. *Bell System Technical Journal*, C. 28(4), 656–715. doi:10.1002/j.1538-7305.1949.tb00928.x.

5th INTERNATIONAL CONFERENCE ON COMPUTATIONAL MATHEMATICS AND ENGINEERING SCIENCES

www.cmescongress.org
cmes2020van@gmail.com